1977

Turbulent mixing with chemical reaction and Collection of inertialess particles on cylinders and spheroids with electrical forces and gravitation

Kenneth Andrew Nielsen
Iowa State University

INFORMATION TO USERS

This was produced from a copy of a document sent to us for microfilming. While the most advanced technological means to photograph and reproduce this document have been used, the quality is heavily dependent upon the quality of the material submitted.

The following explanation of techniques is provided to help you understand markings or notations which may appear on this reproduction.

1. The sign or "target" for pages apparently lacking from the document photographed is "Missing Page(s)". If it was possible to obtain the missing page(s) or section, they are spliced into the film along with adjacent pages. This may have necessitated cutting through an image and duplicating adjacent pages to assure you of complete continuity.

2. When an image on the film is obliterated with a round black mark it is an indication that the film inspector noticed either blurred copy because of movement during exposure, or duplicate copy. Unless we meant to delete copyrighted materials that should not have been filmed, you will find a good image of the page in the adjacent frame.

3. When a map, drawing or chart, etc., is part of the material being photographed the photographer has followed a definite method in "sectioning" the material. It is customary to begin filming at the upper left hand corner of a large sheet and to continue from left to right in equal sections with small overlaps. If necessary, sectioning is continued again–beginning below the first row and continuing on until complete.

4. For any illustrations that cannot be reproduced satisfactorily by xerography, photographic prints can be purchased at additional cost and tipped into your xerographic copy. Requests can be made to our Dissertations Customer Services Department.

5. Some pages in any document may have indistinct print. In all cases we have filmed the best available copy.

University
Microfilms
International

300 N. ZEEB ROAD, ANN ARBOR, MI 48106
18 BEDFORD ROW, LONDON WC1R 4EJ, ENGLAND

NIELSEN, Kenneth Andrew

TURBULENT MIXING WITH CHEMICAL REACTION AND COLLECTION OF INERTIALESS PARTICLES ON CYLINDERS AND SPHEROIDS WITH ELECTRICAL FORCES AND GRAVITATION.

Iowa State University Ph.D. 1977

Turbulent mixing with chemical reaction

and

Collection of inertialess particles on cylinders and spheroids with electrical forces and gravitation

by

Kenneth Andrew Nielsen

A Dissertation Submitted to the
Graduate Faculty in Partial Fulfillment of
The Requirements for the Degree of
DOCTOR OF PHILOSOPHY

Department: Chemical Engineering and Nuclear Engineering
Major: Chemical Engineering

Approved:

Signature was redacted for privacy.

In Charge of Major Work

Signature was redacted for privacy.

For the Major Department

Signature was redacted for privacy.

For the Graduate College

Iowa State University
Ames, Iowa

1977

TABLE OF CONTENTS

ABSTRACT

By numerically integrating the Fourier transformed exact conservation equations of reactants over time using a numerical simulation of a homogeneous isotropic turbulent velocity field for the convection velocity, O'Brien's and Toor's statistical independence hypotheses were tested using numerical experiments in which reaction and mixing conditions were carefully controlled. Two simulated turbulent velocity fields that obey continuity were used for the tests. The first has a constant specified energy spectrum (and hence constant time and distance scales) but lacks interaction between Fourier modes. The second velocity field, which is generated using a modified form of the Navier-Stokes equation, has interaction and conserves turbulent energy but the energy spectrum is transient.

For single component second-order reactions, O'Brien's statistical independence hypothesis successfully predicted that the decay of concentration fluctuation intensity for turbulent mixing with reaction can be estimated by the product of the intensity decay for pure mixing without reaction and intensity decay for pure reaction without mixing. The results suggest that counteracting or canceling of two opposing physical tendencies may be responsible for the success of O'Brien's hypothesis. However, O'Brien's hypothesis of Fourier mode independence exhibited significant

error in some cases.

For two-species second-order reactions with stoichiometric reactants and equal diffusivities, Toor's statistical independence hypothesis successfully predicted (within the ability of the turbulence simulation to describe segregation tendencies of the species) that the decay of the covariance of the concentration fluctuations of the two species is insensitive to the rate of reaction and can be approximated by pure mixing results. The deviation of the hypothesis from the actual results that does occur underestimates the covariance decay and is strongly correlated with the deviation of the correlation coefficient from -1. For unequal diffusivities with stoichiometric reactants, Toor's hypothesis shows significant error. A strong correlation exists between the extent of the deviation and the ratio of the correlation coefficient for mixing with reaction to the correlation coefficient for pure mixing. For nonstoichiometric reactants with equal diffusivities, Toor's hypothesis quickly breaks down as the Damköhler number increases from being small. For this case, the extent of the deviation is strongly correlated with the ratio of the fluctuation intensity of the limiting reactant to the fluctuation intensity of the reactant in excess. The results indicate that Toor's hypothesis can be applied to systems that are not initially segregated provided the correlation coefficient of the fluctuations is -1.

Although the mixing characteristics of the two velocity fields differ, deviations of O'Brien's hypothesis and Toor's hypothesis are similar for both mixing fields.

Particle trajectories and collection efficiencies are predicted for the collection of fine, inertialess, charged particles (on a single collecting element) in fibrous filters and wet scrubbers by the combined actions of coulombic and external electric field forces, gravity, and particle interception. Two methods of solution are used that are valid for stationary incompressible flows and solenoidal force fields. The first method, which can only be used for two-dimensional trajectories, determines limiting trajectories using stream functions. The second method, which can be used for nonsymmetrical three-dimensional trajectories, determines the particle flux to the collector.

For collection on fibers, results for circular and elliptical cylinders and ribbons are found for cases of the external fields and the flow being at an arbitrary orientation to each other and the collector. The results reveal how the collection efficiency is affected by such factors as the form of the flow field, the orientation of the external fields and the flow, fiber geometry, and an accumulation of previously collected particles. The analytical solution for particle trajectories is used to investigate the growth of particle chains from the surface of the collector.

For collection on droplets, results for prolate and oblate spheroids and spheres are found for cases of the external fields being parallel to the axis of symmetry but with the flow being at an arbitrary angle to both the axis of symmetry and the external fields.

For single force cases, results are found that are independent of collector geometry. In general, for a given collector geometry, with a combination of the forces, theory indicates that deposition of point particles is the same for all stationary incompressible flows. With the coulombic force alone, particle collection is independent of both collector geometry and the flow field.

The influence of fiber packing density in filters and droplet density in scrubbers on collection is investigated using a cellular model of flow around a circular cylinder or a sphere, and is shown to have little effect on single fiber or droplet collection efficiencies.

PART I. TURBULENT MIXING WITH CHEMICAL REACTION

NOMENCLATURE

In the Introduction, Statistical Description of Turbulence, Pure Mixing, and Literature Review sections, the asterisk, which denotes a dimensional variable in all other sections, is omitted and all variables are dimensional, unless otherwise indicated.

Latin:

$C^*(\underset{\sim}{x}^*,t^*)$	instantaneous physical-space concentration
$C(\underset{\sim}{x},t)$	$= C^*(\underset{\sim}{x}^*,t^*)/\overline{C}_0^*$, dimensionless instantaneous physical-space concentration
$\overline{C}^*(t^*)$	volume-averaged concentration
$\overline{C}(t)$	$= \overline{C}^*(t^*)/\overline{C}_0^*$, dimensionless volume-averaged concentration
$\overline{C}_0^*$	$= \overline{C}^*(0)$
$c^*(\underset{\sim}{x}^*,t^*)$	$= C^*(\underset{\sim}{x}^*,t^*) - \overline{C}^*(t^*)$, instantaneous physical-space concentration fluctuation
$c(\underset{\sim}{x},t)$	$= c^*(\underset{\sim}{x}^*,t^*)/\overline{C}_0^*$, dimensionless instantaneous physical-space concentration fluctuation
$\tilde{c}(t)$	$= [\overline{c(\underset{\sim}{x},t)^2}]^{\frac{1}{2}}$, root-mean-square concentration fluctuation
$\mathcal{C}(\underset{\sim}{k},t)$	$= F[C(\underset{\sim}{x},t)]$, dimensionless Fourier transformed concentration, defined by Equation 596
$\mathcal{C}(\underset{\sim}{0})$	$= \overline{C}(t)$
$\mathfrak{c}(\underset{\sim}{k})$	$= \mathcal{C}(\underset{\sim}{k}) - \mathcal{C}(\underset{\sim}{0})\delta_{\underset{\sim}{k},\underset{\sim}{0}}$, Fourier transform of the instantaneous concentration fluctuation, defined by Equation 600
$\mathfrak{c}^R(\underset{\sim}{k})$	real part of $\mathfrak{c}(\underset{\sim}{k})$
$\mathfrak{c}^I(\underset{\sim}{k})$	imaginary part of $\mathfrak{c}(\underset{\sim}{k})$

D	diffusivity
Da_I	$= K\bar{C}_0^* L_{f\emptyset}^* / \tilde{v}_{\emptyset}^*$, first Damköhler number (for a second-order reaction)
Da_{II}	$= K\bar{C}_0^* L_{f\emptyset}^{*2} / D = Da_I Pe$, second Damköhler number (for a second-order reaction)
$d^2(x)$	defined by Equation 275
$E(k)$	energy spectrum function
$E_{ij}(\underset{\sim}{k})$	$= F[Q_{ij}(\underset{\sim}{r})]$, energy spectrum tensor
E_o	$= \frac{1}{2}\delta_{ii}\tilde{v}^2$, turbulent energy content
$E_s(k)$	concentration spectrum function, defined by Equations 115 and 116
$E_{ss}(\underset{\sim}{k})$	$= F[Q_{ss}(\underset{\sim}{r})]$
F	Fourier transform operator
$F(r)$	defined by Equation 6
$f(r)$	$= \overline{v_r(\underset{\sim}{x}) v_r(\underset{\sim}{x}+\underset{\sim}{r})} / \tilde{v}^2$, longitudinal correlation function
$f_s(r)$	$= Q_{ss}(\underset{\sim}{r}) / \tilde{c}^2$, concentration (scalar) correlation coefficient
$G(r)$	defined by Equation 6
$g(r)$	$= \overline{v_n(\underset{\sim}{x}) v_n(\underset{\sim}{x}+\underset{\sim}{r})} / \tilde{v}^2$, lateral correlation function
i	$= (-1)^{\frac{1}{2}}$
K	reaction rate constant
k	$= \lvert\underset{\sim}{k}\rvert$
$\underset{\sim}{k}^*$ or k_i^*	$= 2\pi\underset{\sim}{n}/L^*$ or $2\pi n_i/L^*$, wave number vector or components
$\underset{\sim}{k}$ or k_i	$= \underset{\sim}{k}^* L_{f\emptyset}^*$ or $k_i^* L_{f\emptyset}^*$, dimensionless wave number vector or components

$k(r)$ = $\overline{v_r(\underset{\sim}{x})v_r(\underset{\sim}{x})v_r(\underset{\sim}{x}+\underset{\sim}{r})}/\tilde{v}^3$, radial triple-velocity correlation function

k_B = $(\epsilon/\nu D^2)^{1/4}$, Batchelor wave number

k_C = $(\epsilon/D^3)^{1/4}$, Corrsin-Obukhov wave number

k_K = $(\epsilon/\nu^3)^{1/4}$, Kolmogorov wave number

k_o wave number corresponding to maximum of energy spectrum

$k_s(r)$ = $\overline{c(\underset{\sim}{x})c(\underset{\sim}{x}+\underset{\sim}{r})v_r(\underset{\sim}{x})}/\tilde{c}^2\tilde{v}$, radial triple correlation coefficient

L^* length of the sides of the unit box of turbulence repeating through space

$L_f(k)$ defined by Equation 567 or 568

L_f longitudinal integral scale of turbulence, defined by Equation 20

L_g lateral integral scale of turbulence, defined by Equation 21

L_s concentration integral scale, defined by Equation 87

N = $L^*/L^*_{f\emptyset}$

$\underset{\sim}{n}$ or n_i = 0, ±1, ±2, ..., integer quantized vector or components

P^* pressure

P = $P^*/\rho\tilde{v}^{*2}_{\emptyset}$, dimensionless pressure

Pe = $Re\,Sc$ = $\tilde{v}^*_{\emptyset}L^*_{f\emptyset}/D$, turbulence Peclet number

$P_{ij}(\underset{\sim}{k})$ = $\delta_{ij} - k_ik_j/k^2$, standard projection operator

$P^+_{ij}(\underset{\sim}{r})$ auxiliary pressure function defined by Equation 64

$Q_{ij}(\underset{\sim}{r})$ = $\overline{v_i(\underset{\sim}{x})v_j(\underset{\sim}{x}+\underset{\sim}{r})}$, velocity correlation tensor

$Q_{ij}(\underset{\sim}{0})$ = $\overline{v_i(\underset{\sim}{x})v_j(\underset{\sim}{x})}$, energy tensor

$Q_{ss}(\underset{\sim}{r})$	$= \overline{c(\underset{\sim}{x})c(\underset{\sim}{x}+\underset{\sim}{r})}$, concentration (scalar) correlation function
Re	$= \tilde{v}^*_{\emptyset} L^*_{f\emptyset}/\nu$, turbulence Reynolds number
$R_{ij}(\underset{\sim}{r})$	$= Q_{ij}(\underset{\sim}{r})/\tilde{v}^2$, velocity correlation coefficient
$R_s(\underset{\sim}{r})$	$= \overline{c(\underset{\sim}{x})c(\underset{\sim}{x})c(\underset{\sim}{x}+\underset{\sim}{r})}$
$R_s(\underset{\sim}{k})$	$= F[R_s(\underset{\sim}{r})]$
r	$= \lvert\underset{\sim}{r}\rvert$
$\underset{\sim}{r}$ or r_i	separation vector or components
Sc	$= \nu/D$, Schmidt number
$S(t,T_{so})$	random step function
$S_i(\underset{\sim}{r})$	$= \overline{c(\underset{\sim}{x})c(\underset{\sim}{x}+\underset{\sim}{r})v_i(\underset{\sim}{x})}$, triple correlation vector
$S_{ij,k}(\underset{\sim}{r})$	$= \overline{v_i(\underset{\sim}{x})v_j(\underset{\sim}{x})v_k(\underset{\sim}{x}+\underset{\sim}{r})}$, triple-velocity correlation tensor
T_{so}	characteristic period of random step function
$T(k)$	energy spectrum transfer function, defined by Equations 74 and 75
$T_{ij}(\underset{\sim}{r})$	auxiliary function defined by Equation 63
$T_{ij}(\underset{\sim}{k})$	$= F[T_{ij}(\underset{\sim}{r})]$
$T_s(k)$	defined by Equations 118 and 119
$T_s(\underset{\sim}{k})$	$= F[\partial S_i(\underset{\sim}{r})/\partial r_i]$
t	$= t^*\tilde{v}^*_{\emptyset}/L^*_{f\emptyset}$, dimensionless time
$u_i(\underset{\sim}{k})$	$= F[v_i(\underset{\sim}{x})]$, dimensionless Fourier transformed velocity, defined by Equation 363
$\tilde{v}$	$= (\overline{v^2})^{1/2}$, root-mean-square velocity fluctuation
$v^*_i(x^*)$	physical-space velocity
$v_i(\underset{\sim}{x})$	$= v^*_i(\underset{\sim}{x}^*)/\tilde{v}^*_{\emptyset}$, dimensionless physical-space velocity

v_K = $(\nu\epsilon)^{1/4}$, Kolmogorov velocity

$\underset{\sim}{x}^*$ or x_i^* rectangular coordinate position vector or components

$\underset{\sim}{x}$ or x_i = $\underset{\sim}{x}^*/L_{f\emptyset}^*$ or $x_i^*/L_{f\emptyset}^*$, dimensionless position vector or components

Danish:

$\emptyset_i^*(\underset{\sim}{x})$ physical-space random convection velocity

$\emptyset_i(\underset{\sim}{x})$ = $\emptyset_i^*(\underset{\sim}{x})/\tilde{v}_\emptyset^*$, dimensionless physical-space random convection velocity

$\emptyset_i(\underset{\sim}{k})$ = $F[\emptyset_i(\underset{\sim}{x})]$, dimensionless Fourier transformed random convection velocity

Icelandic:

Þ = $\overline{c_A c_B}/\bar{c}_A\bar{c}_B$, segregation coefficient

ð = $\overline{c_A c_B}/\tilde{c}_A\tilde{c}_B$, correlation coefficient

Greek:

α = $\bar{c}(0)/\tilde{c}(0)$ in Literature Review section

β = $\bar{c}_{B0}/n\bar{c}_{A0}$, stoichiometric parameter in Literature Review section

ϵ rate of dissipation of turbulent energy, defined by Equation 69

ϵ_s = $-d\tilde{c}^2/dt$, rate of dissipation of concentration fluctuations

ζ dampening ratio for second-order response

$\eta(k)$ defined by Equation 377 or 379

θ angular location in random walk on a circle

λ_f longitudinal microscale of turbulence, defined by Equation 26

λ_g	lateral microscale of turbulence, defined by Equation 27
λ_K	$= 1/k_K$, Kolmogorov microscale
λ_s	concentration fluctuation microscale, defined by Equation 103
μ	viscosity
ν	$= \mu/\rho$, kinematic viscosity
ρ	density
τ	time constant for second-order response
ϕ	distribution function for concentration fluctuations in Literature Review section
ψ	stream function
$\psi^2(x)$	defined by Equation 310
$\mathcal{N}(t)$	defined by Equations 173 and 174

Special symbols:

$\bar{}$	overbar indicates volume average unless otherwise indicated
$\sim$	indicates vector quantity when under variable, root-mean-square symbol when over variable
*	dimensional quantity
3D	three dimensions
2D	two dimensions

Subscripts or superscripts:

A	species A
B	species B
c	continuous basis
d	discrete basis

f	longitudinal
I	imaginary part of complex variable
ind	value calculated using independence hypothesis
mix	pure mixing value
R	real part of complex variable
rxn	pure reaction value
s	concentration (scalar) quantity
Ø	random convection velocity quantity
0	value at t = 0

INTRODUCTION

Turbulent mixing effects on chemical reactions are important in many different types of reaction systems. In designing or scaling up industrial reactors, the prediction of the rate of conversion of chemical reactants undergoing turbulent mixing is often the name of the game. Indeed, various forms of tubular plug-flow reactors, continuous-flow stirred-tank reactors, and jet stirred reactors have been designed to utilize turbulent mixing as a means of contacting reactants. For extremely fast reactions this becomes a virtual necessity since the rate of conversion is completely controlled by the mixing. Turbulent mixing may also be used in a reactor for other reasons such as to aid heat transfer in removing heat released by exothermic reactions. The resulting temperature fluctuations can have a significant effect on local rates of reaction and hence conversion. Other systems in which turbulent reactions are important include combustion chambers, propulsion systems, flow lasers, and reactions between water-born or atmospheric pollutants such as in photochemical smog formation. Despite the importance of turbulent chemical reactions, little fundamental knowledge of interactions between chemical reactions and turbulent mixing is available because of the enormous complexity of the problem. Often empirical methods must be relied upon to obtain even order-of-magnitude

estimates of rates of conversion.

Fortunately, recent advances in the statistical theory of turbulent chemical reactions have led to the proposal of two potentially useful statistical independence hypotheses. For single component second-order reactions, O'Brien's statistical independence hypothesis (60) predicts the statistical characteristics of a chemical reaction undergoing turbulent mixing from the statistical characteristics of the mixing field without reaction and the statistical characteristics of the reaction field without mixing. For two-species second-order reactions, Toor's statistical independence hypothesis (123) predicts that for stoichiometric reactants with equal diffusivities the rate of decay of the covariance of the concentration fluctuations of the two species is independent of the rate of reaction and is the same as that for pure mixing. If they are valid these two independence hypotheses would be extremely useful since rates of conversion for turbulent chemical reactions could then be predicted from either tracer studies of a reactor or pure mixing theory. Rigorous experimental testing of the independence hypotheses has proven to be very difficult and has yet to be accomplished. In fact, no data is available whatsoever with which O'Brien's hypothesis can be tested. This is due to a variety of reasons, among which are difficulty in accurately measuring rapidly fluctuating chemical concentrations, eliminating temperature fluctua-

tion effects due to exothermic reactions, and maintaining identical flow conditions for both the mixing with reaction experiment and the corresponding pure mixing experiment. Experimental investigation of the hypotheses over a wide range of conditions is also an extensive undertaking.

In this study, O'Brien's hypothesis and Toor's hypothesis are tested using definitive computer experiments in which reaction and mixing conditions are carefully controlled. This is done by numerically integrating the Fourier transformed exact conservation equations of the reactants over time using a numerical simulation of a homogeneous isotropic turbulent velocity field for the convection velocity. For a variety of conditions the results of the computer experiment for turbulent mixing with reaction are then compared with results predicted using the statistical independence hypothesis and a turbulent mixing computer experiment that uses the same turbulent velocity field and the same initial concentration field.

In the first section that follows, statistical quantities and relations used to describe turbulent velocity fields are derived and reviewed that will be used later in formulating a numerical simulation model of turbulence that has requisite statistical properties. In the next section, the statistical theory of turbulent mixing and quantities used to describe turbulent concentration fields are reviewed. Following that the literature on the statistical theory of

turbulent chemical reactions is reviewed and finally the statistical independence hypotheses are described in detail. In the remaining sections, turbulent velocity field simulation models are developed, the Fourier transformed concentration field equations are derived, numerical integration procedures described, and the results presented and discussed.

STATISTICAL DESCRIPTION OF TURBULENCE

In this section the principal statistical quantities used to describe incompressible homogeneous isotropic turbulence are defined and useful relations between them derived. Careful examination of these definitions and derivations is warranted since many turbulence relations developed in three dimensions do not hold for two-dimensional turbulence, a case of interest in this study because of reduced computational requirements. Additional discussion of the statistical theory of turbulence is given by Brodkey (8), Hinze (38), Batchelor (5), and Leslie (60).

Throughout this study the indices i, j, k, m, and n (which should not be confused with subscripts) take the values 1, 2, and 3 for three dimensions but only 1 and 2 for two dimensions. The summation convention is used for repeated indices. Equations that are only valid in three dimensions (two dimensions) are indicated by 3D (2D) appearing with the equation number. Statistical averages are obtained by volume averaging (indicated by an overbar) except where otherwise stated.

Physical Space Quantities

A quantity of great importance in the statistical theory of turbulence is the correlation between the velocities at two points in space. A measure of this correlation

on the average is given by the velocity correlation tensor

$$Q_{ij}(\underset{\sim}{r}) \equiv \overline{v_i(\underset{\sim}{x})v_j(\underset{\sim}{x}+\underset{\sim}{r})} \tag{1}$$

where $\underset{\sim}{r}$ is the space vector between the points. If the separation between the points is small compared to eddy size, there will be a high degree of correlation between the velocities, whereas, if the separation is large compared to eddy size, little correlation can be expected. In fact, an "eddy" can be defined as a region of high correlation between the fluid velocities at two points. The velocity correlation tensor gives the spatial correlation for an "average" eddy. The highest degree of correlation occurs for zero separation, for which $Q_{ij}(\underset{\sim}{r})$ reduces to the energy tensor

$$Q_{ij}(\underset{\sim}{0}) = \overline{v_i(\underset{\sim}{x})v_j(\underset{\sim}{x})} \tag{2}$$

A complete determination of this would permit evaluation of the energy associated with the various velocity fluctuations.

Normalizing the velocity correlation tensor using the root-mean-square of the velocity fluctuation components gives the velocity correlation coefficient

$$R_{ij}(\underset{\sim}{r}) \equiv \overline{v_i(\underset{\sim}{x})v_j(\underset{\sim}{x}+\underset{\sim}{r})}/\tilde{v}^2 \tag{3}$$

$$R_{ij}(\underset{\sim}{0}) = 1, \quad |R_{ij}(\underset{\sim}{r})| \leq 1, \quad R_{ij}(\underset{\sim}{r}) = R_{ji}(-\underset{\sim}{r})$$

$$\tilde{v}^2 \equiv \overline{v_1^2} = \overline{v_2^2} = \overline{v_3^2} \tag{4}$$

The continuity condition for an incompressible fluid gives the two requirements

$$\frac{\partial R_{ij}(\underset{\sim}{r})}{\partial r_i} = \frac{\partial R_{ij}(\underset{\sim}{r})}{\partial r_j} = 0 \tag{5}$$

From the condition of isotropy $R_{ij}(\underset{\sim}{r})$ is restricted to the form (5)

$$R_{ij}(\underset{\sim}{r}) = F(r) r_i r_j + G(r) \delta_{ij} \tag{6}$$

Combining this with the continuity condition gives

$$\frac{\partial R_{ij}(\underset{\sim}{r})}{\partial r_i} = F(r) \frac{\partial (r_i r_j)}{\partial r_i} + r_i r_j \frac{\partial r}{\partial r_i} \frac{\partial F(r)}{\partial r} + \frac{\partial r}{\partial r_i} \frac{\partial G(r)}{\partial r} \delta_{ij} \tag{7}$$

$$\frac{\partial r}{\partial r_i} = \frac{\partial (r_n r_n)^{\frac{1}{2}}}{\partial r_i} = \tfrac{1}{2} r^{-1} \frac{\partial (r_n r_n)}{\partial r_i} = \frac{r_i}{r} \tag{8}$$

$$\frac{\partial (r_i r_j)}{\partial r_i} = \delta_{ii} r_j + r_i \frac{\partial r_j}{\partial r_i} = \delta_{ii} r_j + r_j = (\delta_{ii} + 1) r_j \tag{9}$$

and finally

$$\frac{\partial R_{ij}(\underset{\sim}{r})}{\partial r_i} = r_j \left[(\delta_{ii} + 1) F(r) + r \frac{\partial F(r)}{\partial r} + r^{-1} \frac{\partial G(r)}{\partial r} \right] = 0 \tag{10}$$

This shows that in incompressible isotropic turbulence only one scalar function is necessary to specify the velocity correlation. This is usually taken as either the longitu-

dinal correlation function

$$f(r) \equiv \overline{v_r(\underset{\sim}{x})v_r(\underset{\sim}{x}+\underset{\sim}{r})}/\tilde{v}^2, \quad f(0) = 1 \tag{11}$$

or the lateral correlation function

$$g(r) \equiv \overline{v_n(\underset{\sim}{x})v_n(\underset{\sim}{x}+\underset{\sim}{r})}/\tilde{v}^2, \quad g(0) = 1 \tag{12}$$

f(r) is usually positive and slowly approaches zero for large r, but g(r) becomes negative and approaches zero from the negative side. The negative correlation portion of g(r) arises because the velocities on opposite sides of an eddy are generally in opposite directions. From Equation 6 f(r), g(r), F(r), and G(r) are related as

$$\overline{v_r(\underset{\sim}{x})v_r(\underset{\sim}{x}+\underset{\sim}{r})}/\tilde{v}^2 = r^2F(r) + G(r) = f(r) \tag{13}$$

$$\overline{v_n(\underset{\sim}{x})v_n(\underset{\sim}{x}+\underset{\sim}{r})}/\tilde{v}^2 = G(r) = g(r) \tag{14}$$

$$F(r) = [f(r) - g(r)]/r^2 \tag{15}$$

In terms of f(r) and g(r), Equations 6 and 10 become

$$R_{ij}(\underset{\sim}{r}) = [f(r) - g(r)]r_i r_j/r^2 + g(r)\delta_{ij} \tag{16}$$

$$g(r) = f(r) + \tfrac{1}{2}r\frac{\partial f(r)}{\partial r} = \tfrac{1}{2}f(r) + \tfrac{1}{2}\frac{\partial [rf(r)]}{\partial r} \tag{17,3D}$$

$$g(r) = f(r) + r\frac{\partial f(r)}{\partial r} = \frac{\partial [rf(r)]}{\partial r} \tag{18,2D}$$

Using Equation 17 or 18 a useful relation results from contracting indices in Equation 16

$$R_{ii}(\underset{\sim}{r}) = Q_{ii}(\underset{\sim}{r})/\tilde{v}^2 = f(r) + (\delta_{ii} - 1)g(r)$$
$$= (\delta_{ii} + r\frac{\partial}{\partial r})f(r) \qquad (19)$$

The longitudinal integral scale of turbulence, L_f, and lateral integral scale, L_g, are defined by

$$L_f \equiv \int_0^\infty f(r)dr, \quad L_g \equiv \int_0^\infty g(r)dr \qquad (20,21)$$

Integrating Equations 17 and 18 over all r gives

$$L_g = \tfrac{1}{2}L_f, \quad L_g = 0 \qquad (22,3D;23,2D)$$

since $rf(r) \to 0$ as $r \to \infty$. In two-dimensional turbulence there must be as much area below the axis as above in g(r) versus r.

Since f(r) and g(r) are even functions, their series expansions contain only even powers of r

$$f(r) = 1 + \frac{r^2}{2!}\left(\frac{\partial^2 f(r)}{\partial r^2}\right)_{r=0} + \frac{r^4}{4!}\left(\frac{\partial^4 f(r)}{\partial r^4}\right)_{r=0} + \cdots \qquad (24)$$

$$g(r) = 1 + \frac{r^2}{2!}\left(\frac{\partial^2 g(r)}{\partial r^2}\right)_{r=0} + \frac{r^4}{4!}\left(\frac{\partial^4 g(r)}{\partial r^4}\right)_{r=0} + \cdots \qquad (25)$$

The second derivatives at r = 0 are a measure of the curvature of the correlation curves at r = 0 and can be used to define microscales for the velocity fluctuations, λ_f and λ_g, which are measures of the energy dissipation length

$$\frac{2}{\lambda_f^2} \equiv -\left(\frac{\partial^2 f(r)}{\partial r^2}\right)_{r=0}, \quad \frac{2}{\lambda_g^2} \equiv -\left(\frac{\partial^2 g(r)}{\partial r^2}\right)_{r=0} \qquad (26,27)$$

λ_f and λ_g correspond to the abscissa between the origin and the point of intersection with the osculation parabola at the vertex of their respective correlation curves. Differentiating Equations 17 and 18 twice and taking the limit $r = 0$ gives

$$\lambda_f^2 = 2\lambda_g^2, \quad \lambda_f^2 = 3\lambda_g^2 \qquad (28,3D;29,2D)$$

A two-point triple-velocity correlation tensor can be defined as

$$S_{ij,k}(\underset{\sim}{r}) \equiv \overline{v_i(\underset{\sim}{x})v_j(\underset{\sim}{x})v_k(\underset{\sim}{x}+\underset{\sim}{r})} \qquad (30)$$

$$S_{i,kj}(-\underset{\sim}{r}) = -S_{kj,i}(\underset{\sim}{r}) = -S_{jk,i}(\underset{\sim}{r}) \qquad (31)$$

For incompressible isotropic turbulence the third-order correlation is also determined by a single scalar function (5). Three possibilities are the triple-velocity correlation functions

$$k(r) \equiv \overline{v_r(\underset{\sim}{x})v_r(\underset{\sim}{x})v_r(\underset{\sim}{x}+\underset{\sim}{r})}/\tilde{v}^3 \qquad (32)$$

$$h(r) \equiv \overline{v_n(\underset{\sim}{x})v_n(\underset{\sim}{x})v_r(\underset{\sim}{x}+\underset{\sim}{r})}/\tilde{v}^3 \qquad (33)$$

$$q(r) \equiv \overline{v_r(\underset{\sim}{x})v_n(\underset{\sim}{x})v_n(\underset{\sim}{x}+\underset{\sim}{r})}/\tilde{v}^3 \qquad (34)$$

Using isotropy and continuity conditions these can be shown to be interrelated as

$$h(r) = -(\delta_{nn} - 1)^{-1} k(r) \tag{35}$$

$$q(r) = \tfrac{1}{2}k(r) + \tfrac{1}{2}(\delta_{nn} - 1)^{-1} r \frac{\partial k(r)}{\partial r} \tag{36}$$

and the triple-velocity correlation tensor can be written as

$$\begin{aligned} S_{ij,k}(\underset{\sim}{r}) = &- \frac{\tilde{v}^3}{r^3}\left[2q(r) + \delta_{nn}h(r)\right] r_i r_j r_k \\ &+ \frac{\tilde{v}^3 q(r)}{r}\left(r_i\delta_{jk} + r_j\delta_{ik}\right) + \frac{\tilde{v}^3 h(r)}{r} r_k \delta_{ij} \end{aligned} \tag{37}$$

Contracting indices i and k in Equation 37 gives

$$\begin{aligned} S_{ij,i}(\underset{\sim}{r}) &= \tilde{v}^3 (r_j/r)\left[k(r) + (\delta_{nn} - 1)q(r)\right] \\ &= \tilde{v}^3 (r_j/2r)(\delta_{nn} + 1 + r\frac{\partial}{\partial r})k(r) \end{aligned} \tag{38}$$

The series expansion of k(r) is of the form

$$k(r) = \frac{r^3}{3!}\left(\frac{\partial^3 k(r)}{\partial r^3}\right)_{r=0} + \frac{r^5}{5!}\left(\frac{\partial^5 k(r)}{\partial r^5}\right)_{r=0} + \cdots \tag{39}$$

since it is an odd function and its first derivative is zero at r = 0.

An important description of a turbulent field is the probability distribution of the turbulent fluctuations. Experiments (5) indicate a normal distribution for the velocity fluctuations at a single point.

Fourier Space Quantities

The use of Fourier transforms considerably simplifies the mathematics of isotropic turbulence. The Fourier transformation of a function from physical space to wave number space is given by

$$f(\underset{\sim}{k}) \equiv (2\pi)^{-\delta_{nn}} \int_{\underset{\sim}{x}} f(\underset{\sim}{x})\exp(-i\underset{\sim}{k}\cdot\underset{\sim}{x})d\underset{\sim}{x} = F[f(\underset{\sim}{x})] \qquad (40)$$

where $\underset{\sim}{k}$ is the wave number vector. The corresponding inverse integral transform is

$$f(\underset{\sim}{x}) = \int_{\underset{\sim}{k}} f(\underset{\sim}{k})\exp(i\underset{\sim}{k}\cdot\underset{\sim}{x})d\underset{\sim}{k} = F^{-1}[f(\underset{\sim}{k})] \qquad (41)$$

In order for the Fourier integral to exist the condition

$$\int_{-\infty}^{\infty} |f(\underset{\sim}{x})|\, d\underset{\sim}{x} = \text{finite} \qquad (42)$$

must be met. This condition is not satisfied when $f(\underset{\sim}{x})$ is a homogeneous random function of position and infinite in extent; to be rigorously correct mathematically a Fourier-Stieltjes integral transform must be used. In practice, however, use of the Fourier transform with infinite limits in theoretical work presents no difficulty. Equation 42 can be satisfied by considering hypothetical fields which differ from real fields in physically trivial respects only; for instance, if $f(\underset{\sim}{x})$ is regarded as being zero outside a very large but finite volume, a Fourier integral may be used. Further discussion on the adequacy of the Fourier transform

is given by Batchelor (5).

The transform can be viewed as a representation of the complicated random waveform of turbulent motion by a sum of sine waves of various amplitudes and frequencies that is equivalent to the original waveform. The wave number vector components are proportional to the frequency of the corresponding sine wave and are related to the wave length by $k_i = 2\pi/\lambda_i$, hence the wave number has units of reciprocal length.

The Fourier transform of the velocity correlation tensor is called the energy spectrum tensor

$$E_{ij}(\underset{\sim}{k}) \equiv F[Q_{ij}(\underset{\sim}{r})] = F[\overline{v_i(\underset{\sim}{x})v_j(\underset{\sim}{x}+\underset{\sim}{r})}] \qquad (43)$$

It indicates how the turbulent energy associated with each velocity component is distributed over various wave numbers. The wave number can be pictured in a rough sense as an inverse eddy size. The larger the wave number, the smaller the scale of turbulent motion that is represented. The energy spectrum tensor can be pictured as being an energy density in wave number space; integrating $E_{ij}(\underset{\sim}{k})$ over all wave numbers gives the energy tensor

$$Q_{ij}(\underset{\sim}{0}) = \overline{v_i(\underset{\sim}{x})v_j(\underset{\sim}{x})} = \int_{-\infty}^{\infty} E_{ij}(\underset{\sim}{k})d\underset{\sim}{k} \qquad (44)$$

From the Fourier transform of Equation 5 the continuity condition for an incompressible fluid becomes

$$k_i E_{ij}(\underset{\sim}{k}) = k_j E_{ij}(\underset{\sim}{k}) = 0 \tag{45}$$

A quantity that can be readily obtained experimentally is the one-dimensional spectrum function $E_{ij}(k_1)$, defined by

$$E_{ij}(k_1) = \int_{-\infty}^{\infty}\int_{-\infty}^{\infty} E_{ij}(\underset{\sim}{k})dk_m dk_n \tag{46,3D}$$

It can also be obtained as the Fourier transform of the corresponding one-dimensional velocity correlation

$$E_{ij}(k_1) = F[Q_{ij}(r_1)] \tag{47}$$

The energy spectrum tensor is a function of the vector $\underset{\sim}{k}$. The integrated energy spectrum tensor, which is a function of the scalar variable k, is obtained by integrating the energy spectrum tensor over constant $k = |\underset{\sim}{k}|$ in wave number space

$$\overset{o}{E}_{ij}(k) = \int_0^{2\pi}\int_0^{\pi} E_{ij}(\underset{\sim}{k})k d\theta d\phi = 4\pi k^2 E_{ij}(\underset{\sim}{k}) \tag{48,3D}$$

$$\overset{o}{E}_{ij}(k) = \int_0^{2\pi} E_{ij}(\underset{\sim}{k})k d\theta = 2\pi k\, E_{ij}(\underset{\sim}{k}) \tag{49,2D}$$

$\overset{o}{E}_{ij}(k)$ can be pictured as the energy contribution per wave number; the energy tensor is obtained by integration over all wave numbers k

$$Q_{ij}(0) = \int_0^{\infty} \overset{o}{E}_{ij}(k)dk \tag{50}$$

A widely used simple quantity is the energy spectrum function, defined as

$$E(k) \equiv \tfrac{1}{2}\overset{\circ}{E}_{ii}(k), \quad E(k) \equiv \overset{\circ}{E}_{ii}(k) \qquad (51,3D;52,2D)$$

For isotropic turbulence

$$E(k) = 4\pi k^2 \tfrac{1}{2}E_{ii}(\underset{\sim}{k}), \quad E(k) = 2\pi k\, E_{ii}(\underset{\sim}{k}) \qquad (53,3D;54,2D)$$

It is equivalent to the kinetic energy density per wave number, and is normalized to give the total kinetic energy by integration over all wave numbers

$$E_o = \frac{3}{2}\overset{\circ}{v}^2 = \int_0^\infty E(k)dk \qquad (55,3D)$$

$$E_o = \overset{\circ}{v}^2 = \int_0^\infty E(k)dk \qquad (56,2D)$$

The von Karman-Howarth Equation

An equation giving the decay of the velocity correlation tensor can be derived using the Navier-Stokes equation. The Navier-Stokes equation at one point is (unprimed, associated with index i)

$$\frac{\partial v_i}{\partial t} + \frac{\partial(v_k v_i)}{\partial x_k} = -\frac{1}{\rho}\frac{\partial P}{\partial x_i} + \nu \frac{\partial^2 v_i}{\partial x_k^2} \qquad (57)$$

and at a second point is (primed, associated with index j)

$$\frac{\partial v_j'}{\partial t} + \frac{\partial(v_k' v_j')}{\partial x_k'} = -\frac{1}{\rho}\frac{\partial P'}{\partial x_j'} + \frac{\partial^2 v_j'}{\partial x_k'^2} \qquad (58)$$

Multiplying Equation 57 by v_j' and Equation 58 by v_i and adding gives

$$\frac{\partial(v_i v_j')}{\partial t} + \left(\frac{\partial(v_i v_k v_j')}{\partial x_k} + \frac{\partial(v_i v_k' v_j')}{\partial x_k'}\right)$$

$$= -\frac{1}{\rho}\left(\frac{\partial(P v_j')}{\partial x_i} + \frac{\partial(P' v_i)}{\partial x_j'}\right) + \nu\left(\frac{\partial^2(v_i v_j')}{\partial x_k^2} + \frac{\partial^2(v_i v_j')}{\partial x_k'^2}\right) \tag{59}$$

Rewriting in terms of the separation vector $r_i = x_i' - x_i$ with

$$\frac{\partial}{\partial x_i} = -\frac{\partial}{\partial r_i}, \quad \frac{\partial}{\partial x_i'} = \frac{\partial}{\partial r_i}, \quad \frac{\partial^2}{\partial x_k^2} = \frac{\partial^2}{\partial x_k'^2} = \frac{\partial^2}{\partial r_k^2} \tag{60}$$

and volume averaging gives

$$\frac{\partial \overline{v_i v_j'}}{\partial t} + \frac{\partial}{\partial r_k}(\overline{v_i v_k' v_j'} - \overline{v_i v_k v_j'})$$

$$= -\frac{1}{\rho}\left(\frac{\partial \overline{P' v_i}}{\partial r_j} - \frac{\partial \overline{P v_j'}}{\partial r_i}\right) + 2\nu \frac{\partial^2 \overline{v_i v_j'}}{\partial r_k^2} \tag{61}$$

In averaging the differentials of two-point quantities the following averaging property is used

$$\overline{\frac{\partial f_i(\underset{\sim}{x},\underset{\sim}{x}')}{\partial r_i}} = \overline{\frac{\partial f_i(\underset{\sim}{x},\underset{\sim}{x}+\underset{\sim}{r})}{\partial r_i}} = \lim_{V\to\infty} \frac{1}{V}\int_V \frac{\partial f_i(\underset{\sim}{x},\underset{\sim}{x}+\underset{\sim}{r})}{\partial r_i}\, d\underset{\sim}{x}$$

$$= \frac{\partial}{\partial r_i}\left[\lim_{V\to\infty} \frac{1}{V}\int_V f_i(\underset{\sim}{x},\underset{\sim}{x}+\underset{\sim}{r})\, d\underset{\sim}{x}\right] = \frac{\partial \overline{f_i(\underset{\sim}{x},\underset{\sim}{x}+\underset{\sim}{r})}}{\partial r_i} = \frac{\partial f_i(\underset{\sim}{r})}{\partial r_i} \tag{62}$$

Equation 59 can be simplified by defining the auxiliary functions

$$T_{ij}(\underset{\sim}{r}) \equiv \frac{\partial}{\partial r_k}(\overline{v_i v_k v_j'} - \overline{v_i v_k' v_j'}) = \frac{\partial}{\partial r_k}\left[S_{ik,j}(\underset{\sim}{r}) - S_{i,kj}(-\underset{\sim}{r})\right] \tag{63}$$

$$P^{+}_{ij}(\underset{\sim}{r}) \equiv \frac{1}{\rho}\left(\frac{\partial\overline{P'v_i}}{\partial r_j} - \frac{\partial\overline{Pv_j'}}{\partial r_i}\right) \tag{64}$$

and identifying $Q_{ij}(\underset{\sim}{r}) = \overline{v_i v_j'}$ to give

$$\frac{\partial Q_{ij}(\underset{\sim}{r})}{\partial t} = T_{ij}(\underset{\sim}{r}) - P^{+}_{ij}(\underset{\sim}{r}) + 2\nu\frac{\partial^2 Q_{ij}(\underset{\sim}{r})}{\partial r_k^2} \tag{65}$$

For incompressible isotropic turbulence $P^{+}_{ij}(\underset{\sim}{r}) = 0$ and the other terms are known to reduce to scalar functions. Therefore, contracting indices in Equation 65 and using Equations 8, 19, 31, and 38 gives

$$\begin{aligned}(\delta_{nn} + r\frac{\partial}{\partial r})\Bigg\{\frac{\partial[\tilde{v}^2 f(r)]}{\partial t} - \tilde{v}^3\left[\frac{(\delta_{kk}+1)}{r} + \frac{\partial}{\partial r}\right]k(r) \\ - 2\nu\tilde{v}^2\left[\frac{(\delta_{kk}+1)}{r}\frac{\partial}{\partial r} + \frac{\partial^2}{\partial r^2}\right]f(r)\Bigg\} = 0\end{aligned} \tag{66}$$

Integrating this and setting the integration constant equal to zero so that the function remains finite at $r = 0$ gives the final form

$$\begin{aligned}\frac{\partial[\tilde{v}^2 f(r)]}{\partial t} - \tilde{v}^3\left[\frac{(\delta_{kk}+1)}{r} + \frac{\partial}{\partial r}\right]k(r) \\ = 2\nu\tilde{v}^2\left[\frac{(\delta_{kk}+1)}{r}\frac{\partial}{\partial r} + \frac{\partial^2}{\partial r^2}\right]f(r)\end{aligned} \tag{67}$$

which is known as the von Karman-Howarth equation for isotropic turbulence. All quantities in it can be measured experimentally.

Equation 67 can not be solved because it contains two

unknowns. An equation for the triple-velocity correlation can be constructed in a manner similar to that for the double-velocity correlation, but inertial terms of the fourth order appear because of nonlinearity. An infinite hierarchy of dynamical equations can be constructed in like manner, but there is always one more unknown than there are equations. This constitutes one of the major problems of the statistical approach to turbulence and is called the closure problem of turbulence theory. Various approximation techniques have been proposed for achieving closure, but all have met with only limited and varying success. These are discussed in detail by Leslie (60).

Using Equations 24, 26, and 39, Equation 67 reduces to

$$\frac{d\tilde{v}^2}{dt} = 2(\delta_{nn} + 2)\nu\tilde{v}^2\left(\frac{\partial^2 f(r)}{\partial r^2}\right)_{r=0} = -4(\delta_{nn} + 2)\nu\tilde{v}^2/\lambda_f(t)^2 \qquad (68)$$

in the limit $r = 0$. But the rate of dissipation of turbulent energy is defined as

$$\epsilon \equiv -\frac{\delta_{nn}}{2}\frac{d\tilde{v}^2}{dt} \qquad (69)$$

so that

$$\lambda_f(t)^2 = 2\delta_{nn}(\delta_{kk} + 2)\nu\tilde{v}^2/\epsilon \qquad (70)$$

In the final period of turbulence the velocity fluctuations decay as (5)

$$\tilde{v}^2 \propto t^{-5/2} \qquad (71,3D)$$

Spectrum Equation

Taking the Fourier transform of Equation 65 gives

$$\frac{\partial E_{ij}(\underset{\sim}{k})}{\partial t} = T_{ij}(\underset{\sim}{k}) - P^{+}_{ij}(\underset{\sim}{k}) - 2\nu k^2 E_{ij}(\underset{\sim}{k}) \tag{72}$$

where $T_{ij}(\underset{\sim}{k}) \equiv F[T_{ij}(\underset{\sim}{r})]$ is the energy spectrum transfer tensor and $P^{+}_{ij}(\underset{\sim}{k}) \equiv F[P^{+}_{ij}(\underset{\sim}{r})]$. The nonlinear term $T_{ij}(\underset{\sim}{k})$ indicates a flow of energy between different wave numbers (for the same velocity component). It changes the wave number density of contributions to the energy tensor $\overline{v_i v_j}$, but does not affect the total contribution; its integral over all wave numbers is zero. Mathematics does not define the direction of transfer, but reasoning shows that the effect of inertia is directed toward the large wave numbers or small eddies, where energy is lost due to viscous dissipation. The nonlinear pressure term $P^{+}_{ij}(\underset{\sim}{k})$ indicates a transfer of energy between different velocity components (for the same wavenumber), but it is zero for incompressible isotropic turbulence. The effect of pressure is to tend to equalize the mean square velocity values.

The spectrum equation can be reduced by contracting indices to give

$$\frac{\partial E_{ii}(\underset{\sim}{k})}{\partial t} = T_{ii}(\underset{\sim}{k}) - 2\nu k^2 E_{ii}(\underset{\sim}{k}) \tag{73}$$

Multiplying through by $2\pi k^2$ or $2\pi k$, using Equation 53 or 54,

and defining the scalar transfer function

$$T(k) \equiv 4\pi k^2 \tfrac{1}{2} T_{ii}(\underset{\sim}{k}), \quad T(k) \equiv 2\pi k T_{ii}(\underset{\sim}{k}) \quad (74,3D;75,2D)$$

gives

$$\frac{\partial E(k)}{\partial t} = T(k) - 2\nu k^2 E(k) \qquad (76)$$

which is the Fourier transform equivalent of the von Karman-Howarth equation. The scalar T(k) is associated with the transfer of energy between wave numbers or eddy sizes. It does not affect the total amount of energy since its integral over all wave numbers is zero.

The time rate of change of the kinetic energy of turbulent motion can be established by integrating Equation 75 over all wave numbers

$$\frac{\partial}{\partial t} \int_0^\infty E(k)dk = \int_0^\infty T(k)dk - 2\nu \int_0^\infty k^2 E(k)dk \qquad (77)$$

or

$$-\tfrac{1}{2} \frac{\partial \overline{v_i^2}}{\partial t} = -\tfrac{1}{2}\delta_{nn} \frac{\partial \tilde{v}^2}{\partial t} = 2\nu \int_0^\infty k^2 E(k)dk = \epsilon \qquad (78)$$

where ϵ is the rate of dissipation of turbulent energy. Viscous dissipation reduces the energy from components of any one wave number, but has no effect on the transfer between wave numbers. Further, this energy dissipation is selective toward the high wave numbers, or small eddies, because of the strong effect of the k^2 factor.

Substituting Equation 55 or 56 for $\tilde{v}^2$ and Equation 78

for ϵ into Equation 70 gives

$$\frac{1}{\lambda_f(t)^2} = \frac{1}{\delta_{nn}(\delta_{mm}+2)\bar{v}^2}\int_0^\infty k^2E(k)dk = \frac{\int_0^\infty k^2E(k)dk}{2(\delta_{nn}+2)\int_0^\infty E(k)dk} \tag{79}$$

Spectral Theory

The energy spectrum function for fully developed turbulence is illustrated qualitatively in Figure 1. The energy-containing eddies are associated with the maximum of the spectrum and contain most of the turbulent energy. Although the more permanent large eddies contain much less energy, their energy is by no means negligible and may amount to as much as twenty percent of the total kinetic energy (29). In analysing the energy cascade from large to small eddies, the concept of an eddy Reynolds number that varies with eddy size and velocity is useful. For extensive eddies the eddy Reynolds number is large, viscosity has little influence on the motion, and no appreciable viscous dissipation of energy occurs. The viscosity becomes determinative only when the eddy Reynolds number is of order unity or less. Thus dissipation of energy occurs in the smallest eddies, which are unimportant in determining the general flow pattern. The smallest eddies are not influenced by outside forces but owe their existence to inertial interactions of the larger scale motions. Unless the large scale eddies receive energy from an outside source, the total amount of

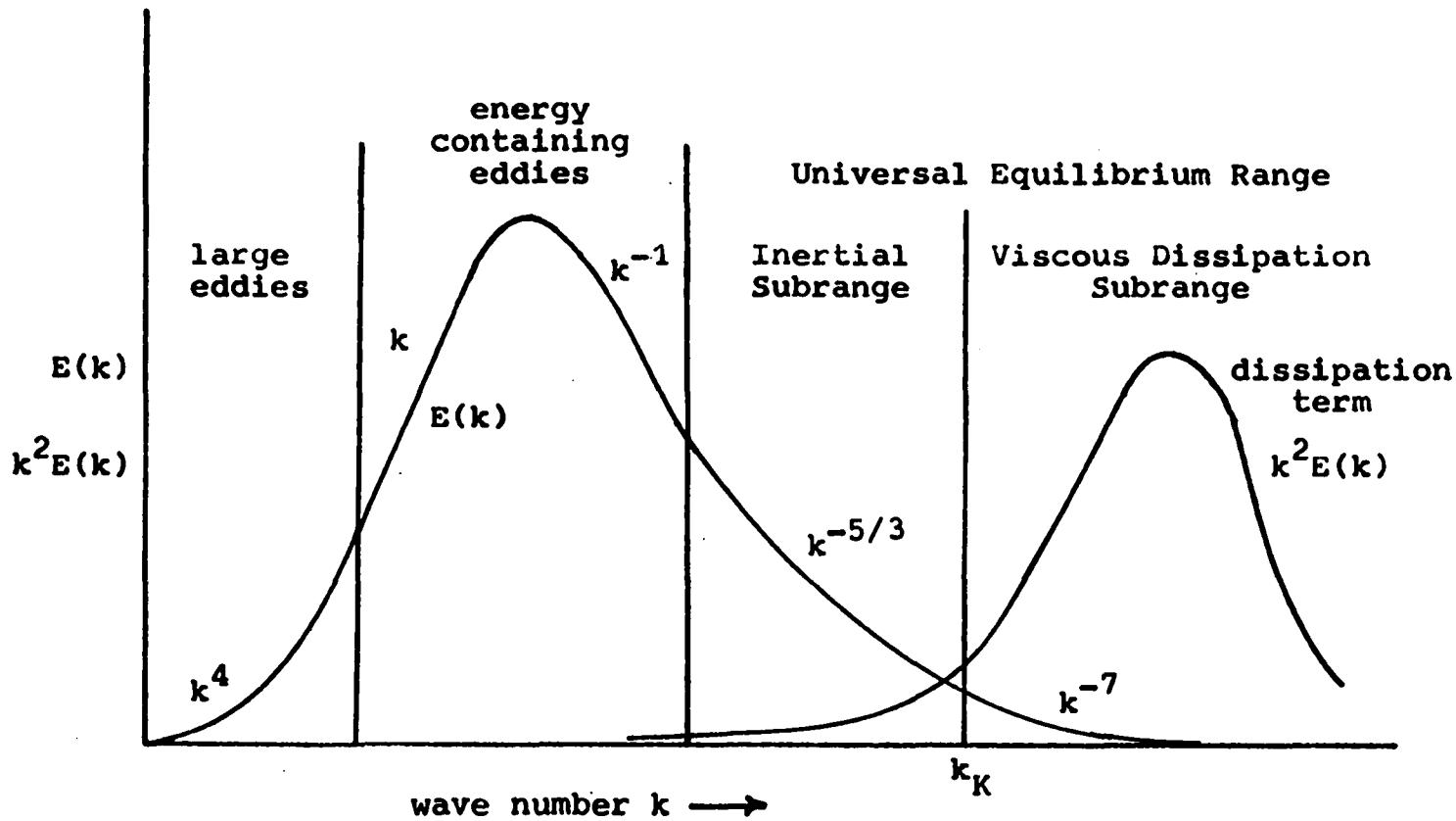

Figure 1. General form of the energy spectrum function E(k) and dissipation term $k^2E(k)$ for fully developed isotropic turbulence

turbulent energy decays with time.

In the universal equilibrium range, which exists only for very large turbulence Reynolds numbers, the decay process is relatively slow compared to eddy motion, and the turbulence may be considered to be statistically steady. Kolmogorov (46,47) was the first to postulate that the dynamics of this equilibrium state depend only on the rate of energy dissipation ϵ and the kinematic viscosity. Furthermore, even if the large scale flow is anisotropic, this small scale motion may be considered to be locally isotropic. Length and velocity parameters characteristic of this range are the Kolmogorov microscale and velocity $\lambda_K \equiv (\nu^3/\epsilon)^{1/4}$ and $v_K \equiv (\nu\epsilon)^{1/4}$. Whereas the integral scale L_f is associated with the region of maximum $E(k)$, λ_K is associated with the viscous dissipation group $k^2E(k)$. The Kolmogorov wavenumber

$$k_K \equiv 1/\lambda_K = (\epsilon/\nu^3)^{1/4} \tag{80}$$

defines the separation between the inertial and viscous dissipation subranges.

From dimensional analysis Kolmogorov found $E(k) \sim k^{-5/3}$ in the inertial subrange, where inertial forces are controlling and $E(k)$ is independent of ν. Tchen (117) divided the equilibrium range into three subranges and showed by an approximate harmonic analysis that $E(k)$ is proportional to k^{-1}, $k^{-5/3}$, and k^{-7}, respectively, in the three subranges.

In the viscous dissipation subrange the k^{-7} dependence had also been obtained by Heisenberg (35), who assumed an explicit functional form for the energy transfer function. However, the -7 decay law has not been verified experimentally. In the large eddies range Batchelor (2 , 3) showed that $E(k) \sim k^4$. Von Karman and Lin (41) postulated the existence of a parameter D_o which characterizes the energy transfer mechanism and showed by dimensional analysis that $E(k) \sim D_o^2 k$ in the subrange where E(k) depends only on D_o.

PURE MIXING

The statistical theory of turbulent mixing has been developed parallel to the turbulent motion problem, but is simpler since a scalar quantity rather than a vector quantity is involved. The equations describing the mixing of a chemical species in the absence of reaction are also of the same form as equations describing temperature fluctuations in a turbulent fluid. Therefore experimental studies of pure mixing can be done by measuring temperature fluctuations in analogous heat transfer experiments, eliminating the difficult task of measuring concentration fluctuations. Indeed, much of the theory of pure mixing has been developed in terms of the turbulent temperature fluctuation problems. Turbulent mixing theory usually considers only the period after initial contacting of the two fluids (as either two different species or one species and a diluent) when the mixing parameters are approximately uniform over the mixing field. General reviews of mixing are given by Brodkey (8) and Hinze (38).

Conservation Equation Analysis

Analysis of the pure mixing problem begins with the mass conservation equation for a single species in an incompressible isotropic turbulent velocity field

$$\frac{\partial C}{\partial t} + v_i \frac{\partial C}{\partial x_i} = D \frac{\partial^2 C}{\partial x_i^2} \tag{81}$$

where C and v_i are both random functions of position and time. The mixing process is assumed to be passive (does not affect the turbulent velocity field) with constant mass diffusivity. This restricts us to problems of low concentration fluctuation (or small temperature variation) but it also uncouples the component mass conservation equation (with a given velocity field) from the Navier-Stokes equation, which is a great simplification.

As was done with the instantaneous velocity, it is convenient to write the instantaneous concentration as the sum of a volume-averaged concentration $\overline{C}$ and concentration fluctuation c

$$C(\underset{\sim}{x},t) = \overline{C}(t) + c(\underset{\sim}{x},t) \tag{82}$$

Incorporating this into Equation 81 and subtracting out the volume-average of Equation 81 gives

$$\frac{\partial \overline{C}}{\partial t} = 0, \quad \frac{\partial c}{\partial t} + v_i \frac{\partial c}{\partial x_i} = D \frac{\partial^2 c}{\partial x_i^2} \tag{83,84}$$

which shows that the mean concentration remains constant through the mixing process. A quantity of primary importance is the average squared concentration fluctuation $\overline{c^2}$. An equation for $\overline{c^2}$ can be obtained by multiplying Equation 84 by c, rearranging the convection term using continuity, and averaging to give

$$\frac{d\overline{c^2}}{dt} = -2D\ \overline{\left(\frac{\partial c}{\partial x_i}\right)\left(\frac{\partial c}{\partial x_i}\right)} \qquad (85)$$

The terms in Equation 84 indicate that the species is distributed throughout the turbulent velocity field by two actions: turbulent dispersion and molecular diffusion.

Turbulent dispersion (or turbulent diffusion) is the dispersion of a scalar quantity by turbulent motion only and is represented by the convective term of the mass conservation equation; it is not due to molecular diffusion. In turbulent mixing, the dispersive action is always present and can occur in the absence of molecular diffusion, as in the mixing of two immiscible liquids. One way in which it enhances submicroscopic mixing is by providing an increased area for diffusion. It is well established that turbulent convection stretches the iso-concentration surfaces continuously on the average. This in turn tends to bring the surfaces even closer together, increasing the scalar gradient fluctuation level and enhancing molecular diffusion further. (From the Fourier analysis viewpoint this is propagation to higher and higher wave number in the spectrum of the concentration field.) Although the convective term in the mass conservation equation is linear, this particular behavior resembles that of a nonlinear phenomenon. An inherent feature of this process is a continual reduction of the length-scale of concentration variations (size of unmixed clumps of fluid). However, because of the macro-

scopic nature of turbulence, dispersion can only spread out unmixed fluid elements to an ultimate level that is nowhere near the molecular realm.

Equation 85 shows that dissipation of average concentration fluctuation, and hence ultimate mixing on a molecular scale, is due entirely to molecular diffusion. Without diffusion $\overline{c^2}$ would remain constant regardless of the level of turbulent dispersion. Although the turbulent velocity does not appear explicitly in Equation 85, its mixing action is of course felt through dispersive concentration gradient steepening, which tends to increase the mean square derivatives. Molecular diffusion allows the movement of different molecules across the iso-concentration surfaces, thus smearing out the fluctuation gradients or reducing the concentration difference between elements of fluid. This reduction in intensity will occur with or without turbulence.

Danckwerts (18) has presented two quantitative measures of the "goodness" of mixing that are based on dispersion and diffusion effects: first, the degree to which the material to be mixed by turbulent action has been spread out, as measured by the scale of segregation; second, the approach to uniformity by the action of molecular diffusion, as measured by the intensity of segregation.

Scale of segregation

The scale of segregation is a measure of the size of unmixed clumps of pure components; as these clumps are spread out, the scale of mixing is reduced. It is analogous to the scale of turbulence, but there is only one concentration coefficient, defined as

$$f_s(r) \equiv \overline{c(\underset{\sim}{x})c(\underset{\sim}{x}+\underset{\sim}{r})}/\tilde{c}^2 \qquad (86)$$

where $\tilde{c}$ is the root-mean-square concentration fluctuation, with which to define a concentration integral scale

$$L_s \equiv \int_0^\infty f_s(r)dr \qquad (87)$$

Since by definition there is good correlation between the concentrations of two points within the same concentration eddy, L_s is a measure of the average concentration eddy size; it is a good measure of the large scale process of eddy breakup, but not of the small scale diffusional process.

In a liquid system with slow molecular diffusion, the scale would decrease rapidly to some small value (smallest eddy size), and then increase slowly as molecular diffusion completes the mixing. The increase in scale is due to an apparent increase in eddy size because of outward diffusion. The scale increases indefinitely with time since $f_s(r) \to 1$ for all r as a uniform medium is approached.

In a gas with rapid molecular diffusion, the scale may

not be reduced appreciably before diffusional effects become controlling. For the gas system and in the latter part of the liquid mixing process the intensity of segregation gives a better description of the degree of mixing.

Intensity of segregation

The intensity of segregation is defined as

$$I \equiv -\overline{c_A c_B}/\bar{c}_A\bar{c}_B = 1 - \overline{C_A C_B}/\bar{C}_A\bar{C}_B \tag{88}$$

for the mixing of two species. It is a good measure of the degree of mixing at the molecular level (micromixing) because I varies from zero for a uniform solution to one when A and B do not coexist anywhere (complete segregation). For the mixing of a single species with pure diluent (nonpremixed case) it follows that I can be written as

$$I = \overline{c^2}/\overline{c_0^2} \tag{89}$$

where $\overline{c_0^2}$ is the initial fluctuation level. I then varies from one when mixing is initiated to zero when mixing is complete.

The intensity of segregation describes the effect of molecular diffusion on the mixing process and may be viewed as a measure of the difference in concentration between neighboring clumps of fluid. In systems where reaction is to occur between two nonpremixed reactants, the need for submicroscopic mixing as measured by the intensity of

segregation is apparent, for without it the only chemical reaction that could occur would be on the surface of the fluid clumps. In the mixing of two reactants the intensity of segregation often needs to be reduced rapidly in order to avoid local spots of concentrated reactant and the undesirable side reactions usually associated with such spots.

Two-Point Correlation: The Mixing von Karman-Howarth Equation

Equation 84 is an example of an equation describing the behavior of the concentration fluctuation at a single point. It is also instructive to examine the correlation between the concentration fluctuations at two different points in the turbulent field. An equation that describes this can be developed as follows. The mass conservation equation at one point (unprimed) is

$$\frac{\partial c}{\partial t} + v_i \frac{\partial c}{\partial x_i} = D \frac{\partial^2 c}{\partial x_i^2} \tag{90}$$

while at a second point (primed) at the same time it is

$$\frac{\partial c'}{\partial t} + v_i' \frac{\partial c'}{\partial x_i'} = D \frac{\partial^2 c'}{\partial x_i'^2} \tag{91}$$

Multiplying the first equation by c' and the second by c, using continuity to rearrange the convection terms, and adding the two equations gives

$$\frac{\partial(cc')}{\partial t} + \left[\frac{\partial(cc'v_i)}{\partial x_i} + \frac{\partial(cc'v_i')}{\partial x_i'}\right] = D\left[\frac{\partial^2(cc')}{\partial x_i^2} + \frac{\partial^2(cc')}{\partial x_i'^2}\right] \tag{92}$$

Rewriting in terms of the separation vector $r_i = x_i' - x_i$ and noting that

$$\frac{\partial\overline{(cc'v_i)}}{\partial x_i} = \frac{\partial\overline{(cc'v_i')}}{\partial x_i'} \tag{93}$$

gives

$$\frac{\partial\overline{cc'}}{\partial t} + 2\frac{\partial\overline{cc'v_i}}{\partial r_i} = 2D\frac{\partial^2\overline{cc'}}{\partial r_i^2} \tag{94}$$

upon averaging.

A two-point concentration (scalar) correlation function can be defined as

$$Q_{ss}(\underset{\sim}{r}) \equiv \overline{c(\underset{\sim}{x})c(\underset{\sim}{x}+\underset{\sim}{r})} = \overline{cc'}(\underset{\sim}{r}) \tag{95}$$

and a two-point triple correlation vector as

$$S_i(\underset{\sim}{r}) \equiv \overline{c(\underset{\sim}{x})c(\underset{\sim}{x}+\underset{\sim}{r})v_i(\underset{\sim}{x})} = \overline{cc'v}_i(\underset{\sim}{r}) \tag{96}$$

In isotropic turbulence it can be shown that $Q_{ss}(\underset{\sim}{r})$ and $S_i(\underset{\sim}{r})$ can be expressed by single scalar functions. Let these be defined as the concentration (scalar) correlation coefficient

$$f_s(r) \equiv \overline{c(\underset{\sim}{x})c(\underset{\sim}{x}+\underset{\sim}{r})}/\overline{c}^2 \tag{97}$$

and the radial triple correlation coefficient

$$k_s(r) \equiv \overline{c(\underset{\sim}{x})c(\underset{\sim}{x}+\underset{\sim}{r})v_r(\underset{\sim}{x})}/\tilde{c}^2\tilde{v} \tag{98}$$

It can be shown that $f_s(r)$, $Q_{ss}(\underset{\sim}{r})$, $k_s(r)$, and $S_i(\underset{\sim}{r})$ are related by (38)

$$f_s(r) = Q_{ss}(\underset{\sim}{r})/\tilde{c}^2 \tag{99}$$

$$S_i(\underset{\sim}{r}) = \tilde{c}^2\tilde{v}\, k_s(r)r_i/r, \quad S_i(\underset{\sim}{r})^2 = (\tilde{c}^2\tilde{v})^2 k_s(r)^2 \tag{100,101}$$

Since $f_s(r)$ is an even function its series expansion contains only even powers of r

$$f_s(r) = 1 + \frac{r^2}{2!}\left(\frac{\partial^2 f_s(r)}{\partial r^2}\right)_{r=0} + \frac{r^4}{4!}\left(\frac{\partial^4 f_s(r)}{\partial r^4}\right)_{r=0} + \ldots \tag{102}$$

As was done in the turbulence problem, the second derivative at $r = 0$ can be used to define a concentration fluctuation microscale, λ_s, which is a measure of the fluctuation dissipation length

$$\frac{2}{\lambda_s} \equiv -\left(\frac{\partial^2 f_s(r)}{\partial r^2}\right)_{r=0} \tag{103}$$

However, $k_s(r)$ is an odd function and its first derivative is zero at $r = 0$ (38), giving

$$k_s(r) = \frac{r^3}{3!}\left(\frac{\partial^3 k_s(r)}{\partial r^3}\right)_{r=0} + \frac{r^5}{5!}\left(\frac{\partial^5 k_s(r)}{\partial r^5}\right)_{r=0} + \ldots \tag{104}$$

Substituting $Q_{ss}(\underset{\sim}{r})$ and $S_i(\underset{\sim}{r})$ into Equation 94 gives

$$\frac{\partial Q_{ss}(\underset{\sim}{r})}{\partial t} - 2\frac{\partial S_i(\underset{\sim}{r})}{\partial r_i} = 2D\frac{\partial^2 Q_{ss}(\underset{\sim}{r})}{\partial r_i^2} \tag{105}$$

In terms of the correlation coefficients Equation 105 becomes

$$\frac{\partial[\tilde{c}^2 f_s(r)]}{\partial t} - 2\tilde{c}^2\tilde{v}\left[(\delta_{ii} - 1)/r + \frac{\partial}{\partial r}\right]k_s(r) = 2\tilde{c}^2 D\left[(\delta_{ii} - 1)\frac{1}{r}\frac{\partial}{\partial r} + \frac{\partial^2}{\partial r^2}\right]f_s(r) \tag{106}$$

This is the mixing equivalent of the von Karman-Howarth equation and it is expressed entirely in terms of measurable values.

As in the turbulence problem, Equation 106 can not be solved because it contains two unknowns. A hierarchy of equations for expressing low order correlations or moments in terms of higher order moments can be written, but a closed set of equations is never obtained. The closure problem in mixing is similar to that of the motion problem, but it arises for a different reason. In turbulence, the closure problem is a direct consequence of the nonlinearity of the original equation of motion. In mixing, however, it is caused by the nonlinearity in the stochastic variables, even though the scalar conservation equation is essentially linear, and results from using a statistical approach. Various assumptions have been proposed for achieving closure, but all have met with limited and varying success.

Decay Laws

Using Equations 101, 102, and 103, in the limit $r = 0$ Equation 106 reduces to

$$\frac{d\tilde{c}^2}{dt} = 2\delta_{ii}D\tilde{c}^2\left(\frac{\partial^2 f_s(r)}{\partial r^2}\right)_{r=0} = -4\delta_{ii}D\tilde{c}^2/\lambda_s^2 \qquad (107)$$

In order to integrate this the time dependence of λ_s^2 is needed. For constant λ_s integration gives

$$\tilde{c}^2 = \tilde{c}_0^2 \exp(-4\delta_{ii}Dt/\lambda_s^2) \qquad (108)$$

Corrsin (11) has suggested that for low Schmidt number

$$\lambda_s^2/\lambda_g^2 \sim 2D/\nu = 2Sc \qquad (109)$$

Since λ_g is constant for stationary turbulence, λ_s is pseudoconstant and the decay of the concentration field is expressible entirely in terms of the turbulence. Various spectral analyses have been devised to give λ_s for high Schmidt numbers and hence the time constant of decay (8).

For decaying isotropic turbulent velocity fields, the relative rate of decay of the concentration fluctuations can be found by dividing Equation 68 for the decay of $\tilde{v}^2$ into Equation 107, giving

$$\frac{d\tilde{c}^2/\tilde{c}^2}{d\tilde{v}^2/\tilde{v}^2} = \frac{\delta_{ii}}{(\delta_{nn}+2)Sc}\left(\frac{\lambda_f(t)}{\lambda_s(t)}\right)^2 \sim O(1) \qquad (110)$$

valid for Sc unity or less (17).

The decay law of concentration fluctuations in homogeneous turbulence before the final period has been determined to be

$$\overline{c^2} = A(t - t_0)^{-3/2} + B(t - t_0)^{-5} \qquad (111)$$

where A and t_0 are constants determined by the initial conditions and the constant B depends on both initial conditions and the Schmidt number (67). For large times the last term becomes negligible, leaving the -3/2 power decay law for the final period (10). Hinze (38) has determined that a -3/2 power decay law for the decay of $\overline{c^2}$ also holds in the initial period of decay of the velocity field.

Concentration Spectrum Equation

Insight into the distribution of concentration fluctuations over the frequencies of fluctuations can be gained from the Fourier transform of Equation 105

$$\frac{\partial E_{ss}(\underset{\sim}{k})}{\partial t} = 2T_{ss}(\underset{\sim}{k}) - 2Dk^2 E_{ss}(\underset{\sim}{k}) \qquad (112)$$

$$E_{ss}(\underset{\sim}{k}) \equiv F[Q_{ss}(\underset{\sim}{r})], \quad T_{ss}(\underset{\sim}{k}) \equiv F[\partial S_i(\underset{\sim}{r})/\partial r_i] \qquad (113,114)$$

The concentration spectrum function is defined as

$$E_s(k) = \int_0^{2\pi}\int_0^{\pi} E_{ss}(\underset{\sim}{k}) k d\theta d\phi = 4\pi k^2 E_{ss}(\underset{\sim}{k}) \qquad (115,3D)$$

$$E_s(k) = \int_0^{2\pi} E_{ss}(\underset{\sim}{k}) k d\theta = 2\pi k\, E_{ss}(\underset{\sim}{k}) \qquad (116,2D)$$

and is normalized to give

$$\tilde{c}^2 = \int_0^\infty E_s(k)dk \qquad (117)$$

Similarly the transfer function can be defined by

$$T_s(k) \equiv 8\pi k^2 T_{ss}(\underset{\sim}{k}),\ T_s(k) \equiv 4\pi k\, T_{ss}(\underset{\sim}{k}) \quad (118,3D;119,2D)$$

Incorporating these definitions into Equation 112 gives the basic relation

$$\frac{\partial E_s(k)}{\partial t} = T_s(k) - 2Dk^2 E_s(k) \qquad (120)$$

which is the mixing analog of the Fourier transformed and reduced von Karman-Howarth equation. Integrating Equation 120 over all k gives

$$-\frac{d\tilde{c}^2}{dt} = 2D\int_0^\infty k^2 E_s(k)dk \equiv \epsilon_s \qquad (121)$$

where ϵ_s is the rate of dissipation of the concentration fluctuations by diffusion. Incorporating Equation 121 for ϵ_s and Equation 117 for $\tilde{c}^2$ into Equation 107 gives

$$1/\lambda_s^2 = \epsilon_s/4\delta_{ii}D\tilde{c}^2 = (1/2\delta_{ii}\tilde{c}^2)\int_0^\infty k^2 E_s(k)dk$$

$$= (1/2\delta_{ii})\frac{\int_0^\infty k^2 E_s(k)dk}{\int_0^\infty E_s(k)dk} \qquad (122)$$

As with the turbulence transfer term, $T_s(k)$ is associated with the transfer of concentration "energy" or "stuff"

between wave numbers or eddy sizes, but its integral over all wave numbers is zero. The diffusion-dissipation term causes no transfer through the spectrum but its effect is selective towards the high wave numbers, or small concentration eddies, because of the k^2 factor. The concentration spectrum function $E_s(k)$ is the fundamental description of the mixing process whether in gases or liquids. A large part of mixing theory has been devoted to the prediction of its form under different conditions.

Spectral Theories of Mixing

Spectral theories of mixing attempt to predict $E_s(k)$ for a stationary (nondecaying) isotropic concentration field in a stationary isotropic turbulence. Examination of such an imaginary state is justified by reasoning similar to that connected with Kolmogorov's hypothesis: for large turbulence Reynolds numbers, the small-scale components (small eddies) of the concentration field are statistically steady, isotropic, and independent of the detailed structure of the large-scale components (big eddies). Unless concentration variations on some definite length scale are supplied continually by some external agency, the statistical properties of the concentration distribution can not be exactly steady; however, the properties of the small-scale components will be approximately steady in general, because convective distortion and concentration gradient steepening

occur much faster than the overall decay of the concentration field. The continual steepening of concentration gradients is checked by the smoothing action of mass diffusion, and a statistically steady state is maintained in the small-scale components as the large-scale components decay.

The part of the concentration spectrum just described emerges for large Peclet numbers and is called the mixing universal equilibrium range. It can be further divided into four subranges, with each characterized by the dominant feature (convection or diffusion) affecting the concentration and turbulence spectra. Figure 2 shows a composite plot of theoretical results for the subranges along with the turbulence spectrum. The Schmidt number, a measure of the relative rates of diffusion of mass and momentum, has a strong influence on the shape of the concentration spectrum. Characteristic limits of the subranges are the cutoff wave numbers of Kolmogorov $k_K \equiv (\epsilon/\nu^3)^{1/4}$, Corrsin-Obukhov $k_C \equiv (\epsilon/D^3)^{1/4} = k_K Sc^{3/4}$, and Batchelor $k_B \equiv (\epsilon/\nu D^2)^{1/4} = k_K Sc^{1/2}$.

Inertial-convective subrange

The velocity spectrum is of the Kolmogorov type ($E(k) \sim k^{-5/3}$) and is influenced by inertial forces, while in the concentration field spectral transfer is purely convective (diffusion transport is negligible). Largely by dimensional reasoning and intuitive arguments, Corrsin (10) and Obukhov (98) determined the concentration spectrum to be

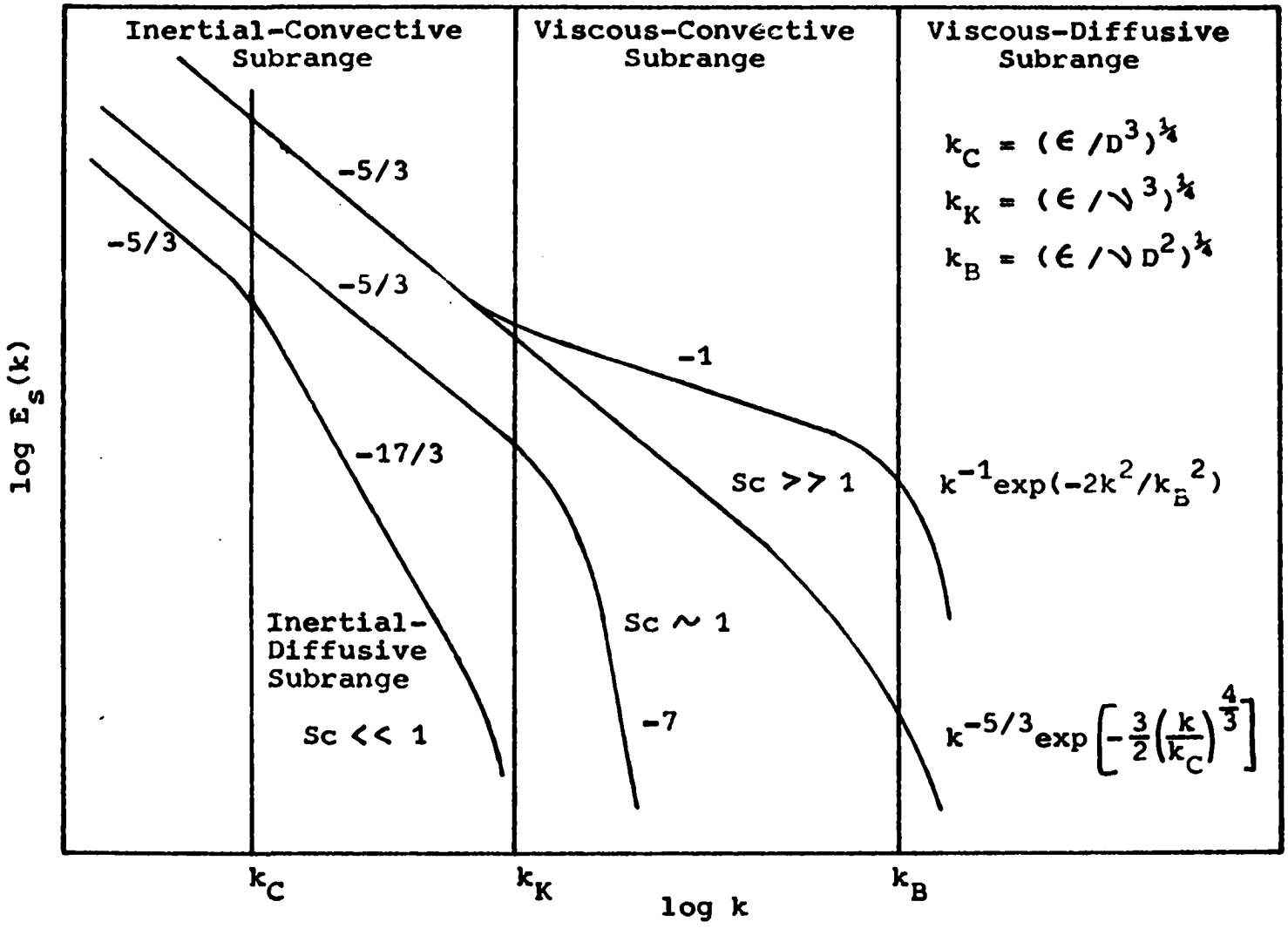

Figure 2. Pure mixing energy spectrum functions $E_s(k)$

$$E_s(k) \sim \epsilon_s \epsilon^{-1/3} k^{-5/3}, \quad k_o << k << k_c \qquad (123)$$

where k_o is a wave number characteristic of the energy containing eddies. Batchelor (4) later clarified that this was true for Sc << 1, but for Sc $\geq$ 1 Equation 123 holds over the extended range $k_o << k << k_K$.

Viscous subrange

In the viscous subrange for the velocity field ($k >> k_K$), the velocity spectrum is strongly affected by viscous forces. The wave number range within this where the concentration spectrum is strongly affected by diffusion is called the viscous-diffusive subrange. For Schmidt numbers about one the wave number dependence of the concentration spectrum and velocity spectrum are similar. For large Schmidt number, however, mass diffusion begins to affect the concentration spectrum only at wave numbers much larger than k_K, and the viscous-diffusive subrange exists only for $k >> k_B$. For $k_K << k << k_B$ the viscous-convective subrange appears, where the velocity spectrum is strongly affected by viscous forces but the concentration field transfer is predominantly convective and is probably due to distortion or straining of fluid elements.

In the viscous subrange Heisenberg (35) found $E(k) \sim k^{-7}$ for the velocity spectrum. Using the same method and dimensional reasoning, Corrsin (10) found a -7 power law for the viscous-diffusive subrange with Sc ~ 1. Batchelor,

however, has pointed out that basic assumptions in Heisenberg's method are not entirely accurate; hence the validity of the -7 power laws has not been established.

For large Schmidt numbers, Batchelor (4) presented arguments that the velocity field can be regarded as a persistent uniform straining motion for the small-scale variation of the concentration field. Using a uniform straining model he derived by both dimensional and analytical means the concentration spectrum for the entire viscous range

$$E_s(k) \sim 2\epsilon_s(\nu/\epsilon)^{\frac{1}{2}}k^{-1}\exp(-2k^2/k_B^2),\ k >> k_K \qquad (124)$$

For the viscous-convective subrange this reduces to the -1 power law

$$E_s(k) \sim 2\epsilon_s(\nu/\epsilon)^{\frac{1}{2}}\, k^{-1},\ k_K << k << k_B \qquad (125)$$

Pao (104,105) has presented a continuous spectral cascading concept for transferring turbulent energy and passive scalar quantities at large wave numbers. This concept, in essence, is a modification and extension of the spectral jump concepts proposed by Onsager (99,100) and Corrsin (14, 16). The deduced concentration spectrum function is

$$E_s(k) \sim \epsilon_s\epsilon^{-1/3}k^{-5/3}\exp\left[-\frac{3}{2}(k/k_c)^{4/3}\right],\ k > k_o \qquad (126)$$

which is independent of viscosity and claimed to be valid for the whole universal equilibrium range. However,

measurements by Nye and Brodkey (83) in the viscous-convective subrange support Batchelor's -1 power law and do not agree with the cascading process suggested by Pao.

Kraichnan (50) has reexamined Batchelor's persistent uniform straining model to see the effects of spatial and temporal fluctuations in the rate of strain. The -1 power law viscous-convective subrange spectrum is unaltered, except for the constant of proportionality, but the spectrum in the viscous-diffusive subrange displays a sensitivity to fluctuations which increases with wave number. Other analyses have also been given by Kraichnan (51).

Inertial-diffusive subrange

In the inertial-diffusive subrange that exists for very small Schmidt numbers the velocity spectrum follows the -5/3 power law and is influenced by inertial forces, but the concentration spectrum is strongly diffusive and falls off more rapidly. The analogous heat transfer case (for very small Prandtl numbers) is heat transfer in liquid metals. Starting from the equation of balance between transfer by turbulence convection and molecular diffusion, Batchelor, Howells, and Townsend (6) obtained

$$D^2k^4E_s(k) = (\epsilon_s/3D)E(k) \qquad (127)$$

by making the hypothesis that the main contribution to a Fourier component of the c-spectrum is given by the Fourier

component of the same order of the velocity spectrum. Substituting in the -5/3 power law for E(k) gives

$$E_s(k) \sim (\epsilon_s \epsilon^{2/3}/D^3)\, k^{-17/3},\quad k_C << k << k_K \qquad (128)$$

Gibson (28,29) has examined the physical mechanisms by which the fine structure of scalar fields is produced by turbulent convection and from this has proposed universal similarity hypotheses based on local straining mechanisms, Kolmogorov's local isotropy theory, and the mixing theories of Obukhov, Corrsin, and Batchelor. Three sets of similarity coordinates are found that depend on five fundamental parameters of turbulent mixing: the turbulence dissipation rate, the scalar fluctuation dissipation rate, the local strain rate, the kinematic viscosity, and the molecular diffusivity. Transformations between coordinate systems depend only on the Schmidt number as a mapping parameter. When the similarity hypotheses are used to predict the scalar spectrum function the inertial-convective subrange -5/3 power law and the viscous-convective subrange (for large Sc) -1 power law are reproduced; however, for small Sc values, a new inertial-diffusive subrange arises with a -3 power dependence. The Batchelor, Howells, and Townsend model gives a faster decay (-17/3 power law) since it excludes from consideration portions of the scalar field where convective transport is dominant (regions where the scalar gradient is small or zero), whereas the effect of

minimal gradient straining is taken into account in Gibson's analysis. The -3 power law was shown to be consistent with temperature fluctuation spectra measured in mercury.

Kraichnan (50) has treated the concentration fluctuation spectrum by the Lagrangian history direct-interaction approximation. The -5/3, -1, and -17/3 power laws are all recovered, but it gives a faster-than-algebraic spectrum decay in the viscous-diffusive subrange.

Differences between the mixing characteristics of gases and liquids arise primarily because of differences in Schmidt number and hence concentration spectra. In the inertial-convective subrange the spectra are independent of Schmidt number and both gases and liquids obey the -5/3 decay law. The difference between gases and liquids is manifested in the viscous-convective subrange where gases follow (approximately) the -7 power law ($Sc \sim 1$), whereas the liquid spectrum follows the -1 power law ($Sc >> 1$). However, most of the details of the spectrum are lost when quantities such as $\overline{c^2}$ are obtained by integrating over it.

LITERATURE REVIEW

The main problems considered in the statistical theory of turbulent mixing with chemical reaction are single-species first- and second-order reactions and premixed or nonpremixed two-species second-order reactions. In analyses it is assumed that reactants and products are dilute enough so that diffusivities are constant and the reaction is effectively isothermal and passive. In order to simplify analysis (indeed to obtain any solution at all) it is often assumed that the diffusivities of all reactants and products are equal. The quantities of primary interest are $\overline{C}(t)$, $\overline{c^2}(t)$, and for two-species reactions $\overline{c_A c_B}(t)$: $\overline{C}(t)$ represents the average unconverted reactant per unit volume, $\overline{c^2}(t)$ is a measure of the nonuniformity of this residual and tells the approach to detailed spatial homogeneity of the species, and $\overline{c_A c_B}(t)$ indicates how well the two reactants are correlated. Sources of randomness in the concentration field are statistical initial conditions, the stochastic velocity field, and the self-interaction of nonlinear reactions. Concentration fluctuations increase the rate of conversion over that for uniform solutions for premixed single- or two-species second-order reactions but decrease the conversion rate for nonpremixed two-species reactions.

Since turbulence is a macroscopic continuum phenomenon, the kinetic rate expressions developed for uniform solutions

can be used to give the rate expression at a point in the turbulent fluid, as is done in nonturbulent fluid dynamics. The reaction term is a local function of the concentration of the reacting species and does not depend upon gradients, hence it has no length scale. Because of this, turbulence has no direct influence on the reaction rate. By writing the mass conservation equation of a reactant in Lagrangian coordinates it can be shown that an invariance property exists for D = 0: in the absence of molecular diffusion the fluid motion has no effect on the rate of reaction. Since C is a nonnegative random variable, the distribution of C becomes highly skewed during reactive decay; this has an important consequence in formulating statistical solutions, for in order to guarantee realizability of a solution (that is, to avoid unphysical results such as negative concentrations) the following inequality between the moments of C must be satisfied (88)

$$(\overline{C^m})^{1-n} \leq (\overline{C^n})^{1-m}(\overline{C^1})^{m-n}, \quad 1 > m > n \geq 0 \qquad (129)$$

The first-order reaction has the well-behaved property of linearity, consequently mean conversion is independent of concentration fluctuations and the mean-square fluctuations are given by simple extension of the pure mixing case. Much of the theory has been devoted to developing spectra for stationary, reacting concentration fields.

The second-order single-component reaction is the

simplest nonlinear reaction case for studying turbulence effects. Much effort has gone into developing a successful closure approximation for the infinite hierarchy of equations that results from nonlinearity, but with only limited success.

Turbulent mixing has the strongest effects in the case of two-species reactions, with diffusion playing an important role in the initially unmixed case. Much work has been devoted to connecting the properties of systems with reaction to the corresponding nonreaction pure mixing case. The most fruitful results have come from predicting the conversion of nonpremixed reactants in a turbulent tubular flow reactor for very rapid reactions.

Recent reviews of homogeneous turbulent mixing with chemical reaction have been given by Hill (36b), Murthy (78), and Brodkey (9).

First-Order Reactions

Conservation equation analysis of a single reaction system

The mass conservation equations for the reactant (A) and product (B) of the first-order irreversible reaction

$$A \rightarrow B \tag{130}$$

with rate constant K in an isotropic turbulent velocity field are

$$\frac{\partial C_A}{\partial t} + v_i \frac{\partial C_A}{\partial x_i} = D_A \frac{\partial^2 C_A}{\partial x_i^2} - K C_A \qquad (131)$$

$$\frac{\partial C_B}{\partial t} + v_i \frac{\partial C_B}{\partial x_i} = D_B \frac{\partial^2 C_B}{\partial x_i^2} + K C_A \qquad (132)$$

For first-order reactions the conservation equations have the useful property of linearity in concentration, which simplifies analysis considerably.

Decay equations Averaging Equations 131 and 132 and restricting to homogeneity gives

$$\frac{d\overline{C}_A}{dt} = -K\overline{C}_A, \quad \frac{d\overline{C}_B}{dt} = K\overline{C}_A \qquad (133,134)$$

with the direct solutions

$$\overline{C}_A(t) = \overline{C}_{A0}\exp(-Kt) \qquad (135)$$

$$\overline{C}_B(t) = \overline{C}_{B0} + \overline{C}_{A0}[1 - \exp(-Kt)] \qquad (136)$$

which are the well known results for uniform solutions. Mean conversion of reactant and mean production of product are independent of concentration fluctuations. Setting $C_A = \overline{C}_A + c_A$, $C_B = \overline{C}_B + c_B$ in Equations 131 and 132 and subtracting out the averaged Equations 133 and 134, respectively, gives

$$\frac{\partial c_A}{\partial t} + v_i \frac{\partial c_A}{\partial x_i} = D_A \frac{\partial^2 c_A}{\partial x_i^2} - K c_A \qquad (137)$$

$$\frac{\partial c_B}{\partial t} + v_i \frac{\partial c_B}{\partial x_i} = D_B \frac{\partial^2 c_B}{\partial x_i^2} + K c_A \tag{138}$$

Equations for $\overline{c_A^2}$ and $\overline{c_B^2}$, developed in the manner of Equation 85, are

$$\frac{d\overline{c_A^2}}{dt} = -2D_A \overline{\left(\frac{\partial c_A}{\partial x_i}\right)\left(\frac{\partial c_A}{\partial x_i}\right)} - 2K\overline{c_A^2} \tag{139}$$

$$\frac{d\overline{c_B^2}}{dt} = -2D_B \overline{\left(\frac{\partial c_B}{\partial x_i}\right)\left(\frac{\partial c_B}{\partial x_i}\right)} + 2K\overline{c_A c_B} \tag{140}$$

An equation for $\overline{c_A c_B}$ is obtained by cross-multiplying Equations 131 and 132, adding, and averaging

$$\frac{d\overline{c_A c_B}}{dt} = D_A \overline{c_B \frac{\partial^2 c_A}{\partial x_i^2}} + D_B \overline{c_A \frac{\partial^2 c_B}{\partial x_i^2}} + K(\overline{c_A^2} - \overline{c_A c_B}) \tag{141}$$

Equation 139 shows that the dissipation of average reactant concentration fluctuation is due to both diffusion and reaction. Equation 140 shows that diffusion always dissipates the average product concentration fluctuation, but that the reaction term can either increase or decrease $\overline{c_B^2}$ depending upon whether the cross-correlation $\overline{c_A c_B}$ is positive or negative, respectively. At the beginning of the reaction, for no B present initially, A and B are well correlated and hence $\overline{c_A c_B}$ must be initially positive. Equation 141 shows that $\overline{c_A c_B}$ is created by interdiffusion of the species and from $\overline{c_A^2}$ through reaction, but that it is

also self-dissipating through reaction.

Solution of the decay equations without diffusion

In the limit of no diffusion ($D_A = D_B = 0$) the set of Equations 139-141 becomes determinant, with the solutions

$$\overline{c_A^2}(t) = \overline{c_{A0}^2}\,\bar{C}_A(t)^2/\bar{C}_{A0}^2 \qquad (142)$$

$$\overline{c_A c_B}(t) = \overline{c_{A0}^2}[\exp(-Kt) - \exp(-2Kt)] \qquad (143)$$

$$\overline{c_B^2}(t) = \overline{c_{A0}^2}\,\bar{C}_B(t)^2/\bar{C}_{A0}^2 \qquad (144)$$

$$\overline{c_A c_B}(0) = \overline{c_B^2}(0) = \bar{C}_B(0) = 0 \qquad (145)$$

This system has several interesting properties. Equations 142 and 144 show that the relative intensities of reactant and product concentration fluctuations, $\overline{c_A^2}/\bar{C}_A^2$ and $\overline{c_B^2}/\bar{C}_B^2$, remain constant at the initial relative intensity $\overline{c_{A0}^2}/\bar{C}_{A0}^2$, during decay and growth, respectively. Also, the two concentration fields are always perfectly correlated since $\overline{c_A c_B} = (\overline{c_A^2})^{1/2}(\overline{c_B^2})^{1/2}$. The fluctuation levels are also related by

$$\overline{c_{A0}^2} = \overline{c_A^2}(t) + 2\overline{c_A c_B}(t) + \overline{c_B^2}(t) = \overline{(c_A + c_B)^2} \qquad (146)$$

$\overline{c_A c_B}(t)$ is always positive and reaches a maximum value of

$$\overline{c_A c_B}(t_{max}) = \overline{c_{A0}^2}\,(2^{2/3} - 2^{1/3})/2 = 0.164\,\overline{c_{A0}^2} \qquad (147)$$

$$t_{max} = (\ln 2)/3K \qquad (148)$$

for all values of K. $\overline{c_B^2}(t)$ is not formed immediately but depends on development of $\overline{c_A c_B}(t)$, which acts like an intermediate between the decay of $\overline{c_A^2}(t)$ and growth of $\overline{c_B^2}(t)$. Fluctuation intensity is conserved in the absence of diffusion since at the completion of the reaction $\overline{c_B^2}(\infty) = \overline{c_A^2}(0)$.

Solutions using a characteristic diffusion length

Corrsin (13) has extended the analysis of Equation 139 by characterizing the diffusion term by the characteristic length $\lambda_s(t)$

$$-\overline{\left(\frac{\partial c_A}{\partial t}\right)\left(\frac{\partial c_A}{\partial t}\right)} = \delta_{ii}\,\overline{c_A^2}\left(\frac{\partial^2 f_s(r)}{\partial r^2}\right)_{r=0} = -2\delta_{ii}\,\overline{c_A^2}/\lambda_s(t)^2 \tag{149}$$

to give

$$\frac{d\overline{c_A^2}}{dt} = -2\overline{c_A^2}\left[2\delta_{ii}D_A/\lambda_s(t)^2 + K\right] \tag{150}$$

or upon integrating

$$\overline{c_A^2}(t) = \overline{c_{A0}^2}\,\exp\left[-4\delta_{ii}D_A\int_0^t dt_1/\lambda_s(t_1)^2\right]\exp(-2Kt) \tag{151}$$

Corrsin then reasons that since a first-order reaction is a simple linear phenomena, it should not be spectrally selective and hence the presence of the reaction should not affect characteristic lengths; $\lambda_s(t)$ used above with a first-order reaction should be the same as $\lambda_s(t)$ for pure mixing. With this Equation 151 can be expressed as a pure mixing result times the reaction exponential. In general

first-order reactions obey decay or growth laws of the form

$$\overline{c}(t) = \overline{c}_m(t)\mathcal{N}(t), \quad \overline{c^2}(t) = \overline{c_m^2}(t)\mathcal{N}^2(t) \qquad (152,153)$$

where $\overline{c}_m(t)$ and $\overline{c_m^2}(t)$ are the values for pure mixing and diffusion without reaction under the same conditions, and $\mathcal{N}(t)$ depends only on the chemical kinetics.

In order to carry out the integration in Equation 151 the time dependence of $\lambda_s^2(t)$ must be known. Corrsin (13) gives some approximate solutions. For stationary isotropic turbulence, using the pure mixing approximation given by Equation 109 gives

$$\overline{c_A^2} = \overline{c_{A0}^2} \exp[-2(K + 3\nu/\lambda_g^2)t] \qquad (154,3D)$$

For decaying turbulence other approximations for λ_s must be used. In the turbulence close behind a grid both the turbulence Reynolds ($\tilde{v}\lambda_g/\nu$) and Peclet ($\tilde{v}\lambda_s/D$) numbers remain fairly constant; this postulate gives $\lambda_s^2(t) = \lambda_s^2(0) + 20\,D_A t$ for pure mixing and hence

$$\overline{c_A^2}(t) = \overline{c_{A0}^2}\,[1 + 20D_A t/\lambda_s^2(0)]^{-3/5}\exp(-2Kt) \qquad (155)$$

In the final period of turbulence decay, both Re and Pe are small and $\lambda_s^2 = 8D_A t$, giving

$$\overline{c_A^2}(t) \sim t^{-3/2}\exp(-2Kt) \qquad (156,3D)$$

Solution in terms of pure mixing for $D_A = D_B$ For the case of equal diffusivities ($D_A = D_A$) it can be shown (15,102) that the reactant and product concentration fields are perfectly correlated and that a solution can be obtained in terms of a pure mixing case. Equation 131 for the reactant can be reduced to a pure mixing case by the transformation

$$c_A(\underset{\sim}{x},t) = c_m(\underset{\sim}{x},t) \exp(-Kt) \tag{157}$$

to give

$$\frac{\partial c_m}{\partial t} + v_i \frac{\partial c_m}{\partial x_i} = D \frac{\partial^2 c_m}{\partial x_i^2} \tag{158}$$

where $c_m(\underset{\sim}{x},t)$ is the solution of the corresponding pure mixing problem. Likewise, when $D = D_A = D_B$, the transformation

$$c_B(\underset{\sim}{x},t) = c_m(\underset{\sim}{x},t) \left[1 - \exp(-Kt)\right] \tag{159}$$

reduces the product equation, Equation 132, to Equation 158. With these transformations it is easily shown that $\overline{c_A c_B} = (\overline{c_A^2})^{\frac{1}{2}}(\overline{c_B^2})^{\frac{1}{2}}$ is satisfied since

$$\overline{c_A^2}(t) = \overline{c_m^2}(t) \exp(-2Kt) \tag{160}$$

$$\overline{c_B^2}(t) = \overline{c_m^2}(t) \left[1 - \exp(-Kt)\right]^2 \tag{161}$$

$$\overline{c_A c_B}(t) = \overline{c_m^2}(t) \left[\exp(-Kt) - \exp(-2Kt)\right] \tag{162}$$

Comparison of these expressions with Equations 142-144 for

the no diffusion case shows that the time dependence due to reaction is the same for both cases. With diffusion the reactant fluctuations decay more quickly; the product fluctuations grow and then die out. The linearity of the reaction specifies that for each fluid material point, C_B is created at a rate proportional to the C_A already there. In the absence of diffusion this would certainly result in perfect correlation. The equality of the diffusivities guarantees that although the two constituents actually diffuse, they diffuse together.

Two-point correlation equation The two-point correlation equation with a first-order reaction is

$$\frac{\partial[\tilde{c}_A^2 f_s(r)]}{\partial t} - 2\tilde{c}_A^2\tilde{v}\left[(\delta_{ii}-1)/r + \frac{\partial}{\partial r}\right]k_s(r)$$

$$= 2D_A\tilde{c}_A^2\left[(\delta_{ii}-1)\frac{1}{r}\frac{\partial}{\partial r} + \frac{\partial^2}{\partial r^2}\right]f_s(r) - 2K\tilde{c}_A^2 f_s(r) \qquad (163)$$

Corrsin (13) has solved this for the limiting case of small Peclet number. For very small Pe, local convection is negligible compared to molecular transport effects and the triple correlation terms can be neglected. Letting $Q_{ss}(r) = \tilde{c}_A^2 f_s(r)$, Equation 163 becomes

$$\frac{\partial Q_{ss}(r)}{\partial t} = 2D_A\left(\frac{2}{r}\frac{\partial}{\partial r} + \frac{\partial^2}{\partial r^2}\right)Q_{ss}(r) - 2KQ_{ss}(r) \qquad (164,3D)$$

with the solution

$$Q_{ss}(r,t) = (32\pi)^{-1/2} Q_o (D_A t)^{-3/2} \exp[-(r^2/8D_A t) - 2Kt] \quad (165,3D)$$

$$Q_o = \int_0^\infty r^2 Q_{ss}(r,0)dr$$

This is the corresponding pure mixing result times the reaction exponential. Notice that the reaction does not influence the spatial dependence. Taking the limit $r = 0$ gives

$$\tilde{c}_A(t)^2 = (32\pi)^{-1/2} Q_o (D_A t)^{-3/2} \exp(-2Kt) \quad (166,3D)$$

$$\lambda_s(t)^2 = 8D_A t \quad (167,3D)$$

Characteristic lengths are unaffected by first-order reactions but concentration fluctuations die out much more rapidly than in the pure mixing case. Of course this case with negligible convection is not actually a turbulence phenomenon.

Decay laws For large times, the fluctuation intensity of a reactant undergoing a first-order reaction decays according to

$$\overline{c_A^2}(t) \sim [at^{-3/2} + bt^{-5} + ct^{-15/2}] \exp(-2Kt) \quad (168,3D)$$

The first term in Equation 168 is the -3/2 final period decay law (no velocity field), first given by Corrsin (13); the other terms are for slightly earlier times and were evaluated by Kumar and Patel (52,53) and Patel (106). These were obtained from a set of two-, three-, and four-point

single time correlation equations made determinant by neglecting quintuple correlation terms. The first term in Equation 168 corresponds to the concentration "energy" for the two-point equation, the second term is due to the three-point correlation, and the third term comes from the four-point correlation. The terms associated with the higher-order correlations die out faster than those associated with the lower order ones.

Multireaction system with equal diffusivities

Using the simplification of equal diffusivities for all species, Pao (103) has shown that for certain conditions the concentration fields of all species in a multicomponent mixture undergoing different types of first-order reactions can be solved for in terms of pure mixing solutions.

The mass conservation equation for the rth component is

$$\frac{\partial C_r}{\partial t} + \underset{\sim}{v} \cdot \nabla C_r = D_r \nabla^2 C_r + \sum_{s=1}^{n} K_{rs} C_s \qquad (169)$$

for r = 1, 2, ..., n reacting species, and for a nonreacting species (pure mixing)

$$\frac{\partial C_m}{\partial t} + \underset{\sim}{v} \cdot \nabla C_m = D \nabla^2 C_m \qquad (170)$$

$$C_r(\underset{\sim}{x},t) = \overline{C}_r(t) + c_r(\underset{\sim}{x},t) \qquad (171)$$

$$C_m(\underset{\sim}{x},t) = \overline{C}_m(t) + c_m(\underset{\sim}{x},t) \qquad (172)$$

Let the initial conditions for all species r be

$$C_r(\underset{\sim}{x},0) = C_m(\underset{\sim}{x},0)\mathcal{N}_r(0) \tag{173}$$

This initial condition suggests a possible relation

$$C_r(\underset{\sim}{x},t) = C_m(\underset{\sim}{x},t)\mathcal{N}_r(t) \tag{174}$$

for all species r where $\mathcal{N}_r(t)$ is a function to be determined. Substituting Equation 174 into Equation 169 gives

$$C_m\frac{\partial \mathcal{N}_r}{\partial t} + \mathcal{N}_r\frac{\partial C_m}{\partial t} + \mathcal{N}_r\,\underset{\sim}{v}\cdot\nabla C_m = \mathcal{N}_r D_r \nabla^2 C_m + \sum_{s=1}^{n} K_{rs} C_m \mathcal{N}_s \tag{175}$$

or

$$\frac{\partial C_m}{\partial t} + \underset{\sim}{v}\cdot\nabla C_m = D\nabla^2 C_m + \frac{C_m}{\mathcal{N}_r}\left(\sum_{s=1}^{n} K_{rs}\mathcal{N}_s - \frac{\partial \mathcal{N}_r}{\partial t}\right) \tag{176}$$

Therefore, by demanding that

$$\sum_{s=1}^{n} K_{rs}\mathcal{N}_s - \frac{d\mathcal{N}_r}{dt} = 0 \tag{177}$$

and $D = D_r$ for all species r, then Equation 176 reduces to the pure mixing equation. Thus, we have shown that, for the initial condition Equation 173, $C_r(\underset{\sim}{x},t)$ can be related to $C_m(\underset{\sim}{x},t)$ for properly chosen $\mathcal{N}_r(t)$. $\mathcal{N}_r(t)$ is determined by solving the set of simultaneous first-order ordinary differential equations defined by Equation 177. Averaging Equation 174 gives

$$\overline{C}_r(t) = \overline{C}_m(t)\mathcal{N}_r(t) \tag{178}$$

but

$$[\bar{C}_r(t) + c_r(\underset{\sim}{x},t)] = [\bar{C}_m(t) + c_m(\underset{\sim}{x},t)]\,\mathcal{N}_r(t) \qquad (179)$$

The difference of these two equations is

$$c_r(\underset{\sim}{x},t) = c_m(\underset{\sim}{x},t)\,\mathcal{N}_r(t) \qquad (180)$$

Consequently the desired statistical relations are

$$\overline{c_r^2}(t) = \overline{c_m^2}(t)\,\mathcal{N}_r^2(t) \qquad (181)$$

$$\overline{c_r(\underset{\sim}{x},t)c_s(\underset{\sim}{x}',t)} = \overline{c_m(\underset{\sim}{x},t)c_m(\underset{\sim}{x}',t)}\,\mathcal{N}_r(t)\,\mathcal{N}_s(t) \qquad (182)$$

and so on. Pao also generalizes this approach to include cases where the C_r field is, initially, a linear combination of pure mixing fields

$$C_r(\underset{\sim}{x},0) = \sum_{I=1}^{J} C_{mI}(\underset{\sim}{x},0)\,\mathcal{N}_{rI}(0) \qquad (183)$$

As an example of Pao's method, consider the first-order reversible reaction

$$A \rightleftharpoons B \qquad (184)$$

with forward rate constant K_A and reverse rate constant K_B. The mass conservation equations are

$$\frac{\partial C_A}{\partial t} + \underset{\sim}{v}\cdot\nabla C_A = D\nabla^2 C_A - K_A C_A + K_B C_B \qquad (185)$$

$$\frac{\partial C_B}{\partial t} + \underset{\sim}{v}\cdot\nabla C_B = D\nabla^2 C_B + K_A C_A - K_B C_B \qquad (186)$$

Substitution of the transformations

$$C_A(\underset{\sim}{x},t) = C_m(\underset{\sim}{x},t)\mathcal{N}_A(t), \quad C_B(\underset{\sim}{x},t) = C_m(\underset{\sim}{x},t)\mathcal{N}_B(t) \qquad (187,188)$$

into Equations 185 and 186 gives the requirement that

$$\frac{d\mathcal{N}_A}{dt} = -K_A\mathcal{N}_A + K_B\mathcal{N}_B, \quad \frac{d\mathcal{N}_B}{dt} = K_A\mathcal{N}_A - K_B\mathcal{N}_B \qquad (189,190)$$

with initial conditions

$$C_A(\underset{\sim}{x},0) = C_m(\underset{\sim}{x},0)\mathcal{N}_A(0), \quad C_B(\underset{\sim}{x},0) = C_m(\underset{\sim}{x},0)\mathcal{N}_B(0) \qquad (191,192)$$

in order for the transformed equations to reduce to the pure mixing equation. Solving Equations 189 and 190 simultaneously gives

$$\mathcal{N}_A(t) = \frac{K_A[\mathcal{N}_A(0) + \mathcal{N}_B(0)]}{K_A + K_B} + \frac{[K_A\mathcal{N}_A(0) - K_B\mathcal{N}_B(0)]}{K_A + K_B} e^{-(K_A + K_B)t} \qquad (193)$$

The equation for $\mathcal{N}_B(t)$ is obtained from Equation 193 by interchanging the subscripts A and B. The desired concentration fluctuation growth and decay relations are then

$$\overline{c_A^2}(t) = \overline{c_m^2}(t)\mathcal{N}_A^2(t), \quad \overline{c_B^2}(t) = \overline{c_m^2}(t)\mathcal{N}_B^2(t) \qquad (194,195)$$

$$\overline{c_A c_B}(t) = \overline{c_m^2}(t)\mathcal{N}_A(t)\mathcal{N}_B(t) \qquad (196)$$

Concentration spectrum equation

With a first-order reaction the concentration spectrum equation becomes

$$\frac{\partial E_s(k)}{\partial t} + 2\left[Dk^2 + K\right]E_s(k) = T_s(k) \qquad (197)$$

Integrating Equation 197 over all k gives

$$-\frac{d\tilde{c}^2}{dt} = 2D\int_0^\infty k^2 E_s(k)dk + 2K\int_0^\infty E_s(k)dk = \epsilon_s \qquad (198)$$

Taking the limit $r = 0$ of the two-point correlation equation, Equation 163, gives

$$\lambda_s^2 = 4\delta_{ii}D\tilde{c}_A^2/(\epsilon_s - 2K\tilde{c}_A^2) \qquad (199)$$

Upon substituting Equation 198 into Equation 199, Equation 122 is recovered.

Since it is a linear phenomenon, a first-order reaction is not spectrally selective in the case of freely decaying fields. Therefore, its occurrence should not affect the relative spectral distribution of concentration fluctuations. Indeed, it can be shown (84) that for a first-order reaction the (nonstationary) concentration spectrum has the same wave number dependence as in the corresponding pure mixing case. For a first-order reaction the conservation equation for the reactant gives (Equation 137)

$$\frac{\partial c}{\partial t} + v_i\frac{\partial c}{\partial x_i} = D\frac{\partial^2 c}{\partial x_i^2} - Kc \qquad (200)$$

Let $c_m(\underset{\sim}{x},t)$ be a solution of the pure mixing equation

$$\frac{\partial c_m}{\partial t} + v_i \frac{\partial c_m}{\partial x_i} = D \frac{\partial^2 c_m}{\partial x_i^2} \tag{201}$$

Then $c_m(\underset{\sim}{x},t)\exp(-Kt)$ is a solution of the reaction equation as can be verified by direct substitution. Similarly, if the reaction equation at another point (primed)

$$\frac{\partial c'}{\partial t} + v_i' \frac{\partial c'}{\partial x_i'} = D \frac{\partial^2 c'}{\partial x_i'^2} - Kc' \tag{202}$$

is assumed to have a solution, it can be of the form $c_m'(\underset{\sim}{x},t)\exp(-Kt)$ where $c_m'(\underset{\sim}{x},t)$ satisfies

$$\frac{\partial c_m'}{\partial t} + v_i' \frac{\partial c_m'}{\partial x_i'} = D \frac{\partial^2 c_m'}{\partial x_i'^2} \tag{203}$$

Multiplying the two solutions and averaging then gives

$$\overline{cc'}(\underset{\sim}{r}) = \overline{c_m c_m'}(\underset{\sim}{r})\exp(-2Kt) \tag{204}$$

The Fourier transform of this is

$$E_s(\underset{\sim}{k}) = E_s(\underset{\sim}{k})_m \exp(-2Kt) \tag{205}$$

or from isotropy

$$E_s(k) = E_s(k)_m \exp(-2Kt) \tag{206}$$

From this it is evident that the (nonstationary) concentration spectrum function for a fluctuating field with a first-order reaction has the same k dependence as the (nonstation-

ary) spectrum function for a nonreactive fluctuating field.

O'Brien (84) has attempted to investigate the statistical behavior of the reactant of a first-order irreversible reaction in isotropic turbulence through numerical integration of the concentration spectrum equation. In order to make calculation feasible, only Equation 197 and the next higher moment equation in the infinite hierarchy were used. As a closure approximation it was assumed that all fourth-order moments are related to second-order ones in the same manner as for Gaussian variables (zero fourth-order cumulant approximation). Under this hypothesis the mean of any four fluctuating components a, b, c, and d will satisfy the equation

$$\overline{abcd} = \overline{ab}\cdot\overline{cd} + \overline{ac}\cdot\overline{bd} + \overline{ad}\cdot\overline{bc} \qquad (207)$$

If a, b, c, and d were true Gaussian variables any odd order mean would be zero. However, to require this would completely eliminate inertial transfer effects and thus destroy the very property of interest in the problem. Using the resultant determinant set of equations, the small time behavior of the concentration spectrum transfer function was calculated for several initial velocity and concentration spectra. However, numerical calculation (96) showed that the approximation leads to negative concentration spectrum functions (an unphysical result).

Spectral theories

Simple dimensional reasoning does not work in deducing the spectrum function when reaction occurs because of added parameters like the reaction rate constant. To handle the reacting cases, Corrsin (14,15) extended Onsager's (100) spectral transfer concepts for turbulence dynamics to turbulent mixing with or without reaction. Onsager introduced the crude concept of a spectral "energy cascade", in which spectral elements (local sections of the spectrum "content" that can be thought of as being "tagged" upon entering the spectrum) "jump" to successively larger wave numbers as time goes on. In a stationary field, large scale fluctuations are continuously introduced which decay to progressively smaller scale fluctuations and finally dissipate. Following a spectral element through the spectrum (from low to high wave numbers) can be thought of as following a "tagged" fluctuation through the decay process. Assumptions made in the Corrsin-Onsager analysis are:

1) The cascade wave number sequence is a geometrical progression, so that the size of the jump is given by $\Delta k \sim k$. For turbulence dynamics this is suggested by the nonlinearity of the Navier-Stokes equation; here it is suggested by the nonlinear statistical characteristics of the convection term of the mass conservation equation.

2) The part of the $\overline{c^2}$-spectrum transferred in a jump at wave number k is $E_s(k)\,\Delta k$, where Δk is the width of the

spectral "slab" being followed. Since the upper and lower wave number limits of the slab jump to new wave numbers proportional to their previous values, $\Delta k \sim k$.

3) The characteristic time for each jump depends on the velocity spectrum E(k). For the inertial part of the velocity spectrum, Onsager chose the simplest dimensional possibility, $\Delta\tau(k) = k^{-3/2}E(k)^{-1/2}$. In other parts of the spectrum the spectral local convection time will be different and dependent upon the characteristics of the subranges.

4) A decrease (reactant) or gain (product) in $\overline{c^2}$-spectrum content for the progressing slab results from the chemical reaction. This rate of decrease or gain with k must be determined in some manner.

The rate of transfer of spectral content through a wave number k is proportional to the quantity "jumping", $E_s(k)\Delta k \sim E_s(k)k$, divided by the time for the jump $\Delta\tau(k)$. In the inertial-convective and viscous-convective subranges, the spectral content is conserved for the nonreacting case because dissipation does not occur, therefore

$$\frac{d}{dk}\left[E_s(k)k/\Delta\tau(k)\right] = 0 \qquad (208)$$

For the reacting case Corrsin further proposed that

$$\frac{d}{dk}\left[E_s(k)k\,f(k)/\Delta\tau(k)\right] = 0 \qquad (209)$$

f(k) is compensation for the decrease or increase in spectral content with k due to reaction. One difficulty of

this approach is deducing the form of f(k) by suitable arguments.

Pao's (103) unified concept of spectral transfer uses a continuous spectral cascade rather than a geometric progression. The rate at which a $\overline{c^2}$-spectral element is transferred across k is defined as $s(k) = dk/d\mathcal{T}$. The rate of spectral flux across k is then $E_s(k)s(k)$. s(k) is obtained for the various subranges by physical reasoning. Since the integral of the transfer function $T_s(k)$ from k to infinity is equal to the spectral flux across k, it can be shown that $T_s(k) = -d[E_s(k)s(k)]/dk$, and the stationary concentration spectrum equation for pure mixing can be written as

$$2Dk^2E_s(k) = -d[E_s(k)s(k)]/dk \qquad (210)$$

from which $E_s(k)$ can be found for a given form of s(k). Using this approach Pao developed analogous equations for the case of first-order reactions and used the expressions for s(k) developed for pure mixing to obtain solutions.

Pao (104,105) has also developed a simple continuous spectral cascading concept for turbulent energy and scalar quantities. By dimensional reasoning s(k) is chosen to be $s(k) \sim \epsilon^{1/3}k^{5/3}$ and it is argued that the resulting scalar spectrum function for pure mixing is valid for the whole universal equilibrium range for any Schmidt number (experiments by Nye and Brodkey (83) do not agree with this, however). In obtaining this it has essentially been postulated

that the small-scale of the concentration field is dependent on ϵ, ϵ_s, and D, but not on the viscosity.

In addition to the spectral cascade concepts above, physical reasoning and dimensional arguments are used in determining quantities such as $\Delta\gamma(k)$, f(k), and s(k) in the different subranges. In the inertial-convective subrange the transfer of spectral elements is purely convective and the cascade is expected to depend mainly upon the turbulent dissipation ϵ. Since viscous and diffusive effects are negligible, the diffusion term is dropped from the mass conservation equation in finding f(k). In the viscous subranges Batchelor's uniform straining model is used since the turbulent straining action can be considered as locally uniform for a limited time; the local least turbulent straining rate is an important parameter. In the viscous-convective range diffusive effects are negligible; simplification is achieved by setting D = 0. Two different routes have been used in analyzing the inertial-diffusive subrange. The first uses the spectral cascade argument, where the cascading process is again dependent on the turbulent dissipation ϵ, but the diffusion term in the mass conservation equation can no longer be neglected. The second does not use the spectral cascade method but instead follows the arguments and procedure established by Batchelor, Howells, and Townsend (6) for the pure mixing case with appropriate reaction terms added. The two routes generally yield dif-

ferent results.

Reaction spectra

Calculations of the concentration spectrum functions of the reactant, G(k), and the product, H(k), of a first-order irreversible reaction (with rate constant a) have been made by Corrsin (14,15,16) and Pao (102) using the Corrsin-Onsager method, by Pao (103) using Pao's unified concept of spectral transfer, by Kumar and Paul (54) using Pao's simple continuous spectral cascading concept, and by Tchen (118) and Menkes and Tchen (73). Additional results for the inertial-diffusive subrange have been obtained by Corrsin (14) and Pao (102,103) using the technique of Batchelor, Howells, and Townsend (6). For the first-order irreversible reaction the results of the three spectral theories reduce to the same wave number dependence, although the constants of proportionality vary. A summary of the results for the different analyses is presented in Table 1.

The reactant and product concentration spectrum functions are depicted qualitatively in Figures 3 and 4 for large and small Schmidt numbers, respectively. Evidently in the inertial-convective subrange, for wave numbers well above the characteristic reaction wave number $k_a \equiv (a^3/\epsilon)^{\frac{1}{2}}$, the effect of reaction on spectral shape is negligible since both the reactant and product spectra approach the pure mixing dependence on wave number. k_a locates the spectral

Table 1. First-order irreversible reaction spectrum functions

---

Inertial-Convective Subrange

Corrsin (14,15), Pao (103), Kumar and Paul (54)

$$G(k) \sim k^{-5/3} \exp\left[3(k_a/k)^{2/3}\right]$$

$$H(k) \sim k^{-5/3} \left\{1 - N(a) \exp\left[3(k_a/k)^{2/3}\right]\right\}^2$$

$k_a \equiv (a^3/\epsilon)^{1/2}$ = characteristic reaction wave number

$N(a)$ = collection of constants, $N(0) = 0$

Viscous Subrange

Corrsin (14,15), Pao (103), Kumar and Paul (54)

$$G(k) \sim k^{-(1 + 4N_a)} \exp(-2k^2/k_B^2)$$

Pao (102,103), Corrsin (14,15), Kumar and Paul (54)

$$H(k) \sim k^{-1} \left\{1 - L(a)(k_K/k)^{2N_a}\right\}^2 \exp(-2k^2/k_B^2)$$

$N_a \equiv a(\nu/\epsilon)^{1/2}$ = reaction parameter

$L(a)$ = collection of constants, $L(0) = 0$

In the viscous-convective range the above expressions simplify since $\exp(-2k^2/k_B^2) \sim 1$

Table 1. (Continued)

Inertial-Diffusive Subrange

Corrsin (14), Pao (103)

$$G(k) \sim k^{-17/3} \left[Dk^2/(Dk^2 + a)\right]^2$$

Pao (102,103)

$$H(k) \sim k^{-17/3} \left[N_1 + aN_2(Dk^2 + a)^{-1}\right]^2$$

Corrsin (16), Kumar and Paul (54)

$$G(k) \sim k^{-5/3} \exp\left[3(k_a/k)^{2/3} - (3/2)(k/k_c)^{4/3}\right]$$

Kumar and Paul (54)

$$H(k) \sim k^{-5/3} \left\{N_1' a^2 - N_2' a \exp\left[(3/2)(k_a/k)^{2/3}\right] + N_3' \exp\left[3(k_a/k)^{2/3}\right]\right\} \exp\left[-(3/2)(k/k_c)^{4/3}\right]$$

$$k_a \equiv (a^3/\epsilon)^{1/2}$$

N_1, N_2, N_1', N_2', N_3' = collection of constants

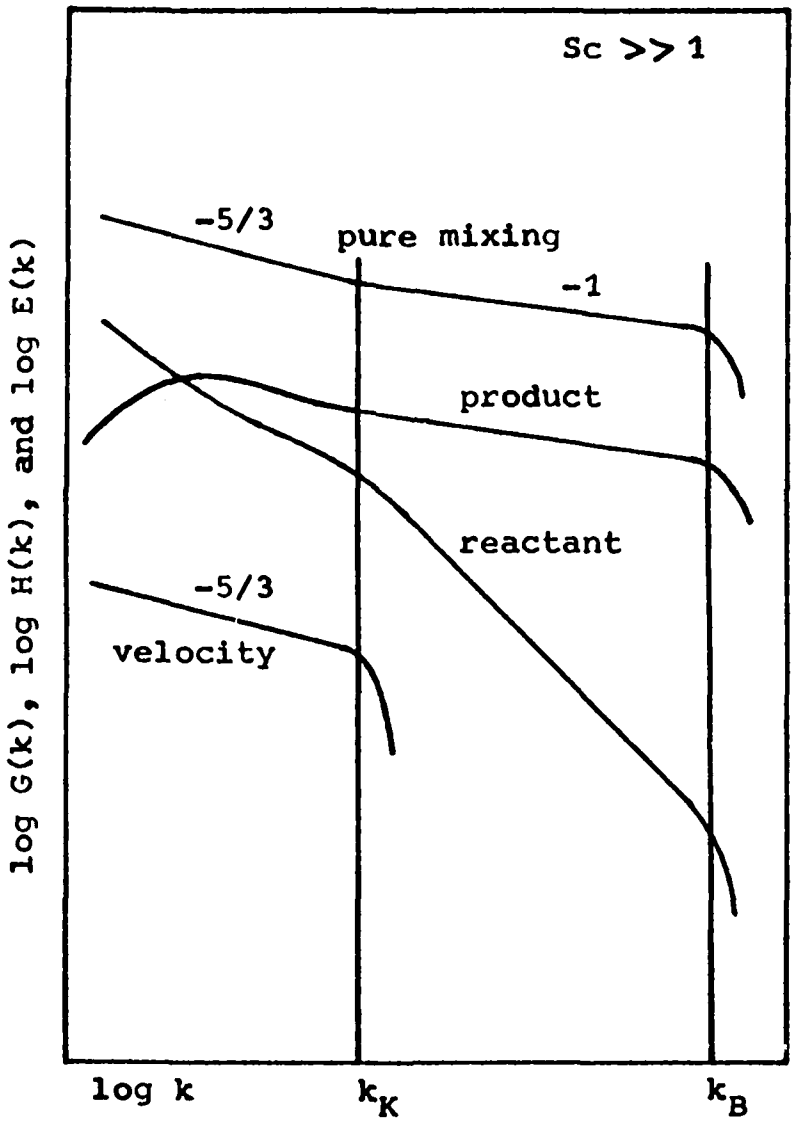

Figure 3. First-order reactant and product spectra for Sc >> 1

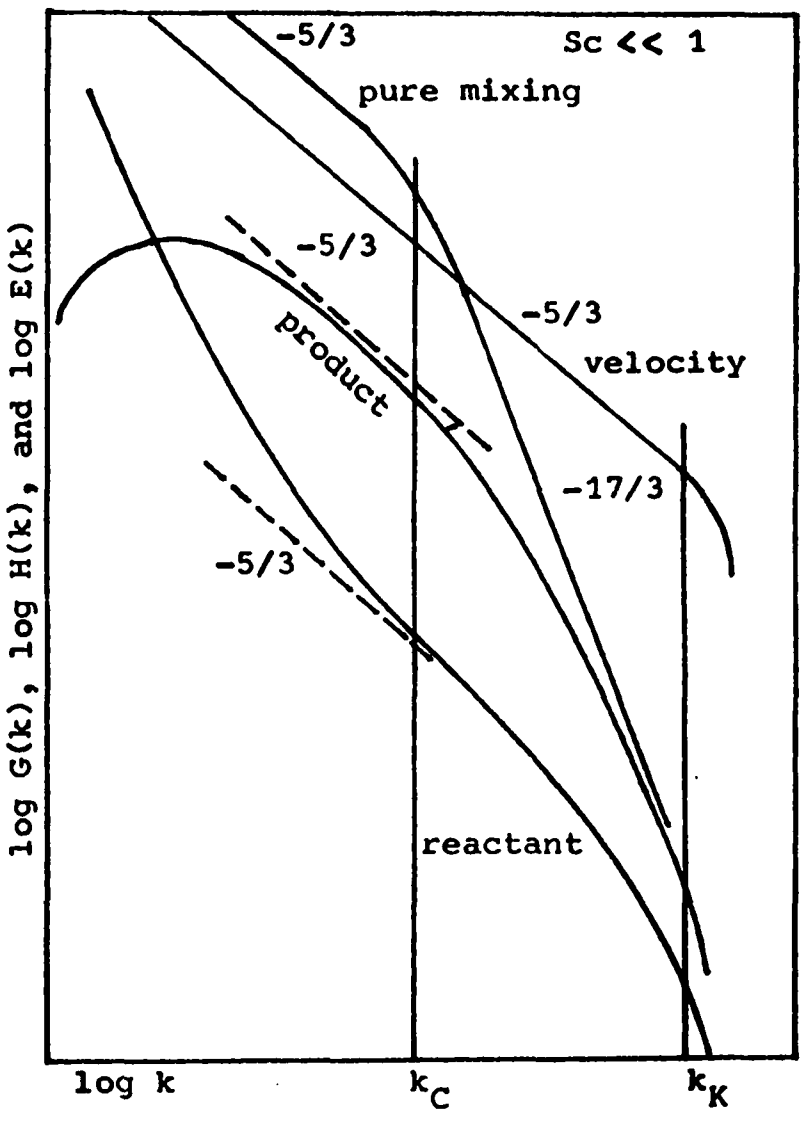

Figure 4. First-order reactant and product spectra for Sc << 1

region in which the rate of reactive loss (or gain) is of the same order as the rate of convective spectral transfer. The dominant feature in the low wave number range is the transfer of reactant spectral content to the product spectral content during the flux to higher wave numbers. The product spectrum should be independent of the product diffusivity to reactant diffusivity ratio since molecular diffusion is of no concern in this range.

In the viscous-convective subrange the reaction wave number k_a does not influence the shape of the reactant spectrum; the spectrum remains linear but with increased slope on a log-log plot. It does, however, affect the entire local level through the constant of proportionality. In general the reactant spectrum decreases more rapidly than for simple mixing, while the product spectrum decreases less rapidly. As in the inertial-convective subrange, the product spectrum is independent of diffusivity. For the viscous-diffusive subrange molecular diffusion is important, but no closed form solution for the product spectrum is known for the case of nonequal diffusivities; in this case a numerical solution is necessary, using the equations developed by Pao (103), for instance.

In the inertial-diffusive subrange both reactant and product spectra approximate the pure-mixing form (-17/3 law) in the wave number range $k >> (a/D)^{\frac{1}{2}}$, which is a measure of the spectral location where reactive and diffusive loss

rates are comparable. At the beginning of the subrange both approximate the -5/3 mixing law due to matching with the inertial-convective subrange. For nonequal diffusivities no closed form for the product spectrum exists.

Spectra for multiple reaction cases (with equal reactant and product diffusivities) have also been investigated. The reversible first-order reaction case has been solved by Pao (102) using the Corrsin-Onsager method, Pao (103) using Pao's unified concept of spectral transfer, and Kumar and Paul (55) using Pao's simple continuous spectral cascading concept. The parallel irreversible first-order reaction and consecutive irreversible first-order reaction cases have been solved for the inertial-diffusive subrange by Paul (108) using Batchelor, Howells, and Townsend's (6) method and for the other subranges by Kumar and Paul (55) using Pao's continuous spectral cascading concept.

It should be emphasized that none of these results has been tested experimentally. The fact that very few turbulent mixing with chemical reaction theoretical results have been checked against experimental results of any kind points to a strong need for new methods of detecting rapidly fluctuating chemical concentrations.

Second-Order Single Component Reaction

Decay equations

The mass conservation equation for the reactant of a single component second-order irreversible reaction with rate constant K is

$$\frac{\partial C}{\partial t} + v_i \frac{\partial C}{\partial x_i} = D \frac{\partial^2 C}{\partial x_i^2} - K C^2 \qquad (211)$$

Averaging and restricting to homogeneity gives

$$\frac{d\overline{C}}{dt} = -K(\overline{C}^2 + \overline{c^2}) \qquad (212)$$

and the total rate of conversion of reactant depends explicitly upon concentration fluctuations: concentration fluctuations increase the rate of conversion. Setting $C = \overline{C} + c$ in Equation 211 and subtracting out the averaged Equation 212 gives

$$\frac{\partial c}{\partial t} + v_i \frac{\partial c}{\partial x_i} = D \frac{\partial^2 c}{\partial x_i^2} - 2K\overline{C}c - K c^2 + K\overline{c^2} \qquad (213)$$

The corresponding equation for the dissipation of average concentration fluctuation is

$$\frac{d\overline{c^2}}{dt} = -2D \overline{\left(\frac{\partial c}{\partial x_i}\right)\left(\frac{\partial c}{\partial x_i}\right)} - 4K\overline{C}\,\overline{c^2} - 2K\overline{c^3} \qquad (214)$$

which shows that the dissipation of average concentration fluctuation of a second-order reaction is influenced by higher order fluctuation terms as well. $\overline{c^3}$ may be either

positive or negative, but consideration of the conservation equation without convection or diffusion, $dC/dt = -KC^2$, shows that the reaction tends to make $\overline{c^3} < 0$. Hence the $\overline{c^3}$ term may slow the decay of $\overline{c^2}$. Due to the nonlinearity of the reaction term, even in the limit of no diffusion ($D = 0$) Equations 212 and 214 are not determinant and a closure problem exists. An equation for $\overline{c^3}$ can be obtained by multiplying Equation 213 through by c^2, rearranging the convection and diffusion terms, averaging, and restricting to homogeneity

$$\frac{d\overline{c^3}}{dt} = 3D\,\overline{c^2\frac{\partial^2 c}{\partial x_i^2}} - 6K\bar{C}\,\overline{c^3} - 3K\overline{c^4} + 3K(\overline{c^2})^2 \qquad (215)$$

Corrsin (13) has examined simplifications of Equations 212, 214, and 215 for three different limiting conditions. The diffussive terms in Equations 214 and 215 are handled by introducing characteristic lengths

$$\overline{\left(\frac{\partial c}{\partial x_i}\right)\left(\frac{\partial c}{\partial x_i}\right)} = 2\delta_{ii}\overline{c^2}/\lambda_s(t)^2, \quad \overline{c^2\frac{\partial^2 c}{\partial x_i^2}} \equiv \delta_{ii}\overline{c^3}/p^2(t) \qquad (216,217)$$

so that Equations 214 and 215 become

$$\frac{d\overline{c^2}}{dt} = -2\left[2\delta_{ii}D/\lambda_s(t)^2 + 2K\bar{C}\right]\overline{c^2} - 2K\overline{c^3} \qquad (218)$$

$$\frac{d\overline{c^3}}{dt} = 3\left[\delta_{ii}D/p^2(t) - 2K\bar{C}\right]\overline{c^3} - 3K\left[\overline{c^4} - (\overline{c^2})^2\right] \qquad (219)$$

Due to the presence of $\overline{c^3}(t)$ and $\lambda_s(t)$ in Equation 218,

strong restrictions or assumptions are necessary for even rough estimates to be made. Hopefully, introducing a rough approximation into an equation for a higher moment of c will have less effect than an approximation in the equation for $\overline{c^2}$. The three limiting cases considered by Corrsin are:

1) Extremely low fluctuation level ($\tilde{c}/\bar{C} \ll 1$). This implies that the system is well mixed. For $\tilde{c}/\bar{C} \ll 1$, the system of equations becomes

$$\frac{d\bar{C}}{dt} \approx -K\bar{C}^2, \quad \frac{d\overline{c^2}}{dt} \approx -2\left[2\delta_{ii}D/\lambda_s(t)^2 + 2K\bar{C}\right]\overline{c^2} \qquad (220,221)$$

$$\frac{d\overline{c^3}}{dt} \approx 3\left[\delta_{ii}D/p^2(t) - 2K\bar{C}\right]\overline{c^3} \qquad (222)$$

and the mean concentration decays in the manner of a uniform mixture. The equations for the fluctuation terms no longer depend on higher order moments, but solution for $\overline{c^2}$ still requires information on $\lambda_s(t)$. Unlike the first-order reaction, it can not be assumed a priori that $\lambda_s(t)$ is set only by the balance between convective and diffusive actions; the nonlinearity of a second-order reaction must influence the size structure of the concentration field.

2) Very slow reaction ($K\bar{C} \ll D/\lambda_s^2$). In addition, the dominance of diffusion should keep the skewness factor small: $\overline{c^3}/(\overline{c^2})^{3/2} \ll 1$. Therefore, in the early stages of such a reaction (before $\tilde{c}/\bar{C} \ll 1$) it may be possible to neglect $\overline{c^3}$ in the equation for $\overline{c^2}$ and to consider $\lambda_s(t)^2$ to

be given by pure mixing results, giving

$$\frac{d\bar{C}}{dt} = -K(\bar{C}^2 + \overline{c^2}), \quad \frac{d\overline{c^2}}{dt} \approx -4\delta_{ii}\overline{c^2}/\lambda_s(t)^2 \quad (223,224)$$

3) Very fast reaction ($K\bar{C} >> \delta_{ii}D/\lambda_s^2$, $2K\bar{C} >> \delta_{ii}D/p^2$). If the rate of decrease of $\overline{c^2}$ due to chemical reaction is much greater than that due to diffusion, the $\overline{c^3}$ term is important but the diffusive terms may be negligible in both fluctuation equations. An assumption for $\overline{c^4}$ is necessary to make the equations determinant. A crude assumption is that c is Gaussian, so that $\overline{c^4} \approx 3(\overline{c^2})^2$. Therefore

$$\frac{d\bar{C}}{dt} = -K(\bar{C}^2 + \overline{c^2}), \quad \frac{d\overline{c^2}}{dt} \approx -4K\bar{C}\,\overline{c^2} - 2K\overline{c^3} \quad (225,226)$$

$$\frac{d\overline{c^3}}{dt} \approx -6K\bar{C}\,\overline{c^3} - 6K(\overline{c^2})^2 \quad (227)$$

In final period turbulence, Equation 220 shows that the mean field decays according to $\bar{C}(t) \sim t^{-1}$, as it does for a nonturbulent reaction. O'Brien (87) has shown that the intensity follows $\overline{c^2}(t) \sim t^{-4}$ for $D = 0$ and $\sim t^{-11/2}$ for $D \neq 0$.

Closure theories, stochastic type reactions

As can be seen from the above simple analyses, achieving closure of the mass conservation equation is a central problem in the theory of second-order reactions in turbulence. Developing closure techniques that satisfy

various statistical restraints imposed by the physical nature of turbulence and the concentration field while also being accurate and solvable has proved to be a difficult task. In order to understand the closure problem associated with the reaction term, there have been several studies of the equation

$$\frac{dC}{dt} = -K C^2 \tag{228}$$

The problem is made stochastic by assigning initial conditions in a statistical manner. Homogeneity and isotropy are assigned to the initial statistics so that the concentration probability density function $P[C(\underset{\sim}{x},0)]$ is independent of $\underset{\sim}{x}$ and the joint probability density $P[C(\underset{\sim}{x},0), C(\underset{\sim}{x}',0)]$ is a function of $|\underset{\sim}{x} - \underset{\sim}{x}'|$ only.

The introduction of spatial dependence into a problem in which there is no spatial variable in the defining equation is somewhat artificial. It means, for example, that isotropy is guaranteed throughout the decay if it is embodied in the initial conditions, that there is no spatial scale to the problem except in the initial prescription, and that spectral transfer only depends on the shape of the initial concentration spectrum (86). But in the sense that reaction terms never involve spatial operators, such behavior is typical of the instantaneous spectral transfer action of second-order reactions in a real turbulence.

The solution of Equation 228 with a deterministic

initial condition $C(\underset{\sim}{x},0)$ is simply

$$C(\underset{\sim}{x},t) = C(\underset{\sim}{x},0)/[1 + C(\underset{\sim}{x},0)Kt] \tag{229}$$

Thus, typical stochastic solutions, in terms of initial probability densities, can be written

$$\overline{C^n(\underset{\sim}{x},t)} = \int_0^\infty [C_1/(1 + C_1Kt)]^n \, P[C_1(\underset{\sim}{x},0)]dC_1 \tag{230}$$

$$\overline{C^n(\underset{\sim}{x},t)C^m(\underset{\sim}{x}',t')} = \int_0^\infty \int_0^\infty [C_1/(1 + C_1Kt)]^n \, [C_2/(1 + C_2Kt')]^m \tag{231}$$

$$\cdot \, P[C_1(\underset{\sim}{x},0),C_2(\underset{\sim}{x}',0)] \, dC_1dC_2$$

For fluctuations in concentration defined in the usual way, $c(\underset{\sim}{x},t) = C(\underset{\sim}{x},t) - \overline{C}(t)$, the behaviors of the mean and moments of the fluctuation field follow immediately from Equations 230 and 231 once specific initial probability densities are assigned. Asymptotic decay limits (as $t \to \infty$) that follow from Equation 230 are

$$\overline{C}(t) \sim t^{-1}, \; \overline{c^2}(t) \sim t^{-4}, \; \overline{c^3}(t) \sim -t^{-6} \tag{232}$$

The appropriate form of the moment equations to be solved by the approximate closure methods are

$$\frac{d\overline{C}}{dt} = -K\overline{C}^2 - K\overline{c^2} \tag{233}$$

$$\frac{d\overline{c^2}}{dt} = -4K\overline{C}\,\overline{c^2} - 2K\overline{c^3} \tag{234}$$

$$\frac{d\overline{c^3}}{dt} = -6K\bar{c}\,\overline{c^3} - 3K[\overline{c^4} - (\overline{c^2})^2] \qquad (235)$$

and so on, where the initial moments $\bar{c}(0)$, $\overline{c^2}(0)$, $\overline{c^3}(0)$, ..., are prescribed.

O'Brien (86) has compared the exact solution of Equation 226, using an initial multivariate normal probability distribution, with various closure approximations that have been employed in the study of turbulence:

1) The zero-third-moment approximation, which simply sets $\overline{c^3} = 0$ in Equation 234.

2) The joint normal distribution hypothesis, which assumes that all fourth-order moments are related to second-order ones in the same manner as for Gaussian variables (Equation 207). It has been shown to have unphysical results in the turbulence problem, but in this problem it introduces no such difficulties provided $\bar{c}(0)/\tilde{c}(0)$ is not large.

3) Kraichnan's (49) direct-interaction hypothesis.

The direct-interaction hypothesis provides a satisfactory description of the mean, root-mean-square, and correlation function of the concentration field as does the joint normal distribution hypothesis. However, the former is slightly superior even in this problem in which energetic difficulties of the latter are not apparent. The zero-third-moment approximation is less satisfactory. In order to obtain realizable results for the normal distribution,

the initial relative intensity $\tilde{c}/\bar{C}$ was limited to values of 0.4 or less; this serves to lessen the distinction between the closures.

O'Brien (90) has shown that the direct-interaction hypothesis, when applied to Equation 211, fails to preserve, even approximately, an important statistical invariance. Namely, that in the absence of molecular diffusion the decay of single-point statistical functions of the concentration field should be independent of the turbulence. To remedy this, O'Brien (89) applied the Lagrangian history direct-interaction approximation which does preserve this property. In the limit of a stochastically distributed second-order reaction the equations reduce to those of direct-interaction.

In order to guarantee a well-behaved system for any value of the relative intensity of the initial fluctuations, O'Brien (88) developed a closure at the third-order moment that satisfies the statistical realizability conditions for a nonnegative random variable. It is supposed that $\bar{C}(0)$, $\overline{c^2}(0)$, and $\overline{c^3}(0)$ are prescribed, and it is desired to replace $\overline{c^3}$ by specified functions of $\bar{C}$ and $\overline{c^2}$ whose forms do not depend on the initial data, but are such that the first two moment equations yield physically acceptable descriptions of the first three moments. The proposed closure is

$$\overline{c^3} = A_1(\overline{c^2})^2/\bar{C} - A_0(\overline{c^2})^{3/2} \qquad (236)$$

The constant A_1 is obtained from A_0, $\overline{c}(0)$, $\overline{c^2}(0)$, and $\overline{c^3}(0)$. O'Brien and Eng (95) generalized the closure for reactions of order R where $1 \leq R \leq 3$. Lin (63) has also proposed a third-order moment closure that satisfies the realizability conditions; although it is asymptotically less exact than O'Brien's it is easily generalized to include spatial correlation and two-species reactions.

Lee (59) has developed a generalized direct-interaction approximation devised to close off the hierarchy of moment equations at the arbitrary moment level, and the results of such a closure technique have been compared term-by-term with the exact moment solutions for the system of Equation 228. A quantitative comparison indicates that the direct-interaction equations closed at the triple moment level represent a meaningful statistical approximation of the lowest order for this second-order reaction problem.

Reaction with turbulence and diffusion using direct-interaction

Lee (58) used the direct-interaction approximation to compute the decay of $\overline{c}$ and $\overline{c^2}$ for a second-order reaction with turbulence and diffusion. The parameter dependence and component terms of the direct-interaction equations can be summarized as follows (in dimensionless variables)

Mean concentration

$$\frac{d\overline{c}(t)}{dt} = -Da_{II}\overline{c}(t)^2 - (2^{\frac{1}{2}}Da_{II}/\alpha^2\pi^{\frac{1}{2}}) \int_0^\infty k^2 S(k,t,t)dk \qquad (237)$$

Concentration covariance (fluctuations)

$$\left[\frac{\partial}{\partial t} + k^2 + 2Da_{II}\bar{\mathcal{Z}}(t)\right] S(k,t,t')$$

$$= (2k\,Pe^2/\pi^{1/2}) \left[\begin{matrix}\text{nonlinear convective} \\ \text{D-I terms}\end{matrix}\right] \qquad (238)$$

$$+ (2^{1/2}Da_{II}{}^2/\pi^{1/2}\alpha^2 k) \left[\begin{matrix}\text{nonlinear reactive} \\ \text{D-I terms}\end{matrix}\right]$$

$$S(k,t,t') \equiv [(2^{1/2}\pi^{1/2}k_o)^3/\tilde{c}^2(0)]\, F[c(\underset{\sim}{x},t)c(\underset{\sim}{x}',t')]$$

$$\alpha \equiv \bar{C}(0)/\tilde{c}(0),\quad t \equiv t^*Dk_o^2,\quad \bar{\mathcal{Z}}(t) \equiv F[\bar{C}(t)/\bar{C}(0)]$$

$$Da_{II} \equiv K\bar{C}(0)/Dk_o^2 = \text{second Damköhler number}$$

$$Pe \equiv \tilde{v}/Dk_o = \text{Peclet number}$$

$$k_o = \text{characteristic energy spectrum wave number}$$

In addition there is a third equation for a direct-interaction response function, which resembles the covariance equation. The response function appears in the nonlinear terms of the covariance equation.

In the limit of $Da_{II} = 0$, the equations reduce to those of pure mixing; therefore, the effect of reaction on the decay dynamics becomes increasingly important as Da_{II} becomes large. In Equation 238, Da_{II} appears with a linear reaction term and nonlinear reactive direct-interaction terms. The linear term gives rise to an exponential decay upon integration; however, the reactive direct-interaction term, which is typically positive, will cause divergence

without modulation by the exponential. An important parameter categorizing the decay dynamics is the first Damköhler number $Da_I \equiv Da_{II}/Pe$. The evolved concentration spectra display accelerated decay with increasing Da_I. Using a steady velocity field having a given velocity spectrum and an imposed initial concentration fluctuation spectrum, Lee calculated the decay of $\bar{C}$ and $\overline{c^2}$ for different Da_I and α.

Overall field structure dependence on Da_I was elucidated from changes in the scalar integral scale and microscale during decay. With $Da_I = 10$, length scales remained virtually unchanged during the entire decay period due to the exponential reaction term, which induces a severe decay independently of wave number. Hence, the reactant field at large Da_I may be said to be structurally frozen. As Da_I becomes small, both the exponential decay and the nonlinear interactions become mutually important so that the concentration field undergoes a fuller structural evolution. The scales for small Da_I change considerably (decrease) during the decay period.

For large α (weak initial relative intensity) it was found that the uniform mixture result $\bar{C}(t) = (1 + Da_{II}t)^{-1}$ was a close upper bound to the mean field decay. An even better approximation was achieved through approximating the fluctuation intensity term in Equation 237 by $S(k,t,t) = S(k,0,0)(1 + Da_{II}t)^{-4}$, an approximation valid at large Da_I (as shown later). Integrating Equation 237 over k gives

$$\frac{d\bar{C}(t)}{dt} = -Da_{II}\bar{C}(t)^2 - Da_{II}\alpha^{-2}(1 + Da_{II}t)^{-4} \qquad (239)$$

the solution of which is (Riccati's equation)

$$\bar{C}(g) = F(g)^{-1}\frac{dF(g)}{dg},\ g \equiv 1 + Da_{II}t \qquad (240)$$

$$F(g) \equiv g\cot(1/g)\cos(1/\alpha g) + g\sin(1/\alpha g) \qquad (241)$$

This was found to agree very closely with the exact direct-interaction result for all Da_{II} (0.01-10) and α (≥ 2) considered. The asymptotic result $\bar{C}(g) = 1/g$ is recovered as $\alpha \to \infty$.

It was observed that the fluctuation intensity, $\overline{c^2}(t)/\overline{c^2}(0)$, begins to fall off rapidly in time as Da_I increases from zero to near unity, and that for larger Da_I the decay curves have the same shape. This suggests a fluctuation decay mechanism at large Da_I in which the linear reaction term in Equation 238 is most dominant. Dropping the k^2 diffusion term and the convective and reactive direct-interaction terms before integrating over all k gives

$$\overline{c^2}(t)/\overline{c^2}(0) = \exp\left[-4Da_{II}\int_0^t \bar{C}(t_1)dt_1\right] \qquad (242)$$

Substituting $\bar{C}(t) = (1 + Da_{II}t)^{-1}$ gives the result (used earlier, after taking the Fourier transform)

$$\overline{c^2}(t)/\overline{c^2}(0) = (1 + Da_{II}t)^{-4} \qquad (243)$$

valid for large Da_{II}. With $Da_I > 1$, this result approx-

imates the direct-interaction results. The implication is that the convective and reactive nonlinear interactions simply do not contribute enough to make the closure hypothesis critical. Lee also improved upon this result using a quasinormal (fourth cumulant discard) approximation for $\overline{c^4}$ to give

$$\overline{c^2}(t)/\overline{c^2}(0) = g^{-4}\left[1 + 6\alpha^{-2}(1 - 2/g + 1/g^2)\right] \qquad (244)$$

$$g \equiv 1 + Da_{II}t$$

This results in much closer agreement with the exact value (for $Da_I > 1$).

For the other extreme of small Da_I, the reactive nonlinear interaction becomes negligible, but the exponential decay still makes a sizable contribution. Therefore, the fluctuation decay is expected to depend on both the decay rate of turbulent mixing, $\overline{c_m^2}(t)/\overline{c_m^2}(0)$, and the exponential decay, so that

$$\overline{c^2}(t)/\overline{c^2}(0) = (1 + Da_{II}t)^{-4}\ \overline{c_m^2}(t)/\overline{c_m^2}(0) \qquad (245)$$

With values of the mixing decay previously reported, this provided a simple decay prediction for the calculated results with $Da_I \leq 0.1$.

Calculations using $\alpha < 2$ were not done because of realizability difficulties.

Spectral results

In addition to causing a loss in spectral content during spectral cascade through wave number space (as does the first-order reaction), the nonlinearity of the second-order reaction term causes additional spectral transfer. Corrsin (16) accounted for this by combining the spectral flux due to convection (or diffusion) with a spectral flux due to reaction in a dual cascade. For simplicity it was assumed that the two fluxes do not interact, except in that they act on the same spectral content, and thus can be summed linearly. However, analytical solution of the resulting equation for the concentration spectrum was not possible. Numerical integration indicated several qualitative features for the inertial-convective-reactive range: the asymptotic behavior for large k is pure mixing, the asymptotic behavior for small k presumably indicates that in this limit reactive transfer is more influential than reactive loss, and in the middle of the range reactive loss is more important than reactive transfer.

O'Brien (85) has made a high wave number analysis of the equations resulting from application of Kraichnan's direct-interaction hypothesis. The direct-interaction equations give rise to four time scales: viscous decay $(Dk^2)^{-1}$, reactive decay $[2K\bar{C}(0)]^{-1}$, spectral transfer by convection $(k\tilde{v})^{-1}$, spectral transfer by reaction $(2K\tilde{c})^{-1}$. For a

first-order reaction the reactive decay time scale becomes $[2\bar{C}(0)]^{-1}$ and spectral transfer by reaction does not occur. Thus in the wave number range $k >> 2K\tilde{c}/\tilde{v}$, first- and second-order reactions have similar response functions and perhaps similar spectral transfer behaviors. In terms of the direct-interaction hypothesis, second-order reactions produce a positive contribution to the spectral intensity growth at all wave numbers.

Dash (19) has calculated reactant and product spectra for a second-order reaction using a moment-discard closure and the simple continuous spectral cascading process of Pao. The reactant spectra are shown in Table 2. Comparison with first-order spectra in Table 1 shows that the k dependence for all subranges is similar except for the leading terms in the second-order spectra. Therefore the leading terms can be interpreted as arising from spectral transfer by reaction; the other reaction terms are due to reactive decay. The inertial-convective subrange result reduces to pure mixing for k much larger than the characteristic reaction wave number, in keeping with the qualitative results of Corrsin.

Table 2. Single component second-order reaction spectrum functions

---

Inertial-Convective Subrange

$$G(k) \sim \left[N_1 + N_2(k_a/k)^{2/3}\right] k^{-5/3} \exp\left[3(k_a/k)^{2/3}\right]$$

$k_a \equiv \left[8K^3\bar{C}(0)^3/\epsilon\right]^{1/2}$ = characteristic reaction wave number

Viscous Subrange

$$G(k) \sim \left[N_3 - N_4 k_K \ln k\right] k^{-(1+4N_a)} \exp(-2k^2/k_B^2)$$

$N_a \equiv 2K\bar{C}(0)\nu^{1/2}/\epsilon^{1/2}$ = reaction parameter

$\exp(-2k^2/k_B^2) = 1$ in the viscous-diffusive subrange

Inertial-Diffusive Subrange

$$G(k) \sim \left[N_1 + N_2(k_a/k)^{2/3}\right] k^{-5/3} \exp\left[3(k_a/k)^{2/3} - (3/2)(k/k_C)^{4/3}\right]$$

Two-Species Reaction

The case of irreversible reaction between two chemical species A and B, with rate constant K and stoichiometry

$$A + nB \rightarrow \text{products} \tag{246}$$

is inherently more complex than the single-component cases because two mass conservation equations

$$\frac{\partial C_A}{\partial t} + v_i \frac{\partial C_A}{\partial x_i} = D_A \frac{\partial^2 C_A}{\partial x_i^2} - K C_A C_B \tag{247}$$

$$\frac{\partial C_B}{\partial t} + v_i \frac{\partial C_B}{\partial x_i} = D_B \frac{\partial^2 C_B}{\partial x_i^2} - K n C_A C_B \tag{248}$$

must be solved. The influence of concentration fluctuations on conversion can be seen by substituting $C_A = \overline{C}_A + c_A$, $C_B = \overline{C}_B + c_B$ into Equations 247 and 248, averaging, and invoking homogeneity

$$\frac{\partial \overline{C}_A}{\partial t} = -K(\overline{C}_A \overline{C}_B + \overline{c_A c_B}) \tag{249}$$

$$\frac{\partial \overline{C}_B}{\partial t} = -Kn(\overline{C}_A \overline{C}_B + \overline{c_A c_B}) \tag{250}$$

The joint correlation in the fluctuations of C_A and C_B either enhances or suppresses the rate of conversion. Only when these fluctuations either do not exist or are uncorrelated is the mean reaction rate the same as that for a uniform mixture. In general $\overline{c_A c_B}$ is positive for premixed

reactants and negative for separately introduced (nonpremixed) reactants.

Equations for the instantaneous fluctuations are

$$\frac{\partial c_A}{\partial t} + v_i \frac{\partial c_A}{\partial x_i} = D_A \frac{\partial^2 c_A}{\partial x_i^2} - K(\bar{C}_A c_B + \bar{C}_B c_A + c_A c_B - \overline{c_A c_B}) \quad (251)$$

$$\frac{\partial c_B}{\partial t} + v_i \frac{\partial c_B}{\partial x_i} = D_B \frac{\partial^2 c_B}{\partial x_i^2} - Kn(\bar{C}_A c_B + \bar{C}_B c_A + c_A c_B - \overline{c_A c_B}) \quad (252)$$

The corresponding equations for the dissipation of average concentration fluctuations are

$$\frac{d\overline{c_A^2}}{dt} = -2D_A \overline{\left(\frac{\partial c_A}{\partial x_i}\right)\left(\frac{\partial c_A}{\partial x_i}\right)} - 2K(\bar{C}_A \overline{c_A c_B} + \bar{C}_B \overline{c_A^2} + \overline{c_B c_A^2}) \quad (253)$$

$$\frac{d\overline{c_B^2}}{dt} = -2D_B \overline{\left(\frac{\partial c_B}{\partial x_i}\right)\left(\frac{\partial c_B}{\partial x_i}\right)} - 2Kn(\bar{C}_B \overline{c_A c_B} + \bar{C}_A \overline{c_B^2} + \overline{c_A c_B^2}) \quad (254)$$

$$\frac{d\overline{c_A c_B}}{dt} = D_A \overline{c_B \frac{\partial^2 c_A}{\partial x_i^2}} + D_B \overline{c_A \frac{\partial^2 c_B}{\partial x_i^2}} - K(\bar{C}_A \overline{c_B^2} + \bar{C}_B \overline{c_A c_B} + \overline{c_A c_B^2}) \quad (255)$$

$$- Kn(\bar{C}_B \overline{c_A^2} + \bar{C}_A \overline{c_A c_B} + \overline{c_B c_A^2})$$

which reveal the complexity of the interactions between the two species.

Decay rate analyses

In order to investigate the magnitude of concentration fluctuation effects on conversion, Donaldson and Hilst (22) solved Equations 249, 250, and 253-255 simultaneously for

the nondiffusive case ($D_A = D_B = 0$) using a zero-third-moment closure approximation. As expected, the greater the initial fluctuation level and lack of correlation between species, the less the reaction goes to completion. However, the results point toward an important role for fluctuations of concentration in controlling chemical reaction rates. The effect of diffusion and scale was investigated qualitatively (21) by characterizing the diffusion terms in Equation 255 by a characteristic length. It was shown that in many laboratory flows, the dissipative or diffusive scale of turbulence is very small, so that neglect of $\overline{c_A c_B}$ in the kinetic equations is permissible. On the other hand, if the laboratory experiment is just increased in size, holding all other parameters such as velocity, temperature, et cetera, constant, the character of the flow changes and fluctuation effects become important.

O'Brien (92) has considered the problem of very rapid two-species reactions in isothermal homogeneous turbulence where the reactants are hypothetically premixed before reaction is initiated in some manner. The concentration fields were found to decay in two stages. In the hypothetical first stage the reaction rate is kinetically controlled since the reaction time scale $(C_0 K)^{-1}$ is much less than the shortest time scale of turbulent convection and diffusion (τ_T). Exact expressions for the concentration moments can be obtained if the initial concentrations are prescribed

stochastically in terms of a joint probability density. O'Brien obtained asymptotic results approached in a time τ where $(C_0K)^{-1} < \tau < \tau_T$. At the end of this first stage the fluctuations become highly intense compared with the mean and the probability distribution of the concentration field can not be considered to be even approximately normal. This corresponds to a state of spatial segregation of the species. In the limit of an instantaneous reaction (or no molecular diffusion) segregation is the physical situation which arises, unless the two reacting species are perfectly correlated or in concentrations far from the stoichiometric balance assumed here.

In the second stage, interspecies diffusion, enhanced by the line and surface stretching characteristic of turbulent motions, is rate controlling. For this stage O'Brien obtained exact solutions in terms of the turbulent mixing of a nonreacting species when the molecular diffusivities of the species are equal. The asymptotic behavior of the initial stage was used to provide explicit initial stochastic information for the final stage of decay. For final period turbulence an approximate solution for unequal diffusivities predicts that very fast stoichiometric reactions in the diffusion controlled limit will decay at a rate determined by the smaller of two widely different diffusivities.

Dopazo and O'Brien (24) have generalized the above formulation to include the passive effects of an exothermic chemical reaction with an Arrhenius type rate constant. Both the temperature and concentration fields were found to decay in two stages: kinetically driven and diffusion controlled. Stochastic solutions show that only a weak concentration-temperature correlation is generated in the first stage. For the special case of equal mass diffusivities and a Lewis number of one the solution to the second stage was obtained in terms of a nonreacting binary mixing problem. An approximate solution for Lewis numbers other than one indicated that the temperature field seems to decay with an effective thermal diffusivity determined by the smaller of the mass and thermal diffusivities. In general, it was shown that starting from a uniform temperature field significant temperature fluctuations can be generated due solely to the random nature of the initial concentration fields. The concentration and temperature fluctuations decay at a rate dictated entirely by the time scale of the turbulent binary mixing problem.

Lin and O'Brien (65) have proposed an approximation technique for solving for the evolution of the first moments, co-spectra, and cross-spectra of the concentration fields for a two-species second-order isothermal reaction in a turbulent fluid. An inequality preserving closure approx-

imation was devised which accurately predicts the exact behavior of stochastically distributed (nondiffusing) reactants, which preserves all established statistical inequalities and invariances, and which adequately predicts the diffusion controlled behavior of very rapid reactions.

Decay rates in final period turbulence

O'Brien (93) derived asymptotic decay rates for an isothermal, very rapid, two-species reaction in final period turbulence. Reactant diffusivities were assumed equal. The approach used (described in detail later) is similar to that of Toor (121). Central to the method is the assumption that the random variable

$$C_t(\underset{\sim}{x},t) \equiv nC_A(\underset{\sim}{x},t) - C_B(\underset{\sim}{x},t) \tag{256}$$

is normally distributed, and hence the probability density of $C_t = \bar{C}_t + c_t$ is

$$P(C_t,t) = [2\pi\overline{c_t^2}(t)]^{-\frac{1}{2}} \exp[-c_t^2(t)/2\overline{c_t^2}(t)] \tag{257}$$

where, from the theory of pure mixing in final period turbulence,

$$\overline{c_t^2}(t) \sim t^{-3/2} \tag{258}$$

as $t \to \infty$. For stoichiometric reactants, $\bar{C}_t = 0$, and the asymptotic limits are (63,93,97)

$$n\bar{C}_A = \bar{C}_B = [\overline{c_t^2}(t)/2\pi]^{\frac{1}{2}} \sim t^{-3/4} \tag{259}$$

$$n^2\overline{c_A^2} = \overline{c_B^2} = \overline{c_t^2}(t)/2\pi \sim t^{-3/2} \tag{260}$$

$$\overline{c_A^2}/\bar{C}_A^2 = \overline{c_B^2}/\bar{C}_B^2 = \pi - 1 \tag{261}$$

$$n\overline{c_A c_B} = -n\bar{C}_A\bar{C}_B = -\overline{c_t^2}(t)/2\pi \sim -t^{-3/2} \tag{262}$$

For nonstoichiometric reactants, $\bar{C}_t \neq 0$, and with B as the underrepresented species

$$n\bar{C}_A - \bar{C}_t \sim [t^{-9/4}\exp(-Kt^{3/2})], \quad \bar{C}_B \sim t^{-9/4}\exp(-Kt^{3/2}) \tag{263,264}$$

$$n^2\overline{c_A^2} - \bar{C}_t^2 - \overline{c_t^2} \sim t^{-15/4}\exp(-Kt^{3/2}) \tag{265}$$

$$\overline{c_B^2} \sim t^{-15/4}\exp(-Kt^{3/2}) \tag{266}$$

$$\overline{c_A^2}/\bar{C}_A^2 \sim t^{-3/2}, \quad \overline{c_B^2}/\bar{C}_B^2 \to \infty \tag{267,268}$$

$$n\overline{c_A c_B} = -n\bar{C}_A\bar{C}_B \sim -t^{-9/4}\exp(-Kt^{3/2}) \tag{269}$$

The above results indicate that one consequence of very rapid, diffusion-controlled reactions is to deplete the mean concentration field of each species as rapidly as the fluctuation field, with the result that relative intensities of order unity and higher will be common. Another consequence is that even stoichiometric turbulent reaction fields of this kind can be expected to exhibit pronounced spottiness or intermittency where local nonstoichiometry produces marked depletion of one species and excess of the other.

Toor's theory for turbulent flow tubular reactors, part I

Toor (121) has presented a very useful analysis of the turbulent mixing of two very rapidly reacting chemical species in a turbulent flow tubular reactor. Assuming equal reactant diffusivities, the statistics of the reacting system are determined from those of an identical but non-reacting system. Apparently Beek and Miller (7) were the first to make the very important point that the yield of a chemical reaction in a flow reactor is related to the decay of concentration fluctuations of a tracer introduced under identical flow conditions. They suggested that concentration data can be used to scale turbulent flow reactors but offered no details as to how this could be done quantitatively.

For a reaction with the stoichiometry of Equation 246, the rates at which A and B react are related by $nr_A - r_B = 0$. Therefore, subtracting Equation 248 from n times Equation 247 gives

$$\frac{\partial(nC_A - C_B)}{\partial t} + v_i \frac{\partial(nC_A - C_B)}{\partial x_i} = D_A \frac{\partial^2(nC_A)}{\partial x_i^2} - D_B \frac{\partial^2 C_B}{\partial x_i^2} \quad (270)$$

For the case of equal diffusivities, $D_A = D_B = D$, this reduces to

$$\frac{\partial C_t}{\partial t} + v_i \frac{\partial C_t}{\partial x_i} = D \frac{\partial^2 C_t}{\partial x_i^2} \quad (271)$$

where $C_t \equiv nC_A - C_B$. This equation for C_t is the same as

that for the pure mixing of a nonreacting component C_m; the quantity C_t is conserved by the reaction, and solution for C_t can be obtained from the equivalent pure mixing problem. The equivalent pure mixing problem is one in which mass transfer takes place in the absence of reaction with the velocity field, geometry, diffusivity, and form of the boundary conditions the same as in the reaction problem.

The above results are valid for fast or slow reactions in both laminar and turbulent flow. In order to obtain useful information about the progress of the reaction, however, it is necessary to relate C_t to either C_A or C_B. This is only possible in the case of irreversible reactions that proceed so fast as compared to diffusion processes that the reactants can not coexist at the same spot (that is, $\overline{C_A C_B} = 0$, which corresponds to an infinitely fast reaction). In this case the reactants remain separated from each other by a reaction surface (or surfaces). The conversion is completely controlled by the mixing. At points where A is present $C_t = nC_A$, $C_B = 0$; where B is present $C_t = -C_B$, $C_A = 0$.

For turbulent flow systems the instantaneous concentrations can be divided into time averaged and fluctuating quantities: $C_A = \overline{C}_A + c_A$, $C_B = \overline{C}_B + c_B$, $C_t = \overline{C}_t + c_t$, $C_m = \overline{C}_m + c_m$. The instantaneous reaction surface is defined by $C_t = 0$ and fluctuates due to the turbulence. Thus on an average basis there is no continuous reaction surface but

rather a reactive volume, and the surface $\overline{C}_t$ must lie inside this volume. It follows that the time average behavior of a nonreacting system does not allow a complete determination of the time average behavior of a reacting system, even for rapid reactions.

If the solution of a pure mixing problem is given by

$$(C_m - C_{m1})/(C_{m2} - C_{m1}) = f(x) \tag{272}$$

where C_{m1} and C_{m2} are concentrations at suitable boundaries, then when a reaction takes place in the same reactor under the same conditions with analogous boundary conditions,

$$(C_t - C_{t1})/(C_{t2} - C_{t1}) = f(x) \tag{273}$$

since the solution to both problems must be the same. Averaging the pure mixing solution and subtracting the averaged equation from the unaveraged gives

$$(C_m - \overline{C}_m)/(C_{m2} - C_{m1}) = c_m/(C_{m2} - C_{m1}) = f(x) - \overline{f(x)} \tag{274}$$

where it is assumed that $\overline{C}_{m1} = C_{m1}$ and $\overline{C}_{m2} = C_{m2}$. Squaring and averaging this result gives

$$\overline{c_m^2}/(C_{m2} - C_{m1})^2 = \overline{f^2(x)} + \overline{f(x)}^2 \equiv d^2(x) \tag{275}$$

Similarly,

$$\overline{c_t^2}/(C_{t2} - C_{t1})^2 = d^2(x) \tag{276}$$

Dividing these equations by their respective values at

$x = x_o$ (values at the entrance to the reactor, for instance) gives

$$\overline{c_m^2}/\overline{c_{mo}^2} = \overline{c_t^2}/\overline{c_{to}^2} = d^2(x)/d^2(x_o) \qquad (277)$$

When species A is present $C_t = nC_A$, $C_B = 0$; when species B is present $C_t = -C_B$, $C_A = 0$. Thus when $C_t = \bar{C}_t + c_t > 0$, then $C_A = C_t/n = (\bar{C}_t + c_t)/n$; when C_t is negative $C_A = 0$. When $\bar{C}_t$ is positive then C_A is zero except when $c_t > -\bar{C}_t$. Using this condition we obtain

$$\bar{C}_A = \frac{1}{n}\int_{-\infty}^{\infty} (\bar{C}_A + c_A)\,\phi(c_A)dc_A = \frac{1}{n}\int_{-\bar{C}_t}^{\infty} (\bar{C}_t + c_t)\,\phi(c_t)dc_t \qquad (278)$$

where $\phi(c_A)$ and $\phi(c_t)$ are the distribution functions of the fluctuating quantities. Since the distribution of c_t about $\bar{C}_t$ must be the same as the distribution of c_m about $\bar{C}_m$, $\phi(c_t)$ is of the same form as $\phi(c_m)$. Toor was able to integrate the above expression by assuming that c_m is normally distributed about $\bar{C}_m$, and hence c_t is normally distributed about $\bar{C}_t$. Therefore, the distribution function is assumed to be of the form

$$\phi(c_t) = (2\pi\tilde{c}_t^2)^{-\frac{1}{2}} \exp(-c_t^2/2\tilde{c}_t^2) \qquad (279)$$

where $\tilde{c}_t \equiv (\overline{c_t^2})^{\frac{1}{2}}$ is the root-mean-square fluctuation. Integration gives

$$n\bar{C}_A/\bar{C}_t = 1 + \hat{g}(\tilde{c}_t/\bar{C}_t) \qquad (280)$$

$$\hat{g}(y) = (y/2^{\frac{1}{2}})\ \text{ierfc}(1/2^{\frac{1}{2}}y) \tag{281}$$

where ierfc is the first integral of the complementary error function. For a stoichiometric feed ratio this result reduces to

$$\overline{C}_A = \tilde{c}_t/n(2\pi)^{\frac{1}{2}} \tag{282}$$

For the case of a stoichiometric feed ratio Equations 277 and 282 can be combined to give the result

$$\overline{C}_A/\overline{C}_{Ao} = \tilde{c}_t/\tilde{c}_{to} = \tilde{c}_m/\tilde{c}_{mo} \tag{283}$$

This remarkable result shows that the conversion of an infinitely fast reaction can be predicted from the decay of concentration fluctuations without reaction. That is, the fractional conversion along the reactor (measured from x_o) is equal to the accomplished mixing:

$$\begin{matrix}\text{fractional}\\ \text{conversion}\end{matrix} = 1 - \overline{C}_A/\overline{C}_{Ao} = 1 - \tilde{c}_m/\tilde{c}_{mo} = \begin{matrix}\text{accomplished}\\ \text{mixing}\end{matrix} \tag{284}$$

For a nonstoichiometric feed ratio Equations 277 and 280 can be combined and rearranged to give

$$1 - \overline{C}_A/\overline{C}_{Ao} = 1 + (\beta - 1)\ [1 + \hat{g}(\tilde{c}_{to}\tilde{c}_m/\overline{C}_t\tilde{c}_{mo})] \tag{285}$$

with stoichiometric parameter $\beta \equiv \overline{C}_{Bo}/n\overline{C}_{Ao}$ and

$$\hat{g}(\tilde{c}_{to}/\overline{C}_t) = \beta/(1-\beta) \tag{286}$$

at the reactor entrance ($x = x_o$). Species A is taken as the

limiting reactant. The fractional conversion versus accomplished mixing for different β is shown in Figure 5.

These results relate conversion to accomplished mixing; to obtain conversion as a function of distance the turbulence field must be specified and the mass transfer problem of relating accomplished mixing to distance solved. The Reynolds and Schmidt numbers will appear only in this latter relationship.

Extending Toor's technique, Lin and O'Brien (66) have shown two-species, irreversible, very rapid reactions with mild heat release in a turbulent shear flow to be analogous to the transport of two nonreacting species by the same shear field. Expressions for the probability density functions of the reacting species, the product species, and the reaction-generated thermal field were obtained in terms of the joint probability density functions of the two nonreacting species.

Experimental investigations of Toor's theory

Gibson and Libby (30) have experimentally investigated the structure of the reaction surface between two reactants undergoing a very rapid reaction. Theoretical analysis of a model for the distribution of a weakly diffusive product near the reaction zone (62) led to the conclusion that the reaction zone will be much smaller than the diffusive zone. Corresponding length scales (see Figure 6) are

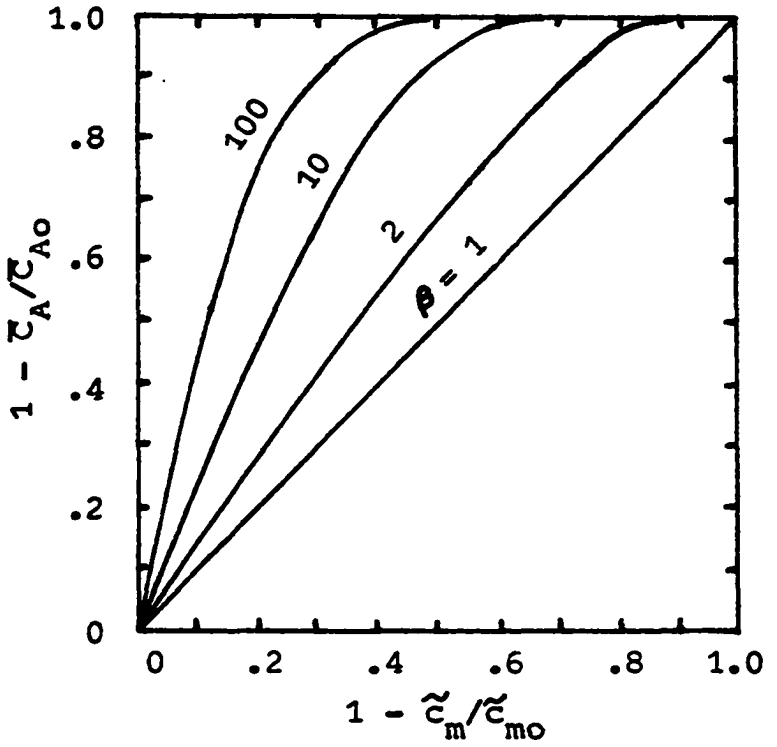

Figure 5. Fractional conversion versus accomplished mixing for different feed ratios

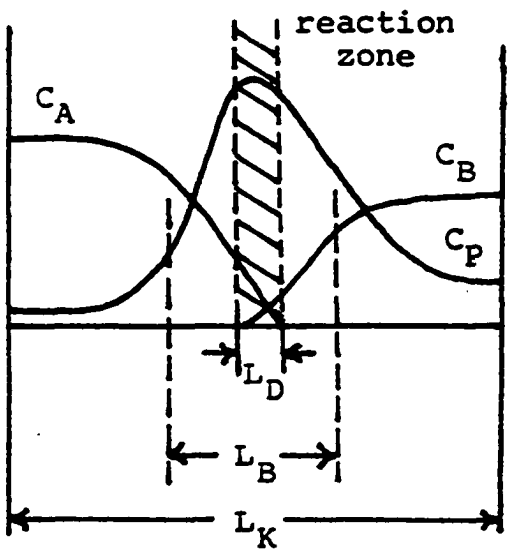

Figure 6. Distribution of reactants and product near a reacting surface for the reaction A + B → P

$L_K \equiv (K/\gamma)^{1/3} L_B$, L_B, and $L_D \equiv (\nu/D)^{1/2} L_B$, respectively, where $L_B = (D/\gamma)^{1/2}$ is the Batchelor length scale, $\gamma = (\epsilon/\nu)^{1/2}$ is the rate of strain, and K is the rate constant. Measurements of the product of the neutralization of a weak-acid, weak-base showed very small scale features which are not inconsistent with the analysis. Sharp spikes in product concentration were observed that correspond to an interface crossing a probe sensitive to product. The spikes became less prominent at later stages in the reaction as the average concentration level of the product increases and it becomes more uniformly distributed by diffusion and straining of previous interfacial surfaces. A particularly small probe showed a number of features which were of a scale small compared to the diffusive scale and are probably related to the presence of reacting surfaces.

Keeler et al.(43) experimentally verified Toor's theory by measuring (using a microconductivity probe) the scalar decay law and fractional conversion for the very rapid reaction of NH_4OH and acetic acid in the turbulent field behind a grid. The fractional conversion was successfully predicted from the accomplished mixing using Toor's relation (Equation 284 or 285) for both stoichiometric and non-stoichiometric feed ratios. Unfortunately data were not obtained for values of the fractional completion of mixing less than 0.5. Torrest and Ranz (126) obtained the same results using a similar system and the same reaction.

Using an experimental procedure and apparatus similar to that of Keeler et al., Miyairi et al. (75) studied the effect of the condition of agitation on the mixing state and extent of reaction between two miscible liquids undergoing a very rapid reaction in a tubular flow reactor. They visualized the process of turbulent mixing as occuring in two steps. In the first step reaction takes place between concentrated masses that are distributed nonuniformly. In the second step reaction takes place in a state in which the distribution of the concentration masses is uniform on a coarse scale. Mixing in the first step was investigated qualitatively using rods or mesh grids of various sizes to alter the flow. It was found that step one plays an important role in determining the overall mixing capacity of the reactor, that the method of turbulence generation strongly influences the point of conversion from step one to step two, and that significant conversion can occur in step one. The experimental results in step two agreed well with Toor's relation between conversion and accomplished mixing.

Vassilatos and Toor (127) experimentally verified Toor's theory using a multiple jet mixing head to produce a turbulent field that was homogeneous on a course scale after about four jet diameters from the inlet. Four different very rapid acid-base reactions were studied. The progress of the reaction was followed by determining the temperature change along the reactor caused by the heat of reaction.

Since the diameter of the thermal couple probe was slightly larger than the diameter of the inlet jets, concentration fluctuations were not measured and the theory could not be checked directly as had been done by Keeler et al. Instead, a further check of the theory was obtained by comparing the conversion obtained with a nonstoichiometric feed ratio ($\beta > 1$) at a given location in the reactor to the conversion measured with a stoichiometric feed ratio ($\beta = 1$) at the same location. This is equivalent to assuming that Toor's theory holds for $\beta = 1$ and using the theory to predict the conversion for $\beta > 1$. Agreement was good, but data were not obtained for values of the fractional completion of mixing less than 0.5. The results were the same for the four different reactions. Data were also obtained for two intermediate rate reactions and one slow reaction. The slow reaction effectively followed a homogeneous rate law, as was expected since the reaction rate was very slow compared to the rate of mixing. Both reaction rate and rate of mixing were found to be important for the intermediate rate reactions.

McKelvey (72) examined the concentration and velocity fields of a reactor identical to the one used by Vassilatos and Toor. The velocity field was found to be highly anisotropic and to be characterized by a strong jetting through the central portion of the reactor. Also, the axial velocity intensity along the centerline of the reactor did not

follow the "-1 power" law which describes the decay of more isotropic flow fields. There were also indications of a preferential eddy size which is probably associated with the break-up of the small jets from the mixing head. The concentration field was found (using a light probe) to obey the "-3/2 power" decay law despite the anisotropic velocity field. The decay of the concentration field was accurately related by Toor's theory to the conversion of the very rapid reactions studied by Vassilatos and Toor. Both the concentration and velocity fluctuations were found to be normally distributed.

Miyawaki et al.(76) measured concentration fluctuations in a multinozzle injection tubular mixer and found the probability density distribution function of the fluctuations to be normally distributed. This result affirms the basis of Toor's theory. Validity of Equation 284 was also demonstrated.

Mixing model simulation of Vassilatos and Toor's data

Kattan and Adler (42) developed a stochastic mixing model for homogeneous, turbulent, tubular reactors that is based on random coalescence and redispersion of fluid elements. The model's parameters, which reflect the mixing characteristics of the reactor, are determined from instantaneous reaction data. The model successfully simulates the conversion data obtained by Vassilatos and Toor over the

complete range of very fast, intermediate, and slow reactions. Of special significance is the ability of the model to predict results of intermediate rates where both mixing and reaction rates are comparable. Harris and Shrivastava (32) presented a similar model.

The success of the simple mixing model of Kattan and Adler, which avoided molecular diffusion as an explicit step, led to speculation that perhaps conversion is not a sensitive function of the details of the mixing, at least for the system of Vassilatos and Toor. To test this idea Mao and Toor (70) developed a simple pure molecular diffusion model which represents almost the opposite extreme of the Kattan and Adler model. The model is based on simultaneous interdiffusion and reaction between alternate slabs of reactants, with slab sizes chosen to fit the conversion data for very rapid reactions in a stoichiometric mixture. The diffusion model was in close agreement to both the data of Vassilatos and Toor and the stochastic mixing model for all reaction rates; it was therefore concluded that the conversion in a mixing process is not very sensitive to the details of the mixing. However, although the two types of models are very different in concept, Rao and Edwards (113) have presented arguments that the diffusion model and the coalescence-dispersion models are equivalent, and hence would be expected to lead to the same results.

Yet another model which represents the data of

Vassilatos and Toor was developed by Rao and Dunn (111). It uses a Monte Carlo coalescence model to simulate both axial and radial dispersion in a tubular reactor.

Toor's theory, part II - Independence hypothesis

Toor (123) has shown that the decay of $\overline{c_A c_B}$ along a turbulent, tubular reactor is the same for very slow and very rapid stoichiometric second-order reactions provided that the diffusivities of A and B are the same. A slow reaction can be defined as one in which $-\overline{c_A c_B} \ll \overline{c}_A \overline{c}_B$. In the limit $K \to 0$, a very slow reaction can be defined as one in which $\overline{c_A c_B}$ does not depend upon the chemical reaction.

Very slow reactions This limit is treated by considering the mixing of two species which do not react at all. This includes all cases between completely premixed and completely nonpremixed.

Consider a mixing device that is divided into two types of inlets: inlets 1 contain species A and B at concentrations C_{A1} and C_{B1}, inlets 2 contain A and B at C_{A2} and C_{B2}. Since the diffusivities of A and B are assumed equal, the mass conservation equations are also identical

$$L(C_A) = L(C_B) = 0 \tag{287}$$

$$L \equiv \frac{\partial}{\partial t} + v_i \frac{\partial}{\partial x_i} - D \frac{\partial^2}{\partial x_i^2} \tag{288}$$

The boundary conditions are

$$C_A = C_{A1},\ C_B = C_{B1} \text{ at the "1" inlets} \tag{289}$$

$$C_A = C_{A2},\ C_B = C_{B2} \text{ at the "2" inlets} \tag{290}$$

with no mass transfer occurring at other boundaries. Let

$$f_A \equiv (C_A - C_{A1})/(C_{A2} - C_{A1}) \tag{291}$$

$$f_B \equiv (C_B - C_{B1})/(C_{B2} - C_{B1}) \tag{292}$$

then

$$L(f_A) = L(f_B) = 0 \tag{293}$$

$$f_A = f_B = 0 \text{ at the "1" inlets} \tag{294}$$

$$f_A = f_B = 1 \text{ at the "2" inlets} \tag{295}$$

Therefore, everywhere in the reactor at every instant of time $f_A = f_B$ and

$$C_A - C_{A1} = (\Delta C_A/\Delta C_B)(C_B - C_{B1}) \tag{296}$$

$$\Delta C_A \equiv C_{A2} - C_{A1};\ \Delta C_B \equiv C_{B2} - C_{B1}$$

Subtracting out the average of Equation 296 from Equation 296 gives

$$c_A = (\Delta C_A/\Delta C_B)c_B \tag{297}$$

From this we get

$$\overline{c_A^2} = (\Delta C_A/\Delta C_B)^2\ \overline{c_B^2} \tag{298}$$

$$\overline{c_A c_B} = (\Delta C_A/\Delta C_B)\overline{c_B^2} = (\Delta C_B/\Delta C_A)\overline{c_A^2} = \pm \tilde{c}_A \tilde{c}_B \qquad (299)$$

where the sign is the same as the sign of $(\Delta C_A/\Delta C_B)/|\Delta C_A/\Delta C_B|$; the correlation coefficient $R_{AB} = \pm 1$.

When the feed is not premixed, $C_{A2} = C_{B1} = 0$, so that

$$\overline{c_A c_B} = -(C_{A1}/C_{B2})\overline{c_B^2} = -(C_{B2}/C_{A1})\overline{c_A^2} = -\tilde{c}_A \tilde{c}_B \qquad (300)$$

Since there is no chemical reaction, the decay of $\overline{c_A^2}$ or $\overline{c_B^2}$ with time or distance describes the mixing in the reactor. For a flow reactor in which all averaged quantities depend only upon the axial distance, Z, then

$$\overline{c_A c_B}/(\overline{c_A c_B})_0 = \overline{c_A^2}/\overline{c_{A0}^2} = \overline{c_B^2}/\overline{c_{B0}^2} = d^2(Z),\ d(0) = 1 \qquad (301)$$

where the subscript zero refers to the inlet of the reactor. d(Z) defines the decay law of the reactor and is measured by using A or B as a tracer in either set of jets, or by measuring the conversion with a very rapid reaction between A and B, with A and B fed separately. Toor (122) proved that the scalar decay law is the same whether the tracer is added to the "1" inlets or to the "2" inlets of the mixer.

Very rapid reactions For very fast reactions in which the reactants are fed in stoichiometric ratio

$$\overline{C}_A/\overline{C}_{A0} = \tilde{c}_t/\tilde{c}_{t0} = \tilde{c}_m/\tilde{c}_{m0} = d(Z),\ d(0) = 1 \qquad (302)$$

Since the reactants are fed in stoichiometric ratio, $\overline{C}_{B0} = n\overline{C}_{A0}$, and by stoichiometry, everywhere along the reactor

$$\bar{C}_B = n\bar{C}_A \text{ or } n\bar{C}_A^2 = \bar{C}_A\bar{C}_B \tag{303}$$

Since the reaction rate remains finite as the rate constant approaches infinity, for nonpremixed very rapid reactions

$$\overline{c_A c_B} = -\bar{C}_A\bar{C}_B \tag{304}$$

This result can also be obtained from the observation that for very rapid reactions the reactants A and B will not coexist at one point, thus $\overline{c_A c_B} = 0$. Combining Equations 302-304 leads to

$$\overline{c_A c_B}/(\overline{c_A c_B})_0 = \bar{C}_A\bar{C}_B/\bar{C}_{A0}\bar{C}_{B0} = \bar{C}_A^2/\bar{C}_{A0}^2 = d^2(Z) \tag{305}$$

for a very rapid reaction. Comparison with Equation 301 leads to the surprising result that $\overline{c_A c_B}$ at any position Z is the same for a very slow reaction as for a very rapid stoichiometric second-order reaction with equal diffusivities. This suggests that $\overline{c_A c_B}$ is independent of the rate of the reaction when the reactants are fed in stoichiometric proportion. If this is the case, the problem of predicting reactions with intermediate rates would be solved for stoichiometric mixtures. Substituting Equation 305 into the expression for the averaged rate of reaction and making use of the relation $(\overline{c_A c_B})_0 = -\bar{C}_{A0}\bar{C}_{B0}$ gives

$$\bar{r}_A = -K(\bar{C}_A\bar{C}_B + \overline{c_A c_B}) = -K\bar{C}_{A0}\bar{C}_{B0}[\bar{C}_A\bar{C}_B/\bar{C}_{A0}\bar{C}_{B0} - d^2(Z)] \tag{306}$$

where $d^2(Z) = \overline{c_m^2}/c_{m0}^2$ describes the mixing characteristics

of the reactor. Assuming plug flow and no axial dispersion in the tubular reactor gives

$$d\bar{C}_A/dZ = -(Kn\bar{C}_{A0}{}^2/v)\left[\bar{C}_A{}^2/\bar{C}_{A0}{}^2 - d^2(Z)\right] \qquad (307)$$

With the decay law known, the conversion-distance curve is completely specified. This equation can be written in dimensionless terms as

$$d\bar{C}_A{}^*/dZ^* = -Da_I\left[\bar{C}_A{}^{*2} - d^2(Z^*)\right],\ d(0) = 1 \qquad (308)$$

$C_A{}^* = C_A/C_{A0}$, $Z^* = Z/Z_m$

$Da_I = Kn\bar{C}_{A0}Z_m/v$ = first Damköhler number

Z_m = mixing distance for the reactor, the distance required for d(Z) to fall to some specified value (0.02 for Vassilatos and Toor)

The form of the decay law can also be expressed as $d^2(Z^*) = \bar{C}_A^{*\infty}(Z^*)$, where $\bar{C}_A^{*\infty} = \bar{C}_A^{\infty}/\bar{C}_{A0}^{\infty}$ is the dimensionless conversion of a stoichiometric very fast reaction as obtained by experiment, for example. Toor integrated Equation 308 for different values of the Damköhler number using the very rapid stoichiometric data of Vassilatos and Toor to give $d(Z^*)$. For Da_I less than about one, the conversion is not appreciably different from the homogeneous conversion, and for Da_I greater than 100, it is not appreciably different from the conversion for very rapid reactions. Unfortunately stoichiometric conditions were not used in Vassilatos and

Toor's measurements for the intermediate reaction rates, so that a valid comparison with the integrated equation could not be made. However, an approximate analysis indicated that $-\overline{c_A c_B}$ apparently goes through a maximum as Da_I varies from very small to very large values, but further data with stoichiometric mixtures were needed to settle this point.

Investigations of Toor's hypothesis

Mao and Toor (71) carried out experiments designed to test Toor's hypothesis. The mixing device used was quite similar to that used by Vassilatos and Toor except more tubes were packed into the same area. The purpose of this modification was to reduce back flow in the regions between the jets as well as to improve the gross flow in the reactor. The reactions were followed by measuring the small temperature rise along the axis of the tube. Mixing characteristics of the reactor, $d^2(Z^*,Re) = \tilde{c}_m^2/\tilde{c}_{m0}^2$, were determined from measurements of the conversion of stoichiometric very rapid reactions, $\bar{C}_A^{*\infty}$, using the identity $d(Z^*,Re) = \bar{C}_A^{*\infty}$ derived earlier. The conversions of stoichiometric intermediate rate reactions were then measured and $\overline{c_A c_B}$ determined from the relation

$$d\bar{C}_A^*/dZ^* = -Da_I\,[\bar{C}_A^{*2} - \Psi^2(Z^*,Da_I,\beta=1,Re)] \qquad (309)$$

$$\Psi^2 \equiv \overline{c_A c_B}/(\overline{c_A c_B})_0,\quad Da_I = K\bar{C}_{B0}Z_m/v \qquad (310,311)$$

for a plug flow tubular reactor with no axial dispersion. The mixing length Z_m is the distance required for the fraction unmixed for no reaction or the fraction unreacted for a very rapid reaction to fall to ½. Since $K\bar{C}_{B0}/v$ is the reciprocal distance required for the fraction unreacted to fall to ½ when the reaction is homogeneous, Da_I is then the ratio of a mixing distance (time) to a reaction distance (time). The velocity v was taken as constant at the bulk average value. The values of ψ^2 for the intermediate rate reactions were consistently somewhat above the very rapid reaction values at the same flow rate. The differences were small enough, however, that at worst Toor's hypothesis is a useful approximation and at best an invariance result. As an alternate test the relation

$$d\bar{C}_A^*/dZ^* = -Da_I\left[\bar{C}_A^{*2} - d^2(Z^*,Re)\right] \qquad (312)$$

was integrated along the reactor and the results compared with the conversion profiles of the stoichiometric intermediate rate reactions. The conversion predicted by the above model was slightly higher along the reactor than the measured conversion, but the correspondence was considered good enough to support the view that Toor's hypothesis is sufficiently accurate to allow reliable predictions of conversion for stoichiometric reactions.

Data were also obtained for nonstoichiometric reactions

to see to what extent Toor's hypothesis applies for non-stoichiometric conditions. The statistical model for very rapid reactions shows that $\overline{c_A c_B}$ depends on the stoichiometric parameter $\beta = \bar{C}_{B0}/n\bar{C}_{A0}$, while it is independent of β for very slow reactions. The reactor model is

$$d\bar{C}_A^*/dZ^* = -Da_I \left[\bar{C}_A^*(\bar{C}_A^* + \beta - 1)/\beta - d^2(Z^*,Re) \right] \qquad (313)$$

For very rapid reactions this reduces to

$$\bar{C}_A^*(\bar{C}_A^* + \beta - 1)/\beta = d^2(Z^*,Re) \qquad (314)$$

which is quadratic in $\bar{C}_A^*$. From a comparison of predicted and experimental conversions for reactions with β = 1.5 and 3.0, it was concluded that Toor's hypothesis is reasonably valid for $1 \leq \beta \leq 3$ and that the reactor model leads to reliable predictions of the conversion. The model would be expected to be less accurate at higher values of β, particularly for large values of Da_I.

Yieh (131) offers support for Toor's hypothesis by showing that for a steady state plug flow tubular reactor the decay of $\overline{c_A c_B}$ is independent of reaction under the assumptions of equal diffusivities, uncorrelated velocity and concentration fluctuations, and evenly distributed products of reaction (zero product concentration fluctuations); however, the last two assumptions are of doubtful validity. By incorporating a variable mean axial velocity into the reactor model of Mao and Toor instead of using the

constant bulk average velocity, Yieh obtained better agreement between predicted and measured conversion for $1 \leq \beta \leq 3$ than obtained by Mao and Toor's analysis. This refinement improves their confirmation of Toor's hypothesis.

For reactions between gases Ajmera's (1) conclusions concerning Toor's hypothesis were similar to those of Mao and Toor for liquid reactions. The intermediate rate second-order reaction between nitric oxide and ozone was studied in a turbulent gas flow reactor with the reactants fed separately. In order to measure the rate of reaction along the reactor, the time-averaged temperature rise due to the highly exothermic reaction was measured instead of concentration. A study of $\overline{c_A c_B}$ decay under different conditions indicated this process to be relatively invariant to the Damköhler number, stoichiometric ratio ($1 \leq \beta \leq 3$), and Reynolds number within the ranges of these variables considered.

Rao and Edwards (112) compared stoichiometric concentration profiles in a tubular reactor calculated from the Monte Carlo coalescence model of Rao and Dunn (111) with those calculated using Toor's hypothesis with the very rapid reaction data of Vassilatos and Toor for various Damköhler numbers. The Monte Carlo model was also used to obtain root-mean-square concentration fluctuations as a function of distance for a tracer input. These results were then used to calculate conversions for a very rapid reaction for β =

1.0, 1.5, and 3.0. Because the results agree well with Vassilatos and Toor's data, the use of the Monte Carlo model for obtaining $\overline{c_A c_B}$ for different conditions is suggested.

In order to determine the effect of reactor scale on conversion at constant Reynolds numbers, Toor and Singh (125) measured conversion in two geometrically similar tubular reactors whose scales differed by a factor of 2.13. A unique curve resulted for conversion versus distance made dimensionless by the half-mixing distance, which scales linearly with the diameter of the reactor. Conversion over a range of Reynolds numbers was measured and a small Reynolds number effect was found; however, the range was too narrow to determine the dependence. Scaling of reactors at constant Reynolds number was also discussed. The design equation for a one-dimensional turbulent flow reactor has been given as Equation 313. In the dimensionless Z^* coordinate system the effect of scale appears only in the Damköhler number, which can be shown to increase as the square of the reactor size

$$(Da_I)_2 = (Da_I)_1 \, (Z_{m2}/Z_{m1})^2 \qquad (315)$$

At low values of Da_I (<0.02 for Toor and Singh's reactor) the chemical reaction is slow compared to the mixing, so that the system is reaction controlled; the second term in the square brackets is much less than the first. The design equation then reduces to the normal design equation for a

homogeneous plug flow reactor. Since this is expressible in dimensionless time coordinates, there is no effect of reactor size. At high values of Da_I (>50) the reaction is mixing controlled and Equation 314 applies. The conversion then depends upon reactor size in a simple manner: in dimensionless length coordinates the conversion-distance curve is invariant to scale. An interesting result of this analysis is that a small reactor which shows no mixing effects may, upon scaling up, become strongly influenced by mixing effects. In scaling up reactors with a variable Reynolds number it was suggested that one could guarantee that a reaction-controlled system would remain such by holding Da_I constant during scaling by increasing the Reynolds number appropriately.

In order to compare liquid and gaseous mixing, Singh (115) conducted experiments using liquids in the reactor used earlier by Ajmera for gases. Upon comparing the scalar decay law of the liquid system, as obtained from very rapid stoichiometric reaction data, to the gaseous system data of Ajmera, it was concluded that the decay laws of liquids and gases on the length scale are approximately equal for equal Reynolds numbers, that is, $d_l^2(Z^*) \approx d_g^2(Z^*)$. Using the stoichiometric parameter and Damköhler number for the gaseous system but the decay law of the liquid system at the same Reynolds number, the conversion profile obtained by numerical solution of the reactor model was compared with

the experimental conversions of Ajmera and found to be in good agreement. Therefore, in a one-dimensional reactor the conversion in gases as well as liquids can be predicted by using the decay law of the liquid. This is useful since it is easy to obtain the decay law from a very rapid liquid reaction.

Singh has extended the principles developed for one-dimensional plug flow tubular reactors to the two-dimensional case of a coflowing confined jet reactor. In the reactor studied, reactant A is fed through a tube, forms a jet at the plane $Z = 0$, mixes with the external stream of reactant B, and reacts. Singh has developed a model to predict the time-average concentration profiles of the species A and B in the field of interest starting from the initial plane, $Z = 0$. Because of the axisymmetry, the variables depend only on axial and radial coordinates. In developing the model, the eddy diffusivity concept is introduced to relate the velocity-concentration fluctuation correlation of a species to the gradient of the mean average concentration of the species. The eddy diffusivities were assumed to be equal and independent of reaction; and so they could be obtained from the nonreaction case. In practise they were obtained from a measurement of the time-average temperature field for two streams entering the reactor at different temperatures. The eddy distribution used was that which reproduced the temperature profile. The molecular

diffusivity was neglected compared to the eddy diffusivity and the axial dispersion term was neglected compared to the radial dispersion term. In order to handle the mean product of the concentration term, Singh advanced arguments to justify extending Toor's independence hypothesis, developed for one-dimensional systems, to two dimensions. Therefore, the scalar mixing decay in the reactor as determined from two-dimensional stoichiometric very rapid reaction conversion data was used for $\overline{c_A c_B}$ for the intermediate rate reaction investigated. From this the model was used to predict the two-dimensional conversion profiles of reactants A and B, which were then compared to measured conversion profiles. Since the comparison was favorable, it was concluded that the model developed can satisfactorily predict the time-average concentration profiles of reactants undergoing an intermediate rate reaction in a two-dimensional field. The results also added credence to the extension of Toor's independence hypothesis to two dimensions.

Pavlica's (109) experiments, in which the completion of an acid-base reaction versus downstream position was measured photometrically, showed that for very fast reactions in a turbulence downstream from a grid much slower conversion is obtained in a viscoelastic fluid than in water with similar conditions. A simple model was developed in which the eddy stretching process determines the overall rate of

reaction. The model adequately describes both the visco-elastic and Newtonian data in terms of an experimental Kolmogorov cutoff wave number and the fluid deformation rate.

Taking a point of view which translates and rotates with the turbulent liquid, Fisher (26) developed a laminae stretching model to describe very rapid reactions occurring in a tubular flow reactor. The model assumes that reactants contact one another in adjacent sheets of fluid which are subjected to a stretching flow. Measurements of the extent of reaction were made downstream of various multi-jet mixing devices in a tubular reactor. Effects of Reynolds number, mixing head geometry, stoichiometry, reagent diffusivity, and common ion were investigated and the results were shown to be consistent with the model behavior.

STATISTICAL INDEPENDENCE HYPOTHESES

The prediction of the rate of conversion of chemical reactants undergoing a second-order reaction in a turbulent mixing field is an extremely difficult problem that has defied rigorous solution. One approach towards simplifying the solution process has been to attempt to describe the turbulent mixing with reaction problem in terms of its component parts, namely, turbulent mixing without reaction and pure reaction without mixing. Statistical independence of reaction and mixing holds exactly in the case of first-order reactions and is expressed by Equations 152 and 153 in terms of physical-space quantities and Equation 206 in terms of Fourier-space quantities. In the case of second-order reactions two potentially useful statistical independence hypotheses have been proposed: O'Brien's (91) hypothesis for single component reactions and Toor's (123) hypothesis for two species reactions.

O'Brien's Hypothesis

The basic premise of O'Brien's hypothesis is that the concentration fluctuation intensity spectrum is given by the product of relative intensity due to mixing and intensity due to reaction where both act like statistically independent phenomena. This is the same point of view as

in Corrsin's (16) use of a noninteracting dual cascade of spectral flux due to convection (or diffusion) with a spectral flux due to reaction in deducing the inertial-convection-reactive range spectrum.

O'Brien's premise (given by O'Brien without proof) can be expressed in more precise terms by considering the first two moment equations of the reactant mass conservation equation (the second-moment equation is the same as Equation 105 with second-order reaction terms added)

$$\frac{d\overline{C}}{dt} = -K(\overline{C}^2 + \overline{c^2}) \tag{316}$$

$$\left(\frac{\partial}{\partial t} + 4K\overline{C} - 2D\frac{\partial^2}{\partial r_i^2}\right) Q_{ss}(\underset{\sim}{r}) + 2KR_s(\underset{\sim}{r}) = 2\frac{\partial S_i(\underset{\sim}{r})}{\partial r_i} \tag{317}$$

$$Q_{ss}(\underset{\sim}{r}) \equiv \overline{c(\underset{\sim}{x})c(\underset{\sim}{x}+\underset{\sim}{r})}$$

$$R_s(\underset{\sim}{r}) \equiv \overline{c(\underset{\sim}{x})c(\underset{\sim}{x})c(\underset{\sim}{x}+\underset{\sim}{r})}$$

$$S_i(\underset{\sim}{r}) \equiv \overline{c(\underset{\sim}{x})c(\underset{\sim}{x}+\underset{\sim}{r})v_i(\underset{\sim}{x})}$$

Taking the Fourier transform of Equation 317 gives the concentration spectrum equation

$$\left(\frac{\partial}{\partial t} + 4K\overline{C} + 2D\,k^2\right) E_{ss}(\underset{\sim}{k},t) + 2KR_s(\underset{\sim}{k}) = 2T_s(\underset{\sim}{k}) \tag{318}$$

$$E_{ss}(\underset{\sim}{k},t) \equiv F[Q_{ss}(\underset{\sim}{r},t)],\quad R_s(\underset{\sim}{k}) \equiv F[R_s(\underset{\sim}{r})]$$

$$T_s(\underset{\sim}{k}) \equiv F[T_s(\underset{\sim}{r})] = F[\partial S_i(\underset{\sim}{r})/\partial r_i]$$

The independence hypothesis can then be stated as: if $E_{ss}(\underset{\sim}{k},t)_{rxn}$ is the solution of Equations 316 and 318 when $D = 0$, $v_i = 0$ (the so-called stochastically distributed reactant or frozen field problem),

$$d\overline{C}_{rxn}/dt = -K(\overline{C}_{rxn}^2 + \overline{c^2}_{rxn}) \tag{319}$$

$$(\frac{\partial}{\partial t} + 4K\overline{C}_{rxn})\, E_{ss}(\underset{\sim}{k},t)_{rxn} + 2K R_s(\underset{\sim}{k})_{rxn} = 0 \tag{320}$$

and if $E_{ss}(\underset{\sim}{k},0)_{rxn}M(\underset{\sim}{k},t)_{mix}$ is the solution of the same equations when $K = 0$ (no reaction), $M(\underset{\sim}{k},0)_{mix} = 1$,

$$\overline{C}(t)_{mix} = \overline{C}(0)_{mix} \tag{321}$$

$$(\frac{\partial}{\partial t} + 2Dk^2)E_{ss}(\underset{\sim}{k},0)_{rxn}M(\underset{\sim}{k},t)_{mix} = 2T_s(\underset{\sim}{k})_{mix} \tag{322}$$

then an approximation to the actual solution, $E_{ss}(\underset{\sim}{k},t)$, of the equations for reaction with arbitrary D and v_i is given by

$$E_{ss}(\underset{\sim}{k},t)_{ind} = E_{ss}(\underset{\sim}{k},t)_{rxn}M(\underset{\sim}{k},t)_{mix} \tag{323}$$

with

$$d\overline{C}_{ind}/dt = -K(\overline{C}_{ind}^2 + \overline{c^2}_{ind}) \tag{324}$$

$$(\frac{\partial}{\partial t} + 4K\overline{C}_{ind} + 2Dk^2)E_{ss}(\underset{\sim}{k},t)_{rxn}M(\underset{\sim}{k},t)_{mix} + 2K R_s(\underset{\sim}{k})_{ind} \doteq 2T_s(\underset{\sim}{k}) \tag{325}$$

One property of the actual solution, $E_{ss}(\underset{\sim}{k},t)$, is that integration of Equation 318 over all wave numbers gives the result

$$\frac{\partial}{\partial t}\int_{\underset{\sim}{k}} E_{ss}(\underset{\sim}{k},t)d\underset{\sim}{k} + \int_{\underset{\sim}{k}} (4K\bar{C} + 2D\,k^2)E_{ss}(\underset{\sim}{k},t)d\underset{\sim}{k} + 2K\int_{\underset{\sim}{k}} R_s(\underset{\sim}{k})d\underset{\sim}{k} = 0 \tag{326}$$

that is, the integral of the left side of the equation is zero because the actual scalar transfer function $T_s(\underset{\sim}{k})$ is known to integrate to zero.

$$\int_{\underset{\sim}{k}} T_s(\underset{\sim}{k})d\underset{\sim}{k} = 0 \tag{327}$$

This property of the actual solution creates a consistency condition that any acceptable approximation to $E_{ss}(\underset{\sim}{k},t)$ must satisfy. Therefore, in order for the proposed statistical independence solution, Equation 323, to be an acceptable approximation, the left side of Equation 325 should integrate to zero.

$$\frac{\partial}{\partial t}\int_{\underset{\sim}{k}} E_{ss}(\underset{\sim}{k},t)_{rxn}M(\underset{\sim}{k},t)_{mix}d\underset{\sim}{k} + \int_{\underset{\sim}{k}} (4K\bar{C}_{ind} + 2Dk^2)E_{ss}(\underset{\sim}{k},t)_{rxn}M(\underset{\sim}{k},t)_{mix}d\underset{\sim}{k} + 2K\int_{\underset{\sim}{k}} R_s(\underset{\sim}{k})_{ind}d\underset{\sim}{k} = 0 \tag{328}$$

In regards to this, since by definition the mixing solution $E_{ss}(\underset{\sim}{k},0)_{rxn}M(\underset{\sim}{k},t)_{mix}$ is an actual solution of Equation 322, then

$$\frac{\partial}{\partial t}\int_{\underset{\sim}{k}} E_{ss}(\underset{\sim}{k},0)_{rxn}M(\underset{\sim}{k},t)_{mix}d\underset{\sim}{k} + 2D\int_{\underset{\sim}{k}} k^2 E_{ss}(\underset{\sim}{k},0)_{rxn}M(\underset{\sim}{k},t)_{mix}d\underset{\sim}{k} = 0 \tag{329}$$

is an exact result. Similarly, for the reaction solution $E_{ss}(\underset{\sim}{k},t)_{rxn}$, from Equation 320 it follows that

$$\frac{\partial}{\partial t}\int_{\underset{\sim}{k}} E_{ss}(\underset{\sim}{k},t)_{rxn}d\underset{\sim}{k} + 4K\bar{C}_{rxn}\int_{k} E_{ss}(\underset{\sim}{k},t)_{rxn}d\underset{\sim}{k} + 2K\int_{\underset{\sim}{k}} R_s(\underset{\sim}{k})_{rxn}d\underset{\sim}{k} = 0 \tag{330}$$

Through an imprecise analysis of the consistency condition resulting from the property of the scalar transfer function expressed by Equation 327, O'Brien claims that by imposing the restriction that the time and wave number dependence of the reaction solution be separable,

$$E_{ss}(\underset{\sim}{k},t)_{rxn} = F(t)E_{ss}(\underset{\sim}{k},0)_{rxn} \tag{331}$$

$$F(0) = 1$$

the consistency condition is satisfied. If this were true then the independence solution would become

$$E_{ss}(\underset{\sim}{k},t)_{ind} = F(t)E_{ss}(\underset{\sim}{k},0)_{rxn}M(\underset{\sim}{k},t)_{mix} \tag{332}$$

and integration over all wave numbers would give the result

$$\frac{\tilde{c}(t)^2_{ind}}{\tilde{c}(0)^2} = \frac{\tilde{c}(t)^2_{rxn}}{\tilde{c}(0)^2} \cdot \frac{\tilde{c}(t)^2_{mix}}{\tilde{c}(0)^2} \tag{333}$$

But clearly this is not the case; the imposition of separability does not satisfy the consistency condition. Substituting Equation 332 into Equation 328 gives

$$\left[\frac{\partial F(t)}{\partial t} + F(t)\frac{\partial}{\partial t}\right] \int_{\underset{\sim}{k}} E_{ss}(\underset{\sim}{k},0)_{rxn} M(\underset{\sim}{k},t)_{mix} d\underset{\sim}{k}$$

$$+ \int_{\underset{\sim}{k}} (4K\bar{C}_{ind} + 2Dk^2)F(t)E_{ss}(\underset{\sim}{k},0)_{rxn} M(\underset{\sim}{k},t)_{mix} d\underset{\sim}{k} \tag{334}$$

$$+ 2K \int_{\underset{\sim}{k}} R_s(\underset{\sim}{k})_{ind} d\underset{\sim}{k} \stackrel{?}{=} 0$$

This can be simplified by multiplying the mixing relation, Equation 329, by F(t) and subtracting the result from Equation 334, giving

$$\frac{\partial F(t)}{\partial t} \int_{\underset{\sim}{k}} E_{ss}(\underset{\sim}{k},0)_{rxn} M(\underset{\sim}{k},t)_{mix} d\underset{\sim}{k}$$

$$+ 4K\bar{C}_{ind} \int_{\underset{\sim}{k}} F(t)E_{ss}(\underset{\sim}{k},0)_{rxn} M(\underset{\sim}{k},t)_{mix} d\underset{\sim}{k} + 2K \int_{\underset{\sim}{k}} R_s(\underset{\sim}{k})_{ind} d\underset{\sim}{k} \stackrel{?}{=} 0 \tag{335}$$

Substituting Equation 331 into the reaction relation, Equation 330, and subtracting the result from Equation 335 gives

$$\frac{\partial F(t)}{\partial t} \int_{\underset{\sim}{k}} E_{ss}(\underset{\sim}{k},0)_{rxn} [M(\underset{\sim}{k},t)_{mix} - 1] d\underset{\sim}{k}$$

$$+ 4K F(t) \int_{\underset{\sim}{k}} E_{ss}(\underset{\sim}{k},0)[\bar{C}_{ind} M(\underset{\sim}{k},t)_{mix} - \bar{C}_{rxn}] d\underset{\sim}{k}$$

$$+ 2K \int_{\underset{\sim}{k}} [R_s(\underset{\sim}{k})_{ind} - R_s(\underset{\sim}{k})_{rxn}]d\underset{\sim}{k} \stackrel{?}{=} 0 \qquad (336)$$

$\bar{c}_{rxn}$ = mean field decay with just reaction ($D = v_i = 0$)

$\bar{c}_{ind}$ = mean field decay with reaction and mixing

Recognizing that

$$\tilde{c}(0)^2_{rxn} = \int_{\underset{\sim}{k}} E_{ss}(\underset{\sim}{k},0)_{rxn} d\underset{\sim}{k} \qquad (337)$$

$$\tilde{c}(t)^2_{mix} = \int_{\underset{\sim}{k}} E_{ss}(\underset{\sim}{k},0)_{rxn} M(\underset{\sim}{k},t)_{mix} d\underset{\sim}{k} \qquad (338)$$

converts Equation 336 to the form

$$\frac{\partial F(t)}{\partial t}\left[\tilde{c}(t)^2_{mix} - \tilde{c}(0)^2_{rxn}\right] + 4K F(t)\left[\bar{c}_{ind}\tilde{c}(t)^2_{mix} - \bar{c}_{rxn}\tilde{c}(0)^2_{rxn}\right]$$
$$+ 2K \int_k [R_s(\underset{\sim}{k})_{ind} - R_s(\underset{\sim}{k})_{rxn}]dk \stackrel{?}{=} 0 \qquad (339)$$

Clearly Equation 339 (or 336) does not form an identity even under crude assumptions. Only in the limit of zero diffusivity, when Equation 328 and 330 become similar and $\tilde{c}(t)^2_{mix} = \tilde{c}(0)^2_{mix} = \tilde{c}(0)^2_{rxn}$, does Equation 339 become an identity.

O'Brien has compared the initial time behaviors of the actual solution, $E_{ss}(\underset{\sim}{k},t)$, and independence solution $E_{ss}(\underset{\sim}{k},t)_{ind}$, as given by Equation 332, using the difference of the Taylor series expansions of each.

$$E_{ss}(\underset{\sim}{k},t) - E_{ss}(\underset{\sim}{k},t)_{ind} = \frac{\partial}{\partial t}\left[E_{ss}(\underset{\sim}{k},t) - E_{ss}(\underset{\sim}{k},t)_{ind}\right]_{t=0} t + \tfrac{1}{2}\frac{\partial^2}{\partial t^2}\left[E_{ss}(\underset{\sim}{k},t) - E_{ss}(\underset{\sim}{k},t)_{ind}\right]_{t=0} t^2 + \cdots \quad (340)$$

$$E_{ss}(\underset{\sim}{k},0) \equiv E_{ss}(\underset{\sim}{k},0)_{ind}$$

The first time derivative in Equation 340 is zero, but comparison of Equations 318 and 325 at $t = 0$ shows this to be a direct consequence of using identical initial conditions for the two solutions. Integration over all $\underset{\sim}{k}$ converts Equation 340 to the form

$$\overline{c^2}(t) - \overline{c^2}(t)_{ind} = \tfrac{1}{2}\frac{\partial^2}{\partial t^2}\left[\overline{c^2}(t) - \overline{c^2}(t)_{ind}\right]_{t=0} t^2 + \cdots \quad (341)$$

O'Brien concludes that the second- and higher-order terms in the expansion are nonzero and proportional to the diffusivity; hence after the initial period the time behaviors of the actual and independence solutions diverge and only in the limit of no diffusion are they the same.

Some support for the independence hypothesis comes from Lee's (58) direct-interaction calculations. For small values of Da_I, it was found that the results could be expressed by Equation 245, which is of the same form as Equation 333.

Unfortunately no experimental data exists with which the statistical independence hypothesis can be compared so that its validity and usefulness in either the modal decay

or fluctuation intensity decay forms remains a matter for investigation. Evidence would come from an experimental study of simple mixing and reactive mixing under the same turbulent conditions. Although Equation 332 for individual modes had been shown to be of doubtful validity, the behavior of the independence hypothesis in the form of Equation 333 remains of interest. In particular, Equation 333 predicts that the faster of the two phenomena, mixing and reaction, will dominate the decay of fluctuations; hence it holds in the limit of very large and very small Damköhler numbers. One of the purposes of this study is to investigate the behavior of the hypothesis over a range of intermediate Damköhler numbers by conducting computer experiments under carefully controlled reaction and mixing conditions.

Toor's Hypothesis

The development of Toor's statistical independence hypothesis for two species second-order reactions has already been presented in the Literature Review section in terms of decay along a turbulent flow tubular reactor. The analysis can also be developed in terms of a statistically homogeneous system in which the concentrations of reactants decays with time, the case that will be considered in this study. (This follows from considering a frame of reference that translates down the reactor with the flow.)

Toor has shown that the decay of $\overline{c_A c_B}$ over time is the same for very slow and very rapid stoichiometric second-order reactions when the diffusivities of A and B are equal. Furthermore, in these limits the rate of decay of $\overline{c_A c_B}$ is the same as that of $\overline{c_m^2}$ for a nonreacting species in the same mixing field with the same diffusivity. Therefore, Toor hypothesized that the relation

$$\overline{c_A c_B}(t)/\overline{c_A c_B}(0) = \overline{c_m^2}(t)/\overline{c_m^2}(0) \qquad (342)$$

may provide a useful approximation for intermediate rate stoichiometric reactions with equal diffusivities. This approximation would be extremely useful since reaction behavior under turbulent mixing conditions could then be predicted from either tracer studies of a reactor or pure mixing theory. Due to various difficulties experimental testing of this hypothesis has yielded unconclusive results: at best Equation 342 may be a valid independence hypothesis or at worst it may be a useful approximation. Experiments also suggest that the requirement of stoichiometric reactants may be relaxed. A second purpose of this study is to investigate the validity of Toor's hypothesis over a range of intermediate reaction rates and to examine its sensitivity to changes in reactant stoichiometry and diffusivities by means of reaction and mixing computer experiments.

DEVELOPMENT OF TURBULENT VELOCITY FIELD SIMULATION MODELS

In this section two simple models are developed for generating a simulated turbulent velocity field. The first, referred to as the random convection velocity, obeys continuity and has a constant specified energy spectrum (and hence constant time and distance scales) but lacks interaction between Fourier modes. The second model has interaction and satisfies continuity but the transient nature of its energy spectrum is unknown. The model is based on a modified form of the Navier-Stokes equation; notable differences are convection of the flow velocity by the random convection velocity (instead of self-convection) and absence of the viscous-dissipation term.

The numerical calculations are performed in Fourier-transformed space. The Fourier transform has the convenient property of converting spatial gradient terms in the momentum and species mass conservation equations into wave number algebraic quantities, and hence only integration over time is necessary. Before proceeding to the development of the models, the Fourier transform and Fourier-space quantities are defined and relations are derived for calculating physical-space quantities from Fourier-space ones. Both two and three dimensional cases are considered.

Definitions of Quantities

The Fourier transform (and its inverse) used in the Statistical Description of Turbulence, Pure Mixing, and Literature Review sections and defined by Equations 40 and 41 is for an unbounded isotropic turbulence and it is inherently assumed that the integrations in Equations 40 and 41 exist despite this. The wave number in the transform definition is thus a continuous variable. However, in numerical simulations of turbulence this produces great difficulties, which are normally avoided by supposing that the turbulence is confined to the insides of a large box (of side length L) and repeats itself throughout space, obeying cyclic boundary conditions on the sides of the box. In this case the wave number k^* (* denotes a dimensional variable or parameter) is a discrete variable of the form

$$k_i^* \equiv 2\pi n_i/L^*, \; n_i = 0, \pm 1, \pm 2, \ldots \tag{343}$$

where n_i is a vector having integer components.

For numerical computations the discrete form of the Fourier transform of a function is used. It is defined by

$$a^*(k^*) \equiv L^{*-\delta_{nn}} \int_{\underset{\sim}{x}^*} a^*(\underset{\sim}{x}^*) \exp(-i\underset{\sim}{k}^* \cdot \underset{\sim}{x}^*) d\underset{\sim}{x}^* \tag{344}$$

where

$$\underset{\sim}{k}^* = (k_1^*, k_2^*, k_3^*), \; \underset{\sim}{x}^* = (x_1^*, x_2^*, x_3^*), \; \delta_{nn} = 3 \tag{345,3D}$$

$$d\underset{\sim}{x}^* = dx_1^* dx_2^* dx_3^*, \quad \int_{\underset{\sim}{x}^*} = \int_{x_1^*} \int_{x_2^*} \int_{x_3^*}$$

in three dimensions and

$$\underset{\sim}{k}^* = (k_1^*, k_2^*), \quad \underset{\sim}{x}^* = (x_1^*, x_2^*), \quad \delta_{nn} = 2$$
$$d\underset{\sim}{x}^* = dx_1^* dx_2^*, \quad \int_{\underset{\sim}{x}^*} = \int_{x_1^*} \int_{x_2^*} \qquad (346,2D)$$

in two dimensions. Integration over $\underset{\sim}{x}^*$ is confined to the volume of the box. The discrete form of the inverse Fourier transform is

$$a^*(\underset{\sim}{x}^*) = \sum_{k^*} a^*(\underset{\sim}{k}^*) \exp(i\underset{\sim}{k}^* \cdot \underset{\sim}{x}^*) \qquad (347)$$

where

$$\sum_{\underset{\sim}{k}^*} = \sum_{k_1^*} \sum_{k_2^*} \sum_{k_3^*} \qquad (348,3D)$$

in three dimensions and

$$\sum_{\underset{\sim}{k}^*} = \sum_{k_1^*} \sum_{k_2^*} \qquad (349,2D)$$

in two dimensions. Summation is over all wave numbers $\underset{\sim}{k}^*$. In derivations it is sometimes convenient to approximate the summation over $\underset{\sim}{k}^*$ in the inverse transform by an integral, a procedure that becomes more accurate as $\underset{\sim}{L}^*$ becomes large. Equation 347 becomes

$$a^*(\underset{\sim}{x}^*) = (L^*/2\pi)^{\delta_{nn}} \int_{\underset{\sim}{k}^*} a^*(\underset{\sim}{k}^*) \exp(i\underset{\sim}{k}^* \cdot \underset{\sim}{x}^*) d\underset{\sim}{k}^* \qquad (350)$$

where

$$\Delta n_i = 1 = (L^*/2\pi)\Delta k_i^* \rightarrow (L^*/2\pi)dk_i^* \tag{351}$$

as L^* becomes large has been used. Comparison of Equations 344 and 350 with Equations 40 and 41, respectively, reveals the identification of

$$(L^*/2\pi)^{\delta_{nn}}\, a^*(\underset{\sim}{k}^*) \rightarrow f(\underset{\sim}{k}) \tag{352}$$

as L^* approaches infinity.

The Fourier transform will be made dimensionless using the as yet unspecified reference length $L_{f\emptyset}^*$. The dimensionless Fourier transform of a dimensionless quantity is then defined by

$$a(\underset{\sim}{k}) \equiv N^{-\delta_{nn}} \int_{\underset{\sim}{x}} a(\underset{\sim}{x})\, \exp(-i\underset{\sim}{k}\cdot\underset{\sim}{x})d\underset{\sim}{x} = F[a(\underset{\sim}{x})] \tag{353}$$

$$k_i \equiv L_{f\emptyset}^* k_i^* = 2\pi n_i/N,\ n_i = 0, \pm 1, \pm 2, \ldots \tag{354}$$

$$N \equiv L^*/L_{f\emptyset}^*,\ x_i \equiv x_i^*/L_{f\emptyset}^* \tag{355}$$

The discrete and integral approximation forms of the dimensionless inverse Fourier transform are, respectively

$$a(\underset{\sim}{x}) = \sum_{\underset{\sim}{k}} a(\underset{\sim}{k})\, \exp(i\underset{\sim}{k}\cdot\underset{\sim}{x}) = F^{-1}[a(\underset{\sim}{k})] \tag{356}$$

$$a(\underset{\sim}{x}) = (N/2\pi)^{\delta_{nn}} \int_{\underset{\sim}{k}} a(\underset{\sim}{k})\, \exp(i\underset{\sim}{k}\cdot\underset{\sim}{x})d\underset{\sim}{x} \tag{357}$$

A dimensionless longitudinal integral scale and a dimensionless longitudinal microscale can be written using

$L^*_{f\emptyset}$ as

$$L_f(t) \equiv L^*_f(t^*)/L^*_{f\emptyset}, \quad \lambda_f(t) \equiv \lambda^*_f(t^*)/L^*_{f\emptyset}$$

$$L_f(t) = \int_0^\infty f(r,t)dr, \quad r \equiv r^*/L^*_{f\emptyset} \tag{358}$$

$$2/\lambda_f(t)^2 = -\left(\frac{\partial^2 f(r,t)}{\partial r^2}\right)_{r=0} \tag{359}$$

Velocity quantities will be made dimensionless using the as yet unspecified reference velocity $\tilde{v}^*_\emptyset$. The dimensionless fluid velocity is

$$v_i(\underset{\sim}{x}) \equiv v^*_i(\underset{\sim}{x}^*)/\tilde{v}^*_\emptyset \tag{360}$$

with dimensionless root-mean-square velocity $\tilde{v}(t) \equiv \tilde{v}^*(t^*)/\tilde{v}^*_\emptyset$. The longitudinal and lateral correlation functions can then be expressed in terms of dimensionless quantities as

$$f(r,t) = \overline{v_r(x)v_r(x+r)}/\tilde{v}(t)^2 \tag{361}$$

$$g(r,t) = \overline{v_n(x)v_n(x+r)}/\tilde{v}(t)^2 \tag{362}$$

The dimensionless Fourier velocity is

$$u_i(\underset{\sim}{k}) \equiv N^{-\delta_{nn}} \int_{\underset{\sim}{x}} v_i(\underset{\sim}{x}) \exp(-i\underset{\sim}{k}\cdot\underset{\sim}{x})d\underset{\sim}{x} \tag{363}$$

with the corresponding discrete and integral approximation inverse relations

$$v_i(\underset{\sim}{x}) = \sum_{\underset{\sim}{k}} u_i(\underset{\sim}{k}) \exp(i\underset{\sim}{k}\cdot\underset{\sim}{x}) \tag{364}$$

$$v_i(\underset{\sim}{x}) = (N/2\pi)^{\delta_{nn}} \int_{\underset{\sim}{k}} u_i(\underset{\sim}{k}) \exp(i\underset{\sim}{k}\cdot\underset{\sim}{x}) d\underset{\sim}{k} \tag{365}$$

The dimensionless velocity correlation tensor is

$$Q_{ij}(\underset{\sim}{r}) \equiv Q^*_{ij}(\underset{\sim}{r}^*)/\tilde{v}^{*2}_{\emptyset} = \overline{v_i(\underset{\sim}{x}) v_j(\underset{\sim}{x}+\underset{\sim}{r})} \tag{366}$$

The dimensionless energy spectrum tensor is then defined by

$$E_{ij}(\underset{\sim}{k}) = E^*_{ij}(\underset{\sim}{k}^*)/\tilde{v}^{*2}_{\emptyset} = F[Q_{ij}(\underset{\sim}{r})]$$

$$E_{ij}(\underset{\sim}{k}) \equiv N^{-\delta_{nn}} \int_{\underset{\sim}{r}} Q_{ij}(\underset{\sim}{r}) \exp(-i\underset{\sim}{k}\cdot\underset{\sim}{r}) d\underset{\sim}{r} \tag{367}$$

The discrete and integral approximation inverse relations are

$$Q_{ij}(\underset{\sim}{r}) = \sum_{\underset{\sim}{k}} E_{ij}(\underset{\sim}{k})_d \exp(i\underset{\sim}{k}\cdot\underset{\sim}{r}) \tag{368}$$

$$Q_{ij}(\underset{\sim}{r}) = (N/2\pi)^{\delta_{nn}} \int_{\underset{\sim}{k}} E_{ij}(\underset{\sim}{k})_c \exp(i\underset{\sim}{k}\cdot\underset{\sim}{r}) d\underset{\sim}{r} \tag{369}$$

where the subscript d denotes a discrete basis and the subscript c denotes a continuous basis.

The energy spectrum function E(k) is usually defined as a continuous function and normalized by integration as

$$E(k)_c \equiv E(k^*)^*_c / L^*_{f\emptyset} \tilde{v}^{*2}_{\emptyset}$$

$$E_o = \tfrac{1}{2}\delta_{ii}\tilde{v}(t)^2 = \int_0^{\infty} E(k)_c dk \tag{370}$$

where $k^2 = k_i k_i$ and the subscript c denotes normalization on a continuous basis. Although $E(k)_c$ and $E_{ij}(\underset{\sim}{k})_c$ are defined independently, they both describe the distribution of turbulent energy in the velocity field and thus are interrelated. On a continuous basis this interrelation can be established from

$$E_o = \frac{3}{2}\tilde{v}(t)^2 = \tfrac{1}{2}Q_{ii}(\underset{\sim}{0}) = \tfrac{1}{2}(N/2\pi)^3 \int_{\underset{\sim}{k}} E_{ii}(\underset{\sim}{k})_c d\underset{\sim}{k}$$
$$= \tfrac{1}{2}(N/2\pi)^3 \int_0^\infty 4\pi k^2 E_{ii}(\underset{\sim}{k})_c dk = \int_0^\infty E(k)_c dk \qquad (371,3D)$$

in three dimensions and

$$E_o = \tilde{v}(t)^2 = \tfrac{1}{2}Q_{ii}(\underset{\sim}{0}) = \tfrac{1}{2}(N/2\pi)^2 \int_{\underset{\sim}{k}} E_{ii}(\underset{\sim}{k})_c d\underset{\sim}{k}$$
$$= \tfrac{1}{2}(N/2\pi)^2 \int_0^\infty 2\pi k\, E_{ii}(\underset{\sim}{k})_c dk = \int_0^\infty E(k)_c dk \qquad (372,2D)$$

in two dimensions, giving

$$E(k)_c = (N/2\pi)^3 2\pi k^2 E_{ii}(\underset{\sim}{k})_c \qquad (373,3D)$$

$$E(k)_c = (N/2\pi)^2 \pi k\, E_{ii}(\underset{\sim}{k})_c \qquad (374,2D)$$

A discrete energy spectrum function $E(k)_d$ can also be defined that is normalized by summation over the discrete values of k

$$E(k)_d \equiv E(k^*)^*_d / \tilde{v}^{*2}_\emptyset$$

$$E_o = \tfrac{1}{2}\delta_{ii}\tilde{v}(t)^2 = \sum_k E(k)_d \tag{375}$$

The relation between $E(k)_d$ and $E_{ij}(\underset{\sim}{k})_d$ can be established from

$$E_o = \frac{3}{2}\tilde{v}(t)^2 = \tfrac{1}{2}Q_{ii}(\underset{\sim}{0}) = \tfrac{1}{2}\sum_{\underset{\sim}{k}} E_{ii}(\underset{\sim}{k})_d \tag{376,3D}$$

$$= \tfrac{1}{2}\sum_{k_1}\sum_{k_2}\sum_{k_3} E_{ii}(\underset{\sim}{k})_d = \tfrac{1}{2}\sum_k \sum_{\theta_{\underset{\sim}{k}}}\sum_{\phi_{\underset{\sim}{k}}} E_{ii}(\underset{\sim}{k})_d$$

$$= \tfrac{1}{2}\sum_k \eta(k)E_{ii}(\underset{\sim}{k})_d = \sum_k E(k)_d$$

$$\eta(k) \equiv \sum_{\theta_{\underset{\sim}{k}}}\sum_{\phi_{\underset{\sim}{k}}} 1 = \text{number of discrete points on the spherical surface } k = |\underset{\sim}{k}| = \text{constant} \tag{377,3D}$$

in three dimensions and

$$E_o = \tilde{v}(t)^2 = \tfrac{1}{2}Q_{ii}(\underset{\sim}{0}) = \tfrac{1}{2}\sum_{\underset{\sim}{k}} E_{ii}(\underset{\sim}{k})_d$$

$$= \tfrac{1}{2}\sum_{k_1}\sum_{k_2} E_{ii}(\underset{\sim}{k})_d = \tfrac{1}{2}\sum_k\sum_{\theta_{\underset{\sim}{k}}} E_{ii}(\underset{\sim}{k})_d \tag{378,2D}$$

$$= \tfrac{1}{2}\sum_k \eta(k)E_{ii}(\underset{\sim}{k})_d = \sum_k E(k)_d$$

$$\eta(k) \equiv \sum_{\theta_{\underset{\sim}{k}}} 1 = \text{number of discrete points on the curve } k = |\underset{\sim}{k}| = \text{constant} \tag{379,2D}$$

in two dimensions, giving

$$E(k)_d = \tfrac{1}{2}\eta(k)E_{ii}(\underset{\sim}{k})_d \tag{380}$$

This discrete form of the energy spectrum is useful

because it can be calculated exactly from the discrete Fourier velocity components; integral approximation with averaging over volumes in $\underset{\sim}{k}$-space is not used. Tabulated values of $\eta(k)$ are given in Appendix A along with analysis of the interconversion process between the discrete and continuous forms of the energy spectrum. Comparison of the discrete and continuous forms shows the following quantities to be analogous

$$(N/2\pi)^{\delta_{nn}} E_{ii}(\underset{\sim}{k})_c \leftrightarrow E_{ii}(\underset{\sim}{k})_d \tag{381}$$

$$4\pi k^2 \leftrightarrow \eta(k) \tag{382,3D}$$

$$2\pi k \leftrightarrow \eta(k) \tag{383,2D}$$

Calculation of the Energy Spectrum Tensor

In order to be able to assign initial conditions and follow the evolution of the generated velocity field, it is necessary to be able to calculate the energy spectrum and other quantities directly from the Fourier velocity modes. In this section the energy spectrum tensor is found.

From the definition of $u_i(\underset{\sim}{k})$, it follows that

$$u_i(\underset{\sim}{k})u_j(\underset{\sim}{k}') = N^{-2\delta_{nn}} \int_{\underset{\sim}{x}} \int_{\underset{\sim}{x}'} v_i(\underset{\sim}{x})v_j(\underset{\sim}{x}') \exp[-i(\underset{\sim}{k}\cdot\underset{\sim}{x} + \underset{\sim}{k}'\cdot\underset{\sim}{x}')]d\underset{\sim}{x}\, d\underset{\sim}{x}' \tag{384}$$

Letting $\underset{\sim}{r} = \underset{\sim}{x} - \underset{\sim}{x}'$, we get

$$u_i(\underset{\sim}{k})u_j(\underset{\sim}{k}')$$

$$= N^{-2\delta_{nn}} \int_{\underset{\sim}{r}} \int_{\underset{\sim}{x}'} v_i(\underset{\sim}{x}' + \underset{\sim}{r})v_j(\underset{\sim}{x}')\exp[-i(\underset{\sim}{k} + \underset{\sim}{k}')\cdot\underset{\sim}{x}']d\underset{\sim}{x}' \quad (385)$$

$$\cdot \exp(-i\underset{\sim}{k}\cdot\underset{\sim}{r})d\underset{\sim}{r}$$

In order for the integral over $\underset{\sim}{x}'$ to become a volume average, the condition $\underset{\sim}{k} + \underset{\sim}{k}' = \underset{\sim}{0}$ must be imposed, giving

$$u_i(\underset{\sim}{k})u_j(-\underset{\sim}{k})$$

$$= N^{-\delta_{nn}} \int_{\underset{\sim}{r}} N^{-\delta_{nn}} \int_{\underset{\sim}{x}'} v_i(\underset{\sim}{x}' + \underset{\sim}{r})v_j(\underset{\sim}{x}')d\underset{\sim}{x}' \exp(-i\underset{\sim}{k}\cdot\underset{\sim}{r})d\underset{\sim}{r} \quad (386)$$

$$= N^{-\delta_{nn}} \int_{\underset{\sim}{r}} Q_{ij}(\underset{\sim}{r}) \exp(-i\underset{\sim}{k}\cdot\underset{\sim}{r})d\underset{\sim}{r} = E_{ij}(\underset{\sim}{k})$$

Hence

$$E_{ij}(\underset{\sim}{k}) = u_i(\underset{\sim}{k})u_j(-\underset{\sim}{k}) \quad (387)$$

Energy Content of the Turbulence

From the inverse Fourier transform of $u_i(\underset{\sim}{k})$, it follows that

$$v_i(\underset{\sim}{x})v_j(\underset{\sim}{x}) = \sum_{\underset{\sim}{k}} \sum_{\underset{\sim}{k}'} u_i(\underset{\sim}{k})u_j(\underset{\sim}{k}') \exp[i(\underset{\sim}{k} + \underset{\sim}{k}')\cdot\underset{\sim}{x}] \quad (388)$$

Volume averaging both sides gives

$$\overline{v_i(\underset{\sim}{x})v_j(\underset{\sim}{x})} = N^{-\delta_{nn}} \int_{\underset{\sim}{x}} v_i(\underset{\sim}{x})v_j(\underset{\sim}{x})d\underset{\sim}{x}$$

$$= \sum_{\underset{\sim}{k}} \sum_{\underset{\sim}{k}'} u_i(\underset{\sim}{k})u_j(\underset{\sim}{k}')\, N^{-\delta_{nn}} \int_{\underset{\sim}{x}} \exp[i(\underset{\sim}{k}+\underset{\sim}{k}')\cdot\underset{\sim}{x}]d\underset{\sim}{x} \qquad (389)$$

But

$$\delta_{\underset{\sim}{k}+\underset{\sim}{k}',\underset{\sim}{0}} = N^{-\delta_{nn}} \int_{\underset{\sim}{x}} \exp[i(\underset{\sim}{k}+\underset{\sim}{k}')\cdot\underset{\sim}{x}]d\underset{\sim}{x} \qquad (390)$$

Therefore,

$$\overline{v_i(\underset{\sim}{x})v_j(\underset{\sim}{x})} = \sum_{\underset{\sim}{k}} \sum_{\underset{\sim}{k}'} \delta_{\underset{\sim}{k}+\underset{\sim}{k}',\underset{\sim}{0}}\, u_i(\underset{\sim}{k})u_j(\underset{\sim}{k}') \qquad (391)$$

For constant $\underset{\sim}{k}$, in the summation over $\underset{\sim}{k}'$, there is only one value of $\underset{\sim}{k}'$ that has a nonzero result, namely $-\underset{\sim}{k}$, so that the double summation over both $\underset{\sim}{k}$ and $\underset{\sim}{k}'$ reduces to a single summation over $\underset{\sim}{k}$, with the condition $\underset{\sim}{k}' = -\underset{\sim}{k}$, giving

$$\overline{v_i(\underset{\sim}{x})v_j(\underset{\sim}{x})} = \sum_{\underset{\sim}{k}} u_i(\underset{\sim}{k})u_j(-\underset{\sim}{k}) = \sum_{\underset{\sim}{k}} E_{ij}(\underset{\sim}{k}) \qquad (392)$$

and hence

$$E_o = \tfrac{1}{2}\delta_{ii}\tilde{v}(t)^2 = \tfrac{1}{2}\,\overline{v_i(\underset{\sim}{x})v_i(\underset{\sim}{x})} = \tfrac{1}{2}\sum_{\underset{\sim}{k}} u_i(\underset{\sim}{k})u_i(-\underset{\sim}{k}) = \tfrac{1}{2}\sum_{\underset{\sim}{k}} E_{ii}(\underset{\sim}{k}) \qquad (393)$$

Calculation of the Energy Spectrum

The form of $E_{ij}(\underset{\sim}{k})$ is restricted by the requirement of isotropy and the continuity condition expressed by Equation 45. A form of $E_{ij}(\underset{\sim}{k})$ that satisfies these requirements is

$$u_i(\underset{\sim}{k})u_j(-\underset{\sim}{k}) = E_{ij}(\underset{\sim}{k}) = P_{ij}(\underset{\sim}{k})\hat{E}(k) \qquad (394)$$

where

$$P_{ij}(\underset{\sim}{k}) \equiv \delta_{ij} - k_i k_j/k^2 \tag{395}$$

is the standard projection operator. $\hat{E}(k)$ is a scalar function of a scalar variable, but it must be identified with some meaningful quantity to be useful.

Continuous energy spectrum in three dimensions

From Equations 392 and 394 we have

$$\overline{v_i(\underset{\sim}{x})v_j(\underset{\sim}{x})} = \sum_{\underset{\sim}{k}} P_{ij}(\underset{\sim}{k})\, \hat{E}(k) \tag{396}$$

In order to relate $\hat{E}(k)$ to the continuously defined energy spectrum function $E(k)_c$, it is first necessary to convert the summation into the continuous integral approximation. Using

$$1 = (N/2\pi)\,\Delta k_i \rightarrow (N/2\pi)\,dk_i \tag{397}$$

as N gets large we get

$$\overline{v_i(\underset{\sim}{x})v_j(\underset{\sim}{x})} = (N/2\pi)^3 \int_{\underset{\sim}{k}} P_{ij}(\underset{\sim}{k})\hat{E}(k)d\underset{\sim}{k} \tag{398,3D}$$

Equation 398 can be converted into a form dependent only on scalar k (instead of $\underset{\sim}{k}$) by integrating over a spherical surface of radius k in $\underset{\sim}{k}$-space. (Polar coordinates have x_1 direction as axis.)

$$\overline{v_i(\underset{\sim}{x})v_j(\underset{\sim}{x})} = (N/2\pi)^3 \int_k k^2\hat{E}(k)dk \int_0^{\pi}\int_0^{2\pi} (\delta_{ij} - k_i k_j/k^2)\sin\theta \; d\phi\, d\theta \tag{399,3D}$$

The components of $\underset{\sim}{k}$ can be written as

$$k_1 = k\cos\theta,\ k_2 = k\sin\theta\cos\phi,\ k_3 = k\sin\theta\sin\phi \qquad (400,3D)$$

Consider the 1,1-component of the tensor

$$\overline{v_1(\underset{\sim}{x})v_1(\underset{\sim}{x})}$$

$$= (N/2\pi)^3 \int_k k^2\hat{E}(k)dk \int_0^{\pi}\int_0^{2\pi} (1 - \cos^2\theta)\sin\theta\, d\phi\, d\theta \qquad (401,3D)$$

$$= (N/2\pi)^3\ (8\pi/3) \int_k k^2\hat{E}(k)dk$$

Values of $\overline{v_2(\underset{\sim}{x})v_2(\underset{\sim}{x})}$ and $\overline{v_3(\underset{\sim}{x})v_3(\underset{\sim}{x})}$ are the same as this. Now consider an off-diagonal component of the tensor,

$$\overline{v_1(\underset{\sim}{x})v_2(\underset{\sim}{x})} \qquad (402,3D)$$

$$= (N/2\pi)^3 \int_k k^2\hat{E}(k)dk \int_0^{\pi}\int_0^{2\pi} (-\cos\theta\ \sin^2\theta)d\phi\ d\theta = 0$$

The other off-diagonal components are also zero. Therefore,

$$\overline{v_i(\underset{\sim}{x})v_j(\underset{\sim}{x})} = (N/2\pi)^3\ (8\pi/3)\,\delta_{ij} \int_k k^2\hat{E}(k)dk \qquad (403,3D)$$

The energy content of the flow is thus

$$E_o = \frac{3}{2}\,\tilde{v}(t)^2 = \tfrac{1}{2}\ \overline{v_i(\underset{\sim}{x})v_i(\underset{\sim}{x})} \qquad (404,3D)$$

$$= (N/2\pi)^3 \int_k 4\pi k^2\ \hat{E}(k)dk = \int_k E(k)_c dk$$

Therefore,

$$\hat{E}(k) = (2\pi/N)^3\ E(k)_c/4\pi k^2 \qquad (405,3D)$$

giving a relation that can be used for calculating $E(k)_c$ directly from the Fourier velocity modes

$$E_{ij}(\underset{\sim}{k}) = u_i(\underset{\sim}{k})u_j(-\underset{\sim}{k}) = (2\pi/N)^3 P_{ij}(\underset{\sim}{k})E(k)_c/4\pi k^2 \quad (406,3D)$$

Continuous energy spectrum in two dimensions

In two dimensions Equation 396 becomes

$$\overline{v_i(\underset{\sim}{x})v_j(\underset{\sim}{x})} = (N/2\pi)^2 \int_{\underset{\sim}{k}} P_{ij}(\underset{\sim}{k})\hat{E}(k)d\underset{\sim}{k} \quad (407,2D)$$

in the integral approximation. Integration over a circle of radius k gives

$$\overline{v_i(\underset{\sim}{x})v_j(\underset{\sim}{x})} = (N/2\pi)^2 \int_k k\hat{E}(k)dk \int_0^{2\pi} (\delta_{ij} - k_i k_j/k^2)d\theta \quad (408,2D)$$

The components of $\underset{\sim}{k}$ can be written as

$$k_1 = k\cos\theta, \quad k_2 = k\sin\theta \quad (409,2D)$$

Consider the 1,1-component of the tensor

$$\overline{v_1(x)v_1(x)} = (N/2\pi)^2 \int_k k\hat{E}(k)dk \int_0^{2\pi} (1 - \cos^2\theta)d\theta \quad (410,2D)$$

$$= (N/2\pi)^2 \pi \int_k k\hat{E}(k)dk = \overline{v_2(\underset{\sim}{x})v_2(\underset{\sim}{x})}$$

Consider the 1,2-component of the tensor

$$\overline{v_1(\underset{\sim}{x})v_2(\underset{\sim}{x})} = (N/2\pi)^2 \int_k k\hat{E}(k)dk \int_0^{2\pi} (-\cos\theta\sin\theta)d\theta = 0 \quad (411,2D)$$

The 2,1-component is also zero. Therefore,

$$\overline{v_i(\underset{\sim}{x})v_j(\underset{\sim}{x})} = (N/2\pi)^2 \pi \delta_{ij} \int_k k\hat{E}(k)dk \qquad (412,2D)$$

The energy content of the flow is then

$$E_o = \tilde{v}(t)^2 = \tfrac{1}{2} \overline{v_i(\underset{\sim}{x})v_i(\underset{\sim}{x})}$$

$$= (N/2\pi)^2 \pi \int_k k\hat{E}(k)dk = \int_k E(k)_c dk \qquad (413,2D)$$

Therefore,

$$\hat{E}(k) = (2\pi/N)^2 E(k)_c/\pi k \qquad (414,2D)$$

which gives

$$E_{ij}(\underset{\sim}{k}) = \hat{u}_i(\underset{\sim}{k})u_j(-\underset{\sim}{k}) = (2\pi/N)^2 P_{ij}(\underset{\sim}{k})E(k)_c/\pi k \qquad (415,2D)$$

Discrete energy spectrum in three dimensions

The discrete energy spectrum function $E(k)_d$ is useful because it can be calculated in exact form directly from the Fourier velocity modes without the use of approximations. In order to relate $E(k)_d$ to $\hat{E}(k)$, it is necessary to express Equation 396 in terms of k (and $\theta_{\underset{\sim}{k}}$, $\phi_{\underset{\sim}{k}}$) instead of k_1, k_2, and k_3. The components of $\underset{\sim}{k}$ can be written as

$$k_1 = k\cos\theta_{\underset{\sim}{k}}, \quad k_2 = k\sin\theta_{\underset{\sim}{k}}\cos\phi_{\underset{\sim}{k}}, \quad k_3 = k\sin\theta_{\underset{\sim}{k}}\sin\phi_{\underset{\sim}{k}} \qquad (416,3D)$$

where $\theta_{\underset{\sim}{k}}$ and $\phi_{\underset{\sim}{k}}$ are discrete angles and known for each $\underset{\sim}{k}$. For example, $\theta_{\underset{\sim}{k}} = \cos^{-1}(k_1/k)$ and $\phi_{\underset{\sim}{k}} = \tan^{-1}(k_3/k_2)$.

Considering the diagonal components of $Q_{ij}(\underset{\sim}{0})$, we

find

$$\overline{v_1(\underset{\sim}{x})v_1(\underset{\sim}{x})} = \sum_{k_1}\sum_{k_2}\sum_{k_3}(1 - k_1k_1/k^2)\hat{E}(k) \tag{417,3D}$$

$$= \sum_{k}\sum_{\theta_{\underset{\sim}{k}}}\sum_{\phi_{\underset{\sim}{k}}}(1 - \cos^2\theta_{\underset{\sim}{k}})\hat{E}(k) = \sum_{k}\sum_{\theta_{\underset{\sim}{k}}}\sum_{\phi_{\underset{\sim}{k}}}\sin^2\theta_{\underset{\sim}{k}}\,\hat{E}(k)$$

$$\overline{v_2(\underset{\sim}{x})v_2(\underset{\sim}{x})} = \sum_{k_1}\sum_{k_2}\sum_{k_3}(1 - k_2k_2/k^2)\hat{E}(k) \tag{418,3D}$$

$$= \sum_{k}\sum_{\theta_{\underset{\sim}{k}}}\sum_{\phi_{\underset{\sim}{k}}}(1 - \sin^2\theta_{\underset{\sim}{k}}\cos^2\phi_{\underset{\sim}{k}})\hat{E}(k)$$

$$\overline{v_3(\underset{\sim}{x})v_3(\underset{\sim}{x})} = \sum_{k_1}\sum_{k_2}\sum_{k_3}(1 - k_3k_3/k^2)\hat{E}(k) \tag{419,3D}$$

$$= \sum_{k}\sum_{\theta_{\underset{\sim}{k}}}\sum_{\phi_{\underset{\sim}{k}}}(1 - \sin^2\theta_{\underset{\sim}{k}}\sin^2\phi_{\underset{\sim}{k}})\hat{E}(k)$$

Consider the off-diagonal 1,2-component,

$$\overline{v_1(\underset{\sim}{x})v_2(\underset{\sim}{x})} = \sum_{k_1}\sum_{k_2}\sum_{k_3}(-k_1k_2/k^2)\hat{E}(k) \tag{420,3D}$$

$$= \sum_{k}\sum_{\theta_{\underset{\sim}{k}}}\sum_{\phi_{\underset{\sim}{k}}}(-\cos\theta_{\underset{\sim}{k}}\sin\theta_{\underset{\sim}{k}}\cos\phi_{\underset{\sim}{k}})\hat{E}(k) = 0$$

It is zero because for points located on the k_1-axis and $k_1 = 0$ plane, $\cos\theta_{\underset{\sim}{k}}\sin\theta_{\underset{\sim}{k}}\cos\phi_{\underset{\sim}{k}} = 0$. During the summation over $\theta_{\underset{\sim}{k}}$ and $\phi_{\underset{\sim}{k}}$ for constant k, points $(k, \theta_{\underset{\sim}{k}}, \phi_{\underset{\sim}{k}})$ lying on the sphere k = constant in the half-space $k_1 > 0$, cancel with the mirror image points $(k, \pi - \theta_{\underset{\sim}{k}}, \phi_{\underset{\sim}{k}})$ in the half-space $k_1 < 0$. This can be seen from

$$\cos\theta_{\underset{\sim}{k}} \sin\theta_{\underset{\sim}{k}} \cos\phi_{\underset{\sim}{k}} + \cos(\pi - \theta_{\underset{\sim}{k}})\sin(\pi - \theta_{\underset{\sim}{k}})\cos\phi_{\underset{\sim}{k}} = 0 \quad (421)$$

The off-diagonal 1,3-component,

$$\overline{v_1(\underset{\sim}{x})v_3(\underset{\sim}{x})} = \sum_{k_1}\sum_{k_2}\sum_{k_3} (-k_1k_3/k^2)\hat{E}(k)$$

$$= \sum_{k}\sum_{\theta_{\underset{\sim}{k}}}\sum_{\phi_{\underset{\sim}{k}}} (-\cos\theta_{\underset{\sim}{k}} \sin\theta_{\underset{\sim}{k}} \sin\phi_{\underset{\sim}{k}})\hat{E}(k) = 0 \quad (422,3D)$$

is zero by the same arguments.

Consider the off-diagonal 2,3-component,

$$\overline{v_2(\underset{\sim}{x})v_3(\underset{\sim}{x})} = \sum_{k_1}\sum_{k_2}\sum_{k_3} (-k_2k_3/k^2)\hat{E}(k)$$

$$= \sum_{k}\sum_{\theta_{\underset{\sim}{k}}}\sum_{\phi_{\underset{\sim}{k}}} (-\sin^2\theta_{\underset{\sim}{k}} \cos\phi_{\underset{\sim}{k}} \sin\phi_{\underset{\sim}{k}})\hat{E}(k) = 0 \quad (423,3D)$$

It is also zero. Points located on the k_3-axis and $k_3 = 0$ plane have $\sin^2\theta_{\underset{\sim}{k}} \cos\phi_{\underset{\sim}{k}} \sin\phi_{\underset{\sim}{k}} = 0$. During the summation over $\theta_{\underset{\sim}{k}}$ and $\phi_{\underset{\sim}{k}}$ for constant k, points $(k, \theta_{\underset{\sim}{k}}, \phi_{\underset{\sim}{k}})$ in the half-space $k_3 > 0$ cancel exactly with the mirror image points $(k, \theta_{\underset{\sim}{k}}, 2\pi - \phi_{\underset{\sim}{k}})$ in the half-space $k_3 < 0$. This can be seen from

$$\sin^2\theta_{\underset{\sim}{k}} \cos\phi_{\underset{\sim}{k}} \sin\phi_{\underset{\sim}{k}} + \sin^2\theta_{\underset{\sim}{k}} \cos(2\pi - \phi_{\underset{\sim}{k}})\sin(2\pi - \phi_{\underset{\sim}{k}}) = 0 \quad (424)$$

Likewise, the other off-diagonal components (2,1), (3,1), and (3,2) are all zero. Therefore, the energy content of the flow is

$$E_o = \frac{3}{2}\,\tilde{v}(t)^2 = \tfrac{1}{2}\,\overline{v_i(\underset{\sim}{x})v_i(\underset{\sim}{x})}$$

$$= \tfrac{1}{2}\sum_k \sum_{\theta_{\underset{\sim}{k}}} \sum_{\phi_{\underset{\sim}{k}}} [\sin^2\theta_{\underset{\sim}{k}} + (1 - \sin^2\theta_{\underset{\sim}{k}}\cos^2\phi_{\underset{\sim}{k}})$$

$$+ (1 - \sin^2\theta_{\underset{\sim}{k}}\sin^2\phi_{\underset{\sim}{k}})]\,\hat{E}(k) \qquad (425,3D)$$

$$= \sum_k \sum_{\theta_{\underset{\sim}{k}}} \sum_{\phi_{\underset{\sim}{k}}} \hat{E}(k) = \sum_k \eta(k)\hat{E}(k) = \sum_k E(k)_d$$

and

$$\hat{E}(k) = E(k)_d/\eta(k) \qquad (426,3D)$$

The discrete energy spectrum function can be calculated from

$$E_{ij}(\underset{\sim}{k})_d = u_i(\underset{\sim}{k})u_j(-\underset{\sim}{k}) = P_{ij}(\underset{\sim}{k})E(k)_d/\eta(k) \qquad (427,3D)$$

Discrete energy spectrum in two dimensions

In order to relate $E(k)_d$ to $\hat{E}(k)$ in two dimensions it is necessary to express Equation 396 in terms of k (and $\theta_{\underset{\sim}{k}}$) instead of k_1 and k_2. The components of $\underset{\sim}{k}$ can be written as

$$k_1 = k\cos\theta_{\underset{\sim}{k}}, \quad k_2 = k\sin\theta_{\underset{\sim}{k}} \qquad (428,2D)$$

where $\theta_{\underset{\sim}{k}}$ is discrete and known for each $\underset{\sim}{k}$. Considering the diagonal components of the tensor gives

$$\overline{v_1(\underset{\sim}{x})v_1(\underset{\sim}{x})} = \sum_{k_1}\sum_{k_2} (1 - k_1k_1/k^2)\hat{E}(k) \qquad (429,2D)$$

$$= \sum_k \sum_{\theta_{\underset{\sim}{k}}} (1 - \cos^2\theta_{\underset{\sim}{k}})\hat{E}(k) = \sum_k \sum_{\theta_{\underset{\sim}{k}}} \sin^2\theta_{\underset{\sim}{k}}\,\hat{E}(K)$$

$$\overline{v_2(\underset{\sim}{x})v_2(\underset{\sim}{x})} = \sum_{k_1}\sum_{k_2}(1 - k_2k_2/k^2)\hat{E}(k)$$

$$= \sum_{k}\sum_{\theta_{\underset{\sim}{k}}}(1 - \sin^2\theta_{\underset{\sim}{k}})\hat{E}(k) = \sum_{k}\sum_{\theta_{\underset{\sim}{k}}}\cos^2\theta_{\underset{\sim}{k}}\,\hat{E}(k) \qquad (430,2D)$$

Consider the off-diagonal 1,2-component

$$\overline{v_1(\underset{\sim}{x})v_2(\underset{\sim}{x})} = \sum_{k_1}\sum_{k_2}(-k_1k_2/k^2)\hat{E}(k)$$

$$= \sum_{k}\sum_{\theta_{\underset{\sim}{k}}}(-\cos\theta_{\underset{\sim}{k}}\sin\theta_{\underset{\sim}{k}})\hat{E}(k) = 0 \qquad (431,2D)$$

Points on the k_1-axis have $\cos\theta_{\underset{\sim}{k}}\sin\theta_{\underset{\sim}{k}} = 0$. In the summation over $\theta_{\underset{\sim}{k}}$ for constant k, points $(k, \theta_{\underset{\sim}{k}})$ lying on the circular curve k = constant in the half-plane $k_2 > 0$ cancel with the mirror image points $(k, -\theta_{\underset{\sim}{k}})$ in the half plane $k_2 < 0$. This can be seen from

$$\cos\theta_{\underset{\sim}{k}}\sin\theta_{\underset{\sim}{k}} + \cos(-\theta_{\underset{\sim}{k}})\sin(-\theta_{\underset{\sim}{k}}) = 0 \qquad (432)$$

Likewise, the 2,1-component is also zero.

Therefore,

$$E_o = \tilde{v}(t)^2 = \tfrac{1}{2}\,\overline{v_i(\underset{\sim}{x})v_i(\underset{\sim}{x})}$$

$$= \tfrac{1}{2}\sum_{k}\sum_{\theta_{\underset{\sim}{k}}}(\sin^2\theta_{\underset{\sim}{k}} + \cos^2\theta_{\underset{\sim}{k}})\hat{E}(k) = \tfrac{1}{2}\sum_{k}\sum_{\theta_{\underset{\sim}{k}}}\hat{E}(k) = \sum_{k}E(k)_d \qquad (433,2D)$$

and

$$\hat{E}(k) = 2E(k)_d/\eta(k) \qquad (434,2D)$$

and the discrete energy spectrum function can be calculated from

$$E_{ij}(\underset{\sim}{k})_d = u_i(\underset{\sim}{k})u_i(-\underset{\sim}{k}) = 2P_{ij}(\underset{\sim}{k})E(k)_d/\eta(k) \qquad (435,2D)$$

Calculation of $Q_{ij}(r)$ and $f(r)$

The integral approximation of the inverse Fourier transform gives $Q_{ij}(\underset{\sim}{r})$ from $E_{ij}(\underset{\sim}{k})$. The angular dependence can be removed from Equation 369 by integrating over the surface $k = |\underset{\sim}{k}| = \text{constant}$, using the relations

$$\underset{\sim}{k}\cdot\underset{\sim}{r} = kr\cos\theta, \quad d\underset{\sim}{k} = k^2\sin\theta\, d\theta\, d\phi\, dk \qquad (436,3D)$$

$$\underset{\sim}{k}\cdot\underset{\sim}{r} = kr\cos\theta, \quad d\underset{\sim}{k} = k\, d\theta\, dk \qquad (437,2D)$$

where θ is the angle between $\underset{\sim}{k}$ and $\underset{\sim}{r}$. This gives

$$Q_{ij}(r) = (N/2\pi)^3 \int_k \int_0^{2\pi}\int_0^{\pi} k^2 E_{ij}(k)_c \sin\theta\, \exp(ikr\cos\theta)\, d\theta\, d\phi\, dk$$

$$= (N/2\pi)^3\, 2\pi \int_k \int_0^{\pi} k^2 E_{ij}(k)_c \sin\theta\, \cos(kr\cos\theta)\, d\theta\, dk \qquad (438,3D)$$

$$+ (N/2\pi)^3\, 2\pi i \int_k \int_0^{\pi} k^2 E_{ij}(\underset{\sim}{k})_c \sin\theta\, \sin(kr\cos\theta)\, d\theta\, dk$$

$$Q_{ij}(r) = (N/2\pi)^2 \int_k kE_{ij}(k)_c \int_0^{2\pi} \exp(ikr\cos\theta)\, d\theta\, dk \qquad (439,2D)$$

and finally

$$Q_{ij}(r) = (N/2\pi)^3\, 4\pi \int_k k^2 E_{ij}(k)_c \frac{\sin(kr)}{kr}\, dk \qquad (440,3D)$$

$$Q_{ij}(r) = (N/2\pi)^2 \, 2\pi \int_k k E_{ij}(k)_c \, J_0(kr) dk \qquad (441,2D)$$

where

$$\int_0^{2\pi} \exp(ikr\cos\theta)\, d\theta = \int_0^{2\pi} \cos(kr\cos\theta)\, d\theta = 2\pi\, J_0(kr) \qquad (442)$$

has been used to get Equation 441 and where $J_0(kr)$ is the zero-order Bessel function of the first kind. Converting Equations 440 and 441 back to discrete form gives

$$Q_{ij}(r) = \sum_k \eta(k) E_{ij}(k)_d \frac{\sin(kr)}{kr} \qquad (443,3D)$$

$$Q_{ij}(r) = \sum_k \eta(k) E_{ij}(k)_d \, J_0(kr) \qquad (444,2D)$$

Using Equation 373 (374) converts Equation 440 (441) to

$$Q_{ii}(r) = 2 \int_0^{\infty} E(k)_c \frac{\sin(kr)}{kr} dk \qquad (445,3D)$$

$$Q_{ii}(r) = 2 \int_0^{\infty} E(k)_c \, J_0(kr)\, dk \qquad (446,2D)$$

and using Equation 380 converts Equations 443 and 444 to

$$Q_{ii}(r) = 2 \sum_k E(k)_d \frac{\sin(kr)}{kr} \qquad (447,3D)$$

$$Q_{ii}(r) = 2 \sum_k E(k)_d \, J_0(kr) \qquad (448,2D)$$

Integrating Equation 19 gives $f(r)$ from $Q_{ii}(r)$

$$f(r) = (1/\tilde{v}^2 r^{\delta_{nn}}) \int_0^r r_1^{(\delta_{nn}-1)} Q_{ii}(r_1) dr_1 \qquad (449)$$

Incorporating Equations 445 - 448 into Equation 449 gives expressions for calculating f(r) directly from the discrete or continuous energy spectrum,

$$f(r) = (2/\tilde{v}^2) \int_0^\infty E(k)_c \left[\frac{\sin(kr)}{(kr)^3} - \frac{\cos(kr)}{(kr)^2}\right] dk \qquad (450,3D)$$

$$f(r) = (2/\tilde{v}^2) \int_0^\infty E(k)_c \left[J_1(kr)/kr\right] dk \qquad (451,2D)$$

$$f(r) = (2/\tilde{v}^2) \sum_k E(k)_d \left[\frac{\sin(kr)}{(kr)^3} - \frac{\cos(kr)}{(kr)^2}\right] \qquad (452,3D)$$

$$f(r) = (2/\tilde{v}^2) \sum_k E(k)_d \, J_1(kr)/kr \qquad (453,2D)$$

Using Equations 380 and 387 and the definition of $\eta(k)$ converts Equations 452 and 453 to a form from which f(r) can be calculated directly from the Fourier velocity modes,

$$f(r) = (1/\tilde{v}^2) \sum_{\tilde{k}} u_i(\tilde{k}) u_i(-\tilde{k}) \left[\frac{\sin(kr)}{(kr)^3} - \frac{\cos(kr)}{(kr)^2}\right] \qquad (454,3D)$$

$$f(r) = (1/\tilde{v}^2) \sum_{\tilde{k}} u_i(\tilde{k}) u_i(-\tilde{k}) \, J_1(kr)/kr \qquad (455,2D)$$

Calculation of $E_{ij}(k)$ and $E(k)$ from $Q_{ij}(r)$ and $f(r)$

$E_{ij}(\tilde{k})$ is given by the Fourier transform of $Q_{ij}(\tilde{r})$. The angular dependence can be removed from Equation 367 by integrating over the surface $r = |\tilde{r}|$ = constant, giving

$$E_{ij}(k) = N^{-3}\int_r \int_0^{2\pi}\int_0^{\pi} r^2 Q_{ij}(r)\sin\theta \exp(-ikr\cos\theta)\, d\theta\, d\phi\, dr \qquad (456,3D)$$

$$E_{ij}(k) = N^{-2}\int_r \int_0^{2\pi} rQ_{ij}(r) \exp(-ikr\cos\theta)\, d\theta\, dr \qquad (457,2D)$$

and finally

$$E_{ij}(k) = (4\pi/N^3) \int_0^{\infty} r^2 Q_{ij}(r) \frac{\sin(kr)}{kr}\, dr \qquad (458,3D)$$

$$E_{ij}(k) = (2\pi/N^2) \int_0^{\infty} r\, Q_{ij}(r)\, J_0(kr)\, dr \qquad (459,2D)$$

Combining Equation 373 (374) and Equation 458 (459) gives

$$E(k)_c = (1/\pi) \int_0^{\infty} kr\, Q_{ii}(r)\, \sin(kr)\, dr \qquad (460,3D)$$

$$E(k)_c = \tfrac{1}{2} \int_0^{\infty} kr\, Q_{ii}(r)\, J_0(kr)\, dr \qquad (461,2D)$$

Substituting Equation 19 into Equations 460 and 461 and simplifying the results using integration by parts gives expressions for calculating the energy spectrum directly from f(r),

$$E(k)_c = (\tilde{v}^2/\pi) \int_0^{\infty} f(r)[kr\, \sin(kr) - k^2r^2\cos(kr)]\, dr \qquad (462,3D)$$

$$E(k)_c = (\tilde{v}^2/2) \int_0^{\infty} f(r)\, k^2r^2\, J_1(kr)\, dr \qquad (463,2D)$$

Calculation of the Longitudinal Integral Scale

The longitudinal integral scale has been defined by Equation 358 and can be found directly through integration of Equations 450 - 455 over all r.

$$L_f(t) = (\pi/2\tilde{v}^2) \int_0^\infty k^{-1}E(k)_c dk \qquad (464,3D)$$

$$L_f(t) = (2/\tilde{v}^2) \int_0^\infty k^{-1}E(k)_c dk \qquad (465,2D)$$

$$L_f(t) = (\pi/2\tilde{v}^2) \sum_k k^{-1}E(k)_d \qquad (466,3D)$$

$$L_f(t) = (2/\tilde{v}^2) \sum_k k^{-1}E(k)_d \qquad (467,2D)$$

$$L_f(t) = (\pi/4\tilde{v}^2) \sum_{\underset{\sim}{k}} k^{-1}u_i(\underset{\sim}{k})u_i(-\underset{\sim}{k}) \qquad (468,3D)$$

$$L_f(t) = (1/\tilde{v}^2) \sum_{\underset{\sim}{k}} k^{-1}u_i(\underset{\sim}{k})u_i(-\underset{\sim}{k}) \qquad (469,2D)$$

Calculation of the Longitudinal Microscale

The longitudinal microscale has been defined by Equation 359 and can be found through differentiating Equations 450 - 455 twice and taking the limit r = 0.

$$\lambda_f(t)^{-2} = (1/15\tilde{v}^2) \int_0^\infty k^2E(k)_c dk \qquad (470,3D)$$

$$\lambda_f(t)^{-2} = (1/8\tilde{v}^2) \int_0^\infty k^2E(k)_c dk \qquad (471,2D)$$

$$\lambda_f(t)^{-2} = (1/15\tilde{v}^2) \sum_k k^2 E(k)_d \qquad (472,3D)$$

$$\lambda_f(t)^{-2} = (1/8\tilde{v}^2) \sum_k k^2 E(k)_d \qquad (473,2D)$$

$$\lambda_f(t)^{-2} = (1/30\tilde{v}^2) \sum_{\underset{\sim}{k}} k^2 u_i(\underset{\sim}{k}) u_i(-\underset{\sim}{k}) \qquad (474,3D)$$

$$\lambda_f(t)^{-2} = (1/16\tilde{v}^2) \sum_{\underset{\sim}{k}} k^2 u_i(\underset{\sim}{k}) u_i(-\underset{\sim}{k}) \qquad (475,2D)$$

Navier-Stokes Equation

In formulating a model for the simulation of isotropic turbulence, it is useful to first examine the Navier-Stokes equation in wave number space. For incompressible flows, the Navier-Stokes and continuity equations in physical space are

$$\frac{\partial v_i^*}{\partial t^*} + \frac{\partial (v_i^* v_j^*)}{\partial x_j^*} = - \frac{1}{\rho} \frac{\partial P^*}{\partial x_i^*} + \nu \frac{\partial^2 v_i^*}{\partial x_j^{*2}} \qquad (476)$$

$$\partial v_i^* / \partial x_i^* = 0 \qquad (477)$$

Using the reference length $L_{f\emptyset}^*$ and reference velocity $\tilde{v}_\emptyset^*$, dimensionless variables can be defined as

$$t \equiv t^* \tilde{v}_\emptyset^* / L_{f\emptyset}^*, \quad x_i \equiv x_i^* / L_{f\emptyset}^*, \quad v_i \equiv v_i^* / \tilde{v}_\emptyset^*, \quad P \equiv P^* / \rho \tilde{v}_\emptyset^{*2} \qquad (478)$$

and the Navier-Stokes equation can be made dimensionless,

$$\frac{\partial v_i}{\partial t} + \frac{\partial (v_i v_j)}{\partial x_j} = - \frac{\partial P}{\partial x_i} + \frac{1}{Re} \frac{\partial^2 v_i}{\partial x_j^2} \qquad (479)$$

$$Re \equiv \tilde{v}_{\emptyset}^{*} L_{f\emptyset}^{*} / \nu \tag{480}$$

The Fourier transform of Equation 479 is (see Appendix B for properties of the Fourier transform)

$$\frac{\partial u_i(\underset{\sim}{k})}{\partial t} + ik_j \sum_{\underset{\sim}{p}+\underset{\sim}{q}=\underset{\sim}{k}} u_i(\underset{\sim}{p}) u_j(\underset{\sim}{q}) = -ik_i P(\underset{\sim}{k}) - \frac{1}{Re} k^2 u_i(\underset{\sim}{k}) \tag{481}$$

where $P(\underset{\sim}{k}) \equiv F[P(\underset{\sim}{x})]$. The Fourier transformed continuity equation is

$$k_i u_i(\underset{\sim}{k}) = 0 \tag{482}$$

The summation over the inertial terms is restricted by the requirement that $\underset{\sim}{k} = \underset{\sim}{p} + \underset{\sim}{q}$. The term involving this sum indicates that two Fourier modes with wave numbers $\underset{\sim}{p}$ and $\underset{\sim}{q}$ can interact to put energy into, or take energy out of, a third mode with wave number $\underset{\sim}{k}$ provided that $\underset{\sim}{k}$, $\underset{\sim}{p}$, and $\underset{\sim}{q}$ satisfy the triangle relation $\underset{\sim}{k} = \underset{\sim}{p} + \underset{\sim}{q}$. This interaction between modes is a consequence of the nonlinearity of the Navier-Stokes equations and is central to the problem of turbulence, having no analogue in linear systems.

By taking the inner product of Equation 481 and k_i, the pressure term can be solved for and eliminated by using the continuity equation

$$\frac{\partial [k_i u_i(\underset{\sim}{k})]}{\partial t} + ik_i k_j \sum_{\underset{\sim}{p}+\underset{\sim}{q}=\underset{\sim}{k}} u_i(\underset{\sim}{p}) u_j(\underset{\sim}{q}) = -ik^2 P(\underset{\sim}{k}) - \frac{1}{Re} k^2 [k_i u_i(k)] \tag{483}$$

$$P(\underset{\sim}{k}) = -(k_n k_j/k^2) \sum_{\underset{\sim}{p}+\underset{\sim}{q}=\underset{\sim}{k}} u_n(\underset{\sim}{p})u_j(\underset{\sim}{q}) \tag{484}$$

Substituting Equation 484 into Equation 481 gives (with rearranging)

$$\frac{\partial u_i(\underset{\sim}{k})}{\partial t} + \frac{1}{Re} k^2 u_i(\underset{\sim}{k}) = -ik_j \sum_{\underset{\sim}{p}+\underset{\sim}{q}=\underset{\sim}{k}} u_i(\underset{\sim}{p})u_j(\underset{\sim}{q}) + i(k_i k_j k_n/k^2) \sum_{\underset{\sim}{p}+\underset{\sim}{q}=\underset{\sim}{k}} u_n(\underset{\sim}{p})u_j(\underset{\sim}{q}) \tag{485}$$

Upon using the identities

$$-ik_j \sum_{\underset{\sim}{p}+\underset{\sim}{q}=\underset{\sim}{k}} u_i(\underset{\sim}{p})u_j(\underset{\sim}{q}) = -ik_n \sum_{\underset{\sim}{p}+\underset{\sim}{q}=\underset{\sim}{k}} u_i(\underset{\sim}{p})u_n(\underset{\sim}{q})$$

$$= -ik_n \sum_{\underset{\sim}{p}+\underset{\sim}{q}=\underset{\sim}{k}} u_i(\underset{\sim}{q})u_n(\underset{\sim}{p}) = -ik_n \sum_{\underset{\sim}{p}+\underset{\sim}{q}=\underset{\sim}{k}} u_n(\underset{\sim}{p})\delta_{ij}u_j(\underset{\sim}{q})$$

Equation 485 becomes

$$\frac{\partial u_i(\underset{\sim}{k})}{\partial t} + \frac{1}{Re} k^2 u_i(\underset{\sim}{k}) = -i(\delta_{ij} - k_i k_j/k^2)k_n \sum_{\underset{\sim}{p}+\underset{\sim}{q}=\underset{\sim}{k}} u_n(\underset{\sim}{p})u_j(\underset{\sim}{q}) \tag{486}$$

or, finally,

$$\frac{\partial u_i(\underset{\sim}{k})}{\partial t} + \frac{1}{Re} k^2 u_i(\underset{\sim}{k}) = -i P_{ij}(\underset{\sim}{k}) \sum_{\underset{\sim}{p}} k_n u_n(\underset{\sim}{p})u_j(\underset{\sim}{k}-\underset{\sim}{p}) \tag{487}$$

One feature of the Navier-Stokes equation, Equation 487, is that it cannot describe stationary isotropic turbulence since it contains no input of energy to balance the

dissipative effect of viscosity. Therefore, turbulent energy and hence the intensity of turbulent mixing decays over time. In real flows, energy input is provided by effects, such as the interaction of the mean velocity gradient with the Reynolds stress, which are incompatible with the ideas of homogeneity and isotropy. This difficulty is sometimes avoided by introducing a hypothetical homogeneous isotropic stirring force. It is important to realize that this stirring force is not a real force, rather it is a compensation for the unreality of the model.

Using Equation 393, it can be shown that turbulent energy is conserved by the Navier-Stokes equation for the case of infinite Reynolds number (no viscous dissipation). From Equation 486

$$\frac{\partial u_i(\underset{\sim}{k})}{\partial t} = -iP_{ij}(\underset{\sim}{k})k_n \sum_{\underset{\sim}{p}+\underset{\sim}{q}=\underset{\sim}{k}} u_n(\underset{\sim}{p})u_j(\underset{\sim}{q}) \tag{488}$$

$$\frac{\partial u_i(-\underset{\sim}{k})}{\partial t} = +iP_{ij}(-\underset{\sim}{k})k_n \sum_{\underset{\sim}{p}+\underset{\sim}{q}=\underset{\sim}{k}} u_n(-\underset{\sim}{p})u_j(-\underset{\sim}{q}) \tag{489}$$

Taking the inner product of Equation 488 and $u_i(-\underset{\sim}{k})$ and the inner product of Equation 489 and $u_i(\underset{\sim}{k})$, adding the resulting equations, and summing over $\underset{\sim}{k}$ gives

$$2\frac{dE_o}{dt} = \frac{d}{dt}\sum_{\underset{\sim}{k}} u_i(\underset{\sim}{k})u_i(-\underset{\sim}{k})$$

$$= -i \sum_{\underset{\sim}{k}} \sum_{\underset{\sim}{p}+\underset{\sim}{q}=\underset{\sim}{k}} P_{ij}(\underset{\sim}{k}) k_n \left[u_n(\underset{\sim}{p}) u_j(\underset{\sim}{q}) u_i(-\underset{\sim}{k})\right]$$

$$+ i \sum_{\underset{\sim}{k}} \sum_{\underset{\sim}{p}+\underset{\sim}{q}=\underset{\sim}{k}} P_{ij}(\underset{\sim}{k}) k_n \left[u_n(-\underset{\sim}{p}) u_j(-\underset{\sim}{q}) u_i(\underset{\sim}{k})\right] = 0 \qquad (490)$$

the two summations being equal by symmetry arguments and where $P_{ij}(\underset{\sim}{k}) = P_{ij}(-\underset{\sim}{k})$ has been used.

Turbulent Velocity Field Generation Equation

In this study, one simulated turbulent velocity field will be generated using a modified form of the Navier-Stokes equation

$$\frac{\partial v_i}{\partial t} + \frac{\partial (v_i \phi_j)}{\partial x_j} = - \frac{\partial P}{\partial x_i} \qquad (491)$$

Notable features of this model are convection of the flow velocity $v_i(\underset{\sim}{x})$ by a random convection velocity $\phi_j(\underset{\sim}{x})$ (instead of self-convection) and absence of the viscous-dissipation term. The Fourier transform of Equation 491 is

$$\frac{\partial u_i(\underset{\sim}{k})}{\partial t} + ik_j \sum_{\underset{\sim}{p}+\underset{\sim}{q}=\underset{\sim}{k}} u_i(\underset{\sim}{p}) \phi_j(\underset{\sim}{q}) = -ik_i P(\underset{\sim}{k}) \qquad (492)$$

Solving for and eliminating the pressure term as before

$$\partial [k_i u_i(\underset{\sim}{k})]/\partial t + ik_i k_j \sum_{\underset{\sim}{p}+\underset{\sim}{q}=\underset{\sim}{k}} u_i(\underset{\sim}{p}) \phi_j(\underset{\sim}{q}) = -ik^2 P(\underset{\sim}{k}) \qquad (493)$$

$$P(\underset{\sim}{k}) = -(k_n k_j / k^2) \sum_{\underset{\sim}{p}+\underset{\sim}{q}=\underset{\sim}{k}} u_n(\underset{\sim}{p}) \phi_j(\underset{\sim}{q}) \qquad (494)$$

gives

$$\partial u_i(\underset{\sim}{k})/\partial t = -ik_j \sum_{\underset{\sim}{p}+\underset{\sim}{q}=\underset{\sim}{k}} u_i(\underset{\sim}{p})\phi_j(\underset{\sim}{q})$$

$$+ i(k_i k_j k_n/k^2) \sum_{\underset{\sim}{p}+\underset{\sim}{q}=\underset{\sim}{k}} u_n(\underset{\sim}{p})\phi_j(\underset{\sim}{q})$$

$$= -ik_j \sum_{\underset{\sim}{p}+\underset{\sim}{q}=\underset{\sim}{k}} \delta_{in} u_n(\underset{\sim}{p})\phi_j(\underset{\sim}{q})$$

$$+ i(k_i k_j k_n/k^2) \sum_{\underset{\sim}{p}+\underset{\sim}{q}=\underset{\sim}{k}} u_n(\underset{\sim}{p})\phi_j(\underset{\sim}{q})$$

$$= -i(\delta_{in} - k_i k_n/k^2)k_j \sum_{\underset{\sim}{p}+\underset{\sim}{q}=\underset{\sim}{k}} \phi_j(\underset{\sim}{q})u_n(\underset{\sim}{p})$$

$$= -i(\delta_{ij} - k_i k_j/k^2)k_n \sum_{\underset{\sim}{p}+\underset{\sim}{q}=\underset{\sim}{k}} \phi_n(\underset{\sim}{q})u_j(\underset{\sim}{p})$$

and

$$\partial u_i(\underset{\sim}{k})/\partial t = -i P_{ij}(\underset{\sim}{k})\, k_n \sum_{\underset{\sim}{p}+\underset{\sim}{q}=\underset{\sim}{k}} \phi_n(\underset{\sim}{p})u_j(\underset{\sim}{q}) \qquad (495)$$

or finally

$$\partial u_i(\underset{\sim}{k})/\partial t = -i P_{ij}(\underset{\sim}{k})\, k_n \sum_{\underset{\sim}{p}} \phi_n(\underset{\sim}{p})u_j(\underset{\sim}{k}-\underset{\sim}{p}) \qquad (496)$$

for generating the velocity field directly in wave number space.

That the velocity field generated obeys continuity can by shown by taking the inner product of Equation 496 and k_i

$$\partial[k_i u_i(\underset{\sim}{k})]/\partial t = -i(k_i\delta_{ij} - k_j)k_n \sum_{\underset{\sim}{p}} \phi_n(\underset{\sim}{p})u_j(\underset{\sim}{k}-\underset{\sim}{p}) = 0 \qquad (497)$$

which gives

$$k_i u_i(\underset{\sim}{k},t) = k_i u_i(\underset{\sim}{k},0) \qquad (498)$$

Therefore, continuity is obeyed over all time if it is obeyed initially.

It can also be shown that turbulent energy is conserved. From Equation 495,

$$\partial u_i(-\underset{\sim}{k})/\partial t = +i P_{ij}(-\underset{\sim}{k})\, k_n \sum_{\underset{\sim}{p}+\underset{\sim}{q}=\underset{\sim}{k}} \phi_n(-\underset{\sim}{p}) u_j(-\underset{\sim}{q}) \qquad (499)$$

Taking the inner product of Equation 495 and $u_i(-\underset{\sim}{k})$ and the inner product of Equation 499 and $u_i(\underset{\sim}{k})$, adding the resulting equations, and summing over $\underset{\sim}{k}$ gives

$$2\frac{dE_o}{dt} = \frac{d}{dt}\sum_{\underset{\sim}{k}} u_i(\underset{\sim}{k})u_i(-\underset{\sim}{k})$$

$$= -i \sum_{\underset{\sim}{k}} \sum_{\underset{\sim}{p}+\underset{\sim}{q}=\underset{\sim}{k}} P_{ij}(\underset{\sim}{k})k_n \left[\phi_n(\underset{\sim}{p})u_j(\underset{\sim}{q})u_i(-\underset{\sim}{k})\right] \qquad (500)$$

$$+ i \sum_{\underset{\sim}{k}} \sum_{\underset{\sim}{p}+\underset{\sim}{q}=\underset{\sim}{k}} P_{ij}(\underset{\sim}{k})k_n \left[\phi_n(-\underset{\sim}{p})u_j(-\underset{\sim}{q})u_i(\underset{\sim}{k})\right] = 0$$

That the random convection or forcing velocity does not pump energy into the flow or extract energy from it stands to reason; it is a purely convective action and merely transports turbulent energy about the flow. Notice that this also means that $\tilde{v}(t)$ should remain constant over time.

Although exclusion of the viscous-dissipation term in the Navier-Stokes equation would result in turbulent energy conservation, with self-convection integration over time would still result in equipartitioning of turbulent energy over all wave numbers: the initial shell-averaged energy

spectrum would decay to a uniform distribution over the finite number of wave number modes used in the calculation. In Equation 496, the random convection velocity field (with constant energy spectrum and fluctuation intensity) acts like a forcing function on the $v_i(\underset{\sim}{x})$ field energy spectrum and a statistically steady velocity field might be reached by integration over time. Use of the random convection velocity should also guarantee that the turbulent mixing field remains complicated over time.

Velocity Field Expressions in Terms of Real and Imaginary Parts

The Fourier transformed velocity is a complex variable and can be written in terms of real and imaginary parts as

$$u_i(\underset{\sim}{k}) = u_i^R(\underset{\sim}{k}) + i\, u_i^I(\underset{\sim}{k}) \tag{501}$$

Substituting this into

$$v_i(\underset{\sim}{x}) = \sum_{\underset{\sim}{k}} u_i(\underset{\sim}{k})\, \exp(i\underset{\sim}{k}\cdot\underset{\sim}{x}) \tag{502}$$

we get

$$\begin{aligned} v_i(\underset{\sim}{x}) &= \sum_{\underset{\sim}{k}} [u_i^R(\underset{\sim}{k}) + i\, u_i^I(\underset{\sim}{k})][\cos(\underset{\sim}{k}\cdot\underset{\sim}{x}) + i \sin(\underset{\sim}{k}\cdot\underset{\sim}{x})] \\ &= \sum_{\underset{\sim}{k}} [u_i^R(\underset{\sim}{k})\cos(\underset{\sim}{k}\cdot\underset{\sim}{x}) - u_i^I(\underset{\sim}{k})\sin(\underset{\sim}{k}\cdot\underset{\sim}{x})] \\ &\quad + i \sum_{\underset{\sim}{k}} [u_i^R(\underset{\sim}{k})\sin(\underset{\sim}{k}\cdot\underset{\sim}{x}) + u_i^I(\underset{\sim}{k})\cos(\underset{\sim}{k}\cdot\underset{\sim}{x})] \end{aligned} \tag{503}$$

However, since $v_i(\underset{\sim}{x})$ is a real variable, we must have

$$v_i(\underset{\sim}{x}) = \sum_{\underset{\sim}{k}} [u_i^R(\underset{\sim}{k})\cos(\underset{\sim}{k}\cdot\underset{\sim}{x}) - u_i^I(\underset{\sim}{k})\sin(\underset{\sim}{k}\cdot\underset{\sim}{x})] \tag{504}$$

$$0 = \sum_{\underset{\sim}{k}} [u_i^R(\underset{\sim}{k})\sin(\underset{\sim}{k}\cdot\underset{\sim}{x}) + u_i^I(\underset{\sim}{k})\cos(\underset{\sim}{k}\cdot\underset{\sim}{x})] \tag{505}$$

Furthermore,

$$\overline{v_i(\underset{\sim}{x})} = N^{-3}\int_{\underset{\sim}{x}} v_i(\underset{\sim}{x})\exp(-i\underset{\sim}{0}\cdot\underset{\sim}{x})d\underset{\sim}{x} = u_i(\underset{\sim}{0}) = \underset{\sim}{0} \tag{506}$$

so that

$$u_i^R(\underset{\sim}{0}) = u_i^I(\underset{\sim}{0}) = \underset{\sim}{0} \tag{507}$$

Also,

$$\sin(-\underset{\sim}{k}\cdot\underset{\sim}{x}) = -\sin(\underset{\sim}{k}\cdot\underset{\sim}{x}),\ \cos(-\underset{\sim}{k}\cdot\underset{\sim}{x}) = \cos(\underset{\sim}{k}\cdot\underset{\sim}{x}) \tag{508}$$

so that Equation 505 gives the requirement

$$u_i^R(\underset{\sim}{k}) = u_i^R(-\underset{\sim}{k}),\ u_i^I(\underset{\sim}{k}) = -u_i^I(-\underset{\sim}{k}) \tag{509}$$

With

$$\phi_i(\underset{\sim}{k}) = \phi_i^R(\underset{\sim}{k}) + i\,\phi_i^I(\underset{\sim}{k}) \tag{510}$$

the velocity field generation equation, Equation 496, can be written in real and imaginary parts,

$$\begin{aligned}\frac{\partial u_i^R(\underset{\sim}{k})}{\partial t} &= P_{ij}(\underset{\sim}{k})k_n \sum_{\underset{\sim}{p}} [\phi_n^R(\underset{\sim}{p})u_j^I(\underset{\sim}{k}-\underset{\sim}{p}) + \phi_n^I(\underset{\sim}{p})u_j^R(\underset{\sim}{k}-\underset{\sim}{p})] \\ \frac{\partial u_i^I(\underset{\sim}{k})}{\partial t} &= -P_{ij}(\underset{\sim}{k})k_n \sum_{\underset{\sim}{p}} [\phi_n^R(\underset{\sim}{p})u_j^R(\underset{\sim}{k}-\underset{\sim}{p}) - \phi_n^I(\underset{\sim}{p})u_j^I(\underset{\sim}{k}-\underset{\sim}{p})]\end{aligned} \tag{511}$$

The equation of continuity gives

$$k_i u_i^R(\underset{\sim}{k}) = k_i u_i^I(\underset{\sim}{k}) = 0 \tag{512}$$

The energy spectrum tensor becomes

$$E_{ij}(\underset{\sim}{k}) = [u_i^R(\underset{\sim}{k})u_j^R(\underset{\sim}{k}) + u_i^I(\underset{\sim}{k})u_j^I(\underset{\sim}{k})] + i\,[u_i^I(\underset{\sim}{k})u_j^R(\underset{\sim}{k}) - u_i^R(\underset{\sim}{k})u_j^I(\underset{\sim}{k})] \tag{513}$$

By using the identity

$$E_{ii}(\underset{\sim}{k}) = u_i(\underset{\sim}{k})u_i(-\underset{\sim}{k}) = u_i^R(\underset{\sim}{k})^2 + u_i^I(\underset{\sim}{k})^2 \tag{514}$$

the energy spectrum function, energy content, and longitudinal correlation function, integral scale, and microscale can be calculated directly from the real and imaginary Fourier velocity components using the expressions derived previously.

Calculation of the Stream Function

In two dimensions, the stream function exists and is defined by

$$v_1(\underset{\sim}{x}) = \frac{\partial \Psi(\underset{\sim}{x})}{\partial x_2}, \quad v_2(\underset{\sim}{x}) = -\frac{\partial \Psi(\underset{\sim}{x})}{\partial x_1} \tag{515,2D}$$

Taking the Fourier transform of Equation 515 gives

$$\Psi(\underset{\sim}{k}) = -i\, u_1(\underset{\sim}{k})/k_2 = i\, u_2(\underset{\sim}{k})/k_1 \tag{516,2D}$$

where $\Psi(\underset{\sim}{k}) \equiv F[\Psi(\underset{\sim}{x})]$. The right hand equality in Equation

516 simply reproduces the continuity condition. In terms of real and imaginary parts, Equation 516 becomes

$$\Psi^R(\underset{\sim}{k}) = u_1^I(\underset{\sim}{k})/k_2 = -u_2^I(\underset{\sim}{k})/k_1 \qquad (517,2D)$$

$$\Psi^I(\underset{\sim}{k}) = -u_1^R(\underset{\sim}{k})/k_2 = u_2^R(\underset{\sim}{k})/k_1 \qquad (518,2D)$$

The physical-space stream function is found using the inverse Fourier transform

$$\Psi(\underset{\sim}{x}) = \sum_{\underset{\sim}{k}} [\Psi^R(\underset{\sim}{k})\cos(\underset{\sim}{k}\cdot\underset{\sim}{x}) - \Psi^I(\underset{\sim}{k})\sin(\underset{\sim}{k}\cdot\underset{\sim}{x})] \qquad (519,2D)$$

Substituting in Equations 508 and 509 gives the final expression

$$\Psi(\underset{\sim}{x}) = \sum_{k_1} \sum_{k_2 \neq 0} [u_1^I(\underset{\sim}{k})\cos(\underset{\sim}{k}\cdot\underset{\sim}{x}) + u_1^R(\underset{\sim}{k})\sin(\underset{\sim}{k}\cdot\underset{\sim}{x})]/k_2 \qquad (520,2D)$$

$$- \sum_{\substack{k_1 \neq 0 \\ k_2 = 0}} [u_2^I(\underset{\sim}{k})\cos(\underset{\sim}{k}\cdot\underset{\sim}{x}) + u_2^R(\underset{\sim}{k})\sin(\underset{\sim}{k}\cdot\underset{\sim}{x})]/k_1 + \Psi(\underset{\sim}{0})$$

The physical-space velocity field is found using Equation 504. The fluctuation in velocity over time can be obtained in simple manner at the single point $\underset{\sim}{x} = \underset{\sim}{0}$, since Equation 504 reduces to

$$v_i(\underset{\sim}{0},t) = \sum_{\underset{\sim}{k}} u_i^R(\underset{\sim}{k},t) \qquad (521)$$

Numerical Calculation Considerations

Truncation of the infinite system of equations

Equations 511 involve an infinite system of equations that clearly cannot be implemented on a finite computer. In the Fourier transformed Navier-Stokes equation, a natural truncation of the system is to cut off artificially all wave number summations of the type in Equations 511. Such a cutoff would result if the viscosity acting on modes above the cutoff were allowed to become infinite. An asymptotic ordering argument (101) indicates that modes subject to such a viscosity are indeed cut off - in effect, they can never be excited. A finite set of ordinary differential equations for a finite set of dynamical quantities is therefore obtained by setting $u_i^R(\underset{\sim}{k}) = u_i^I(\underset{\sim}{k}) \equiv 0$ for $|\underset{\sim}{k}| > k_{max}$, where k_{max} is the cutoff wave number. The dynamical quantities retained in the simulation are $u_i(\underset{\sim}{k})$ for $|\underset{\sim}{k}| \leq k_{max}$. This truncation is clearly the most natural for isotropic turbulence.

Assignment of flow initial conditions

The principal requirements or constraints placed on the initial values of the Fourier velocity modes are that they give the desired energy spectrum and obey the continuity equation. In three dimensions, these constraints can be expressed in terms of the real and imaginary parts of the velocity modes as the system of equations

$$u_1^R(\underset{\sim}{k},0)^2 + u_1^I(\underset{\sim}{k},0)^2 = P_{11}(\underset{\sim}{k})E(k,0)_d/\eta(k) \qquad (522,3D)$$

$$u_2^R(\underset{\sim}{k},0)^2 + u_2^I(\underset{\sim}{k},0)^2 = P_{22}(\underset{\sim}{k})E(k,0)_d/\eta(k) \qquad (523,3D)$$

$$u_3^R(\underset{\sim}{k},0)^2 + u_3^I(\underset{\sim}{k},0)^2 = P_{33}(\underset{\sim}{k})E(k,0)_d/\eta(k) \qquad (524,3D)$$

$$k_1u_1^R(\underset{\sim}{k},0) + k_2u_2^R(\underset{\sim}{k},0) + k_3u_3^R(\underset{\sim}{k},0) = 0 \qquad (525,3D)$$

$$k_1u_1^I(\underset{\sim}{k},0) + k_2u_2^I(\underset{\sim}{k},0) + k_3u_3^I(\underset{\sim}{k},0) = 0 \qquad (526,3D)$$

This system of six variables and five independent equations leaves one degree of freedom with which an ensemble of initial flows can be created, each obeying continuity and having the same energy spectrum. Notice that Equations 522 - 524 indicate that values of $u_i^R(\underset{\sim}{k},0)$ and $u_i^I(\underset{\sim}{k},0)$ always lie on a circle of radius $[P_{ii}(\underset{\sim}{k})E(k,0)_d/\eta(k)]^{\frac{1}{2}}$ (no summation over i) in $u_i^R(\underset{\sim}{k})$, $u_i^I(\underset{\sim}{k})$-space. Since there is one degree of freedom available, one of the six variables must be specified arbitrarily. Therefore, values of $u_1^R(\underset{\sim}{k},0)$ and $u_1^I(\underset{\sim}{k},0)$ will be determined by random selection of a point on the circle determined by Equation 522. This leaves the system of Equations 523 - 526 to be solved simultaneously for the variables $u_2^R(\underset{\sim}{k},0)$, $u_2^I(\underset{\sim}{k},0)$, $u_3^R(\underset{\sim}{k},0)$, and $u_3^I(\underset{\sim}{k},0)$. The solution of this system is (for $k_2 = k_3 \neq 0$)

$\underline{k_2 = k_3 \neq 0}$

$$u_2^R(\underset{\sim}{k},0) = [-k_1k_2u_1^R(\underset{\sim}{k},0) \pm kk_3u_1^I(\underset{\sim}{k},0)]/(k^2 - k_1^2) \quad (527,3D)$$

$$u_2^I(\underset{\sim}{k},0) = [-k_1k_2u_1^I(\underset{\sim}{k},0) \mp kk_3u_1^R(\underset{\sim}{k},0)]/(k^2 - k_1^2) \quad (528,3D)$$

$$u_3^R(\underset{\sim}{k},0) = [-k_1k_3u_1^R(\underset{\sim}{k},0) \mp kk_2u_1^I(\underset{\sim}{k},0)]/(k^2 - k_1^2) \quad (529,3D)$$

$$u_3^I(\underset{\sim}{k},0) = [-k_1k_3u_1^I(\underset{\sim}{k},0) \pm kk_2u_1^R(\underset{\sim}{k},0)]/(k^2 - k_1^2) \quad (530,3D)$$

The special solution for the cases $k_2 = k_3 = 0$ (k_1-axis) is found by rotating indices ($1 \rightarrow 2$, $2 \rightarrow 3$, $3 \rightarrow 1$) in the previous solution and simplifying,

$\underline{k_2 = k_3 = 0,\ k_1 \neq 0}$

$$u_2^R(\underset{\sim}{k},0)^2 + u_2^I(\underset{\sim}{k},0)^2 = E(k,0)_d/\eta(k) \quad (531,3D)$$

$$u_3^R(\underset{\sim}{k},0) = \pm u_2^I(\underset{\sim}{k},0),\ u_3^I(\underset{\sim}{k},0) = \mp u_2^R(\underset{\sim}{k},0) \quad (532,3D)$$

$$u_1^R(\underset{\sim}{k},0) = u_1^I(\underset{\sim}{k},0) = 0 \quad (533,3D)$$

$\underline{k_1 = k_2 = k_3 = 0}$

$$u_1^R(\underset{\sim}{0},0) = u_1^I(\underset{\sim}{0},0) = 0 \quad (534,3D)$$

In this case, $u_2^R(\underset{\sim}{k},0)$ and $u_2^I(\underset{\sim}{k},0)$ are chosen arbitrarily from the circle determined by Equation 531.

In two dimensions, the system of independent constraint equations is

$$u_1^R(\underset{\sim}{k},0)^2 + u_1^I(\underset{\sim}{k},0)^2 = 2P_{11}(\underset{\sim}{k})E(k,0)_d/\eta(k) \qquad (535,2D)$$

$$k_1 u_1^R(\underset{\sim}{k},0) + k_2 u_2^R(\underset{\sim}{k},0) = 0 \qquad (536,2D)$$

$$k_1 u_1^I(\underset{\sim}{k},0) + k_2 u_2^I(\underset{\sim}{k},0) = 0 \qquad (537,2D)$$

The fourth constraint equation

$$u_2^R(\underset{\sim}{k},0)^2 + u_2^I(\underset{\sim}{k},0)^2 = 2P_{22}(\underset{\sim}{k})E(k,0)_d/\eta(k) \qquad (538,2D)$$

is not independent of the first three. This system of four variables and three independent equations also leaves one degree of freedom with which an ensemble of initial flows can be created, each obeying continuity and having the same energy spectrum. Solution of this system of equations is trivial,

$\underline{k_2 \neq 0}$

$$u_1^R(\underset{\sim}{k},0)^2 + u_1^I(\underset{\sim}{k},0)^2 = 2(1 - k_1^2/k^2)E(k,0)_d/\eta(k) \qquad (539,2D)$$

$$u_2^R(\underset{\sim}{k},0) = -k_1 u_1^R(\underset{\sim}{k},0)/k_2 \qquad (540,2D)$$

$$u_2^I(\underset{\sim}{k},0) = -k_1 u_1^I(\underset{\sim}{k},0)/k_2 \qquad (541,2D)$$

$\underline{k_2 = 0,\ k_1 \neq 0}$

$$u_2^R(\underset{\sim}{k},0)^2 + u_2^I(\underset{\sim}{k},0)^2 = 2E(k,0)_d/\eta(k) \qquad (542,2D)$$

$$u_1^R(\underset{\sim}{k},0) = u_1^I(\underset{\sim}{k},0) = 0 \qquad (543,2D)$$

$k_1 = k_2 = 0$

$$u_i^R(\underset{\sim}{0},0) = u_i^I(\underset{\sim}{0},0) = 0 \qquad (544,2D)$$

For $k_2 \neq 0$, $u_1^R(\underset{\sim}{k},0)$ and $u_1^I(\underset{\sim}{k},0)$ are chosen arbitrarily from the circle determined by Equation 539; for $k_2 = 0$, $u_2^R(\underset{\sim}{k},0)$ and $u_2^I(\underset{\sim}{k},0)$ are chosen arbitrarily from the circle determined by Equation 542.

Generation of the Random Convection Velocity

Constraint equations

It is desirable for the random convection velocity $\phi_i(\underset{\sim}{k},t)$ to obey continuity and to have a constant energy spectrum, and hence a constant fluctuation intensity $\tilde{\phi}(t)$, over time. The constraint equations that result from continuity and assignment of an energy spectrum are the same as Equations 522 - 526 and 535 - 537 with $\phi_i^R(\underset{\sim}{k},t)$, $\phi_i^I(\underset{\sim}{k},t)$, and $E(k)_{d\phi}$ replacing $u_i^R(\underset{\sim}{k},0)$, $u_i^I(\underset{\sim}{k},0)$, and $E(k,0)_d$, respectively. In three dimensions, the corresponding solution of the constraint equations over time is

$k_2 = k_3 \neq 0$

$$\phi_1^R(\underset{\sim}{k},t)^2 + \phi_1^I(\underset{\sim}{k},t)^2 = (1 - k_1^2/k^2)E(k)_{d\phi}/\eta(k) \qquad (545,3D)$$

$$\phi_2^R(\underset{\sim}{k},t) = [-k_1k_2\phi_1^R(\underset{\sim}{k},t) \pm kk_3\phi_1^I(\underset{\sim}{k},t)]/(k^2 - k_1^2) \qquad (546,3D)$$

$$\phi_2^I(\underset{\sim}{k},t) = [-k_1k_2\phi_1^I(\underset{\sim}{k},t) \mp kk_3\phi_1^I(\underset{\sim}{k},t)]/(k^2 - k_1^2) \qquad (547,3D)$$

$$\phi_3^R(\underset{\sim}{k},t) = [-k_1k_3\phi_1^R(\underset{\sim}{k},t) \mp kk_2\phi_1^I(\underset{\sim}{k},t)]/(k^2 - k_1^2) \quad (548,3D)$$

$$\phi_3^I(\underset{\sim}{k},t) = [-k_1k_3\phi_1^I(\underset{\sim}{k},t) \pm kk_2\phi_1^R(\underset{\sim}{k},t)]/(k^2 - k_1^2) \quad (549,3D)$$

$\underline{k_2 = k_3 = 0,\ k_1 \neq 0}$

$$\phi_2^R(\underset{\sim}{k},t)^2 + \phi_2^I(\underset{\sim}{k},t)^2 = E(k)_{d\phi}/\eta(k) \quad (550,3D)$$

$$\phi_3^R(\underset{\sim}{k},t) = \pm \phi_2^I(\underset{\sim}{k},t),\ \phi_3^I(\underset{\sim}{k},t) = \mp \phi_2^R(\underset{\sim}{k},t) \quad (551,3D)$$

$$\phi_1^R(\underset{\sim}{k},t) = \phi_1^I(\underset{\sim}{k},t) = 0 \quad (552,3D)$$

$\underline{k_1 = k_2 = k_3 = 0}$

$$\phi_i^R(\underset{\sim}{0},t) = \phi_i^I(\underset{\sim}{0},t) = 0 \quad (553,3D)$$

For $k_2 = k_3 \neq 0$, values of $\phi_1^R(\underset{\sim}{k},t)$ and $\phi_1^I(\underset{\sim}{k},t)$ will be generated over time by a point making a random walk on the circle determined by Equation 545 in $\phi_1^R(\underset{\sim}{k})$, $\phi_1^I(\underset{\sim}{k})$ - space; for $k_2 = k_3 = 0$, $k_1 \neq 0$, values of $\phi_2^R(\underset{\sim}{k},t)$ and $\phi_2^I(\underset{\sim}{k},t)$ will be similarly generated using Equation 550.

In two dimensions, we have

$\underline{k_2 \neq 0}$

$$\phi_1^R(\underset{\sim}{k},t)^2 + \phi_1^I(\underset{\sim}{k},t)^2 = 2(1 - k_1^2/k^2)E(k)_{d\phi}/\eta(k) \quad (554,2D)$$

$$\phi_2^R(\underset{\sim}{k},t) = -k_1\phi_1^R(\underset{\sim}{k},t)/k_2 \quad (555,2D)$$

$$\phi_2^I(\underset{\sim}{k},t) = -k_1\phi_1^I(\underset{\sim}{k},t)/k_2 \quad (556,2D)$$

$\underline{k_2 = 0,\ k_1 \neq 0}$

$$\phi_2^R(\underset{\sim}{k},t)^2 + \phi_2^I(\underset{\sim}{k},t)^2 = 2E(k)_{d\phi}/\eta(k) \qquad (557,2D)$$

$$\phi_1^R(\underset{\sim}{k},t) = \phi_1^I(\underset{\sim}{k},t) = 0 \qquad (558,2D)$$

$\underline{k_1 = k_2 = 0}$

$$\phi_i^R(\underset{\sim}{0},t) = \phi_i^I(\underset{\sim}{0},t) = 0 \qquad (559,2D)$$

Values of $\phi_1^R(\underset{\sim}{k},t)$ and $\phi_1^I(\underset{\sim}{k},t)$ (for $k_2 \neq 0$) are generated using Equation 554 by the same random walk method used in three dimensions; for $k_2 = 0$, values of $\phi_2^R(\underset{\sim}{k},t)$ and $\phi_2^I(\underset{\sim}{k},t)$ are similarly generated using Equation 557.

Random walk on a circle

The location of a point making a random walk on a circle given by

$$\phi_1^R(\underset{\sim}{k},t)^2 + \phi_1^I(\underset{\sim}{k},t)^2 = (4 - \delta_{nn})P_{11}(\underset{\sim}{k})E(k)_{d\phi}/\eta(k) \equiv R(k)^2 \qquad (560)$$

in $\phi_1^R(\underset{\sim}{k})$, $\phi_1^I(\underset{\sim}{k})$ - space is given by its angular coordinate $\theta(\underset{\sim}{k},t)$. From this it follows that

$$\phi_1^R(\underset{\sim}{k},t) = R(k)\cos\theta(\underset{\sim}{k},t),\ \phi_1^I(\underset{\sim}{k},t) = R(k)\sin\theta(\underset{\sim}{k},t) \qquad (561)$$

A random walk in $\theta(\underset{\sim}{k},t)$ that exhibits inertia and temporal continuity can be generated as the second-order response to the integral of the random step forcing function $s(t,T_{so})$

$$\tau^2 \frac{d^2\theta}{dt^2} + 2\tau\zeta \frac{d\theta}{dt} + \theta = 2\pi S(t,T_{so}) \tag{562}$$

$$S(t,T_{so}) = A\int_0^t s(t,T_{so})dt \tag{563}$$

$$\tau \equiv \tau^* \tilde{v}^*_\emptyset / L^*_{f\emptyset},\ t \equiv t^* \tilde{v}^*_\emptyset / L^*_{f\emptyset},\ A \equiv A^* L^*_{f\emptyset} / \tilde{v}^*_\emptyset,\ T_{so} \equiv T^*_{so} \tilde{v}^*_\emptyset / L^*_{f\emptyset} \tag{564}$$

The random step function $s(t,T_{so})$ is generated by successively choosing random numbers from a uniform distribution having the range $-0.5 \leq s \leq 0.5$. A is a scaling constant. The duration of each individual step T_s is chosen successively from a Poisson distribution of characteristic period T_{so}. From Equation 563, the value of $S(t,T_{so})$ in the $j+1$ period is given from the value in the jth period by

$$S_{j+1} = S_j + a s_{j+1} \tag{565}$$

where a is a scaling constant. Each step generated has an equal probability of being in the forward or backward direction along the circle and the magnitude and direction of each step is independent of prior step history. Over time the random walk shows equal preference for all locations on the circle; the time average of $S(t,T_{so})$ depends explicitly on the averaging interval used and so infinite time averages of S and θ do not exist.

A random walk needs to be generated for each value of

$\underset{\sim}{k}$ and values of τ, the time constant of the response, must be assigned accordingly. The value of T_{so} will be assigned as being proportional to τ. The value of ζ, the dampening ratio of the second-order response, can be used to control the time-smoothness of the response and will be assigned a constant value for all $\underset{\sim}{k}$.

The value of τ is to be associated with the local convection time of the turbulence. The square-root of the energy spectrum, $E(k)_d^{\frac{1}{2}}$, is a measure of the local velocity; this can be combined with a measure of the local length scale to get a local time. One measure of the local length scale is the inverse wave number, k^{-1}; this gives

$$\tau_k = \tau_k^* \tilde{v}_\emptyset^* / L_{f\emptyset}^* = B/kE(k)_d^{\frac{1}{2}} \qquad (566)$$

where B is a constant of proportionality which must be assigned. τ_k decreases with wave number as k increases from zero, but passes through a minimum and increases for large k; it is valid in the low wave number range (energy containing eddies) but not for large wave numbers.

Another local length scale can be defined using the longitudinal integral scale. $L_f(t)$ is found by summing over all wave numbers using

$$L_f(t) = (\pi/2\tilde{v}^2) \sum_k k^{-1} E(k)_d \equiv \sum_k L_f(k) \qquad (567,3D)$$

$$L_f(t) = (2/\tilde{v}^2) \sum_k k^{-1} E(k)_d \equiv \sum_k L_f(k) \qquad (568,2D)$$

Therefore, it can also be imagined that $L_f(t)$ is equal to a sum of local length scales, which are given by

$$L_f(k) = \pi E(k)_d / 2\tilde{v}^2 k \qquad (569,3D)$$

$$L_f(k) = 2E(k)_d / \tilde{v}^2 k \qquad (570,2D)$$

Using this gives

$$\gamma_f = B_f \pi E(k)_d^{\frac{1}{2}} / 2\tilde{v}^2 k \qquad (571,3D)$$

$$\gamma_f = B_f 2E(k)_d^{\frac{1}{2}} / \tilde{v}^2 k \qquad (572,2D)$$

where B_f is a constant of proportionality. After passing through a maximum at small wave numbers, γ_f falls off for large wave numbers; it behaves properly at large wave numbers but not at small wave numbers.

By matching the wave number dependence of γ_k and γ_f at intermediate wave numbers, we can get an expression for γ that behaves properly for all wave numbers. For a smooth matching of γ_k and γ_f, it is necessary to find the value of the wave number k_o at which

$$\gamma_k = \gamma_f \text{ and } \frac{d\gamma_k}{dk} = \frac{d\gamma_f}{dk} \qquad (573)$$

From the first requirement, we get

$$B = B_f \pi E(k_o)_d / 2\tilde{v}^2 \qquad (574,3D)$$

$$B = B_f 2E(k_o)_d / \tilde{v}^2 \qquad (575,2D)$$

Using this, the second requirement gives the condition

$$\left(\frac{dE(k)_d}{dk}\right)_{k_o} = 0 \qquad (576)$$

Smooth matching of γ_k and γ_f occurs at the wave number k_o that corresponds to the maximum in the energy spectrum $E(k)_d$. Therefore, γ is given by

$$\gamma = (B_f \pi/2\tilde{v}^2 k)\ E(k_o)_d/E(k)_d^{\frac{1}{2}} \quad \text{for } k \leq k_o \qquad (577,3D)$$

$$\gamma = (B_f 2/\tilde{v}^2 k)\ E(k_o)_d/E(k)_d^{\frac{1}{2}} \quad \text{for } k \leq k_o \qquad (578,2D)$$

$$\gamma = (B_f \pi/2\tilde{v}^2 k)\ E(k)_d^{\frac{1}{2}} \quad \text{for } k \geq k_o \qquad (579,3D)$$

$$\gamma = (B_f 2/\tilde{v}^2 k)\ E(k)_d^{\frac{1}{2}} \quad \text{for } k \geq k_o \qquad (580,2D)$$

The proportionality constant B_f must be assigned in some manner.

Self-consistency requirements

The velocity field equations that have been developed have been made dimensionless using the reference velocity $\tilde{v}^*_\phi$ and reference length $L^*_{f\phi}$, quantities that have not yet been defined. Since the energy spectrum and fluctuation intensity of the random convection velocity ϕ_i are held constant in time, let $\tilde{v}^*_\phi$ be defined as the root-mean-square velocity fluctuation of ϕ_i and let $L^*_{f\phi}$ be defined as the longitudinal integral scale of ϕ_i. Two self-consistency requirements on the values of the random convection

velocity Fourier modes then follow from this assignment, namely that

$$\tilde{\phi}(t) \equiv \tilde{\phi}^*(t^*)/\tilde{v}^*_\phi = 1 \tag{581}$$

$$L_{f\phi}(t) \equiv L^*_{f\phi}(t^*)/L^*_{f\phi} = 1 \tag{582}$$

The requirement of $\tilde{\phi}(t) = 1$ is satisfied by normalization of the energy spectrum of ϕ_i and hence proper normalization of the Fourier modes, as seen from

$$\begin{aligned} E_o &= \tfrac{1}{2}\,\delta_{nn}\tilde{\phi}(t)^2 \equiv \tfrac{1}{2}\delta_{nn} \equiv \sum_k E(k)_{d\phi} \\ &= \tfrac{1}{2}\sum_k \eta(k)E_{ii}(\underset{\sim}{k})_{d\phi} = \tfrac{1}{2}\sum_{\underset{\sim}{k}} E_{ii}(\underset{\sim}{k})_{d\phi} \\ &= \tfrac{1}{2}\sum_{\underset{\sim}{k}} \phi_i(\underset{\sim}{k})\phi_i(-\underset{\sim}{k}) = \tfrac{1}{2}\sum_{\underset{\sim}{k}} [\phi_i^R(\underset{\sim}{k},t)^2 + \phi_i^I(\underset{\sim}{k},t)^2] \end{aligned} \tag{583}$$

For the requirement of $L_{f\phi} = 1$ to be satisfied, it is necessary that

$$\begin{aligned} L_{f\phi}(t) = 1 &= (\pi/2)\sum_k k^{-1}E(k)_{d\phi} \\ &= (\pi/4)\sum_{\underset{\sim}{k}} k^{-1}[\phi_i^R(\underset{\sim}{k},t)^2 + \phi_i^I(\underset{\sim}{k},t)^2] \end{aligned} \tag{584,3D}$$

The values of the velocity modes, however, have already been fixed by normalization of the energy spectrum. The only variable left for adjustment is the as yet unspecified value of N in the dimensionless wave number $k_i \equiv 2\pi n_i/N$, which is the number of ϕ_i - field longitudinal integral scales equal

to the length of the repeating unit box of turbulence. Therefore, the required value of N is given by

$$8/N = 2\sum_{n} n^{-1}E(n)_{d\phi} = \sum_{n} n^{-1}[\phi_i^R(\underset{\sim}{n},t)^2 + \phi_i^I(\underset{\sim}{n},t)^2] \quad (585,3D)$$

$$2\pi/N = 2\sum_{n} n^{-1}E(n)_{d\phi} = \sum_{n} n^{-1}[\phi_i^R(\underset{\sim}{n},t)^2 + \phi_i^I(\underset{\sim}{n},t)^2] \quad (586,2D)$$

where $n^2 = n_i n_i$. By dimensional arguments, it can be shown that in any expression for the discrete energy spectrum, the wave number k always appears in ratio with some reference wave number k_{ref}, so that $k/k_{ref} = n/n_{ref}$ and N does not appear. Therefore, $E(k)_{d\phi}$ can be written equally well as $E(n)_{d\phi}$ in Equations 585 and 586. Likewise, the correspondence of $\phi_i(\underset{\sim}{k})$ with $\phi_i(\underset{\sim}{n})$ presents no problem.

Equations 585 and 586 can also be used to show that a lower limit exists for the value of N. Since

$$\sum_{k} E(k)_d = \sum_{n} E(n)_d = \tfrac{1}{2}\delta_{ii} \quad (587)$$

and $n^{-1}E(n)_d \leq E(n)_d$ because $n \geq 1$, it follows that

$$\sum_{n} n^{-1}E(n)_d \leq \tfrac{1}{2}\delta_{ii} \quad (588)$$

and hence

$$N \geq 8/3 \quad (589,3D)$$

$$N \geq \pi \quad (590,2D)$$

DEVELOPMENT OF THE CONCENTRATION FIELD EQUATIONS

In this section, Fourier-space quantities that describe the concentration fields of the reactants are developed, relations for calculating concentration field physical-space quantities from Fourier-space quantities are derived, and the Fourier transformed mass conservation equations of the reactants are formed.

Definitions of Quantities

The instantaneous concentration of the reacting species $C^*(\underset{\sim}{x}^*,t^*)$ can be written as the sum of the volume averaged concentration $\overline{C}^*(t^*)$ and instantaneous concentration fluctuation $c^*(\underset{\sim}{x}^*,t^*)$

$$C^*(\underset{\sim}{x}^*,t^*) = \overline{C}^*(t^*) + c^*(\underset{\sim}{x}^*,t^*) \tag{591}$$

Dimensionless concentrations will be defined using the initial average concentration $\overline{C}_0^* \equiv \overline{C}^*(0)$

$$C(\underset{\sim}{x},t) \equiv C^*(\underset{\sim}{x}^*,t^*)/\overline{C}_0^* \tag{592}$$

$$c(\underset{\sim}{x},t) \equiv c^*(\underset{\sim}{x}^*,t^*)/\overline{C}_0^* \tag{593}$$

$$\overline{C}(t) \equiv \overline{C}^*(t^*)/\overline{C}_0^*, \quad \overline{C}(0) \equiv 1 \tag{594}$$

and Equation 591 becomes

$$C(\underset{\sim}{x},t) = \overline{C}(t) + c(\underset{\sim}{x},t) \tag{595}$$

The Fourier transformed concentration is given by

$$\mathcal{C}(\underset{\sim}{k}) \equiv N^{-\delta_{nn}} \int_{\underset{\sim}{x}} C(\underset{\sim}{x}) \exp(-i\underset{\sim}{k}\cdot\underset{\sim}{x})d\underset{\sim}{x} \tag{596}$$

Taking the Fourier transform of Equation 595 gives

$$\mathcal{C}(\underset{\sim}{k}) = \bar{C} N^{-\delta_{nn}} \int_{\underset{\sim}{x}} \exp(-i\underset{\sim}{k}\cdot\underset{\sim}{x})d\underset{\sim}{x} + N^{-\delta_{nn}} \int_{\underset{\sim}{x}} c(\underset{\sim}{x})\exp(-i\underset{\sim}{k}\cdot\underset{\sim}{x})d\underset{\sim}{x} \tag{597}$$

but

$$\delta_{\underset{\sim}{k},\underset{\sim}{0}} = N^{-\delta_{nn}} \int_{\underset{\sim}{x}} \exp(-i\underset{\sim}{k}\cdot\underset{\sim}{x})d\underset{\sim}{x} \tag{598}$$

$$\mathcal{C}(\underset{\sim}{0}) = N^{-\delta_{nn}} \int_{\underset{\sim}{x}} C(\underset{\sim}{x}) \exp(-i\underset{\sim}{0}\cdot\underset{\sim}{x})d\underset{\sim}{x} = \bar{C} \tag{599}$$

and Equation 597 becomes

$$\mathcal{C}(\underset{\sim}{k}) - \mathcal{C}(\underset{\sim}{0})\delta_{\underset{\sim}{k},\underset{\sim}{0}} = \mathcal{c}(\underset{\sim}{k}) \equiv N^{-\delta_{nn}} \int_{\underset{\sim}{x}} c(\underset{\sim}{x}) \exp(-i\underset{\sim}{k}\cdot\underset{\sim}{x})d\underset{\sim}{x} \tag{600}$$

$$\mathcal{c}(\underset{\sim}{0}) = N^{-\delta_{nn}} \int_{\underset{\sim}{x}} c(\underset{\sim}{x}) \exp(-i\underset{\sim}{0}\cdot\underset{\sim}{x})d\underset{\sim}{x} = \bar{c}(\underset{\sim}{x}) \equiv 0 \tag{601}$$

The inverse transform is

$$C(\underset{\sim}{x}) = \sum_{\underset{\sim}{k}} \mathcal{C}(\underset{\sim}{k}) \exp(i\underset{\sim}{k}\cdot\underset{\sim}{x}) \tag{602}$$

Taking the inverse transform of

$$\mathcal{C}(\underset{\sim}{k}) = \mathcal{C}(\underset{\sim}{0})\delta_{\underset{\sim}{k},\underset{\sim}{0}} + \mathcal{c}(\underset{\sim}{k}) \tag{603}$$

gives

$$c(\underset{\sim}{x}) = \sum_{\underset{\sim}{k}} \mathcal{c}(\underset{\sim}{k}) \exp(i\underset{\sim}{k}\cdot\underset{\sim}{x}) \tag{604}$$

The integral approximation of the inverse transform is

$$c(\underset{\sim}{x}) = (N/2\pi)^{\delta_{nn}} \int_{\underset{\sim}{k}} \phi(\underset{\sim}{k}) \exp(i\underset{\sim}{k}\cdot\underset{\sim}{x})d\underset{\sim}{k} \tag{605}$$

The dimensionless concentration correlation function is

$$Q_{ss}(\underset{\sim}{r}) \equiv \overline{c(\underset{\sim}{x})c(\underset{\sim}{x}+\underset{\sim}{r})} \tag{606}$$

with Fourier transform

$$E_{ss}(\underset{\sim}{k}) \equiv N^{-\delta_{nn}} \int_{\underset{\sim}{r}} Q_{ss}(\underset{\sim}{r}) \exp(-i\underset{\sim}{k}\cdot\underset{\sim}{r})d\underset{\sim}{r} \tag{607}$$

The discrete and integral approximation forms of the inverse transform are

$$Q_{ss}(\underset{\sim}{r}) = \sum_{\underset{\sim}{k}} E_{ss}(\underset{\sim}{k})_d \exp(i\underset{\sim}{k}\cdot\underset{\sim}{r}) \tag{608}$$

$$Q_{ss}(\underset{\sim}{r}) = (N/2\pi)^{\delta_{nn}} \int_{\underset{\sim}{k}} E_{ss}(\underset{\sim}{k})_c \exp(i\underset{\sim}{k}\cdot\underset{\sim}{r})d\underset{\sim}{k} \tag{609}$$

The concentration correlation coefficient can be expressed in terms of dimensionless quantities as

$$f_s(r,t) = \overline{c(\underset{\sim}{x})c(\underset{\sim}{x}+\underset{\sim}{r})}/\tilde{c}(t)^2 \tag{610}$$

where $\tilde{c}(t)$ is the root-mean-square concentration fluctuation. A dimensionless concentration integral scale and microscale are defined by

$$L_s(t) = \int_0^{\infty} f_s(r,t)dr \tag{611}$$

$$2/\lambda_s(t)^2 = -\left(\frac{\partial^2 f_s(r)}{\partial r^2}\right)_{r=0} \tag{612}$$

$$L_s(t) \equiv L_s^*(t^*)/L_{f\emptyset}^*, \quad \lambda_s(t) \equiv \lambda_s^*(t^*)/L_{f\emptyset}^*$$

The concentration spectrum function is usually defined as a continuous function and normalized by integration

$$\tilde{c}(t)^2 = \int_0^\infty E_s(k)_c dk \tag{613}$$

$$E_s(k)_c \equiv E_s^*(k^*)_c/L_{f\emptyset}^* \bar{c}_0^2$$

The relationship between $E_{ss}(\underset{\sim}{k})_c$ and $E_s(k)_c$ can be established from

$$\tilde{c}(t)^2 = \overline{c(\underset{\sim}{x})c(\underset{\sim}{x})} = Q_{ss}(\underset{\sim}{0}) = (N/2\pi)^3 \int_{\underset{\sim}{k}} E_{ss}(\underset{\sim}{k})_c d\underset{\sim}{k}$$
$$= (N/2\pi)^3 \int_0^\infty 4\pi k^2 E_{ss}(\underset{\sim}{k})_c dk = \int_0^\infty E_s(k)_c dk \tag{614,3D}$$

in three dimensions and

$$\tilde{c}(t)^2 = (N/2\pi)^2 \int_{\underset{\sim}{k}} E_{ss}(\underset{\sim}{k})_c d\underset{\sim}{k}$$
$$= (N/2\pi)^2 \int_0^\infty 2\pi k\, E_{ss}(\underset{\sim}{k})_c dk = \int_0^\infty E_s(k)_c dk \tag{615,2D}$$

in two dimensions, which gives

$$E_s(k)_c = (N/2\pi)^3\, 4\pi k^2 E_{ss}(\underset{\sim}{k})_c \tag{616,3D}$$

$$E_s(k)_c = (N/2\pi)^2\, 2\pi k\, E_{ss}(\underset{\sim}{k})_c \tag{617,2D}$$

As with the velocity field, it is useful to define a discrete concentration spectrum function $E_s(k)_d$ that is normalized by summation over the discrete values of k

$$\tilde{c}(t)^2 = \sum_k E_s(k)_d \tag{618}$$

The relationship between $E_{ss}(\underset{\sim}{k})_d$ and $E_s(k)_d$ can be established from

$$\tilde{c}(t)^2 = Q_{ss}(\underset{\sim}{0}) = \sum_{\underset{\sim}{k}} E_{ss}(\underset{\sim}{k})_d = \sum_k \eta(k) E_{ss}(\underset{\sim}{k})_d = \sum_k E_s(k)_d \tag{619}$$

which gives

$$E_s(k)_d = \eta(k) E_{ss}(\underset{\sim}{k})_d \tag{620}$$

Calculation of the Concentration Spectrum

An expression for calculating $E_{ss}(\underset{\sim}{k})$ directly from the Fourier concentration modes can be found following the procedure used to find $E_{ij}(\underset{\sim}{k})$ in the velocity field section. From the definition of $\phi(\underset{\sim}{k})$, it follows that

$$\phi(\underset{\sim}{k})\phi(\underset{\sim}{k}') = N^{-2\delta_{nn}} \int_{\underset{\sim}{x}} \int_{\underset{\sim}{x}'} c(\underset{\sim}{x})c(\underset{\sim}{x}') \exp[-i(\underset{\sim}{k}\cdot\underset{\sim}{x} + \underset{\sim}{k}'\cdot\underset{\sim}{x}')] d\underset{\sim}{x}\, d\underset{\sim}{x}' \tag{621}$$

Letting $\underset{\sim}{r} = \underset{\sim}{x} - \underset{\sim}{x}'$, we get

$$\phi(\underset{\sim}{k})\phi(\underset{\sim}{k}') = N^{-2\delta_{nn}} \int_{\underset{\sim}{r}} \int_{\underset{\sim}{x}'} c(\underset{\sim}{x}' + \underset{\sim}{r})c(\underset{\sim}{x}')\exp[-i(\underset{\sim}{k} + \underset{\sim}{k}')\cdot\underset{\sim}{x}'] d\underset{\sim}{x}' \exp(-i\underset{\sim}{k}\cdot\underset{\sim}{r}) d\underset{\sim}{r} \tag{622}$$

In order for the integral over $\underset{\sim}{x}'$ to become a volume average, the condition $\underset{\sim}{k} + \underset{\sim}{k}' = \underset{\sim}{0}$ must be imposed, giving

$$\begin{aligned} \phi(\underset{\sim}{k})\phi(-\underset{\sim}{k}) &= N^{-\delta_{nn}} \int_{\underset{\sim}{r}} N^{-\delta_{nn}} \int_{\underset{\sim}{x}'} c(\underset{\sim}{x}' + \underset{\sim}{r})c(\underset{\sim}{x}')d\underset{\sim}{x}' \exp(-i\underset{\sim}{k}\cdot\underset{\sim}{r})d\underset{\sim}{r} \\ &= N^{-\delta_{nn}} \int_{\underset{\sim}{r}} Q_{ss}(\underset{\sim}{r})\exp(-i\underset{\sim}{k}\cdot\underset{\sim}{r})d\underset{\sim}{r} = E_{ss}(\underset{\sim}{k}) \end{aligned} \tag{623}$$

Hence,

$$E_{ss}(\underset{\sim}{k}) = \phi(\underset{\sim}{k})\phi(-\underset{\sim}{k}) \tag{624}$$

Using Equations 616 and 617 gives the continuous concentration spectrum function

$$E_s(k)_c = (N/2\pi)^3 \, 4\pi k^2 \, \phi(\underset{\sim}{k})\phi(-\underset{\sim}{k}) \tag{625,3D}$$

$$E_s(k)_c = (N/2\pi)^2 \, 2\pi k \, \phi(\underset{\sim}{k})\phi(-\underset{\sim}{k}) \tag{626,2D}$$

and using Equation 620 gives the discrete concentration spectrum function

$$E_s(k)_d = \eta(k) \, \phi(\underset{\sim}{k})\phi(-\underset{\sim}{k}) \tag{627}$$

Summing Equation 627 over the discrete values of k and using the definition of $\eta(k)$ gives the concentration fluctuation intensity

$$\tilde{c}(t)^2 = \overline{c(\underset{\sim}{x})c(\underset{\sim}{x})} = \sum_{\underset{\sim}{k}} \phi(\underset{\sim}{k})\phi(-\underset{\sim}{k}) = \sum_{\underset{\sim}{k}} E_{ss}(\underset{\sim}{k})_d \tag{628}$$

With two species reactions, the single-point correlation between the fluctuations of reactants A and B is also

of interest. From the inverse Fourier transform of $\phi(\underset{\sim}{k})$ we get

$$c_A(\underset{\sim}{x})c_B(\underset{\sim}{x}) = \sum_{\underset{\sim}{k}} \sum_{\underset{\sim}{k}'} \phi_A(\underset{\sim}{k})\phi_B(\underset{\sim}{k}')\exp[i(\underset{\sim}{k} + \underset{\sim}{k}')\cdot\underset{\sim}{x}] \quad (629)$$

Volume averaging both sides gives

$$\overline{c_A(\underset{\sim}{x})c_B(\underset{\sim}{x})} = \sum_{\underset{\sim}{k}} \sum_{\underset{\sim}{k}'} \phi_A(\underset{\sim}{k})\phi_B(\underset{\sim}{k}')\, N^{-\delta_{nn}} \int_{\underset{\sim}{x}} \exp[i(\underset{\sim}{k}+\underset{\sim}{k}')\cdot\underset{\sim}{x}]d\underset{\sim}{x} \quad (630)$$

$$= \sum_{\underset{\sim}{k}} \sum_{\underset{\sim}{k}'} \delta_{\underset{\sim}{k}+\underset{\sim}{k}',\underset{\sim}{0}}\, \phi_A(\underset{\sim}{k})\phi_B(\underset{\sim}{k}') = \sum_{\underset{\sim}{k}} \phi_A(\underset{\sim}{k})\phi_B(-\underset{\sim}{k})$$

Hence,

$$\overline{c_A c_B}(t) = \sum_{\underset{\sim}{k}} \phi_A(\underset{\sim}{k})\phi_B(-\underset{\sim}{k}) \equiv \sum_{k} E_{AB}(k)_d \quad (631)$$

$$E_{AB}(k)_d = \eta(k)\, \phi_A(\underset{\sim}{k})\phi_B(-\underset{\sim}{k}) \quad (632)$$

where $E_{AB}(k)_d$ is the joint fluctuation spectrum.

Calculation of the Concentration Integral Scale and Microscale

$Q_{ss}(r)$ can be related to $E_{ss}(k)_c$ by integrating out the angular dependence of the integral approximation of the inverse Fourier transform of $E_{ss}(\underset{\sim}{k})_c$, as given by Equation 609, with the result

$$Q_{ss}(r) = (N/2\pi)^3\, 4\pi \int_k k^2 E_{ss}(k)_c \frac{\sin(kr)}{kr}\, dk \quad (633,3D)$$

$$Q_{ss}(r) = (N/2\pi)^2\, 2\pi \int_k k\, E_{ss}(k)_c\, J_0(kr)\, dk \quad (634,2D)$$

Converting Equations 633 and 634 back to discrete form gives

$$Q_{ss}(r) = \sum_k \eta(k) E_{ss}(k)_d \frac{\sin(kr)}{kr} \qquad (635,3D)$$

$$Q_{ss}(r) = \sum_k \eta(k) E_{ss}(k)_d J_0(kr) \qquad (636,2D)$$

Using Equation 616 (617) converts Equation 633 (634) to

$$Q_{ss}(r) = \int_0^\infty E_s(k)_c \frac{\sin(kr)}{kr} dk \qquad (637,3D)$$

$$Q_{ss}(r) = \int_0^\infty E_s(k)_c J_0(kr)\, dk \qquad (638,2D)$$

and using Equation 620 converts Equations 635 and 636 to

$$Q_{ss}(r) = \sum_k E_s(k)_d \frac{\sin(kr)}{kr} \qquad (639,3D)$$

$$Q_{ss}(r) = \sum_k E_s(k)_d J_0(kr) \qquad (640,2D)$$

Substituting Equation 624 into Equations 635 and 636 and using the definition of $\eta(k)$ gives a relation for calculating $Q_{ss}(r)$ directly from the Fourier concentration modes

$$Q_{ss}(r) = \tilde{c}^2 f_s(r) = \sum_{\underset{\sim}{k}} \phi(\underset{\sim}{k})\phi(-\underset{\sim}{k}) \frac{\sin(kr)}{kr} \qquad (641,3D)$$

$$Q_{ss}(r) = \tilde{c}^2 f_s(r) = \sum_{\underset{\sim}{k}} \phi(\underset{\sim}{k})\phi(-\underset{\sim}{k}) J_0(kr) \qquad (642,2D)$$

Similarly, integrating out the angular dependence of the Fourier transform of $Q_{ss}(\underset{\sim}{r})$ gives the inverse relations

$$E_{ss}(k) = (4\pi/N^3) \int_0^\infty r^2 Q_{ss}(r) \frac{\sin(kr)}{kr} dr \qquad (643,3D)$$

$$E_{ss}(k) = (2\pi/N^2) \int_0^\infty r\, Q_{ss}(r)\, J_0(kr)\, dr \qquad (644,2D)$$

Using Equations 606, 610, 616, and 617 gives

$$E_s(k)_c = (2\tilde{c}^2/\pi) \int_0^\infty kr\, f_s(r) \sin(kr)\, dr \qquad (645,3D)$$

$$E_s(k)_c = \tilde{c}^2 \int_0^\infty kr\, f_s(r)\, J_0(kr)\, dr \qquad (646,2D)$$

The concentration integral scale has been defined by Equation 611. Using the definition of $f_s(r)$, $L_s(t)$ follows directly from integration of Equations 637 - 642 over all r.

$$L_s(t) = (\pi/2\tilde{c}^2) \int_0^\infty k^{-1} E_s(k)_c dk \qquad (647,3D)$$

$$L_s(t) = (1/\tilde{c}^2) \int_0^\infty k^{-1} E_s(k)_c dk \qquad (648,2D)$$

$$L_s(t) = (\pi/2\tilde{c}^2) \sum_k k^{-1} E_s(k)_d \qquad (649,3D)$$

$$L_s(t) = (1/\tilde{c}^2) \sum_k k^{-1} E_s(k)_d \qquad (650,2D)$$

$$L_s(t) = (\pi/2\tilde{c}^2) \sum_{\underset{\sim}{k}} k^{-1} \phi(\underset{\sim}{k}) \phi(-\underset{\sim}{k}) \qquad (651,3D)$$

$$L_s(t) = (1/\tilde{c}^2) \sum_{\underset{\sim}{k}} k^{-1} \phi(\underset{\sim}{k}) \phi(-\underset{\sim}{k}) \qquad (652,2D)$$

The concentration microscale has been defined by Equation 612. Using the definition of $f_s(r)$, $\lambda_s(t)$ follows directly from differentiating Equations 637 - 642 twice with respect to r and taking the limit r = 0.

$$\lambda_s(t)^{-2} = (1/6\tilde{c}^2) \int_0^\infty k^2 E_s(k)_c dk \qquad (653,3D)$$

$$\lambda_s(t)^{-2} = (1/4\tilde{c}^2) \int_0^\infty k^2 E_s(k)_c dk \qquad (654,2D)$$

$$\lambda_s(t)^{-2} = (1/6\tilde{c}^2) \sum_k k^2 E_s(k)_d \qquad (655,3D)$$

$$\lambda_s(t)^{-2} = (1/4\tilde{c}^2) \sum_k k^2 E_s(k)_d \qquad (656,2D)$$

$$\lambda_s(t)^{-2} = (1/6\tilde{c}^2) \sum_{\tilde{k}} k^2 \, \phi(\tilde{k})\phi(-\tilde{k}) \qquad (657,3D)$$

$$\lambda_s(t)^{-2} = (1/4\tilde{c}^2) \sum_{\tilde{k}} k^2 \, \phi(\tilde{k})\phi(-\tilde{k}) \qquad (658,2D)$$

Concentration Field Expressions in Terms of Real and Imaginary Parts

Like the velocity, the Fourier transformed concentration is a complex variable and can be written in terms of real and imaginary parts as

$$\phi(\tilde{k}) = \phi^R(\tilde{k}) + i \, \phi^I(\tilde{k}) \qquad (659)$$

However, since $c(\tilde{x})$ is a real variable, the real and imaginary parts must obey

$$\phi^R(\underset{\sim}{k}) = \phi^R(-\underset{\sim}{k}), \quad \phi^I(\underset{\sim}{k}) = -\phi^I(-\underset{\sim}{k}) \tag{660}$$

This gives

$$E_{ss}(\underset{\sim}{k}) = \phi(\underset{\sim}{k})\phi(-\underset{\sim}{k}) = \phi^R(\underset{\sim}{k})^2 + \phi^I(\underset{\sim}{k})^2 \tag{661}$$

Using Equation 661, the concentration spectrum function, integral scale, microscale, and $f_s(r)$ can be calculated directly from the real and imaginary Fourier concentration modes. The physical space concentration field is found from

$$c(\underset{\sim}{x}) = \sum_{\underset{\sim}{k}} [\phi^R(\underset{\sim}{k})\cos(\underset{\sim}{k}\cdot\underset{\sim}{x}) - \phi^I(\underset{\sim}{k})\sin(\underset{\sim}{k}\cdot\underset{\sim}{x})] \tag{662}$$

The temporal fluctuation in concentration is easily obtained at the point $\underset{\sim}{x} = \underset{\sim}{0}$ since Equation 662 reduces to

$$c(\underset{\sim}{0},t) = \sum_{\underset{\sim}{k}} \phi^R(\underset{\sim}{k}) \tag{663}$$

Using Equation 662, isoconcentration lines can also be found.

Fourier Transformation of the Conservation Equation for a Single Component Second-Order Reaction

The conservation equation for a single component second-order reaction is

$$\frac{\partial C^*}{\partial t^*} + \frac{\partial(v_i^* C^*)}{\partial x_i^*} = D\frac{\partial^2 C^*}{\partial x_i^{*2}} - K\,C^{*2} \tag{664}$$

Using the reference length $L^*_{f\emptyset}$, reference velocity $\bar{v}^*_{\emptyset}$, and reference concentration $\bar{C}^*_0$, dimensionless variables can be

defined as

$$t \equiv t^{*}\tilde{v}^{*}_{\emptyset}/L^{*}_{f\emptyset},\ x_i \equiv x^{*}_i/L^{*}_{f\emptyset},\ v_i \equiv v^{*}_i/\tilde{v}^{*}_{\emptyset},\ C = C^{*}/\bar{C}^{*}_0 \qquad (665)$$

and the concentration equation can be made dimensionless

$$\frac{\partial C}{\partial t} + \frac{\partial (v_i C)}{\partial x_i} = Pe^{-1} \frac{\partial^2 C}{\partial x_i^2} - Da_I\, C^2 \qquad (666)$$

$$Pe = \tilde{v}^{*}_{\emptyset} L^{*}_{f\emptyset}/D = \text{turbulence Peclet number} \qquad (667)$$

$$Da_I = K\bar{C}^{*}_0 L^{*}_{f\emptyset}/\tilde{v}^{*}_{\emptyset} = \text{first Damköhler number} \qquad (668)$$

Taking the Fourier transform of Equation 666 gives

$$\frac{\partial \mathcal{C}(\underset{\sim}{k})}{\partial t} + ik_i \sum_{\underset{\sim}{p}} u_i(\underset{\sim}{p})\mathcal{C}(\underset{\sim}{k}-\underset{\sim}{p}) = -Pe^{-1} k^2 \mathcal{C}(\underset{\sim}{k}) - Da_I \sum_{\underset{\sim}{p}} \mathcal{C}(\underset{\sim}{p})\mathcal{C}(\underset{\sim}{k}-\underset{\sim}{p}) \qquad (669)$$

Substituting Equation 603 into Equation 669 gives

$$\begin{aligned} &\partial \mathcal{C}(\underset{\sim}{0})/\partial t\ \delta_{\underset{\sim}{k},\underset{\sim}{0}} + \partial c(\underset{\sim}{k})/\partial t + ik_i \sum_{\underset{\sim}{p}} u_i(\underset{\sim}{p})\mathcal{C}(\underset{\sim}{0})\ \delta_{\underset{\sim}{k}-\underset{\sim}{p},\underset{\sim}{0}} \\ &+ ik_i \sum_{\underset{\sim}{p}} u_i(\underset{\sim}{p}) c(\underset{\sim}{k}-\underset{\sim}{p}) + Pe^{-1} k^2 \mathcal{C}(\underset{\sim}{0})\ \delta_{\underset{\sim}{k},\underset{\sim}{0}} + Pe^{-1} k^2 c(\underset{\sim}{k}) \\ &= -Da_I \sum_{\underset{\sim}{p}} \mathcal{C}(\underset{\sim}{0})^2\ \delta_{\underset{\sim}{p},\underset{\sim}{0}}\ \delta_{\underset{\sim}{k}-\underset{\sim}{p},\underset{\sim}{0}} - Da_I \sum_{\underset{\sim}{p}} \mathcal{C}(\underset{\sim}{0}) c(\underset{\sim}{k}-\underset{\sim}{p})\ \delta_{\underset{\sim}{p},\underset{\sim}{0}} \\ &- Da_I \sum_{\underset{\sim}{p}} \mathcal{C}(\underset{\sim}{0}) c(\underset{\sim}{p})\ \delta_{\underset{\sim}{k}-\underset{\sim}{p},\underset{\sim}{0}} - Da_I \sum_{\underset{\sim}{p}} c(\underset{\sim}{p}) c(\underset{\sim}{k}-\underset{\sim}{p}) \end{aligned} \qquad (670)$$

However, with the simplifications

$$ik_i \sum_{\underset{\sim}{p}} u_i(\underset{\sim}{p})\mathcal{L}(\underset{\sim}{0})\delta_{\underset{\sim}{k}-\underset{\sim}{p},\underset{\sim}{0}} = ik_i u_i(\underset{\sim}{k})\mathcal{L}(\underset{\sim}{0}) = 0 \tag{671}$$

$$Pe^{-1}\, k^2 \mathcal{L}(\underset{\sim}{0})\delta_{\underset{\sim}{k},\underset{\sim}{0}} = 0 \tag{672}$$

$$-Da_I \sum_{\underset{\sim}{p}} \mathcal{L}(\underset{\sim}{0})^2 \delta_{\underset{\sim}{p},\underset{\sim}{0}}\delta_{\underset{\sim}{k}-\underset{\sim}{p},\underset{\sim}{0}} = -Da_I\, \mathcal{L}(\underset{\sim}{0})^2 \delta_{\underset{\sim}{k},\underset{\sim}{0}} \tag{673}$$

$$-Da_I \sum_{\underset{\sim}{p}} \mathcal{L}(\underset{\sim}{0})c(\underset{\sim}{k}-\underset{\sim}{p})\,\delta_{\underset{\sim}{p},\underset{\sim}{0}} = -Da_I\, \mathcal{L}(\underset{\sim}{0})c(\underset{\sim}{k}) \tag{674}$$

$$-Da_I \sum_{\underset{\sim}{p}} \mathcal{L}(\underset{\sim}{0})c(\underset{\sim}{p})\,\delta_{\underset{\sim}{k}-\underset{\sim}{p},\underset{\sim}{0}} = -Da_I\, \mathcal{L}(\underset{\sim}{0})c(\underset{\sim}{k}) \tag{675}$$

Equation 670 reduces to

$$\partial\mathcal{L}(\underset{\sim}{0})/\partial t\, \delta_{\underset{\sim}{k},\underset{\sim}{0}} + \partial c(\underset{\sim}{k})/\partial t + ik_i \sum_{\underset{\sim}{p}} u_i(\underset{\sim}{p})c(\underset{\sim}{k}-\underset{\sim}{p}) + Pe^{-1}\, k^2 c(\underset{\sim}{k}) \tag{676}$$

$$= -Da_I\, \mathcal{L}(\underset{\sim}{0})^2\, \delta_{\underset{\sim}{k},\underset{\sim}{0}} - 2Da_I\, \mathcal{L}(\underset{\sim}{0})c(\underset{\sim}{k}) - Da_I \sum_{\underset{\sim}{p}} c(\underset{\sim}{p})c(\underset{\sim}{k}-\underset{\sim}{p})$$

Separated into parts valid for $\underset{\sim}{k} = \underset{\sim}{0}$ and $\underset{\sim}{k} \neq \underset{\sim}{0}$, Equation 676 becomes

$\underline{\underset{\sim}{k} = \underset{\sim}{0}}$

$$\partial\mathcal{L}(\underset{\sim}{0})/\partial t = -Da_I\, \mathcal{L}(\underset{\sim}{0})^2 - Da_I \sum_{\underset{\sim}{p}} c(\underset{\sim}{p})c(-\underset{\sim}{p}) \tag{677}$$

$$c(\underset{\sim}{0}) = 0 \tag{678}$$

$\underset{\sim}{k} \neq \underset{\sim}{0}$

$$\partial \phi(\underset{\sim}{k})/\partial t + ik_i \sum_{\underset{\sim}{p}} u_i(\underset{\sim}{p})\phi(\underset{\sim}{k}-\underset{\sim}{p}) + Pe^{-1} k^2 \phi(\underset{\sim}{k}) = -2Da_I \mathcal{C}(\underset{\sim}{0})\phi(\underset{\sim}{k}) - Da_I \sum_{\underset{\sim}{p}} \phi(\underset{\sim}{p})\phi(\underset{\sim}{k}-\underset{\sim}{p}) \tag{679}$$

Subtracting $\delta_{\underset{\sim}{k},\underset{\sim}{0}}$ times Equation 677 from Equation 676 gives

$$\partial \phi(\underset{\sim}{k})/\partial t + ik_i \sum_{\underset{\sim}{p}} u_i(\underset{\sim}{p})\phi(\underset{\sim}{k}-\underset{\sim}{p}) + Pe^{-1} k^2 \phi(\underset{\sim}{k}) = -2Da_I \mathcal{C}(\underset{\sim}{0})\phi(\underset{\sim}{k}) - Da_I \sum_{\underset{\sim}{p}} \phi(\underset{\sim}{p})\phi(\underset{\sim}{k}-\underset{\sim}{p}) + \delta_{\underset{\sim}{k},\underset{\sim}{0}} Da_I \sum_{\underset{\sim}{p}} \phi(\underset{\sim}{p})\phi(-\underset{\sim}{p}) \tag{680}$$

Equation 680 reduces to Equation 679 for $\underset{\sim}{k} \neq \underset{\sim}{0}$ and reduces to zero for $\underset{\sim}{k} = \underset{\sim}{0}$. As a check on the consistency of the various forms of the fluctuation equation derived, it should be noted that Equation 676 results directly from taking the Fourier transform of Equation 666 after substituting $C = \overline{C} + c$, namely

$$\frac{\partial \overline{C}}{\partial t} + \frac{\partial c}{\partial t} + \frac{\partial (v_i c)}{\partial x_i} - Pe^{-1} \frac{\partial^2 c}{\partial x_i^2} = -Da_I \overline{C}^2 - 2Da_I \overline{C}c - Da_I c^2 \tag{681}$$

Also, Equation 677 results from taking the Fourier transform of the volume average of Equation 681, that is

$$d\overline{C}/dt = -Da_I \overline{C}^2 - Da_I \overline{c^2} \tag{682}$$

and Equation 680 results from the Fourier transform of

Equation 681 minus Equation 682

$$\frac{\partial c}{\partial t} + \frac{\partial (v_i c)}{\partial x_i} - Pe^{-1} \frac{\partial^2 c}{\partial x_i^2} = -2Da_I \bar{C} c - Da_I c^2 + Da_I \overline{c^2} \quad (683)$$

Taking the limit $\underset{\sim}{k} = \underset{\sim}{0}$ in $\underset{\sim}{k}$-space is the same as volume averaging in $\underset{\sim}{x}$-space.

In terms of real and imaginary parts, the Fourier transformed conservation equation becomes

$\underline{\underset{\sim}{k} = \underset{\sim}{0}}$

$$\partial \mathcal{C}(\underset{\sim}{0})/\partial t = -Da_I \mathcal{C}(\underset{\sim}{0})^2 - Da_I \sum_{\underset{\sim}{p}} [c^R(\underset{\sim}{p})^2 + c^I(\underset{\sim}{p})^2] \quad (684)$$

$$c^R(\underset{\sim}{0}) = c^I(\underset{\sim}{0}) = 0 \quad (685)$$

$\underline{\underset{\sim}{k} \neq \underset{\sim}{0}}$

$$\partial c^R(\underset{\sim}{k})/\partial t - k_i \sum_{\underset{\sim}{p}} [u_i^R(\underset{\sim}{p}) c^I(\underset{\sim}{k}-\underset{\sim}{p}) + u_i^I(\underset{\sim}{p}) c^R(\underset{\sim}{k}-\underset{\sim}{p})]$$

$$+ Pe^{-1} k^2 c^R(\underset{\sim}{k}) = -2Da_I \mathcal{C}(\underset{\sim}{0}) c^R(\underset{\sim}{k}) \quad (686)$$

$$- Da_I \sum_{\underset{\sim}{p}} [c^R(\underset{\sim}{p}) c^R(\underset{\sim}{k}-\underset{\sim}{p}) - c^I(\underset{\sim}{p}) c^I(\underset{\sim}{k}-\underset{\sim}{p})]$$

$$\partial c^I(\underset{\sim}{k})/\partial t + k_i \sum_{\underset{\sim}{p}} [u_i^R(\underset{\sim}{p}) c^R(\underset{\sim}{k}-\underset{\sim}{p}) - u_i^I(\underset{\sim}{p}) c^I(\underset{\sim}{k}-\underset{\sim}{p})]$$

$$+ Pe^{-1} k^2 c^I(\underset{\sim}{k}) = -2Da_I \mathcal{C}(\underset{\sim}{0}) c^I(\underset{\sim}{k}) \quad (687)$$

$$- Da_I \sum_{\underset{\sim}{p}} [c^R(\underset{\sim}{p}) c^I(\underset{\sim}{k}-\underset{\sim}{p}) + c^I(\underset{\sim}{p}) c^R(\underset{\sim}{k}-\underset{\sim}{p})]$$

Fourier Transformation of the Conservation Equations for a Two Species Second-Order Reaction

The dimensionless conservation equations for a second-order reaction between species A and B are

$$\frac{\partial C_A}{\partial t} + \frac{\partial (v_i C_A)}{\partial x_i} = Pe_A^{-1} \frac{\partial^2 C_A}{\partial x_i^2} - Da_I C_A C_B \tag{688}$$

$$\frac{\partial C_B}{\partial t} + \frac{\partial (v_i C_B)}{\partial x_i} = Pe_B^{-1} \frac{\partial^2 C_B}{\partial x_i^2} - Da_I C_A C_B \tag{689}$$

where $\bar{C}^*_{A0} \equiv \bar{C}^*_A(0)$ is the reference concentration. By definition, $\bar{C}_A(0) = 1$, and $\bar{C}_B(0)$ gives the initial stoichiometry of the reactants. Taking the Fourier transform of Equations 688 and 689, substituting in

$$\mathcal{C}_A(\underset{\sim}{k}) = \mathcal{C}_A(\underset{\sim}{0})\,\delta_{\underset{\sim}{k},\underset{\sim}{0}} + \mathcal{c}_A(\underset{\sim}{k}) \tag{690}$$

$$\mathcal{C}_B(\underset{\sim}{k}) = \mathcal{C}_B(\underset{\sim}{0})\,\delta_{\underset{\sim}{k},\underset{\sim}{0}} + \mathcal{c}_B(\underset{\sim}{k}) \tag{691}$$

and simplifying gives

$$\frac{\partial \mathcal{C}_A(\underset{\sim}{0})}{\partial t}\,\delta_{\underset{\sim}{k},\underset{\sim}{0}} + \frac{\partial \mathcal{c}_A(\underset{\sim}{k})}{\partial t} + ik_i \sum_{\underset{\sim}{p}} u_i(\underset{\sim}{p})\mathcal{c}_A(\underset{\sim}{k}-\underset{\sim}{p})$$

$$+ Pe_A^{-1} k^2 \mathcal{c}_A(\underset{\sim}{k}) = -Da_I \mathcal{C}_A(\underset{\sim}{0})\mathcal{C}_B(\underset{\sim}{0})\,\delta_{\underset{\sim}{k},\underset{\sim}{0}} - Da_I \mathcal{C}_A(\underset{\sim}{0})\mathcal{c}_B(\underset{\sim}{k}) \tag{692}$$

$$- Da_I \mathcal{C}_B(\underset{\sim}{0})\mathcal{c}_A(\underset{\sim}{k}) - Da_I \sum_{\underset{\sim}{p}} \mathcal{c}_A(\underset{\sim}{p})\mathcal{c}_B(\underset{\sim}{k}-\underset{\sim}{p})$$

$$\frac{\partial \mathcal{C}_B(\underset{\sim}{0})}{\partial t}\,\delta_{\underset{\sim}{k},\underset{\sim}{0}} + \frac{\partial c_B(\underset{\sim}{k})}{\partial t} + ik_i \sum_{\underset{\sim}{p}} u_i(\underset{\sim}{p})c_B(\underset{\sim}{k}-\underset{\sim}{p})$$

$$+ Pe_B^{-1}\, k^2 c_B(\underset{\sim}{k}) = -Da_I \mathcal{C}_A(\underset{\sim}{0})\mathcal{C}_B(\underset{\sim}{0})\,\delta_{\underset{\sim}{k},\underset{\sim}{0}} - Da_I \mathcal{C}_A(\underset{\sim}{0})c_B(\underset{\sim}{k}) \tag{693}$$

$$- Da_I \mathcal{C}_B(\underset{\sim}{0})c_A(\underset{\sim}{k}) - Da_I \sum_{\underset{\sim}{p}} c_A(\underset{\sim}{p})c_B(\underset{\sim}{k}-\underset{\sim}{p})$$

Separated into parts valid for $\underset{\sim}{k} = \underset{\sim}{0}$ and $\underset{\sim}{k} \neq \underset{\sim}{0}$, Equations 692 and 693 become

$\underset{\sim}{k} = \underset{\sim}{0}$

$$\frac{\partial \mathcal{C}_A(\underset{\sim}{0})}{\partial t} = -Da_I \mathcal{C}_A(\underset{\sim}{0})\mathcal{C}_B(\underset{\sim}{0}) - Da_I \sum_{\underset{\sim}{p}} c_A(\underset{\sim}{p})c_B(-\underset{\sim}{p}) \tag{694}$$

$$\frac{\partial \mathcal{C}_B(\underset{\sim}{0})}{\partial t} = -Da_I \mathcal{C}_A(\underset{\sim}{0})\mathcal{C}_B(\underset{\sim}{0}) - Da_I \sum_{\underset{\sim}{p}} c_A(\underset{\sim}{p})c_B(-\underset{\sim}{p}) \tag{695}$$

$$c_A(\underset{\sim}{0}) = c_B(\underset{\sim}{0}) = 0 \tag{696}$$

$\underset{\sim}{k} \neq \underset{\sim}{0}$

$$\frac{\partial c_A(\underset{\sim}{k})}{\partial t} + ik_i \sum_{\underset{\sim}{p}} u_i(\underset{\sim}{p})c_A(\underset{\sim}{k}-\underset{\sim}{p}) + Pe_A^{-1}\, k^2 c_A(\underset{\sim}{k}) \tag{697}$$

$$= -Da_I \mathcal{C}_A(\underset{\sim}{0})c_B(\underset{\sim}{k}) - Da_I \mathcal{C}_B(\underset{\sim}{0})c_A(\underset{\sim}{k}) - Da_I \sum_{\underset{\sim}{p}} c_A(\underset{\sim}{p})c_B(\underset{\sim}{k}-\underset{\sim}{p})$$

$$\frac{\partial c_B(\underset{\sim}{k})}{\partial t} + ik_i \sum_{\underset{\sim}{p}} u_i(\underset{\sim}{p})c_B(\underset{\sim}{k}-\underset{\sim}{p}) + Pe_B^{-1}\, k^2 c_B(\underset{\sim}{k}) \tag{698}$$

$$= - Da_I \mathcal{C}_A(\underset{\sim}{0})c_B(\underset{\sim}{k}) - Da_I \mathcal{C}_B(\underset{\sim}{0})c_A(\underset{\sim}{k}) - Da_I \sum_{\underset{\sim}{p}} c_A(\underset{\sim}{p})c_B(\underset{\sim}{k}-\underset{\sim}{p})$$

In terms of real and imaginary parts, we have

$$\phi_A(\underset{\sim}{k}) = \phi_A^R(\underset{\sim}{k}) + i\,\phi_A^I(\underset{\sim}{k}) \tag{699}$$

$$\phi_B(\underset{\sim}{k}) = \phi_B^R(\underset{\sim}{k}) + i\,\phi_B^I(\underset{\sim}{k}) \tag{700}$$

and the system of Equations 694 - 698 becomes

$\underline{\underset{\sim}{k} = \underset{\sim}{0}}$

$$\frac{\partial \ell_A(\underset{\sim}{0})}{\partial t} = -Da_I \ell_A(\underset{\sim}{0})\ell_B(\underset{\sim}{0}) - Da_I \sum_{\underset{\sim}{p}} [\phi_A^R(\underset{\sim}{p})\phi_B^R(\underset{\sim}{p}) + \phi_A^I(\underset{\sim}{p})\phi_B^I(\underset{\sim}{p})] \tag{701}$$

$$\frac{\partial \ell_B(\underset{\sim}{0})}{\partial t} = -Da_I \ell_A(\underset{\sim}{0})\ell_B(\underset{\sim}{0}) - Da_I \sum_{\underset{\sim}{p}} [\phi_A^R(\underset{\sim}{p})\phi_B^R(\underset{\sim}{p}) + \phi_A^I(\underset{\sim}{p})\phi_B^I(\underset{\sim}{p})] \tag{702}$$

$$\phi_A^R(\underset{\sim}{0}) = \phi_A^I(\underset{\sim}{0}) = \phi_B^R(\underset{\sim}{0}) = \phi_B^I(\underset{\sim}{0}) = 0 \tag{703}$$

$\underline{\underset{\sim}{k} \neq \underset{\sim}{0}}$

$$\frac{\partial \phi_A^R(\underset{\sim}{k})}{\partial t} - k_i \sum_{\underset{\sim}{p}} [u_i^R(\underset{\sim}{p})\phi_A^I(\underset{\sim}{k}-\underset{\sim}{p}) + u_i^I(\underset{\sim}{p})\phi_A^R(\underset{\sim}{k}-\underset{\sim}{p})]$$

$$+ Pe_A^{-1} k^2 \phi_A^R(\underset{\sim}{k}) = -Da_I \ell_A(\underset{\sim}{0})\phi_B^R(\underset{\sim}{k}) - Da_I \ell_B(\underset{\sim}{0})\phi_A^R(\underset{\sim}{k}) \tag{704}$$

$$- Da_I \sum_{\underset{\sim}{p}} [\phi_A^R(\underset{\sim}{p})\phi_B^R(\underset{\sim}{k}-\underset{\sim}{p}) - \phi_A^I(\underset{\sim}{p})\phi_B^I(\underset{\sim}{k}-\underset{\sim}{p})]$$

$$\frac{\partial \phi_A^I(\underset{\sim}{k})}{\partial t} + k_i \sum_{\underset{\sim}{p}} [u_i^R(\underset{\sim}{p})\phi_A^R(\underset{\sim}{k}-\underset{\sim}{p}) - u_i^I(\underset{\sim}{p})\phi_A^I(\underset{\sim}{k}-\underset{\sim}{p})]$$

$$+ Pe_A^{-1} k^2 \phi_A^I(\underset{\sim}{k}) = -Da_I \ell_A(\underset{\sim}{0})\phi_B^I(\underset{\sim}{k}) - Da_I \ell_B(\underset{\sim}{0})\phi_A^I(\underset{\sim}{k}) \tag{705}$$

$$- Da_I \sum_{\underset{\sim}{p}} [\phi_A^R(\underset{\sim}{p})\phi_B^I(\underset{\sim}{k}-\underset{\sim}{p}) + \phi_A^I(\underset{\sim}{p})\phi_B^R(\underset{\sim}{k}-\underset{\sim}{p})]$$

$$\frac{\partial c_B^R(\underset{\sim}{k})}{\partial t} - k_i \sum_{\underset{\sim}{p}} [u_i^R(\underset{\sim}{p}) c_B^I(\underset{\sim}{k}-\underset{\sim}{p}) + u_i^I(\underset{\sim}{p}) c_B^R(\underset{\sim}{k}-\underset{\sim}{p})]$$

$$+ Pe_B^{-1} k^2 c_B^R(\underset{\sim}{k}) = -Da_I \ell_A(\underset{\sim}{0}) c_B^R(\underset{\sim}{k}) - Da_I \ell_B(\underset{\sim}{0}) c_A^R(\underset{\sim}{k}) \qquad (706)$$

$$- Da_I \sum_{\underset{\sim}{p}} [c_A^R(\underset{\sim}{p}) c_B^R(\underset{\sim}{k}-\underset{\sim}{p}) - c_A^I(\underset{\sim}{p}) c_B^I(\underset{\sim}{k}-\underset{\sim}{p})]$$

$$\frac{\partial c_B^I(\underset{\sim}{k})}{\partial t} + k_i \sum_{\underset{\sim}{p}} [u_i^R(\underset{\sim}{p}) c_B^R(\underset{\sim}{k}-\underset{\sim}{p}) - u_i^I(\underset{\sim}{p}) c_B^I(\underset{\sim}{k}-\underset{\sim}{p})]$$

$$+ Pe_B^{-1} k^2 c_B^I(\underset{\sim}{k}) = -Da_I \ell_A(\underset{\sim}{0}) c_B^I(\underset{\sim}{k}) - Da_I \ell_B(\underset{\sim}{0}) c_A^I(\underset{\sim}{k}) \qquad (707)$$

$$- Da_I \sum_{\underset{\sim}{p}} [c_A^R(\underset{\sim}{p}) c_B^I(\underset{\sim}{k}-\underset{\sim}{p}) + c_A^I(\underset{\sim}{p}) c_B^R(\underset{\sim}{k}-\underset{\sim}{p})]$$

Fourier Transformation of the Conservation Equation for a First-Order Reaction

The dimensionless conservation equation for a first-order reaction is

$$\frac{\partial C}{\partial t} + \frac{\partial (v_i C)}{\partial x_i} = Pe^{-1} \frac{\partial^2 C}{\partial x_i^2} - Da_I C \qquad (708)$$

$$Da_I \equiv KL_{f\phi}^{\bullet} / \tilde{v}_{\phi}^{\bullet} \qquad (709)$$

Taking the Fourier transform of Equation 708 gives

$$\frac{\partial \ell(\underset{\sim}{k})}{\partial t} + ik_i \sum_{\underset{\sim}{p}} u_i(\underset{\sim}{p}) \ell(\underset{\sim}{k}-\underset{\sim}{p}) = -Pe^{-1} k^2 \ell(\underset{\sim}{k}) - Da_I \ell(\underset{\sim}{k}) \qquad (710)$$

Substituting in Equation 603, simplifying, and separating the result into parts valid for $\underset{\sim}{k} = \underset{\sim}{0}$ and $\underset{\sim}{k} \neq \underset{\sim}{0}$ gives

$\underset{\sim}{k} = \underset{\sim}{0}$

$$\frac{\partial \mathcal{C}(\underset{\sim}{0})}{\partial t} = -Da_I \, \mathcal{C}(\underset{\sim}{0}), \quad \mathcal{C}(\underset{\sim}{0}) = 0 \tag{711}$$

$\underset{\sim}{k} \neq \underset{\sim}{0}$

$$\frac{\partial \mathcal{C}(\underset{\sim}{k})}{\partial t} + ik_i \sum_{\underset{\sim}{p}} u_i(\underset{\sim}{p})\mathcal{C}(\underset{\sim}{k}-\underset{\sim}{p}) + Pe^{-1} k^2 \mathcal{C}(\underset{\sim}{k}) = -Da_I \mathcal{C}(\underset{\sim}{k}) \tag{712}$$

In terms of real and imaginary parts, the Fourier transformed conservation equation becomes

$\underset{\sim}{k} \neq \underset{\sim}{0}$

$$\frac{\partial \mathcal{C}^R(\underset{\sim}{k})}{\partial t} - k_i \sum_{\underset{\sim}{p}} [u_i^R(\underset{\sim}{p})\mathcal{C}^I(\underset{\sim}{k}-\underset{\sim}{p}) + u_i^I(\underset{\sim}{p})\mathcal{C}^R(\underset{\sim}{k}-\underset{\sim}{p})] + Pe^{-1} k^2 \mathcal{C}^R(\underset{\sim}{k}) = -Da_I \mathcal{C}^R(\underset{\sim}{k}) \tag{713}$$

$$\frac{\partial \mathcal{C}^I(\underset{\sim}{k})}{\partial t} + k_i \sum_{\underset{\sim}{p}} [u_i^R(\underset{\sim}{p})\mathcal{C}^R(\underset{\sim}{k}-\underset{\sim}{p}) - u_i^I(\underset{\sim}{p})\mathcal{C}^I(\underset{\sim}{k}-\underset{\sim}{p})] + Pe^{-1} k^2 \mathcal{C}^I(\underset{\sim}{k}) = -Da_I \mathcal{C}^I(\underset{\sim}{k}) \tag{714}$$

Numerical Calculation Considerations

As was done with the velocity field, a finite system of equations describing the concentration field is obtained by truncations of summations at a cutoff wave number k_{max}.

For single component reactions, the initial value of the average concentration has been defined to be

$$\bar{C}(0) = \mathcal{C}(\underset{\sim}{0},0) = 1 \tag{715}$$

by choice of $\bar{C}_0^* = \bar{C}^*(0)$ as the reference concentration. An important parameter in the calculations is the initial average concentration fluctuation intensity $\tilde{c}(0)$. The assigned initial concentration spectrum must be normalized to give the desired value of $\tilde{c}(0)$. This in turn assures that the assigned initial real and imaginary Fourier concentration modes are properly normalized, as seen from

$$\begin{aligned}\tilde{c}(0)^2 &= \sum_{\underset{\sim}{k}} [\mathcal{C}^R(\underset{\sim}{k},0)^2 + \mathcal{C}^I(\underset{\sim}{k},0)^2] = \sum_{\underset{\sim}{k}} E_{ss}(\underset{\sim}{k},0)_d \\ &= \sum_{\underset{\sim}{k}} E_s(k,0)_d/\eta(k) = \sum_{k} E_s(k,0)_d\end{aligned} \tag{716}$$

since the assignment is made using

$$\mathcal{C}^R(\underset{\sim}{k},0)^2 + \mathcal{C}^I(\underset{\sim}{k},0)^2 = E_s(k,0)_d/\eta(k) \tag{717}$$

Equation 717 contains two variables, so there is one degree of freedom left with which an ensemble of initial concentration distributions can be created, each having the same

concentration fluctuation spectrum. Values of $\phi^R(\underset{\sim}{k},0)$ and $\phi^I(\underset{\sim}{k},0)$ lie on a circle of radius $[E_s(k,0)_d/\eta(k)]^{\frac{1}{2}}$ in $\phi^R(\underset{\sim}{k})$, $\phi^I(\underset{\sim}{k})$ - space and can be chosen by random selection of a point on the circle.

The initial value of the concentration integral scale and microscale are fixed once $E_s(k,0)_d$ and N have been specified; $L_s(0)$ can only be changed by changing the first moment of the concentration spectrum.

For two species reactions, the initial average concentrations are

$$\begin{aligned} \overline{C}_A(0) &= \mathcal{C}_A(\underset{\sim}{0},0) = 1 \\ \overline{C}_B(0) &= \mathcal{C}_B(\underset{\sim}{0},0) = \text{initial stoichiometry} \end{aligned} \tag{718}$$

by choice of $\overline{C}^*_{A0} = \overline{C}^*_A(0)$ as the reference concentration. The initial concentration fluctuation spectra of A and B are normalized to give the desired values of $\tilde{c}_A(0)$ and $\tilde{c}_B(0)$. In addition the initial correlation between the fluctuations of A and B is also of interest. In particular, in testing Toor's hypothesis it is desirable to have A and B uncorrelated initially, so that A and B are not premixed. This condition is expressed by $\overline{C_A C_B} = \overline{C}_A\overline{C}_B + \overline{c_A c_B} = 0$ or $\overline{c_A c_B}(0) = -\overline{C}_A(0)\overline{C}_B(0)$. Therefore, the constraints put on the initial values of the concentration modes can be expressed as the set of equations

$$\phi_A^R(\underset{\sim}{k},0)^2 + \phi_A^I(\underset{\sim}{k},0)^2 = E_A(k,0)_d/\eta(k) \tag{719}$$

$$\phi_B^R(\underset{\sim}{k},0)^2 + \phi_B^I(\underset{\sim}{k},0)^2 = E_B(k,0)_d/\eta(k) \tag{720}$$

$$\phi_A^R(\underset{\sim}{k},0)\phi_B^R(\underset{\sim}{k},0) + \phi_A^I(\underset{\sim}{k},0)\phi_B^I(\underset{\sim}{k},0) = E_{AB}(k,0)_d/\eta(k) \tag{721}$$

where

$$\overline{c_A c_B}(0) = \sum_{\underset{\sim}{k}} E_{AB}(k,0)_d/\eta(k) = \sum_k E_{AB}(k,0)_d \tag{722}$$

This system of four variables and three equations leaves one degree of freedom with which an ensemble of concentration distributions of A and B can be generated, each having the same concentration spectrum and correlation between A and B. Values of $\phi_A^R(\underset{\sim}{k},0)$ and $\phi_A^I(\underset{\sim}{k},0)$ can be determined by random selection of a point on the circle in $\phi_A^R(\underset{\sim}{k})$, $\phi_A^I(\underset{\sim}{k})$-space determined by Equation 719. Values of $\phi_B^R(\underset{\sim}{k},0)$ and $\phi_B^I(\underset{\sim}{k},0)$ are then given by the simultaneous solution of Equations 720 and 721,

$$\phi_B^R(\underset{\sim}{k},0) = \frac{E_{AB}(k)_d}{E_A(k)_d}\,\phi_A^R(\underset{\sim}{k},0) \pm \frac{\left[E_A(k)_d E_B(k)_d - E_{AB}(k)_d^2\right]^{1/2}}{E_A(k)_d}\,\phi_A^I(\underset{\sim}{k},0) \tag{723}$$

$$\phi_B^I(\underset{\sim}{k},0) = \frac{E_{AB}(k)_d}{E_A(k)_d}\,\phi_A^I(\underset{\sim}{k},0) \mp \frac{\left[E_A(k)_d E_B(k)_d - E_{AB}(k)_d^2\right]^{1/2}}{E_A(k)_d}\,\phi_A^R(\underset{\sim}{k},0) \tag{724}$$

for $\quad E_A(k)_d \neq 0 \quad (k \neq 0)$

$$E_A(k)_d E_B(k)_d \geq E_{AB}(k)_d^2$$

TIME SCALED EQUATIONS IN TERMS OF $\underset{\sim}{n}$

The velocity field and concentration field equations can be put into a more convenient form for numerical integration by rewriting them in terms of the integer vector $\underset{\sim}{n}$ instead of the wave number vector $\underset{\sim}{k}$. The resulting appearance of the quantity N in the equations can be removed by time scaling. In addition, quantities which are a function of the discrete scalar values of n are more easily expressed in terms of the integer values n^2.

Velocity Field Equations

Velocity field generation equation

When time scaled and written in terms of $\underset{\sim}{n}$, the velocity field generation equation becomes

$$\frac{\partial u_i^R(\underset{\sim}{n})}{\partial t'} = P_{ij}(\underset{\sim}{n})n_1 \sum_{\underset{\sim}{m}} [\phi_1^R(\underset{\sim}{m})u_j^I(\underset{\sim}{n}-\underset{\sim}{m}) + \phi_1^I(\underset{\sim}{m})u_j^R(\underset{\sim}{n}-\underset{\sim}{m})] \quad (725)$$

$$\frac{\partial u_i^I(\underset{\sim}{n})}{\partial t'} = -P_{ij}(\underset{\sim}{n})n_1 \sum_{\underset{\sim}{m}} [\phi_1^R(\underset{\sim}{m})u_j^R(\underset{\sim}{n}-\underset{\sim}{m}) - \phi_1^I(\underset{\sim}{m})u_j^I(\underset{\sim}{n}-\underset{\sim}{m})] \quad (726)$$

$$t' \equiv (2\pi/N)t \quad (727)$$

In three dimensions, the equations for assigning initial conditions become

$\underline{n_2^2 + n_3^2 \neq 0}$

$$u_1^R(\underset{\sim}{n},0)^2 + u_1^I(\underset{\sim}{n},0)^2 = (1 - n_1^2/n^2)E(n^2,0)_d/\eta(n^2) \equiv R_1(n^2)^2 \tag{728,3D}$$

$$u_1^R(\underset{\sim}{n},0) = R_1(n^2)\cos\theta(\underset{\sim}{n},0) \tag{729,3D}$$

$$u_1^I(\underset{\sim}{n},0) = R_1(n^2)\sin\theta(\underset{\sim}{n},0) \tag{730,3D}$$

$$u_2^R(\underset{\sim}{n},0) = [-n_1n_2u_1^R(\underset{\sim}{n},0) \pm nn_3u_1^I(\underset{\sim}{n},0)]/(n^2 - n_1^2) \tag{731,3D}$$

$$u_2^I(\underset{\sim}{n},0) = [-n_1n_2u_1^I(\underset{\sim}{n},0) \mp nn_3u_1^R(\underset{\sim}{n},0)]/(n^2 - n_1^2) \tag{732,3D}$$

$$u_3^R(\underset{\sim}{n},0) = [-n_1n_3u_1^R(\underset{\sim}{n},0) \mp nn_2u_1^I(\underset{\sim}{n},0)]/(n^2 - n_1^2) \tag{733,3D}$$

$$u_3^I(\underset{\sim}{n},0) = [-n_1n_3u_1^I(\underset{\sim}{n},0) \pm nn_2u_1^R(\underset{\sim}{n},0)]/(n^2 - n_1^2) \tag{734,3D}$$

$\underline{n_2 = n_3 = 0,\ n_1 \neq 0}$

$$u_2^R(\underset{\sim}{n},0)^2 + u_2^I(\underset{\sim}{n},0)^2 = E(n^2,0)_d/\eta(n^2) \equiv R_2(n^2)^2 \tag{735,3D}$$

$$u_2^R(\underset{\sim}{n},0) = R_2(n^2)\cos\theta(\underset{\sim}{n},0) \tag{736,3D}$$

$$u_2^I(\underset{\sim}{n},0) = R_2(n^2)\sin\theta(\underset{\sim}{n},0) \tag{737,3D}$$

$$u_3^R(\underset{\sim}{n},0) = \pm\, u_2^I(\underset{\sim}{n},0),\quad u_3^I(\underset{\sim}{n},0) = \mp\, u_2^R(\underset{\sim}{n},0) \tag{738,3D}$$

$$u_1^R(\underset{\sim}{n},0) = u_1^I(\underset{\sim}{n},0) = 0 \tag{739,3D}$$

$\underline{n_1 = n_2 = n_3 = 0}$

$$u_i^R(\underset{\sim}{0},0) = u_1^I(\underset{\sim}{0},0) = 0 \tag{740,3D}$$

and in two dimensions

$\underline{n_2 \neq 0}$

$$u_1^R(\underset{\sim}{n},0)^2 + u_1^I(\underset{\sim}{n},0)^2 = 2(1 - n_1^2/n^2)E(n^2,0)_d/\eta(n^2) \equiv R_1(n^2)^2 \qquad (741,2D)$$

$$u_1^R(\underset{\sim}{n},0) = R_1(n^2)\cos\theta(\underset{\sim}{n},0) \qquad (742,2D)$$

$$u_1^I(\underset{\sim}{n},0) = R_1(n^2)\sin\theta(\underset{\sim}{n},0) \qquad (743,2D)$$

$$u_2^R(\underset{\sim}{n},0) = -n_1 u_1^R(\underset{\sim}{n},0)/n_2 \qquad (744,2D)$$

$$u_2^I(\underset{\sim}{n},0) = -n_1 u_1^I(\underset{\sim}{n},0)/n_2 \qquad (745,2D)$$

$\underline{n_2 = 0,\ n_1 \neq 0}$

$$u_2^R(\underset{\sim}{n},0)^2 + u_2^I(\underset{\sim}{n},0)^2 = 2E(n^2,0)_d/\eta(n^2) \equiv R_2(n^2)^2 \qquad (746,2D)$$

$$u_2^R(\underset{\sim}{n},0) = R_2(n^2)\cos\theta(\underset{\sim}{n},0) \qquad (747,2D)$$

$$u_2^I(\underset{\sim}{n},0) = R_2(n^2)\sin\theta(\underset{\sim}{n},0) \qquad (748,2D)$$

$$u_1^R(\underset{\sim}{n},0) = u_1^I(\underset{\sim}{n},0) = 0 \qquad (749,2D)$$

$\underline{n_1 = n_2 = 0}$

$$u_1^R(\underset{\sim}{0},0) = u_1^I(\underset{\sim}{0},0) = u_2^R(\underset{\sim}{0},0) = u_2^I(\underset{\sim}{0},0) = 0 \qquad (750,2D)$$

where $\theta(\underset{\sim}{n},0)$ is an angular coordinate that is chosen at random.

Velocity field statistics

In calculating velocity field statistics, it is convenient to write the discrete energy spectrum function $E(n)_d$ in the equivalent form $E(n^2)_d$. Furthermore, let $E(n^2)_d \equiv 0$ for values of n^2 having $\eta(n^2) = 0$, that is, integer values of n^2 that are not given by $n^2 = n_i n_i$ (do not correspond to points on the $\underset{\sim}{n}$-lattice). Then summations over the discrete (noninteger) values of n can be accomplished by summing over all integer values of n^2 within $0 \leq n^2 \leq n_{max}^2$.

In practice, there is no guarantee that the velocity field will remain isotropic as calculations proceed over time. Therefore, let the value of the energy spectrum at the point $\underset{\sim}{n}$ be denoted by $E(\underset{\sim}{n})_d$. Then the average value $E(n^2)_d$ for points on the surface n is given by

$$E(n^2)_d = \eta(n^2)^{-1} \sum_{\theta_{\underset{\sim}{n}}} \sum_{\phi_{\underset{\sim}{n}}} E(\underset{\sim}{n})_d \qquad (751,3D)$$

$$E(n^2)_d = \eta(n^2)^{-1} \sum_{\theta_{\underset{\sim}{n}}} E(\underset{\sim}{n})_d \qquad (752,2D)$$

However, from Equations 427 and 435 we have

$$E_{ii}(\underset{\sim}{n})_d = u_i^R(\underset{\sim}{n})^2 + u_i^I(\underset{\sim}{n})^2 = 2E(\underset{\sim}{n})_d/\eta(n^2) \qquad (753)$$

and hence

$$E(\underset{\sim}{n})_d = \tfrac{1}{2}\,\eta(n^2)[u_i^R(\underset{\sim}{n})^2 + u_i^I(\underset{\sim}{n})^2] \qquad (754)$$

Substituting Equation 754 into Equations 751 and 752 gives the results

$$E(n^2)_d = \tfrac{1}{2} \sum_{\theta_{\underset{\sim}{n}}} \sum_{\phi_{\underset{\sim}{n}}} [u_i^R(\underset{\sim}{n})^2 + u_i^I(\underset{\sim}{n})^2] \qquad (755,3D)$$

$$E(n^2)_d = \tfrac{1}{2} \sum_{\theta_{\underset{\sim}{n}}} [u_i^R(\underset{\sim}{n})^2 + u_i^I(\underset{\sim}{n})^2] \qquad (756,3D)$$

To simplify the summation procedure, the equivalent form

$$E(n^2)_d = \tfrac{1}{2} \sum_{\underset{\sim}{m}} \delta_{n^2,m^2} [u_i^R(\underset{\sim}{m})^2 + u_i^I(\underset{\sim}{m})^2] \qquad (757)$$

can be used. In practice, it is not necessary to sum over all values of $\underset{\sim}{m}$ for each value of n^2; summations for all values of n^2 can be done simultaneously in one operation.

The velocity field statistics can be found directly from $E(n^2)_d$, using

$$E_o(t') = \tfrac{1}{2}\delta_{ii}\tilde{v}(t')^2 = \sum_{n^2=1}^{n_{max}^2} E(n^2,t')_d \qquad (758)$$

$$L_f(t') = [N/4\tilde{v}(t')^2] \sum_{n^2=1}^{n_{max}^2} n^{-1}E(n^2,t')_d \qquad (759,3D)$$

$$L_f(t') = [N/\pi\tilde{v}(t')^2] \sum_{n^2=1}^{n_{max}^2} n^{-1}E(n^2,t')_d \qquad (760,2D)$$

$$\lambda_f(t')^{-2} = [4\pi^2/15N^2\tilde{v}(t')^2] \sum_{n^2=1}^{n_{max}^2} n^2E(n^2,t')_d \qquad (761,3D)$$

$$\lambda_f(t')^{-2} = [\pi^2/2N^2\tilde{v}(t')^2] \sum_{n^2=1}^{n_{max}^2} n^2 E(n^2,t')_d \qquad (762,2D)$$

$$f(r,t') = [2/\tilde{v}(t')^2] \sum_{n^2=1}^{n_{max}^2} E(n^2,t')_d \left[\frac{\sin(kr)}{(kr)^3} - \frac{\cos(kr)}{(kr)^2}\right] \qquad (763,3D)$$

$$f(r,t') = [2/\tilde{v}(t')^2] \sum_{n^2=1}^{n_{max}^2} E(n^2,t')_d \, J_1(kr)/kr \qquad (764,2D)$$

$$kr = (2\pi/N)nr \qquad (765)$$

In calculating the stream function (two dimensions), it is convenient to use the scaled coordinate system $\underset{\sim}{x}' \equiv \underset{\sim}{x}^*/L^*$ that is referenced to the length of the sides of the box. In terms of $\underset{\sim}{x}'$ and $\underset{\sim}{n}$, the stream function is given by

$$\Psi'(\underset{\sim}{x}',t') = (2\pi/N)\,\Psi(\underset{\sim}{x}',t')$$

$$= \sum_{n_1} \sum_{n_2 \neq 0} [u_1^I(\underset{\sim}{n},t')\cos(2\pi \underset{\sim}{n}\cdot\underset{\sim}{x}') + u_1^R(\underset{\sim}{n},t')\sin(2\pi \underset{\sim}{n}\cdot\underset{\sim}{x}')]/n_2 \qquad (766,2D)$$

$$- \sum_{\substack{n_1 \neq 0 \\ n_2 = 0}} [u_2^I(\underset{\sim}{n},t')\cos(2\pi \underset{\sim}{n}\cdot\underset{\sim}{x}') + u_2^R(\underset{\sim}{n},t')\sin(2\pi \underset{\sim}{n}\cdot\underset{\sim}{x}')]/n_1$$

$$+ \Psi'(\underset{\sim}{0})$$

The physical-space velocity at the point $\underset{\sim}{x} = \underset{\sim}{0}$ can be found from

$$v_i(\underset{\sim}{0},t') = \sum_{\underset{\sim}{n}} u_i^R(\underset{\sim}{n},t') \qquad (767)$$

Random convection velocity

The equations for generating the random convection velocity in three dimensions are

$n_2^2 + n_3^2 \neq 0$

$$\phi_1^R(\underset{\sim}{n},t')^2 + \phi_1^I(\underset{\sim}{n},t')^2 = (1 - n_1^2/n^2)E(n^2)_{d\phi}/\eta(n^2) \equiv R_{1\phi}(n^2)^2 \quad (768,3D)$$

$$\phi_1^R(\underset{\sim}{n},t') = R_{1\phi}(n^2)\cos\theta(\underset{\sim}{n},t') \quad (769,3D)$$

$$\phi_1^I(\underset{\sim}{n},t') = R_{1\phi}(n^2)\sin\theta(\underset{\sim}{n},t') \quad (770,3D)$$

$$\phi_2^R(\underset{\sim}{n},t') = [-n_1n_2\phi_1^R(\underset{\sim}{n},t') \pm nn_3\phi_1^I(\underset{\sim}{n},t')]/(n^2 - n_1^2) \quad (771,3D)$$

$$\phi_2^I(\underset{\sim}{n},t') = [-n_1n_2\phi_1^I(\underset{\sim}{n},t') \mp nn_3\phi_1^R(\underset{\sim}{n},t')]/(n^2 - n_1^2) \quad (772,3D)$$

$$\phi_3^R(\underset{\sim}{n},t') = [-n_1n_3\phi_1^R(\underset{\sim}{n},t') \mp nn_2\phi_1^I(\underset{\sim}{n},t')]/(n^2 - n_1^2) \quad (773,3D)$$

$$\phi_3^I(\underset{\sim}{n},t') = [-n_1n_3\phi_1^I(\underset{\sim}{n},t') \pm nn_2\phi_1^R(\underset{\sim}{n},t')]/(n^2 - n_1^2) \quad (774,3D)$$

$n_2 = n_3 = 0,\ n_1 \neq 0$

$$\phi_2^R(\underset{\sim}{n},t')^2 + \phi_2^I(\underset{\sim}{n},t')^2 = E(n^2)_{d\phi}/\eta(n^2) \equiv R_{2\phi}(n^2)^2 \quad (775,3D)$$

$$\phi_2^R(\underset{\sim}{n},t') = R_{2\phi}(n^2)\cos\theta(\underset{\sim}{n},t') \quad (776,3D)$$

$$\phi_2^I(\underset{\sim}{n},t') = R_{2\phi}(n^2)\sin\theta(\underset{\sim}{n},t') \quad (777,3D)$$

$$\phi_3^R(\underset{\sim}{n},t') = \pm\,\phi_2^I(\underset{\sim}{n},t'),\ \phi_3^I(\underset{\sim}{n},t') = \mp\,\phi_2^R(\underset{\sim}{n},t') \quad (778,3D)$$

$$\phi_1^R(\underset{\sim}{n},t') = \phi_1^I(\underset{\sim}{n},t') = 0 \quad (779,3D)$$

$\underline{n_1 = n_2 = n_3 = 0}$

$$\phi_i^R(\underset{\sim}{0},t') = \phi_i^I(\underset{\sim}{0},t') = 0 \qquad (780,3D)$$

and in two dimensions

$\underline{n_2 \neq 0}$

$$\phi_1^R(\underset{\sim}{n},t')^2 + \phi_1^I(\underset{\sim}{n},t')^2 = 2(1-n_1^2/n^2)E(n^2)_{d\phi}/\eta(n^2) \equiv R_{1\phi}(n^2)^2 \qquad (781,2D)$$

$$\phi_1^R(\underset{\sim}{n},t') = R_{1\phi}(n^2)\cos\theta(\underset{\sim}{n},t') \qquad (782,2D)$$

$$\phi_1^I(\underset{\sim}{n},t') = R_{1\phi}(n^2)\sin\theta(\underset{\sim}{n},t') \qquad (783,2D)$$

$$\phi_2^R(\underset{\sim}{n},t') = -n_1\phi_1^R(\underset{\sim}{n},t')/n_2 \qquad (784,2D)$$

$$\phi_2^I(\underset{\sim}{n},t') = -n_1\phi_1^I(\underset{\sim}{n},t')/n_2 \qquad (785,2D)$$

$\underline{n_2 = 0,\ n_1 \neq 0}$

$$\phi_2^R(\underset{\sim}{n},t')^2 + \phi_2^I(\underset{\sim}{n},t')^2 = 2E(n^2,t')_{d\phi}/\eta(n^2) \equiv R_{2\phi}(n^2)^2 \qquad (786,2D)$$

$$\phi_2^R(\underset{\sim}{n},t') = R_{2\phi}(n^2)\cos\theta(\underset{\sim}{n},t') \qquad (787,2D)$$

$$\phi_2^I(\underset{\sim}{n},t') = R_{2\phi}(n^2)\sin\theta(\underset{\sim}{n},t') \qquad (788,2D)$$

$$\phi_1^R(\underset{\sim}{n},t') = \phi_1^I(\underset{\sim}{n},t') = 0 \qquad (789,2D)$$

$\underline{n_1 = n_2 = 0}$

$$\phi_1^R(\underset{\sim}{n},t') = \phi_1^I(\underset{\sim}{n},t') = \phi_2^R(\underset{\sim}{n},t') = \phi_2^I(\underset{\sim}{n},t') = 0 \qquad (790,2D)$$

where values of $\theta(\underset{\sim}{n},t')$ are generated by a random walk on a circle.

The statistical properties of the random convection velocity are held constant and can be calculated directly from the assigned energy spectrum function $E(n^2)_{d\phi}$, using

$$4/N = \sum_{n^2=1}^{n_{max}^2} n^{-1}E(n^2)_{d\phi} \qquad (791,3D)$$

$$\pi/N = \sum_{n^2=1}^{n_{max}^2} n^{-1}E(n^2)_{d\phi} \qquad (792,2D)$$

$$L_{f\phi}(t') = 1, \ \tilde{\phi}(t') = 1 \qquad (793)$$

$$E_o(t')_{\phi} = \tfrac{1}{2}\delta_{ii} = \sum_{n^2=1}^{n_{max}^2} E(n^2)_{d\phi} \qquad (794)$$

$$\lambda_{f\phi}(t')^{-2} = (4\pi^2/15N^2) \sum_{n^2=1}^{n_{max}^2} n^2E(n^2)_{d\phi} \qquad (795,3D)$$

$$\lambda_{f\phi}(t')^{-2} = (\pi^2/2N^2) \sum_{n^2=1}^{n_{max}^2} n^2E(n^2)_{d\phi} \qquad (796,2D)$$

$$f(r)_{\phi} = 2 \sum_{n^2=1}^{n_{max}^2} E(n^2)_{d\phi} \left[\frac{\sin(kr)}{(kr)^3} - \frac{\cos(kr)}{(kr)^2}\right] \qquad (797,3D)$$

$$f(r)_{\phi} = 2 \sum_{n^2=1}^{n_{max}^2} E(n^2)_{d\phi} \, J_1(kr)/kr \qquad (798,2D)$$

Random walk on a circle

The time-scaled equations for generating a random walk on a circle using a second-order response to an integral random step forcing function are

$$\tau'(\underset{\sim}{n})^2 \frac{d^2\theta(\underset{\sim}{n},t')}{dt'^2} + 2\tau'(\underset{\sim}{n})\zeta \frac{d\theta(\underset{\sim}{n},t')}{dt'} + \theta(\underset{\sim}{n},t') = 2\pi\, S(\underset{\sim}{n},t',T'_{so}) \tag{799}$$

$$S_{j+1}(\underset{\sim}{n},t',T'_{so}) = S_j(\underset{\sim}{n},t',T'_{so}) + B\, s_{j+1}(\underset{\sim}{n},t',T'_{so}) \tag{800}$$

$$\tau' \equiv (2\pi/N)\tau, \quad T'_{so} \equiv (2\pi/N)T_{so} \tag{801}$$

$$\tau'(\underset{\sim}{n}) = (B_f\pi/2)n^{-1}E(n_o^2)_{d\emptyset}/E(n^2)_{d\emptyset}^{\frac{1}{2}} \tag{802,3D}$$

for $1 \leq n \leq n_o$

$$\tau'(\underset{\sim}{n}) = (2B_f)n^{-1}E(n_o^2)_{d\emptyset}/E(n^2)_{d\emptyset}^{\frac{1}{2}} \tag{803,2D}$$

$$\tau'(\underset{\sim}{n}) = (B_f\pi/2)n^{-1}E(n^2)_{d\emptyset}^{\frac{1}{2}} \tag{804,3D}$$

for $n_o \leq n \leq n_{max}$

$$\tau'(\underset{\sim}{n}) = (2B_f)n^{-1}E(n^2)_{d\emptyset}^{\frac{1}{2}} \tag{805,2D}$$

Concentration Field Equations

Single component second-order reaction

Written in terms of $\underset{\sim}{n}$, the time-scaled conservation equation for a single component second-order reaction is

$\underset{\sim}{n} = \underset{\sim}{0}$

$$\frac{\partial \mathcal{C}(\underset{\sim}{0})}{\partial t'} = -Da_I' \mathcal{C}(\underset{\sim}{0})^2 - Da_I' \sum_{\underset{\sim}{m}} [c^R(\underset{\sim}{m})^2 + c^I(\underset{\sim}{m})^2] \tag{806}$$

$$c^R(\underset{\sim}{0}) = c^I(\underset{\sim}{0}) = 0 \tag{807}$$

$\underset{\sim}{n} \neq \underset{\sim}{0}$

$$\frac{\partial c^R(\underset{\sim}{n})}{\partial t'} = -Pe'^{-1} n^2 c^R(\underset{\sim}{n}) - 2Da_I' \mathcal{C}(\underset{\sim}{0}) c^R(\underset{\sim}{n})$$

$$+ n_i \sum_{\underset{\sim}{m}} [u_i^R(\underset{\sim}{m}) c^I(\underset{\sim}{n}-\underset{\sim}{m}) + u_i^I(\underset{\sim}{m}) c^R(\underset{\sim}{n}-\underset{\sim}{m})] \tag{808}$$

$$- Da_I' \sum_{\underset{\sim}{m}} [c^R(\underset{\sim}{m}) c^R(\underset{\sim}{n}-\underset{\sim}{m}) - c^I(\underset{\sim}{m}) c^I(\underset{\sim}{n}-\underset{\sim}{m})]$$

$$\frac{\partial c^I(\underset{\sim}{n})}{\partial t'} = -Pe'^{-1} n^2 c^I(\underset{\sim}{n}) - 2Da_I' \mathcal{C}(\underset{\sim}{0}) c^I(\underset{\sim}{n})$$

$$- n_i \sum_{\underset{\sim}{m}} [u_i^R(\underset{\sim}{m}) c^R(\underset{\sim}{n}-\underset{\sim}{m}) - u_i^I(\underset{\sim}{m}) c^I(\underset{\sim}{n}-\underset{\sim}{m})] \tag{809}$$

$$- Da_I' \sum_{\underset{\sim}{m}} [c^R(\underset{\sim}{m}) c^I(\underset{\sim}{n}-\underset{\sim}{m}) + c^I(\underset{\sim}{m}) c^R(\underset{\sim}{n}-\underset{\sim}{m})]$$

$$t' \equiv (2\pi/N)t, \quad Da_I' \equiv (N/2\pi)Da_I, \quad Pe' \equiv (N/2\pi)Pe \tag{810}$$

The initial conditions on the concentration field are assigned using

$$\bar{C}(0) = \mathcal{C}(\underset{\sim}{0},0) = 1 \tag{811}$$

$$\tilde{c}(0)^2 = \sum_{n^2=1}^{n_{max}^2} E_s(n^2,0)_d \tag{812}$$

$$c^R(\underset{\sim}{n},0)^2 + c^I(\underset{\sim}{n},0)^2 = E_s(n^2,0)_d/\eta(n^2) \equiv R_s(n^2)^2 \tag{813}$$

$$c^R(\underset{\sim}{n},0) = R_s(n^2)\cos\theta(\underset{\sim}{n}) \tag{814}$$

$$c^I(\underset{\sim}{n},0) = R_s(n^2)\sin\theta(\underset{\sim}{n}) \tag{815}$$

where $\theta(\underset{\sim}{n})$ is the angular coordinate of a point chosen at random on the circle determined by Equation 813.

First-order reaction

The time-scaled conservation equation in terms of $\underset{\sim}{n}$ for a first-order reaction is

$\underset{\sim}{n} = \underset{\sim}{0}$

$$\frac{\partial \mathcal{C}(\underset{\sim}{0})}{\partial t'} = -Da_I' \mathcal{C}(\underset{\sim}{0}), \quad c^R(\underset{\sim}{0}) = c^I(\underset{\sim}{0}) = 0 \tag{816}$$

$\underset{\sim}{n} \neq \underset{\sim}{0}$

$$\frac{\partial c^R(\underset{\sim}{n})}{\partial t'} = -Pe'^{-1} n^2 c^R(\underset{\sim}{n}) - Da_I' c^R(\underset{\sim}{n}) + n_i \sum_{\underset{\sim}{m}} [u_i^R(\underset{\sim}{m}) c^I(\underset{\sim}{n}-\underset{\sim}{m}) + u_i^I(\underset{\sim}{m}) c^R(\underset{\sim}{n}-\underset{\sim}{m})] \tag{817}$$

$$\frac{\partial c^I(\underset{\sim}{n})}{\partial t'} = -Pe'^{-1} n^2 c^I(\underset{\sim}{n}) - Da'_I\, c^I(\underset{\sim}{n}) - n_i \sum_{\underset{\sim}{m}} [u_i^R(\underset{\sim}{m}) c^R(\underset{\sim}{n}-\underset{\sim}{m}) - u_i^I(\underset{\sim}{m}) c^I(\underset{\sim}{n}-\underset{\sim}{m})] \tag{818}$$

where $Da'_I \equiv (N/2\pi)Da_I$ is the scaled Damköhler number for a first-order reaction. The initial conditions are established using Equations 811 - 815.

Two species second-order reaction

For the reactants of a two species second-order reaction, the time-scaled conservation equations written in terms of $\underset{\sim}{n}$ are

$\underset{\sim}{n} = \underset{\sim}{0}$

$$\frac{\partial \mathcal{C}_A(\underset{\sim}{0})}{\partial t'} = \frac{\partial \mathcal{C}_B(\underset{\sim}{0})}{\partial t'} = -Da'_I\, \mathcal{C}_A(\underset{\sim}{0}) \mathcal{C}_B(\underset{\sim}{0}) - Da'_I \sum_{\underset{\sim}{m}} [c_A^R(\underset{\sim}{m}) c_B^R(\underset{\sim}{m}) + c_A^I(\underset{\sim}{m}) c_B^I(\underset{\sim}{m})] \tag{819}$$

$$c_A^R(\underset{\sim}{0}) = c_A^I(\underset{\sim}{0}) = c_B^R(\underset{\sim}{0}) = c_A^I(\underset{\sim}{0}) = 0 \tag{820}$$

$\underset{\sim}{n} \neq \underset{\sim}{0}$

$$\frac{\partial c_A^R(\underset{\sim}{n})}{\partial t'} = -Pe'^{-1}_A n^2 c_A^R(\underset{\sim}{n}) - Da'_I [\mathcal{C}_A(\underset{\sim}{0}) c_B^R(\underset{\sim}{n}) + \mathcal{C}_B(\underset{\sim}{0}) c_A^R(\underset{\sim}{n})] + n_i \sum_{\underset{\sim}{m}} [u_i^R(\underset{\sim}{m}) c_A^I(\underset{\sim}{n}-\underset{\sim}{m}) + u_i^I(\underset{\sim}{m}) c_A^R(\underset{\sim}{n}-\underset{\sim}{m})] - Da'_I \sum_{\underset{\sim}{m}} [c_A^R(\underset{\sim}{m}) c_B^R(\underset{\sim}{n}-\underset{\sim}{m}) - c_A^I(\underset{\sim}{m}) c_B^I(\underset{\sim}{n}-\underset{\sim}{m})] \tag{821}$$

$$\frac{\partial c_A^I(\underset{\sim}{n})}{\partial t'} = -Pe_A'^{-1} n^2 c_A^I(\underset{\sim}{n}) - Da_I' [\mathcal{C}_A(\underset{\sim}{0}) c_B^I(\underset{\sim}{n}) + \mathcal{C}_B(\underset{\sim}{0}) c_A^I(\underset{\sim}{n})]$$

$$- n_i \sum_{\underset{\sim}{m}} [u_i^R(\underset{\sim}{m}) c_A^R(\underset{\sim}{n}-\underset{\sim}{m}) - u_i^I(\underset{\sim}{m}) c_A^I(\underset{\sim}{n}-\underset{\sim}{m})] \qquad (822)$$

$$- Da_I' \sum_{\underset{\sim}{m}} [c_A^R(\underset{\sim}{m}) c_B^I(\underset{\sim}{n}-\underset{\sim}{m}) + c_A^I(\underset{\sim}{m}) c_B^R(\underset{\sim}{n}-\underset{\sim}{m})]$$

$$\frac{\partial c_B^R(\underset{\sim}{n})}{\partial t'} = -Pe_B'^{-1} n^2 c_B^R(\underset{\sim}{n}) - Da_I' [\mathcal{C}_A(\underset{\sim}{0}) c_B^R(\underset{\sim}{n}) + \mathcal{C}_B(\underset{\sim}{0}) c_A^R(\underset{\sim}{n})]$$

$$+ n_i \sum_{\underset{\sim}{m}} [u_i^R(\underset{\sim}{m}) c_B^I(\underset{\sim}{n}-\underset{\sim}{m}) + u_i^I(\underset{\sim}{m}) c_B^R(\underset{\sim}{n}-\underset{\sim}{m})] \qquad (823)$$

$$- Da_I' \sum_{\underset{\sim}{m}} [c_A^R(\underset{\sim}{m}) c_B^R(\underset{\sim}{n}-\underset{\sim}{m}) - c_A^I(\underset{\sim}{m}) c_B^I(\underset{\sim}{n}-\underset{\sim}{m})]$$

$$\frac{\partial c_B^I(\underset{\sim}{n})}{\partial t'} = -Pe_B'^{-1} n^2 c_B^I(\underset{\sim}{n}) - Da_I' [\mathcal{C}_A(\underset{\sim}{0}) c_B^I(\underset{\sim}{n}) + \mathcal{C}_B(\underset{\sim}{0}) c_A^I(\underset{\sim}{n})]$$

$$- n_i \sum_{\underset{\sim}{m}} [u_i^R(\underset{\sim}{m}) c_B^R(\underset{\sim}{n}-\underset{\sim}{m}) - u_i^I(\underset{\sim}{m}) c_B^I(\underset{\sim}{n}-\underset{\sim}{m})] \qquad (824)$$

$$- Da_I' \sum_{\underset{\sim}{m}} [c_A^R(\underset{\sim}{m}) c_B^I(\underset{\sim}{n}-\underset{\sim}{m}) + c_A^I(\underset{\sim}{m}) c_B^R(\underset{\sim}{n}-\underset{\sim}{m})]$$

$$Pe_A' \equiv (N/2\pi) Pe_A, \quad Pe_B' \equiv (N/2\pi) Pe_B \qquad (825)$$

The initial conditions are assigned using

$$\bar{C}_A(0) = \mathcal{C}_A(\underset{\sim}{0},0) = 1 \qquad (826)$$

$$\bar{C}_B(0) = \mathcal{C}_B(\underset{\sim}{0},0) = \text{initial stoichiometry} \qquad (827)$$

$$\tilde{c}_A(0)^2 = \sum_{n^2=1}^{n_{max}^2} E_A(n^2,0)_d \tag{828}$$

$$\tilde{c}_B(0)^2 = \sum_{n^2=1}^{n_{max}^2} E_B(n^2,0)_d \tag{829}$$

$$\overline{c_A c_B}(0) = \sum_{n^2=1}^{n_{max}^2} E_{AB}(n^2,0)_d \tag{830}$$

$$\phi_A^R(\underset{\sim}{n},0)^2 + \phi_A^I(\underset{\sim}{n},0)^2 = E_A(n^2,0)_d/\eta(n^2) \equiv R_A(n^2)^2 \tag{831}$$

$$\phi_A^R(\underset{\sim}{n},0) = R_A(n^2)\cos\theta(\underset{\sim}{n}) \tag{832}$$

$$\phi_A^I(\underset{\sim}{n},0) = R_A(n^2)\sin\theta(\underset{\sim}{n}) \tag{833}$$

$$\phi_B^R(\underset{\sim}{n},0) = \frac{E_{AB}(n^2,0)_d}{E_A(n^2,0)_d}\phi_A^R(\underset{\sim}{n},0) \pm \frac{[E_A(n^2,0)_d E_B(n^2,0)_d - E_{AB}(n^2,0)_d{}^2]^{\frac{1}{2}}}{E_A(n^2,0)_d}\phi_A^I(\underset{\sim}{n},0) \tag{834}$$

$$\phi_B^I(\underset{\sim}{n},0) = \frac{E_{AB}(n^2,0)_d}{E_A(n^2,0)_d}\phi_A^I(\underset{\sim}{n},0) \mp \frac{[E_A(n^2,0)_d E_B(n^2,0)_d - E_{AB}(n^2,0)_d{}^2]^{\frac{1}{2}}}{E_A(n^2,0)_d}\phi_A^R(n,0) \tag{835}$$

$$\text{for } E_A(n^2,0)_d E_B(n^2,0)_d \geq E_{AB}(n^2,0)_d{}^2, \quad n > 0 \tag{836}$$

Concentration field statistics

The concentration fluctuation spectrum for each reacting species can be calculated using

$$E_s(n^2)_d = \sum_{\theta_{\underset{\sim}{n}}} \sum_{\phi_{\underset{\sim}{n}}} [\phi^R(\underset{\sim}{n})^2 + \phi^I(\underset{\sim}{n})^2] \qquad (837,3D)$$

$$E_s(n^2)_d = \sum_{\theta_{\underset{\sim}{n}}} [\phi^R(\underset{\sim}{n})^2 + \phi^I(\underset{\sim}{n})^2] \qquad (838,2D)$$

or the equivalent form

$$E_s(n^2)_d = \sum_{\underset{\sim}{m}} \delta_{n^2,m^2} [\phi^R(\underset{\sim}{n})^2 + \phi^I(\underset{\sim}{n})^2] \qquad (839)$$

Similarly, for two species reactions the joint correlation spectrum function can be found from

$$E_{AB}(n^2)_d = \sum_{\underset{\sim}{m}} \delta_{n^2,m^2} [\phi_A^R(\underset{\sim}{m})\phi_B^R(\underset{\sim}{m}) + \phi_A^I(\underset{\sim}{m})\phi_B^I(\underset{\sim}{m})] \qquad (840)$$

where $E_s(n^2)_d \equiv 0$ and $E_{AB}(n^2)_d \equiv 0$ for values of n^2 not given by $n^2 = n_i n_i$, that is for which $\eta(n^2) = 0$.

The concentration field statistics can be found using

$$\widetilde{c}(t')^2 = \sum_{n^2=1}^{n_{max}^2} E_s(n^2,t')_d \qquad (841)$$

$$\overline{c_A c_B}(t') = \sum_{n^2=1}^{n_{max}^2} E_{AB}(n^2,t')_d \qquad (842)$$

$$L_s(t') = [N/4\tilde{c}(t')^2] \sum_{n^2=1}^{n_{max}^2} n^{-1} E_s(n^2,t')_d \qquad (843,3D)$$

$$L_s(t') = [N/2\pi\tilde{c}(t')^2] \sum_{n^2=1}^{n_{max}^2} n^{-1} E_s(n^2,t')_d \qquad (844,2D)$$

$$\lambda_s(t')^{-2} = [2\pi^2/3N^2\tilde{c}(t')^2] \sum_{n^2=1}^{n_{max}^2} n^2 E_s(n^2,t')_d \qquad (845,3D)$$

$$\lambda_s(t')^{-2} = [\pi^2/N^2\tilde{c}(t')^2] \sum_{n^2=1}^{n_{max}^2} n^2 E_s(n^2,t')_d \qquad (846,2D)$$

$$f_s(r,t') = [1/\tilde{c}(t')^2] \sum_{n^2=1}^{n_{max}^2} E_s(n^2,t')_d \sin(kr)/kr \qquad (847,3D)$$

$$f_s(r,t') = [1/\tilde{c}(t')^2] \sum_{n^2=1}^{n_{max}^2} E_s(n^2,t')_d \, J_0(kr) \qquad (848,2D)$$

The concentration field isolines are found using

$$c(\underset{\sim}{x}',t') = \sum_{\underset{\sim}{n}} [\phi^R(\underset{\sim}{n},t')\cos(2\pi\underset{\sim}{n}\cdot\underset{\sim}{x}') - \phi^I(\underset{\sim}{n},t')\sin(2\pi\underset{\sim}{n}\cdot\underset{\sim}{x}')] \qquad (849)$$

where $\underset{\sim}{x}' \equiv \underset{\sim}{x}^*/L^*$.

NUMERICAL INTEGRATION PROCEDURE

Due to the very large computational requirements of three-dimensional turbulence, calculations were only made for two-dimensional turbulence. In two dimensions, the discrete values of the integer vector $\underset{\sim}{n}$ can be represented as a lattice of points in $\underset{\sim}{n}$-space, as portrayed in Figure 7 for different values of n_{max}, the spherical (circular) cutoff value of n. Because the real part of a Fourier transformed variable must be symmetric in $\underset{\sim}{n}$ and the imaginary part antisymmetric in $\underset{\sim}{n}$ (the physical-space reality requirement), it is convenient to separate each point and its inversion point into two categories. In Figure 7, the points within the cutoff have been divided into the so-called upper half-space points and lower half-space points. Since Fourier fluctuation variables associated with the point $\underset{\sim}{n} = \underset{\sim}{0}$ are zero for all t, it is immaterial whether the point $\underset{\sim}{n} = \underset{\sim}{0}$ is included in or excluded from either half-space. Therefore, only half of the values of the Fourier modes need to be integrated over time; values of the other half are assigned using the inversion properties and are only used in convolution summations.

Because computation requirements grow rapidly with increasing values of n_{max} even in two dimensions, a cutoff of $n_{max}^2 = 8$ was used in this study, which corresponds to the system of Figure 7c.

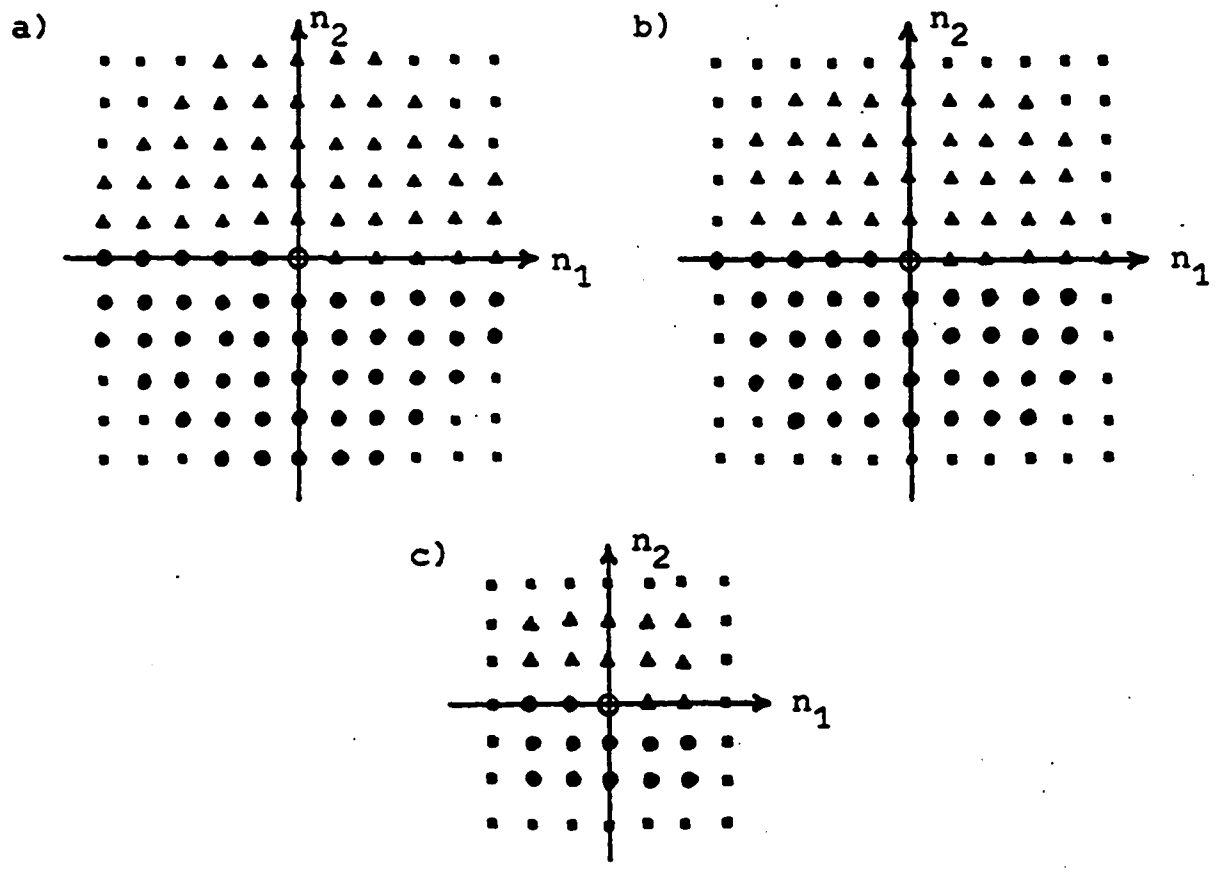

○ $\underset{\sim}{n} = \underset{\sim}{0}$ ▪ excluded points

● lower half-space points, values of Fourier modes associated with these points are obtained by numerical integration over time

▲ upper half-space points, values of Fourier modes associated with these points are assigned using the inversion symmetry properties of real and imaginary parts resulting from the physical-space reality requirement; these values are only used in convolution summations

a) Example of summation limits for cutoff having $n_{max} \neq$ an integer.

b) Example of summation limits for cutoff having $n_{max} =$ an integer. Notice that limits on n_1 are different in summing over just the upper half-space points or lower half-space points.

c) Spherical cutoff used in calculations.

Figure 7. Classification of points in the lattice associated with the integer vector $\underset{\sim}{n}$ for spherical (circular) cutoff of summations over $\underset{\sim}{n}$

Generation of the Turbulent Velocity Fields

Random convection velocity

In order to integrate Equation 799 to find the second-order response to an integrated random step forcing function for each lower half-space value of $\underset{\sim}{n}$, it is convenient to rewrite Equation 799 as two first-order differential equations

$$\gamma'(\underset{\sim}{n})^2 \frac{d\alpha(\underset{\sim}{n},t')}{dt'} + 2\gamma'(\underset{\sim}{n})\zeta\, \alpha(\underset{\sim}{n},t') + \theta(\underset{\sim}{n},t') = 2\pi\, S(\underset{\sim}{n},t',T'_{so}) \tag{850}$$

$$\frac{d\theta(\underset{\sim}{n},t')}{dt'} = \alpha(\underset{\sim}{n},t') \tag{851}$$

Converting Equations 850 and 851 to finite difference form gives

$$\alpha(\underset{\sim}{n},t'_{r+1}) = \alpha(\underset{\sim}{n},t'_r) + \Delta t'_\theta \left[2\pi S(\underset{\sim}{n},t'_r,T'_{so}) - 2\gamma'(\underset{\sim}{n})\zeta\, \alpha(\underset{\sim}{n},t'_r) - \theta(\underset{\sim}{n},t'_r)\right]/\gamma'(\underset{\sim}{n})^2 \tag{852}$$

$$\theta(\underset{\sim}{n},t'_{r+1}) = \theta(\underset{\sim}{n},t'_r) + \Delta t'_\theta\, \alpha(\underset{\sim}{n},t'_r) \tag{853}$$

$$t'_{r+1} = t'_r + \Delta t'_\theta \tag{854}$$

Values of $\phi_i^R(\underset{\sim}{n},t')$ and $\phi_i^I(\underset{\sim}{n},t')$ are found using Equations 781 - 790.

The Gaussian energy spectrum in discrete form assigned

to the random convection velocity for all time is given in Table 3 along with other statistics and numerical integration parameters. The longitudinal correlation function $f(r,t)_{\phi}$ is shown in Figure 8.

Initial values $S(\underset{\sim}{n},0,T'_{so})$ and successive values of $s(\underset{\sim}{n},t',T'_{so})$ were computer generated random numbers chosen from a uniform distribution ranging from -0.5 to 0.5. The initial values $\theta(\underset{\sim}{n},0)$ were generated as random numbers from the same distribution scaled by the factor 2π. The initial values $\alpha(\underset{\sim}{n},0)$ were assigned using

$$\alpha(\underset{\sim}{n},0) = [2\pi\, S(\underset{\sim}{n},0) - \theta(\underset{\sim}{n},0)]/2\mathcal{S}(n^2) \qquad (855)$$

Initial and successive values of $T_s(\underset{\sim}{n})$ were computer generated random numbers chosen from a Poisson distribution having a mean value of 20 and scaled by the factor $T_{so}(n^2)/20$.

Using Equations 781 - 790, 800, and 852 - 854, values of t', $\phi_1^R(\underset{\sim}{n},t')$, $\phi_1^I(\underset{\sim}{n},t')$, $\phi_2^R(\underset{\sim}{n},t')$, and $\phi_2^I(\underset{\sim}{n},t')$ were computed (using an IBM 370/158 computer located at the Iowa State University Computation Center) and recorded on magnetic computer tape. Since only every other set of values of $\phi_i^R(\underset{\sim}{n},t')$ and $\phi_i^I(\underset{\sim}{n},t')$ were recorded on tape, the effective time increment for the random convection velocity values is $\Delta t_{\phi} = 2\Delta t_{\theta}$.

Figure 9 shows an example (for an arbitrary time scale)

Table 3. Assigned random convection velocity numerical integration parameters, statistics, and energy spectrum

Numerical Integration Parameters

time scale factor = $2\pi/N = 1.40442$

$T_{so}(1) = 4.0$, $T_{so}(n^2) = 4\gamma(n^2)$ (assigned)

$\Delta t_\theta = T_{so}(n_{max}^2)/640 = 4\gamma(n_{max}^2)/640 = 5.1532 \times 10^{-4}$

$S = 0.3$, $B = 0.4$

Statistics

$E(n^2,t)_{d\phi} = a_d(n/n_o)^3 \exp[-1.5(n/n_o)^2]$

$n_o^2 = 1.9$, $n_{max}^2 = 8$, $a_d = 1.60254$

$L_{f\phi}(t) = 1.0$, $\lambda_{f\phi}(t) = 1.22911$, $N = 4.47385$

Energy Spectrum and Time Scales

n^2	$\eta(n^2)$	$E(n^2,t)_{d\phi}$	$\gamma(n^2)$
1	4	0.27787	1.00000
2	4	0.35688	0.62269
4	4	0.20813	0.36625
5	8	0.13208	0.23959
8	4	0.02503	0.08245

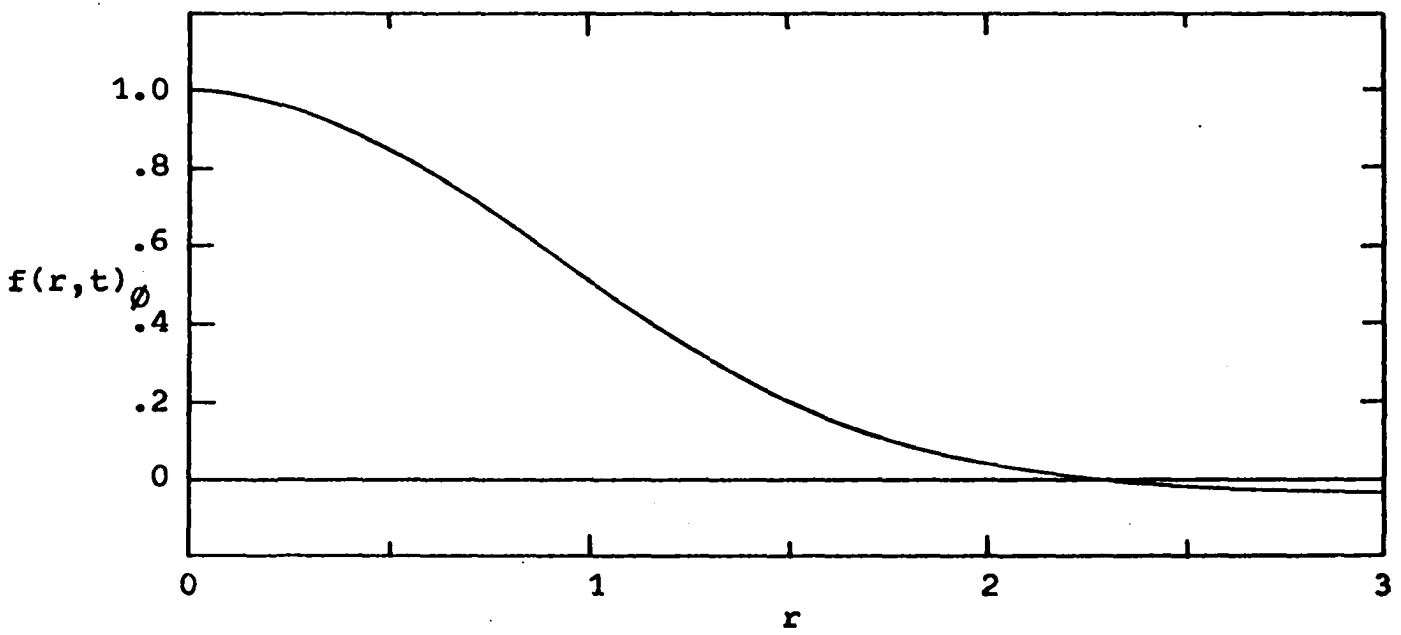

Figure 8. Longitudinal correlation function $f(r,t)_{\phi}$ for the random convection velocity for all t

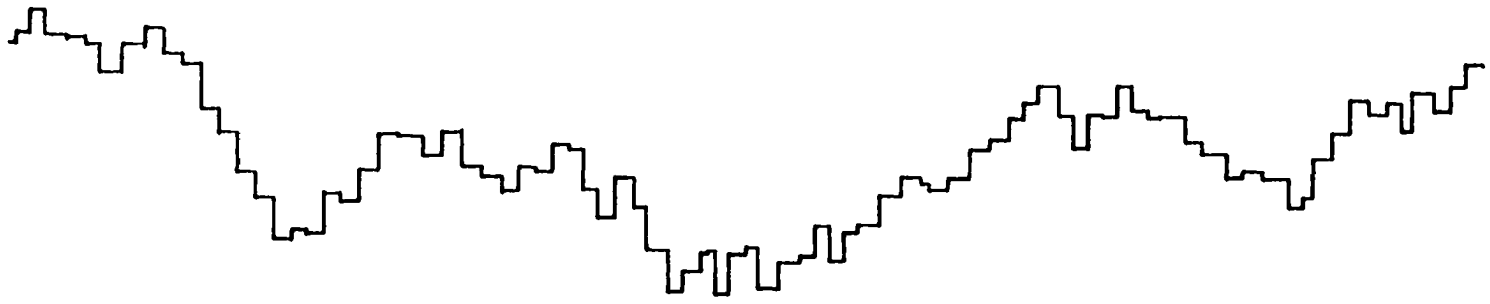

Figure 9. Example of a random step forcing function $S(t,T_{so})$ with successive periods T_s chosen from a Poisson distribution

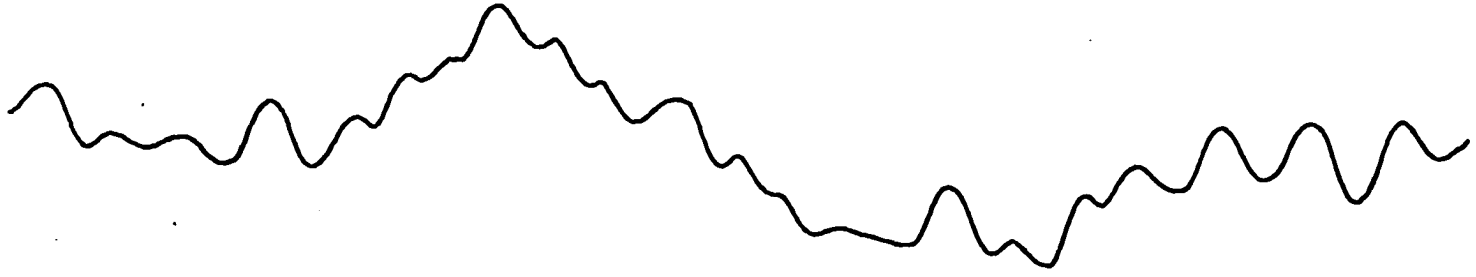

Figure 10. Example of a second-order response to a random step forcing function with constant successive periods $T_s = 4\tau$ and for a dampening ratio $\zeta = 0.3$

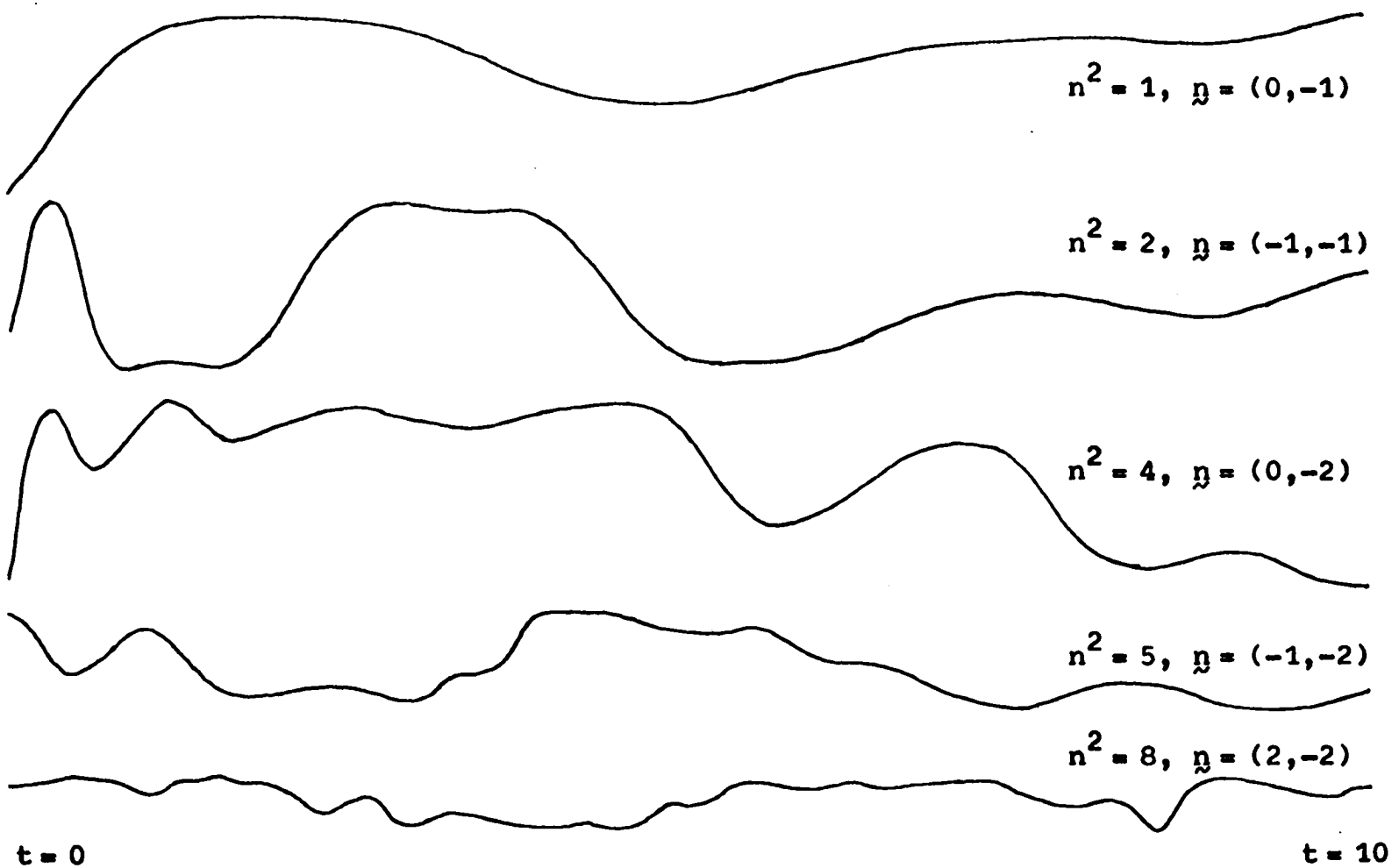

Figure 11. Examples of the time behaviors of the random convection velocity Fourier modes $\phi_1^R(\underset{\sim}{n},t)$ and $\phi_1^I(\underset{\sim}{n},t)$ for different values of $\underset{\sim}{n}$

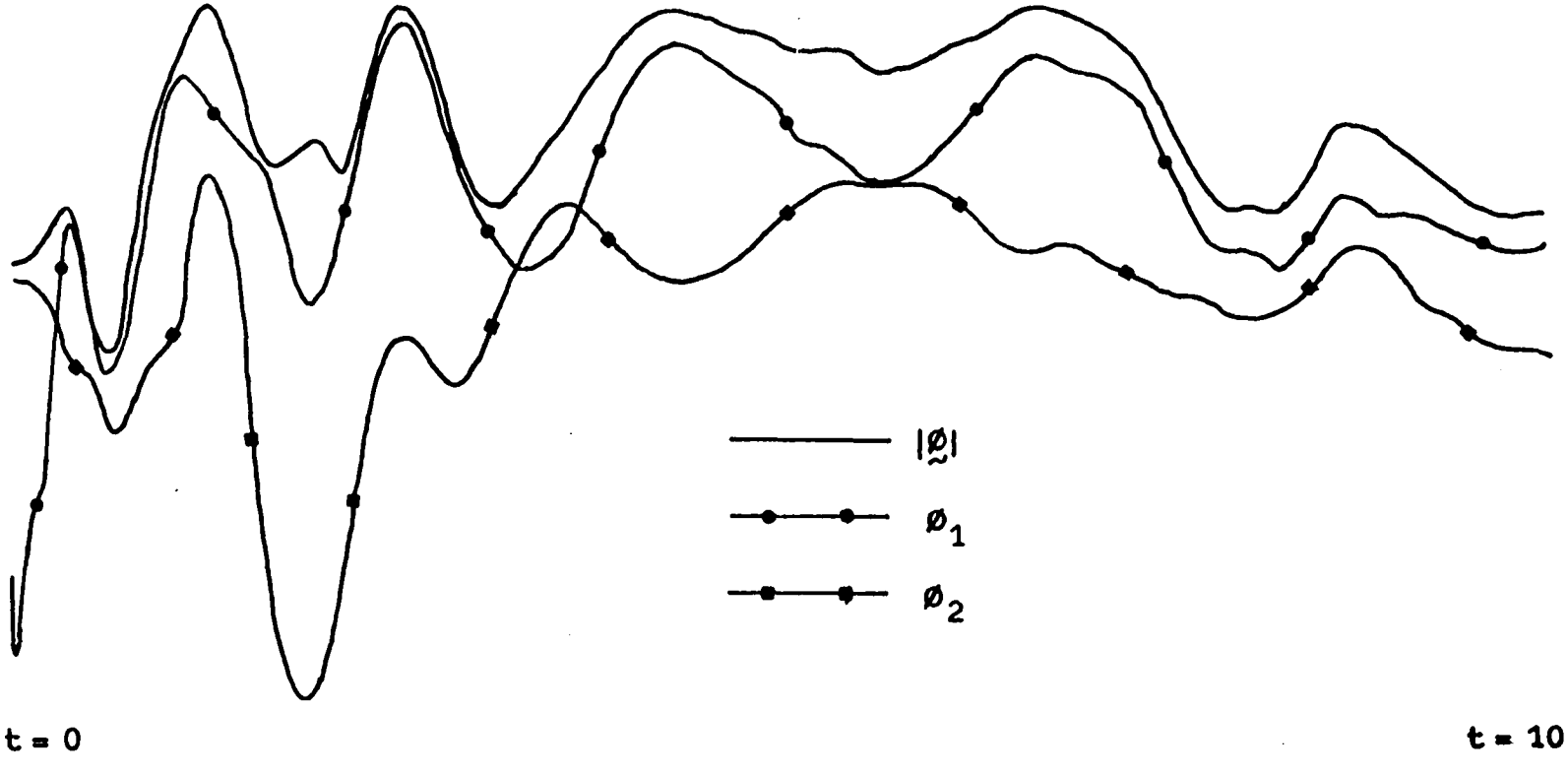

Figure 12. Time behavior of the components and magnitude of the physical-space random convection velocity at the point $\underset{\sim}{x} = \underset{\sim}{0}$

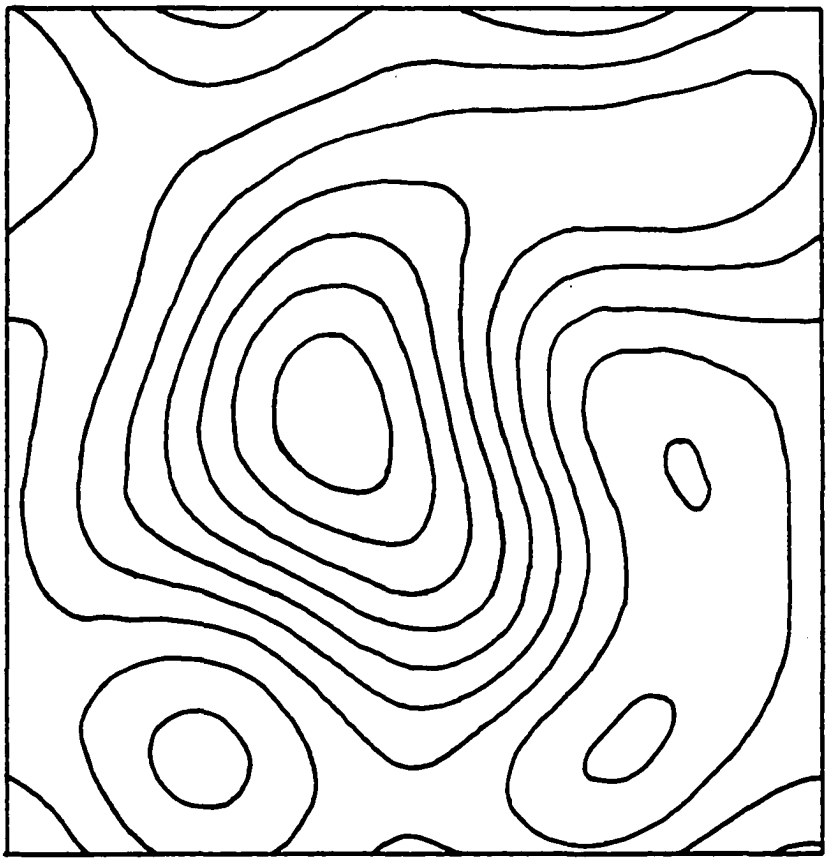

Figure 13. Streamlines for the random convection velocity at $t = 0$

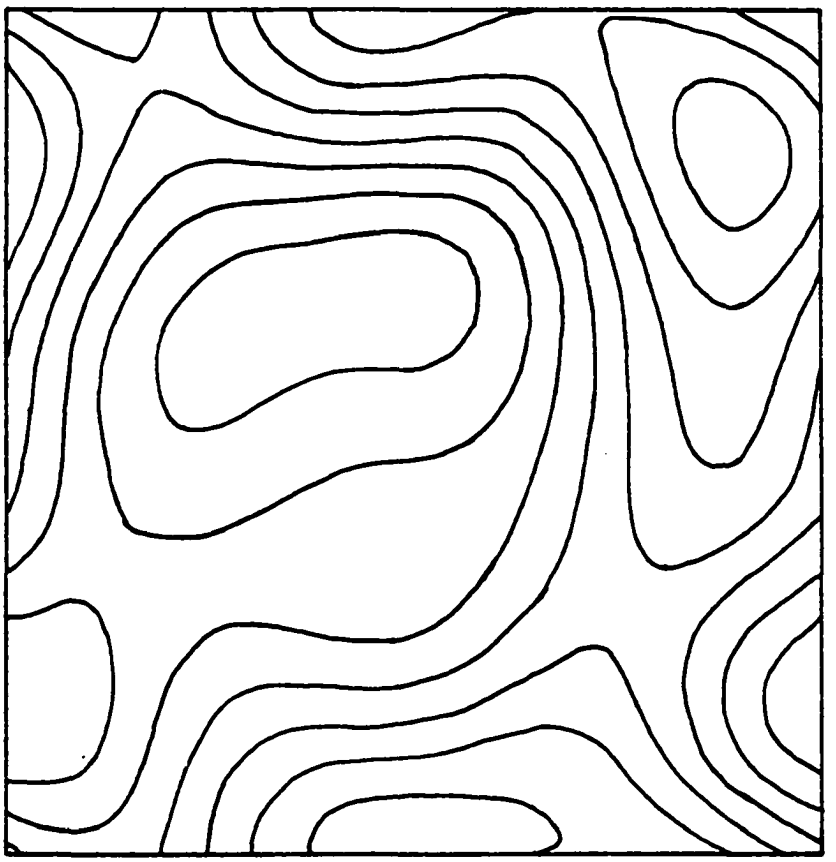

Figure 14. Streamlines for the random convection velocity at t = 5

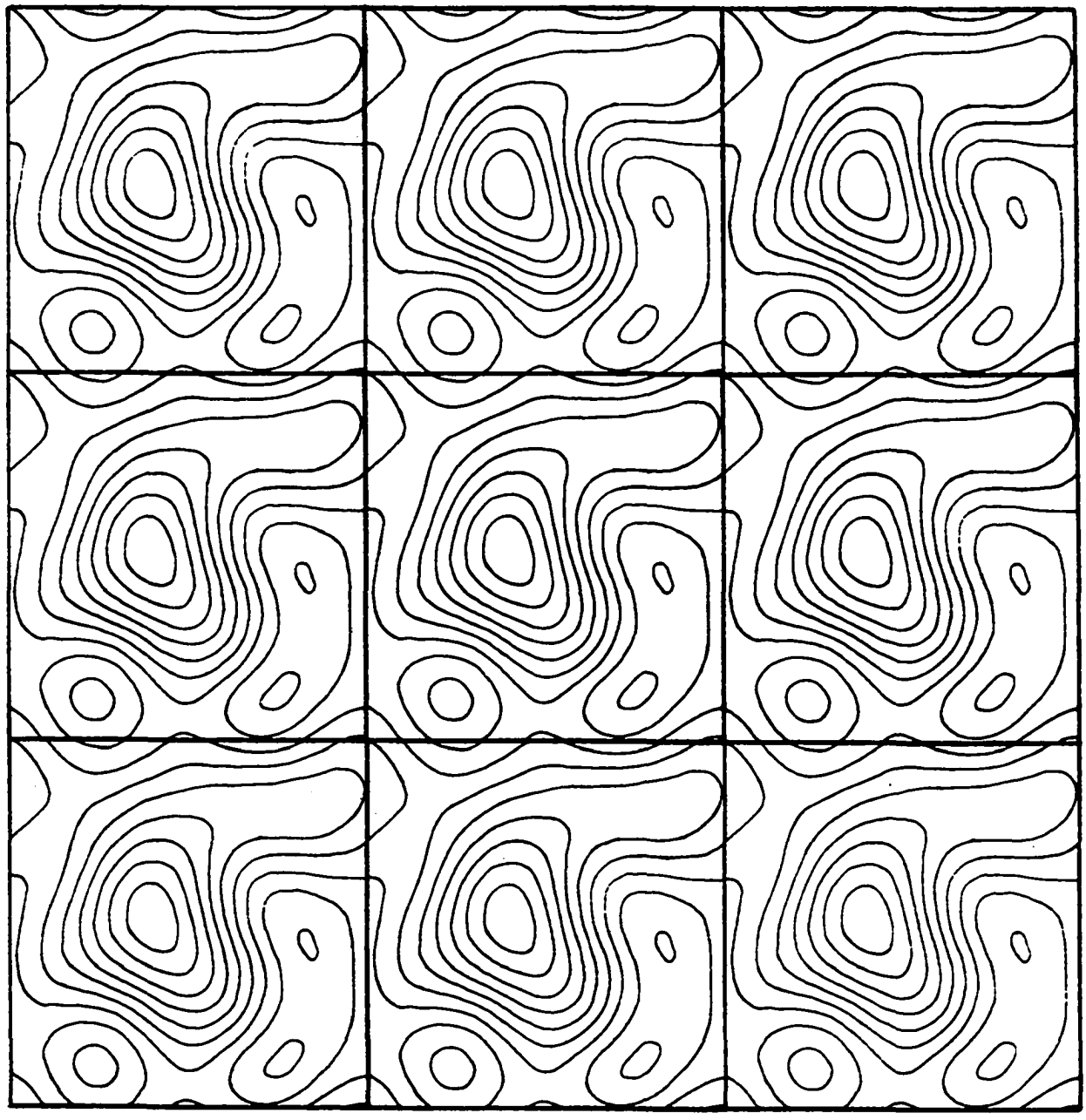

Figure 15. Streamlines for the random convection velocity at t = 0 extended over several unit boxes of turbulence

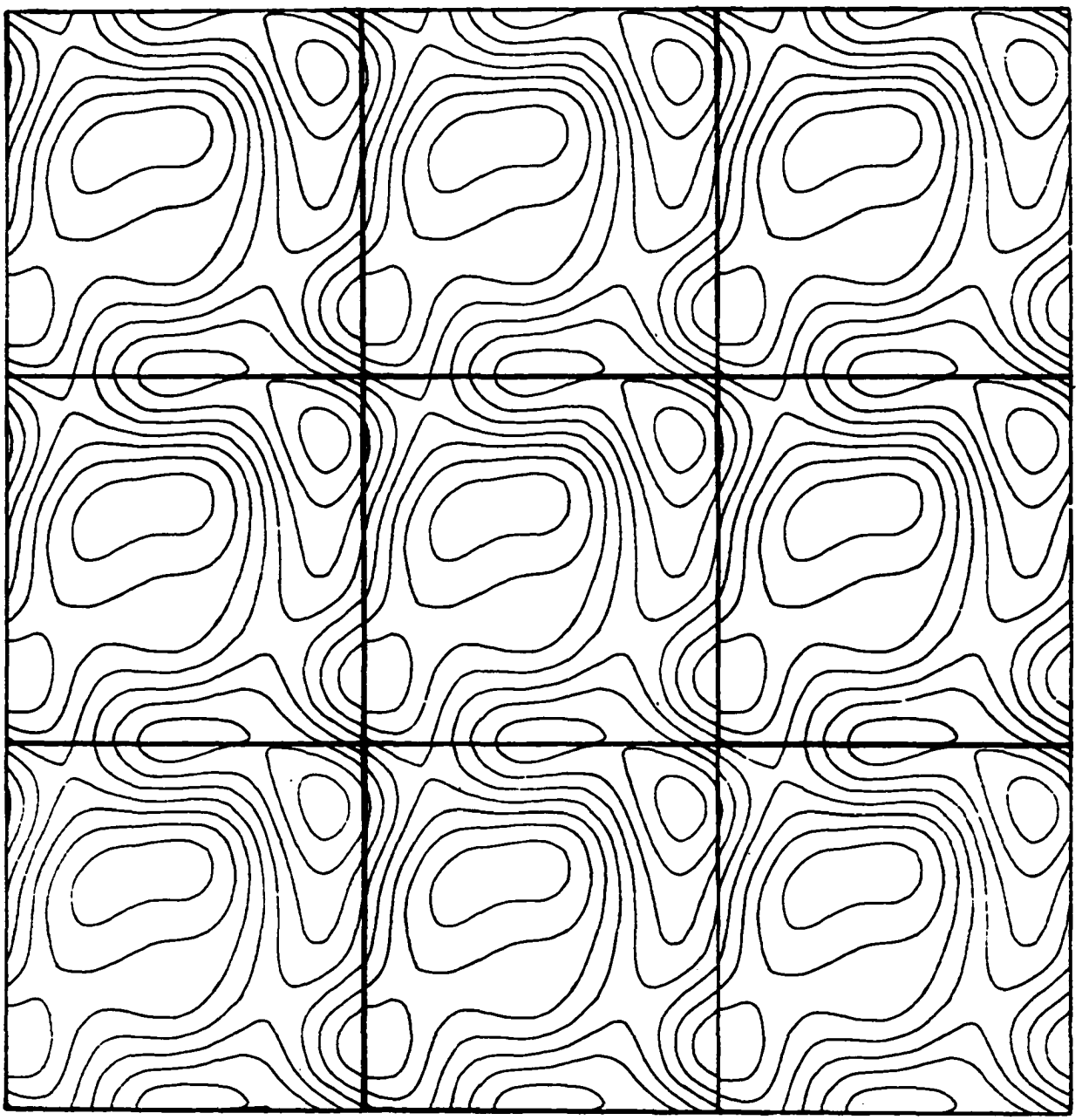

Figure 16. Streamlines for the random convection velocity at t = 5 extended over several unit boxes of turbulence

of a random step forcing function $S(t,T_{so})$ with successive periods T_s chosen from a Poisson distribution. An example of a second-order response to a random step forcing function with constant successive periods T_s, the random walk on a circle with inertia whose location is indicated by $\theta(\underset{\sim}{n},t')$, is illustrated in Figure 10 (for an arbitrary time scale). Figure 11 shows examples of the time behavior of some of the random convection velocity Fourier modes $\phi_1^R(\underset{\sim}{n},t)$ and $\phi_1^I(\underset{\sim}{n},t)$ that were generated and stored on tape. The scale of motion decreases from being largest at the top of the figure (n^2 = 1) to smallest at the bottom (n^2 = 8). The reduction in amplitude of the fluctuations reflects the decrease in energy content of the scales as dictated by the assigned energy spectrum. Likewise, the time scale of the fluctuations decreases with the scale of motion. The time behavior shown is for 10 dimensionless time units or eddy circulation times. The time behavior of the components and magnitude of the physical-space random convection velocity at the point $\underset{\sim}{x} = \underset{\sim}{0}$, found by summing the real parts of the Fourier modes, is shown in Figure 12 for ten eddy circulation times. Streamlines for the physical-space random convection velocity at t = 0 and t = 5 eddy circulation times are shown in Figures 13 and 14, respectively. Streamline patterns extending over several repeating unit boxes of turbulence are shown in Figures 15 and 16.

Convected velocity field with interaction

The velocity field $u_i(\underset{\sim}{n})$ that is convected by the random convection velocity $\phi_i(\underset{\sim}{n})$ and has interaction between Fourier modes, hereafter referred to as the convected velocity field with interaction, is generated by integrating the set of Equations 725 and 726 over time. In two dimensions, Equations 725 and 726 can be written in abbreviated form as the set of equations

$$\frac{\partial u_1^R(\underset{\sim}{n},t')}{\partial t'} = F_1^R(\underset{\sim}{n},t'), \quad \frac{\partial u_1^I(\underset{\sim}{n},t')}{\partial t'} = F_1^I(\underset{\sim}{n},t') \qquad (855,856)$$

$$\frac{\partial u_2^R(\underset{\sim}{n},t')}{\partial t'} = F_2^R(\underset{\sim}{n},t'), \quad \frac{\partial u_2^I(\underset{\sim}{n},t')}{\partial t'} = F_2^I(\underset{\sim}{n},t') \qquad (857,858)$$

with

$$\begin{aligned} F_1^R(\underset{\sim}{n},t') = {} & n_1 P_{11}(\underset{\sim}{n}) \sum_{\underset{\sim}{m}} [\phi_1^R(\underset{\sim}{m}) u_1^I(\underset{\sim}{n}-\underset{\sim}{m}) + \phi_1^I(\underset{\sim}{m}) u_1^R(\underset{\sim}{n}-\underset{\sim}{m})] \\ & + n_1 P_{12}(\underset{\sim}{n}) \sum_{\underset{\sim}{m}} [\phi_1^R(\underset{\sim}{m}) u_2^I(\underset{\sim}{n}-\underset{\sim}{m}) + \phi_1^I(\underset{\sim}{m}) u_2^R(\underset{\sim}{n}-\underset{\sim}{m})] \qquad (859,2D) \\ & + n_2 P_{11}(\underset{\sim}{n}) \sum_{\underset{\sim}{m}} [\phi_2^R(\underset{\sim}{m}) u_1^I(\underset{\sim}{n}-\underset{\sim}{m}) + \phi_2^I(\underset{\sim}{m}) u_1^R(\underset{\sim}{n}-\underset{\sim}{m})] \\ & + n_2 P_{12}(\underset{\sim}{n}) \sum_{\underset{\sim}{m}} [\phi_2^R(\underset{\sim}{m}) u_2^I(\underset{\sim}{n}-\underset{\sim}{m}) + \phi_2^I(\underset{\sim}{m}) u_2^R(\underset{\sim}{n}-\underset{\sim}{m})] \end{aligned}$$

$$\begin{aligned} F_2^R(\underset{\sim}{n},t') = {} & n_1 P_{21}(\underset{\sim}{n}) \sum_{\underset{\sim}{m}} [\phi_1^R(\underset{\sim}{m}) u_1^I(\underset{\sim}{n}-\underset{\sim}{m}) + \phi_1^I(\underset{\sim}{m}) u_1^R(\underset{\sim}{n}-\underset{\sim}{m})] \\ & + n_1 P_{22}(\underset{\sim}{n}) \sum_{\underset{\sim}{m}} [\phi_1^R(\underset{\sim}{m}) u_2^I(\underset{\sim}{n}-\underset{\sim}{m}) + \phi_1^I(\underset{\sim}{m}) u_2^R(\underset{\sim}{n}-\underset{\sim}{m})] \end{aligned}$$

$$+ n_2 P_{21}(\underset{\sim}{n}) \sum_{\underset{\sim}{m}} [\phi_2^R(\underset{\sim}{m}) u_1^I(\underset{\sim}{n}-\underset{\sim}{m}) + \phi_2^I(\underset{\sim}{m}) u_1^R(\underset{\sim}{n}-\underset{\sim}{m})]$$

$$+ n_2 P_{22}(\underset{\sim}{n}) \sum_{\underset{\sim}{m}} [\phi_2^R(\underset{\sim}{m}) u_2^I(\underset{\sim}{n}-\underset{\sim}{m}) + \phi_2^I(\underset{\sim}{m}) u_2^R(\underset{\sim}{n}-\underset{\sim}{m})] \quad (860,2D)$$

$$F_1^I(\underset{\sim}{n},t') = -n_1 P_{11}(\underset{\sim}{n}) \sum_{\underset{\sim}{m}} [\phi_1^R(\underset{\sim}{m}) u_1^R(\underset{\sim}{n}-\underset{\sim}{m}) - \phi_1^I(\underset{\sim}{m}) u_1^I(\underset{\sim}{n}-\underset{\sim}{m})]$$

$$- n_1 P_{12}(\underset{\sim}{n}) \sum_{\underset{\sim}{m}} [\phi_1^R(\underset{\sim}{m}) u_2^R(\underset{\sim}{n}-\underset{\sim}{m}) - \phi_1^I(\underset{\sim}{m}) u_2^I(\underset{\sim}{n}-\underset{\sim}{m})] \quad (861,2D)$$

$$- n_2 P_{11}(\underset{\sim}{n}) \sum_{\underset{\sim}{m}} [\phi_2^R(\underset{\sim}{m}) u_1^R(\underset{\sim}{n}-\underset{\sim}{m}) - \phi_2^I(\underset{\sim}{m}) u_1^I(\underset{\sim}{n}-\underset{\sim}{m})]$$

$$- n_2 P_{12}(\underset{\sim}{n}) \sum_{\underset{\sim}{m}} [\phi_2^R(\underset{\sim}{m}) u_2^R(\underset{\sim}{n}-\underset{\sim}{m}) - \phi_2^I(\underset{\sim}{m}) u_2^I(\underset{\sim}{n}-\underset{\sim}{m})]$$

$$F_2^I(\underset{\sim}{n},t') = -n_1 P_{21}(\underset{\sim}{n}) \sum_{\underset{\sim}{m}} [\phi_1^R(\underset{\sim}{m}) u_1^R(\underset{\sim}{n}-\underset{\sim}{m}) - \phi_1^I(\underset{\sim}{m}) u_1^I(\underset{\sim}{n}-\underset{\sim}{m})]$$

$$- n_1 P_{22}(\underset{\sim}{n}) \sum_{\underset{\sim}{m}} [\phi_1^R(\underset{\sim}{m}) u_2^R(\underset{\sim}{n}-\underset{\sim}{m}) - \phi_1^I(\underset{\sim}{m}) u_2^I(\underset{\sim}{n}-\underset{\sim}{m})] \quad (862,2D)$$

$$- n_2 P_{21}(\underset{\sim}{n}) \sum_{\underset{\sim}{m}} [\phi_2^R(\underset{\sim}{m}) u_1^R(\underset{\sim}{n}-\underset{\sim}{m}) - \phi_2^I(\underset{\sim}{m}) u_1^I(\underset{\sim}{n}-\underset{\sim}{m})]$$

$$- n_2 P_{22}(\underset{\sim}{n}) \sum_{\underset{\sim}{m}} [\phi_2^R(\underset{\sim}{m}) u_2^R(\underset{\sim}{n}-\underset{\sim}{m}) - \phi_2^I(\underset{\sim}{m}) u_2^I(\underset{\sim}{n}-\underset{\sim}{m})]$$

Converting Equations 855 - 858 to finite difference form and using values of $F_i^R(\underset{\sim}{n},t')$ and $F_i^I(\underset{\sim}{n},t')$ that are averaged over time steps t'_r and t'_{r+1} gives

$$[u_i^R(\underset{\sim}{n},t'_{r+1}) - u_i^R(\underset{\sim}{n},t'_r)]/\Delta t' = \tfrac{1}{2}[F_i^R(\underset{\sim}{n},t'_r) + F_i^R(\underset{\sim}{n},t'_{r+1})] \quad (863)$$

$$[u_i^I(\underset{\sim}{n},t'_{r+1}) - u_i^I(\underset{\sim}{n},t'_r)]/\Delta t' = \tfrac{1}{2}[F_i^I(\underset{\sim}{n},t'_r) + F_i^I(\underset{\sim}{n},t'_{r+1})] \quad (864)$$

and hence the set of predictor equations

$$u_i^R(\underset{\sim}{n},t'_{r+1}) = u_i^R(\underset{\sim}{n},t'_r) + \Delta t' \; F_i^R(\underset{\sim}{n},t'_r) \quad (865)$$

$$u_i^I(\underset{\sim}{n},t'_{r+1}) = u_i^I(\underset{\sim}{n},t'_r) + \Delta t' \; F_i^I(\underset{\sim}{n},t'_r) \quad (866)$$

and set of iterative corrector equations

$$u_i^R(\underset{\sim}{n},t'_{r+1}) = u_i^R(\underset{\sim}{n},t'_r) + \tfrac{1}{2}\Delta t' [\, F_i^R(\underset{\sim}{n},t'_r) + F_i^R(\underset{\sim}{n},t'_{r+1}) \,] \quad (867)$$

$$u_i^I(\underset{\sim}{n},t'_{r+1}) = u_i^I(n,t'_r) + \tfrac{1}{2}\Delta t' [\, F_i^I(\underset{\sim}{n},t'_r) + F_i^I(\underset{\sim}{n},t'_{r+1}) \,] \quad (868)$$

The initial conditions for $u_i^R(\underset{\sim}{n})$ and $u_i^I(\underset{\sim}{n})$ are found using Equations 741 - 750 and were generated in the same manner as for the random convection velocity. The initial energy spectrum and other statistics are the same as those given previously for the random convection velocity in Table 3 and Figure 8 but with different (randomly) generated values of the Fourier modes.

By reading the previously calculated values of $\phi_i^R(\underset{\sim}{n},t')$ and $\phi_i^I(\underset{\sim}{n},t')$ from tape and using Equations 865 - 868, values of $u_1^R(\underset{\sim}{n},t')$, $u_1^I(\underset{\sim}{n},t')$, $u_2^R(\underset{\sim}{n},t')$, and $u_2^I(\underset{\sim}{n},t')$ were calculated and recorded on a second magnetic computer tape. In order to avoid significant accumulations of round-off

errors, the calculations were performed in double precision but the values of $u_i^R(\underset{\sim}{n})$ and $u_i^I(\underset{\sim}{n})$ were truncated to single precision for storage on tape. The criteria used to determine iteration convergence of Equations 867 and 868 are given by

$$\left| \frac{u_i^R(\underset{\sim}{n},t'_{r+1})_{j+1} - u_i^R(\underset{\sim}{n},t'_{r+1})_j}{u_i^R(\underset{\sim}{n},t'_{r+1})_{j+1}} \right| < 3 \times 10^{-7} \qquad (869)$$

$$\left| \frac{u_i^I(\underset{\sim}{n},t'_{r+1})_{j+1} - u_i^I(\underset{\sim}{n},t'_{r+1})_j}{u_i^I(\underset{\sim}{n},t'_{r+1})_{j+1}} \right| < 3 \times 10^{-7} \qquad (870)$$

for all $\underset{\sim}{n}$ for the jth iteration.

The time behavior of the components of the physical-space convected velocity field with interaction at the point $\underset{\sim}{x} = \underset{\sim}{0}$ is shown in Figure 17. The streamline pattern for the velocity field at t = 5 eddy circulation times is shown in Figures 18 and 19. The corresponding streamline pattern for the random convection velocity at the same time is shown in Figures 14 and 16.

The energy spectrum and hence time scales and other statistics of the random convection velocity are constant over time. However, the energy spectrum of the convected velocity field with interaction fluctuates randomly with time and does not reach a steady state even after long times. The turbulent energy content remains constant but

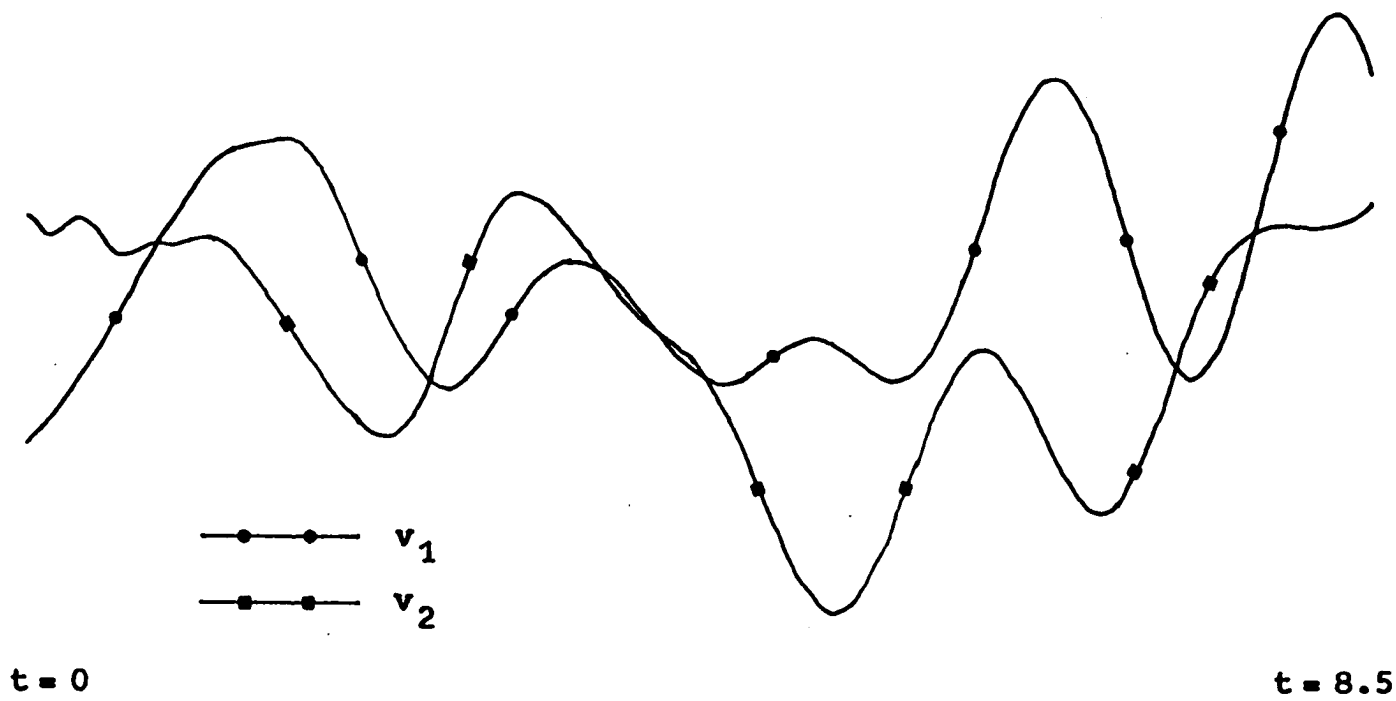

Figure 17. Time behavior of the components of the physical-space convected velocity field with interaction at the point $\underset{\sim}{x} = \underset{\sim}{0}$

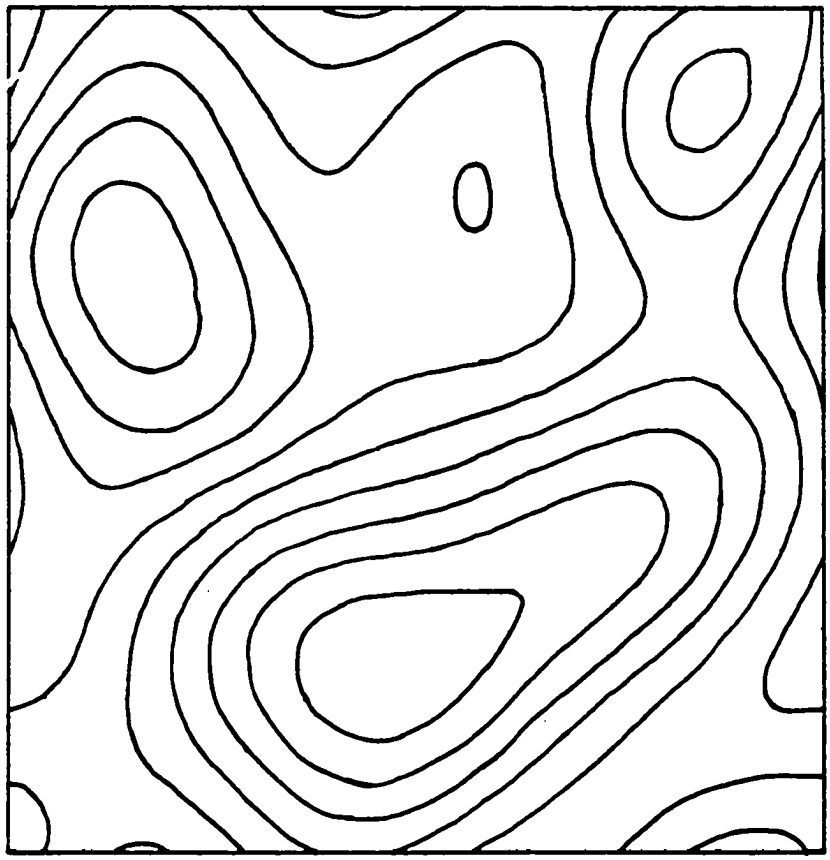

Figure 18. Streamlines for the convected velocity field with interaction at t = 5

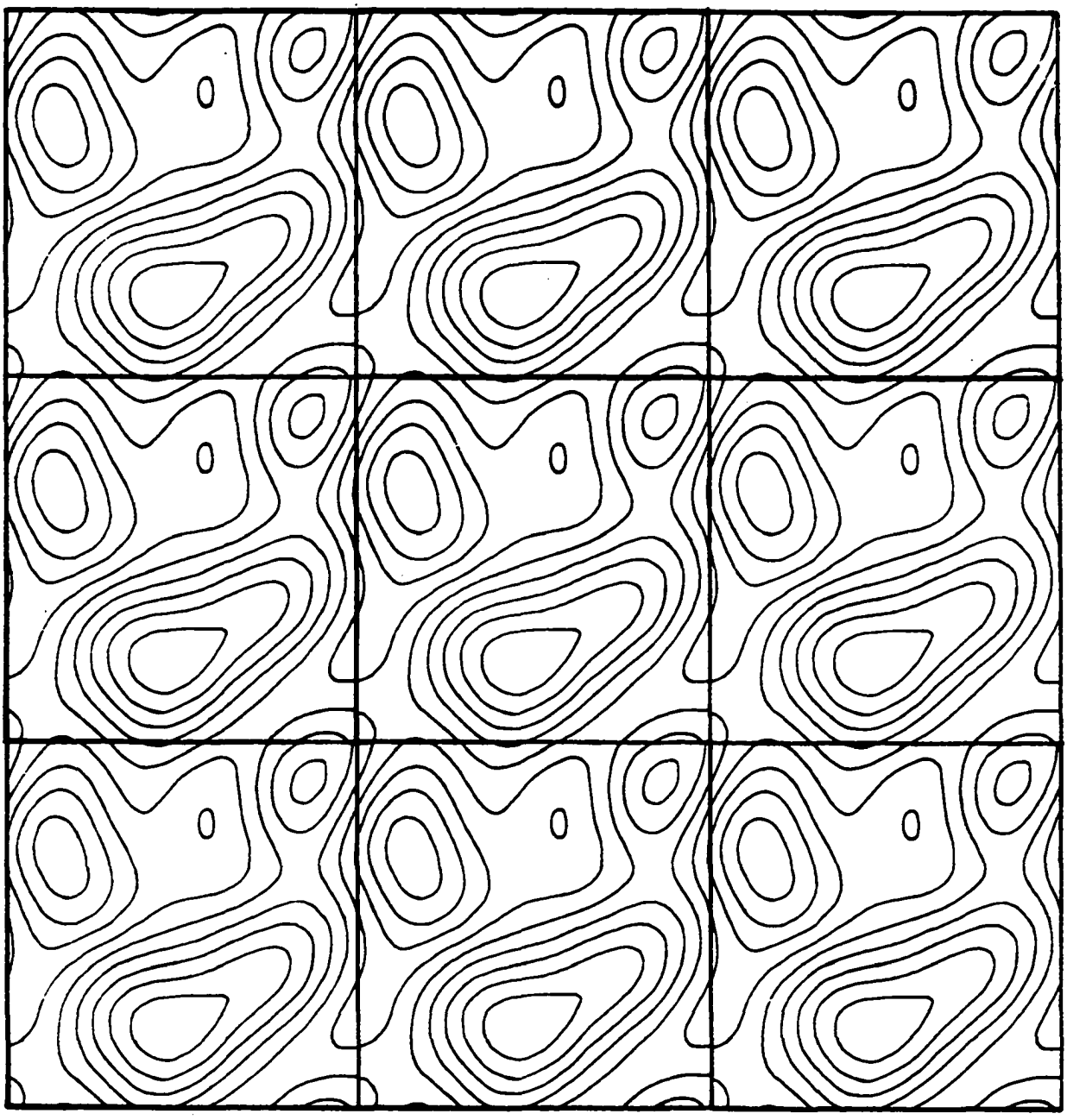

Figure 19. Streamlines for the convected velocity field with interaction at t = 5 extended over several unit boxes of turbulence

the energy spectrum modes freely and randomly exchange energy content between one another, and hence the time scales of the turbulence fluctuate. For this reason, the random convection velocity field was used for most of the concentration field calculations and was used to obtain all results reported, except where otherwise indicated. The convected velocity field with interaction was used in selected cases in order to compare concentration field behaviors for the two velocity fields.

Integration of the Concentration Field Equations

Concentration field initial conditions

For single component reactions the initial concentration field was generated using Equations 811 - 815, whereas for two-species reactions the initial concentration fields A and B were generated using Equations 826 - 836. The values of $\theta(\underset{\sim}{n})$ were computer generated random numbers (scaled by the factor 2π) chosen from a uniform distribution ranging from 0 to 1. In actuality, the initial concentration field used for the single component system was the same as the initial concentration field of species A in the two-species system. The same initial concentration field was used for all cases examined. The initial statistics assigned to the concentration fields are given in Table 4. The initial concentration correlation coefficient $f_s(r,0)$ is shown in

Table 4. Initial assigned statistics for the concentration fields

For single component reactions, the initial concentration field and statistics are identical to the concentration field and statistics for species A for two species reactions.

$\bar{C}_A(0) = 1.0$, $\bar{C}_B(0) =$ initial stoichiometry

correlation coefficient $\gamma(0) = \overline{c_A c_B}(0)/\tilde{c}_A(0)\tilde{c}_B(0) = -1.0$

segregation coefficient $P(0) = \overline{c_A c_B}(0)/\bar{C}_A(0)\bar{C}_B(0) = -0.2$

$\tilde{c}_A(0)^2 = 0.2$, $\overline{c_A c_B}(0) = P(0)\bar{C}_B(0)$

$\tilde{c}_B(0)^2 = [P(0)\bar{C}_B(0)/\gamma(0)\tilde{c}_A(0)]^2$

$L_A(0) = L_B(0) = 0.52772$, $\lambda_A(0) = \lambda_B(0) = 0.90289$

$E_s(n^2,0)_d = a_s\tilde{c}(0)^2\,(n/n_{os})\exp(-n^2/2n_{os}^2)$

$n_{os}^2 = 1.0$, $a_s = 0.61244$

$$E_s(n^2,0)_d/\tilde{c}(0)^2 = E_A(n^2,0)_d/\tilde{c}_A(0)^2 = E_B(n^2,0)_d/\tilde{c}_B(0)^2 = -E_{AB}(n^2,0)_d/\overline{c_A c_B}(0)$$

n^2	$E_s(n^2,0)_d/\tilde{c}(0)^2$
1	0.37146
2	0.31863
4	0.16577
5	0.11241
8	0.03173

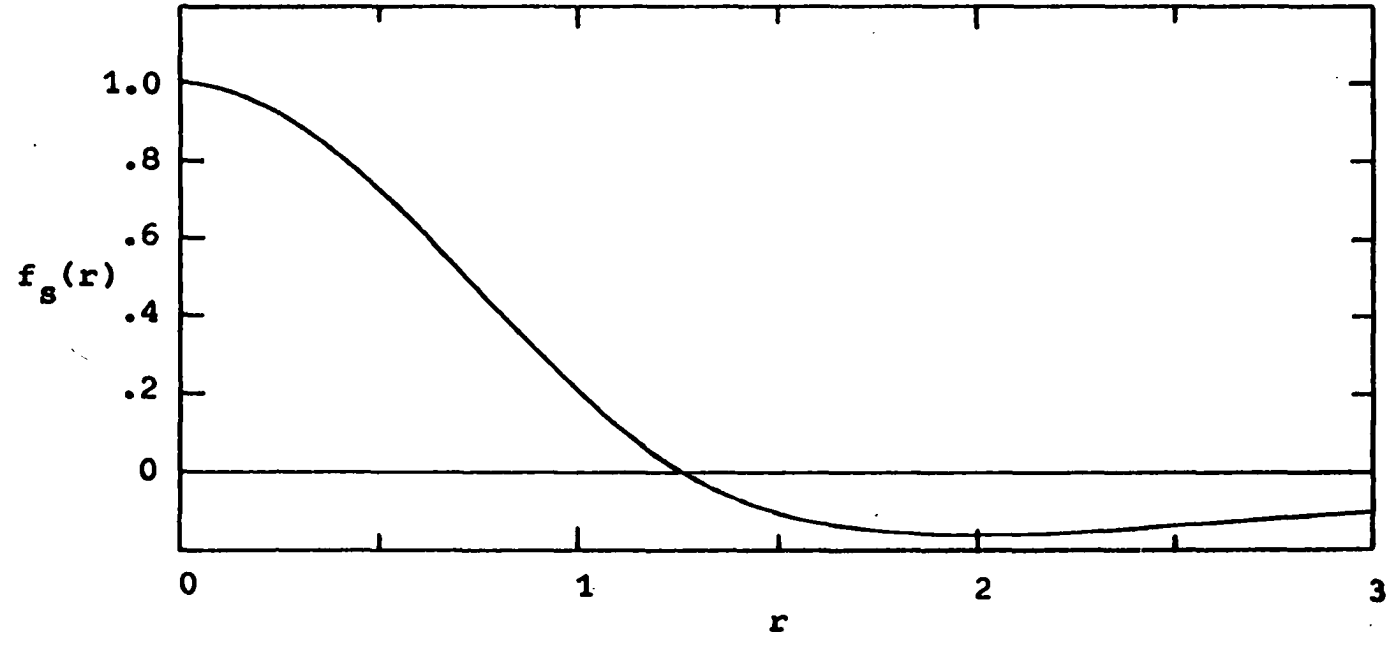

Figure 20. Initial concentration correlation coefficient $f_s(r,0)$

Figure 20. For the two-species system, the wave number dependences of $E_A(n^2,0)_d$, $E_B(n^2,0)_d$, and $E_{AB}(n^2,0)_d$ were taken to be the same. Under this restriction, Equations 834 - 836 reduce to

$$\phi_B^R(\underset{\sim}{n},0) = \frac{\overline{c_A c_B}(0)}{\tilde{c}_A(0)^2}\,\phi_A^R(\underset{\sim}{n},0) \pm \frac{\tilde{c}_A(0)\tilde{c}_B(0)}{\tilde{c}_A(0)^2}[1 - \aleph(0)^2]^{\frac{1}{2}}\,\phi_A^I(\underset{\sim}{n},0) \tag{871}$$

$$\phi_B^I(\underset{\sim}{n},0) = \frac{\overline{c_A c_B}(0)}{\tilde{c}_A(0)^2}\,\phi_A^I(\underset{\sim}{n},0) \mp \frac{\tilde{c}_A(0)\tilde{c}_B(0)}{\tilde{c}_A(0)^2}[1 - \aleph(0)^2]^{\frac{1}{2}}\,\phi_A^R(\underset{\sim}{n},0) \tag{872}$$

$$-1 \leq \aleph(0) \leq 1 \tag{873}$$

In finding initial concentration fields with desired statistics, one fundamental difficulty (related to the nature of the Fourier transform itself) that must be overcome is that of satisfying the requirement of having only positive physical-space concentrations. In this study, this requirement restricted the initial relative intensity of concentration fluctuations to values of approximately $\tilde{c}(0)^2/\bar{c}(0)^2 = 0.2$ or less ($\tilde{c}(0)/\bar{c}(0) \leq 0.447$). Since large relative intensities of fluctuation are desirable, $\tilde{c}(0)^2/\bar{c}(0)^2 = 0.2$ was used, but even at this moderate level of intensity, only one concentration field out of six randomly generated ones did not contain regions of negative physical-space concentration. Furthermore, this restriction on intensity does not seem to arise from the small number of Fourier modes used in this study. Using a much larger

number of modes, at different intensity levels the amount of concentration field negativity was about the same as that for fewer modes and was insensitive to changing the concentration spectrum.

Another related limitation is the degree to which species segregation can be accurately described using the Fourier transform, especially with a small number of modes. For two-species reactions, in order to approximate segregation as much as possible, a correlation coefficient of $\mathcal{P}(0) = \overline{c_A c_B}(0)/\tilde{c}_A(0)\tilde{c}_B(0) = -1$ was used, which corresponds to the concentration fluctuations of A and B being completely out of phase. An initial segregation coefficient value of $\bar{\mathcal{P}}(0) = \overline{c_A c_B}(0)/\bar{c}_A(0)\bar{c}_B(0) = -0.2$ was used.

The initial physical-space concentration fields of A and B used for stoichiometric reactants are shown in Figure 21.

Single component second-order reaction

Equations 806 - 809 for a single component second-order reaction can be written in abbreviated form as

$\underset{\sim}{n} = \underset{\sim}{0}$

$$\frac{\partial \mathcal{C}(t')}{\partial t'} = -Da_I' \left[\mathcal{C}(t')^2 + \tilde{c}(t')^2 \right] \tag{874}$$

$$\tilde{c}(t')^2 = \sum_{\underset{\sim}{m}} \left[\mathcal{C}^R(\underset{\sim}{m},t')^2 + \mathcal{C}^I(\underset{\sim}{m},t')^2 \right] \tag{875}$$

$$\mathcal{C}^R(\underset{\sim}{0},t') = \mathcal{C}^I(\underset{\sim}{0},t') = 0 \tag{876}$$

0.67	1.03	1.29	1.36	1.21	0.88	0.51	0.24	0.17	0.34	0.67
0.51	0.64	1.03	1.35	1.28	0.92	0.62	0.60	0.67	0.61	0.51
0.61	0.45	0.73	1.13	1.21	0.97	0.82	0.99	1.17	1.01	0.61
0.62	0.38	0.46	0.77	1.04	1.10	1.05	1.07	1.09	0.94	0.62
0.54	0.41	0.38	0.65	1.10	1.36	1.21	0.85	0.61	0.57	0.54
0.75	0.66	0.64	0.99	1.51	1.64	1.21	0.64	0.44	0.61	0.75
1.36	1.14	1.11	1.52	1.91	1.72	1.04	0.60	0.79	1.24	1.36
1.91	1.63	1.51	1.78	1.93	1.50	0.80	0.58	1.10	1.77	1.91
1.87	1.79	1.64	1.65	1.58	1.17	0.60	0.42	0.86	1.52	1.87
1.26	1.52	1.52	1.42	1.26	0.94	0.50	0.20	0.30	0.76	1.26
0.67	1.03	1.29	1.36	1.21	0.88	0.51	0.24	0.17	0.34	0.67

A Field

Figure 21. Physical-space concentration fields of A and B at $t = 0$ with $\overline{C}_B(0) = 1.0$, $\widetilde{c}_A(0)^2 = \widetilde{c}_B(0)^2 = 0.2$, and $\overline{c_A c_B}(0) = -0.2$

1.33	0.97	0.71	0.64	0.79	1.11	1.49	1.76	1.83	1.66	1.33
1.49	1.36	0.97	0.65	0.72	1.08	1.38	1.40	1.33	1.39	1.49
1.39	1.55	1.27	0.87	0.79	1.03	1.18	1.01	0.83	0.99	1.39
1.38	1.62	1.54	1.23	0.96	0.90	0.95	0.93	0.91	1.06	1.38
1.46	1.59	1.62	1.35	0.90	0.64	0.79	1.15	1.39	1.43	1.46
1.25	1.34	1.36	1.01	0.49	0.36	0.79	1.36	1.56	1.39	1.25
0.64	0.86	0.89	0.48	0.09	0.28	0.96	1.40	1.21	0.76	0.64
0.09	0.37	0.49	0.22	0.07	0.50	1.20	1.42	0.90	0.23	0.09
0.13	0.21	0.36	0.35	0.42	0.83	1.40	1.58	1.14	0.48	0.13
0.74	0.48	0.48	0.58	0.74	1.06	1.50	1.80	1.70	1.24	0.74
1.33	0.97	0.71	0.64	0.79	1.11	1.49	1.76	1.83	1.66	1.33

B Field

Values shown are concentrations at points in the unit box of turbulence corresponding to a 10 by 10 grid

$\underset{\sim}{n} \neq \underset{\sim}{0}$

$$\frac{\partial c^R(\underset{\sim}{n},t')}{\partial t'} = -[n^2/Pe' + 2Da_I' \ell(t')]c^R(\underset{\sim}{n},t') + F^R(\underset{\sim}{n},t') \quad (877)$$

$$\frac{\partial c^I(\underset{\sim}{n},t')}{\partial t'} = -[n^2/Pe' + 2Da_I' \ell(t')]c^I(\underset{\sim}{n},t') + F^I(\underset{\sim}{n},t') \quad (878)$$

with

$$F^R(\underset{\sim}{n},t') = n_i \sum_{\underset{\sim}{m}} [u_i^R(\underset{\sim}{m})c^I(\underset{\sim}{n}-\underset{\sim}{m}) + u_i^I(\underset{\sim}{m})c^R(\underset{\sim}{n}-\underset{\sim}{m})] - Da_I' \sum_{\underset{\sim}{m}} [c^R(\underset{\sim}{m})c^R(\underset{\sim}{n}-\underset{\sim}{m}) - c^I(\underset{\sim}{m})c^I(\underset{\sim}{n}-\underset{\sim}{m})] \quad (879)$$

$$F^I(\underset{\sim}{n},t') = -n_i \sum_{\underset{\sim}{m}} [u_i^R(\underset{\sim}{m})c^R(\underset{\sim}{n}-\underset{\sim}{m}) - u_i^I(\underset{\sim}{m})c^I(\underset{\sim}{n}-\underset{\sim}{m})] - Da_I' \sum_{\underset{\sim}{m}} [c^R(\underset{\sim}{m})c^I(\underset{\sim}{n}-\underset{\sim}{m}) + c^I(\underset{\sim}{m})c^R(\underset{\sim}{n}-\underset{\sim}{m})] \quad (880)$$

Converting Equations 874, 877, and 878 to finite difference form using values of the right-hand sides averaged over time steps t_r' and t_{r+1}' and solving for $\ell(t_{r+1}')$, $c^R(\underset{\sim}{n},t_{r+1}')$, and $c^I(\underset{\sim}{n},t_{r+1}')$ gives the set of predictor equations

$$\ell(t_{r+1}') = \frac{[1 - \tfrac{1}{2}\Delta t' Da_I' \ell(t_r')]\ell(t_r') - \Delta t' Da_I' \tilde{c}(t_r')^2}{1 + \tfrac{1}{2}\Delta t' Da_I' \ell(t_r')} \quad (881)$$

$$c^R(\underset{\sim}{n},t_{r+1}') = \{[1 - \tfrac{1}{2}\Delta t' n^2/Pe' - \Delta t' Da_I' \ell(t_r')]c^R(\underset{\sim}{n},t_r') + \Delta t' F^R(\underset{\sim}{n},t_r')\}/[1 + \tfrac{1}{2}\Delta t' n^2/Pe' + \Delta t' Da_I' \ell(t_r')] \quad (882)$$

$c^I(\underset{\sim}{n},t_{r+1}')$ = same as Equation 882 with I replacing R (883)

and corrector equations

$$\ell(t'_{r+1}) = \{[1 - \tfrac{1}{2}\Delta t' Da'_I \ell(t'_r)]\ell(t'_r) - \tfrac{1}{2}\Delta t' Da'_I [\tilde{c}(t'_r)^2 + \tilde{c}(t'_{r+1})^2]\}/[1 + \tfrac{1}{2}\Delta t' Da'_I \ell(t'_{r+1})] \tag{884}$$

$$c^R(\underset{\sim}{n}, t'_{r+1}) = \{[1 - \tfrac{1}{2}\Delta t' n^2/Pe' - \Delta t' Da'_I \ell(t'_r)] c^R(\underset{\sim}{n}, t'_r) + \tfrac{1}{2}\Delta t'[F^R(\underset{\sim}{n}, t'_r) + F^R(\underset{\sim}{n}, t'_{r+1})]\} / [1 + \tfrac{1}{2}\Delta t' n^2/Pe' + \Delta t' Da'_I \ell(t'_{r+1})] \tag{885}$$

$$c^I(\underset{\sim}{n}, t'_{r+1}) = \text{same as Equation 885 with I replacing R} \tag{886}$$

First-order reaction

Writing Equations 816 - 818 for a first-order reaction in abbreviated form gives

$\underset{\sim}{n} = \underset{\sim}{0}$

$$\frac{\partial \ell(t')}{\partial t'} = -Da'_I \ell(t') \tag{887}$$

$\underset{\sim}{n} \neq \underset{\sim}{0}$

$$\frac{\partial c^R(\underset{\sim}{n}, t')}{\partial t'} = -(n^2/Pe' + Da'_I) c^R(\underset{\sim}{n}, t') + F^R(\underset{\sim}{n}, t') \tag{888}$$

$$\frac{\partial c^I(\underset{\sim}{n}, t')}{\partial t'} = -(n^2/Pe' + Da'_I) c^I(\underset{\sim}{n}, t') + F^I(\underset{\sim}{n}, t') \tag{889}$$

with

$$F^R(\underset{\sim}{n}, t') = n_i \sum_{\underset{\sim}{m}} [u_i^R(\underset{\sim}{m}) c^I(\underset{\sim}{n}, \underset{\sim}{m}) + u_i^I(\underset{\sim}{m}) c^R(\underset{\sim}{n}-\underset{\sim}{m})] \tag{890}$$

$$F^I(\underset{\sim}{n},t') = -n_i \sum_{\underset{\sim}{m}} [u_i^R(\underset{\sim}{m})c^R(\underset{\sim}{n}-\underset{\sim}{m}) - u_i^I(\underset{\sim}{m})c^I(\underset{\sim}{n}-\underset{\sim}{m})] \quad (891)$$

In terms of finite differences, Equations 887 - 889 give the predictor equations

$$\mathcal{C}(t'_{r+1}) = \frac{(1 - \frac{1}{2}\Delta t' Da'_I)}{(1 + \frac{1}{2}\Delta t' Da'_I)} \mathcal{C}(t'_r) \quad (892)$$

$$c^R(\underset{\sim}{n},t'_{r+1}) = \{[1 - \tfrac{1}{2}\Delta t' n^2/Pe' - \tfrac{1}{2}\Delta t' Da'_I]c^R(\underset{\sim}{n},t'_r) + \Delta t' F^R(\underset{\sim}{n},t'_r)\}/[1 + \tfrac{1}{2}\Delta t' n^2/Pe' + \tfrac{1}{2}\Delta t' Da'_I] \quad (893)$$

$$c^I(\underset{\sim}{n},t'_{r+1}) = \text{same as Equation 893 with I replacing R} \quad (894)$$

and corrector equations

$$c^R(\underset{\sim}{n},t'_{r+1}) = \{[1 - \tfrac{1}{2}\Delta t' n^2/Pe' - \tfrac{1}{2}\Delta t' Da'_I\, c^R(\underset{\sim}{n},t'_r) + \tfrac{1}{2}\Delta t'[F^R(\underset{\sim}{n},t'_r) + F^R(\underset{\sim}{n},t'_{r+1})]\} /[1 + \tfrac{1}{2}\Delta t' n^2/Pe' + \tfrac{1}{2}\Delta t' Da'_I] \quad (895)$$

$$c^I(\underset{\sim}{n},t'_{r+1}) = \text{same as Equation 895 with I replacing R} \quad (896)$$

<u>Two-species second-order reaction</u>

The abbreviated forms of Equations 819 - 824 for a two-species second-order reaction are

$\underset{\sim}{n} = \underset{\sim}{0}$

$$\frac{\partial \mathcal{C}_A(t')}{\partial t'} = -Da'_I[\mathcal{C}_A(t')\mathcal{C}_B(t') + \overline{c_A c_B}(t')] \quad (897)$$

$$\frac{\partial \mathcal{L}_B(t')}{\partial t'} = \text{same as Equation 897} \tag{898}$$

$$\overline{c_A c_B}(t') = \sum_{\underset{\sim}{m}} \left[\phi_A^R(\underset{\sim}{m}) \phi_B^R(\underset{\sim}{m}) + \phi_A^I(\underset{\sim}{m}) \phi_B^I(\underset{\sim}{m}) \right] \tag{899}$$

$\underset{\sim}{n} \neq \underset{\sim}{0}$

$$\frac{\partial \phi_A^R(\underset{\sim}{n},t')}{\partial t'} = -\left[n^2/Pe_A' + Da_I' \mathcal{L}_B(t')\right] \phi_A^R(\underset{\sim}{n},t') - Da_I' \mathcal{L}_A(t') \phi_B^R(\underset{\sim}{n},t') + F_A^R(\underset{\sim}{n},t') \tag{900}$$

$$\frac{\partial \phi_A^I(\underset{\sim}{n},t')}{\partial t'} = -\left[n^2/Pe_A' + Da_I' \mathcal{L}_B(t')\right] \phi_A^I(\underset{\sim}{n},t') - Da_I' \mathcal{L}_A(t') \phi_B^I(\underset{\sim}{n},t') + F_A^I(\underset{\sim}{n},t') \tag{901}$$

$$\frac{\partial \phi_B^R(\underset{\sim}{n},t')}{\partial t'} = -\left[n^2/Pe_B' + Da_I' \mathcal{L}_A(t')\right] \phi_B^R(\underset{\sim}{n},t') - Da_I' \mathcal{L}_B(t') \phi_A^R(\underset{\sim}{n},t') + F_B^R(\underset{\sim}{n},t') \tag{902}$$

$$\frac{\partial \phi_B^I(\underset{\sim}{n},t')}{\partial t'} = -\left[n^2/Pe_B' + Da_I' \mathcal{L}_A(t')\right] \phi_B^I(\underset{\sim}{n},t') - Da_I' \mathcal{L}_B(t') \phi_A^I(\underset{\sim}{n},t') + F_B^I(\underset{\sim}{n},t') \tag{903}$$

with

$$F_A^R(\underset{\sim}{n},t') = n_i \sum_{\underset{\sim}{m}} \left[u_i^R(\underset{\sim}{m}) \phi_A^I(\underset{\sim}{n}-\underset{\sim}{m}) + u_i^I(\underset{\sim}{m}) \phi_A^R(\underset{\sim}{n}-\underset{\sim}{m}) \right] - Da_I' \sum_{\underset{\sim}{m}} \left[\phi_A^R(\underset{\sim}{m}) \phi_B^R(\underset{\sim}{n}-\underset{\sim}{m}) - \phi_A^I(\underset{\sim}{m}) \phi_B^I(\underset{\sim}{n}-\underset{\sim}{m}) \right] \tag{904}$$

$$F_A^I(\underset{\sim}{n},t') = -n_i \sum_{\underset{\sim}{m}} [u_i^R(\underset{\sim}{m})c_A^R(\underset{\sim}{n}-\underset{\sim}{m}) - u_i^I(\underset{\sim}{m})c_A^I(\underset{\sim}{n}-\underset{\sim}{m})]$$
$$- Da_I' \sum_{\underset{\sim}{m}} [c_A^R(\underset{\sim}{m})c_B^I(n-m) + c_A^I(\underset{\sim}{m})c_B^R(\underset{\sim}{n}-\underset{\sim}{m})] \quad (905)$$

$$F_B^R(\underset{\sim}{n},t') = n_i \sum_{\underset{\sim}{m}} [u_i^R(\underset{\sim}{m})c_B^I(\underset{\sim}{n}-\underset{\sim}{m}) + u_i^I(\underset{\sim}{m})c_B^R(\underset{\sim}{n}-\underset{\sim}{m})]$$
$$- Da_I' \sum_{\underset{\sim}{m}} [c_A^R(\underset{\sim}{m})c_B^R(\underset{\sim}{n}-\underset{\sim}{m}) - c_A^I(\underset{\sim}{m})c_B^I(\underset{\sim}{n}-\underset{\sim}{m})] \quad (906)$$

$$F_B^I(\underset{\sim}{n},t') = -n_i \sum_{\underset{\sim}{m}} [u_i^R(\underset{\sim}{m})c_B^R(\underset{\sim}{n}-\underset{\sim}{m}) - u_i^I(\underset{\sim}{m})c_B^I(\underset{\sim}{n}-\underset{\sim}{m})]$$
$$- Da_I' \sum_{\underset{\sim}{m}} [c_A^R(\underset{\sim}{m})c_B^I(\underset{\sim}{n}-\underset{\sim}{m}) + c_A^I(\underset{\sim}{m})c_B^R(\underset{\sim}{n}-\underset{\sim}{m})] \quad (907)$$

Converting Equations 897 - 903 to finite difference form gives the predictor equations

$$\mathcal{C}_A(t'_{r+1}) = \{[1 - \tfrac{1}{2}\Delta t' Da_I' \mathcal{C}_B(t'_r)]\mathcal{C}_A(t'_r) - \Delta t' Da_I' \overline{c_A c_B}(t'_r)\}$$
$$/[1 + \tfrac{1}{2}\Delta t' Da_I' \mathcal{C}_B(t'_r)] \quad (908)$$

$$\mathcal{C}_B(t'_{r+1}) = \{[1 - \tfrac{1}{2}\Delta t' Da_I' \mathcal{C}_A(t'_r)]\mathcal{C}_B(t'_r) - \Delta t' Da_I' \overline{c_A c_B}(t'_r)\}$$
$$/[1 + \tfrac{1}{2}\Delta t' Da_I' \mathcal{C}_A(t'_r)] \quad (909)$$

$$c_A^R(\underset{\sim}{n},t'_{r+1}) = \{[1 - \tfrac{1}{2}\Delta t' n^2/Pe_A' - \tfrac{1}{2}\Delta t' Da_I' \mathcal{C}_B(t'_r)]c_A^R(\underset{\sim}{n},t'_r)$$
$$- \Delta t' Da_I' \mathcal{C}_A(t'_r)c_B^R(\underset{\sim}{n},t'_r) + \Delta t' F_A^R(\underset{\sim}{n},t'_r)\} \quad (910)$$
$$/[1 + \tfrac{1}{2}\Delta t' n^2/Pe_A' + \tfrac{1}{2}\Delta t' Da_I' \mathcal{C}_B(t'_r)]$$

$$\phi_A^I(\underset{\sim}{n},t'_{r+1}) = \text{same as Equation 910 with I replacing R} \quad (911)$$

$$\phi_B^R(\underset{\sim}{n},t'_{r+1}) = \{[1 - \tfrac{1}{2}\Delta t' n^2/Pe'_B - \tfrac{1}{2}\Delta t' Da'_I \ell_A(t'_r)]\phi_B^R(\underset{\sim}{n},t'_r)$$
$$- \Delta t' Da'_I \ell_B(t'_r)\phi_A^R(\underset{\sim}{n},t'_r) + \Delta t' F_B^R(\underset{\sim}{n},t'_r)\} \quad (912)$$
$$/[1 + \tfrac{1}{2}\Delta t' n^2/Pe'_B + \tfrac{1}{2}\Delta t' Da'_I \ell_A(t'_r)]$$

$$\phi_B^I(\underset{\sim}{n},t'_{r+1}) = \text{same as Equation 912 with I replacing R} \quad (913)$$

and corrector equations

$$\ell_A(t'_{r+1}) = \{[1 - \tfrac{1}{2}\Delta t' Da'_I \ell_B(t'_r)]\ell_A(t'_r)$$
$$- \tfrac{1}{2}\Delta t' Da'_I[\overline{c_A c_B}(t'_r) + \overline{c_A c_B}(t'_{r+1})]\} \quad (914)$$
$$/[1 + \tfrac{1}{2}\Delta t' Da'_I \ell_B(t'_{r+1})]$$

$$\ell_B(t'_{r+1}) = \{[1 - \tfrac{1}{2}\Delta t' Da'_I \ell_A(t'_r)]\ell_B(t'_r)$$
$$- \tfrac{1}{2}\Delta t' Da'_I[\overline{c_A c_B}(t'_r) + \overline{c_A c_B}(t'_{r+1})]\} \quad (915)$$
$$/[1 + \tfrac{1}{2}\Delta t' Da'_I \ell_A(t'_{r+1})]$$

$$\phi_A^R(\underset{\sim}{n},t'_{r+1}) = \{[1 - \tfrac{1}{2}\Delta t' n^2/Pe'_A - \tfrac{1}{2}\Delta t' Da'_I \ell_B(t'_r)]\phi_A^R(\underset{\sim}{n},t'_r)$$
$$- \tfrac{1}{2}\Delta t' Da'_I[\ell_A(t'_{r+1})\phi_B^R(\underset{\sim}{n},t'_{r+1}) + \ell_A(t'_r)\phi_B^R(\underset{\sim}{n},t'_r)]$$
$$+ \tfrac{1}{2}\Delta t'[F_A^R(\underset{\sim}{n},t'_{r+1}) + F_A^R(\underset{\sim}{n},t'_r)]\}$$

$$/[1 + \tfrac{1}{2}\Delta t' n^2/Pe'_A + \tfrac{1}{2}\Delta t' Da'_I \mathcal{L}_B(t'_{r+1})] \tag{916}$$

$$\phi^I_A(\underset{\sim}{n}, t'_{r+1}) = \text{same as Equation 916 with I replacing R} \tag{917}$$

$$\begin{aligned}\phi^R_B(\underset{\sim}{n}, t'_{r+1}) = \{&[1 - \tfrac{1}{2}\Delta t' n^2/Pe'_B - \tfrac{1}{2}\Delta t' Da'_I \mathcal{L}_A(t'_r)]\phi^R_B(\underset{\sim}{n}, t'_r) \\ &- \tfrac{1}{2}\Delta t' Da'_I [\mathcal{L}_B(t'_{r+1})\phi^R_A(\underset{\sim}{n}, t'_{r+1}) + \mathcal{L}_B(t'_r)\phi^R_A(\underset{\sim}{n}, t'_r)] \\ &+ \tfrac{1}{2}\Delta t' [F^R_B(\underset{\sim}{n}, t'_{r+1}) + F^R_B(\underset{\sim}{n}, t'_r)]\} \\ &/[1 + \tfrac{1}{2}\Delta t' n^2/Pe'_B + \tfrac{1}{2}\Delta t' Da'_I \mathcal{L}_A(t'_{r+1})]\end{aligned} \tag{918}$$

$$\phi^I_B(\underset{\sim}{n}, t'_{r+1}) = \text{same as Equation 918 with I replacing R} \tag{919}$$

Limiting Cases and Check of Numerical Integration

Using the finite difference equations given in the previous section, the concentration fields were calculated over time using the previously calculated velocity fields stored on magnetic tape and time increments $\Delta t'$ that are an integer multiple of the time increment $\Delta t'_\phi$ corresponding to the velocity field values. To avoid accumulation of round-off errors, the concentration variables were carried in double precision although the velocity field was in single precision. Iterations of the corrector equations were cut-off according to the specifications

$$\left| \frac{\phi^R(\underset{\sim}{n},t'_{r+1})_{j+1} - \phi^R(\underset{\sim}{n},t'_{r+1})_j}{\phi^R(\underset{\sim}{n},t'_{r+1})_{j+1}} \right| < 3 \times 10^{-7} \qquad (920)$$

$$\left| \frac{\phi^I(\underset{\sim}{n},t'_{r+1})_{j+1} - \phi^I(\underset{\sim}{n},t'_{r+1})_j}{\phi^I(\underset{\sim}{n},t'_{r+1})_{j+1}} \right| < 3 \times 10^{-7} \qquad (921)$$

for all $\underset{\sim}{n}$ for the jth iteration.

In order to check the numerical integration of the concentration field equations and properties of the turbulence simulation used in this study, calculations were made for several different mixing and reaction limiting cases. In the limit of no diffusion and no reaction (pure convection), concentration fluctuation intensities and correlation between species should remain constant with time. This is shown in Table 5 for different integration time increments, which gives an indication of the convergence of the concentration field integration with the velocity field present.

For final period turbulence, $\underset{\sim}{u} = \underset{\sim}{0}$ and convection does not occur. In the limit of pure diffusion, the Fourier concentration field equations reduce to

$$\frac{\partial \phi^R(\underset{\sim}{n},t')}{\partial t'} = -(n^2/Pe')\phi^R(\underset{\sim}{n},t') \qquad (922)$$

$$\frac{\partial \phi^I(\underset{\sim}{n},t')}{\partial t'} = -(n^2/Pe')\phi^I(\underset{\sim}{n},t') \qquad (923)$$

which can be integrated exactly to give

Table 5. Convergence of the concentration field integration for different time increments and check of constant species fluctuation intensities for pure convection without diffusion or reaction

t	$\widetilde{c}(t)^2$				
	$\Delta t/\Delta t_\emptyset = 2$	4	8	16	32
0	1.000000	1.000000	1.00000	1.00000	1.00000
0.495	0.999998	0.999993	0.99997	0.99989	0.99957
0.989	0.999997	0.999990	0.99996	0.99983	0.99933
1.484	0.999999	0.999995	0.99998	0.99992	0.99968
1.979	1.000000	0.999999	1.00000	0.99998	0.99994
2.475	1.000001	1.000004	1.00002	1.00006	1.00026
2.968	1.000001	1.000006	1.00002	1.00009	1.00038
3.463	1.000001	1.000005	1.00002	1.00008	1.00030
4.452	1.000001	1.000003	1.00001	1.00005	1.00018
4.947	0.999999	0.999998	0.99999	0.99996	0.99985
5.442	1.000000	0.999998	0.99999	0.99998	0.99990

t	$\overline{c_A c_B}(t)$	$\widetilde{c}_A(t)^2$	$\widetilde{c}_B(t)^2$
0	-0.20000	0.20000	0.20000[a]
0.594	-0.19999	0.19999	0.19999
1.187	-0.20000	0.20000	0.20000
1.781	-0.19999	0.19999	0.19999
2.375	-0.19998	0.19998	0.19998
2.968	-0.19997	0.19997	0.19997
3.562	-0.19994	0.19994	0.19994
4.155	-0.19991	0.19991	0.19991
4.749	-0.19994	0.19994	0.19994
5.343	-0.19997	0.19997	0.19997

[a] $\Delta t = 16\Delta t_\emptyset$.

$$\phi^R(\underset{\sim}{n},t') = \phi^R(\underset{\sim}{n},0)\ \exp[-(n^2/Pe')t'] \tag{924}$$

$$\phi^I(\underset{\sim}{n},t') = \phi^I(\underset{\sim}{n},0)\ \exp[-(n^2/Pe')t'] \tag{925}$$

and hence the decay of fluctuation intensity as

$$\tilde{c}(t')^2 = \sum_{n^2=1}^{n_{max}^2} E_s(n^2,0)_d\ \exp[-2(n^2/Pe')t'] \tag{926}$$

in terms of the initial concentration spectrum. Notice that using the time scale t'/Pe' results in a unique decay for $\tilde{c}^2$. Results for diffusive decay of $\tilde{c}(t)$ obtained by numerical integration and Equation 926 are compared in Table 6. In Figure 22, the exact result as given by Equation 926 is compared with the -3/2 power law for final period turbulence.

For final period turbulence with diffusion and a first-order reaction, the concentration field equations become

$$\frac{\partial \phi^R(\underset{\sim}{n},t')}{\partial t'} = -(n^2/Pe' + Da_I')\phi^R(\underset{\sim}{n},t') \tag{927}$$

$$\frac{\partial \phi^I(\underset{\sim}{n},t')}{\partial t'} = -(n^2/Pe' + Da_I')\phi^I(\underset{\sim}{n},t') \tag{928}$$

and integrate to

$$\phi^R(\underset{\sim}{n},t') = \phi^R(\underset{\sim}{n},0)\ \exp[-(n^2/Pe')t']\ \exp(-Da_I't') \tag{929}$$

$$\phi^I(\underset{\sim}{n},t') = \phi^I(\underset{\sim}{n},0)\ \exp[-(n^2/Pe')t']\ \exp(-Da_I't') \tag{930}$$

This gives

Table 6. Comparison of numerical integration and analytical results for diffusive decay of $\tilde{c}(t)$ with and without a first-order reaction and no convection ($\underset{\sim}{u} = \underset{\sim}{0}$) for Pe = 100

t	Da = 0	Da = 0.1	
	$\tilde{c}(t)^2$	$\bar{c}(t)$	$\tilde{c}(t)^2$
0	0.2000000	1.0000000	0.2000000
0.528	0.1900266	0.9485996	0.1709938[a]
	0.1900265	0.9485996	0.1709938[b]
1.055	0.1807712	0.8998413	0.1463730
	0.1807711	0.8998413	0.1463730
1.979	0.1661061	0.8204669	0.1118170
	0.1661060	0.8204669	0.1118170
3.034	0.1514047	0.7382899	0.0825264
	0.1514046	0.7382900	0.0825264
4.024	0.1393020	0.6687403	0.0622977
	0.1393020	0.6687403	0.0622977
5.013	0.1285716	0.6057424	0.0471760
	0.1285715	0.6057425	0.0471760
6.002	0.1190105	0.5486792	0.0358280
	0.1190104	0.5486793	0.0358280
6.992	0.1104514	0.4969916	0.0272816
	0.1104514	0.4969917	0.0272816
7.981	0.1027557	0.4501732	0.0208240
	0.1027557	0.4501732	0.0208240
9.037	0.0953685	0.4050844	0.0156493
	0.0953685	0.4050844	0.0156493
9.960	0.0895101	0.3693522	0.0122111
	0.0895101	0.3693522	0.0122111

[a]Analytical solution.

[b]Numerical integration.

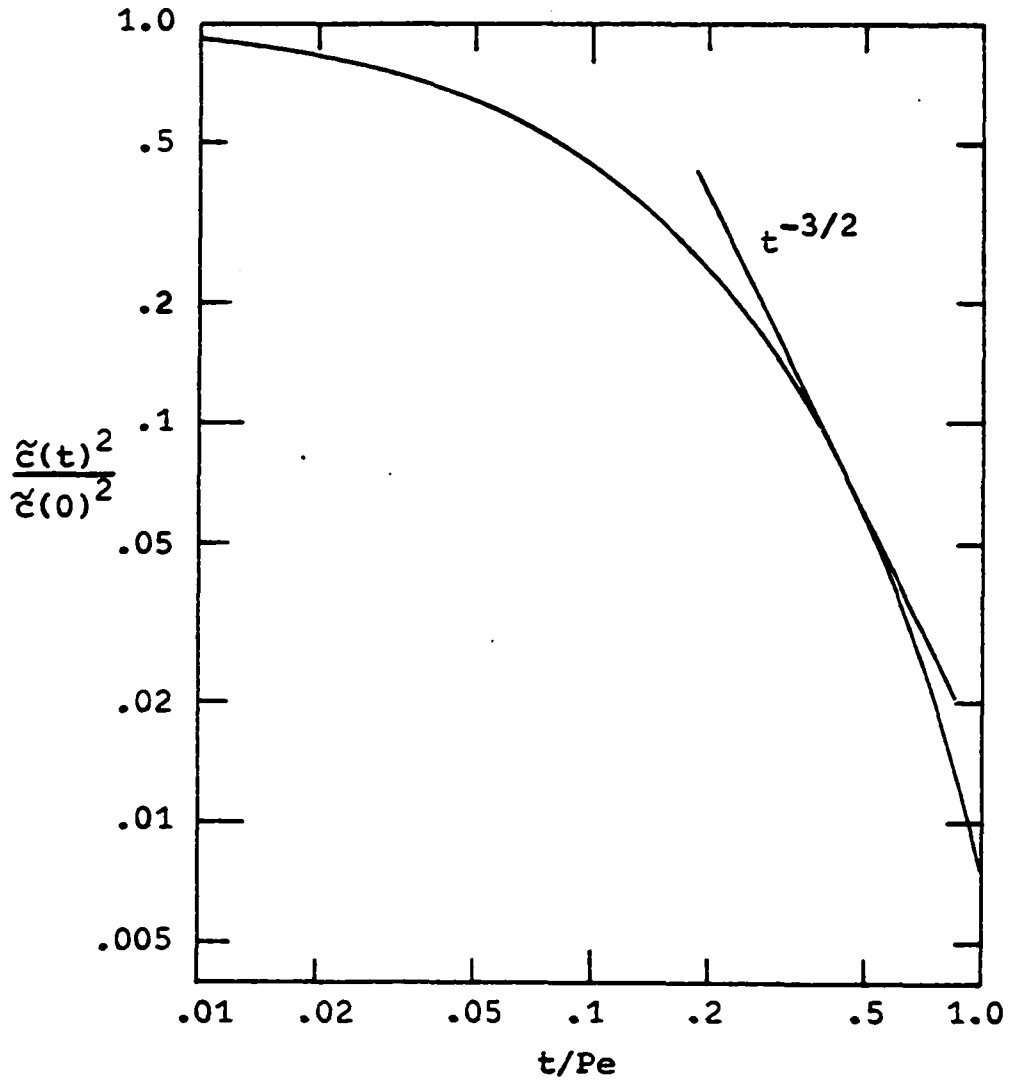

Figure 22. Decay of $\tilde{c}(t)^2$ by diffusion without convection or reaction and comparison with the -3/2 power law for final period turbulence

$$\tilde{c}(t')^2 = \left(\sum_{n^2=1}^{n_{max}^2} E_s(n^2,0)_d \exp[-2(n^2/Pe')t'] \right) \exp(-2Da_I' t') \qquad (931)$$

Results for diffusive decay of $\tilde{c}(t)$ with a first-order reaction as obtained by numerical integration and Equation 931 are also compared in Table 6.

Enhancement of mixing (with no reaction) by the random convection velocity for Peclet numbers of 5, 20, and 100 is shown in Figures 23, 24, and 25, respectively. In addition, the decay of $\tilde{c}(t)^2$ by diffusion with (and without) convection is compared with the -3/2 power law for mixing in the initial period of turbulence decay.

For first-order reactions, statistical independence holds exactly and is expressed by

$$\tilde{c}(t')^2 = \tilde{c}(t')_{mix}^2 \exp(-2Da_I' t') \qquad (932)$$

In Table 7, the decay of $c(t)^2$ for a first-order reaction with convection and diffusion as obtained by numerical integration is compared with that calculated using Equation 932 and the pure mixing decay $\tilde{c}(t)_{mix}^2$. In addition, the concentration integral scale and microscale were found to be unchanged from the pure mixing values by the first-order reaction.

A check of the convergence of the numerical integration of the single component second-order reaction terms is

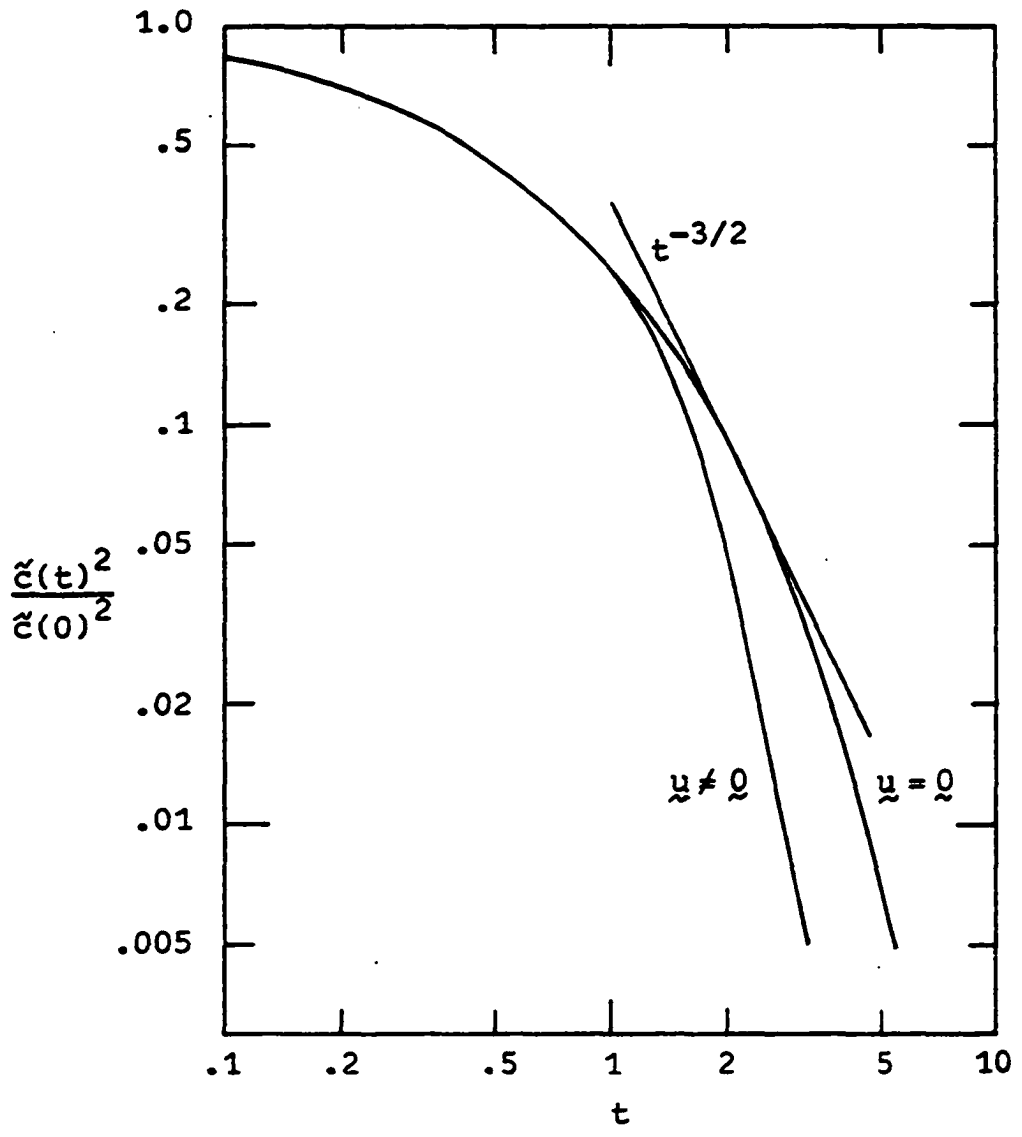

Figure 23. Decay of $\tilde{c}(t)^2$ by diffusion with (and without) convection and no reaction for Pe = 5 and comparison with the initial period -3/2 power law

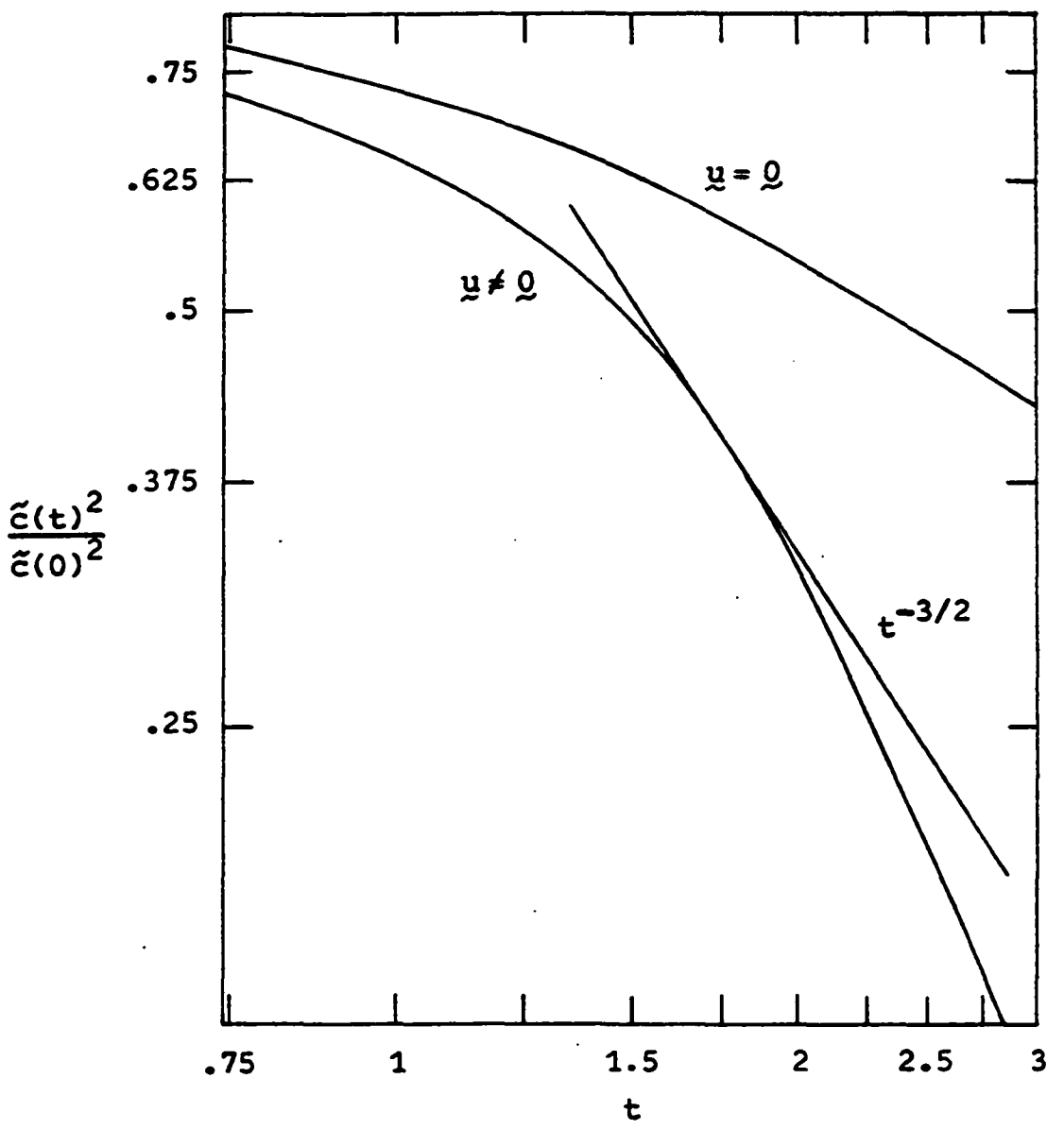

Figure 24. Decay of $\tilde{c}(t)^2$ by diffusion with (and without) convection and no reaction for Pe = 20 and comparison with the initial period -3/2 power law

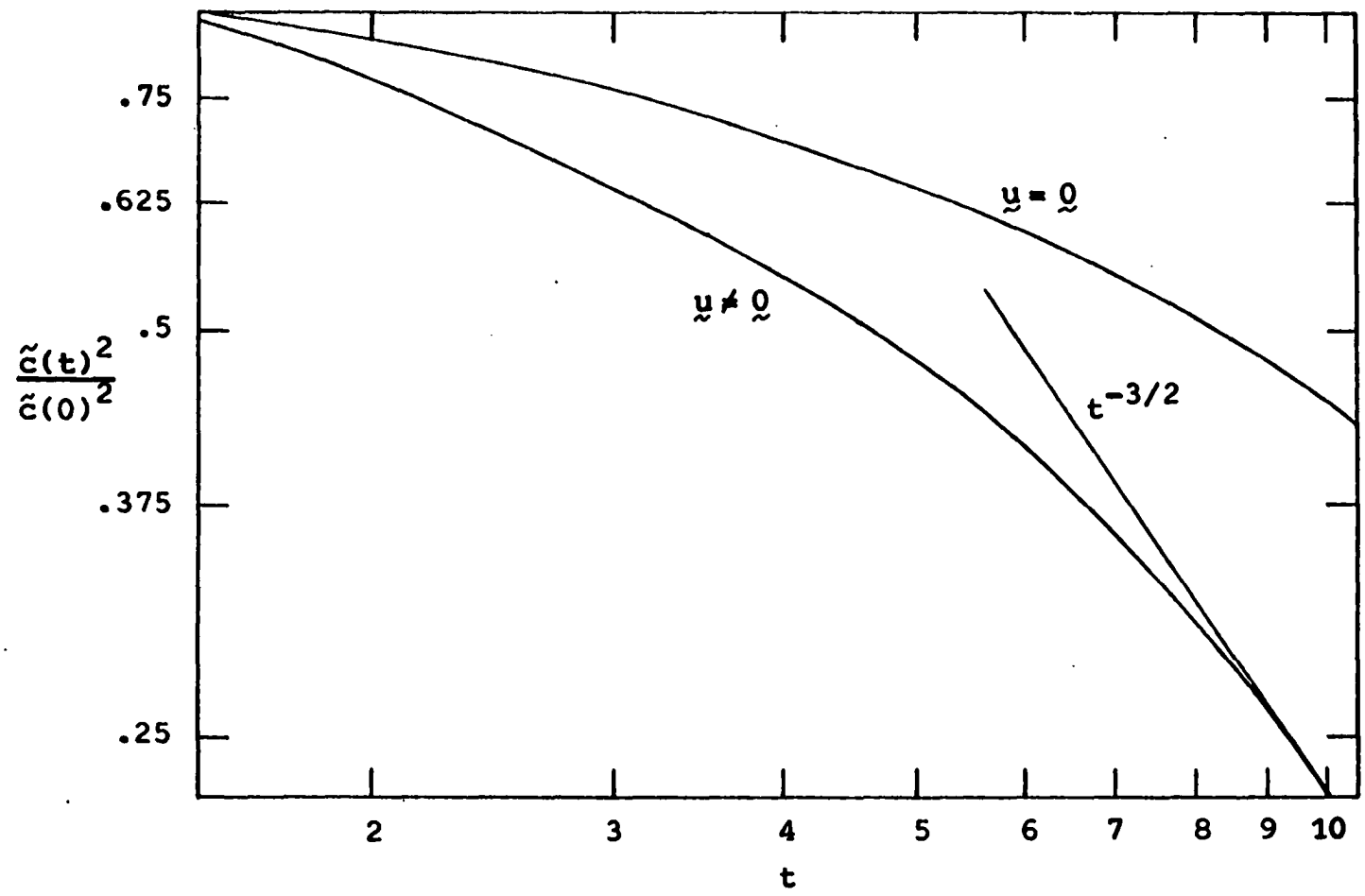

Figure 25. Decay of $\tilde{c}(t)^2$ by diffusion with (and without) convection and no reaction for Pe = 100 and comparison with the initial period -3/2 power law

Table 7. Check of statistical independence for first-order reaction with diffusion and convection

t	$\tilde{c}(t)^2$ for Pe = 20[a]		t	$\tilde{c}(t)^2$ for Pe = 100[b]	
	$Da_I = 0$	$Da_I = 0.5$		$Da_I = 0$	$Da_I = 0.1$
0	0.200000	0.200000	0	0.200000	0.200000
0.247	0.178222	0.139168[c] 0.139168[d]	0.528	0.190358	0.171296[c] 0.171292[d]
0.495	0.160283	0.097734 0.097733	1.055	0.180744	0.146357 0.146351
0.742	0.144603	0.068851 0.068850	1.979	0.155768	0.104867 0.104858
0.989	0.130001	0.048334 0.048334	3.034	0.127251	0.069372 0.069361
1.237	0.115675	0.033584 0.033583	4.024	0.108797	0.048668 0.048655
1.484	0.099505	0.022559 0.022558	5.013	0.094837	0.034810 0.034798
1.731	0.081932	0.014504 0.014504	6.002	0.082742	0.024919 0.024909
1.979	0.065491	0.0090531 0.0090529	6.992	0.070417	0.017402 0.017393
2.226	0.051603	0.0055702 0.0055701	7.981	0.061053	0.012380 0.012373
2.474	0.041128	0.0034667 0.0034666	9.037	0.052377	0.008600 0.008595
2.721	0.033567	0.0022094 0.0022093	9.960	0.045367	0.006193 0.006189
2.968	0.027392	0.0014078 0.0014078			

[a] $\Delta t = 4\,\Delta t_{\emptyset}$.

[b] $\Delta t = 16\,\Delta t_{\emptyset}$.

[c] Numerical integration.

[d] Using mixing result and statistical independence.

Table 8. Check of single component second-order reaction (without convection or diffusion) time and Damköhler number scaling invariance for numerical integration

$Da_I t$	t	Da_I	$\bar{c}(t)$	$\tilde{c}(t)^2$
0.06596	6.596	0.01	0.927293	0.1531772[a]
	0.6596	0.1	0.927293	0.1531771[a]
	0.06596	1.0	0.927292	0.1531764[b]
0.1319	13.19	0.01	0.865422	0.1199332
	1.319	0.1	0.865422	0.1199331
	0.1319	1.0	0.865420	0.1199321
0.2309	2.309	0.1	0.787916	0.0859268
	0.2309	1.0	0.787914	0.0859258
0.4947	4.947	0.1	0.639409	0.0407338
	0.4947	1.0	0.639407	0.0407332
0.9894	9.894	0.1	0.476766	0.0141165
	0.9894	1.0	0.476764	0.0141162

[a] $\Delta t = 16\,\Delta t_{\emptyset}$.

[b] $\Delta t = 4\,\Delta t_{\emptyset}$.

provided by the time and Damköhler number scaling invariance of the reaction when convection and diffusion do not occur. In this limit the decay of $\bar{c}(t)$ and $\tilde{c}(t)^2$ becomes unique when expressed in terms of $Da_I t$. This is shown in Table 8.

One significant test of the turbulent concentration field simulation that shows the affect of only using a finite number of Fourier modes is that for no molecular diffusion the fluid motion should not affect the rate of reaction (36a). This is shown in Table 9 for a single component second-order reaction and in Table 10 for a two-

Table 9. Check of single component second-order reaction invariance to convection for no diffusion and $Da_I = 0.1$

t	$\bar{C}(t)$	$\tilde{c}(t)^2$	t	$\bar{C}(t)$	$\tilde{c}(t)^2$
0	1.000000	0.20000[a]	4.024	0.684043	0.05188
	1.000000	0.20000[b]		0.683977	0.05271
0.528	0.940876	0.16126	5.013	0.636458	0.04006
	0.940870	0.16173		0.636310	0.04123
1.055	0.889041	0.13195	6.002	0.595445	0.03153
	0.889000	0.13269		0.595207	0.03252
1.517	0.848597	0.11186	6.992	0.559682	0.02523
	0.848543	0.11184		0.559382	0.02607
1.979	0.812006	0.09565	7.981	0.528186	0.02046
	0.811968	0.09528		0.527838	0.02132
2.507	0.774197	0.08072	9.037	0.498456	0.01659
	0.774183	0.08036		0.498056	0.01752
3.034	0.740034	0.06872	9.960	0.475179	0.01395
	0.740027	0.06886		0.474732	0.01486
3.496	0.712715	0.06008			
	0.712688	0.06080			

[a] $\underset{\sim}{u} = \underset{\sim}{0}$.

[b] $\underset{\sim}{u} \neq \underset{\sim}{0}$.

species second-order reaction. In both cases the solutions with and without convection are both convergent and differences that appear over time are due to the use of a finite number of Fourier modes in the model and not to numerical integration inaccuracies.

Table 10. Check of two-species second-order reaction invariance to convection for no diffusion and $Da_I = 0.1$

t	$\bar{c}_A, \bar{c}_B$	$\overline{c_A c_B}$	$\tilde{c}_A^2$	$\tilde{c}_B^2$
0	1.000000	-0.20000	0.20000	0.20000
0.594	0.955178	-0.19992	0.20272	0.19748[a]
	0.955178	-0.19991	0.20191	0.19822
1.187	0.915154	-0.19964	0.20534	0.19539
	0.915157	-0.19970	0.20423	0.19636
1.781	0.879236	-0.19926	0.20784	0.19364
	0.879244	-0.19944	0.20819	0.19289
2.375	0.846857	-0.19880	0.21023	0.19217
	0.846883	-0.19929	0.20951	0.19182
2.968	0.817549	-0.19828	0.21251	0.19093
	0.817611	-0.19913	0.20820	0.19340
3.562	0.790923	-0.19772	0.21470	0.18986
	0.791037	-0.19886	0.20483	0.19723
4.155	0.766652	-0.19712	0.21680	0.18896
	0.766828	-0.19858	0.20404	0.19843
4.749	0.744459	-0.19651	0.21881	0.18818
	0.744720	-0.19856	0.20119	0.20145
5.343	0.724109	-0.19587	0.22075	0.18751
	0.724481	-0.19850	0.19748	0.20539
5.936	0.705399	-0.19523	0.22262	0.18693
	0.705908	-0.19851	0.19809	0.20472
6.530	0.688156	-0.19458	0.22441	0.18644
	0.688835	-0.19860	0.19546	0.20713
7.124	0.672229	-0.19392	0.22615	0.18602
	0.673100	-0.19847	0.19508	0.20772
7.717	0.657486	-0.19326	0.22782	0.18566
	0.658568	-0.19834	0.19113	0.21203

[a] $\underset{\sim}{y} = \underset{\sim}{0}$ above and $\underset{\sim}{y} \neq \underset{\sim}{0}$ below.

RESULTS AND DISCUSSION

Test of O'Brien's Statistical Independence Hypothesis

In terms of concentration fluctuation intensities, O'Brien's statistical independence hypothesis for single component second-order reactions is given by Equation 333,

$$\frac{\tilde{c}(t)^2_{ind}}{\tilde{c}(0)^2} = \frac{\tilde{c}(t)^2_{mix}}{\tilde{c}(0)^2} \cdot \frac{\tilde{c}(t)^2_{rxn}}{\tilde{c}(0)^2} \qquad (333)$$

In order to test O'Brien's hypothesis, for given Damköhler and Peclet numbers numerical experiments were made to find:

1) $\tilde{c}(t)^2_{rxn}$, the decay of $\tilde{c}(t)^2$ by pure reaction ($\underset{\sim}{u} = \underset{\sim}{0}$, no diffusion) for given Da_I.

2) $\tilde{c}(t)^2_{mix}$, the decay of $\tilde{c}(t)^2$ by pure mixing (no reaction) for given Pe.

3) $\tilde{c}(t)^2_{actual}$, the actual decay of $\tilde{c}(t)^2$ by mixing with reaction for given Da_I and Pe.

The initial concentration field was the same for all three experiments and the velocity field was identical for the pure mixing and mixing with reaction experiments. Equation 333 was then used to calculate $\tilde{c}(t)^2_{ind}$, the decay of $\tilde{c}(t)^2$ according to the independence hypothesis. Values of $\tilde{c}(t)^2_{actual}$ and $\tilde{c}(t)^2_{ind}$ were then compared by calculating the correction factor on O'Brien's hypothesis at time t, defined by

$$\text{correction factor} = \tilde{c}(t)^2_{\text{actual}} / \tilde{c}(t)^2_{\text{ind}} \qquad (933)$$

The results of the numerical experiments and the correction factors on O'Brien's hypothesis are given in Tables 11 - 13 and 15 - 18 using the random convection velocity and in Table 14 using the convected velocity field with interaction. Calculations were made for the following cases:

Table number	Da_I	Pe
11	0.01	20
12	0.1	100
13	0.1	20
15	0.1	5
16	1.0	100
17	1.0	20
18	10.0	20

The correction factors found for different Damköhler numbers (using Pe = 20) are compared in Table 19 for different values of the relative intensity of fluctuations, $\tilde{c}^2/\bar{c}^2$. Table 20 summarizes the correction factors for different Peclet numbers with constant Da_I.

For constant Peclet number, O'Brien's hypothesis holds in the limit of very small Damköhler numbers, where mixing decay is dominant since mixing is finished before appreciable reaction can occur, and in the limit of very large Damköhler numbers, where reaction decay is dominant because

Table 11. Check of O'Brien's independence hypothesis for $Da_I = 0.01$ and Pe = 20

t	$\bar{c}$	$\tilde{c}^2/\bar{c}^2$	$\tilde{c}(t)^2/\tilde{c}(0)^2$				correction factor
			mix	rxn	ind	actual	
0	1.00000	0.20000	1.00000	1.00000	1.00000	1.00000	1.0000
0.264	0.99688	0.17608	0.88469	0.98891	0.87488	0.87491	1.0000
0.528	0.99383	0.15652	0.79018	0.97799	0.77279	0.77299	1.0003
0.792	0.99085	0.13966	0.70855	0.96723	0.68533	0.68560	1.0004
1.055	0.98792	0.12373	0.63082	0.95663	0.60346	0.60378	1.0005
1.319	0.98506	0.10790	0.55299	0.94618	0.52323	0.52351	1.0005
1.583	0.98225	0.08977	0.46247	0.93588	0.43282	0.43304	1.0005
1.847	0.97951	0.07147	0.37013	0.92574	0.34264	0.34286	1.0006
2.111	0.97683	0.05544	0.28857	0.91574	0.26426	0.26449	1.0009
2.375	0.97419	0.04291	0.22449	0.90589	0.20336	0.20361	1.0012
2.638	0.97160	0.03413	0.17942	0.89618	0.16079	0.16110	1.0019
2.902	0.96904	0.02739	0.14469	0.88660	0.12828	0.12862	1.0026
3.166	0.96651	0.02203	0.11689	0.87717	0.10253	0.10289	1.0035
3.430	0.96400	0.01804	0.096147	0.86787	0.083443	0.083837	1.0047
3.694	0.96151	0.01487	0.079579	0.85870	0.068334	0.068738	1.0059
3.956	0.95905	0.01231	0.066191	0.84966	0.056240	0.056623	1.0068
4.221	0.95660	0.01033	0.055777	0.84074	0.046894	0.047247	1.0075
4.485	0.95417	0.00889	0.048244	0.83195	0.040137	0.040460	1.0081
4.749	0.95175	0.00778	0.042422	0.82329	0.034926	0.035222	1.0085
5.013	0.94935	0.00679	0.037216	0.81474	0.030321	0.030591	1.0089

Table 11. (Continued)

t	$\bar{c}$	$\tilde{c}^2/\bar{c}^2$	$\tilde{c}(t)^2/\tilde{c}(0)^2$				correction factor
			mix	rxn	ind	actual	
5.277	0.94696	0.00595	0.032765	0.80632	0.026419	0.026665	1.0093
5.541	0.94459	0.00521	0.028833	0.79801	0.023009	0.023235	1.0098
5.804	0.94223	0.00447	0.024847	0.78981	0.019624	0.019828	1.0104
6.068	0.93989	0.00373	0.020834	0.78173	0.016287	0.016465	1.0110
6.332	0.93755	0.00305	0.017121	0.77375	0.013247	0.013401	1.0116
6.596	0.93523	0.00248	0.013996	0.76589	0.010719	0.010849	1.0121
6.860	0.93293	0.00205	0.011612	0.75813	0.0088034	0.0089128	1.0124
7.124	0.93063	0.00172	0.0097831	0.75047	0.0073419	0.0074354	1.0127
7.388	0.92835	0.00143	0.0081842	0.74292	0.0060802	0.0061604	1.0132
7.658	0.92608	0.00118	0.0067817	0.73547	0.0049877	0.0050563	1.0137
7.915	0.92382	0.00098	0.0056638	0.72812	0.0041239	0.0041829	1.0143
8.179	0.92157	0.00084	0.0048490	0.72087	0.0034955	0.0035473	1.0148
8.443	0.91933	0.00073	0.0042379	0.71371	0.0030246	0.0030706	1.0152
8.707	0.91711	0.00063	0.0036679	0.70665	0.0025919	0.0026317	1.0153
8.971	0.91489	0.00053	0.0031023	0.69968	0.0021706	0.0022041	1.0154

Table 12. Check of O'Brien's independence hypothesis for Da_I = 0.1 and Pe = 100

t	$\bar{c}$	$\tilde{c}^2/\bar{c}^2$	$\tilde{c}(t)^2/\tilde{c}(0)^2$				correction factor
			mix	rxn	ind	actual	
0	1.00000	0.20000	1.00000	1.00000	1.00000	1.00000	1.0000
0.264	0.96949	0.18600	0.97516	0.89618	0.87392	0.87413	1.0002
0.528	0.94109	0.17378	0.95179	0.80632	0.76744	0.76953	1.0027
0.729	0.91456	0.16239	0.92870	0.72812	0.67621	0.67914	1.0043
1.055	0.88973	0.15139	0.90372	0.65974	0.59622	0.59923	1.0050
1.319	0.86642	0.14031	0.87581	0.59967	0.52519	0.52664	1.0028
1.583	0.84452	0.12873	0.84054	0.54666	0.45949	0.45907	0.9991
1.847	0.82390	0.11742	0.80004	0.49971	0.39979	0.39853	0.9969
2.111	0.80445	0.10679	0.75754	0.45796	0.34692	0.34554	0.9960
2.375	0.78607	0.09716	0.71701	0.42071	0.30165	0.30017	0.9951
2.638	0.76865	0.08913	0.68192	0.38737	0.26415	0.26329	0.9967
2.902	0.75209	0.08218	0.65087	0.35743	0.23264	0.23243	0.9991
3.166	0.73632	0.07609	0.62249	0.33047	0.20571	0.20628	1.0028
3.430	0.72128	0.07084	0.59700	0.30613	0.18276	0.18427	1.0082
3.694	0.70691	0.06586	0.57239	0.28409	0.16261	0.16456	1.0120
3.956	0.69316	0.06117	0.54938	0.26410	0.14509	0.14696	1.0129
4.221	0.67999	0.05697	0.52851	0.24591	0.12996	0.13172	1.0135
4.485	0.66736	0.05323	0.50945	0.22933	0.11683	0.11853	1.0146
4.749	0.65523	0.04984	0.49163	0.21418	0.10530	0.10699	1.0160
5.013	0.64356	0.04670	0.47419	0.20032	0.094988	0.096714	1.0182

Table 12. (Continued)

t	$\bar{c}$	$\tilde{c}^2/\bar{c}^2$	$\tilde{c}(t)^2/\tilde{c}(0)^2$				correction factor
			mix	rxn	ind	actual	
5.277	0.63234	0.04379	0.45772	0.18760	0.085870	0.087552	1.0196
5.541	0.62153	0.04106	0.44213	0.17592	0.077781	0.079306	1.0196
5.804	0.61111	0.03840	0.42631	0.16518	0.070416	0.071703	1.0183
6.068	0.60106	0.03579	0.40929	0.15527	0.063550	0.064645	1.0172
6.332	0.59136	0.03323	0.39086	0.14612	0.057113	0.058109	1.0174
6.596	0.58199	0.03085	0.37327	0.13766	0.051385	0.052246	1.0168
6.860	0.57293	0.02879	0.35856	0.12983	0.046551	0.047246	1.0149
7.124	0.56416	0.02698	0.34577	0.12257	0.042379	0.042937	1.0132
7.388	0.55568	0.02527	0.33273	0.11582	0.038537	0.039015	1.0124
7.658	0.54745	0.02367	0.31985	0.10955	0.035040	0.035477	1.0125
7.915	0.53948	0.02223	0.30806	0.10371	0.031950	0.032348	1.0125
8.179	0.53175	0.02092	0.29721	0.098271	0.029207	0.029573	1.0125
8.443	0.52425	0.01970	0.28693	0.093194	0.026740	0.027078	1.0127
8.707	0.51696	0.01853	0.27636	0.088451	0.024444	0.024763	1.0130
8.971	0.50988	0.01734	0.26486	0.084016	0.022252	0.022543	1.0131
9.234	0.50300	0.01618	0.25310	0.079864	0.020213	0.020465	1.0125
9.498	0.49631	0.01512	0.24234	0.075973	0.018411	0.018626	1.0117
9.762	0.48980	0.01420	0.23295	0.072323	0.016848	0.017028	1.0107

Table 13. Check of O'Brien's independence hypothesis for Da_I = 0.1 and Pe = 20

t	$\bar{c}$	$\tilde{c}^2/\bar{c}^2$	$\tilde{c}(t)^2/\tilde{c}(0)^2$				correction factor
			mix	rxn	ind	actual	
0	1.00000	0.20000	1.00000	1.00000	1.00000	1.00000	1.0000
0.1978	0.97704	0.17567	0.91086	0.92072	0.83865	0.83850	0.9998
0.3958	0.95551	0.15582	0.83618	0.84966	0.71046	0.71133	1.0012
0.5936	0.93523	0.13835	0.76830	0.78576	0.60370	0.60504	1.0022
0.7915	0.91606	0.12328	0.70850	0.72812	0.51587	0.51727	1.0027
0.9894	0.89789	0.10934	0.65000	0.67600	0.43941	0.44076	1.0031
1.1873	0.88064	0.09639	0.59291	0.62875	0.37279	0.37376	1.0026
1.3852	0.86422	0.08349	0.53144	0.58580	0.31131	0.31180	1.0016
1.5830	0.84860	0.07021	0.46242	0.54666	0.25279	0.25281	1.0001
1.7809	0.83370	0.05764	0.39246	0.51092	0.20052	0.20031	0.9990
1.9788	0.81948	0.04657	0.32745	0.47823	0.15660	0.15636	0.9985
2.1767	0.80587	0.03727	0.27063	0.44825	0.12131	0.12103	0.9977
2.3746	0.79280	0.02996	0.22445	0.42071	0.094429	0.094147	0.9970
2.5725	0.78023	0.02453	0.18928	0.39536	0.074834	0.074668	0.9977
2.7703	0.76811	0.02032	0.16123	0.37200	0.059977	0.05994	0.9994
2.9682	0.75640	0.01679	0.13696	0.35042	0.047994	0.04804	1.0010
3.1661	0.74507	0.01395	0.11684	0.33047	0.038612	0.03873	1.0031

Table 14. Check of O'Brien's independence hypothesis for $Da_I = 0.1$ and $Pe = 20$ using convected velocity field with interaction

t	$\bar{c}$	$\tilde{c}^2/\bar{c}^2$	$\tilde{c}(t)^2/\tilde{c}(0)^2$				correction factor
			mix	rxn	ind	actual	
0	1.00000	0.20000	1.00000	1.00000	1.00000	1.00000	1.0000
0.198	0.97705	0.17503	0.90786	0.92072	0.83589	0.83543	0.9995
0.396	0.95555	0.15204	0.81791	0.84965	0.69494	0.69419	0.9988
0.594	0.93537	0.13030	0.72624	0.78575	0.57065	0.57001	0.9989
0.792	0.91637	0.11017	0.63557	0.72812	0.46277	0.46258	0.9996
0.989	0.89844	0.09197	0.54914	0.67600	0.37122	0.37117	0.9999
1.187	0.88145	0.07593	0.46955	0.62875	0.29523	0.29498	0.9991
1.385	0.86532	0.06245	0.39992	0.58579	0.23427	0.23382	0.9981
1.583	0.84994	0.05173	0.34256	0.54666	0.18726	0.18684	0.9977
1.791	0.83522	0.04332	0.29630	0.51092	0.15138	0.15111	0.9982
1.979	0.82111	0.03660	0.25841	0.47823	0.12358	0.12338	0.9984
2.177	0.80755	0.03105	0.22636	0.44825	0.10147	0.10124	0.9978
2.375	0.79449	0.02634	0.19825	0.42071	0.083406	0.083145	0.9969
2.572	0.78190	0.02233	0.17318	0.39536	0.068470	0.068252	0.9968
2.770	0.76974	0.01887	0.15069	0.37200	0.056056	0.055909	0.9974
2.968	0.75800	0.01588	0.13049	0.35042	0.045726	0.045619	0.9977
3.166	0.74664	0.01332	0.11264	0.33047	0.037223	0.037122	0.9973
3.364	0.73563	0.01118	0.097295	0.31199	0.030355	0.030250	0.9965

Table 14. (Continued)

t	$\bar{c}$	$\tilde{c}^2/\bar{c}^2$	$\tilde{c}(t)^2/\tilde{c}(0)^2$				correction factor
			mix	rxn	ind	actual	
3.562	0.72497	0.00943	0.084418	0.29484	0.024890	0.024787	0.9959
3.760	0.71463	0.00800	0.073578	0.27891	0.020522	0.020436	0.9958
3.958	0.70459	0.00680	0.064165	0.26409	0.016946	0.016892	0.9968
4.156	0.69485	0.00578	0.055846	0.25029	0.013978	0.013965	0.9991
4.353	0.68537	0.00493	0.048671	0.23743	0.011556	0.011583	1.0023
4.551	0.67616	0.00423	0.042661	0.22541	0.0096163	0.0096763	1.0062
4.749	0.66720	0.00365	0.037596	0.21418	0.0080522	0.0081332	1.0101
4.947	0.65847	0.00316	0.033168	0.20367	0.0067553	0.0068443	1.0132

Table 15. Check of O'Brien's independence hypothesis for Da_I = 0.1 and Pe = 5

t	$\bar{c}$	$\tilde{c}^2/\bar{c}^2$	$\tilde{c}(t)^2/\tilde{c}(0)^2$				correction factor
			mix	rxn	ind	actual	
0	1.00000	0.20000	1.00000	1.00000	1.00000	1.00000	1.0000
0.066	0.99223	0.17428	0.88213	0.97259	0.85795	0.85792	1.0000
0.132	0.98474	0.15311	0.78468	0.94620	0.74246	0.74240	0.9999
0.198	0.97747	0.13570	0.70409	0.92072	0.64827	0.64826	1.0000
0.264	0.97041	0.12118	0.63661	0.89618	0.57051	0.57059	1.0001
0.330	0.96354	0.10893	0.57938	0.87250	0.50551	0.50564	1.0003
0.396	0.95683	0.09831	0.52951	0.84966	0.44990	0.46001	1.0003
0.462	0.95027	0.08891	0.48497	0.82761	0.40136	0.40143	1.0002
0.528	0.94385	0.08057	0.44507	0.80632	0.35887	0.35888	1.0000
0.594	0.93757	0.07325	0.40976	0.78575	0.32197	0.32195	0.9999
0.660	0.93140	0.06687	0.37873	0.76589	0.29006	0.29003	0.9999
0.726	0.92535	0.06121	0.35104	0.74668	0.26212	0.62608	0.9998
0.729	0.91941	0.05609	0.32561	0.72812	0.23708	0.23706	0.9999
0.857	0.91357	0.05136	0.30182	0.71017	0.21434	0.21434	1.0000
0.923	0.90784	0.04700	0.27953	0.69281	0.19366	0.19369	1.0001
0.989	0.90219	0.04299	0.25875	0.67600	0.17492	0.17497	1.0003
1.055	0.89663	0.03931	0.23939	0.65974	0.15794	0.15803	1.0005
1.121	0.89117	0.03590	0.22120	0.64400	0.14245	0.14257	1.0008
1.187	0.88578	0.03269	0.20377	0.62875	0.12812	0.12825	1.0010
1.253	0.88048	0.02960	0.18669	0.61398	0.11462	0.11475	1.0011

Table 15. (Continued)

t	$\bar{c}$	$\tilde{c}^2/\bar{c}^2$	$\tilde{c}(t)^2/\tilde{c}(0)^2$				correction factor
			mix	rxn	ind	actual	
1.319	0.87525	0.02661	0.16976	0.59967	0.10180	0.10192	1.0012
1.385	0.87010	0.02372	0.15308	0.58579	0.089673	0.089787	1.0013
1.451	0.86503	0.02096	0.13687	0.57235	0.078337	0.078435	1.0013
1.517	0.86002	0.01838	0.12137	0.55931	0.067883	0.067966	1.0012
1.583	0.85509	0.01599	0.10684	0.54666	0.058405	0.058471	1.0011
1.649	0.85022	0.01384	0.093507	0.53439	0.049969	0.050021	1.0010
1.715	0.84542	0.01193	0.081515	0.52248	0.042590	0.042631	1.0010
1.781	0.84068	0.01026	0.070905	0.51093	0.036227	0.036262	1.0010
1.847	0.83600	0.00882	0.061640	0.49971	0.030802	0.030834	1.0010
1.913	0.83138	0.00759	0.053622	0.48881	0.026211	0.026242	1.0012
1.979	0.82681	0.00655	0.046718	0.47823	0.022342	0.022373	1.0014
2.045	0.82230	0.00565	0.040779	0.46795	0.019082	0.019133	1.0016
2.111	0.81784	0.00489	0.035668	0.45796	0.016334	0.016362	1.0017
2.177	0.81343	0.00424	0.031268	0.44825	0.014016	0.014040	1.0017
2.243	0.80907	0.00369	0.027489	0.43881	0.012063	0.012083	1.0016
2.309	0.80476	0.00322	0.024265	0.42963	0.010425	0.010441	1.0015
2.375	0.80050	0.00283	0.021531	0.42071	0.0090583	0.0090700	1.0013
2.441	0.79629	0.00250	0.019214	0.41203	0.0079167	0.0079253	1.0011
2.507	0.79212	0.00222	0.017237	0.40358	0.0069566	0.0069628	1.0009
2.572	0.78799	0.00198	0.015527	0.39537	0.0061388	0.0061431	1.0007

Table 15. (Continued)

t	$\bar{c}$	$\tilde{c}^2/\bar{c}^2$	$\tilde{c}(t)^2/\tilde{c}(0)^2$				correction factor
			mix	rxn	ind	actual	
2.638	0.78391	0.00177	0.014025	0.38737	0.0054328	0.0054357	1.0005
2.704	0.77987	0.00158	0.012691	0.37958	0.0048173	0.0048194	1.0004
2.770	0.77587	0.00142	0.011500	0.37200	0.0042780	0.0042799	1.0004
2.836	0.77192	0.00128	0.010436	0.36462	0.0038052	0.0038072	1.0005
2.902	0.76800	0.00115	0.0094878	0.35743	0.0033912	0.0033938	1.0008
2.968	0.76413	0.00104	0.0086467	0.35043	0.0030300	0.0030332	1.0011
3.034	0.76029	0.00094	0.0079016	0.34360	0.0027150	0.0027189	1.0014
3.100	0.75649	0.00085	0.0072406	0.33695	0.0024397	0.0024443	1.0019
3.166	0.75273	0.00078	0.0066512	0.33047	0.0021980	0.0022032	1.0024

Table 16. Check of O'Brien's independence hypothesis for Da_I = 1.0 and Pe = 100

t	$\bar{c}$	$\tilde{c}^2/\bar{c}^2$	$\tilde{c}(t)^2/\tilde{c}(0)^2$				correction factor
			mix	rxn	ind	actual	
0	1.00000	0.20000	1.00000	1.00000	1.00000	1.00000	1.0000
0.066	0.92731	0.17688	0.99363	0.76588	0.76100	0.76048	0.9993
0.132	0.86552	0.15783	0.98734	0.59966	0.59207	0.59119	0.9985
0.198	0.81220	0.14206	0.98118	0.47822	0.46922	0.46855	0.9986
0.264	0.76563	0.12890	0.97516	0.38736	0.37774	0.37779	1.0001
0.330	0.72452	0.11774	0.96937	0.31799	0.30825	0.30902	1.0025
0.396	0.68794	0.10802	0.96359	0.26409	0.25448	0.25560	1.0044
0.462	0.65513	0.09943	0.95773	0.22158	0.21221	0.21338	1.0055
0.528	0.62551	0.09181	0.95179	0.18760	0.17856	0.17960	1.0058
0.594	0.59863	0.08501	0.94587	0.16012	0.15145	0.15232	1.0058
0.660	0.57410	0.07895	0.94006	0.13766	0.12941	0.13010	1.0054
0.726	0.55162	0.07352	0.93439	0.11913	0.11131	0.11185	1.0048
0.792	0.53093	0.06861	0.92870	0.10371	0.096316	0.096706	1.0040
0.857	0.51181	0.06416	0.92281	0.090781	0.083774	0.084038	1.0032
0.923	0.49410	0.06009	0.91665	0.079862	0.073206	0.073354	1.0020
0.989	0.47762	0.05635	0.91025	0.070581	0.064247	0.064277	1.0005
1.055	0.46226	0.05289	0.90372	0.062645	0.056614	0.056514	0.9982
1.121	0.44791	0.04969	0.89715	0.055822	0.050081	0.049840	0.9952
1.187	0.43445	0.04671	0.89044	0.049926	0.044456	0.044079	0.9915
1.253	0.42182	0.04393	0.88338	0.044805	0.039580	0.039084	0.9875

Table 16. (Continued)

t	$\bar{c}$	$\tilde{c}^2/\bar{c}^2$	$\tilde{c}(t)^2/\tilde{c}(0)^2$				correction factor
			mix	rxn	ind	actual	
1.319	0.40992	0.04134	0.87581	0.040340	0.035330	0.034735	0.9832
1.385	0.39871	0.03891	0.86769	0.036429	0.031609	0.030930	0.9785
1.451	0.38812	0.03663	0.85906	0.032991	0.028341	0.027589	0.9735
1.517	0.37809	0.03449	0.84999	0.029957	0.025463	0.024650	0.9681
1.583	0.36859	0.03248	0.84054	0.027271	0.022923	0.022064	0.9625
1.649	0.35958	0.03061	0.83076	0.024884	0.020673	0.019788	0.9572
1.715	0.35100	0.02887	0.82072	0.022758	0.018678	0.017785	0.9522
1.781	0.34284	0.02726	0.81047	0.020858	0.016905	0.016019	0.9476
1.847	0.33506	0.02576	0.80004	0.019156	0.015326	0.014457	0.9433
1.913	0.32764	0.02435	0.78949	0.017627	0.013916	0.013071	0.9393
1.979	0.32055	0.02304	0.77884	0.016250	0.012656	0.011837	0.9353
2.045	0.31377	0.02181	0.76817	0.015006	0.011527	0.010735	0.9313
2.111	0.30727	0.02066	0.75754	0.013882	0.010516	0.0097509	0.9272
2.177	0.30105	0.01958	0.74703	0.012862	0.0096080	0.0088712	0.9233
2.243	0.29508	0.01857	0.73674	0.011935	0.0087930	0.0080848	0.9195
2.309	0.28934	0.01763	0.72672	0.011092	0.0080605	0.0073817	0.9158
2.375	0.28383	0.01677	0.71701	0.010322	0.0074012	0.0067531	0.9124
2.441	0.27853	0.01596	0.70768	0.0096194	0.0068075	0.0061910	0.9094

Table 17. Check of O'Brien's independence hypothesis for Da_I = 1.0 and Pe = 20

t	$\bar{c}$	$\tilde{c}^2/\bar{c}^2$	$\tilde{c}(t)^2/\tilde{c}(0)^2$				correction factor
			mix	rxn	ind	actual	
0	1.00000	0.20000	1.00000	1.00000	1.00000	1.00000	1.0000
0.050	0.94444	0.17873	0.97619	0.81686	0.79741	0.79711	0.9996
0.099	0.89551	0.16055	0.95332	0.67600	0.64444	0.64377	0.9990
0.148	0.85201	0.14498	0.93156	0.56577	0.52705	0.52623	0.9984
0.198	0.81301	0.13157	0.91086	0.47822	0.43559	0.43484	0.9983
0.247	0.77780	0.11997	0.89111	0.40777	0.36337	0.36289	0.9987
0.297	0.74580	0.10983	0.87221	0.35042	0.30564	0.30545	0.9994
0.346	0.71658	0.10084	0.85397	0.30325	0.25897	0.25891	0.9998
0.396	0.68976	0.09278	0.83618	0.26409	0.22083	0.22072	0.9995
0.445	0.66505	0.08551	0.81866	0.23131	0.18936	0.18911	0.9987
0.495	0.64219	0.07894	0.80142	0.20367	0.16323	0.16277	0.9972
0.544	0.62096	0.07299	0.78458	0.18019	0.14137	0.14073	0.9954
0.594	0.60119	0.06763	0.76831	0.16012	0.12302	0.12222	0.9935
0.643	0.58273	0.06278	0.75269	0.14287	0.10754	0.10660	0.9913
0.693	0.56545	0.05839	0.73767	0.12796	0.094392	0.093348	0.9889
0.742	0.54922	0.05439	0.72302	0.11501	0.083155	0.082029	0.9865
0.792	0.53395	0.05072	0.70850	0.10371	0.073479	0.072297	0.9839
0.841	0.51955	0.04773	0.69394	0.093808	0.065097	0.063881	0.9813
0.890	0.50595	0.04420	0.67931	0.085096	0.057807	0.056573	0.9787
0.940	0.49308	0.04130	0.66463	0.077401	0.051443	0.050207	0.9760

Table 17. (Continued)

t	$\bar{c}$	$\tilde{c}^2/\bar{c}^2$	$\tilde{c}(t)^2/\tilde{c}(0)^2$				correction factor
			mix	rxn	ind	actual	
0.989	0.48088	0.03862	0.65000	0.070581	0.045878	0.044649	0.9732
1.039	0.46930	0.03613	0.63554	0.064517	0.041003	0.039784	0.9703
1.088	0.45829	0.03382	0.62127	0.059107	0.036721	0.035515	0.9671
1.138	0.44781	0.03167	0.60713	0.054268	0.032948	0.031753	0.9637
1.187	0.43781	0.02966	0.59291	0.049926	0.029602	0.028424	0.9602
1.237	0.42827	0.02777	0.57838	0.046020	0.026617	0.025463	0.9566
1.286	0.41915	0.02597	0.56333	0.042498	0.023940	0.022817	0.9531
1.336	0.41042	0.02427	0.54768	0.039314	0.021532	0.020444	0.9495
1.385	0.40207	0.02266	0.53144	0.036429	0.019360	0.018313	0.9459
1.435	0.39406	0.02112	0.51469	0.033810	0.017402	0.016397	0.9423
1.484	0.38637	0.01966	0.49753	0.031427	0.015636	0.014674	0.9385
1.534	0.37899	0.01828	0.48007	0.029255	0.014044	0.013126	0.9346
1.583	0.37190	0.01697	0.46242	0.027271	0.012611	0.011736	0.9306
1.632	0.36507	0.01574	0.44473	0.025455	0.011321	0.010492	0.9268
1.682	0.35850	0.01459	0.42711	0.023791	0.010161	0.0093788	0.9230
1.731	0.35216	0.01352	0.40966	0.022263	0.0091203	0.0083844	0.9193
1.781	0.34606	0.01252	0.39246	0.020858	0.0081859	0.0074965	0.9158
1.830	0.34016	0.01159	0.37559	0.019565	0.0073484	0.0067039	0.9123
1.880	0.33447	0.01072	0.35910	0.018371	0.0065970	0.0059963	0.9089
1.929	0.32897	0.00991	0.34304	0.017269	0.0059240	0.0053644	0.9055
1.979	0.32366	0.00916	0.32745	0.016250	0.0053211	0.0048002	0.9021

Table 17. (Continued)

t	$\bar{c}$	$\tilde{c}^2/\bar{c}^2$	$\tilde{c}(t)^2/\tilde{c}(0)^2$				correction factor
			mix	rxn	ind	actual	
2.028	0.31851	0.00847	0.31238	0.015305	0.0047810	0.0042965	0.8987
2.078	0.31353	0.00783	0.29785	0.014430	0.0042980	0.0038471	0.8951
2.127	0.30871	0.00723	0.28392	0.013617	0.0038661	0.0034467	0.8915
2.177	0.30403	0.00669	0.27063	0.012862	0.0034808	0.0030906	0.8879
2.226	0.29950	0.00619	0.25802	0.012159	0.0031373	0.0027744	0.8843
2.275	0.29510	0.00573	0.24610	0.011504	0.0028311	0.0024941	0.8810
2.325	0.29083	0.00531	0.23491	0.010893	0.0025589	0.0022461	0.8778
2.375	0.28668	0.00493	0.22445	0.019322	0.0023168	0.0020268	0.8748
2.424	0.28266	0.00459	0.21471	0.0097893	0.0021019	0.0018332	0.8722
2.473	0.27874	0.00428	0.20564	0.0092907	0.0019105	0.0016619	0.8699

Table 18. Check of O'Brien's independence hypothesis for Da_I = 10.0 and Pe = 20

t	$\bar{c}$	$\tilde{c}^2/\bar{c}^2$	$\tilde{c}(t)^2/\tilde{c}(0)^2$				correction factor
			mix	rxn	ind	actual	
0	1.00000	0.20000	1.00000	1.00000	1.00000	1.00000	1.0000
0.0330	0.72356	0.11857	0.98403	0.31594	0.31089	0.31038	0.9984
0.0660	0.57315	0.08019	0.96845	0.13660	0.13229	0.13172	0.9957
0.0989	0.47675	0.05832	0.95332	0.070028	0.066759	0.066279	0.9928
0.132	0.40910	0.04443	0.93868	0.040029	0.037575	0.037183	0.9896
0.165	0.35876	0.03498	0.92455	0.024697	0.022834	0.022511	0.9859
0.198	0.31972	0.02823	0.91086	0.016131	0.014693	0.014428	0.9819
0.231	0.28851	0.02323	0.89760	0.011013	0.0098852	0.0096672	0.9779
0.264	0.26295	0.01942	0.84472	0.0077906	0.0068925	0.0067128	0.9739
0.297	0.24162	0.01644	0.87221	0.0056745	0.0049494	0.0047992	0.9697
0.330	0.22353	0.01407	0.85999	0.0042355	0.0036425	0.0035155	0.9651
0.363	0.20799	0.01215	0.84800	0.0032281	0.0027374	0.0026289	0.9603
0.396	0.19450	0.01058	0.83618	0.0025049	0.0020945	0.0020011	0.9554
1.088	0.08266	0.00151	0.62127	0.0000936	0.0000581	0.00005155	0.8865

Table 19. Summary of correction factors on O'Brien's hypothesis - effect of Damköhler number (Pe = 20)

$\tilde{c}^2/\bar{c}^2$	Da_I				
	0.01	0.1	0.1[a]	1.0	10
0.20	1.0000	1.0000	1.0000	1.0000	1.0000
0.18	1.0000	0.9999	0.9996	0.9996	0.9996
0.16	1.0002	1.0009	0.9990	0.9990	0.9992
0.14	1.0004	1.0021	0.9989	0.9984	0.9988
0.12	1.0005	1.0028	0.9993	0.9987	0.9984
0.10	1.0005	1.0027	0.9998	0.9998	0.9971
0.08	1.0006	1.0012	0.9993	0.9974	0.9957
0.06	1.0008	0.9992	0.9980	0.9898	0.9930
0.04	1.0014	0.9979	0.9983	0.9746	0.9879
0.02	1.0041	0.9995	0.9972	0.9394	0.9745
0.01	1.0076		0.9961	0.9059	0.9536
0.008	1.0084		0.9958	0.8961	
0.006	1.0093		0.9986	0.8829	
0.004	1.0108		1.0077	0.8678	
0.002	1.0124				
0.001	1.0142				

[a]Using convected velocity field with interaction.

Table 20. Summary of correction factors on O'Brien's hypothesis - effect of Peclet number

$\tilde{c}^2/\bar{c}^2$	$Da_I = 0.1$			$Da_I = 1.0$	
	Pe = 5	Pe = 20[a]	Pe = 100	Pe = 100	Pe = 20
0.20	1.0000	1.0000	1.0000	1.0000	1.0000
0.18	1.0000	0.9996	1.0014	0.9994	0.9996
0.16	0.9999	0.9990	1.0045	0.9986	0.9990
0.14	1.0000	0.9989	1.0028	0.9988	0.9984
0.12	1.0001	0.9993	0.9974	1.0020	0.9987
0.10	1.0003	0.9998	0.9954	1.0054	0.9998
0.08	1.0000	0.9993	1.0004	1.0055	0.9974
0.06	0.9998	0.9980	1.0131	1.0020	0.9898
0.04	1.0005	0.9983	1.0191	0.9806	0.9746
0.02	1.0013	0.9972	1.0126	0.9248	0.9394
0.01	1.0010	0.9961	1.0061		0.9059
0.008	1.0011	0.9958			0.8961
0.006	1.0015	0.9986			0.8829
0.004	1.0016	1.0077			0.8678
0.002	1.0007				
0.001	1.0012				

[a]Using convected velocity field with interaction.

the reaction goes to completion before appreciable mixing can occur. Similarly, for constant Damköhler number, O'Brien's hypothesis holds exactly in the limit of infinite Peclet number, since diffusion and hence mixing does not occur, and in the limit of a zero Peclet number, since the diffusivity approaches being infinite and the concentration field diffuses to uniformity before appreciable reaction can occur. Therefore, conditions in which both mixing and reaction are significant are of the greatest interest in testing O'Brien's hypothesis.

For $Da_I = 0.01$ and $Pe = 20$, the results in Table 11 show the decay of $\tilde{c}(t)^2$ due to reaction to be very slow compared to the mixing decay. O'Brien's hypothesis underestimates the decay rate by less than one percent throughout most of the decay and the deviation is only 1.5 percent at $\tilde{c}^2/\bar{c}^2 = 0.0005$.

For $Da_I = 0.1$, Tables 12, 13, and 15 give results for Peclet numbers of 100, 20, and 5, respectively, with the mixing decay being slower than, approximately equal to, and faster than the reaction decay. Table 14 gives results for $Da_I = 0.1$ and $Pe = 20$ obtained using the convected velocity field with interaction. Comparison with results in Table 13 for the random convection velocity shows that although mixing is somewhat faster with the convected velocity field, the correction factors obtained are similar for both velocity fields. It is interesting to note that in all four

cases the correction factor oscillates about one throughout the decay. The maximum deviations of O'Brien's hypothesis are 2 percent for Pe = 100, 1 percent for Pe = 20, and less than 0.2 percent for Pe = 5.

For $Da_I = 1.0$, Tables 16 and 17 give results for Peclet numbers of 100 and 20, respectively. In both cases, the reaction decay is much faster than the mixing decay but significant mixing does occur. Initially the correction factor oscillates about (or close to) one, but in the later stages of decay it continually drops off from one. At $\tilde{c}^2/\bar{C}^2 = 0.02$ (10 percent of the initial intensity) the deviation is 6 - 7 percent.

For $Da_I = 10.0$ and Pe = 20, the results in Table 18 show that the decay due to reaction is extremely fast compared to the decay due to mixing, and at initial times the system approaches being a frozen field reaction. The correction factor continually drops off from one with the decay but at a relatively slow rate; the deviations are less than those for $Da_I = 1.0$. At $\tilde{c}^2/\bar{C}^2 = 0.02$, the deviation is 2.5 percent and at $\tilde{c}^2/\bar{C}^2 = 0.002$ approximately 10 percent.

The observation that O'Brien's hypothesis underestimates the decay rate when mixing is dominant, overestimates the decay rate when reaction is dominant, and oscillates between underestimating and overestimating the decay rate for intermediate conditions, suggests that counteracting or canceling of two opposing (physical) factors is responsible

for the success of O'Brien's hypothesis.

One drawback to using O'Brien's independence hypothesis in practice is the need for estimating $\widetilde{c}(t)^2_{rxn}$ for real systems. The elimination of mixing effects from a reacting system would seem to be most difficult. Of course the pure reaction decay rate can be calculated if initial concentration probability densities are known (see Equations 230 and 231), but this information would also seem difficult to obtain.

From analysis of the single component second-order reaction problem using the direct-interaction approximation, Lee (58) obtained the approximate result

$$\widetilde{c}(t)^2_{rxn}/\widetilde{c}(0)^2 \approx (1 + Da_I t)^{-4} \qquad (934)$$

for pure reaction decay (see Equations 243 and 245; notice that Lee's time scale is different from that in this study and hence his Da_I and Da_{II} are defined differently). This approximate result is compared in Table 21 and Figure 26 to the decay of $\widetilde{c}(t)^2_{rxn}$ obtained in this study. Notice that unique decays of $\overline{c}(t)$ and $\widetilde{c}(t)^2$ for pure reaction result if the time scale $Da_I t$ is used. This means that for all values of $\widetilde{c}(t)^2$, the difference between Equation 934 and the results of this study is independent of the rate of reaction. From Figure 26 it can be seen that Lee's approximate result agrees reasonably well with the decay found in this study and may provide a useful order-of-magnitude estimate of

Table 21. Decay of $\tilde{c}(t)^2$ for a single component second-order reaction without convection or diffusion compared to Lee's approximate result

$Da_I t$	$\bar{c}(t)$	$\tilde{c}^2/\bar{c}^2$	$\tilde{c}^2/\tilde{c}_0^2$	$(1 + Da_I t)^{-4}$	ratio[a]
0	1.00000	0.20000	1.00000	1.00000	1.0000
0.01055	0.98751	0.19620	0.95663	0.95888	0.9976
0.02111	0.97537	0.19251	0.91574	0.91984	0.9955
0.03166	0.96356	0.18895	0.87717	0.88278	0.9936
0.05013	0.94365	0.18299	0.81474	0.82229	0.9908
0.07124	0.92198	0.17657	0.75047	0.75938	0.9883
0.1055	0.88904	0.16694	0.65974	0.66943	0.9855
0.2111	0.80218	0.14234	0.45796	0.46485	0.9852
0.3166	0.73200	0.12335	0.33047	0.33279	0.9930
0.5013	0.63646	0.09890	0.20032	0.19685	1.0176
0.7124	0.55525	0.07951	0.12257	0.11630	1.0539
1.006	0.47282	0.06126	0.06848	0.06177	1.1087
2.012	0.31598	0.03127	0.01561	0.01215	1.2846
3.018	0.23836	0.01922	0.00546	0.00384	1.4226
4.947	0.16249	0.00967	0.00128	0.000800	1.5968
6.926	0.12273	0.00578	0.000437	0.000253	1.7193
9.894	0.08985	0.00323	0.000130	0.0000710	1.8374

[a]Ratio of $\tilde{c}^2/\tilde{c}_0^2$ to $(1 + Da_I t)^{-4}$.

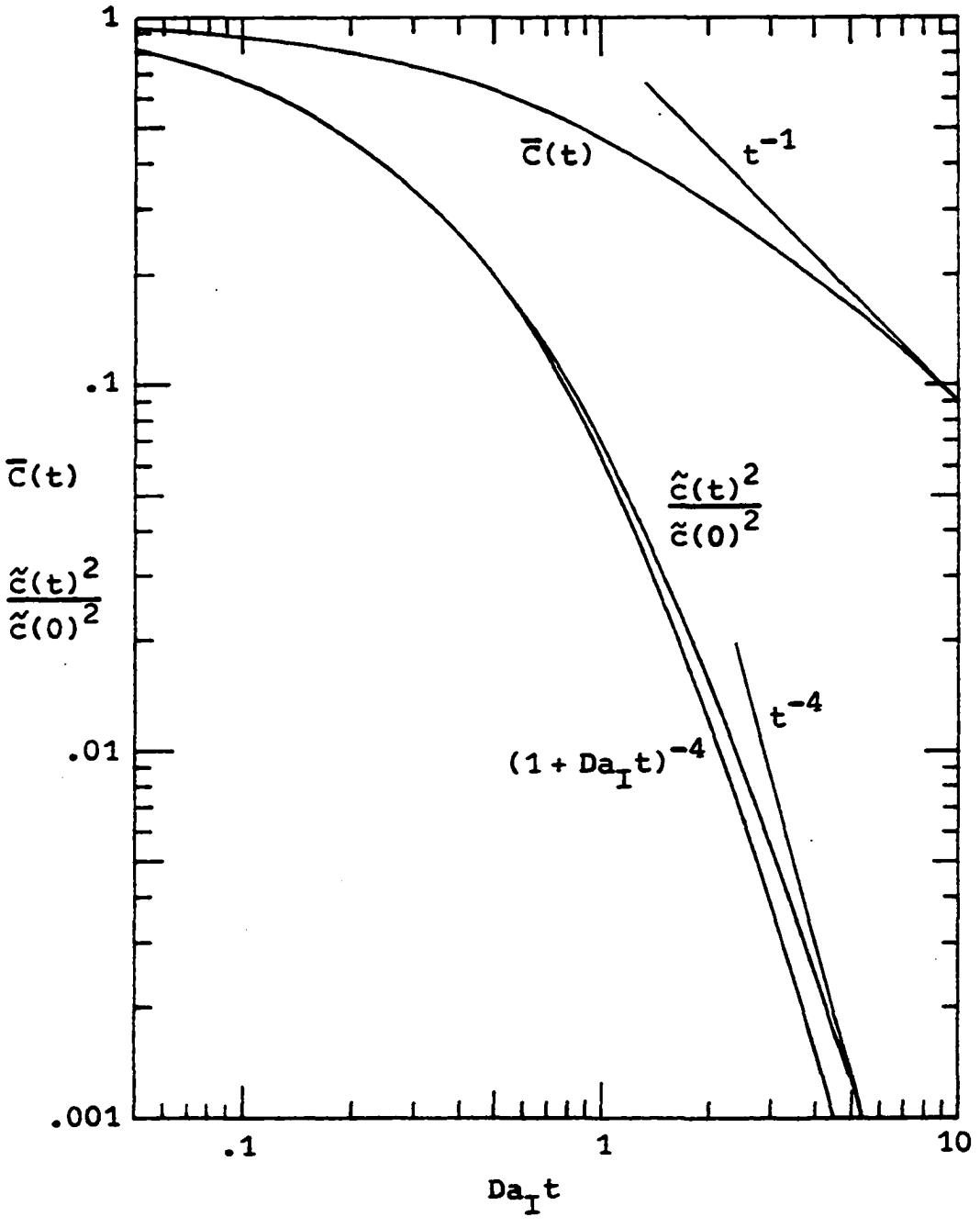

Figure 26. Decay of $\tilde{c}(t)^2$ and $\bar{C}(t)$ by a single component second-order reaction without convection or diffusion and comparison with Lee's approximate result and O'Brien's asymptotic limits

Table 22. Check of O'Brien's hypothesis of modal independence for $Da_I = 0.01$ and $Pe = 20$

t	$E_{ss}(\underset{\sim}{n},t)_d/E_{ss}(\underset{\sim}{n},0)_d$				correction factor
	mix	rxn	ind	actual	
$\underset{\sim}{n} = (0, 1)$, $n^2 = 1$					
0	1.0000	1.0000	1.0000	1.0000	1.0000
0.989	0.6281	0.9529	0.5985	0.6016	1.0053
1.979	0.01486	0.9086	0.01350	0.01372	1.0159
2.968	0.1064	0.8670	0.09222	0.09568	1.0376
3.958	0.06101	0.8278	0.05050	0.05250	1.0396
4.947	0.006139	0.7908	0.004855	0.004990	1.0279
5.936	0.005464	0.7561	0.004131	0.004358	1.0547
6.926	0.000624	0.7232	0.000451	0.000484	1.0725
7.915	0.008818	0.6922	0.006104	0.006524	1.0688
8.905	0.002989	0.6629	0.001981	0.002121	1.0706
$\underset{\sim}{n} = (2, 0)$, $n^2 = 4$					
0	1.0000	1.0000	1.0000	1.0000	1.0000
0.989	0.2054	0.9602	0.1972	0.1970	0.9991
1.979	0.04827	0.9224	0.04452	0.04510	1.0129
2.968	0.01170	0.8866	0.01037	0.01059	1.0204
3.958	0.08426	0.8527	0.07184	0.07243	1.0082
4.947	0.01784	0.8204	0.01464	0.01492	1.0190
5.936	0.01956	0.7897	0.01544	0.01562	1.0116
6.926	0.04110	0.7606	0.03126	0.03154	1.0091
7.915	0.003116	0.7328	0.002284	0.002293	1.0039
8.905	0.002765	0.7064	0.001954	0.001990	1.0188
$\underset{\sim}{n} = (-2, 2)$, $n^2 = 8$					
0	1.0000	1.0000	1.0000	1.0000	1.0000
0.989	0.8854	0.9952	0.8457	0.8620	1.0193
1.979	4.7293	0.9130	4.3176	4.3534	1.0083
2.968	0.9963	0.8732	0.8699	0.8824	1.0143
3.958	0.2029	0.8357	0.1696	0.1739	1.0254
4.947	0.1777	0.8002	0.1422	0.1475	1.0371
5.936	0.03963	0.7668	0.03039	0.03169	1.0427
6.926	0.02384	0.7351	0.01753	0.01826	1.0420
7.915	0.05206	0.7052	0.03671	0.03826	1.0420
8.905	0.002460	0.6768	0.001665	0.001812	1.0880

Table 23. Check of O'Brien's hypothesis of modal independence for $Da_I = 0.1$ and $Pe = 20$

t	$E_{ss}(\underset{\sim}{n},t)_d/E_{ss}(\underset{\sim}{n},0)_d$				correction factor
	mix	rxn	ind	actual	
$\underset{\sim}{n} = (1, -1)$, $n^2 = 2$					
0	1.0000	1.0000	1.0000	1.0000	1.0000
0.495	0.4304	0.8123	0.3496	0.3465	0.9913
0.989	0.03079	0.6684	0.02058	0.01815	0.8819
1.484	0.2896	0.5564	0.1611	0.1622	1.0066
1.979	0.5868	0.4678	0.2745	0.2676	0.9747
2.475	0.2228	0.3968	0.08842	0.08435	0.9540
2.968	0.06769	0.3392	0.02296	0.02320	1.0106
$\underset{\sim}{n} = (2, -1)$, $n^2 = 5$					
0	1.0000	1.0000	1.0000	1.0000	1.0000
0.495	3.9983	0.7814	3.1243	3.2953	1.0547
0.989	2.2344	0.6194	1.3840	1.4867	1.0742
1.484	1.4080	0.4974	0.7003	0.8198	1.1706
1.979	0.2864	0.4039	0.1157	0.1237	1.0691
2.475	0.8491	0.3314	0.2814	0.3603	1.2802
2.968	0.6487	0.2745	0.1781	0.2349	1.3190
$\underset{\sim}{n} = (2, 2)$, $n^2 = 8$					
0	1.0000	1.0000	1.0000	1.0000	1.0000
0.495	0.2576	0.8338	0.2147	0.2337	1.0881
0.989	0.6925	0.7061	0.4890	0.4513	0.9231
1.484	0.2561	0.6057	0.1551	0.1118	0.7205
1.979	1.4102	0.5251	0.7404	0.6905	0.9326
2.475	1.6084	0.4593	0.7388	0.5624	0.7613
2.968	0.05308	0.4049	0.02149	0.01711	0.7962

Table 24. Check of O'Brien's hypothesis of modal independence for $Da_I = 0.1$ and $Pe = 20$ using the velocity field with interaction

t	$E_{ss}(\underset{\sim}{n},t)_d/E_{ss}(\underset{\sim}{n},0)_d$				correction factor
	mix	rxn	ind	actual	
$\underset{\sim}{n} = (1, -1)$, $n^2 = 2$					
0	1.0000	1.0000	1.0000	1.0000	1.0000
0.495	0.2657	0.8123	0.2158	0.2232	1.0342
0.989	0.06885	0.6684	0.04602	0.04219	0.9167
1.484	0.4582	0.5564	0.2549	0.2449	0.9607
1.979	0.7002	0.4678	0.3276	0.3245	0.9908
2.475	0.4913	0.3968	0.1950	0.1978	1.0144
2.968	0.2428	0.3392	0.08238	0.08532	1.0357
3.463	0.1295	0.2921	0.03782	0.04051	1.0708
3.958	0.08788	0.2532	0.02225	0.02399	1.0783
$\underset{\sim}{n} = (2, -1)$, $n^2 = 5$					
0	1.0000	1.0000	1.0000	1.0000	1.0000
0.495	0.9253	0.7814	0.7230	0.7533	1.0419
0.989	0.3049	0.6194	0.1889	0.01892	0.1002
1.484	0.4504	0.4973	0.2240	0.2842	1.2690
1.979	0.4442	0.4039	0.1794	0.2516	1.4022
2.475	0.3193	0.3314	0.1058	0.1562	1.4761
2.968	0.2599	0.2745	0.07136	0.1029	1.4420
3.463	0.2808	0.2294	0.06440	0.08729	1.3556
3.958	0.2047	0.1931	0.03953	0.05230	1.3232
$\underset{\sim}{n} = (2, 2)$, $n^2 = 8$					
0	1.0000	1.0000	1.0000	1.0000	1.0000
0.495	0.1674	0.8338	0.1396	0.1326	0.9505
0.989	2.1491	0.7061	1.5174	1.4277	0.9409
1.484	2.9667	0.6057	1.7968	1.6308	0.9076
1.979	1.6987	0.5251	0.8919	0.7900	0.8857
2.475	1.5043	0.4593	0.6910	0.5904	0.8545
2.968	0.8773	0.4049	0.3552	0.3001	0.8449
3.463	0.2413	0.3592	0.08668	0.07782	0.8977
3.958	0.2302	0.3205	0.07379	0.05844	0.7920

Table 25. Check of O'Brien's hypothesis of modal independence for $Da_I = 1.0$ and $Pe = 20$

t	$E_{ss}(\underset{\sim}{n},t)_d/E_{ss}(\underset{\sim}{n},0)_d$				correction factor
	mix	rxn	ind	actual	
$\underset{\sim}{n} = (1, -1)$, $n^2 = 2$					
0	1.0000	1.0000	1.0000	1.0000	1.0000
0.495	0.4304	0.1935	0.08326	0.07704	0.9252
0.989	0.03079	0.06452	0.001987	0.001483	0.7466
1.484	0.2896	0.02792	0.008087	0.008445	1.0443
1.979	0.5868	0.01413	0.008292	0.006790	0.8189
2.475	0.2228	0.007944	0.001770	0.001254	0.7083
$\underset{\sim}{n} = (2, -1)$, $n^2 = 5$					
0	1.0000	1.0000	1.0000	1.0000	1.0000
0.495	3.9983	0.1398	0.5590	0.8326	1.4895
0.989	2.2344	0.03808	0.08509	0.1268	1.4896
1.484	1.4080	0.01461	0.02058	0.04298	2.0883
1.979	0.2864	0.006897	0.001975	0.002034	1.0298
2.475	0.8491	0.003727	0.003165	0.007631	2.4111
$\underset{\sim}{n} = (2, 2)$, $n^2 = 8$					
0	1.0000	1.0000	1.0000	1.0000	1.0000
0.495	0.2576	0.2589	0.06668	0.09911	1.4862
0.989	0.6925	0.1077	0.07460	0.04640	0.6220
1.484	0.2561	0.05406	0.01384	0.001709	0.1235
1.979	1.4102	0.03033	0.04278	0.02240	0.5237
2.475	1.6084	0.01839	0.02958	0.01140	0.3854

pure reaction decay.

O'Brien's hypothesis of modal independence for single component second-order reactions can be written in the form

$$\frac{E_{ss}(\underset{\sim}{n},t)_{ind}}{E_{ss}(\underset{\sim}{n},0)} = \frac{E_{ss}(\underset{\sim}{n},t)_{mix}}{E_{ss}(\underset{\sim}{n},0)} \cdot \frac{E_{ss}(\underset{\sim}{n},t)_{rxn}}{E_{ss}(\underset{\sim}{n},0)} \qquad (935)$$

This is tested for selected modes of different scales using the random convection velocity and Pe = 20 for Da_I = 0.01, 0.1, and 1.0 in Tables 22, 23, and 25, respectively, and using the convected velocity field with interaction for Pe = 20 and Da_I = 0.1 in Table 24. For Da_I = 0.01, the hypothesis agrees reasonably well with the actual results but the percentage deviation is significantly larger than that found for the hypothesis applied to fluctuation intensities. For the larger Damköhler numbers, Da_I = 0.1 and 1.0, the error in using the hypothesis approaches being substantial.

Test of Toor's Statistical Independence Hypothesis

Toor's statistical independence hypothesis for two-species second-order reactions states that for nonpremixed stoichiometric reactants with equal diffusivities, $\overline{c_A c_B}(t)$ is independent of the rate of reaction and equal to the pure mixing result. Hence, the procedure for testing Toor's hypothesis is quite simple: for given stoichiometry and

Peclet numbers, $\overline{c_A c_B}(t)$ obtained for pure mixing is compared to results obtained for different Damköhler numbers using the same initial concentration fields and the same velocity field. Of course in this study it was not possible to simulate complete species segregation. Therefore, the nonpremixed reactants requirement was relaxed to include premixed reactants with a correlation coefficient of -1, which corresponds to the concentration fluctuations of species A and B being completely out of phase.

Calculations were made using the random convection velocity for the following cases:

Table number	Da_I	Pe_A	Pe_B	$\bar{c}_B(0)$	$\overline{c_A c_B}(0)$
26	0.1	∞	∞	1.0	-0.2
27	0.1	100	100	1.0	-0.2
28	0.1	20	20	1.0	-0.2
29	0.1	20	20	2.0	-0.4
30	0.1	20	20	4.0	-0.8
31	1.0	20	20	1.0	-0.2
33	1.0	20	20	2.0	-0.4
34	1.0	20	5	1.0	-0.2
36	1.0	5	5	1.0	-0.2
37	1.0	5	5	2.0	-0.4
38	10.0	20	20	1.0	-0.2
39	10.0	20	20	1.0	-0.1

In addition, results using the convected velocity field with interaction for $Da_I = 1.0$, $Pe_A = Pe_B = 20$, and $\bar{c}_B(0) = 1.0$ are given in Table 32. The correction factor on Toor's

hypothesis is defined by

$$\text{correction factor} = \overline{c_A c_B}(t)_{Da_I \neq 0} / \overline{c_A c_B}(t)_{Da_I = 0} \qquad (936)$$

Correction factors for stoichiometric reactants and $Pe_A = Pe_B = 20$ are compared for the different Damköhler numbers in Table 41. Correction factors showing the effects of stoichiometry and Peclet number are compared in Table 42 for $Da_I = 0.1$ and Table 43 for $Da_I = 1.0$.

The inability to accurately portray species segregation placed a restriction on the conditions that could be investigated in this study. In particular, very fast reactions or moderately fast reactions with large Peclet numbers could not be used because the reaction drives the system towards segregation and produces regions of negative physical-space concentrations. Because of this, the results reported for $Da_I = 10.0$ are not strictly valid.

For stoichiometric reactants with equal Peclet numbers, Toor's hypothesis was found to behave in a stable manner throughout the course of the reaction. In all cases, after dropping off from one during the initial part of the reaction, the correction factor passes through a minimum and approaches one asymptotically as the reaction nears completion. The maximum deviations are less than 1 percent for $Da_I = 0.1$, 3 - 4 percent for $Da_I = 1.0$, and 19 percent for $Da_I = 10.0$. However, the increase in deviation of Toor's

Table 26. Check of Toor's independence hypothesis for $Da_I = 0.1$, $Pe_A = Pe_B = \infty$, $\bar{c}_B(0) = 1.0$, $\tilde{c}_A(0)^2 = \tilde{c}_B(0)^2 = 0.2$, and $\overline{c_A c_B}(0) = -0.2$

t	$\bar{c}_A, \bar{c}_B$	$\tilde{c}_A^2/\tilde{c}_{A0}^2$	$\tilde{c}_B^2/\tilde{c}_{B0}^2$
0	1.00000	1.00000	1.00000
0.2968	0.97694	1.00622	0.99387
0.5936	0.95518	1.00957	0.99108
0.8965	0.93461	1.01400	0.98782
1.1873	0.91516	1.02117	0.98179
1.4841	0.89672	1.03195	0.97229
1.7809	0.87924	1.04093	0.96445
2.0778	0.86265	1.04464	0.96153
2.3746	0.84688	1.04753	0.95911
2.6714	0.83189	1.04489	0.96214
2.9682	0.81761	1.04101	0.96699
3.2651	0.80401	1.03298	0.97611
3.5619	0.79104	1.02414	0.98616
3.8587	0.77865	1.02200	0.98954
4.1555	0.76683	1.02020	0.99215
4.4523	0.75553	1.01455	0.99815
4.7492	0.74472	1.00596	1.00727
5.0460	0.73438	0.99484	1.01898
5.3428	0.72448	0.98742	1.02693
5.6396	0.71500	0.98727	1.02732
5.9365	0.70591	0.99045	1.02358
6.2333	0.69719	0.98459	1.02846
6.5301	0.68884	0.97730	1.03563
6.8269	0.68081	0.97630	1.03715
7.1237	0.67310	0.97538	1.03858
7.4206	0.66569	0.96677	1.04738
7.7174	0.65857	0.95567	1.06013

$\overline{c_A c_B}/\tilde{c}_A\tilde{c}_B$	$\overline{c_A c_B}/\bar{c}_A\bar{c}_B$	$\overline{c_A c_B}(t)/\overline{c_A c_B}(0)$		correction factor
		$Da_I = 0$	$Da_I \neq 0$	
-1.00000	-0.20000	1.00000	1.00000	1.0000
-0.99977	-0.20951	1.00000	0.99980	0.9998
-0.99926	-0.21911	1.00000	0.99954	0.9995
-0.99838	-0.22878	1.00000	0.99920	0.9992
-0.99721	-0.23844	1.00000	0.99850	0.9985
-0.99606	-0.24816	1.00000	0.99773	0.9977
-0.99527	-0.25799	1.00000	0.99722	0.9972
-0.99465	-0.26791	1.00000	0.99687	0.9969
-0.99413	-0.27787	1.00000	0.99646	0.9965
-0.99346	-0.28788	1.00000	0.99610	0.9961
-0.99237	-0.29789	1.00000	0.99566	0.9957
-0.99098	-0.30787	1.00000	0.99509	0.9951
-0.98936	-0.31779	1.00000	0.99428	0.9943
-0.98786	-0.32770	1.00000	0.99343	0.9934
-0.98691	-0.33771	1.00000	0.99291	0.9929
-0.98666	-0.34788	1.00000	0.99289	0.9929
-0.98629	-0.35802	1.00000	0.99282	0.9928
-0.98593	-0.36812	1.00000	0.99267	0.9927
-0.98560	-0.37818	1.00000	0.99248	0.9925
-0.98532	-0.38821	1.00000	0.99232	0.9923
-0.98577	-0.39837	1.00000	0.99255	0.9925
-0.98688	-0.40861	1.00000	0.99308	0.9931
-0.98704	-0.41855	1.00000	0.99300	0.9930
-0.98646	-0.42832	1.00000	0.99263	0.9926
-0.98598	-0.43807	1.00000	0.99237	0.9924
-0.98614	-0.44785	1.00000	0.99232	0.9923
-0.98523	-0.45730	1.00000	0.99168	0.9917

Table 27. Check of Toor's independence hypothesis for $Da_I = 0.1$, $Pe_A = Pe_B = 100$, $\bar{C}_B(0) = 1.0$, $\tilde{c}_A(0)^2 = \tilde{c}_B(0)^2 = 0.2$, and $\overline{c_A c_B}(0) = -0.2$

t	$\bar{C}_A, \bar{C}_B$	$\tilde{c}_A^2/\tilde{c}_{A0}^2$	$\tilde{c}_B^2/\tilde{c}_{B0}^2$
0	1.00000	1.00000	1.00000
0.2968	0.97686	0.97837	0.96636
0.5936	0.95486	0.95517	0.93729
0.8905	0.93393	0.93289	0.90812
1.1873	0.91396	0.90919	0.87412
1.4841	0.89486	0.88084	0.83168
1.7809	0.87651	0.84181	0.78308
2.0778	0.85883	0.79477	0.73514
2.3746	0.84175	0.74878	0.68962
2.6714	0.82525	0.70627	0.65395
2.9682	0.80933	0.66827	0.62334
3.2651	0.79397	0.63180	0.59847
3.5619	0.77915	0.59740	0.57687
3.8587	0.76484	0.56798	0.55269
4.1555	0.75101	0.54233	0.52987
4.4523	0.73765	0.51813	0.51017
4.7492	0.72475	0.49478	0.49307
5.0460	0.71227	0.47112	0.47740
5.3428	0.70020	0.44997	0.46183

$\overline{c_A c_B}/\tilde{c}_A \tilde{c}_B$	$\overline{c_A c_B}/\bar{c}_A \bar{c}_B$	$\overline{c_A c_B}(t)/\overline{c_A c_B}(0)$		correction factor
		$Da_I = 0$	$Da_I \neq 0$	
-1.00000	-0.20000	1.00000	1.00000	1.0000
-0.99978	-0.20375	0.97225	0.97213	0.9999
-0.99929	-0.20740	0.94587	0.94551	0.9996
-0.99848	-0.21073	0.91977	0.91903	0.9992
-0.99746	-0.21290	0.89044	0.88922	0.9986
-0.99648	-0.21302	0.85456	0.85289	0.9980
-0.99578	-0.21047	0.81047	0.80848	0.9975
-0.99522	-0.20627	0.76284	0.76072	0.9972
-0.99476	-0.20178	0.71701	0.71483	0.9970
-0.99421	-0.19842	0.67789	0.67567	0.9967
-0.99337	-0.19576	0.64347	0.64113	0.9964
-0.99246	-0.19362	0.61271	0.61027	0.9960
-0.99153	-0.19176	0.58461	0.58207	0.9957
-0.99081	-0.18980	0.55773	0.55513	0.9953
-0.99056	-0.18830	0.53355	0.53100	0.9952
-0.99065	-0.18721	0.51174	0.50933	0.9953
-0.99071	-0.18632	0.49163	0.48933	0.9953
-0.99075	-0.18523	0.47206	0.46986	0.9953
-0.99075	-0.18424	0.45378	0.45165	0.9953

Table 27. (Continued)

t	$\bar{c}_A, \bar{c}_B$	$\tilde{c}_A^2/\tilde{c}_{A0}^2$	$\tilde{c}_B^2/\tilde{c}_{B0}^2$
5.6396	0.68852	0.43161	0.44505
5.9365	0.67721	0.41349	0.42632
6.2333	0.66623	0.39183	0.40721
6.5301	0.65555	0.36996	0.38807
6.8269	0.64518	0.35256	0.37096
7.1237	0.63510	0.33797	0.35644
7.4206	0.62531	0.32246	0.34238
7.7174	0.61580	0.30710	0.32919
8.0142	0.60655	0.29361	0.31698
8.3110	0.59755	0.28124	0.30581
8.6079	0.58879	0.26849	0.29551
8.9047	0.58027	0.25458	0.28442
9.2015	0.57196	0.24063	0.27191
9.4983	0.56385	0.22782	0.26034
9.7952	0.55594	0.21672	0.25051

$\overline{c_A c_B}/\tilde{c}_A\tilde{c}_B$	$\overline{c_A c_B}/\bar{c}_A\bar{c}_B$	$\overline{c_A c_B}(t)/\overline{c_A c_B}(0)$		correction factor
		$Da_I = 0$	$Da_I \neq 0$	
-0.99075	-0.18319	0.43628	0.43423	0.9953
-0.99110	-0.18147	0.41801	0.41612	0.9955
-0.99176	-0.17850	0.39784	0.39615	0.9957
-0.99195	-0.17492	0.37743	0.37585	0.9958
-0.99192	-0.17236	0.36024	0.35872	0.9958
-0.99204	-0.17073	0.34577	0.34432	0.9958
-0.99232	-0.16865	0.33107	0.32972	0.9959
-0.99212	-0.16637	0.31680	0.31545	0.9957
-0.99154	-0.16444	0.30389	0.30249	0.9954
-0.99076	-0.16275	0.29204	0.29056	0.9949
-0.98989	-0.16086	0.28042	0.27883	0.9943
-0.98899	-0.15807	0.26781	0.26613	0.9937
-0.98828	-0.15455	0.25453	0.25279	0.9932
-0.98789	-0.15135	0.24234	0.24059	0.9928
-0.98767	-0.14892	0.23187	0.23013	0.9925

Table 28. Check of Toor's independence hypothesis for $Da_I = 0.1$, $Pe_A = Pe_B = 20$, $\bar{c}_B(0) = 1.0$, $\tilde{c}_A(0)^2 = \tilde{c}_B(0)^2 = 0.2$, and $\overline{c_A c_B}(0) = -0.2$

t	$\bar{c}_A, \bar{c}_B$	$\tilde{c}_A^2/\tilde{c}_{A0}^2$	$\tilde{c}_B^2/\tilde{c}_{B0}^2$
0	1.00000	1.00000	1.00000
0.2968	0.97655	0.87767	0.86690
0.5936	0.95376	0.77643	0.76074
0.8905	0.93168	0.68983	0.66986
1.1873	0.91028	0.60519	0.58191
1.4841	0.88948	0.51087	0.48561
1.7809	0.86917	0.40498	0.38144
2.0778	0.84930	0.30787	0.28918
2.3746	0.82991	0.23217	0.21782
2.6714	0.81110	0.18019	0.17007
2.9682	0.79293	0.14082	0.13389
3.2651	0.77540	0.11085	0.10660
3.5619	0.75852	0.088664	0.086640
3.8587	0.74227	0.071461	0.070569
4.1555	0.72664	0.058450	0.057981
4.4523	0.71161	0.049309	0.048971
4.7492	0.69716	0.042630	0.042335
5.0460	0.68325	0.036775	0.036540
5.3428	0.66987	0.031866	0.031716

$\overline{c_A c_B}/\tilde{c}_A \tilde{c}_B$	$\overline{c_A c_B}/\bar{c}_A \bar{c}_B$	$\overline{c_A c_B}(t)/\overline{c_A c_B}(0)$		correction factor
		$Da_I = 0$	$Da_I \neq 0$	
-1.00000	-0.20000	1.00000	1.00000	1.0000
-0.99980	-0.18290	0.87219	0.87209	0.9999
-0.99938	-0.16887	0.76833	0.76807	0.9997
-0.99880	-0.15644	0.67940	0.67896	0.9993
-0.99818	-0.14298	0.59295	0.59235	0.9990
-0.99757	-0.12560	0.49755	0.49687	0.9986
-0.99702	-0.10374	0.39254	0.39186	0.9983
-0.99647	-0.08244	0.29793	0.29733	0.9980
-0.99600	-0.06504	0.22449	0.22398	0.9977
-0.99560	-0.05298	0.17471	0.17429	0.9976
-0.99522	-0.04347	0.13701	0.13666	0.9975
-0.99507	-0.03598	0.10845	0.10817	0.9974
-0.99524	-0.03032	0.087441	0.087229	0.9976
-0.99557	-0.02566	0.070857	0.070699	0.9978
-0.99603	-0.02196	0.058100	0.057984	0.9980
-0.99655	-0.01934	0.049055	0.048970	0.9983
-0.99714	-0.01743	0.042422	0.042361	0.9986
-0.99765	-0.01567	0.036614	0.036571	0.9988
-0.99802	-0.01414	0.031759	0.031728	0.9990

Table 28. (Continued)

t	$\bar{c}_A, \bar{c}_B$	$\tilde{c}_A^2/\tilde{c}_{A0}^2$	$\tilde{c}_B^2/\tilde{c}_{B0}^2$
5.6396	0.65698	0.027405	0.027361
5.9365	0.64456	0.022818	0.022863
6.2333	0.63258	0.018415	0.018534
6.5301	0.62102	0.014642	0.014801
6.8269	0.60985	0.011802	0.011964
7.1237	0.59907	0.0097161	0.0098654
7.4206	0.58866	0.0079379	0.0080651
7.7174	0.57859	0.0064267	0.0065304
8.0142	0.56886	0.0052848	0.0053714
8.3110	0.55944	0.0044963	0.0045688
8.6079	0.55033	0.0038562	0.0039135
8.9047	0.54150	0.0032226	0.0032629
9.2015	0.53295	0.0026434	0.0026675
9.4983	0.52467	0.0021846	0.0021992
9.7952	0.51663	0.0018399	0.0018514

$\overline{c_A c_B}/\tilde{c}_A\tilde{c}_B$	$\overline{c_A c_B}/\bar{c}_A\bar{c}_B$	$\overline{c_A c_B}(t)/\overline{c_A c_B}(0)$		correction factor
		$Da_I = 0$	$Da_I \neq 0$	
-0.99826	-0.01267	0.027359	0.027335	0.9991
-0.99836	-0.01098	0.022822	0.022803	0.9992
-0.99835	-0.009218	0.018459	0.018444	0.9992
-0.99834	-0.007622	0.014709	0.014697	0.9992
-0.99832	-0.006379	0.011873	0.011863	0.9992
-0.99846	-0.005448	0.0097830	0.0097754	0.9992
-0.99857	-0.004611	0.0079956	0.0079898	0.9993
-0.99861	-0.003865	0.0064739	0.0064693	0.9993
-0.99862	-0.003288	0.0053243	0.0053206	0.9993
-0.99876	-0.002892	0.0045295	0.0045264	0.9993
-0.99875	-0.002562	0.0038824	0.0038799	0.9994
-0.99880	-0.002209	0.0032408	0.0032388	0.9994
-0.99887	-0.001868	0.0026540	0.0026524	0.9994
-0.99896	-0.001591	0.0021907	0.0021896	0.9995
-0.99908	-0.001382	0.0018448	0.0018439	0.9995

Table 29. Check of Toor's independence hypothesis for $Da_I = 0.1$, $Pe_A = Pe_B = 20$, $\bar{c}_B(0) = 2.0$, $\tilde{c}_A(0)^2 = 0.2$, $\tilde{c}_B(0)^2 = 0.8$, and $\overline{c_A c_B}(0) = -0.4$

t	$\bar{c}_A$	$\bar{c}_B$	$\tilde{c}_A^2/\tilde{c}_{A0}^2$	$\tilde{c}_B^2/\tilde{c}_{B0}^2$	$\tilde{c}_A/\tilde{c}_B$
0	1.00000	2.00000	1.00000	1.00000	1.00000
0.2968	0.95379	1.95379	0.88200	0.86747	1.00834
0.5936	0.91011	1.91011	0.78109	0.76266	1.01201
0.8905	0.86885	1.86885	0.69358	0.67349	1.01481
1.1873	0.82982	1.82982	0.60734	0.58728	1.01694
1.4841	0.79272	1.79272	0.51120	0.49240	1.01891
1.7809	0.75720	1.75720	0.40285	0.38896	1.01770
2.0778	0.72307	1.72307	0.30292	0.29678	1.01029
2.3746	0.69034	1.69034	0.22543	0.22514	1.00064
2.6714	0.65914	1.65914	0.17191	0.17706	0.98535
2.9682	0.62952	1.62952	0.13185	0.14042	0.96900
3.2651	0.60143	1.60143	0.10152	0.11263	0.94940
3.5619	0.57484	1.57484	0.079151	0.092234	0.92637
3.8587	0.54968	1.54968	0.062294	0.075713	0.90706
4.1555	0.52587	1.52587	0.049855	0.062725	0.89153
4.4523	0.50334	1.50334	0.041175	0.053444	0.87774
4.7492	0.48203	1.48203	0.034838	0.046627	0.86439
5.0460	0.46186	1.46186	0.029379	0.040623	0.85042
5.3428	0.44274	1.44274	0.024862	0.035591	0.83579
5.6396	0.42462	1.42462	0.020862	0.030988	0.82050
5.9365	0.40741	1.40741	0.016942	0.026130	0.80522
6.2333	0.39106	1.39106	0.013323	0.021373	0.78953
6.5301	0.37550	1.37550	0.010316	0.017224	0.77391
6.8269	0.36070	1.36070	0.0080971	0.014051	0.75912
7.1237	0.34660	1.34660	0.0064936	0.011695	0.74515
7.4206	0.33318	1.33318	0.0051718	0.0096488	0.73212

$\overline{c_A c_B}/\tilde{c}_A\tilde{c}_B$	$\overline{c_A c_B}/\bar{c}_A\bar{c}_B$	$\overline{c_A c_B}(t)/\overline{c_A c_B}(0)$		correction factor
		$Da_I = 0$	$Da_I \neq 0$	
-1.00000	-0.20000	1.00000	1.00000	1.0000
-0.99955	-0.18769	0.87219	0.87441	1.0025
-0.99870	-0.17736	0.76833	0.77081	1.0032
-0.99753	-0.16794	0.67940	0.68177	1.0034
-0.99632	-0.15675	0.59295	0.59503	1.0035
-0.99519	-0.14053	0.49755	0.49930	1.0035
-0.99418	-0.11831	0.39254	0.39354	1.0025
-0.99328	-0.095617	0.29793	0.29782	0.9996
-0.99255	-0.076648	0.22449	0.22360	0.9960
-0.99192	-0.063297	0.17471	0.17306	0.9905
-0.99131	-0.052596	0.13701	0.13488	0.9844
-0.99118	-0.044018	0.10845	0.10599	0.9773
-0.99153	-0.037433	0.087440	0.084719	0.9688
-0.99220	-0.031998	0.070857	0.068141	0.9617
-0.99313	-0.027684	0.058100	0.055536	0.9559
-0.99416	-0.024653	0.049055	0.046636	0.9507
-0.99525	-0.022460	0.042422	0.040112	0.9455
-0.99616	-0.020388	0.036614	0.034414	0.9399
-0.99681	-0.018568	0.031759	0.029652	0.9337
-0.99719	-0.016766	0.027359	0.025355	0.9267
-0.99733	-0.014638	0.022822	0.020984	0.9195
-0.99732	-0.012374	0.018459	0.016829	0.9117
-0.99729	-0.010295	0.014709	0.013293	0.9038
-0.99735	-0.0086701	0.011873	0.010638	0.8960
-0.99757	-0.0074503	0.0097830	0.0086934	0.8886
-0.99778	-0.0063472	0.0079957	0.0070485	0.8815

Table 30. Check of Toor's independence hypothesis for $Da_I = 0.1$, $Pe_A = Pe_B = 20$, $\bar{c}_B(0) = 4.0$, $\tilde{c}_A(0)^2 = 0.2$, $\tilde{c}_B(0)^2 = 3.2$, and $\overline{c_A c_B}(0) = -0.8$

t	$\bar{c}_A$	$\bar{c}_B$	$\tilde{c}_A^2/\tilde{c}_{A0}^2$	$\tilde{c}_B^2/\tilde{c}_{B0}^2$	$\tilde{c}_A/\tilde{c}_B$
0	1.00000	4.00000	1.00000	1.00000	1.00000
0.2968	0.91022	3.91022	0.88852	0.86854	1.01144
0.5936	0.82991	3.82991	0.78124	0.76612	1.00982
0.8965	0.75779	3.75779	0.68448	0.67974	1.00348
1.1873	0.69267	3.69267	0.58817	0.59616	0.99328
1.4841	0.63342	3.63342	0.48364	0.50320	0.98037
1.7809	0.57888	3.57888	0.36918	0.40048	0.96013
2.0778	0.52833	3.52833	0.26559	0.30797	0.92865
2.3746	0.48159	3.48159	0.18790	0.23548	0.89328
2.6714	0.43864	3.43864	0.13504	0.18652	0.85088
2.9682	0.39938	3.39938	0.097355	0.14887	0.80868
3.2651	0.36357	3.36357	0.069906	0.12009	0.76296
3.5619	0.33098	3.33098	0.050428	0.098798	0.71443
3.8587	0.30133	3.30133	0.036808	0.081472	0.67215
4.1555	0.27440	3.27440	0.027388	0.067821	0.63547
4.4523	0.24994	3.24994	0.021026	0.058068	0.60174
4.7492	0.22775	3.22775	0.016508	0.050895	0.56952
5.0460	0.20759	3.20759	0.012883	0.044520	0.53794
5.3428	0.18928	3.18928	0.010066	0.039134	0.05717
5.6396	0.17264	3.17264	0.0077824	0.034156	0.047733
5.9365	0.15748	3.15748	0.0058165	0.028853	0.44899
6.2333	0.14368	3.14368	0.0042012	0.023626	0.42169
6.5301	0.13110	3.13110	0.0029820	0.019049	0.39566
6.8269	0.11964	3.11964	0.0021437	0.015546	0.37134
7.1237	0.10919	3.10919	0.0015747	0.012942	0.34882
7.4206	0.099666	3.099666	0.0011508	0.010677	0.32830

$\overline{c_A c_B}/\tilde{c}_A\tilde{c}_B$	$\overline{c_A c_B}/\bar{c}_A\bar{c}_B$	$\overline{c_A c_B}(t)/\overline{c_A c_B}(0)$		correction factor
		$Da_I = 0$	$Da_I \neq 0$	
-1.00000	-0.20000	1.00000	1.00000	1.0000
-0.99884	-0.19723	0.87219	0.87745	1.0060
-0.99676	-0.19409	0.76833	0.77113	1.0036
-0.99410	-0.19050	0.67940	0.67809	0.9981
-0.99151	-0.18364	0.59295	0.58713	0.9902
-0.98919	-0.16963	0.49755	0.48799	0.9808
-0.98716	-0.14657	0.39254	0.37958	0.9670
-0.98559	-0.12097	0.29793	0.28187	0.9461
-0.98439	-0.098800	0.22449	0.20707	0.9224
-0.98325	-0.082766	0.17471	0.15605	0.8932
-0.98215	-0.069672	0.13701	0.11824	0.8630
-0.98194	-0.058857	0.10845	0.089971	0.8296
-0.98255	-0.050325	0.087440	0.069353	0.7931
-0.98396	-0.043331	0.070857	0.053883	0.7604
-0.98602	-0.037838	0.058100	0.042496	0.7314
-0.98833	-0.034011	0.049055	0.034534	0.7040
-0.99064	-0.031250	0.042422	0.028715	0.6769
-0.99246	-0.028556	0.036614	0.023769	0.6492
-0.99372	-0.026137	0.031759	0.019723	0.6210
-0.99441	-0.023681	0.027359	0.016213	0.5926
-0.99460	-0.020729	0.022822	0.012885	0.5646
-0.99452	-0.017549	0.018459	0.0099082	0.5368
-0.99444	-0.014607	0.014709	0.0074951	0.5096
-0.99457	-0.012307	0.011873	0.0057416	0.4836
-0.99505	-0.010585	0.0097830	0.0044920	0.4592
-0.99548	-0.0090358	0.0079957	0.0034893	0.4364

Table 31. Check of Toor's independence hypothesis for $Da_I = 1.0$, $Pe_A = Pe_B = 20$, $\bar{c}_B(0) = 1.0$, $\tilde{c}_A(0)^2 = \tilde{c}_B(0)^2 = 0.2$, and $\overline{c_A c_B}(0) = -0.2$

t	$\bar{c}_A, \bar{c}_B$	$\tilde{c}_A^2/\tilde{c}_{A0}^2$	$\tilde{c}_B^2/\tilde{c}_{B0}^2$
0	1.00000	1.00000	1.00000
0.2968	0.81420	0.92055	0.83624
0.5936	0.69471	0.83123	0.72934
0.8905	0.61096	0.75507	0.63798
1.1873	0.54825	0.67818	0.54768
1.4841	0.49841	0.58652	0.44836
1.7809	0.45619	0.46847	0.35029
2.0778	0.41895	0.34985	0.27116
2.3746	0.38570	0.25866	0.20829
2.6714	0.35620	0.19538	0.16753
2.9682	0.33014	0.14995	0.13443
3.2651	0.30702	0.11428	0.11019
3.5619	0.28650	0.087599	0.093047
3.8587	0.26821	0.069333	0.076631
4.1555	0.25186	0.056794	0.062278
4.4523	0.23722	0.048145	0.051879
4.7492	0.22410	0.041727	0.044447
5.0460	0.21229	0.035880	0.038370
5.3428	0.20158	0.030904	0.033454

$\overline{c_A c_B}/\tilde{c}_A \tilde{c}_B$	$\overline{c_A c_B}/\bar{c}_A \bar{c}_B$	$\overline{c_A c_B}(t)/\overline{c_A c_B}(0)$		correction factor
		$Da_I = 0$	$Da_I \neq 0$	
-1.00000	-0.20000	1.00000	1.00000	1.0000
-0.98701	-0.26126	0.87219	0.86598	0.9929
-0.97142	-0.31344	0.76833	0.75637	0.9844
-0.95421	-0.35485	0.67940	0.66228	0.9748
-0.94015	-0.38125	0.59295	0.57297	0.9663
-0.93148	-0.38458	0.49755	0.47767	0.9600
-0.92744	-0.36106	0.39254	0.37570	0.9571
-0.92644	-0.32514	0.29793	0.28535	0.9578
-0.92845	-0.28972	0.22449	0.21550	0.9600
-0.92838	-0.26476	0.17471	0.16796	0.9614
-0.92845	-0.24190	0.13701	0.13182	0.9621
-0.93264	-0.22206	0.10845	0.10466	0.9650
-0.93660	-0.20603	0.087441	0.084558	0.9670
-0.94295	-0.19109	0.070857	0.068732	0.9700
-0.95277	-0.17866	0.058100	0.056664	0.9753
-0.96240	-0.17094	0.049055	0.048098	0.9805
-0.96959	-0.16629	0.042422	0.041756	0.9843
-0.97305	-0.16023	0.036614	0.036104	0.9861
-0.97471	-0.15425	0.031759	0.031340	0.9868

Table 31. (Continued)

t	$\bar{c}_A, \bar{c}_B$	$\tilde{c}_A^2/\tilde{c}_{A0}^2$	$\tilde{c}_B^2/\tilde{c}_{B0}^2$
5.6396	0.19184	0.026402	0.029017
5.9365	0.18289	0.021869	0.024353
6.2333	0.17462	0.017493	0.019906
6.5301	0.16693	0.013722	0.016101
6.8269	0.15979	0.010921	0.013159
7.1237	0.15315	0.0089515	0.010873
7.4206	0.14699	0.0073144	0.0088000
7.7174	0.14125	0.0060667	0.0070189
8.0142	0.13590	0.0050626	0.0056908
8.3110	0.13091	0.0043550	0.0047849
8.6079	0.12625	0.0037598	0.0040695
8.9047	0.12189	0.0031589	0.0033752
9.2015	0.11780	0.0026073	0.0027429
9.4983	0.11396	0.0021625	0.0022523
9.7952	0.11034	0.0018158	0.0018991

$\overline{c_A c_B}/\tilde{c}_A\tilde{c}_B$	$\overline{c_A c_B}/\bar{c}_A\bar{c}_B$	$\overline{c_A c_B}(t)/\overline{c_A c_B}(0)$		correction factor
		$Da_I = 0$	$Da_I \neq 0$	
-0.97578	-0.14678	0.027359	0.027009	0.9872
-0.97640	-0.13473	0.022822	0.022533	0.9873
-0.97639	-0.11951	0.018459	0.018220	0.9870
-0.97598	-0.10412	0.014709	0.014507	0.9863
-0.97643	-0.09169	0.011873	0.011705	0.9859
-0.97854	-0.08232	0.0097830	0.0096539	0.9868
-0.98062	-0.07314	0.0079956	0.0079019	0.9883
-0.98155	-0.06421	0.0064739	0.0064051	0.9894
-0.98219	-0.05709	0.0053243	0.0052720	0.9902
-0.98336	-0.05239	0.0045295	0.0044890	0.9911
-0.98429	-0.04831	0.0038824	0.0038501	0.9917
-0.98448	-0.4327	0.0032408	0.0032146	0.9919
-0.98449	-0.03794	0.0026540	0.0026328	0.9920
-0.98510	-0.03348	0.0021907	0.0021741	0.9924
-0.98663	-0.03009	0.0018448	0.0018321	0.9931

Table 32. Check of Toor's independence hypothesis using convected velocity field with interaction for $Da_I = 1.0$, $Pe_A = Pe_B = 20$, $\bar{c}_B(0) = 1.0$, $\tilde{c}_A(0)^2 = \tilde{c}_B(0)^2 = 0.2$, and $\overline{c_A c_B}(0) = -0.2$

t	$\bar{c}_A, \bar{c}_B$	$\tilde{c}_A^2/\tilde{c}_{A0}^2$	$\tilde{c}_B^2/\tilde{c}_{B0}^2$
0	1.00000	1.00000	1.00000
0.2968	0.81407	0.92318	0.81662
0.5936	0.69333	0.80598	0.67341
0.8905	0.60672	0.66698	0.54779
1.1873	0.54000	0.54240	0.42410
1.4841	0.48612	0.43592	0.32513
1.7809	0.44150	0.34520	0.26249
2.0778	0.40408	0.27624	0.21749
2.3746	0.37218	0.22492	0.18004
2.6714	0.34452	0.17841	0.15261
2.9682	0.32020	0.13913	0.12873
3.2651	0.29857	0.10966	0.10561
3.5619	0.27924	0.087792	0.085946
3.8587	0.26193	0.070760	0.070594
4.1555	0.24635	0.056315	0.058523
4.4523	0.23227	0.044680	0.048991
4.7492	0.21952	0.036098	0.041226
5.0460	0.20795	0.029492	0.034357
5.3428	0.19739	0.023651	0.027605

$\overline{c_A c_B}/\tilde{c}_A \tilde{c}_B$	$\overline{c_A c_B}/\bar{c}_A \bar{c}_B$	$\overline{c_A c_B}(t)/\overline{c_A c_B}(0)$		correction factor
		$Da_I = 0$	$Da_I \neq 0$	
-1.00000	-0.20000	1.00000	1.00000	1.0000
-0.98619	-0.25842	0.86309	0.85628	0.9921
-0.96751	-0.29655	0.72624	0.71278	0.9815
-0.95288	-0.31293	0.59167	0.57597	0.9735
-0.95048	0.32166	0.46956	0.45586	0.9708
-0.93525	-0.30373	0.36970	0.35887	0.9707
-0.95922	-0.29626	0.29630	0.28874	0.9745
-0.96581	-0.28997	0.24180	0.23673	0.9790
-0.96420	-0.28014	0.19825	0.19403	0.9787
-0.95611	-0.26583	0.16164	0.15776	0.9760
-0.94933	-0.24783	0.13049	0.12705	0.9736
-0.94470	-0.22808	0.10465	0.10166	0.9714
-0.94362	-0.21024	0.084418	0.081967	0.9710
-0.94476	-0.19466	0.068725	0.066773	0.9716
-0.94537	-0.17885	0.055846	0.054272	0.9718
-0.94525	-0.16394	0.045530	0.044224	0.9713
-0.94692	-0.15160	0.037596	0.036529	0.9716
-0.95040	-0.13992	0.031089	0.030253	0.9731
-0.95390	-0.12512	0.025001	0.024374	0.9749

Table 32. (Continued)

t	$\bar{c}_A, \bar{c}_B$	$\tilde{c}_A^2/\tilde{c}_{A0}^2$	$\tilde{c}_B^2/\tilde{c}_{B0}^2$
5.6396	0.18767	0.018425	0.021423
5.9365	0.17872	0.014541	0.016752
6.2333	0.17048	0.011950	0.013681
6.5301	0.16291	0.010035	0.011539
6.8269	0.15594	0.0083694	0.0097351
7.1237	0.14950	0.0070007	0.0082630
7.4206	0.14354	0.0060622	0.0071822
7.7174	0.13803	0.0053824	0.0063486
8.0142	0.13290	0.0048078	0.0056676
8.3110	0.12814	0.0042439	0.0050003
8.6079	0.12368	0.0036137	0.0042293

$\overline{c_A c_B}/\tilde{c}_A \tilde{c}_B$	$\overline{c_A c_B}/\bar{c}_A \bar{c}_B$	$\overline{c_A c_B}(t)/\overline{c_A c_B}(0)$		correction factor
		$Da_I = 0$	$Da_I \neq 0$	
-0.95696	-0.10796	0.019468	0.019013	0.9766
-0.96118	-0.093936	0.015324	0.015001	0.9789
-0.96656	-0.085044	0.012587	0.012358	0.9818
-0.97222	-0.078838	0.010624	0.010462	0.9847
-0.97683	-0.072518	0.0089348	0.0088174	0.9868
-0.97986	-0.066686	0.0075432	0.0074524	0.9880
-0.98231	-0.062915	0.0065520	0.0064817	0.9893
-0.98397	-0.060384	0.0058087	0.0057519	0.9902
-0.98593	-0.058275	0.0051922	0.0051466	0.9912
-0.98788	-0.055434	0.0045865	0.0045508	0.9922
-0.98898	-0.050549	0.0038939	0.0038663	0.9929

Table 33. Check of Toor's independence hypothesis for $Da_I = 1.0$, $Pe_A = Pe_B = 20$, $\bar{c}_B(0) = 2.0$, $\tilde{c}_A(0)^2 = 0.2$, $\tilde{c}_B(0)^2 = 0.8$, and $\overline{c_A c_B}(0) = -0.4$

t	$\bar{c}_A$	$\bar{c}_B$	$\tilde{c}_A^2/\tilde{c}_{A0}^2$	$\tilde{c}_B^2/\tilde{c}_{B0}^2$	$\tilde{c}_A/\tilde{c}_B$
0	1.00000	2.00000	1.00000	1.00000	1.00000
0.2968	0.66947	1.66947	0.90342	0.87053	1.01872
0.5936	0.49509	1.49509	0.72939	0.81265	0.94739
0.8905	0.38831	1.38831	0.59069	0.75867	0.88238
1.1873	0.31575	1.31575	0.47426	0.69244	0.82759
1.4841	0.26202	1.26202	0.36727	0.60397	0.77980
1.7809	0.21793	1.21793	0.25411	0.50148	0.71184
2.0778	0.17936	1.17936	0.15384	0.40788	0.61414
2.3746	0.14564	1.14564	0.090128	0.32808	0.52413
2.6714	0.11704	1.11704	0.053292	0.27212	0.44254
2.9682	0.093417	1.093417	0.031812	0.22495	0.37606
3.2651	0.074047	1.074047	0.017988	0.18784	0.30945
3.5619	0.058281	1.058281	0.0098691	0.15918	0.24900
3.8587	0.045617	1.045617	0.0055800	0.13366	0.20432
4.1555	0.035586	1.035586	0.0032211	0.11258	0.16915
4.4523	0.027703	1.027703	0.0018912	0.097295	0.13942
4.7492	0.021544	1.021544	0.0011312	0.085878	0.11477
5.0460	0.016728	1.016728	0.00066711	0.075490	0.094006
5.3428	0.012960	1.012960	0.00038978	0.066527	0.076544
5.6396	0.010015	1.010015	0.00022259	0.058088	0.061903
5.9365	0.007712	1.007712	0.00011203	0.048999	0.047816
6.2333	0.005912	1.005912	0.00006365	0.040005	0.039890
6.5031	0.004510	1.004510	0.00003208	0.032127	0.031603
6.8269	0.003427	1.003427	0.00001622	0.026093	0.024939
7.1237	0.002595	1.002595	0.00000844	0.021603	0.019772
7.4206	0.001961	1.001961	0.00000449	0.017719	0.015922

$\overline{c_A c_B}/\tilde{c}_A\tilde{c}_B$	$\overline{c_A c_B}/\bar{c}_A\bar{c}_B$	$\overline{c_A c_B}(t)/\overline{c_A c_B}(0)$		correction factor
		$Da_I = 0$	$Da_I \neq 0$	
-1.00000	-0.20000	1.00000	1.00000	1.0000
-0.97657	-0.30995	0.87219	0.86604	0.9929
-0.95304	-0.39651	0.76833	0.73374	0.9550
-0.92962	-0.46174	0.67940	0.62231	0.9160
-0.91289	-0.50368	0.59295	0.52314	0.8823
-0.89962	-0.51252	0.49755	0.42370	0.8516
-0.89136	-0.47954	0.39254	0.31820	0.8106
-0.89422	-0.42358	0.29793	0.22399	0.7518
-0.89843	-0.37036	0.22449	0.15449	0.6882
-0.89399	-0.32936	0.17471	0.10766	0.6162
-0.89080	-0.29510	0.13701	0.075357	0.5500
-0.88878	-0.25985	0.10845	0.051664	0.4764
-0.88534	-0.22758	0.087441	0.035091	0.4013
-0.89249	-0.20440	0.070857	0.024374	0.3440
-0.91025	-0.18814	0.058100	0.017334	0.2983
-0.92931	-0.17711	0.049055	0.012606	0.2570
-0.94231	-0.16880	0.042422	0.0092875	0.2189
-0.94768	-0.15817	0.036614	0.0067252	0.1837
-0.94935	-0.14729	0.031759	0.0048343	0.1522
-0.94958	-0.13502	0.027359	0.0034145	0.1248
-0.94882	-0.11941	0.022822	0.0023202	0.1017
-0.94787	-0.10173	0.018459	0.0015126	0.08194
-0.94684	-0.084862	0.014709	0.00096133	0.06536
-0.94780	-0.071739	0.011873	0.00061676	0.05195
-0.95208	-0.062505	0.0097830	0.00040668	0.04157
-0.95659	-0.054919	0.0079956	0.00026988	0.03375

Table 34. Check of Toor's independence hypothesis for $Da_I = 1.0$, $Pe_A = 20$, $Pe_B = 5$, $\bar{c}_B(0) = 1.0$, $\tilde{c}_A(0)^2 = \tilde{c}_B(0)^2 = 0.2$, and $\overline{c_A c_B}(0) = -0.2$

t	$\bar{c}_A, \bar{c}_B$	$\tilde{c}_A^2/\tilde{c}_{A0}^2$	$\tilde{c}_B^2/\tilde{c}_{B0}^2$
0	1.00000	1.00000	1.00000
0.1319	0.90502		
0.2968	0.80999	0.88229	0.60296
0.4617	0.73394		
0.5936	0.68312	0.74577	0.42422
0.7256	0.63918		
0.8905	0.59193	0.63074	0.31733
1.0554	0.55131		
1.1873	0.52259	0.52544	0.23621
1.3192	0.49657		
1.4841	0.46704	0.41925	0.15869
1.6490	0.44014		
1.7809	0.42020	0.30885	0.093176
1.9129	0.40156		
2.0778	0.37994	0.21362	0.053853
2.2427	0.36008		
2.3746	0.34538	0.14532	0.032038
2.5065	0.33168		
2.6714	0.31584	0.10154	0.020541
2.8363	0.30131		

$\overline{c_A c_B}/\tilde{c}_A \tilde{c}_B$	$\overline{c_A c_B}/\bar{c}_A \bar{c}_B$	$\overline{c_A c_B}(t)/\overline{c_A c_B}(0)$		correction factor
		$Da_I = 0$	$Da_I \neq 0$	
-1.00000	-0.20000	1.00000	1.00000	1.0000
	-0.20876	0.85668	0.85494	0.9980
-0.98587	-0.21920	0.72177	0.71907	0.9962
	-0.22874	0.61757	0.61607	0.9976
-0.97279	-0.23451	0.54757	0.54717	0.9993
	-0.24001	0.48970	0.49029	1.0012
-0.95779	-0.24459	0.42640	0.42850	1.0049
	-0.24521	0.36903	0.37264	1.0098
-0.94185	-0.24300	0.32736	0.33181	1.0136
	-0.23596	0.28557	0.29092	1.0187
-0.92285	-0.21826	0.23122	0.23804	1.0295
	-0.19364	0.17892	0.18756	1.0483
-0.89817	-0.17258	0.14218	0.15236	1.0716
	-0.15241	0.11135	0.12288	1.1036
-0.87250	-0.12965	0.080921	0.093581	1.1564
	-0.11036	0.058407	0.071546	1.2250
-0.85703	-0.098046	0.045339	0.058478	1.2898
	-0.088521	0.035826	0.048690	1.3591
-0.85990	-0.078733	0.027140	0.039271	1.4470
	-0.069368	0.020467	0.031489	1.5385

Table 34. (Continued)

t	$\bar{c}_A, \bar{c}_B$	$\tilde{c}_A^2/\tilde{c}_{A0}^2$	$\tilde{c}_B^2/\tilde{c}_{B0}^2$
2.9682	0.29052	0.071973	0.013035
3.1001	0.28041		
3.2651	0.26866	0.051757	0.0088143
3.4300	0.25779		
3.5619	0.24968	0.037963	0.0063979
3.6938	0.24204		
3.8587	0.23309	0.028092	0.0046715
4.0236	0.22475		
4.1555	0.21848	0.021032	0.0033006
4.2874	0.21253		
4.4523	0.20552	0.016303	0.0024004
4.6172	0.19895		
4.7492	0.19399	0.013055	0.0018834
4.8811	0.18926		
5.0460	0.18366	0.010540	0.0015381
5.2109	0.17837		
5.3428	0.17435	0.0085810	0.0012445

$\overline{c_A c_B}/\tilde{c}_A \tilde{c}_B$	$\overline{c_A c_B}/\bar{c}_A \bar{c}_B$	$\overline{c_A c_B}(t)/\overline{c_A c_B}(0)$		correction factor
		$Da_I = 0$	$Da_I \neq 0$	
-0.85930	-0.062367	0.016282	0.026320	1.6165
	-0.056452	0.013090	0.022195	1.6955
-0.85745	-0.050749	0.010235	0.018314	1.7894
	-0.046267	0.0082042	0.015373	1.8738
-0.86226	-0.043114	0.0069642	0.013438	1.9296
	-0.040153	0.0059564	0.011761	1.9745
-0.86561	-0.036503	0.0048962	0.0099161	2.0253
	-0.032920	0.0039986	0.0083144	2.0793
-0.86871	-0.030327	0.0034101	0.0072379	2.1225
	-0.028205	0.0029535	0.0063700	2.1567
-0.88774	-0.026295	0.0025470	0.0055534	2.1804
	-0.024944	0.0022594	0.0049367	2.1850
-0.91176	-0.024029	0.0020823	0.0045211	2.1712
	-0.023173	0.0019428	0.0041500	2.1361
-0.92841	-0.022165	0.0018050	0.0037381	2.0710
	-0.021163	0.0016738	0.0033667	2.0114
-0.94251	-0.020264	0.0015512	0.0030800	1.9856

Table 35. Comparison of the ratio of the correlation coefficients for mixing with reaction and pure mixing with the correction factor on Toor's hypothesis for $Da_I = 1.0$, $Pe_A = 20$, $Pe_B = 5$, $\bar{c}_B(0) = 1.0$, $\tilde{c}_A(0)^2 = \tilde{c}_B(0)^2 = 0.2$, and $\overline{c_A c_B}(0) = -0.2$

t	$Da_I = 0$		
	$\tilde{c}_A^{\,2}/\tilde{c}_{A0}^{\,2}$	$\tilde{c}_B^{\,2}/\tilde{c}_{B0}^{\,2}$	$\overline{c_A c_B}/\overline{c_A c_B}\,0$
0	1.00000	1.00000	1.00000
0.2968	0.87219	0.60694	0.72177
0.5936	0.76833	0.40982	0.54757
0.8905	0.67940	0.29055	0.42640
1.1873	0.59295	0.20381	0.32736
1.4841	0.49755	0.12905	0.23122
1.7809	0.39254	0.070941	0.14218
2.0778	0.29793	0.038145	0.080921
2.3746	0.22449	0.021542	0.045339
2.6714	0.17471	0.013347	0.027140
2.9682	0.13701	0.0086528	0.016282
3.2651	0.10845	0.0058805	0.010235
3.5619	0.087440	0.0040858	0.0069620
3.8587	0.070857	0.0027830	0.0048962
4.1555	0.058100	0.0017915	0.0034101
4.4523	0.049055	0.0011028	0.0025470
4.7492	0.042422	0.00068844	0.0020823
5.0460	0.036614	0.00044363	0.0018050
5.3428	0.031759	0.00028369	0.0015512

$\gamma(Da_I) = \overline{c_A c_B}/\tilde{c}_A\tilde{c}_B$		$\frac{\gamma(1.0)}{\gamma(0)}$	correction factor
$Da_I = 0$	$Da_I = 1.0$		
-1.00000	-1.00000	1.00000	1.0000
-0.99202	-0.98587	0.99380	0.9962
-0.97582	-0.97279	0.99689	0.9993
-0.95972	-0.95779	0.99799	1.0049
-0.94169	-0.94185	1.00017	1.0136
-0.91248	-0.92285	1.01136	1.0295
-0.85201	-0.89817	1.05418	1.0716
-0.75908	-0.87250	1.14942	1.1564
-0.65197	-0.85703	1.31452	1.2898
-0.56204	-0.85990	1.52996	1.4470
-0.47288	-0.85930	1.81716	1.6165
-0.40530	-0.85745	2.1156	1.7894
-0.36845	-0.86226	2.3402	1.9296
-0.34867	-0.86561	2.4826	2.0253
-0.33425	-0.86871	2.5990	2.1225
-0.34628	-0.88774	2.5636	2.1804
-0.38532	-0.91176	2.3662	2.1712
-0.44787	-0.92841	2.0729	2.0710
-0.51677	-0.94251	1.8238	1.9856

Table 36. Check of Toor's independence hypothesis for $Da_I = 1.0$, $Pe_A = Pe_B = 5$, $\bar{c}_B(0) = 1.0$, $\tilde{c}_A(0)^2 = \tilde{c}_B(0)^2 = 0.2$, and $\overline{c_A c_B}(0) = -0.2$

t	$\bar{c}_A, \bar{c}_B$	$\tilde{c}_A^2/\tilde{c}_{A0}^2$	$\tilde{c}_B^2/\tilde{c}_{B0}^2$
0	1.00000	1.00000	1.00000
0.1319	0.90406		
0.2968	0.80646	0.64053	0.57996
0.4617	0.72749		
0.5936	0.67441	0.44715	0.38129
0.7256	0.62839		
0.8905	0.57881	0.32256	0.26707
1.0554	0.53621		
1.1873	0.50614	0.22708	0.18765
1.3192	0.47899		
1.4841	0.44839	0.14432	0.11918
1.6490	0.42083		
1.7809	0.40069	0.079496	0.065858
1.9129	0.38209		
2.0778	0.36081	0.042123	0.036014
2.2427	0.34153		
2.3746	0.32741	0.023403	0.020613
2.5065	0.31433		
2.6714	0.29931	0.014355	0.012825
2.8363	0.28559		

$\overline{c_A c_B}/\tilde{c}_A \tilde{c}_B$	$\overline{c_A c_B}/\bar{c}_A \bar{c}_B$	$\overline{c_A c_B}(t)/\overline{c_A c_B}(0)$		correction factor
		$Da_I = 0$	$Da_I \neq 0$	
-1.00000	-0.20000	1.00000	1.00000	1.0000
	-0.19167	0.78476	0.78330	0.9981
-0.99037	-0.18562	0.60694	0.60363	0.9945
	-0.18173	0.48504	0.48090	0.9915
-0.98189	-0.17828	0.40982	0.40543	0.9893
	-0.17558	0.35110	0.34666	0.9873
-0.97542	-0.17091	0.29055	0.28629	0.9853
	-0.16383	0.23943	0.23552	0.9837
-0.97010	-0.15634	0.20381	0.20025	0.9825
	-0.14524	0.16980	0.16662	0.9812
-0.96345	-0.12569	0.12905	0.12636	0.9791
	-0.10319	0.093547	0.091379	0.9768
-0.95644	-0.08628	0.070941	0.069205	0.9755
	-0.071669	0.053649	0.052315	0.9751
-0.95567	-0.057184	0.038145	0.037222	0.9758
	-0.046076	0.027502	0.026873	0.9771
-0.95962	-0.039323	0.021542	0.021077	0.9784
	-0.034210	0.017247	0.016900	0.9799
-0.96579	-0.029256	0.013347	0.013104	0.9818
	-0.025188	0.010443	0.010272	0.9836

Table 36. (Continued)

t	$\bar{c}_A, \bar{c}_B$	$\tilde{c}_A^2/\tilde{c}_{A0}^2$	$\tilde{c}_B^2/\tilde{c}_{B0}^2$
2.9682	0.27546	0.0092339	0.0083289
3.1001	0.26600		
3.2651	0.25503	0.0062000	0.0056918
3.4300	0.24490		
3.5619	0.23735	0.0042536	0.0039816
3.6938	0.23024		
3.8587	0.22192	0.0028702	0.0027288
4.0236	0.21416		
4.1555	0.20833	0.0018418	0.0017599

$\overline{c_A c_B}/\tilde{c}_A\tilde{c}_B$	$\overline{c_A c_B}/\bar{c}_A\bar{c}_B$	$\overline{c_A c_B}(t)/\overline{c_A c_B}(0)$		correction factor
		$Da_I = 0$	$Da_I \neq 0$	
-0.97200	-0.022468	0.0086528	0.0085242	0.9851
	-0.020209	0.0072458	0.0071498	0.9867
-0.97889	-0.017882	0.0058805	0.0058151	0.9889
	-0.015874	0.0048043	0.0047604	0.9909
-0.98507	-0.014392	0.0040858	0.0040539	0.9922
	-0.012972	0.0034617	0.0034382	0.9932
-0.98857	-0.011236	0.0027830	0.0027666	0.9941
	-0.0095283	0.0021970	0.0021850	0.9946
-0.98992	-0.0082131	0.0017915	0.0017822	0.9948

Table 37. Check of Toor's independence hypothesis for $Da_I = 1.0$, $Pe_A = Pe_B = 5$, $\bar{c}_B(0) = 2.0$, $\tilde{c}_A(0)^2 = 0.2$, $\tilde{c}_B(0)^2 = 0.8$, and $\overline{c_A c_B}(0) = -0.4$

t	$\bar{c}_A$	$\bar{c}_B$	$\tilde{c}_A^2/\tilde{c}_{A0}^2$	$\tilde{c}_B^2/\tilde{c}_{B0}^2$	$\tilde{c}_A/\tilde{c}_B$
0	1.00000	2.00000	1.00000	1.00000	1.00000
0.1319	0.81912	1.81912			
0.2968	0.65500	1.65500	0.62384	0.60566	1.01490
0.4617	0.53474	1.53474			
0.5936	0.45966	1.45966	0.38366	0.43169	0.94273
0.7256	0.39810	1.39810			
0.8905	0.33536	1.33536	0.23406	0.32906	0.84339
1.0554	0.28432	1.28432			
1.1873	0.24992	1.24992	0.13515	0.25008	0.73514
1.3192	0.22001	1.22001			
1.4841	0.18761	1.18761	0.069591	0.17068	0.63854
1.6490	0.15973	1.15973			
1.7809	0.14020	1.14020	0.030514	0.10066	0.55058
1.9129	0.12290	1.12290			
2.0778	0.10410	1.10410	0.012181	0.058201	0.45748
2.2427	0.088108	1.088108			
2.3746	0.077078	1.077078	0.0048986	0.035093	0.37362
2.5065	0.067430	1.067430			
2.6714	0.057063	1.057063	0.0021272	0.022967	0.30434
2.8363	0.048306	1.048306			

$\overline{c_A c_B}/\tilde{c}_A\tilde{c}_B$	$\overline{c_A c_B}/\bar{c}_A\bar{c}_B$	$\overline{c_A c_B}(t)/\overline{c_A c_B}(0)$		correction factor
		$Da_I = 0$	$Da_I \neq 0$	
-1.00000	-0.20000	1.00000	1.00000	1.0000
	-0.21178	0.78476	0.78894	1.0053
-0.98259	-0.22287	0.60694	0.60399	0.9951
	-0.23133	0.48504	0.47462	0.9785
-0.96939	-0.23519	0.40982	0.39450	0.9626
	-0.23817	0.35110	0.33140	0.9439
-0.95908	-0.23774	0.29055	0.26617	0.9161
	-0.23189	0.23943	0.21169	0.8842
-0.95029	-0.22371	0.20381	0.17470	0.8572
	-0.20981	0.16980	0.14078	0.8291
-0.93855	-0.18363	0.12905	0.10229	0.7926
	-0.15254	0.093547	0.070642	0.7551
-0.92606	-0.12843	0.070941	0.051325	0.7235
	-0.10722	0.053649	0.036991	0.6895
-0.92316	-0.085539	0.038145	0.024580	0.6444
	-0.068744	0.027502	0.016476	0.5991
-0.92688	-0.058553	0.021542	0.012153	0.5641
	-0.050824	0.017247	0.0091453	0.5302
-0.93453	-0.043317	0.013347	0.0065321	0.4894
	-0.037132	0.010443	0.0047009	0.4501

Table 37. (Continued)

t	$\bar{c}_A$	$\bar{c}_B$	$\tilde{c}_A^2/\tilde{c}_{A0}^2$	$\tilde{c}_B^2/\tilde{c}_{B0}^2$	$\tilde{c}_A/\tilde{c}_B$
2.9682	0.042287	1.042287	0.00094814	0.015602	0.24652
3.1001	0.037026	1.037026			
3.2651	0.031367	1.031367	0.00042782	0.011048	0.19678
3.4300	0.026580	1.026580			
3.5619	0.023286	1.023286	0.00019282	0.0079488	0.15575
3.6938	0.020401	1.020401			
3.8587	0.017294	1.017294	0.00008481	0.0055723	0.12337
4.0236	0.014660	1.014660			
4.1555	0.012845	1.012845	0.00003554	0.0036703	0.09840

$\overline{c_A c_B}/\tilde{c}_A \tilde{c}_B$	$\overline{c_A c_B}/\bar{c}_A \bar{c}_B$	$\overline{c_A c_B}(t)/\overline{c_A c_B}(0)$		correction factor
		$Da_I = 0$	$Da_I \neq 0$	
-0.94383	-0.032944	0.0086528	0.0036301	0.4195
	-0.029400	0.0072458	0.0028221	0.3895
-0.95510	-0.025674	0.0058805	0.0020764	0.3531
	-0.022442	0.0048043	0.0015309	0.3186
-0.96600	-0.020076	0.0040858	0.0011959	0.2927
	-0.017847	0.0034617	0.0092880	0.2683
-0.97219	-0.015195	0.0027830	0.00066833	0.2401
	-0.012684	0.0021970	0.00047170	0.2147
-0.97414	-0.010817	0.0017915	0.00035182	0.1964

Table 38. Check of Toor's independence hypothesis for $Da_I = 10.0$, $Pe_A = Pe_B = 20$, $\bar{c}_B(0) = 1.0$, $\tilde{c}_A(0)^2 = \tilde{c}_B(0)^2 = 0.2$, and $\overline{c_A c_B}(0) = -0.2$

t	$\bar{c}_A, \bar{c}_B$	$\tilde{c}_A^2/\tilde{c}_{A0}^2$	$\tilde{c}_B^2/\tilde{c}_{B0}^2$
0	1.00000	1.00000	1.00000
0.0660	0.68328		
0.1319	0.55535		
0.1979	0.48973		
0.2638	0.45149		
0.2968	0.43814	1.10137	0.83001
0.3298	0.42731		
0.3958	0.41076		
0.4617	0.39843		
0.5277	0.38852		
0.5936	0.37994	1.00200	0.75133
0.7256	0.36464		
0.7915	0.35762		
0.8905	0.34805	0.93182	0.66546
0.9894	0.33943		
1.1873	0.32322	0.85864	0.54796
1.4841	0.30014	0.72872	0.44155
1.7809	0.27344	0.54830	0.37061
2.0778	0.24574	0.37207	0.30502
2.3746	0.21918	0.26925	0.23893
2.6714	0.19288	0.20535	0.20467
2.9682	0.17130	0.15388	0.16392
3.2651	0.15410	0.10529	0.14495

$\overline{c_A c_B}/\tilde{c}_A\tilde{c}_B$	$\overline{c_A c_B}/\bar{c}_A\bar{c}_B$	$\overline{c_A c_B}(t)/\overline{c_A c_B}(0)$		correction factor
		$Da_I = 0$	$Da_I \neq 0$	
-1.00000	-0.20000	1.00000	1.00000	1.0000
	-0.40336	0.96851	0.94159	0.9722
	-0.57066	0.93875	0.88001	0.9374
	-0.69261	0.91089	0.83056	0.9118
	-0.77884	0.88469	0.79382	0.8973
-0.81443	-0.81127	0.87219	0.77869	0.8928
	-0.83740	0.86000	0.76452	0.8890
	-0.87395	0.83621	0.73728	0.8817
	-0.89599	0.81293	0.71119	0.8748
	-0.90855	0.79018	0.68571	0.8678
-0.76066	-0.91441	0.76833	0.65999	0.8590
	-0.91747	0.72788	0.60995	0.8380
	-0.91968	0.70855	0.58810	0.8300
-0.71135	-0.92485	0.67940	0.56016	0.8245
	-0.92688	0.65008	0.53394	0.8213
-0.70357	-0.92389	0.59295	0.48260	0.8139
-0.72274	-0.91022	0.49755	0.40997	0.8240
-0.72236	-0.87100	0.39254	0.32562	0.8295
-0.76379	-0.85220	0.29793	0.25731	0.8637
-0.76836	-0.81134	0.22449	0.19488	0.8681
-0.70441	-0.77636	0.17471	0.14441	0.8266
-0.72482	-0.78463	0.13701	0.11511	0.8402
-0.74287	-0.77296	0.10845	0.091773	0.8462

Table 39. Check of Toor's independence hypothesis for $Da_I = 10.0$, $Pe_A = Pe_B = 20$, $\bar{c}_B(0) = 1.0$, $\tilde{c}_A(0)^2 = \tilde{c}_B(0)^2 = 0.1$, and $\overline{c_A c_B}(0) = -0.1$

t	$\bar{c}_A, \bar{c}_B$	$\tilde{c}_A^2/\tilde{c}_{A0}^2$	$\tilde{c}_B^2/\tilde{c}_{B0}^2$
0	1.00000	1.00000	1.00000
0.0660	0.64257		
0.1319	0.49523		
0.1979	0.41772		
0.2638	0.37140		
0.2968	0.35489	1.05254	0.81775
0.3298	0.34139		
0.3958	0.32070		
0.4617	0.30561		
0.5277	0.29404		
0.5936	0.28471	0.97000	0.73992
0.7256	0.26993		
0.7915	0.26374		
0.8905	0.25553	0.90914	0.65741
0.9894	0.24829		
1.1873	0.23541	0.83812	0.54795
1.4841	0.21798	0.71883	0.43892
1.7809	0.19934	0.54599	0.36178
2.0778	0.17983	0.37488	0.29858
2.3746	0.16113	0.26866	0.23365
2.6714	0.14342	0.20274	0.19769
2.9682	0.12817	0.15344	0.15866
3.2651	0.11552	0.10729	0.13858
3.5619	0.10455	0.077034	0.12283
3.8587	0.095214	0.062961	0.096250

$\overline{c_A c_B}/\tilde{c}_A\tilde{c}_B$	$\overline{c_A c_B}/\bar{c}_A\bar{c}_B$	$\overline{c_A c_B}(t)/\overline{c_A c_B}(0)$		correction factor
		$Da_I = 0$	$Da_I \neq 0$	
-1.00000	-0.10000	1.00000	1.00000	1.0000
	-0.23116	0.96851	0.95445	0.9855
	-0.36930	0.93875	0.90571	0.9648
	-0.49406	0.91089	0.86208	0.9464
	-0.59839	0.88469	0.82541	0.9330
-0.87225	-0.64250	0.87219	0.80923	0.9278
	-0.68115	0.86000	0.79386	0.9231
	-0.74314	0.83621	0.76431	0.9140
	-0.78805	0.81293	0.73602	0.9054
	-0.81964	0.79018	0.70866	0.8968
-0.80466	-0.84098	0.76833	0.68170	0.8872
	-0.86445	0.72788	0.62986	0.8653
	-0.87194	0.70855	0.60651	0.8560
-0.74444	-0.88142	0.67940	0.57552	0.8471
	-0.88709	0.65008	0.54687	0.8412
-0.72729	-0.88937	0.59295	0.49287	0.8312
-0.74103	-0.87601	0.49755	0.41624	0.8366
-0.74520	-0.83348	0.39254	0.33119	0.8437
-0.77450	-0.80127	0.29793	0.25912	0.8697
-0.78957	-0.76193	0.22449	0.19782	0.8812
-0.74528	-0.72539	0.17471	0.14920	0.8540
-0.75601	-0.71801	0.13701	0.11796	0.8610
-0.77055	-0.70408	0.10845	0.093958	0.8664
-0.77051	-0.68563	0.087441	0.074950	0.8571
-0.79783	-0.68509	0.070857	0.062108	0.8765

Table 40. Growth of two species correlation and segregation by reaction from zero values initially for $Da_I = 0.5$, $Pe_A = Pe_B = 50$, $\bar{c}_B(0) = 1.0$, $\tilde{c}_A(0)^2 = \tilde{c}_B(0)^2 = 0.2$, and $\overline{c_A c_B}(0) = 0$

t	$\bar{c}_A, \bar{c}_B$	$\tilde{c}_A^2$	$\tilde{c}_B^2$	$\overline{c_A c_B}(t)$	δ	β
0	1.00000	0.20000	0.20000	0	0	0
0.297	0.87393	0.14876	0.14849	-0.041123	-0.2767	-0.0538
0.594	0.78042	0.12286	0.12092	-0.059173	-0.4855	-0.0972
0.890	0.70789	0.10790	0.10344	-0.066370	-0.6282	-0.1324
1.187	0.64968	0.09608	0.09194	-0.067923	-0.7227	-0.1609
1.484	0.60165	0.08641	0.08141	-0.065733	-0.7837	-0.1816
1.781	0.56102	0.07790	0.07136	-0.061531	-0.8253	-0.1955
2.078	0.52600	0.06896	0.06293	-0.056504	-0.8577	-0.2042
2.375	0.49533	0.06093	0.05539	-0.051383	-0.8845	-0.2094
2.671	0.46820	0.05523	0.04846	-0.047027	-0.9090	-0.2145
2.968	0.44408	0.05160	0.04311	-0.043832	-0.9293	-0.2223
3.265	0.42255	0.04921	0.03915	-0.041380	-0.9428	-0.2318
3.562	0.40324	0.04739	0.03617	-0.039313	-0.9495	-0.2418
3.859	0.38584	0.04603	0.03351	-0.037283	-0.9494	-0.2504
4.156	0.37003	0.04466	0.03077	-0.035144	-0.9480	-0.2567
4.452	0.35557	0.04319	0.02840	-0.033179	-0.9472	-0.2624
4.749	0.34230	0.04179	0.02643	-0.031460	-0.9467	-0.2685
5.046	0.33008	0.04012	0.02469	-0.029791	-0.9465	-0.2734
5.343	0.31876	0.03811	0.02309	-0.028132	-0.9483	-0.2769
5.640	0.30823	0.03537	0.02157	-0.026299	-0.9520	-0.2768
5.936	0.29832	0.03202	0.01988	-0.024113	-0.9558	-0.2709
6.233	0.28893	0.02852	0.01796	-0.021688	-0.9582	-0.2598
6.530	0.27997	0.02522	0.01618	-0.019371	-0.9590	-0.2471
6.827	0.27142	0.02240	0.01482	-0.017472	-0.9591	-0.2372
7.124	0.26329	0.02011	0.01375	-0.015951	-0.9592	-0.2301

Table 41. Summary of correction factors on Toor's hypothesis - effect of Damköhler number for $Pe_A = Pe_B = 20$ and $\bar{C}_B(0) = 1.0$

t	Da_I				
	0.1	1.0	1.0[a]	10.0	10.0[b]
0	1.0000	1.0000	1.0000	1.0000	1.0000
0.2968	0.9999	0.9929	0.9921	0.8928	0.9278
0.5936	0.9997	0.9844	0.9815	0.8590	0.8872
0.8905	0.9993	0.9748	0.9735	0.8245	0.8471
1.1873	0.9990	0.9663	0.9708	0.8139	0.8312
1.4841	0.9986	0.9600	0.9707	0.8240	0.8366
1.7809	0.9983	0.9571	0.9745	0.8295	0.8437
2.0778	0.9980	0.9578	0.9790	0.8637	0.8697
2.3746	0.9977	0.9600	0.9787	0.8681	0.8812
2.6714	0.9976	0.9614	0.9760	0.8266	0.8540
2.9682	0.9975	0.9621	0.9736	0.8402	0.8610
3.2651	0.9974	0.9650	0.9715	0.8462	0.8664
3.5619	0.9976	0.9670	0.9710		0.8571
3.8587	0.9978	0.9700	0.9716		0.8765
4.1555	0.9980	0.9753	0.9718		
4.4523	0.9983	0.9805	0.9713		
4.7492	0.9986	0.9843	0.9716		
5.0460	0.9988	0.9861	0.9731		

[a] using convected velocity field with interaction.

[b] $\overline{c_A c_B}(0) = -0.1$, $\tilde{c}_A(0)^2 = \tilde{c}_B(0)^2 = 0.1$.

Table 41. (Continued)

t	Da_I				
	0.1	1.0	1.0[a]	10.0	10.0
5.3428	0.9990	0.9868	0.9749		
5.6396	0.9991	0.9872	0.9766		
5.9365	0.9992	0.9873	0.9790		
6.2333	0.9992	0.9870	0.9818		
6.5301	0.9992	0.9863	0.9847		
6.8269	0.9992	0.9859	0.9869		
7.1237	0.9992	0.9868	0.9880		
7.4206	0.9993	0.9883	0.9893		
7.7174	0.9993	0.9894	0.9902		
8.0142	0.9993	0.9902	0.9912		
8.3110	0.9993	0.9911	0.9922		
8.6079	0.9994	0.9917	0.9929		
8.9047	0.9994	0.9919			
9.2015	0.9994	0.9920			
9.4983	0.9995	0.9924			
9.7952	0.9995	0.9931			

[a]using convected velocity field with interaction.

Table 42. Summary of correction factors on Toor's hypothesis - effect of Peclet number and stoichiometry for $Da_I = 0.1$

	$Pe_A = Pe_B$				
	100		20		
t	$\bar{C}_{B0} = 1$	$\bar{C}_{B0} = 1$	$\bar{C}_{B0} = 1$	$\bar{C}_{B0} = 2$	$\bar{C}_{B0} = 4$
0	1.0000	1.0000	1.0000	1.0000	1.0000
0.2968	0.9998	0.9999	0.9999	1.0026	1.0060
0.5936	0.9995	0.9996	0.9997	1.0032	1.0036
0.8905	0.9992	0.9992	0.9993	1.0035	0.9981
1.1873	0.9985	0.9986	0.9990	1.0035	0.9902
1.4841	0.9977	0.9981	0.9986	1.0035	0.9808
1.7809	0.9972	0.9975	0.9983	1.0025	0.9670
2.0778	0.9969	0.9972	0.9980	0.9996	0.9461
2.3746	0.9965	0.9970	0.9977	0.9960	0.9224
2.6714	0.9961	0.9967	0.9976	0.9905	0.8932
2.9682	0.9957	0.9964	0.9975	0.9845	0.8630
3.2651	0.9951	0.9960	0.9974	0.9773	0.8296
3.5619	0.9943	0.9957	0.9976	0.9689	0.7932
3.8587	0.9934	0.9953	0.9978	0.9617	0.7604
4.1555	0.9929	0.9952	0.9980	0.9559	0.7314
4.4523	0.9929	0.9953	0.9983	0.9507	0.7040
4.7492	0.9928	0.9953	0.9986	0.9456	0.6769
5.0460	0.9927	0.9953	0.9988	0.9399	0.6492

Table 42. (Continued)

	$Pe_A = Pe_B$				
		100		20	
t	$\bar{C}_{B0} = 1$	$\bar{C}_{B0} = 1$	$\bar{C}_{B0} = 1$	$\bar{C}_{B0} = 2$	$\bar{C}_{B0} = 4$
5.3428	0.9925	0.9953	0.9990	0.9337	0.6210
5.6396	0.9923	0.9953	0.9991	0.9267	0.5926
5.9365	0.9926	0.9955	0.9992	0.9195	0.5646
6.2333	0.9931	0.9958	0.9992	0.9117	0.5368
6.5301	0.9930	0.9958	0.9992	0.9038	0.5096
6.8269	0.9926	0.9958	0.9992	0.8960	0.4836
7.1237	0.9924	0.9958	0.9992	0.8886	0.4592
7.4206	0.9923	0.9959	0.9993	0.8815	0.4364
7.7174	0.9917	0.9957	0.9993		
8.0142		0.9954	0.9993		
8.3110		0.9949	0.9993		
8.6079		0.9943	0.9994		
8.9047		0.9937	0.9994		
9.2015		0.9932	0.9994		
9.4983		0.9928	0.9995		
9.7952		0.9925	0.9995		

Table 43. Summary of correction factors on Toor's hypothesis - effect of Peclet number and stoichiometry for $Da_I = 1.0$

	$Pe_A = Pe_B = 20$		$Pe_A = 20$ $Pe_B = 5$	$Pe_A = Pe_B = 5$	
t	$\bar{C}_{B0} = 2$	$\bar{C}_{B0} = 1$	$\bar{C}_{B0} = 1$	$\bar{C}_{B0} = 1$	$\bar{C}_{B0} = 2$
0	1.0000	1.0000	1.0000	1.0000	1.0000
0.1319			0.9980	0.9981	1.0053
0.2968	0.9930	0.9929	0.9963	0.9945	0.9951
0.4617			0.9976	0.9915	0.9785
0.5936	0.9550	0.9844	0.9993	0.9893	0.9626
0.7256			1.0012	0.9874	0.9439
0.8905	0.9160	0.9748	1.0049	0.9853	0.9161
1.0554			1.0098	0.9837	0.8842
1.1873	0.8823	0.9663	1.0136	0.9826	0.8572
1.3192			1.0187	0.9812	0.8281
1.4841	0.8516	0.9600	1.0295	0.9791	0.7926
1.6490			1.0483	0.9768	0.7552
1.7809	0.8106	0.9571	1.0716	0.9755	0.7235
1.9129			1.1036	0.9751	0.6895
2.0778	0.7518	0.9578	1.1565	0.9758	0.6444
2.2427			1.2250	0.9771	0.5991
2.3746	0.6882	0.9600	1.2898	0.9784	0.5641
2.5065			1.3591	0.9799	0.5303
2.6714	0.6162	0.9614	1.4470	0.9818	0.4894
2.8363			1.5385	0.9836	0.4502

Table 43. (Continued)

t	$Pe_A = Pe_B = 20$		$Pe_A = 20$, $Pe_B = 5$	$Pe_A = Pe_B = 5$	
	$\bar{C}_{B0} = 2$	$\bar{C}_{B0} = 1$	$\bar{C}_{B0} = 1$	$\bar{C}_{B0} = 1$	$\bar{C}_{B0} = 2$
2.9682	0.5500	0.9621	1.6165	0.9851	0.4195
3.1001			1.6955	0.9867	0.3895
3.2651	0.4764	0.9650	1.7894	0.9889	0.3531
3.4300			1.8738	0.9909	0.3187
3.5619	0.4013	0.9670	1.9296	0.9922	0.2927
3.6938			1.9745	0.9932	0.2683
3.8587	0.3440	0.9700	2.0252	0.9941	0.2402
4.0236			2.0793	0.9946	0.2147
4.1555	0.2984	0.9753	2.1225	0.9948	0.1964
4.2874			2.1568		
4.4523	0.2570	0.9805	2.1804		
4.6172			2.1850		
4.7492	0.2189	0.9843	2.1712		
4.8811			2.1361		
5.0460	0.1837	0.9861	2.0710		
5.2109			2.0114		
5.3428	0.1522	0.9868	1.9856		

hypothesis with Damköhler number may be due to poorer simulation of the increasingly segregated states. The results for $Da_I = 1.0$ using the convected velocity field with interaction are similar to the results using the random convection velocity field. It is interesting to note that there is a strong correlation between the deviation of the correction factor from one and the deviation of the correlation coefficient from -1.

Using unequal Peclet numbers of $Pe_A = 20$ and $Pe_B = 5$ with stoichiometric reactants resulted in poorer results than for the equal diffusivity case. After dropping slightly below one initially, the correction factor increases fairly quickly to about 2 and then begins to decrease during the last part of the reaction. For this case of nonequal diffusivities, there is a strong correlation between the deviation of the correction factor from one and the deviation of the ratio of the correlation coefficient with reaction to the pure mixing correlation coefficient, as shown in Table 35. Of course for equal diffusivities the pure mixing correlation coefficient remains at the initial value of -1.

For nonstoichiometric reactants with equal Peclet numbers, Toor's hypothesis quickly breaks down as the Damköhler number increases from being small, as shown in Tables 42 and 43. For nonstoichiometric reactants the deviation of the correction factor is strongly correlated with the ratio

$\tilde{c}_A/\tilde{c}_B$, where A is the limiting reactant.

In this study, the initial concentration fluctuations of A and B were totally out of phase and the species were partially segregated, with $\gamma(0) = -1.0$ and $P(0) = -0.2$. In order to verify the growth of species correlation and segregation as caused by reaction, calculations were made for an initially uncorrelated system having $\overline{c_A c_B}(0) = \gamma(0) = P(0) = 0$ for $Da_I = 0.5$ and $Pe_A = Pe_B = 50$. The results are given in Table 40 and Figure 27. For this system, the correlation coefficient quickly increases in magnitude from zero and approaches -1.0 asymptotically. The species become partially segregated but the growth of segregation is halted in the later stages of reaction when mixing effects become more important as the rate of reaction decreases. For reaction without diffusion growth of segregation is unchecked, as shown in Table 26 for $Da_I = 0.1$ and $Pe_A = Pe_B = \infty$. In Figure 27, since $\overline{c_A c_B}(0) = 0$, initially the rate of conversion is the same as that for a uniform system. However, the rate of conversion is soon retarded by the growth of species segregation.

Further examples of mean field decays with and without concentration fluctuations and growth and decay of segregation for some of the test cases of Toor's hypothesis are shown in Figures 28 - 30. In Figure 28, with $Da_I = 0.1$ and $Pe_A = Pe_B = 100$, growth of segregation by reaction and decay of segregation by mixing are approximately balanced since

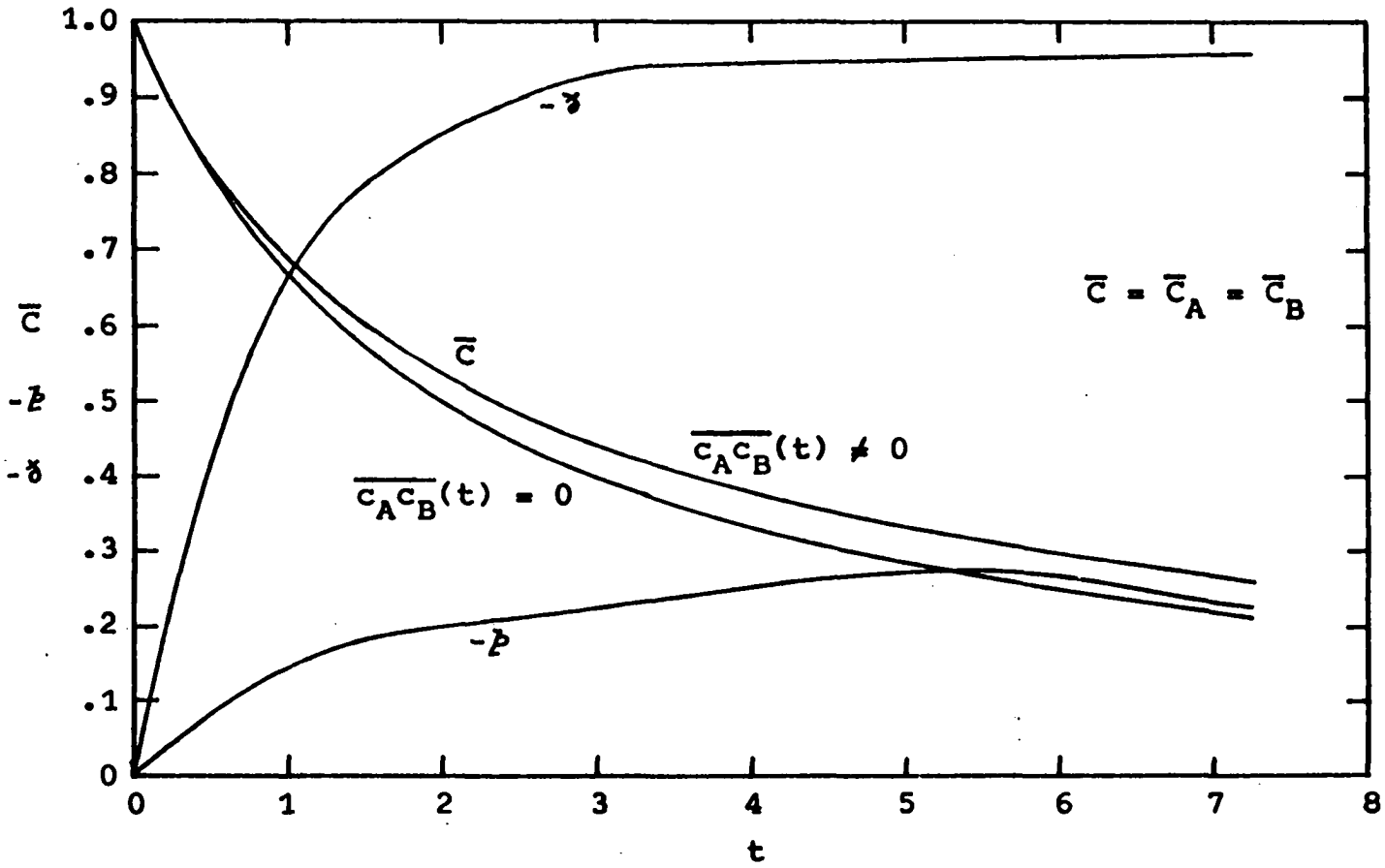

Figure 27. Mean field decay with and without concentration fluctuations and growth of the segregation and correlation coefficients from zero initial correlation of fluctuations of A and B for a second-order reaction with $Da_I = 0.5$, $Pe_A = Pe_B = 50$, $\bar{C}_A(0) = \bar{C}_B(0) = 1.0$, $\tilde{c}_A(0)^2 = \tilde{c}_B(0)^2 = 0.2$, and $\overline{c_A c_B}(0) = 0$

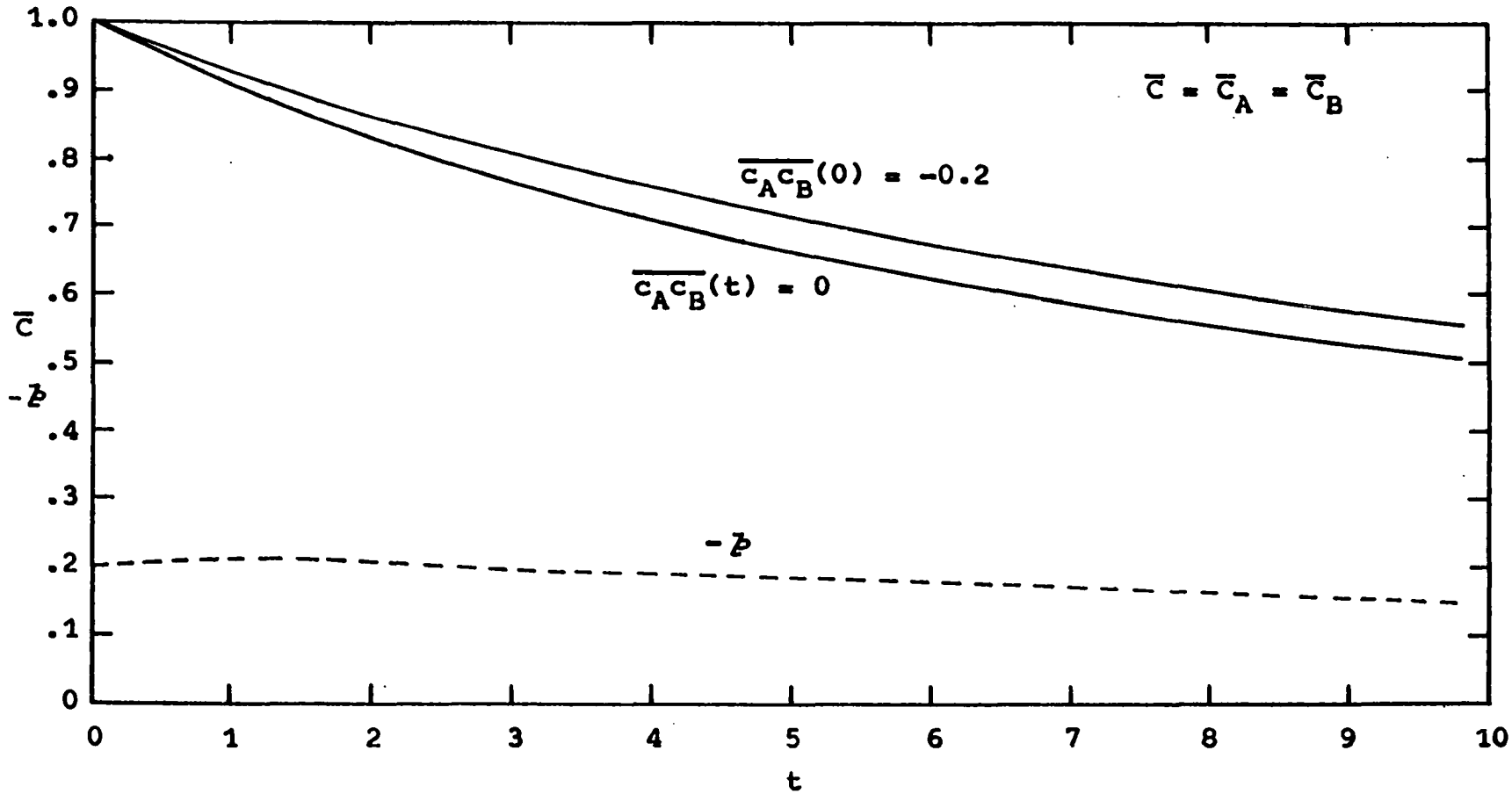

Figure 28. Mean field decay (solid lines) with and without concentration fluctuations and growth of the segregation coefficient (dashed line) for a two-species second-order reaction with $Da_I = 0.1$, $Pe_A = Pe_B = 100$, $\overline{c}_A(0) = \overline{c}_B(0) = 1.0$, $\tilde{c}_A(0)^2 = \tilde{c}_B(0)^2 = 0.2$, and $\overline{c_A c_B}(0) = -0.2$

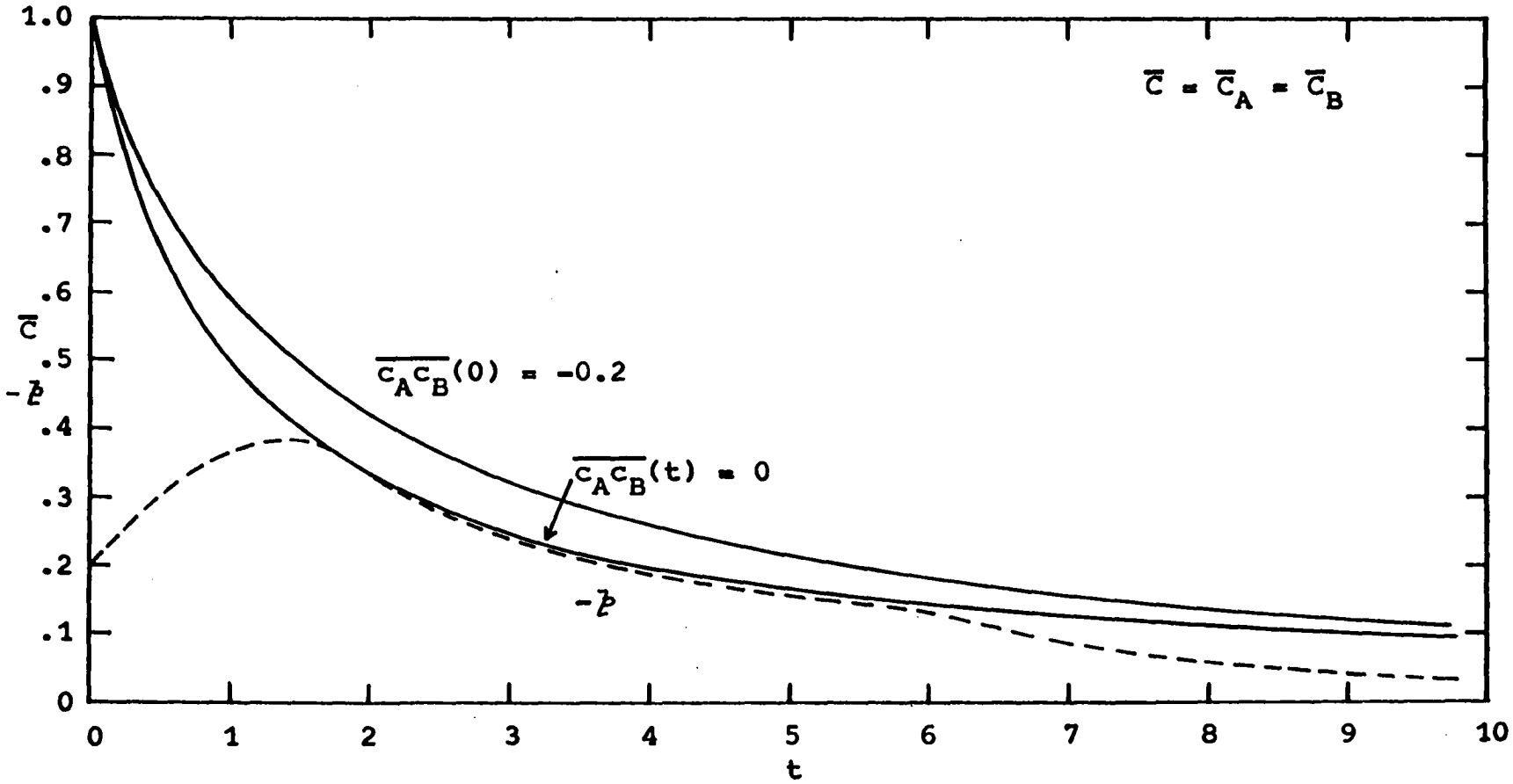

Figure 29. Mean field decay (solid lines) with and without concentration fluctuations and growth of the segregation coefficient (dashed line) for a two-species second-order reaction with $Da_I = 1.0$, $Pe_A = Pe_B = 20$, $\overline{c}_A(0) = \overline{c}_B(0) = 1.0$, $\tilde{c}_A(0)^2 = \tilde{c}_B(0)^2 = 0.2$, and $\overline{c_A c_B}(0) = -0.2$

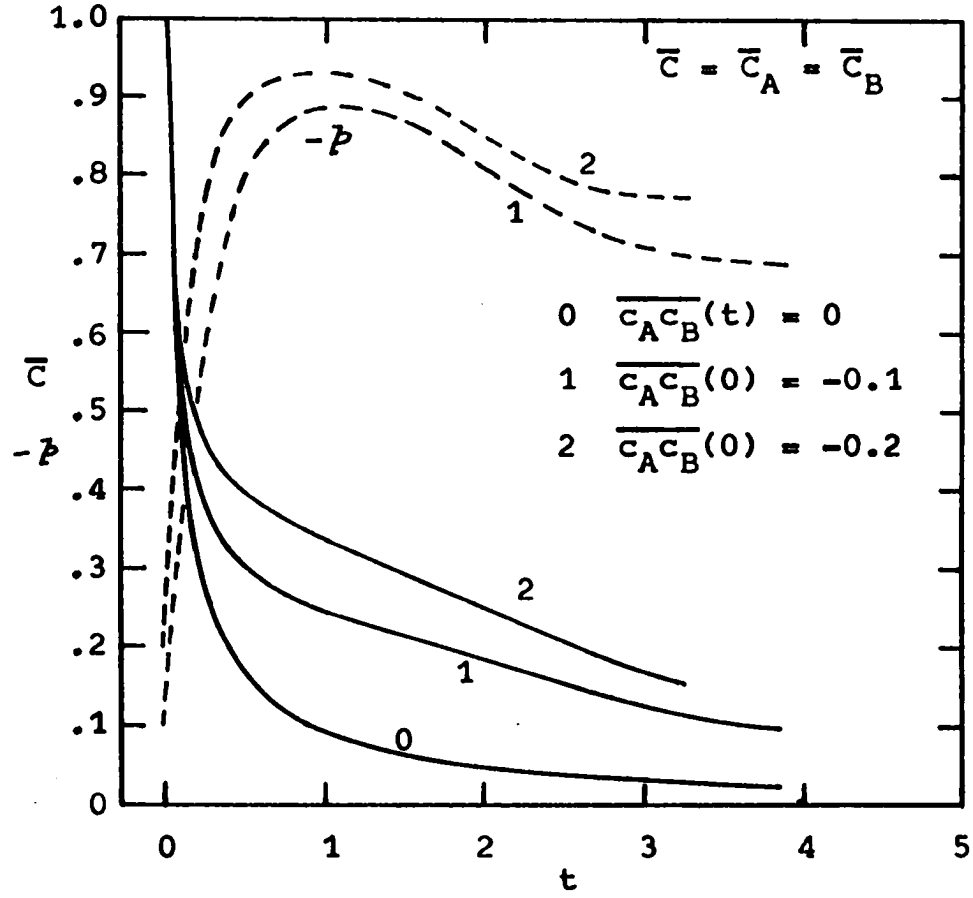

Figure 30. Mean field decay (solid lines) with and without concentration fluctuations and growth of the segregation coefficient (dashed lines) for a two-species second-order reaction with $Da_I = 10.0$, $Pe_A = Pe_B = 20$, $\overline{C}_A(0) = \overline{C}_B(0) = 1.0$, $\tilde{c}_A(0)^2 = \tilde{c}_B(0)^2 = 0.2$ (0.1), and $\overline{c_A c_B}(0) = -0.2$ (-0.1)

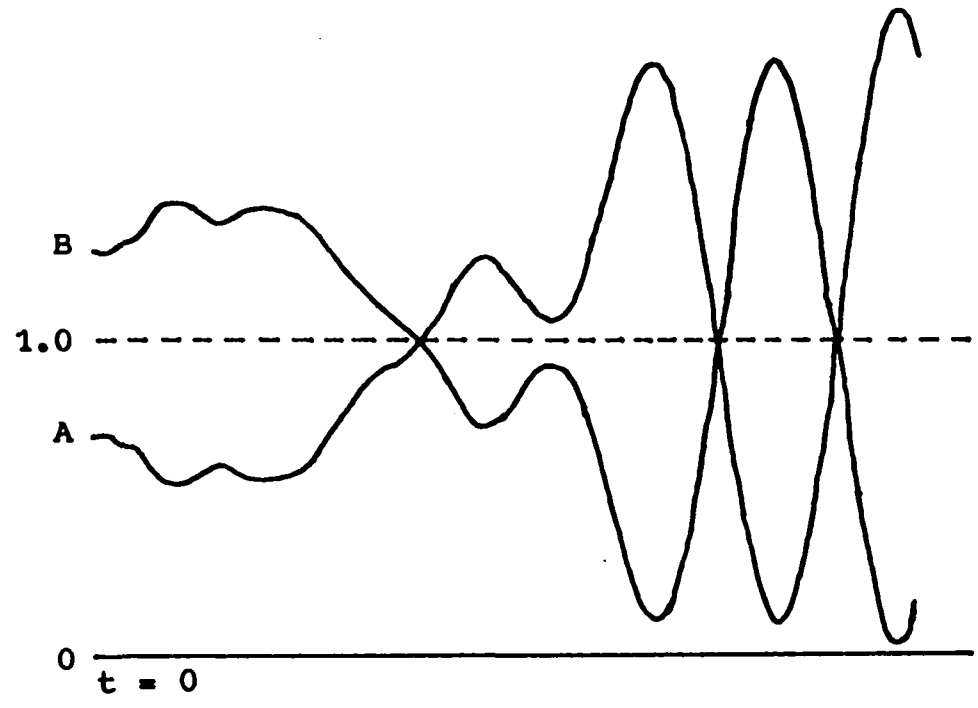

Figure 31. Physical-space concentration fluctuations of A and B at $\underset{\sim}{x} = \underset{\sim}{0}$ (solid lines) and mean field (dashed line) for convection without diffusion or reaction and $\overline{c}_A(0) = \overline{c}_B(0) = 1.0$, $\widetilde{c}_A(0)^2 = \widetilde{c}_B(0)^2 = 0.2$, and $\overline{c_A c_B}(0) = -0.2$

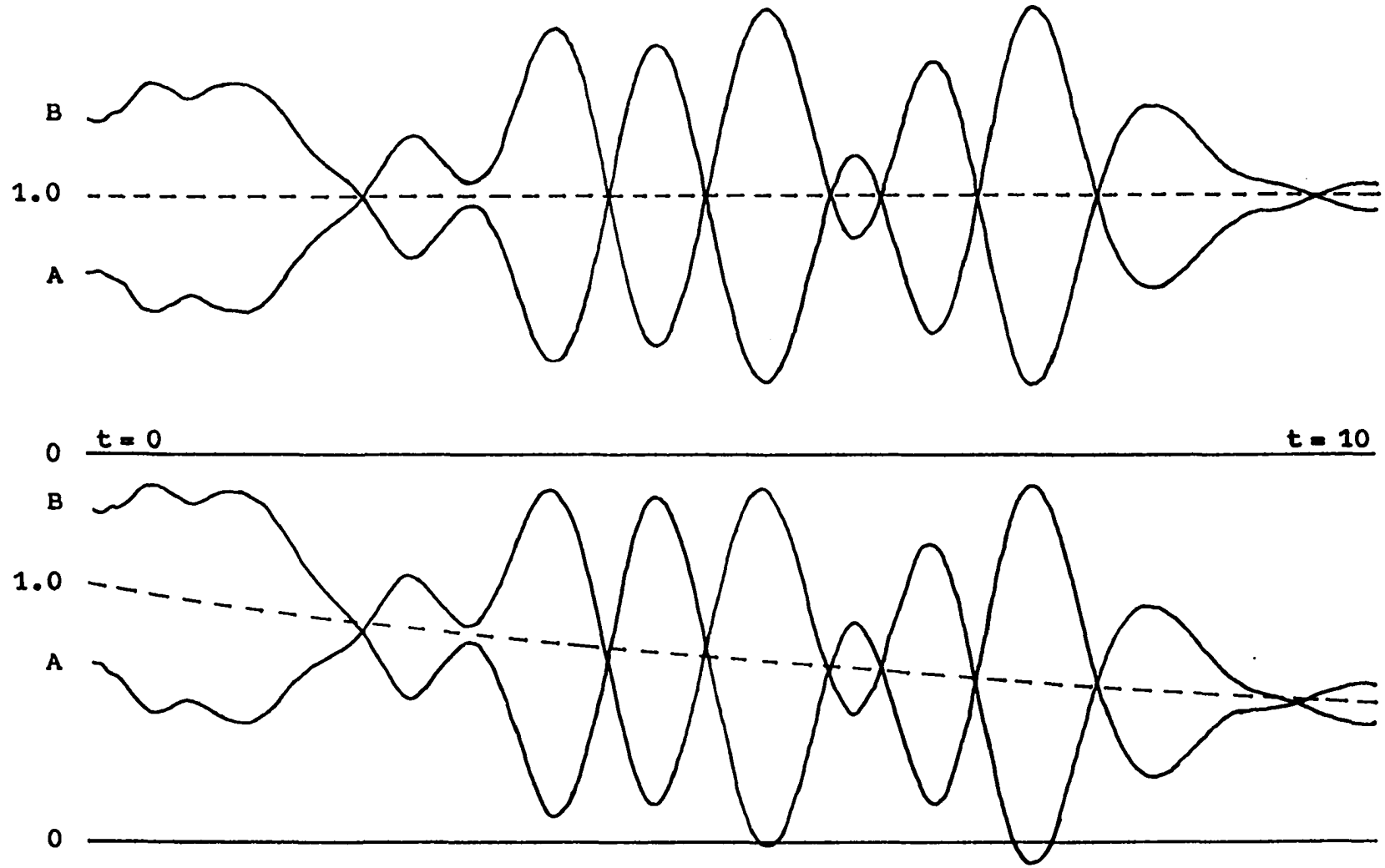

Figure 32. Physical-space concentration fluctuations of A and B at $\underset{\sim}{x} = \underset{\sim}{0}$ (solid lines) and mean field decay (dashed line) for $Da_I = 0$ (above) and $Da_I = 0.1$ (below) and $Pe_A = Pe_B = 100$, $\overline{C}_A(0) = \overline{C}_B(0) = 1.0$, $\widetilde{c}_A(0)^2 = \widetilde{c}_B(0)^2 = 0.2$, and $\overline{c_A c_B}(0) = -0.2$

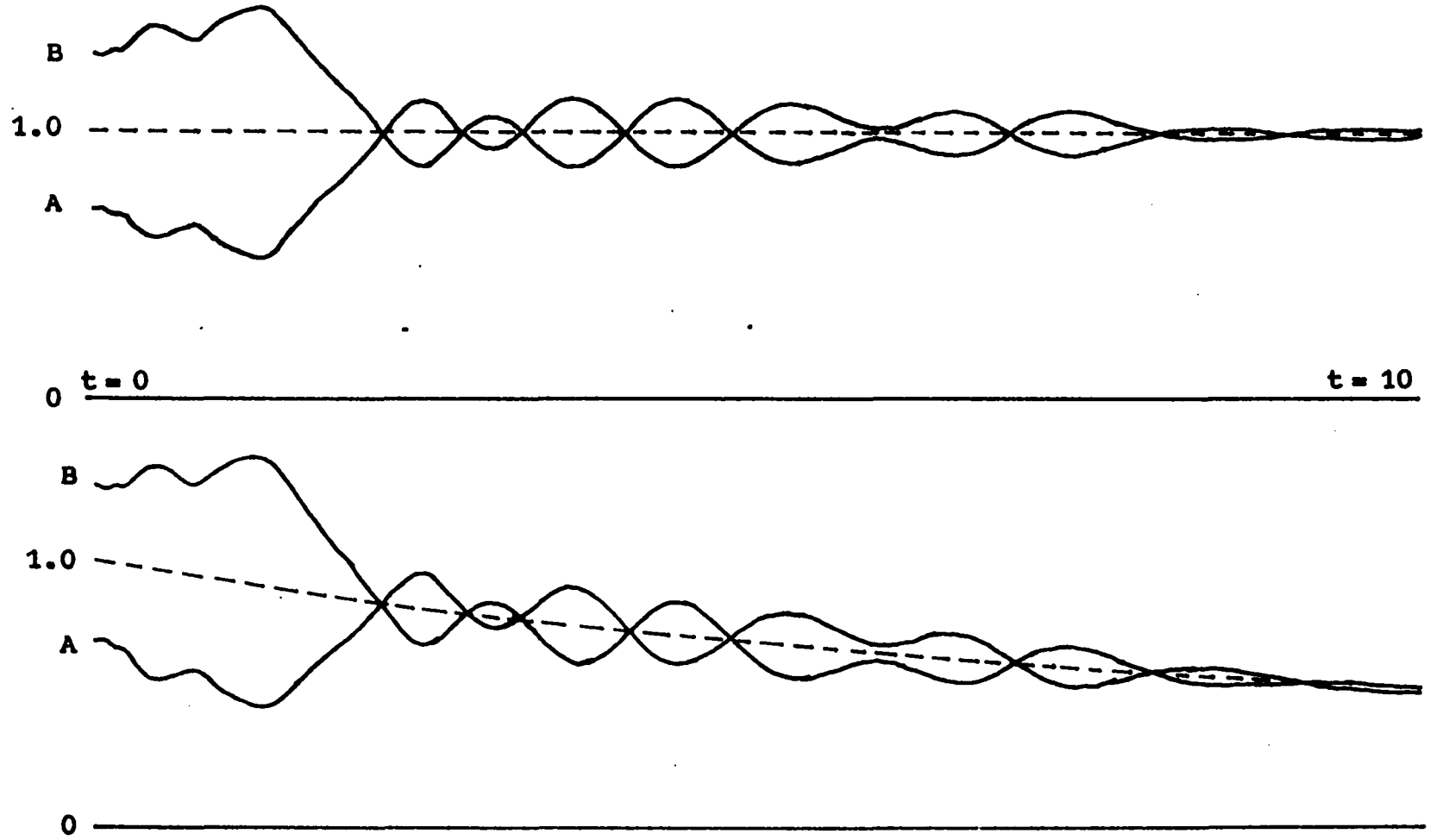

Figure 33. Physical-space concentration fluctuations of A and B at $\underline{x} = \underline{0}$ (solid lines) and mean field decay (dashed line) for $Da_I = 0$ (above) and $Da_I = 0.1$ (below) and $Pe_A = Pe_B = 20$, $\overline{c}_A(0) = \overline{c}_B(0) = 1.0$, $\tilde{c}_A(0)^2 = \tilde{c}_B(0)^2 = 0.2$, and $\overline{c_A c_B}(0) = -0.2$

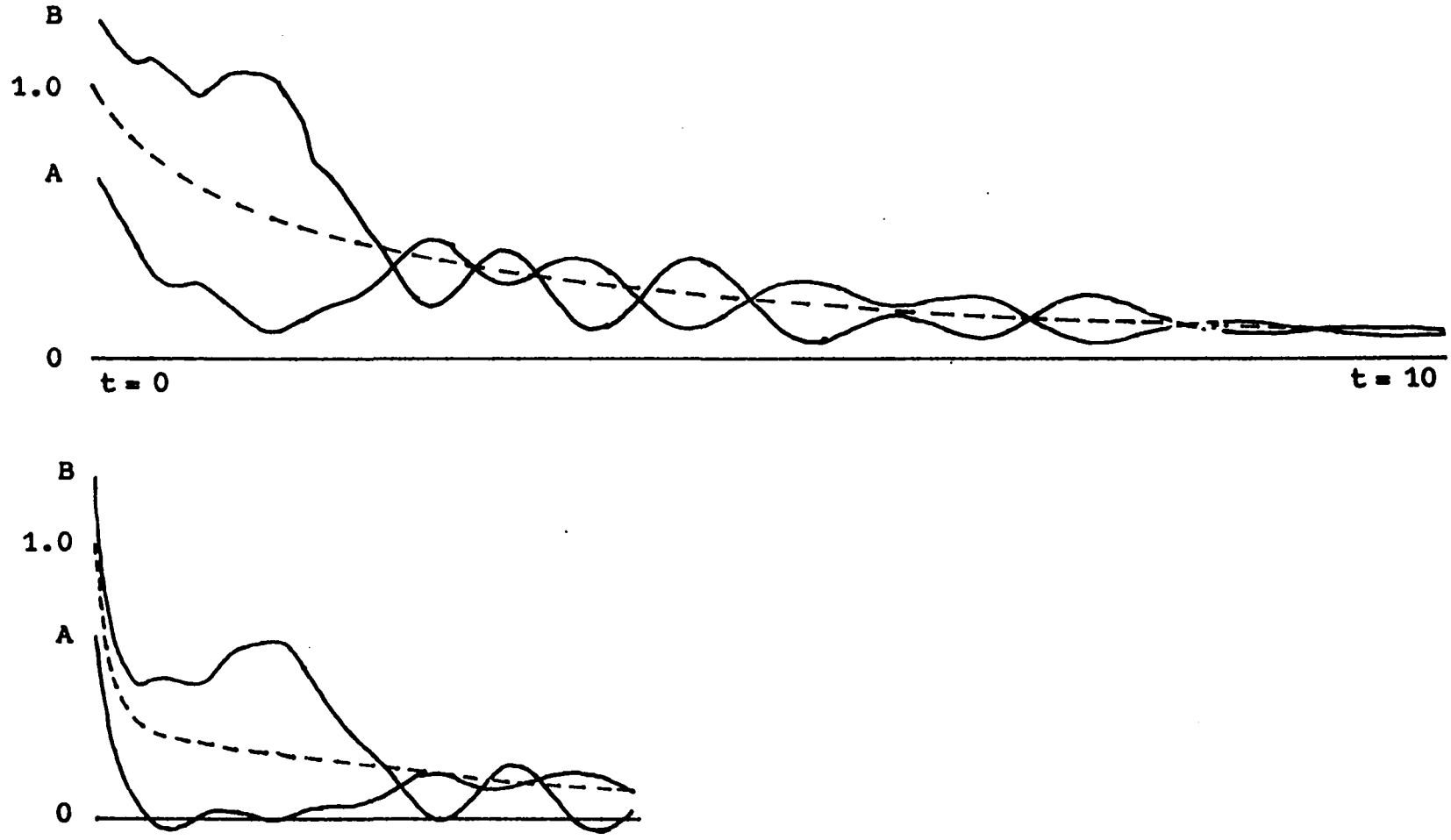

Figure 34. Physical-space concentration fluctuations of A and B at $\underline{x} = \underline{0}$ (solid lines) and mean field decay (dashed line) for $Da_I = 1.0$ (above) and $Da_I = 10.0$ (below) and $Pe_A = Pe_B = 20$, $\overline{c}_A(0) = \overline{c}_B(0) = 1.0$, $\widetilde{c}_A(0)^2 = \widetilde{c}_B(0)^2 = 0.2$, and $\overline{c_A c_B}(0) = -0.2$

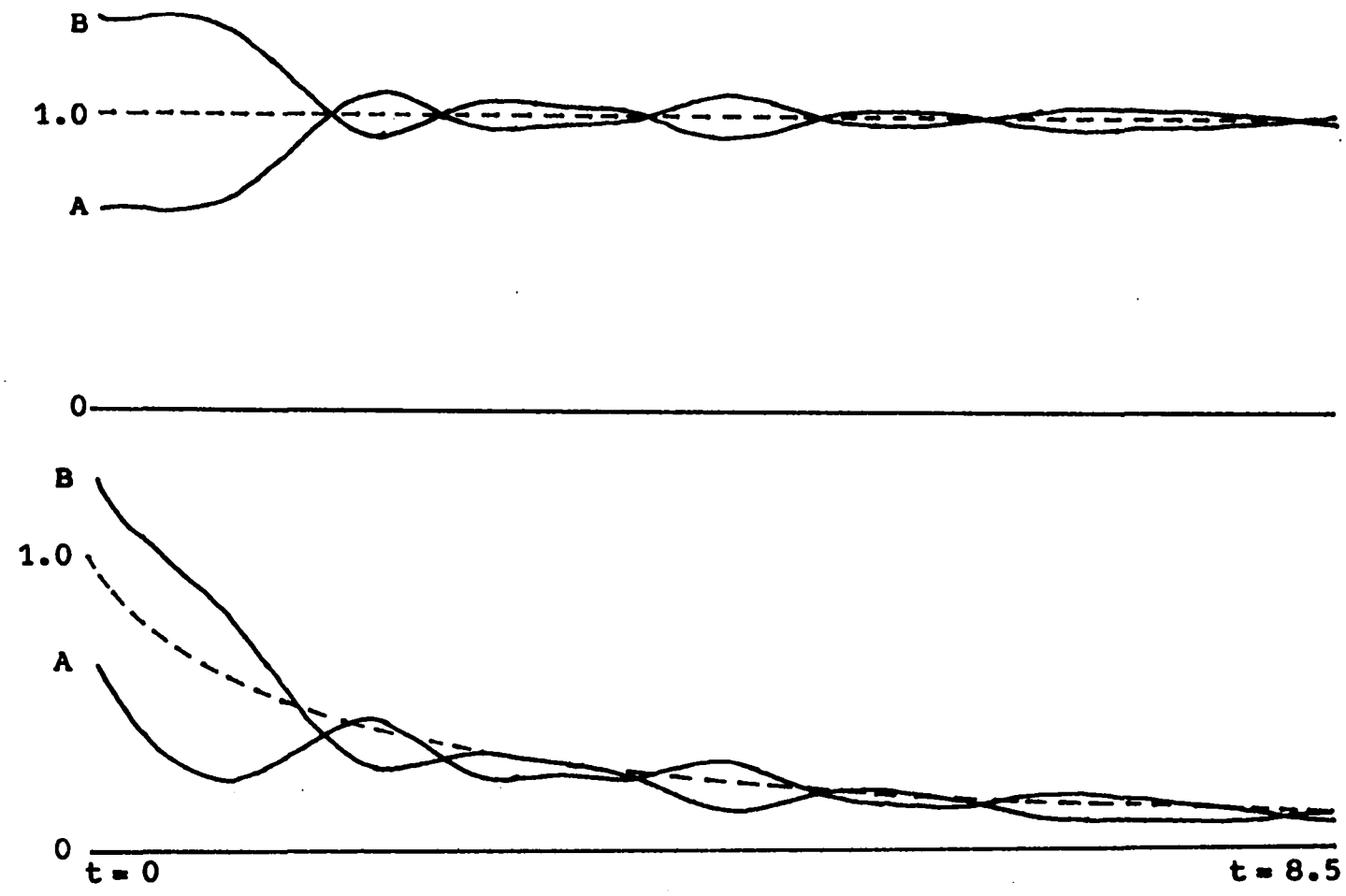

Figure 35. Physical-space concentration fluctuations of A and B at $\underset{\sim}{x} = \underset{\sim}{0}$ (solid lines) and mean field decay (dashed line) with the integrated velocity field with interaction for $Da_I = 0$ (above) and $Da_I = 1.0$ (below) and $Pe_A = Pe_B = 20$, $\overline{c}_A(0) = \overline{c}_B(0) = 1.0$, $\widetilde{c}_A(0)^2 = \widetilde{c}_B(0)^2 = 0.2$, and $\overline{\widetilde{c}_A \widetilde{c}_B}(0) = -0.2$

0.29 0.44 0.37 0.20 0.14 0.21 0.25 0.14 0.02 0.07 0.29

0.33 0.22 0.14 0.18 0.25 0.24 0.15 0.13 0.22 0.34 0.33

0.29 0.05 0.08 0.29 0.42 0.36 0.30 0.41 0.58 0.55 0.29

0.31 0.13 0.24 0.46 0.52 0.42 0.41 0.59 0.73 0.62 0.31

0.44 0.32 0.37 0.49 0.50 0.38 0.32 0.42 0.59 0.60 0.44

0.52 0.34 0.27 0.36 0.44 0.35 0.19 0.19 0.39 0.57 0.52

0.40 0.17 0.07 0.20 0.40 0.42 0.31 0.26 0.38 0.49 0.40

0.17 0.07 0.06 0.17 0.36 0.53 0.61 0.58 0.47 0.31 0.17

0.05 0.21 0.29 0.24 0.27 0.51 0.76 0.72 0.39 0.08 0.05

0.14 0.43 0.47 0.26 0.16 0.35 0.57 0.48 0.14 0.04 0.14

0.29 0.44 0.37 0.20 0.14 0.21 0.25 0.14 0.02 0.07 0.29

A Field

Figure 36. Physical-space concentration fields of A and B at t = 3 ($\overline{C}_A = \overline{C}_B = 0.33$, $\hat{\rho} = -0.24$, $\delta = -0.93$) for $Da_I = 1.0$, $Pe_A = Pe_B = 20$, $\overline{C}_B(0) = 1.0$, $\tilde{c}_A(0)^2 = \tilde{c}_B(0)^2 = 0.2$, and $\overline{c_A c_B}(0) = -0.2$

0.40	0.17	0.23	0.46	0.54	0.43	0.38	0.55	0.76	0.70	0.40
0.26	0.35	0.51	0.54	0.44	0.39	0.47	0.57	0.52	0.35	0.26
0.28	0.56	0.61	0.41	0.22	0.26	0.38	0.34	0.15	0.08	0.28
0.33	0.54	0.45	0.19	0.08	0.18	0.26	0.15	0.01	0.05	0.33
0.28	0.36	0.27	0.13	0.10	0.21	0.28	0.21	0.12	0.15	0.28
0.18	0.27	0.32	0.27	0.21	0.26	0.36	0.38	0.27	0.17	0.18
0.20	0.39	0.51	0.43	0.27	0.24	0.33	0.37	0.27	0.15	0.20
0.40	0.51	0.53	0.42	0.28	0.18	0.17	0.19	0.23	0.29	0.40
0.60	0.43	0.31	0.32	0.33	0.21	0.07	0.12	0.37	0.60	0.60
0.58	0.22	0.13	0.32	0.46	0.33	0.17	0.30	0.65	0.82	0.58
0.40	0.17	0.23	0.46	0.54	0.43	0.38	0.55	0.76	0.70	0.40

B Field

0.01	-0.01	0.39	1.01	1.29	0.93	0.29	-0.06	-0.01	0.09	0.01
0.01	0.06	0.32	0.60	0.62	0.35	0.06	-0.04	0.02	0.05	0.01
-0.10	-0.03	0.14	0.22	0.11	-0.05	-0.08	0.01	0.06	-0.02	-0.10
0.00	-0.03	-0.05	-0.02	0.05	0.11	0.11	0.06	0.03	0.01	0.00
0.47	0.38	0.02	-0.10	0.22	0.57	0.50	0.10	-0.08	0.16	0.47
0.97	1.04	0.45	0.01	0.29	0.81	0.76	0.14	-0.19	0.27	0.97
1.01	1.36	0.92	0.35	0.34	0.70	0.71	0.18	-0.20	0.19	1.01
0.56	1.02	1.06	0.82	0.67	0.64	0.51	0.16	-0.12	0.03	0.56
0.07	0.37	0.82	1.20	0.88	0.41	0.08	-0.04	-0.04	0.04	0.07
-0.08	-0.02	0.53	1.27	1.56	1.12	0.39	-0.02	-0.01	0.02	-0.08
0.01	-0.01	0.39	1.01	1.29	0.93	0.29	-0.06	-0.01	0.09	0.01

A Field

Figure 37. Physical-space concentration fields of A and B at $t = 1.0$ ($\bar{C}_A = \bar{C}_B = 0.34$, $\mathcal{P} = -0.93$, $\mathcal{S} = -0.71$) showing growth of species segregation by reaction for $Da_I = 10.0$, $Pe_A = Pe_B = 20$, $\bar{C}_B(0) = 1$, $\tilde{c}_A(0)^2 = \tilde{c}_A(0)^2 = 0.2$, and $\overline{c_A c_B}(0) = -0.2$

0.83	0.59	0.23	-0.03	-0.07	0.06	0.25	0.45	0.66	0.84	0.83
1.27	1.04	0.33	-0.12	0.01	0.35	0.38	0.18	0.29	0.84	1.27
1.34	1.04	0.37	0.01	0.18	0.45	0.41	0.24	0.44	1.00	1.34
0.89	0.59	0.35	0.30	0.30	0.26	0.27	0.48	0.82	1.01	0.89
0.25	0.09	0.30	0.46	0.28	0.00	0.09	0.55	0.87	0.69	0.25
-0.09	-0.09	0.19	0.35	0.15	-0.09	0.02	0.39	0.54	0.27	-0.09
-0.02	-0.06	0.05	0.12	0.05	-0.01	0.09	0.28	0.34	0.18	-0.02
0.18	-0.05	-0.06	0.02	0.02	0.02	0.17	0.46	0.65	0.51	0.18
0.30	-0.08	-0.05	0.08	0.01	-0.08	0.17	0.74	1.11	0.88	0.30
0.46	0.11	0.07	0.09	-0.04	-0.12	0.16	0.74	1.13	0.96	0.46
0.83	0.59	0.23	-0.03	-0.07	0.06	0.25	0.45	0.66	0.84	0.83

B Field

0.67	1.03	1.29	1.36	1.21	0.88	0.51	0.24	0.17	0.34	0.67
0.51	0.64	1.03	1.35	1.28	0.92	0.62	0.60	0.67	0.61	0.51
0.61	0.45	0.73	1.13	1.21	0.97	0.82	0.99	1.17	1.01	0.61
0.62	0.38	0.46	0.77	1.04	1.10	1.05	1.07	1.09	0.94	0.62
0.54	0.41	0.38	0.65	1.10	1.36	1.21	0.85	0.61	0.57	0.54
0.75	0.66	0.64	0.99	1.51	1.64	1.21	0.64	0.44	0.61	0.75
1.36	1.14	1.11	1.52	1.91	1.72	1.04	0.60	0.79	1.24	1.36
1.91	1.63	1.51	1.78	1.93	1.50	0.80	0.58	1.10	1.77	1.91
1.87	1.79	1.64	1.65	1.58	1.17	0.60	0.42	0.86	1.52	1.87
1.26	1.52	1.52	1.42	1.26	0.94	0.50	0.20	0.30	0.76	1.26
0.67	1.03	1.29	1.36	1.21	0.88	0.51	0.24	0.17	0.34	0.67

A Field

Figure 38. Physical-space concentration fields of A and B at $t = 0$ for $\overline{c}_B(0) = 2.0$, $\widetilde{c}_A(0)^2 = 0.2$, $\widetilde{c}_B(0)^2 = 0.8$, and $\overline{\widetilde{c}_A \widetilde{c}_B}(0) = -0.4$

2.67	1.94	1.42	1.28	1.58	2.23	2.97	3.52	3.65	3.32	2.67
2.99	2.73	1.95	1.31	1.44	2.17	2.75	2.80	2.67	2.79	2.99
2.77	3.11	2.54	1.74	1.59	2.07	2.36	2.03	1.66	1.97	2.77
2.77	3.24	3.09	2.45	1.92	1.81	1.90	1.87	1.83	2.13	2.77
2.93	3.17	3.23	2.69	1.79	1.28	1.57	2.30	2.78	2.87	2.93
2.51	2.69	2.73	2.02	0.99	0.72	1.58	2.73	3.12	2.78	2.51
1.28	1.73	1.79	0.96	0.17	0.57	1.92	2.81	2.42	1.51	1.28
0.17	0.75	0.98	0.44	0.13	0.99	2.40	2.83	1.79	0.46	0.17
0.27	0.42	0.71	0.70	0.83	1.67	2.80	3.17	2.29	0.95	0.27
1.48	0.97	0.95	1.15	1.49	2.12	3.00	3.59	3.39	2.47	1.48
2.67	1.94	1.42	1.28	1.58	2.23	2.97	3.52	3.65	3.32	2.67

B Field

0.03	0.03	0.02	0.02	0.01	0.01	0.01	0.01	0.02	0.02	0.03
0.02	0.04	0.03	0.00	0.00	0.02	0.03	0.02	0.00	0.00	0.02
0.05	0.07	0.04	0.00	0.00	0.06	0.09	0.06	0.00	0.00	0.05
0.08	0.09	0.05	0.00	0.01	0.08	0.13	0.10	0.04	0.03	0.08
0.08	0.07	0.04	0.01	0.03	0.07	0.10	0.10	0.07	0.07	0.08
0.04	0.02	0.02	0.04	0.06	0.06	0.06	0.07	0.08	0.07	0.04
0.01	0.00	0.01	0.06	0.09	0.08	0.05	0.04	0.06	0.05	0.01
0.02	0.00	0.01	0.06	0.10	0.11	0.07	0.04	0.03	0.03	0.02
0.04	0.02	0.02	0.04	0.09	0.10	0.08	0.04	0.03	0.04	0.04
0.04	0.03	0.02	0.03	0.05	0.06	0.04	0.03	0.03	0.04	0.04
0.03	0.03	0.02	0.02	0.01	0.01	0.01	0.01	0.02	0.02	0.03

A Field

Figure 39. Physical-space concentration fields of A and B at $t = 4$ ($\overline{C}_A = 0.043$, $\overline{C}_B = 1.043$, $\mathcal{P} = -0.20$, $\mathcal{S} = -0.90$) showing near depletion of A for $Da_I = 1.0$, $Pe_A = Pe_B = 20$, $\overline{C}_B(0) = 2.0$, $\widetilde{c}_A(0)^2 = 0.2$, $\widetilde{c}_B(0)^2 = 0.8$, and $\overline{c_A c_B}(0) = -0.4$

0.91	0.91	1.22	1.47	1.40	1.18	1.15	1.33	1.42	1.20	0.91
1.17	0.91	1.09	1.48	1.56	1.27	1.03	1.21	1.53	1.54	1.17
1.03	0.69	0.94	1.41	1.42	0.98	0.70	1.01	1.51	1.52	1.03
0.60	0.45	0.86	1.26	1.12	0.63	0.46	0.83	1.22	1.08	0.60
0.51	0.63	0.95	1.09	0.87	0.56	0.52	0.72	0.83	0.68	0.51
0.99	1.23	1.21	0.95	0.72	0.69	0.75	0.73	0.65	0.72	0.99
1.55	1.77	1.46	0.90	0.62	0.73	0.88	0.84	0.79	1.06	1.55
1.56	1.77	1.54	0.99	0.58	0.60	0.85	1.03	1.07	1.23	1.56
1.08	1.33	1.46	1.17	0.71	0.56	0.86	1.22	1.26	1.08	1.08
0.75	0.97	1.33	1.36	1.03	0.82	1.01	1.34	1.33	0.98	0.75
0.91	0.91	1.22	1.47	1.40	1.18	1.15	1.33	1.42	1.20	0.91

B Field

convected velocity field with interaction are shown in Figure 35 for $Pe_A = Pe_B = 20$ and $Da_I = 0$ and 1.0. In each case the mixing with reaction fluctuations about the mean resemble the pure mixing fluctuations.

Physical-space concentration fields of A and B are illustrated in Figures 36 - 39 for some cases of interest. For stoichiometric reactants, Figure 36 shows the concentration fields obtained after 3 eddy circulation times for $Da_I = 1.0$ and $Pe_A = Pe_B = 20$. Figure 37 illustrates the growth of species segregation by a fast reaction after one eddy circulation time for $Da_I = 10.0$ and $Pe_A = Pe_B = 20$. The initial concentration fields corresponding to Figures 36 and 37 are shown in Figure 21. The decay of concentration fields for nonstoichiometric reactants with $\overline{c}_B(0) = 2$ is shown in Figures 38 and 39. For the initial concentration fields shown in Figure 38, Figure 39 shows the near depletion of species A that occurs after 4 eddy circulation times for $Da_I = 1.0$ and $Pe_A = Pe_B = 20$.

Toor's statistical independence hypothesis can be extremely useful because it can be applied to experimental work relatively easily. Since for pure mixing

$$\frac{\overline{c_A c_B}(t)_{mix}}{\overline{c_A c_B}(0)_{mix}} = \frac{\tilde{c}_A(t)^2_{mix}}{\tilde{c}_A(0)^2_{mix}} = \frac{\tilde{c}_B(t)^2_{mix}}{\tilde{c}_B(0)^2_{mix}} = \frac{\tilde{c}_m(t)^2}{\tilde{c}_m(0)^2}$$

the pure mixing dependence of $\overline{c_A c_B}(t)$ can be determined by

measuring the fluctuation intensity decay of a nonreacting tracer with the same diffusivity in the same mixing field, for instance species A or B alone (with diluent for the other mixing stream). Alternatively, Toor has shown that the pure mixing dependence can be obtained using extremely fast stoichiometric reactions.

The breakdown of Toor's hypothesis for nonstoichiometric reactants whenever the Damköhler number is not very small contradicts the tentative experimental observation that the hypothesis might hold well for intermediate rate reactions for stoichiometric ratios up to 3. The less severe breakdown of Toor's hypothesis for widely different reactant diffusivities also places possible limitations on applications of the hypothesis. Despite these difficulties, Toor's hypothesis provides a convenient starting point for analysing and characterizing turbulent chemical reaction behavior.

CONCLUSIONS

In this study, O'Brien's statistical independence hypothesis successfully predicted the decay of concentration fluctuation intensities for turbulent mixing with a single component second-order reaction. The results suggest that counteracting or canceling of two opposing physical tendencies may be responsible for the success of O'Brien's hypothesis. However, O'Brien's hypothesis of modal independence exhibited significant error in some cases.

Toor's statistical independence hypothesis for two-species second-order reactions with stoichiometric reactants and equal diffusivities successfully predicted that $\overline{c_A c_B}(t)$ is insensitive to the rate of reaction (within the ability of the turbulence simulation to describe segregation tendencies of the species) and can be approximated by pure mixing results. The deviation of the hypothesis from the actual results that does occur underestimates the decay of $\overline{c_A c_B}(t)$ and is strongly correlated with the deviation of the correlation coefficient from -1. For unequal diffusivities with stoichiometric reactants, Toor's hypothesis shows significant error. A strong correlation exists between the extent of the deviation and the ratio of the correlation coefficient for mixing with reaction to the correlation coefficient for pure mixing. For nonstoichiometric reactants with equal diffusivities, Toor's hypothesis quickly breaks down

as the Damköhler number increases from being small. For this case the extent of the deviation is strongly correlated with the ratio $\tilde{c}_A/\tilde{c}_B$, where A is the limiting reactant. From these results it follows that Toor's hypothesis can be applied to systems that are not initially segregated provided the correlation coefficient of the fluctuations is -1.

Although mixing is somewhat faster for the convected velocity field with interaction than for the random convection velocity, the deviations of O'Brien's hypothesis and Toor's hypothesis are similar for both mixing fields.

On the basis of the success of O'Brien's and Toor's hypotheses as found in this study, further testing of the hypotheses is warranted using improved turbulence simulations. A fundamental problem that needs to be resolved, however, is how to generate initial concentration fields having higher fluctuation intensities but without negative physical-space concentrations. Since this study used two-dimensional turbulence with a limited number of Fourier modes, two-dimensional calculations should be made using a larger number of Fourier modes so that smaller scale fluctuations and hence species segregation can be more accurately portrayed. Calculations should then be extended to three dimensions since in two-dimensions vortex stretching does not occur and hence there is less formation of new reaction surfaces for two-species reactions than for three-

dimensional turbulence. In addition ensemble repetitions of the calculations should be made.

Additional problems that can be considered include studies of the effect of turbulent mixing on selectivity in competing parallel-consecutive type reactions and inclusion of temperature fluctuation effects arising from exothermic reactions.

APPENDIX A. RELATIONS BETWEEN DISCRETE AND CONTINUOUS SYSTEMS

Tabulated values of $\eta(k)$ are given in Tables 44 and 45 for three and two dimensions, respectively. The number of $\underset{\sim}{n}$-lattice points for a discrete system for different values of the cutoff wave number are given in Table 46.

The quantity $\eta(k)$ for discrete systems has been shown to be analogous to the quantities $2\pi k$ in two dimensions and $4\pi k^2$ in three dimensions for continuous systems. The relationship between these quantities is purely geometric and can be established from

$$\sum_{k=k'}^{k''} \eta(k) = \sum_{k=k'}^{k''} \sum_{\theta_{\underset{\sim}{k}}} \sum_{\phi_{\underset{\sim}{k}}} 1 = (N/2\pi)^3 \sum_{k' \le |\underset{\sim}{k}| \le k''} \Delta\underset{\sim}{k}$$

$$\Rightarrow (N/2\pi)^3 \int_{k' \le |\underset{\sim}{k}| \le k''} d\underset{\sim}{k} = (N/2\pi)^3 \int_{k'}^{k''} 4\pi k^2 dk \qquad (937,3D)$$

$$= (N/2\pi)^3 (4\pi/3)(k''^3 - k'^3)$$

in three dimensions and

$$\sum_{k=k'}^{k''} \eta(k) = \sum_{k=k'}^{k''} \sum_{\theta_{\underset{\sim}{k}}} 1 = (N/2\pi)^2 \sum_{k' \le |\underset{\sim}{k}| \le k''} \Delta\underset{\sim}{k}$$

$$\Rightarrow (N/2\pi)^2 \int_{k' \le |\underset{\sim}{k}| \le k''} d\underset{\sim}{k} = (N/2\pi)^2 \int_{k'}^{k''} 2\pi k \, dk \qquad (938,2D)$$

$$= (N/2\pi)^2 \pi (k''^2 - k'^2)$$

Table 44. Values of $\eta(n)$ in three dimensions

n^2	η	n^2	η	n^2	η	n^2	η	n^2	η
0	1	35	48	70	48	105	96	140	48
1	6	36	30	71	0	106	72	141	96
2	12	37	24	72	36	107	72	142	48
3	8	38	72	73	48	108	32	143	0
4	6	39	0	74	120	109	72	144	30
5	24	40	24	75	56	110	144	145	96
6	24	41	96	76	24	111	0	146	192
7	0	42	48	77	96	112	0	147	56
8	12	43	24	78	48	113	96	148	24
9	30	44	24	79	0	114	96	149	168
10	24	45	72	80	24	115	48	150	120
11	24	46	48	81	102	116	72	151	0
12	8	47	0	82	48	117	120	152	72
13	24	48	8	83	72	118	72	153	144
14	48	49	54	84	48	119	0	154	96
15	0	50	84	85	48	120	48	155	96
16	6	51	48	86	120	121	78	156	0
17	48	52	24	87	0	122	120	157	72
18	36	53	72	88	24	123	48	158	96
19	24	54	96	89	144	124	0	159	0
20	24	55	0	90	120	125	144	160	24
21	48	56	48	91	48	126	144	161	192
22	24	57	48	92	0	127	0	162	108
23	0	58	24	93	48	128	12	163	24
24	24	59	72	94	96	129	144	164	96
25	30	60	0	95	0	130	48	165	96
26	72	61	72	96	24	131	120	166	120
27	32	62	96	97	48	132	48	167	0
28	0	63	0	98	108	133	48	168	48
29	72	64	6	99	72	134	168	169	78
30	48	65	96	100	30	135	0	170	144
31	0	66	96	101	168	136	48	171	120
32	12	67	24	102	48	137	96	172	24
33	48	68	48	103	0	138	96		
34	48	69	96	104	72	139	72		

Table 45. Nonzero values of $\eta(n)$ in two dimensions

n^2	η	n^2	η	n^2	η	n^2	η	n^2	η
0	1	80	8	173	8	277	8	388	8
1	4	81	4	178	8	281	8	389	8
2	4	82	8	180	8	288	4	392	4
4	4	85	16	181	8	289	12	394	8
5	8	89	8	185	16	290	16	397	8
8	4	90	8	193	8	292	8	400	12
9	4	97	8	194	8	293	8	401	8
10	8	98	4	196	4	296	8	404	8
13	8	100	12	197	8	298	8	405	8
16	4	101	8	200	12	305	16	409	8
17	8	104	8	202	8	306	8	410	16
18	4	106	8	205	16	313	8	416	8
20	8	109	8	208	8	314	8	421	8
25	12	113	8	212	8	317	8	424	8
26	8	116	8	218	8	320	8	425	24
29	8	117	8	221	16	324	4	433	8
32	4	121	4	225	12	325	24	436	8
34	8	122	8	226	8	328	8	441	4
36	4	125	16	229	8	333	8		
37	8	128	4	232	8	337	8		
40	8	130	16	233	8	338	12		
41	8	136	8	234	8	340	16		
45	8	137	8	241	8	346	8		
49	4	144	4	242	4	349	8		
50	12	145	16	244	8	353	8		
52	8	146	8	245	8	356	8		
53	8	148	8	250	16	360	8		
58	8	149	8	256	4	361	4		
61	8	153	8	257	8	362	8		
64	4	157	8	260	16	365	16		
65	16	160	8	261	8	369	8		
68	8	162	4	265	16	370	16		
72	4	164	8	269	8	373	8		
73	8	169	12	272	8	377	16		
74	8	170	16	274	8	386	8		

Table 46. Number of $\underset{\sim}{n}$-lattice points within $1 \leq |\underset{\sim}{n}| \leq n_{max}$

n_{max}	number of points 2D	3D	n_{max}	number of points 2D	3D
1	4	6	11	376	5574
2	12	32	12	440	7152
3	28	122	13	528	9170
4	48	256	14	612	
5	80	514	15	708	
6	112	924	16	796	
7	148	1418	17	900	
8	196	2108	18	1008	
9	252	3070	19	1128	
10	316	4168	20	1256	
			21	1372	

Table 47. Comparison of values of S and I for small n for three dimensions

n	S(0,n)	$\frac{S(0,n)}{I(0,n)}$	$\frac{S(n-1,n+1)}{I(n-1,n+1)}$
0	1		
1	7	1.6711	0.9549
2	33	0.9847	1.0651
3	123	1.0876	0.9549
4	257	0.9587	0.9549
5	515	0.9836	1.0492
6	925	1.0223	0.9900
7	1419	0.9876	0.9549
8	2109	0.9834	1.0217
9	3071	1.0057	1.0078
10	4169	0.9953	0.9930
11	5574	0.9999	0.9785
12	7153	0.9882	0.9913
13	9171	0.9965	

Table 48. Comparison of values of S and I for small n for two dimensions

n	S(0,n)	$\frac{S(0,n)}{I(0,n)}$	$\frac{S(n-1,n+1)}{I(n-1,n+1)}$	$\frac{S(n-2,n+2)}{I(n-2,n+2)}$
0	1			
1	5	1.5915	1.0345	
2	13	1.0345	0.9549	0.9549
3	29	1.0257	0.9549	1.0080
4	49	0.9748	1.0345	0.9947
5	81	1.0313	1.0186	0.9549
6	113	0.9991	0.9019	0.9815
7	149	0.9679	0.9549	0.9777
8	197	0.9798	1.0345	1.0146
9	253	0.9942	1.0610	1.0080
10	317	1.0090	0.9868	0.9708
11	377	0.9918	0.8971	0.9983
12	441	0.9748	1.0080	0.9814
13	529	0.9964	1.0529	1.0161
14	613	0.9955	1.0231	1.0118
15	709	1.0030	0.9762	0.9868
16	797	0.9910	0.9549	0.9848
17	901	0.9924	0.9924	0.9830
18	1009	0.9913	1.0080	1.0168
19	1129	0.9955	1.0387	0.9884
20	1257	1.0003	0.9708	
21	1373	0.9910		

in two dimensions. Rewriting the results in terms of n instead of k gives

$$S(n',n'') \equiv \sum_{n=n'}^{n''} \eta(n) \Rightarrow (4\pi/3)(n''^3 - n'^3) \equiv I(n',n'') \qquad (939,3D)$$

$$S(n',n'') \equiv \sum_{n=n'}^{n''} \eta(n) \Rightarrow \pi(n''^2 - n'^2) \equiv I(n',n'') \qquad (940,2D)$$

With $n' = 0$, we get

$$S(0,n'') = \sum_{n=0}^{n''} \eta(n) \Rightarrow (4\pi/3)n''^3 = I(0,n'') \qquad (941,3D)$$

$$S(0,n'') = \sum_{n=0}^{n''} \eta(n) \Rightarrow \pi n''^2 = I(0,n'') \qquad (942,2D)$$

For small n", S oscillates about I in value as n" increases; values of S and I are compared in Tables 47 and 48 for three and two dimensions, respectively. For very large n", Equations 939 - 942 become identities.

Similarly, the relationship between the discrete energy spectrum function $E(k)_d$ and the continuous energy spectrum function $E(k)_c$ can be established from

$$\sum_{k=k'}^{k''} \eta(k)E(k)_d = \sum_{k=k'}^{k''} \sum_{\theta_{\underset{\sim}{k}}} \sum_{\phi_{\underset{\sim}{k}}} E(k)_d$$

$$= (N/2\pi)^3 \sum_{k' \leq |\underset{\sim}{k}| \leq k''} E(k)_d \Delta\underset{\sim}{k} = (N/2\pi)^3 \int_{k' \leq |\underset{\sim}{k}| \leq k''} (a_d/a_c)E(k)_c d\underset{\sim}{k}$$

$$= (N/2\pi)^3 \int_{k'}^{k''} 4\pi k^2 (a_d/a_c)E(k)_c dk \qquad (943,3D)$$

in three dimensions and

$$\sum_{k=k'}^{k''} \eta(k)E(k)_d = \sum_{k=k'}^{k''} \sum_{\theta_{\underset{\sim}{k}}} E(k)_d$$

$$= (N/2\pi)^2 \sum_{k' \le |\underset{\sim}{k}| \le k''} E(k)_d \Delta\underset{\sim}{k} \Rightarrow (N/2\pi)^2 \int_{k' \le |\underset{\sim}{k}| \le k''} (a_d/a_c)E(k)_c d\underset{\sim}{k} \tag{944,2D}$$

$$= (N/2\pi)^2 \int_{k'}^{k''} 2\pi k (a_d/a_c)E(k)_c dk$$

in two dimensions, where a_d and a_c are the normalization constants of the discrete and continuous energy spectra, respectively (required for a finite number of modes). Rewriting the results in terms of n instead of k gives

$$S_E(n',n'') \equiv \sum_{n=n'}^{n''} \eta(n)E(n)_d \tag{945,3D}$$

$$\Rightarrow 4\pi \int_{n'}^{n''} n^2 (a_d/a_c)E(n)_c dn \equiv I_E(n',n'')$$

$$S_E(n',n'') \equiv \sum_{n=n'}^{n''} \eta(n)E(n)_d \tag{946,2D}$$

$$\Rightarrow 2\pi \int_{n'}^{n''} n\,(a_d/a_c)E(n)_c dn \equiv I_E(n',n'')$$

One fundamental problem in numerical computations of turbulent fields is that the numerical calculations are in terms of a discrete Fourier transform system, whereas turbulence theory deals with a continuous Fourier transform system, and discrete statistical quantities must be related

to their continuous counterparts. Usually quantities such as the energy spectrum function are computed by averaging discrete values over shells in Fourier space, and the shell-averaged discrete value is associated (after renormalization) with the average continuous value over the shell; the shell-averaged discrete quantity is assumed to have the same functionality as the continuous quantity. This is also suggested in Equations 943 (944) and 945 (946). Therefore, the Gaussian continuous energy spectrum, given by

$$E(n)_c = \tilde{v}^2\ 16(2/\pi)^{\frac{1}{2}}(n^4/n_o{}^5)\exp[-2(n/n_o)^2] \qquad (947,3D)$$

$$E(n)_c = \tilde{v}^2\ (9/2)(n^3/n_o{}^4)\exp[-\tfrac{3}{2}(n/n_o)^2] \qquad (948,2D)$$

where n_o is the peak wave number, has the discrete counterpart

$$E(n)_d = \tilde{v}^2\ a_d(n/n_o)^4\exp[-2(n/n_o)^2] \qquad (949,3D)$$

$$E(n)_d = \tilde{v}^2\ a_d(n/n_o)^3\exp[-\tfrac{3}{2}(n/n_o)^2] \qquad (950,2D)$$

where a_d is the normalization constant. Equations 447 (948) and 949 (950) can be used to compare values of S_E and I_E in Equations 945 (946). Substituting Equation 947 (948) into Equation 945 (946) and carrying out the integration gives

Table 49. Comparison of values of S_E and I_E for small n for a Gaussian energy spectrum in three dimensions

Conditions used are: $n_o = 5$, $n_{max} = 13$, $a_d = 0.2844410$

n	$E(n)_d$	$S_E(0,n)$	$I_E(0,n)$	$\frac{S_E(0,n)}{I_E(0,n)}$	$S_E(n-1,n+1)$	$I_E(n-1,n+1)$	$\frac{S_E(n-1,n+1)}{I_E(n-1,n+1)}$
0	0	0	0				
1	0.00042	0.0025	0.0008	3.1461	0.0786	0.0817	0.9630
2	0.00529	0.0786	0.0817	0.9630	1.2251	1.0285	1.1911
3	0.01794	1.2276	1.0293	1.1926	4.6325	5.0033	0.9259
4	0.03239	4.7111	5.0850	0.9265	12.8882	13.4222	0.9602
5	0.03849	14.1158	14.4516	0.9768	24.3022	23.2616	1.0447
6	0.03311	29.0133	28.3466	1.0235	28.3536	28.4056	0.9982
7	0.02168	42.4694	42.8572	0.9910	24.7104	25.7674	0.9590
8	0.01114	53.7237	54.1140	0.9928	18.4382	17.9691	1.0261
9	0.00458	60.9077	60.8263	1.0013	10.2153	9.8604	1.0360
10	0.00153	63.9394	63.9744	0.9995	4.2473	4.3283	0.9813
11	0.00042	65.1550	65.1546	1.0000	1.5658	1.5381	1.0180
12	0.00009	65.5051	65.5125	0.9999	0.4455	0.4465	0.9978
13	0.00002	65.6005	65.6011	1.0000			

Table 50. Comparison of values of S_E and I_E for small n for a Gaussian energy spectrum in two dimensions

Conditions used are: $n_o = 8$, $n_{max} = 21$, $a_d = 0.0851093$

n	$E(n)_d$	$S_E(0,n)$	$I_E(0,n)$	$\frac{S_E(0,n)}{I_E(0,n)}$	$S_E(n-1,n+1)$	$I_E(n-1,n+1)$	$\frac{S_E(n-1,n+1)}{I_E(n-1,n+1)}$
0	0	0	0				
1	0.00063	0.0013	0.0002	6.3058	0.0079	0.0063	1.270
2	0.00179	0.0079	0.0062	1.2701	0.0451	0.0435	1.036
3	0.00394	0.0482	0.0437	1.1022	0.1487	0.1579	0.942
4	0.00831	0.1566	0.1642	0.9542	0.4176	0.3893	1.073
5	0.01190	0.4657	0.4330	1.0756	0.7477	0.7400	1.010
6	0.01382	0.9043	0.9042	1.0002	1.0417	1.1625	0.896
7	0.01700	1.5075	1.5955	0.9449	1.4957	1.5724	0.951
8	0.01931	2.4000	2.4766	0.9691	1.9408	1.8797	1.032
9	0.01893	3.4483	3.4752	0.9923	2.1406	2.0207	1.059
10	0.01563	4.5406	4.4973	1.0096	1.9637	1.9775	0.993
11	0.01172	5.4120	5.4527	0.9925	1.6202	1.7772	0.912
12	0.00996	6.1608	6.2745	0.9819	1.5019	1.4766	1.017
13	0.00759	6.9139	6.9293	0.9978	1.2406	1.1399	1.088
14	0.00479	7.4014	7.4014	0.9982	0.8419	0.8210	1.025
15	0.00294	7.7557	7.7502	1.0007	0.5547	0.5533	1.002
16	0.00168	7.9560	7.9678	0.9985	0.3378	0.3499	0.966
17	0.00101	8.0935	8.1001	0.9992	0.2158	0.2080	1.037
18	0.00054	8.1718	8.1758	0.9995	0.1224	0.1165	1.051
19	0.00028	8.2159	8.2166	0.9999	0.0661	0.0615	1.074
20	0.00012	8.2379	8.2373	1.0001	0.0314	0.0307	1.023
21	0.00005	8.2473	8.2473	1.0000			

$$I_E(0,n'') = (\pi a_d n_o^3 \tilde{v}^2/2^{\frac{1}{2}}16)[(15\pi^{\frac{1}{2}}/2)\mathrm{erf}(X'') - (15 + 10X''^2 + 4X''^4)X'' \exp(-X''^2)] \quad (951,3D)$$

$$X'' = 2^{\frac{1}{2}}(n''/n_o)$$

$$I_E(0,n'') = (2^{\frac{1}{2}}2\pi a_d n_o^2 \tilde{v}^2/3^{\frac{1}{2}}9)[(3\pi^{\frac{1}{2}}/2)\mathrm{erf}(X'') - (3 + 2X''^2)X'' \exp(-X''^2)] \quad (952,2D)$$

$$X'' = (3/2)^{\frac{1}{2}}(n''/n_o)$$

with $I_E(n',n'') = I_E(0,n') - I_E(0,n'')$. Values of S_E and I_E obtained using Equations 945 - 950 are compared in Tables 49 and 50.

In three dimensions, the longitudinal correlation function can be calculated from the discrete and continuous energy spectra using

$$f(r)_d = (2/\tilde{v}^2) \sum_k E(k)_d \left[\frac{\sin(kr)}{(kr)^3} - \frac{\cos(kr)}{(kr)^2}\right] \quad (953,3D)$$

$$f(r)_c = (2/\tilde{v}^2) \int_0^\infty E(k)_c \left[\frac{\sin(kr)}{(kr)^3} - \frac{\cos(kr)}{(kr)^2}\right] \quad (954,3D)$$

Substituting the continuous Gaussian energy spectrum, Equation 947, into Equation 954, gives

$$f(r)_c = \exp(-\pi r^2/4) \quad (955,3D)$$

Values of $f(r)_d$ must be calculated numerically after substituting the discrete Gaussian energy spectrum, Equation 949,

into Equation 953. Values of $f(r)_c$ and $f(r)_d$ are compared in Table 51 and are found to be similar.

Table 51. Comparison of $f(r)_c$ and $f(r)_d$ as obtained from Gaussian continuous and discrete energy spectra in three dimensions

Conditions used are: $n_o = 5$, $n_{max} = 13$, $a_d = 0.2844410$

$N_d = 14.12685$, $N_c = 12.533$

r	$f(r)_d$	$f(r)_c$	$f(r)_d/f(r)_c$
0.0	1.00000	1.00000	1.000
0.2	0.97084	0.96907	1.002
0.4	0.88814	0.88191	1.007
0.6	0.76498	0.75371	1.015
0.8	0.61948	0.60492	1.024
1.0	0.47054	0.45594	1.032
1.2	0.33400	0.32272	1.035
1.4	0.22024	0.21451	1.027
1.6	0.13355	0.13391	0.997
1.8	0.07308	0.07850	0.931
2.0	0.03464	0.04321	0.802

APPENDIX B. PROPERTIES OF THE FOURIER TRANSFORM

In terms of dimensionless variables, the discrete form of the Fourier transform of a function is defined by

$$a(\underset{\sim}{k}) \equiv N^{-\delta_{nn}} \int_{\underset{\sim}{x}} a(\underset{\sim}{x}) \exp(-i\underset{\sim}{k}\cdot\underset{\sim}{x})d\underset{\sim}{x} = F[a(\underset{\sim}{x})] \tag{956}$$

where the integration in $\underset{\sim}{x}$ is over the unit box of turbulence and where F is the Fourier transform operator. Let the $\underset{\sim}{x}$ coordinate system be centered at the corner of the box, with $0 \leq x_i \leq N$, where N is the dimensionless length of the sides of the box.

Normalized Delta Function

With $a(\underset{\sim}{x}) = 1$, Equation 956 reduces to the normalized delta function

$$\delta_{\underset{\sim}{k},\underset{\sim}{0}} \equiv N^{-\delta_{nn}} \int_{\underset{\sim}{x}} \exp(-i\underset{\sim}{k}\cdot\underset{\sim}{x})d\underset{\sim}{x} \tag{957}$$

which has the properties

$$\begin{aligned} \delta_{\underset{\sim}{k},\underset{\sim}{0}} &= 1 \quad \text{if } \underset{\sim}{k} = \underset{\sim}{0} \\ &= 0 \quad \text{if } \underset{\sim}{k} \neq \underset{\sim}{0} \end{aligned} \tag{958}$$

This can be shown as follows. For $\underset{\sim}{k} = \underset{\sim}{0}$, Equation 957 reduces to

$$\delta_{\underset{\sim}{0},\underset{\sim}{0}} = N^{-\delta_{nn}} \int_{\underset{\sim}{x}} d\underset{\sim}{x} = 1 \tag{959}$$

For $\underset{\sim}{k} \neq \underset{\sim}{0}$, writing Equation 957 in long form gives

$$\delta_{\underset{\sim}{k},\underset{\sim}{0}} = (1/N) \int_0^N \exp(-ik_1x_1)dx_1 \ \ldots$$

$$= (1/N) \int_0^N [\cos(k_1x_1) - i \sin(k_1x_1)]dx_1 \ \ldots$$

$$= (1/Nk_1) [\sin(k_1x_1) + i \cos(k_1x_1)]\Big|_0^N \ \ldots \tag{960}$$

$$= (1/Nk_1) \{[\sin(2\pi n_1) - 0] + i [\cos(2\pi n_1) - 1]\} \ \ldots = 0$$

Linear Operations

The Fourier transform of a derivative in time gives

$$F\left(\frac{\partial a(\underset{\sim}{x})}{\partial t}\right) = \frac{\partial a(\underset{\sim}{k})}{\partial t} \tag{961}$$

as can be seen from

$$F\left(\frac{\partial a(\underset{\sim}{x})}{\partial t}\right) = N^{-\delta_{nn}} \int_{\underset{\sim}{x}} \left(\frac{\partial a(\underset{\sim}{x})}{\partial t}\right) \exp(-i\underset{\sim}{k}\cdot\underset{\sim}{x})d\underset{\sim}{x}$$

$$= \frac{\partial}{\partial t}\left(N^{-\delta_{nn}} \int_{\underset{\sim}{x}} a(\underset{\sim}{x})\exp(-i\underset{\sim}{k}\cdot\underset{\sim}{x})d\underset{\sim}{x}\right) = \frac{\partial a(\underset{\sim}{k})}{\partial t} \tag{962}$$

The Fourier transform of a first-order derivative in space gives

$$F\left(\frac{\partial a(\underset{\sim}{x})}{\partial x_i}\right) = ik_i a(\underset{\sim}{k}) \tag{963}$$

for cyclic boundary conditions. By definition,

$$F\left(\frac{\partial a(\underset{\sim}{x})}{\partial x_1}\right) = N^{-3} \int_0^N \int_0^N \left\{\int_0^N \frac{\partial a(\underset{\sim}{x})}{\partial x_1} \exp(-ik_1x_1)dx_1\right\} \tag{964}$$

$$\cdot \exp[-i(k_2x_2 + k_3x_3)]\, dx_2\, dx_3$$

Integration by parts gives

$$\int_0^N \frac{\partial a(\underset{\sim}{x})}{\partial x_1} \exp(-ik_1x_1)dx_1 = ik_i \int_0^N a(\underset{\sim}{x})\exp(-ik_1x_1)dx_1 \tag{965}$$

since

$$a(\underset{\sim}{x})\exp(-ik_1x_1)\Big|_0^N = a(\underset{\sim}{x})\Big|_{x_1 = N} - a(\underset{\sim}{x})\Big|_{x_1 = 0} = 0 \tag{966}$$

for cyclic boundary conditions. Substituting Equation 965 into Equation 964 gives Equation 963 .

Similarly, the Fourier transform of a second-order derivative in space gives

$$F\left(\frac{\partial^2 a(\underset{\sim}{x})}{\partial x_i^2}\right) = -k_i^2\, a(\underset{\sim}{k}) \tag{967}$$

for cyclic boundary conditions.

Convolution Summations

The Fourier transform of the product of two functions results in a convolution summation of the product of the transforms of the functions. By definition,

$$F[v_i(\underset{\sim}{x})\phi_j(\underset{\sim}{x})] = N^{-\delta_{nn}} \int_{\underset{\sim}{x}} v_i(\underset{\sim}{x})\phi_j(\underset{\sim}{x}) \exp(-i\underset{\sim}{k}\cdot\underset{\sim}{x})d\underset{\sim}{x} \tag{968}$$

But from the inverse transforms, we have

$$v_i(\underset{\sim}{x}) = \sum_{\underset{\sim}{p}} u_i(\underset{\sim}{p}) \exp(i\underset{\sim}{p}\cdot\underset{\sim}{x}) \tag{969}$$

$$\phi_j(\underset{\sim}{x}) = \sum_{\underset{\sim}{q}} \phi_j(\underset{\sim}{q}) \exp(i\underset{\sim}{q}\cdot\underset{\sim}{x}) \tag{970}$$

where $\underset{\sim}{p}$ and $\underset{\sim}{q}$ are dummy variables. Substitution and simplification gives

$$\begin{aligned} &F[v_i(\underset{\sim}{x})\phi_j(\underset{\sim}{x})] \\ &= N^{-\delta_{nn}} \sum_{\underset{\sim}{p}} \sum_{\underset{\sim}{q}} u_i(\underset{\sim}{p})\phi_j(\underset{\sim}{q}) \int_{\underset{\sim}{x}} \exp[-i(\underset{\sim}{k}-\underset{\sim}{p}-\underset{\sim}{q})\cdot\underset{\sim}{x}]\, d\underset{\sim}{x} \\ &= \sum_{\underset{\sim}{p}} \sum_{\underset{\sim}{q}} u_i(\underset{\sim}{p})\phi_j(\underset{\sim}{q})\, \delta_{\underset{\sim}{k},\underset{\sim}{p}+\underset{\sim}{q}} = \sum_{\underset{\sim}{p}} u_i(\underset{\sim}{p})\phi_j(\underset{\sim}{k}-\underset{\sim}{p}) \end{aligned} \tag{971}$$

Since $\underset{\sim}{p}$ and $\underset{\sim}{q}$ are dummy variables, the following identities exist for the convolution summation,

$$\begin{aligned} F[v_i\phi_j] &= \sum_{\underset{\sim}{p}} \sum_{\underset{\sim}{q}} u_i(\underset{\sim}{p})\phi_j(\underset{\sim}{q})\, \delta_{\underset{\sim}{k},\underset{\sim}{p}+\underset{\sim}{q}} = \sum_{\underset{\sim}{q}} \sum_{\underset{\sim}{p}} u_i(\underset{\sim}{q})\phi_j(\underset{\sim}{p})\, \delta_{\underset{\sim}{k},\underset{\sim}{p}+\underset{\sim}{q}} \\ &= \sum_{\underset{\sim}{p}+\underset{\sim}{q}=\underset{\sim}{k}} u_i(\underset{\sim}{p})\phi_j(\underset{\sim}{q}) = \sum_{\underset{\sim}{p}+\underset{\sim}{q}=\underset{\sim}{k}} u_i(\underset{\sim}{q})\phi_j(\underset{\sim}{p}) \\ &= \sum_{\underset{\sim}{p}} u_i(\underset{\sim}{p})\phi_j(\underset{\sim}{k}-\underset{\sim}{p}) = \sum_{\underset{\sim}{q}} u_i(\underset{\sim}{k}-\underset{\sim}{p})\phi_j(\underset{\sim}{q}) = \sum_{\underset{\sim}{p}} u_i(\underset{\sim}{k}-\underset{\sim}{p})\phi_j(\underset{\sim}{p}) \end{aligned} \tag{972}$$

For systems with a cutoff wave number k_{max}, the summations are subject to the restrictions that

$$0 \le |\underset{\sim}{k},\ \underset{\sim}{p},\ \underset{\sim}{q},\ \underset{\sim}{k}-\underset{\sim}{p},\ \underset{\sim}{k}-\underset{\sim}{q}| \le k_{max} \tag{973}$$

PART II. COLLECTION OF INERTIALESS PARTICLES ON CYLINDERS AND SPHEROIDS WITH ELECTRICAL FORCES AND GRAVITATION

The second part of this dissertation examines the collection of fine, charged particles in electrified fibrous filters and wet scrubbers under conditions in which particle inertia is negligible. Particle trajectories and collection efficiencies are calculated for a system consisting of a single fiber or droplet collector in a particle laden gaseous flow field. In the first two sections, two-dimensional cases of particle collection on fibers are examined using circular cylinders and, to determine the effect of fiber geometry, elliptical cylinders and ribbons. The results are also extended to include irregular cylindrical collectors. In the final section, collection in scrubbers is examined first for two-dimensional (axisymmetric) cases of collection on prolate and oblate spheroids and then three-dimensional cases of collection on spheroids and spheres. Finally, for single force cases results are obtained for arbitrary collector geometry.

NOMENCLATURE

Nomenclature in Common

a = length of major semiaxis

b = length of minor semiaxis

c = one half the focal distance

C = Stokes-Cunningham particle slip correction factor

$\underset{\sim}{E}$ = electric field intensity

E_o = uniform external electric field strength

$\underset{\sim}{f}_e$ = dimensionless spatial dependence of electrical or gravitational force, with e = c, ex, g

$\underset{\sim}{F}_e$ = electrical or gravitational force on particle

g = gravitational acceleration

K = $2C\rho_p U_o R_p^2/9\mu R_{rf}$ = Stokes number

K_c = $\rho_c Q_p C/12\pi^2 \epsilon_f R_p \mu U_o R_{rf}$ = coulombic force parameter for cylinders

K_c = $Q_c Q_p C/24\pi^2 \epsilon_f R_p \mu U_o R_{rf}^2$ = coulombic force parameter for bodies of revolution

K_e = dimensionless particle mobility (force parameter) corresponding to $\underset{\sim}{F}_e$, with e = c, ex, g

K_{ex} = $Q_p E_o C/6\pi R_p \mu U_o$ = external electric field force parameter

K_g = $2R_p^2 \rho_p g C/9\mu U_o$ = gravitational force parameter

Q_p = particle charge

$\mathcal{R}$ = R_p/R_{rf} = interception parameter

R_p = spherical particle radius

R_{rf} = collector reference length

T = tU_o/R_{rf} = dimensionless time

$\underset{\sim}{U}$ = $\underset{\sim}{u}/U_o$ = dimensionless local mean fluid velocity

U_o = free-stream velocity

$\underset{\sim}{V}$ = $\underset{\sim}{v}/U_o$ = dimensionless particle velocity

Greek letters:

ϵ_c = collector dielectric constant

ϵ_f = fluid dielectric constant

μ = viscosity

ρ_p = particle mass density

Ψ = dimensionless stream function for particle trajectory

Ψ_e = dimensionless force stream function, with e = c, ex, g

Ψ_f = $\psi/U_o R_{rf}$ = dimensionless stream function for fluid flow

Subscripts:

c = coulombic force

e = any of the forces

ex = external electric field force

f = fluid

g = gravitational force

i = limiting trajectory

m = grazing trajectory

0 = value with R = 0

Nomenclature for Circular Cylinders

A = defined by Equation 21

B = defined by Equation 53

Eu = 0.5772157... = Euler's constant

G = defined by Equation 10

$h(r)$ = defined in Table 52

h_m = coefficients in series expansion of generalized flow velocity, defined in Table 52

H = $h(R^*)$

H_0 = $h(1)$

Ku = Kuwabara's constant, defined by Equation 46

L = R_{cl}/R_c = dimensionless cell radius

$p(R)$ = defined by Equation 15

P = $p(R^*)$

P_0 = $p(1)$

R = r/R_c = dimensionless radial coordinate

$\mathcal{R}$ = R_p/R_c = interception parameter

R^* = $1 + \mathcal{R}$ = radial coordinate at impaction

R_c = circular cylinder collector radius

R_{cl} = radius of flow cell

Re = $2R_cU_o\rho/\mu$ = collector Reynolds number

R_n = radial coordinate of velocity node

s = defined in Table 52

W = defined by Equation 19

X = x/R_c = dimensionless fixed rectangular coordinate

$\hat{X}$ = $X \cos\beta - Z \sin\beta$ = dimensionless rotated rectangular coordinate system

$\hat{X}_i$ = value of $\hat{X}_o$ for limiting trajectory

X_1 = value of X at R = L

$\hat{X}_o$ = value of $\hat{X}$ at $Z = -\infty$

Y = defined by Equation 20

Y* = defined by Equation 34

Z = z/R_c = dimensionless fixed rectangular coordinate

$\hat{Z}$ = $Z \cos\beta + X \sin\beta$ = dimensionless rotated rectangular coordinate system

Greek letters:

α = cylindrical angle between the uniform external fields and the Z-axis

α^* = volume fraction of fibers (packing density) in filter mat

β = cylindrical angle between rectilinear particle trajectories far upstream and Z-axis

γ = $(\epsilon_c - \epsilon_f)/(\epsilon_c + \epsilon_f)$ = circular cylinder polarization coefficient

$\zeta(\theta)$ = deposition density function, defined by Equation 5

$\hat{\eta}$ = $(\hat{X}_{i+} - \hat{X}_{i-})/2$ = collection efficiency based on undisturbed cross-sectional area perpendicular to rectilinear particle paths

θ = cylindrical angle of particle position from the positive Z-axis

θ_i = angular coordinate at impaction on surface of collector of particles on a limiting trajectory

θ_{li} = value of θ at R = L for limiting trajectory

θ_m = angular location at impaction of a grazing limiting trajectory

θ_n = angular coordinate of velocity node

ρ_c = collector charge density per unit length

τ = $K_c^2/(1 + K_{ex})^2$

Ψ_o = value of Ψ at Z = $-\infty$

Ψ_l = value of Ψ at R = L

ϕ = defined by Equation 52

Subscripts:

l = value at R = L

n = velocity node

o = condition at $\hat{Z} = -\infty$

\+ = corresponding to the limiting trajectory most positive in $\hat{X}_o$

\- = corresponding to the limiting trajectory most negative in $\hat{X}_o$

^ = corresponding to the rotated coordinate system $\hat{Z}$, $\hat{X}$

Nomenclature for Elliptical Cylinders

A = defined by Equation 84

A* = defined in Table

d = generalized reference collector half-width

D = d/c

G = defined by Equation 75

W = defined by Equation 82

X = x/d = dimensionless fixed rectangular coordinate

$\hat{X}$ = $X \cos\beta - Z \sin\beta$ = dimensionless rotated rectangular coordinate

$\hat{X}_i$ = value of $\hat{X}_o$ for limiting trajectory

$\hat{X}_o$ = value of $\hat{X}$ at $\hat{Z} = -\infty$

Y = defined by Equation 83

Z = z/d = dimensionless fixed rectangular coordinate

$\hat{Z}$ = $Z \cos\beta + X \sin\beta$ = dimensionless rotated rectangular coordinate

Greek letters:

α = circular cylindrical angle between uniform external fields and Z-axis

β = circular cylindrical angle between rectilinear particle trajectories far upstream and Z-axis

Γ_0 = polarization coefficient in direction of major axis, defined in Table 54

Γ_{90} = polarization coefficient in direction of minor axis, defined in Table 54

δ = circular cylindrical angle between free-stream velocity and Z-axis

$\hat{\eta}$ = $(\hat{X}_{i+} - \hat{X}_{i-})/2$ = collection efficiency

λ = elliptical-cylinder coordinate angle of particle

position from positive Z-axis

λ_i = elliptical angular coordinate at impaction of particles on limiting trajectory

λ_m = elliptical angular coordinate of grazing trajectory at impaction

λ_n = elliptical angular coordinate of velocity node

$\mathfrak{N}$ = defined by Equation 72

ξ = elliptical-cylinder radial coordinate

ξ_0 = value of ξ at surface of elliptical-cylinder collector

ρ_c = collector charge density per unit length

ω_0 = defined by Equation 79

ω_{90} = defined by Equation 80

Subscripts:

n = velocity node

o = condition at $\hat{Z} = -\infty$

\+ = corresponding to limiting trajectory most positive in $\hat{X}_o$

\- = corresponding to limiting trajectory most negative in $\hat{X}_o$

^ = corresponding to rotated coordinate system $\hat{Z}$, $\hat{X}$

Nomenclature for Spheroids

A = defined by Equation 144

h = generalized fluid velocity function

H = $h(R^*)$

I = particle flux to collector

I_{rf} = reference particle flux

L = dimensionless outer radius of fluid cell

n_o = particle density upstream

p = external electric field force function

P = $K_{ex}(1 + \Upsilon/R^{*3}) + K_g$

$P(R)$ = defined by Equation 162

Q_c = collector charge

Q = K_c/R^{*2}

R = r/R_c = dimensionless radial coordinate for sphere

R^* = $1 + \delta$

R_c = radius of spherical collector

R_{rf} = reference length

S_{rf} = reference area for particle flux

V_o = dimensionless particle approach velocity, defined by Equation 131

W = $-K_c/R^{*2}P(R^*)$

W_0 = defined by Equation 119

X = dimensionless rectangular coordinate

X_o = value of X at $Z = -\infty$

Z = dimensionless rectangular coordinate

Greek letters:

α = angle between $\underset{\sim}{E}_o$ and $\underset{\sim}{U}_o$

Υ = polarization coefficient for a sphere, defined in

Table 62

Γ = polarization coefficient for prolate or oblate spheroid, defined in Table 59 or 60

η = X_i^2 = collection efficiency for axisymmetric cases

$\hat{\eta}$ = I/I_{rf} = collection efficiency for nonaxisymmetric cases, becomes η for $\alpha = 0$

θ = angular coordinate for sphere

λ = prolate or oblate spheroid angular coordinate

ν = defined by Equation 143

ξ = prolate or oblate spheroid radial coordinate

ξ_0 = value of ξ for prolate or oblate spheroid collector surface

ϕ = angular coordinate for sphere

$\mathfrak{T}(\xi_0)$ = geometrical polarization function for prolate or oblate spheroid, defined in Table 59 or 60

Ω = defined by Equation 106 or 108

Subscripts:

1 = value at R = L

n = normal to surface

o = condition at Z = $-\infty$

• = value with interception

' = dimensionless function

^ = rotated coordinate system

PARTICLE COLLECTION ON CIRCULAR CYLINDERS

Introduction and Review of Previous Studies

Many experimental studies (33, 40, 44, 68, 69, 119, 128, 129, 132) have shown that electrical forces can significantly enhance the collection of fine particles in electrified filters. In theoretical analyses, however, the effects of electrical forces have received relatively little attention. Kraemer (48) derived the collection efficiency of charged, inertialess, point particles in uniform flow past a charged cylinder. Natanson (79) showed that Kraemer's result is also valid for other flow fields such as potential flow. Stenhouse (116) computed collection efficiencies for the cases of both the particle and the cylinder being charged, or either one being charged with the other neutral, using a cellular flow field. Zebel (133) examined the collection of small, inertialess, charged particles on a neutral cylinder in the presence of an external electric field applied parallel to the flow field about the collector. It was found that the collection efficiency is the same for both potential flow and Lamb's (57) solution for Oseen flow.

Hochrainer, et al., (39) conducted a photographic study of the motion of small, essentially inertialess, charged particles flowing slowly around either a charged or a

neutral circular cylinder in the presence of an external electric field directed parallel to the flow. The tangential and radial components of particle velocity were evaluated from motion pictures and compared with predictions given by Lamb's solution for Oseen flow. Good agreement was obtained between theory and experiment, which adds credibility to the theoretical calculation of collection efficiencies for slow flows.

A general review of the literature on electrified filters has been given by Davies (20).

In this section the work of these authors is extended. Collection efficiencies are calculated for the capture of fine, inertialess particles on a single, circular cylinder in a gaseous flow field by the combined influences of electrical forces and gravity. The two electrical forces considered are the force between a charged particle and a charged collector, hereafter referred to as the coulombic force, and the force on a charged particle in the presence of a neutral collector by a uniform external electric field directed at an arbitrary angle to the flow.

Mathematical Model

Equations of motion

The equation of motion for a spherical particle of radius R_p and density ρ_p is given by

$$\frac{4}{3}\pi R_p^3 \rho_p \frac{d\underset{\sim}{v}}{dt} = -(6\pi\mu R_p/C)(\underset{\sim}{v} - \underset{\sim}{u}) + \sum_e \underset{\sim}{F}_e \qquad (1)$$

where $\underset{\sim}{v}$ is the particle velocity, $\underset{\sim}{u}$ the local mean fluid velocity, and the $\underset{\sim}{F}_e$'s the electrical and gravitational forces on the particle. In using Equation 1, it is assumed that the particle Reynolds number is very small and the acceleration of displaced fluid and unsteady contributions to the Stokes drag force are negligible (27). Using the collector radius R_c and undisturbed free-stream velocity U_o to make Equation 1 dimensionless gives the Stokes number, $K \equiv 2C\rho_p U_o R_p^2/9\mu R_c$, as the inertial parameter on the left hand side of Equation 1. This study considers motions in which particle inertia is negligible ($K = 0$) so that Equation 1 reduces to

$$\underset{\sim}{V} = \underset{\sim}{U} + \sum_e K_e \underset{\sim}{f}_e \qquad (2)$$

where K_e is a dimensionless characteristic particle mobility corresponding to $\underset{\sim}{F}_e$, which has dimensionless spatial dependence $\underset{\sim}{f}_e$. The coordinate system is shown in Figure 40, with the flow always from left to right.

For any two-dimensional, steady, incompressible flow, the fluid velocity field $\underset{\sim}{U}$ can be written in terms of the stream function,

$$U_r \equiv \frac{1}{R}\frac{\partial \Psi_f}{\partial \theta}, \quad U_\theta \equiv -\frac{\partial \Psi_f}{\partial R} \qquad (3)$$

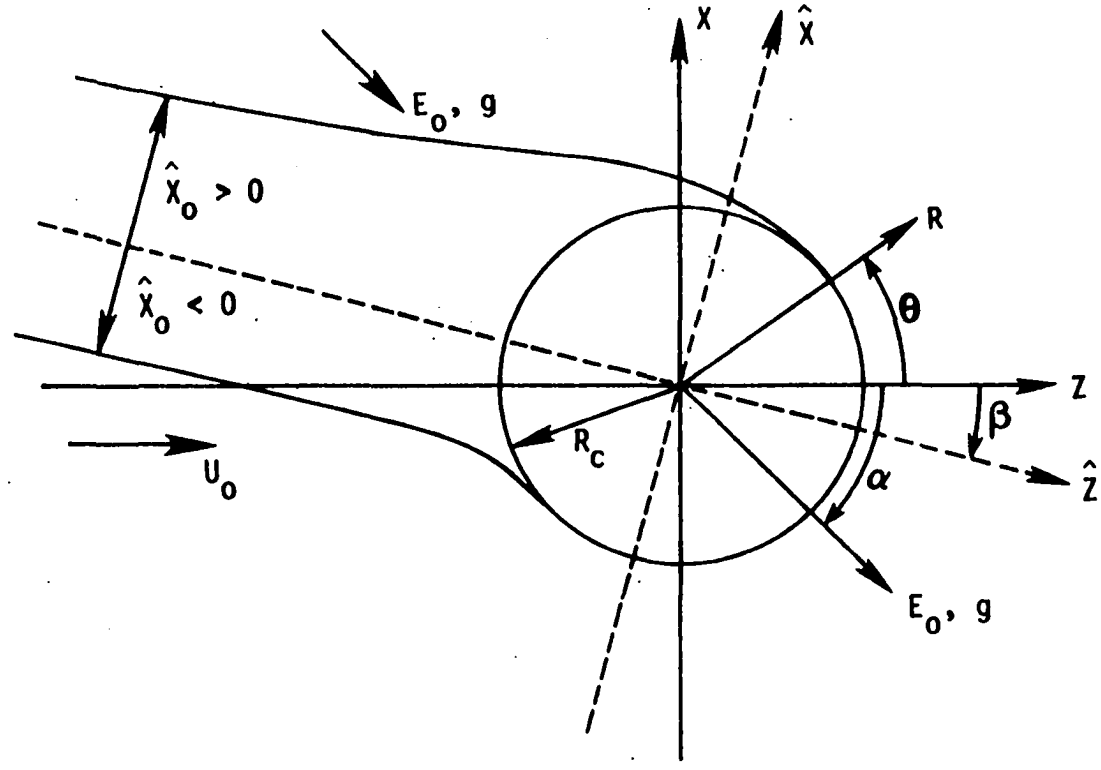

Figure 40. Coordinate system for mathematical model of particle collection by a circular cylinder of radius R_c

(Limiting trajectories are shown for external electric field force with $\alpha = -45^o$, $K_{ex} = 0.5$ in potential flow, case 1)

where dimensionless variables have been used, $U_r = u_r/U_o$, $U_\theta = u_\theta/U_o$, $\Psi_f = \psi_f/R_c U_o$. This study is concerned primarily with symmetrical flows possessing a stream function, with potential flow (zero vorticity), Lamb's solution for Oseen flow (small collector Reynolds number), and uniform flow considered as specific examples. The dimensionless fluid velocities and stream functions for these flows are given in Table 52. Streamlines are shown in Figure 41 for potential flow and Figure 42 for Oseen flow with Re = 0.1. The so-called generalized description encompasses potential flow ($h_2 = -1$) and uniform flow, with $h_0 = 1$ and other h's not mentioned equal to zero; for Lamb's solution for Oseen flow we define

$$h(R) = (\ln R^2 + 1/R^2 - 1)/2s \qquad (4)$$

Since Lamb's solution is an inner solution valid only in the vicinity of the cylinder, in finding initial conditions at infinite distances upstream, Lamb's solution is matched with an outer solution that approaches uniform flow, with the constant value of Ψ_f for a given streamline remaining the same through the matching process (110).

The dimensionless forces are expressed in terms of radial and polar components as $K_e \underset{\sim}{f}_e = K_e(f_e^r \underset{\sim}{a}_r + f_e^\theta \underset{\sim}{a}_\theta)$, with the parameters K_e and force components f_e^r and f_e^θ given in Table 53 for the coulombic force, the external electric field force, and the gravitational force. In

Table 52. Circular cylinder dimensionless fluid velocities and stream functions

POTENTIAL FLOW

$$U_r = \cos\theta\,(1 - 1/R^2)$$

$$U_\theta = -\sin\theta\,(1 + 1/R^2)$$

$$\Psi_f = R\sin\theta\,(1 - 1/R^2)$$

LAMB'S SOLUTION FOR OSEEN FLOW

$$U_r = \cos\theta\,(\ln R^2 + 1/R^2 - 1)/2s$$

$$U_\theta = -\sin\theta\,(\ln R^2 - 1/R^2 + 1)/2s$$

$$\Psi_f = R\sin\theta\,(\ln R^2 + 1/R^2 - 1)/2s$$

$$s = \ln 8 + \tfrac{1}{2} - Eu - \ln Re$$

UNIFORM FLOW

$$U_r = \cos\theta$$

$$U_\theta = -\sin\theta$$

$$\Psi_f = R\sin\theta$$

"GENERALIZED" FLOW

$$U_r = \cos\theta \sum_{m=0}^{\infty} h_m R^{-m} = h(R)\cos\theta$$

$$U_\theta = -\sin\theta \sum_{m=0}^{\infty} (1 - m)h_m R^{-m}$$

$$\Psi_f = R\sin\theta\, h(R);\ h_0 = 1$$

TOMOTIKA AND AOI STATIONARY-VORTEX FLOW (APPROXIMATE EXPRESSION)

$$U_r = \cos\theta\,(\ln R^2 + 1/R^2 - 1)/2s + Re\,R(1 - 2\sin^2\theta)\,[\ln R^2 - 2s(1 - 1/R^4)]/16s$$

$$U_\theta = -\sin\theta\,(\ln R^2 - 1/R^2 + 1)/2s - Re\,R\sin\theta\cos\theta\,[\ln R^2 - 2s(1 + 1/R^4) + 1]/8s$$

$$\Psi_f = R\sin\theta\,(\ln R^2 + 1/R^2 - 1)/2s + Re\,R^2\sin\theta\cos\theta\,[\ln R^2 - 2s(1 - 1/R^4)]/16s$$

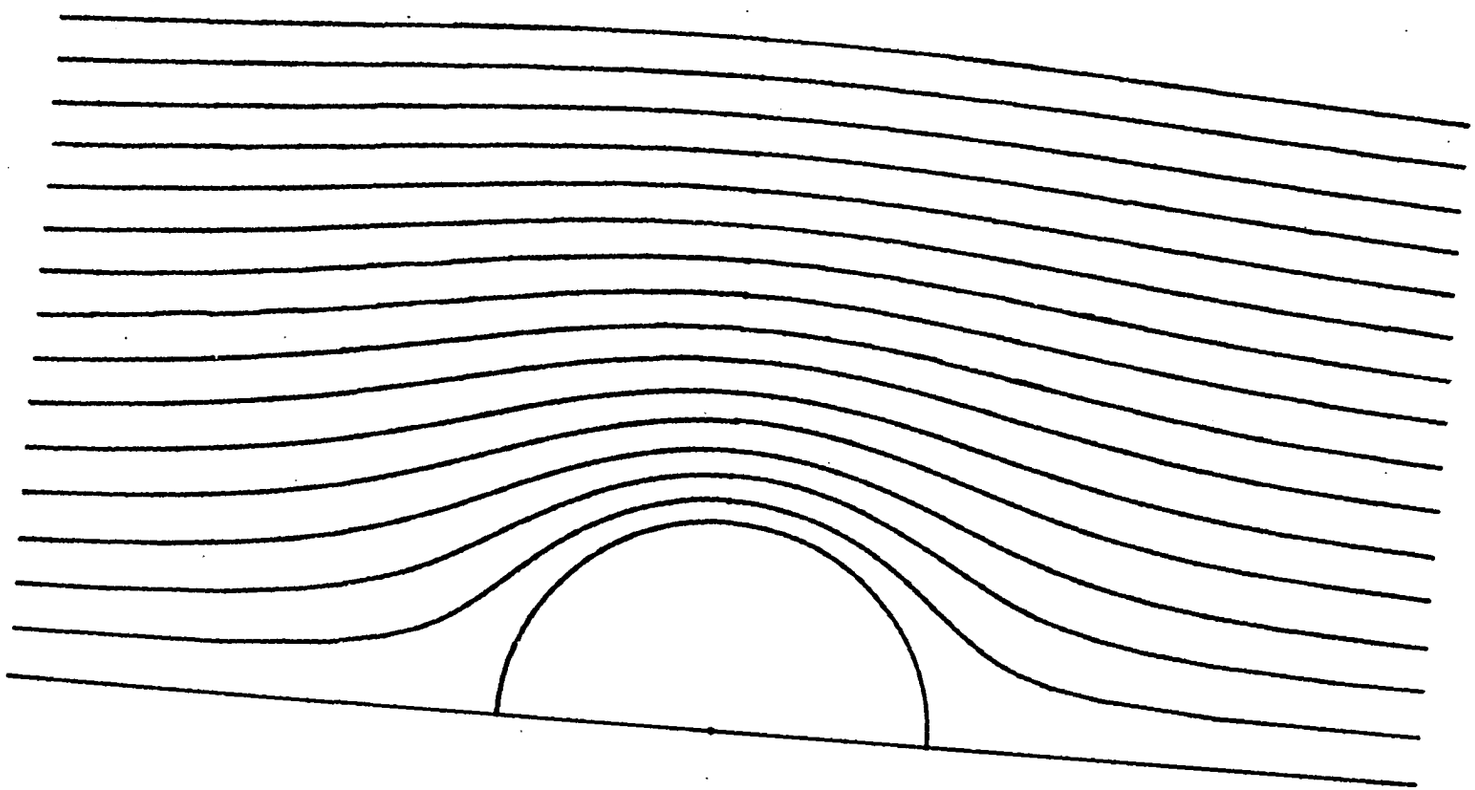

Figure 41. Potential flow streamlines for a circular cylinder

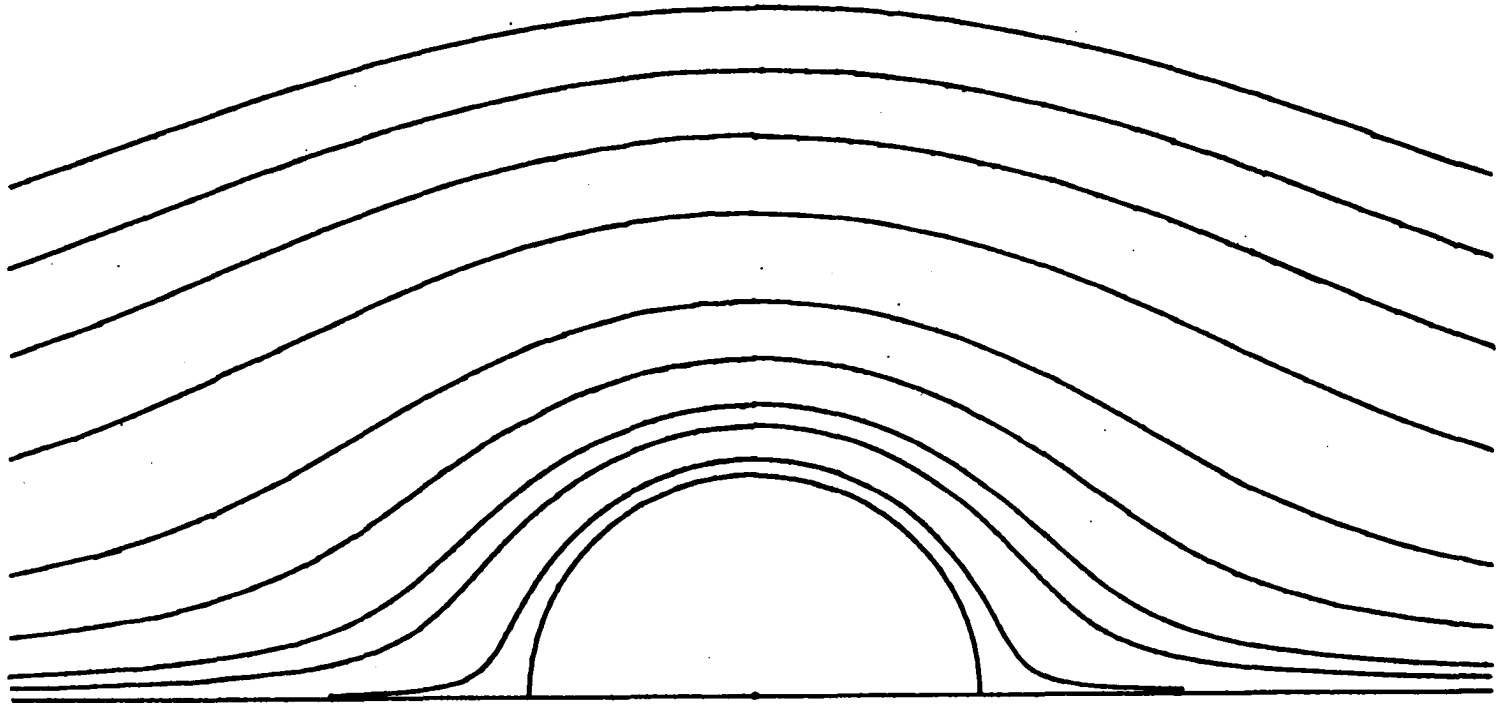

Figure 42. Oseen flow streamlines for a circular cylinder, with Re = 0.1

Table 53. Circular cylinder force expressions

CHARGED-COLLECTOR AND CHARGED-PARTICLE (COULOMBIC) FORCE

$$K_c = \rho_c Q_p C/12\pi^2 \epsilon_f R_c R_p \mu U_o$$

$$f_c^r = 1/R$$

$$f_c^\theta = 0$$

$$\Psi_c = K_c \theta$$

EXTERNAL ELECTRIC FIELD FORCE

$$K_{ex} = Q_p E_o C/6\pi\mu R_p U_o$$

$$f_{ex}^r = (1 + \Upsilon/R^2) \cos(\theta - \alpha)$$

$$f_{ex}^\theta = -(1 - \Upsilon/R^2) \sin(\theta - \alpha)$$

$$\Psi_{ex} = K_{ex} R(1 + \Upsilon/R^2) \sin(\theta - \alpha)$$

$$\Upsilon \equiv (\epsilon_c - \epsilon_f)/(\epsilon_c + \epsilon_f)$$

GRAVITATIONAL FORCE

$$K_g = 2R_p^2 \rho_p g C/9\mu U_o$$

$$f_g^r = \cos(\theta - \alpha)$$

$$f_g^\theta = -\sin(\theta - \alpha)$$

$$\Psi_g = K_g R \sin(\theta - \alpha)$$

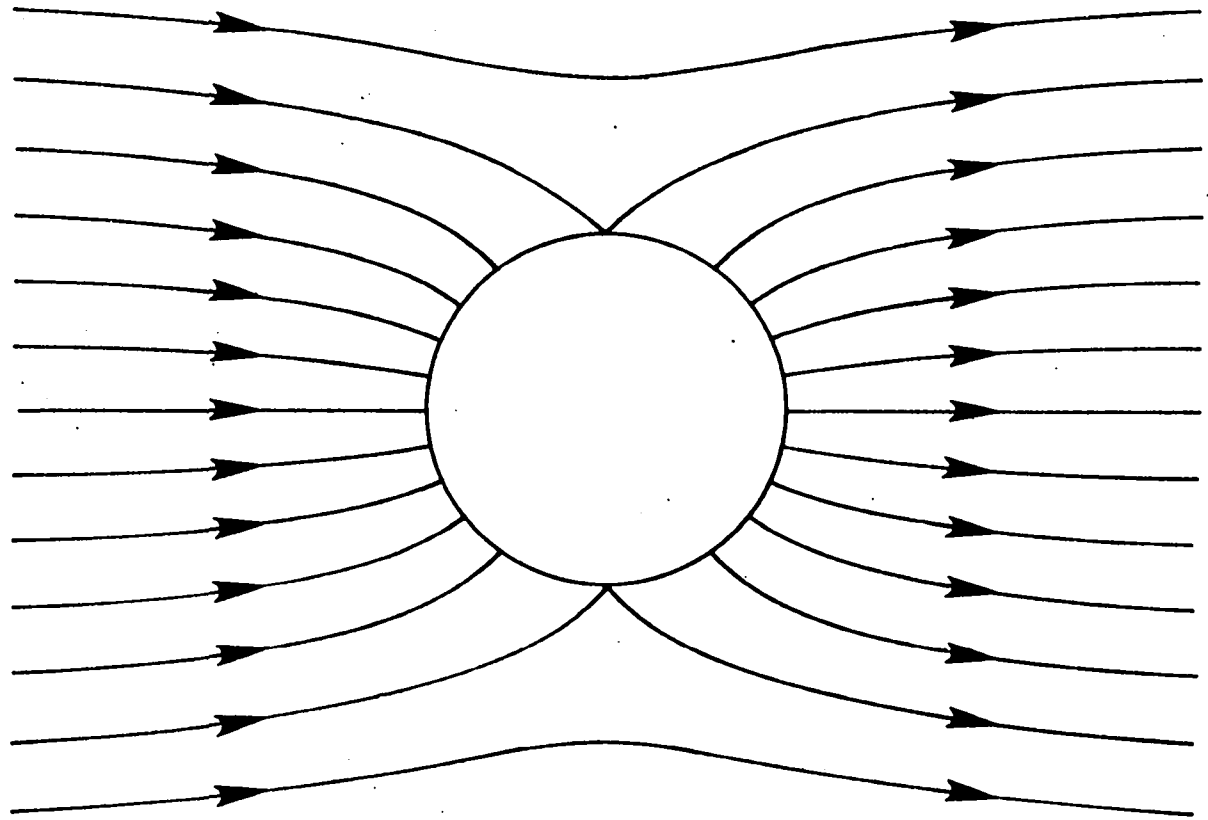

Figure 43. External electric field lines of force for a circular cylinder

Table 53, $\Upsilon \equiv (\epsilon_c - \epsilon_f)/(\epsilon_c + \epsilon_f)$ is the polarization coefficient of the collector. The uniform external electric field and gravity are parallel to each other and directed at an arbitrary angle to the free-stream velocity. E_o and g are considered positive when the Z components of the uniform fields are in the same direction as U_o. The external electric field force lines are shown in Figure 43. The force is attractive on one half of the collector but repulsive on the other half, like the gravitational force. The coulombic force is radial and falls off in intensity as 1/R.

The initial condition for the determination of particle trajectories from Equation 2 is that $V_z = 1 + (K_{ex} + K_g)\cos\alpha$ and $V_x = (K_{ex} + K_g)\sin\alpha$ far upstream.

Collection efficiencies

In this section the efficiency of particle collection is defined as the ratio of the cross-sectional area perpendicular to the particle paths far upstream from which all particles of a given size are collected, to the cross-sectional area of the collector. When the external electric field or gravity is not parallel to the flow, the particle paths far upstream are at an angle β to the flow direction and the particle trajectories are not symmetric (see Figure 40). Therefore, the collection efficiency must be expressed in terms of two limiting trajectories for particle collection. Particles having trajectories within the limiting

trajectories will be collected, but particles on trajectories outside the limiting trajectories will not be collected. In order to express the collection efficiency in terms of the limiting trajectories, it is useful to consider a rotated coordinate system $\hat{Z}$, $\hat{X}$, centered at the cylinder, where the angle between the $\hat{Z}$-axis and the flow direction is β. At distances far upstream the particle paths are parallel to the $\hat{Z}$-axis and are designated by their initial displacement coordinate, $\hat{X}_o$. The collection efficiency, $\hat{\eta}$, is then $\hat{\eta} \equiv (\hat{X}_{i+} - \hat{X}_{i-})/2$, where $\hat{X}_{i+}$ is the dimensionless initial displacement from the $\hat{Z}$-axis of the limiting trajectory most positive in $\hat{X}_o$, and $\hat{X}_{i-}$ is the same but for the limiting trajectory most negative in $\hat{X}_o$.

The efficiency just defined is the total collection efficiency. The deposition density function $S(\theta)$ is the local collection efficiency at the location θ on the cylinder and is evaluated from the derivative of Equation 17 with respect to θ. The total collection efficiency is given by

$$\hat{\eta} = \tfrac{1}{2} \int_{\theta_{i+}}^{\theta_{i-}} S(\theta)\, d\theta \qquad (5)$$

where $S(\theta)$ is zero at locations where no particle collection occurs.

When the trajectory of the center of a particle does not intersect the collector but passes within a distance of one particle radius, the particle will still collide with

the collector due to its finite size. This is the mechanism of collection by particle interception.

Solution for the Trajectory Equation

The approach used to solve Equation 2 for a combination of the coulombic force, external electric field force, and gravitational force depends upon the fact that the forces $\underset{\sim}{f}_e$ and the fluid motion $\underset{\sim}{U}$ are solenoidal with respect to particle position coordinates ($\underset{\sim}{\nabla} \cdot \underset{\sim}{U} = \underset{\sim}{\nabla} \cdot \underset{\sim}{f}_e = 0$). Because $\underset{\sim}{U}$, $\underset{\sim}{f}_e$, and consequently, $\underset{\sim}{V}$ are solenoidal vector fields and the system is two-dimensional, stream functions for the fields exist, which give the vector field components by Equation 3 with obvious changes in nomenclature. The stream function Ψ for particle trajectories is given by superposition as

$$\Psi = \Psi_f + \Psi_c + \Psi_{ex} + \Psi_g \tag{6}$$

where Ψ_c, Ψ_{ex}, and Ψ_g are taken from Table 53. This technique has been used previously by Nielsen and Hill (81) and Whipple and Chalmers (130) in studying the influence of electrical forces on particle capture by spherical droplets dispersed in an air stream. To illustrate the method, the generalized flow description given in Table 52 will be used.

Since Ψ is constant along a particle trajectory, the upstream or initial value Ψ_o is used to evaluate the left hand side of Equation 6. In the limit as $Z \rightarrow -\infty$, $h(R) \rightarrow 1$

and $\theta \to \beta + \pi$; using $X = R\sin\theta$, $Z = R\cos\theta$ gives

$$\Psi_o = \lim_{Z\to-\infty}\{X[1 + (K_{ex} + K_g)\cos\alpha] - Z(K_{ex} + K_g)\sin\alpha\} + K_c(\beta + \pi) \tag{7}$$

At this point it is convenient to use the rotated coordinate system, $\hat{Z}$, $\hat{X}$, that is at an angle β to the Z, X coordinate system

$$X = \hat{Z}\sin\beta + \hat{X}\cos\beta,\quad Z = \hat{Z}\cos\beta - \hat{X}\sin\beta \tag{8}$$

to give

$$\Psi_o = \lim_{Z\to-\infty}\hat{X}[\cos\beta + (K_{ex} + K_g)\cos(\beta - \alpha)] + \lim_{Z\to-\infty}\hat{Z}[\sin\beta + (K_{ex} + K_g)\sin(\beta - \alpha)] + K_c(\beta + \pi) \tag{9}$$

The value of β can be found from the initial condition on the particle velocity. At distances far upstream, particle paths are rectilinear with rectangular velocity components $V_z = 1\ (K_{ex} + K_g)\cos\alpha$ and $V_x = (K_{ex} + K_g)\sin\alpha$, so that

$$|\underset{\sim}{V}| = [1 + 2(K_{ex} + K_g)\cos\alpha + (K_{ex} + K_g)^2]^{\frac{1}{2}} \equiv G \tag{10}$$

The radial components of the particle velocity far upstream are

$$V_r = \cos\theta + (K_{ex} + K_g)\cos(\theta - \alpha) \tag{11}$$

$$V_\theta = -\sin\theta - (K_{ex} + K_g)\sin(\theta - \alpha)$$

For the particle trajectory far upstream that lies along the $\hat{Z}$-axis, $V_\theta = 0$ and $V_r = -G$, so that particles along this trajectory have $\theta = \beta + \pi$. From this, $\sin\beta$ and $\cos\beta$ are found to be

$$\begin{aligned} \sin\beta &= [(K_{ex} + K_g)\sin\alpha]/G \\ \cos\beta &= [1 + (K_{ex} + K_g)\cos\alpha]/G \end{aligned} \tag{12}$$

Substituting these quantities into Equation 9 gives

$$\Psi_o = \hat{X}_o G + K_c(\beta + \pi) \tag{13}$$

Therefore, the particle trajectory is completely defined by the relation

$$\hat{X}_o = [R\,h(R)\sin\theta + R\,p(R)\sin(\theta - \alpha) + K_c(\theta - \pi - \beta)]/G \tag{14}$$

where

$$p(R) = K_{ex}(1 + \gamma/R^2) + K_g \tag{15}$$

$$\beta = \tan^{-1}\left(\frac{(K_{ex} + K_g)\sin\alpha}{1 + (K_{ex} + K_g)\cos\alpha}\right) \tag{16}$$

The condition for impaction is $R = 1 + \mathcal{R} \equiv R^*$, where $\mathcal{R} \equiv R_p/R_c$ is the interception parameter.

Limiting Trajectories and Collection Efficiencies

Analysis of Equation 14 reveals two types of limiting trajectories, whose occurrence depends upon the relative magnitudes and signs of the forces, the orientation of the external electric field and gravity with respect to the flow direction, and interception. The first type of limiting trajectory will be called a grazing limiting trajectory, because a particle following it merely grazes the surface of the collector. Point particles graze the collector at a point where the radial force at the surface changes from attraction to repulsion. The existence of such a point, however, does not mean that a limiting trajectory necessarily impacts there. With interception a grazing limiting trajectory can occur even if the radial force is entirely attractive or repulsive over the surface of the collector. The second type of limiting trajectory will be called a nodal limiting trajectory, since it ends at a velocity node, which is a point located away from the surface of the collector where the particle velocity goes to zero. At the nodal point, the drag force on the particle is exactly opposed by the electrical and gravitational forces. The existence of the velocity node can only be determined using Equation 2 and Tables 52 and 53.

Since the collection efficiency is computed from two limiting trajectory values, the existence of two types of

limiting trajectories creates three types of particle collection behavior. In the first case there are two grazing limiting trajectories, in the second case two nodal limiting trajectories ending at the same particle velocity node, and in the third case both types of limiting trajectories are present.

In the analysis that follows, α is restricted to the range $-\pi/2 \leq \alpha \leq 0$, and K_{ex} and K_g are both positive.

Case 1: Two grazing limiting trajectories

At impaction $R = 1 + \mathcal{R} \equiv R^*$, and Equation 14 becomes

$$\hat{X}_o = [R^*(H + P\cos\alpha)\sin\theta - R^*P\sin\alpha\cos\theta + K_c(\theta - \pi - \beta)]/G \tag{17}$$

where $H \equiv h(R^*)$ and $P \equiv p(R^*)$. For $\mathcal{R} << 1$, $H = 2\mathcal{R}$ for potential flow, $H = 2\mathcal{R}^2$ for Oseen flow, and $P = (1 + \gamma)K_{ex} + K_g$. The grazing limiting trajectory values of $\hat{X}_o$ correspond to a relative maximum and relative minimum in $\hat{X}_o(\theta, R^*)$. The angular location at impaction of either of the limiting trajectories will be denoted by θ_m; in particular, θ_{m+} will correspond to $\hat{X}_{i+}$ and θ_{m-} to $\hat{X}_{i-}$. The two values of θ_m can be found from

$$G\, d\hat{X}_o/d\theta = 0 = R^*(H + P\cos\alpha)\cos\theta_m + R^*P\sin\theta_m + K_c \tag{18}$$

Solving for $\cos\theta_m$ and $\sin\theta_m$ yields

$$\cos\theta_{m\pm} = R^*[-K_c(H + P\cos\alpha) \mp P\sin\alpha(A - K_c^2)^{1/2}]/A \equiv W_{\pm} \qquad (19)$$

or, equivalently,

$$\sin\theta_{m\pm} = R^*[-K_c P\sin\alpha \pm (H + P\cos\alpha)(A - K_c^2)^{1/2}]/A \equiv Y_{\pm} \qquad (20)$$

$$A \equiv R^*[(H + P\cos\alpha)^2 + P^2\sin^2\alpha] \qquad (21)$$

where the top signs correspond to θ_{m+} and the bottom signs correspond to θ_{m-}. The values of $\hat{X}_i$ for the grazing limiting trajectories are given by

$$\hat{X}_{i\pm} = \hat{X}_o(\theta_{m\pm}) = [\pm(A - K_c^2)^{1/2} + K_c(\theta_{m\pm} - \pi - \beta)]/G \qquad (22)$$

$0 \le K_c \le A^{1/2}$: $\theta_{m+} = \cos^{-1}W_+$ $\quad 0 \le \theta_{m+} \le 180^\circ$

$\theta_{m-} = \pi - \sin^{-1}Y_-$ $\quad 90^\circ \le \theta_{m-} \le 270^\circ$

$-A^{1/2} \le K_c \le 0$: $\theta_{m+} = \sin^{-1}Y_+$ $\quad -90^\circ \le \theta_{m+} \le 90^\circ$

$\theta_{m-} = 2\pi - \cos^{-1}W_-$ $\quad 180^\circ \le \theta_{m-} \le 360^\circ$

subject to the condition $-A^{1/2} \le K_c \le A^{1/2}$. The collection efficiency is readily calculated as $\hat{\eta} = (\hat{X}_{i+} - \hat{X}_{i-})/2$.

For point particles ($R = 0$), the expressions given above simplify, since $P = P_0 \equiv (1 + \gamma)K_{ex} + K_g$ and $H = H_0 \equiv h(1)$. Furthermore, for $H_0 = 0$, $A = P_0^2$ and $\hat{\eta}$ is given by

$$\hat{\eta} = \{(P_0^2 - K_c^2)^{1/2} - K_c[\pi - \cos^{-1}(-K_c/P_0)]\}/G \qquad (23)$$

for $-P_0 \leq K_c \leq P_0$. Notice that due to the symmetry of the collector, the orientation of the electric field only affects the value of G in Equation 23. For potential and Oseen flows, $H_0 = 0$ and the influence of the velocity field disappears: θ_{m+}, θ_{m-}, $\hat{x}_{i+}$, $\hat{x}_{i-}$, $\hat{\eta}$, and $S(\theta)$ are the same for both flows. These results are quite surprising, considering the differences in behavior of the two flows. Further consideration of Equations 6 and 13 reveals that when this case is applicable, the results for $S(\theta)$ and $\hat{\eta}$ hold for any flow for which $\Psi_f = 0$ (the stagnation streamline) on the surface of the collector, including even stationary, recirculating vortex motions. This insensitivity of the collection to the form of the flow is similar to that found by Nielsen and Hill (81) for collection on spherical droplets.

Considering only the external electric field and gravitational forces ($K_c = 0$), point particles ($R = 0$), and flows with $H_0 = 0$, Equation 19 reduces to $\cos\theta_{m\pm} = \pm \sin\alpha$ or $\theta_{m\pm} = \alpha + \pi \pm \pi/2$, with collection occurring over the attractive half of the collector. The collection efficiency is

$$\hat{\eta} = \frac{(1 + \gamma)K_{ex} + K_g}{[1 + 2(K_{ex} + K_g)\cos\alpha + (K_{ex} + K_g)^2]^{\frac{1}{2}}} \qquad (24)$$

The efficiency $\hat{\eta}$ is a minimum when the external and flow fields are aligned ($\alpha = 0$) and increases with angle of separation to a maximum when the external and flow fields are perpendicular ($\alpha = -90^\circ$). Notice that Equation 24

predicts a maximum value of $\hat{\eta} = 2$ for a perfectly conducting collector. With the external electric field force alone and $\alpha = 0$, $\hat{\eta} = (1 + \gamma)K_{ex}/(1 + K_{ex})$, a result found by Zebel (133).

An interesting situation arises with potential flow and $K_c = \alpha = 0$, because for $K_{ex} = 1/\gamma$ the collection efficiency is not affected by particle inertia. For these conditions Equation 1 becomes

$$K \frac{dV_z}{dT} + V_z = 1 + K_{ex} + K_g + (1 - \gamma K_{ex})(X^2 - Z^2)/R^4 \qquad (25)$$

$$K \frac{dV_x}{dT} + V_x = -(1 - \gamma K_{ex})2ZX/R^4 \qquad (26)$$

and it can be seen that if $K_{ex} = 1/\gamma$, the viscous drag on the particle is exactly opposed by the electrical force, the particle velocity remains constant, and the collection efficiency is given by $\hat{\eta} = 1 + R$ for all values of the Stokes number.

For the external electric field force alone, Figure 44 shows trajectories when E_o is perpendicular to U_o ($\alpha = -90^o$) in potential flow and the limiting trajectories for Oseen flow. The particle trajectories with Oseen flow only begin to approach conditions at infinity at a considerable distance upstream. Limiting trajectories for potential flow and $\alpha = -45^o$ are shown in Figure 40. The reader is referred to the paper by Zebel (133) for trajectories with E_o and U_o

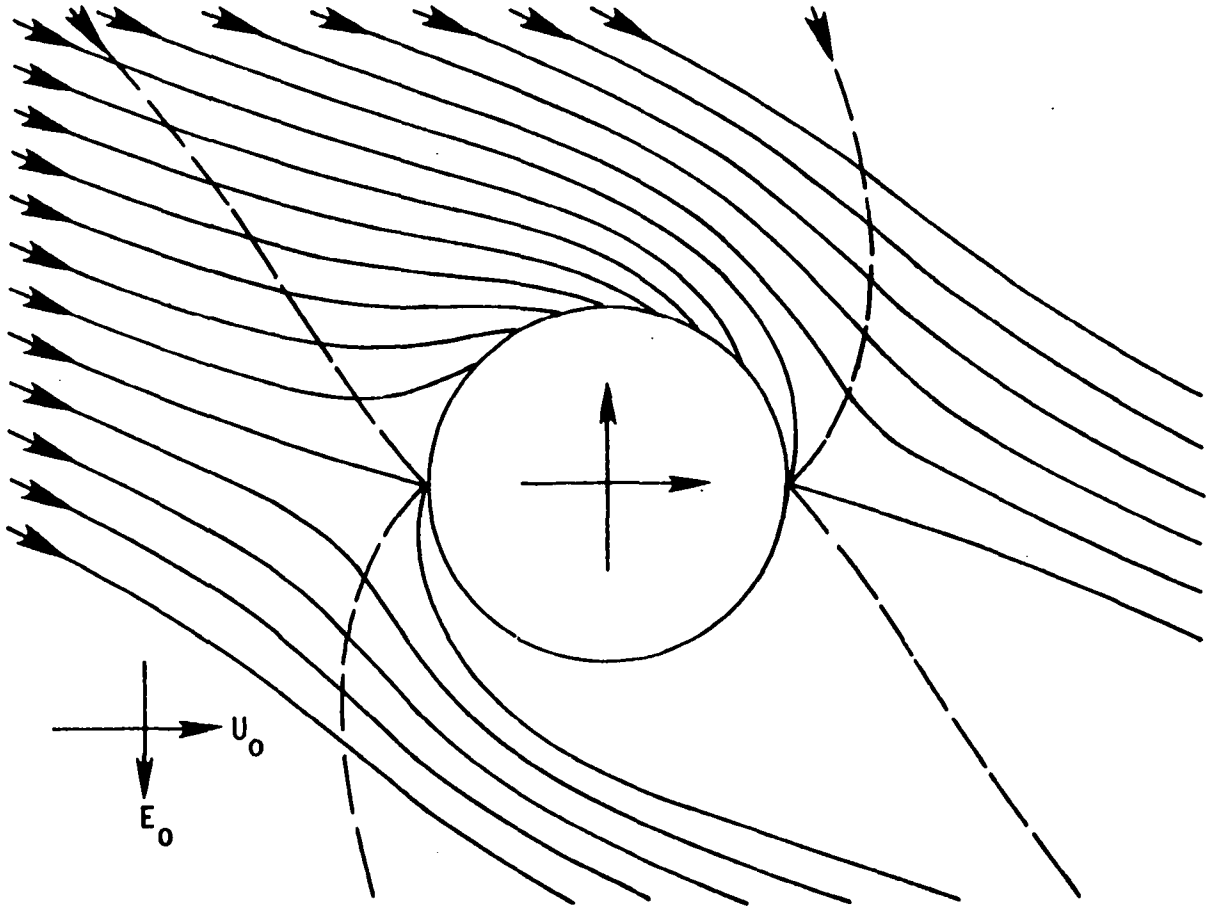

Figure 44. Particle trajectories with an external electric field force in potential flow (solid lines) and limiting trajectories for Oseen flow (dashed lines), with $\alpha = -90^o$, $K_{ex} = 0.5$, $Y = 1.0$, and $Re = 0.1$ (case 1)

aligned.

Case 1 occurs whenever $-A^{\frac{1}{2}} \leq K_c \leq A^{\frac{1}{2}}$ and a particle velocity node does not exist. However, when a velocity node does exist and $-A^{\frac{1}{2}} \leq K_c \leq A^{\frac{1}{2}}$, it is possible that either case 2 or case 3 applies, particularly when the external electric field and the gravitational field are directed perpendicular to the flow. Case 1 may continue to apply when interception is important. Criteria for determining the applicable case are given after case 3.

Case 2: Two nodal limiting trajectories

With $K_c > A^{\frac{1}{2}}$, there are only repulsive forces at the collector surface, and particles do not approach the collector close enough for interception to occur. In this case $\hat{\eta} = 0$ and the two limiting trajectories do not exist, although they could be considered to be coincident and to end at the velocity node located upstream from the collector.

With $K_c < -A^{\frac{1}{2}}$, both limiting trajectories end at the same velocity node located downstream from the collector. There are only attractive forces at the collector surface, but particles following the limiting trajectories do not approach the collector close enough for interception to occur before they reach the velocity node. Let θ_{i+} be the limiting value of the angular location at impaction of particles following a trajectory that lies just within and

approaches being the limiting trajectory corresponding to $\hat{X}_{i+}$, and let θ_{i-} be the analogous value corresponding to $\hat{X}_{i-}$. For the two nodal limiting trajectories present, the values of θ_{i+} and θ_{i-} correspond to the same location on the collector surface and are related by $\theta_{i-} = \theta_{i+} + 2\pi$. Therefore, it is not necessary to find values for $\hat{X}_{i+}$ and $\hat{X}_{i-}$ in computing $\hat{\eta}$. The collection efficiency is found directly to be

$$\hat{\eta} = \frac{-\pi K_c}{[1 + 2(K_{ex} + K_g)\cos\alpha + (K_{ex} + K_g)^2]^{\frac{1}{2}}} \qquad (27)$$

A remarkable feature of Equation 27 is that $\hat{\eta}$ is independent of the flow field and interception. For the coulombic force alone $\hat{\eta} = -\pi K_c$ for all flows considered, provided $1 + \mathcal{R} \leq R_n$, where R_n is the radial coordinate of the velocity node. This result was found by Kraemer (48) and Natanson (79).

Figure 45 shows trajectories for the coulombic force with potential flow. The corresponding trajectories for Oseen flow are similar, but with trajectories generally displaced further from the collector and approaching the surface at a greater angle. Although the flows differ, the distribution of particle collection is the same. In the vicinity of the velocity node, particle trajectories are very sensitive to small changes in $\hat{X}_o$, acting almost as if particles are "repelled" by the node.

So far K_{ex} has been restricted to positive values with

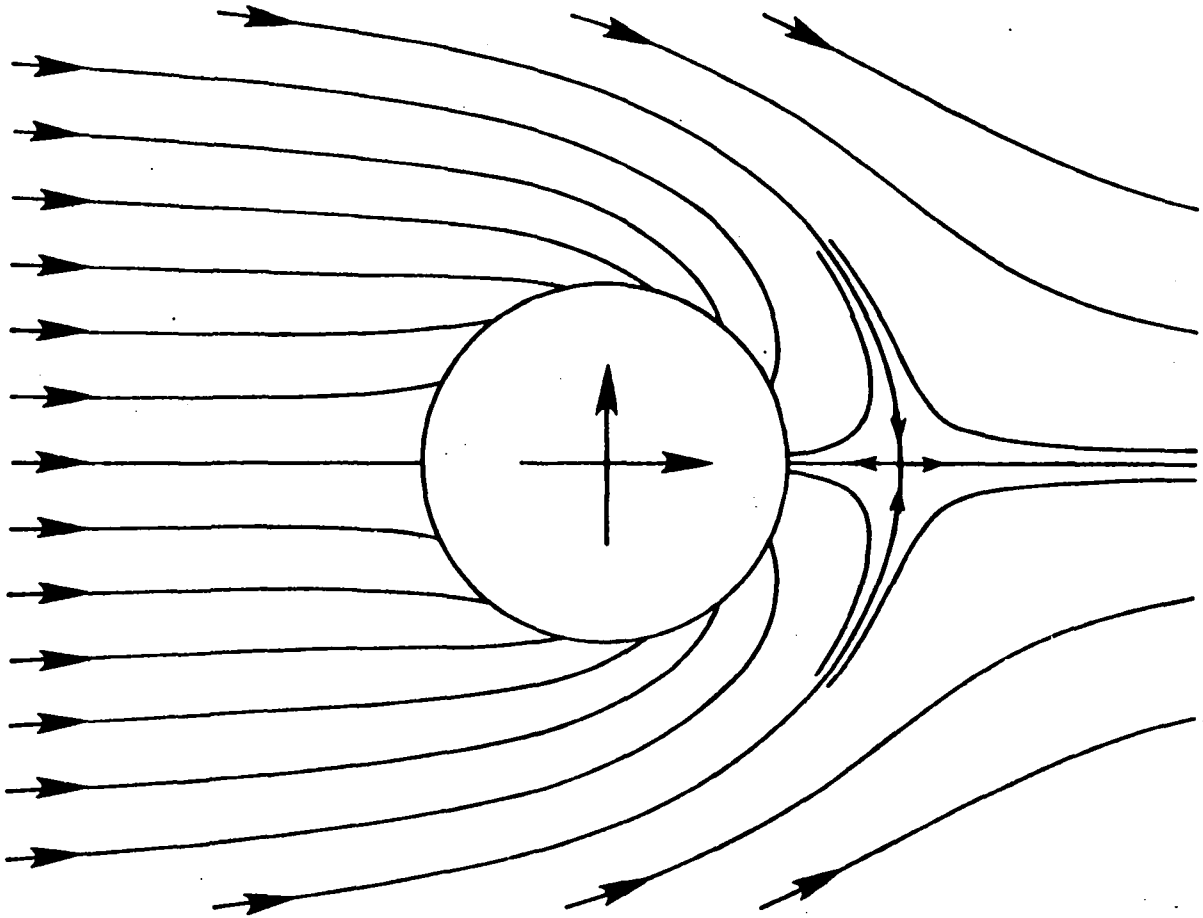

Figure 45. Particle trajectories for an attractive coulombic force with $K_c = -1.0$ in potential flow (case 2)

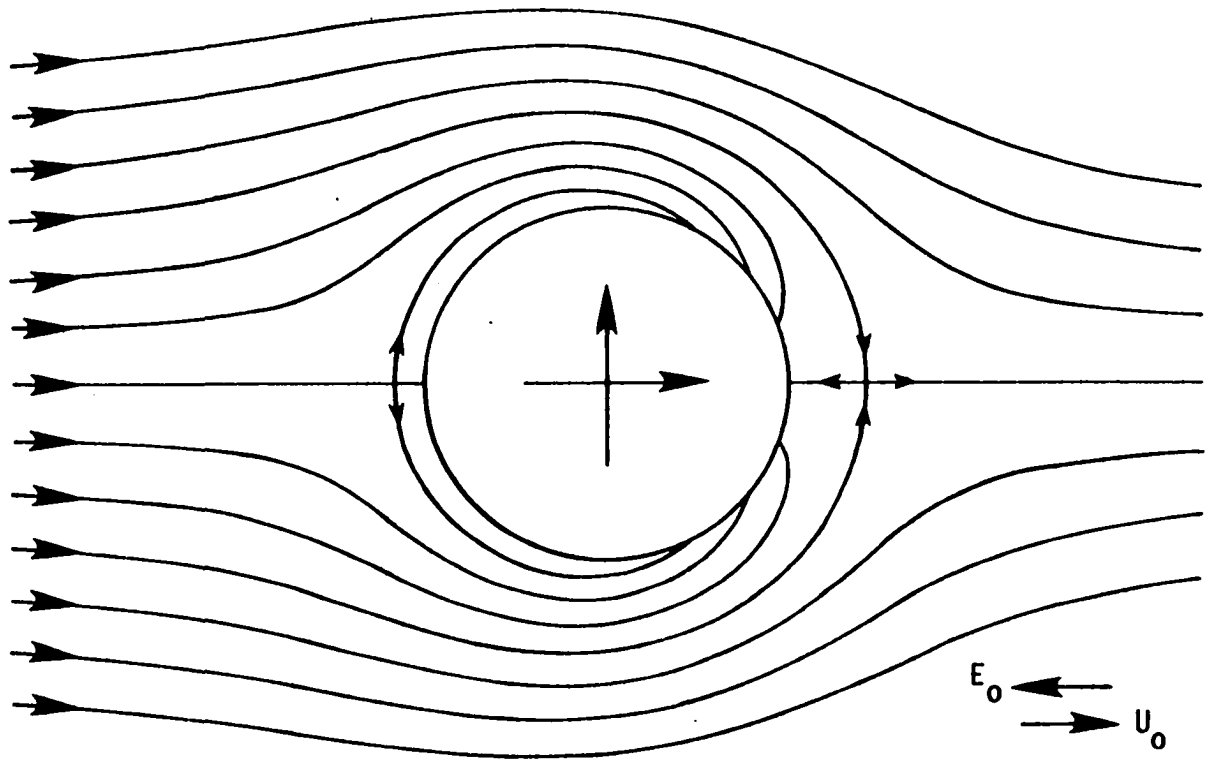

Figure 46. Particle trajectories for combined coulombic and external electric field forces in potential flow, with $\alpha = 0$, $K_{ex} = -0.25$, $K_C = -0.2$, and $\Upsilon = 1.0$ (case 2)

$-90^{\circ} \leq \alpha \leq 0$. However, some interesting and potentially useful features appear with $-1 < K_{ex} < 0$ and $\alpha = 0$ that warrant special consideration. Under these conditions the external electric field is aligned with the flow but it opposes the motion of the particle; the particle velocity far upstream, as given by $1 + K_{ex}$, is less than the free-stream velocity. This condition is advantageous, however, when an attractive coulombic force is present, for then the efficiency, as given by $\hat{\eta} = -\pi K_c/(1 + K_{ex})$, is increased over what it would be if K_{ex} were positive or zero. This case is illustrated in Figure 46. For the particular conditions chosen, collection occurs exclusively on the downstream portion of the collector in the region $-60^{\circ} \leq \theta \leq 60^{\circ}$. The layer void of particles has been noted previously by Zebel (133) and is similar to that illustrated for spheres by Nielsen and Hill (81).

When only the opposing external electric field is present, for symmetrical flows the collector is surrounded by a cylindrical surface that has $V_r = 0$. This creates a layer void of particles about the collector surface. For Oseen flow, an unusual feature under these conditions is the existence of a vortex point within this layer at $\theta = \pm 90^{\circ}$. If particles were present within this layer, they would describe ellipsoidal trajectories centered at the vortex point. Hochrainer, et al., (39) have experimentally verified the existence of such closed particle orbits by

suddenly switching on the electrical field when a particle is near the vortex point location.

With $-A^{\frac{1}{2}} \leq K_c \leq 0$, it is also possible for both limiting trajectories to end at a particle velocity node, particularly when the external electric field is directed perpendicular to the flow. In this case both attractive and repulsive forces are present on the collector surface but $\hat{\eta}$ is still given by Equation 27. The criteria following case 3 should be consulted.

Case 3: One grazing and one nodal limiting trajectory

Case 3 can occur whenever $-A^{\frac{1}{2}} \leq K_c \leq A^{\frac{1}{2}}$, the external electric field and gravity are perpendicular or nearly perpendicular to the flow, and the coulombic force is present. A particle velocity node may arise from the external forces exactly opposing the drag force. With a repulsive coulombic force the limiting trajectory corresponding to $\hat{X}_{i-}$ ends at a velocity node upstream from the collector, while the limiting trajectory corresponding to $\hat{X}_{i+}$ grazes the collector. This situation is illustrated for potential flow in Figure 47. Notice that collection does not occur over the entire attractive force region and that under identical force conditions case 1 applies for Oseen flow (dashed-line limiting trajectories). Despite the different behaviors for the two flows, the value of $\hat{X}_{i+}$ is the same for both, although the values of $\hat{X}_{i-}$ are different. With an attractive coulom-

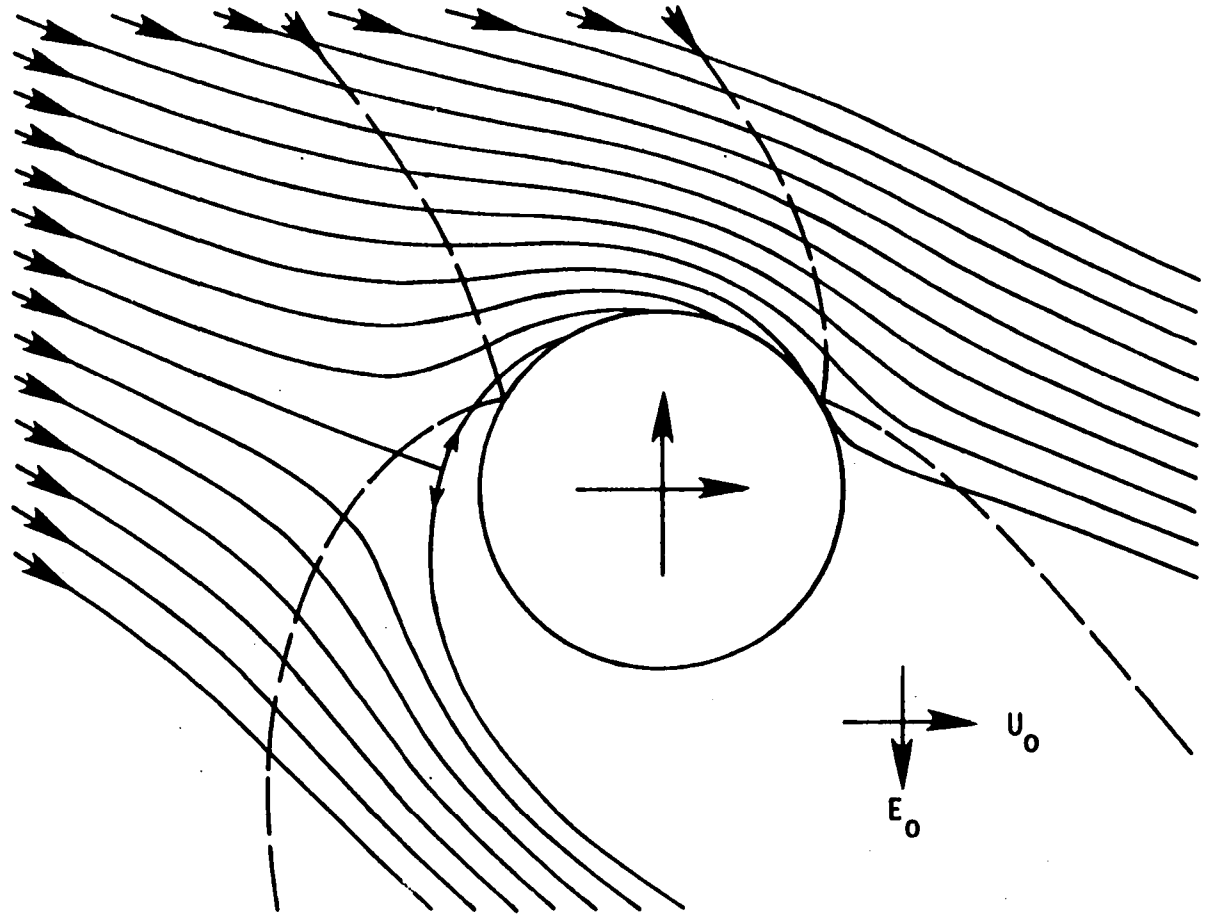

Figure 47. Particle trajectories for combined (repulsive) coulombic and external electric field forces in potential flow (solid lines, case 3) and limiting trajectories for Oseen flow (dashed lines, case 1), with $\alpha = -90^o$, $K_{ex} = 0.5$, $K_c = 0.5$, $\gamma = 1.0$, and $Re = 0.1$

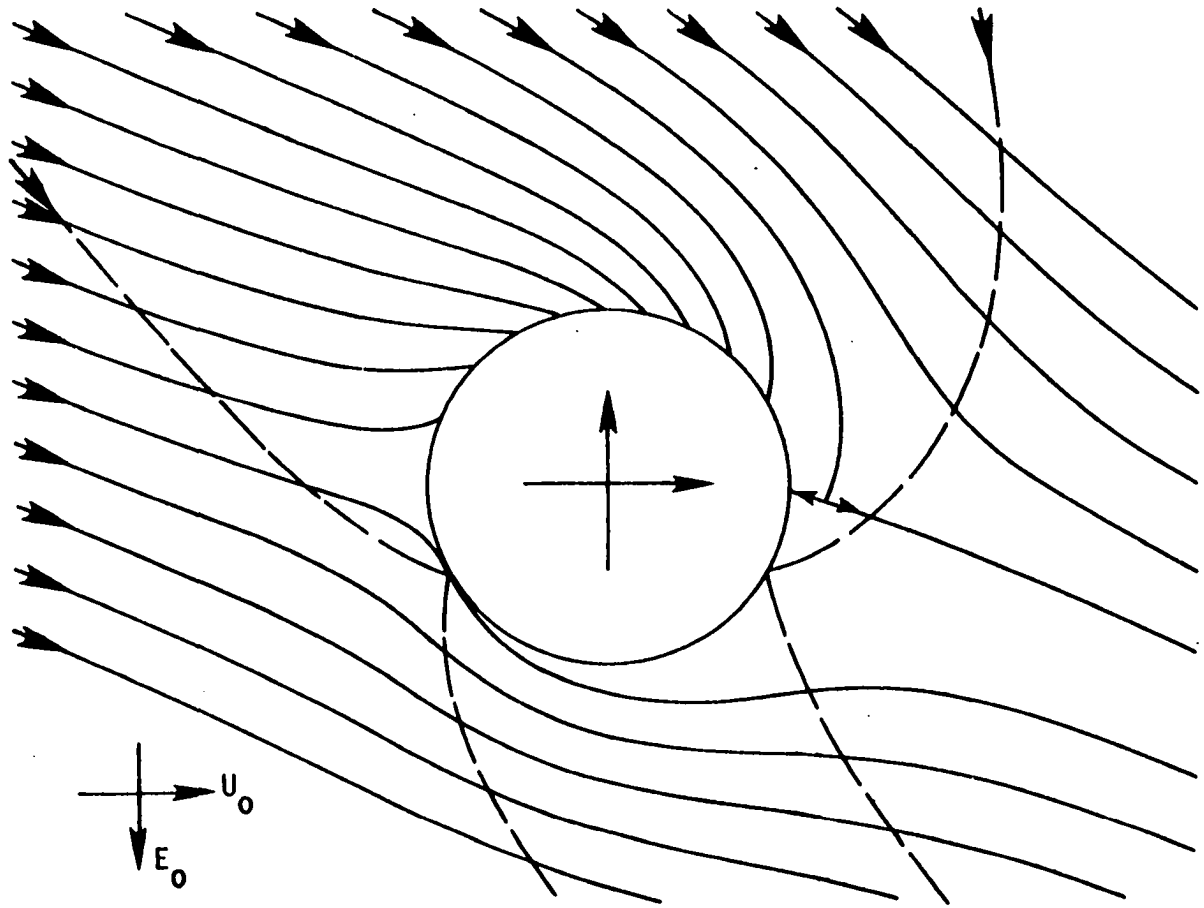

Figure 48. Particle trajectories for combined (attractive) coulombic and external electric field forces in potential flow (solid lines, case 3) and limiting trajectories for Oseen flow (dashed lines, case 1), with $\alpha = -90^o$, $K_{ex} = 0.5$, $K_c = -0.5$, $\Upsilon = 1.0$, and $Re = 0.1$

bic force the limiting trajectory corresponding to $\hat{X}_{i+}$ ends at a node downstream from the collector and the limiting trajectory corresponding to $\hat{X}_{i-}$ grazes the collector. This situation is illustrated in Figure 49. Criteria for determining if case 3 applies are given in the next section.

In order to calculate $\hat{\eta}$, it is necessary to determine the values of $\hat{X}_i$ for both types of limiting trajectories. Values of $\hat{X}_i$ were found in case 1, but it was not necessary to do so in case 2, so the problem of finding values of $\hat{X}_i$ for nodal limiting trajectories remains. Unfortunately, a solution using the general form of the flow field used for cases 1 and 2 is not known. In fact, an analytical solution using a specific flow field is only known for potential flow. Numerical methods must be utilized for Oseen and other flows of interest. Fortunately, a straightforward technique is available. By systematic means the angular and radial coordinates of the particle velocity node, θ_n and R_n, respectively, are determined using the relations $V_r = 0$ and $V_\theta = 0$. These values are then substituted into Equation 14 for the particle trajectory to yield $\hat{X}_i = \hat{X}_o(\theta_n, R_n)$.

The analytical solution for potential flow is possible because Equation 14 is then quadratic in R and the trajectory equation can be put into the explicit form $R = f(\hat{X}_o, \theta)$

$$R = [-B^* \pm (B^{*2} - 4A^*C^*)^{\frac{1}{2}}]/2A^* \qquad (28)$$

$$A^* \equiv [1 + (K_{ex} + K_g)\cos\alpha]\sin\theta - (K_{ex} + K_g)\sin\alpha\cos\theta \quad (29)$$

$$B^* \equiv -\hat{X}_o G + K_c(\theta - \pi - \beta) \quad (30)$$

$$C^* \equiv (\gamma K_{ex}\cos\alpha - 1)\sin\theta - \gamma K_{ex}\sin\alpha\cos\theta \quad (31)$$

where the correct sign depends upon the location of the particle along the trajectory. Examination reveals that for a given trajectory, Equation 28 has two real roots for R (that are greater than one) for a given value of $\dot{\theta}$ whenever θ is close to θ_n in value; i.e., the trajectory doubles backward in the vicinity of the velocity node. At the point of doubling back, $\dot{\theta}$ is at its minimum (or maximum) value for the trajectory, $V_\theta = 0$, and Equation 28 has a double root for R. The value of θ at this double root location will be denoted by θ_r. The double root of Equation 28 occurs when $B^{*2} - 4A^*C^* = 0$. This requirement gives the locus of values of θ_r for different trajectories as

$$\hat{X}_o(\theta_r) = [K_c(\theta_r - \pi - \beta) \pm 2(A^*C^*)^{1/2}]/G \quad (32)$$

where the plus sign is used if $K_c < 0$ and the minus sign is used if $K_c > 0$. It has been determined that the limiting trajectory corresponds to the maximum (or minimum) value of $\hat{X}_o(\theta_r)$, giving $\theta_r = \theta_n$ and $\hat{X}_i = \hat{X}_o(\theta_r = \theta_n)$. Therefore, θ_n can be found from

$$G\, d\hat{X}_o/d\theta_r = 0 = K_c \pm (A^*dC^*/d\theta_r + C^*dA^*/d\theta_r)/(A^*C^*)^{1/2} \quad (33)$$

In general, Equation 33 must be solved numerically for θ_n. For the special conditions of $K_g = 0$, $\alpha = -90^o$, and $Y = 1$, however, an analytical solution is possible, which gives

$$\sin\theta_n = -\{(\sigma/4 + 1)/2 - [(\sigma/4 + 1)^2 - K_{ex}{}^2\sigma]^{1/2}/2\}^{1/2} \equiv Y^* \quad (34)$$

$$\sigma \equiv K_c{}^2/(1 + K_{ex}{}^2)$$

$$\theta_{n+} = \sin^{-1}Y^* \text{ for } K_c < 0$$

$$\theta_{n-} = \pi + \sin^{-1}Y^* \text{ for } K_c > 0$$

In physical terms, the trajectory pattern of case 3 is intermediate to those of cases 1 and 2. With a constant external electric field perpendicular to a given flow field, the relative strength of the coulombic force governs which pattern occurs. For $K_c = 0$, the two grazing limiting trajectories of case 1 are present, as shown in Figure 44. When $|K_c|$ is increased from zero, transition to case 3 occurs due to separation of a velocity node from the surface of the collector, as shown in Figures 47 and 48. As K_c is made more positive, the remaining grazing limiting trajectory approaches the nodal limiting trajectory until merger and separation from the collector occurs, and collection ceases. When K_c is made more negative, the transition pattern shown in Figure 49 is reached. One limiting trajectory both grazes the upstream surface of the collector and ends at the same velocity node downstream as the other

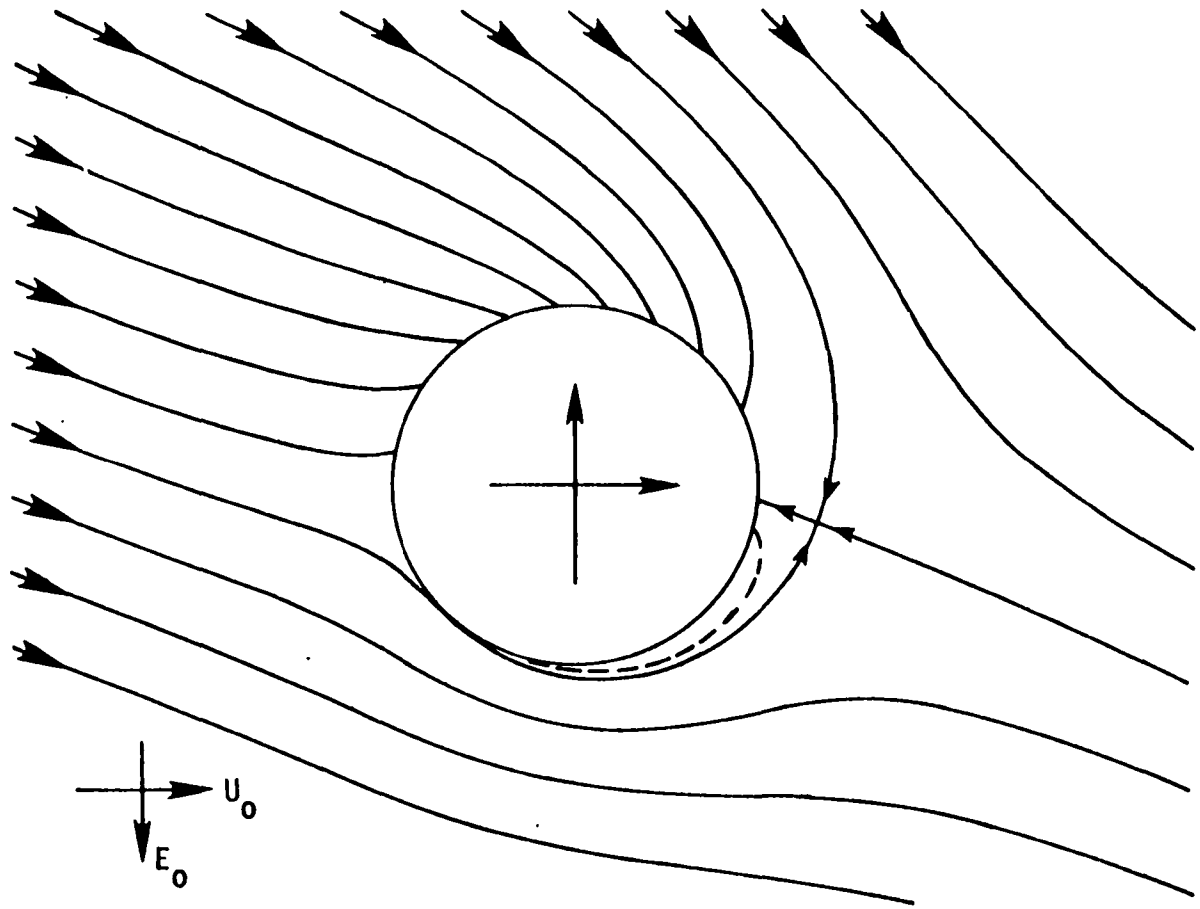

Figure 49. Particle trajectories for combined coulombic and external electric field forces in potential flow showing transition between cases 2 and 3, with $\alpha = -90^{o}$, $K_{ex} = 0.5$, $K_{c} = -0.75$, and $\Upsilon = 1.0$ (Dashed line is trajectory within layer void of particles)

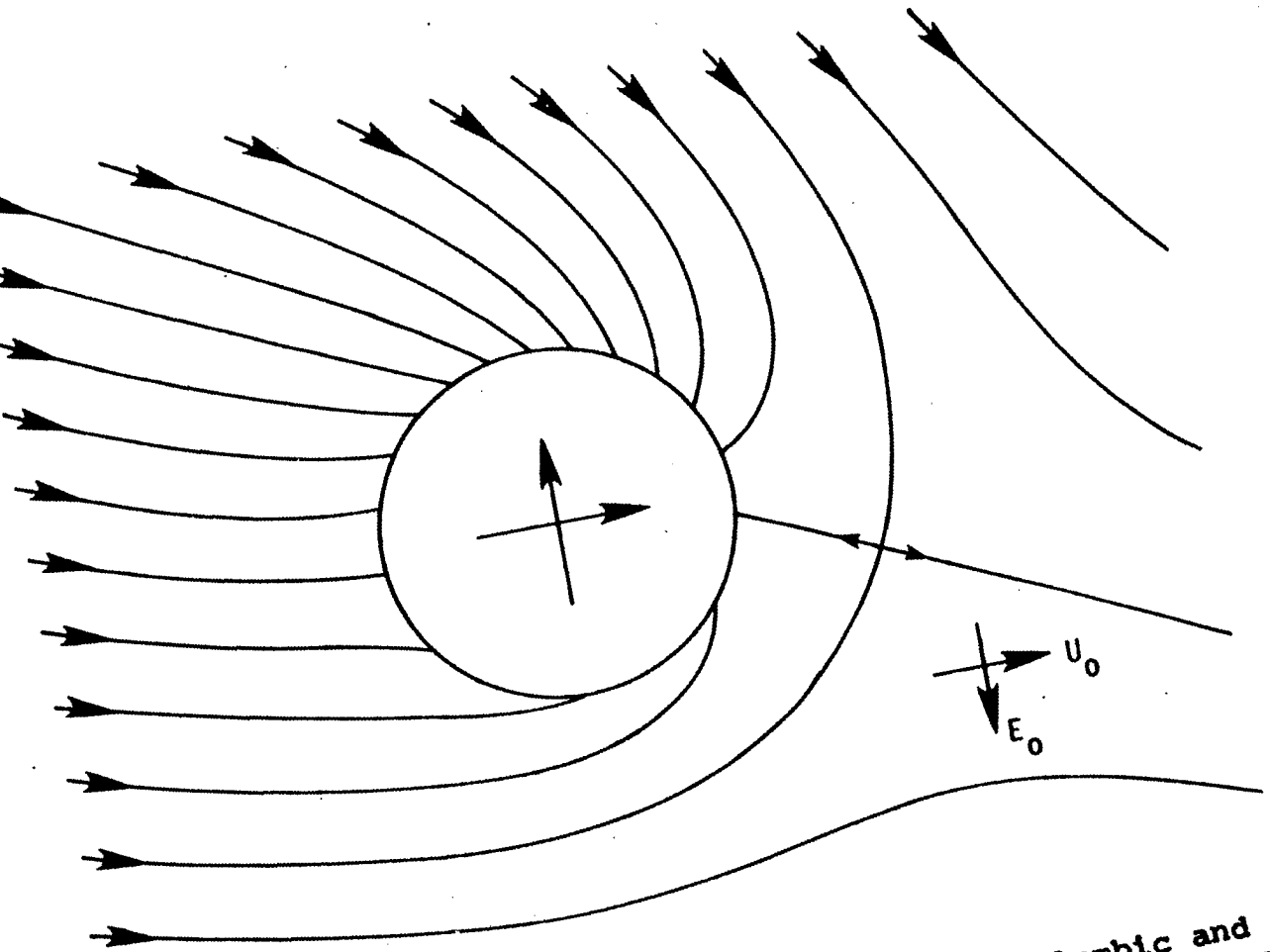

Figure 50. Particle trajectories for combined coulombic and external electric field forces in potential flow, with $\alpha = -90^o$, $K_{ex} = 0.5$, $K_c = -1.5$, and $\Upsilon = 1.0$ (case 2)

limiting trajectory. Figure 50 shows that for still larger $-K_c$, case 2 occurs with two nodal limiting trajectories. For examples of trajectories with E_o parallel to U_o, for which case 3 does not occur, the reader is referred to the paper by Hochrainer, et al., (39).

For case 1, it was found that the collection efficiency for point particles is the same for all flow fields having the same value of H_0. For case 2, it was found that $\hat{\eta}$ is the same for all of the flow fields considered. However, for case 3, there is no basis for concluding that the collection efficiency of point particles will be the same for flow fields having the same value of H_0. Indeed, calculations indicate that $\hat{\eta}$ does vary with the form of the flow. The value of $\hat{X}_i$ for the grazing limiting trajectory is independent of the flow, but the value of $\hat{X}_i$ for the nodal limiting trajectory changes with flow field.

Collection efficiency: Case criteria

When a velocity node is present and $-A^{1/2} \leq K_c \leq A^{1/2}$, no simple relation exists between K_c, K_{ex}, K_g, and $\mathcal{R}$ for determining which of the cases 1, 2, or 3 applies. Instead, it is necessary to compare the value of $\hat{X}_o(\theta_m)$, as determined from Equation 22, with the value of $\hat{X}_o(\theta_n)$, as determined from Equation 32 for potential flow or numerically from Equation 14 for other flows, to determine $\hat{X}_i$. Criteria for the cases in terms of K_c, A, $\hat{X}_o(\theta_m)$, and $\hat{X}_o(\theta_n)$ are:

1) For $K_c < -A^{1/2}$, case 2 always applies and $\hat{\eta}$ is given by Equation 27.

2) For $-A^{1/2} \leq K_c \leq 0$, any of the cases 1, 2, or 3 may apply. If there is no velocity node, case 1 always applies and $\hat{\eta}$ is given by Equation 22. If a velocity node is present, any of the cases may still apply: $\hat{X}_{i+} = \hat{X}_o(\theta_{n+})$ if $R_n > 1 + \mathcal{R}$, otherwise $\hat{X}_{i+} = \hat{X}_o(\theta_{m+})$; $\hat{X}_{i-}$ is the most negative of $\hat{X}_o(\theta_{m-})$ and $\hat{X}_o(\theta_{n-})$.

3) For $K_c = 0$, case 1 always applies and $\hat{\eta}$ is found from Equation 22 for $\mathcal{R} > 0$ or Equation 24 for $\mathcal{R} = 0$.

4) For $0 < K_c \leq A^{1/2}$, either case 1 or case 3 applies. If there is no velocity node, case 1 always applies and $\hat{\eta}$ is found from Equation 22. If a velocity node is present either case may still apply: $\hat{X}_{i-}$ is the least negative of $\hat{X}_o(\theta_{m-})$ and $\hat{X}_o(\theta_{n-})$ if $\theta_{m-} \leq \theta_{n-}$ ($R_n \geq 1 + \mathcal{R}$), or the most negative of $\hat{X}_o(\theta_{m-})$ and $\hat{X}_o(\theta_{n-})$ if $\theta_{m-} > \theta_{n-}$ ($R_n < 1 + \mathcal{R}$); $\hat{X}_{i+} = \hat{X}_o(\theta_{m+})$ always.

5) For $K_c > A^{1/2}$, $\hat{\eta} = 0$ always (case 2).

When the external fields and the flow are aligned ($\alpha = 0$), the criteria are much simpler, since case 3 does not occur. For $K_c < -A^{1/2}$ case 2 always applies; for $-A^{1/2} \leq K_c \leq A^{1/2}$ case 1 always applies; and for $K_c > A^{1/2}$ no collection occurs (case 2).

Deposition Density

When the interception parameter $\mathcal{R}$ is zero, the value of $\hat{X}_o$ for a trajectory intersecting the collector at the angular location θ is given by

$$\hat{X}_o = \{[(1+\Upsilon)K_{ex} + K_g]\sin(\theta - \alpha) + K_c(\theta - \pi - \beta)\}/G \qquad (35)$$

for all flows with $H_0 = 0$ over all θ for which collection occurs. This indicates that the local collection efficiency or deposition density $\mathcal{S}(\theta)$ in all three cases is independent of the flow (for point particles) over the range of θ in which collection occurs for all flows. This result is not in contradiction with the observation that for case 3 the collection efficiency, in particular the value of $\hat{X}_i$ for the nodal limiting trajectory, varies with the types of flow. It merely indicates that the area over which deposition occurs varies with the types of flow; i.e., the larger the collection efficiency the greater the area over which deposition occurs. A notable feature in case 3 is that collection does not occur over the entire region of attractive radial force at the surface.

For the coulombic force alone ($K_{ex} = K_g = \mathcal{R} = 0$), deposition occurs uniformly over the entire collector surface

$$\mathcal{S}(\theta) = -K_c \text{ for all } \theta \qquad (36)$$

It is interesting to note that the radial velocity at impac-

tion is also constant and equal to K_c. For the external electric field and gravity forces alone ($K_c = R = 0$) deposition occurs symmetrically with respect to $\theta = \alpha + \pi$ over half of the collector ($\alpha + \pi/2 \leq \theta \leq \alpha + 3\pi/2$)

$$S(\theta) = [(1 + \Upsilon)K_{ex} + K_g](\cos\alpha \sin\theta)/G \qquad (37)$$

With the external electric field parallel to the flow field, K_{ex} negative, and an attractive coulombic force, it is possible for all collection to occur exclusively on the downstream half of the collector (see Figure 46). The angle at which particles diverted from the stagnation streamline intersect the collector can be found from Equation 35 by setting $\hat{X}_o = \alpha = \beta = K_g = 0$. Therefore, for $0 < K_c/(1 + \Upsilon)K_{ex} \leq 2/\pi$ collection occurs only on the downstream half of the collector.

Particle Collection With Asymmetric Flows

The preceding results are useful in calculating collection efficiencies for symmetric flows (flows having the downstream half and upstream half as mirror images of each other). Because the flow is often not symmetric, it is of interest to learn how asymmetric flow affects collection, especially on the downstream half of the collector. Of particular interest is the effect of trailing, stationary, laminar vortex-rings, which are present for Reynolds numbers in the range 4-40 (114). Tomotika and Aoi (120) have

derived an exact solution for the stream function based on Oseen's linearized equations of motion. Approximate forms of the exact solutions for the stream function and flow velocity are given in Table 52. Although Tomotika and Aoi's expressions behave improperly, in that they give two standing eddies (although of very weak strength) even for very small Reynolds numbers, their expressions are useful as a model or simulation of stationary-vortex flows. They contain the essential features of actual vortex flow, and the Reynolds number can be used parametrically to adjust the size of the vortex to approximate that of the actual flow. The flow pattern given by the approximate form of the solution (for Re = 0.5) is shown in Figure 52b; the size of the vortex increases with increasing Reynolds number.

The approximate expression for the stationary-vortex flow stream function can be written in the form

$$\Psi_f = R \sin\theta[h(R) + Re\, m(R)\cos\theta] \qquad (38)$$

from which it can be seen that Ψ_f reduces to Oseen flow for small Reynolds numbers. Incorporating Equation 38 into Equation 6 and following the procedure established to find Equations 7 through 13 give an expression defining the particle trajectory that is similar to Equation 14, with obvious changes. Since for point particles $h(1) = m(1) = 0$, the results of case 1 and case 2 for $\hat{\eta}$ and $S(\theta)$ apply to the stationary vortex flow and the technique outlined in case 3

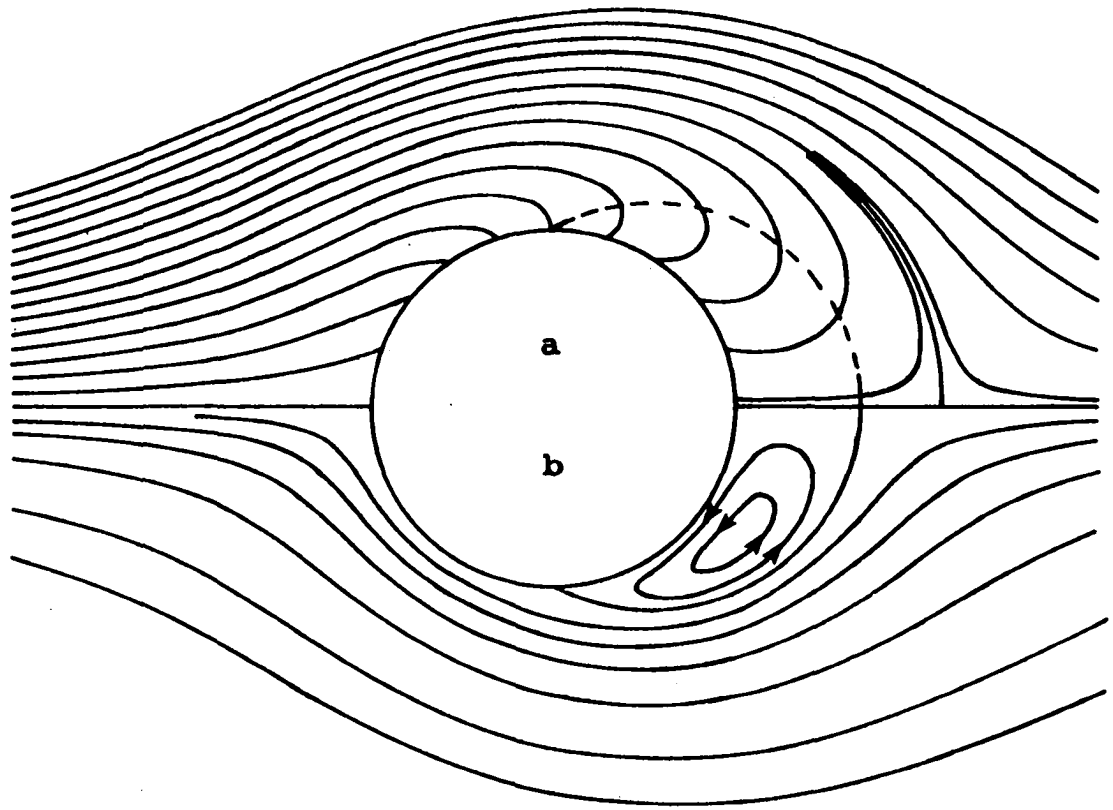

Figure 51. Particle trajectories for an attractive coulombic force with $K_C = -0.1$ (a) and corresponding flow streamlines (b) for particle capture from a stationary-vortex flow with Re = 0.5

for numerical solution of Oseen flow can be applied as well. The deposition density in case 3 is the same as for other flows considered having $H_0 = 0$. As with Oseen flow, the collection efficiency is independent of the Reynolds number.

As an illustration of particle behavior within the standing eddies, Figure 51a shows particle trajectories for the coulombic force with the flow in Figure 12b. The particles within the eddy follow the flow reversal, but the collection efficiency and deposition density remain the same as for Oseen flow and potential flow. The velocity node has shifted farther downstream, outside the eddy.

Particle Collection With Cellular Flows

Another flow pattern of interest is Kuwabara's (56) cellular model of flow through a filter. The model takes into account the influence of neighboring fibers but utilizes the Stokes approximation of a zero collector Reynolds number. Boundary conditions for the cellular flow around a single fiber are $U_r = \cos\theta$ with zero fluid vorticity at $R = L \equiv R_{cl}/R_c$, where R_{cl} is the radius of the outer surface of the cell; $U_r = U_\theta = 0$ at the surface of the collector. The ratio of cell radius to fiber radius, L, is related to α^*, the volume fraction of fibers (packing density) in the filter mat (20), by $L^2 = 1/\alpha^*$; the smaller the packing density the larger the equivalent cell radius. The stream

function is given by

$$\Psi_f = R\, h(R)\sin\theta \tag{39}$$

$$h(R) = a^*/R^2 + b^* + c^*\ln R + d^*R^2 \tag{40}$$

$$h(1) = 0,\ h(L) = 1 \tag{41}$$

$$a^* \equiv (1 - 1/2L^2)/2Ku \tag{42}$$

$$b^* \equiv -(1 - 1/L^2)/2Ku \tag{43}$$

$$c^* \equiv 1/Ku \tag{44}$$

$$d^* \equiv -1/4L^2Ku \tag{45}$$

$$Ku \equiv \ln L - 3/4 + 1/L^2 - 1/L^4 \tag{46}$$

Streamlines for Kuwabara flow are shown in Figure 52.

The stream function for particle trajectories is obtained by substituting Equation 39 into Equation 6. Because the flow field and hence the particle trajectories are only defined within the cell, solution for the limiting trajectories requires a generalization of the technique used for infinite flows. In particular, values of β and G cannot be defined because undisturbed conditions at infinity cannot be used. Instead, the limit $R \to L$, $\theta \to \theta_1$ $(\pi/2 \leq \theta_1 \leq 3\pi/2)$ is used to define the constant value of Ψ for a given particle trajectory

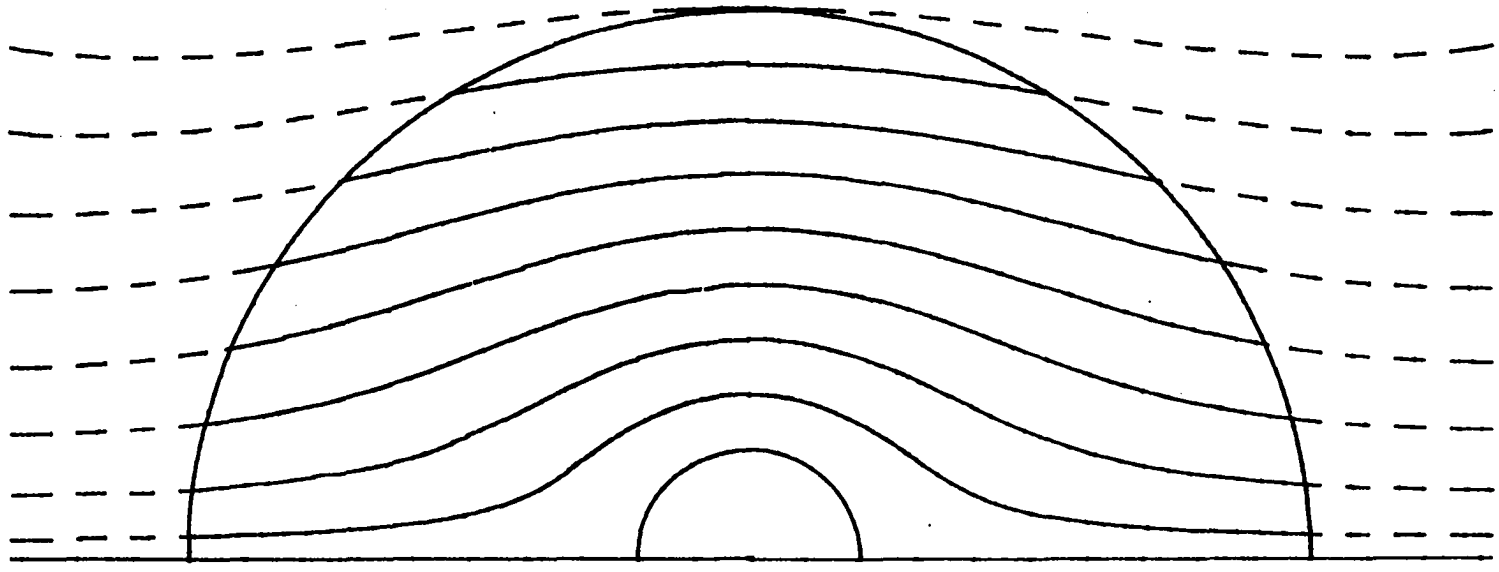

Figure 52. Kuwabara flow streamlines around a circular cylinder for L = 5. Dashed lines illustrate streamline behavior outside the flow cell, where the stream function is not defined

$$\Psi_1(\theta_1;L,\theta_1) = L\sin\theta_1 + L\,p(L)\sin(\theta_1 - \alpha) + K_c\,\theta_1 \qquad (47)$$

$$\Psi_1(\theta_1;R,\theta) = R\,h(R)\sin\theta + R\,p(R)\sin(\theta - \alpha) + K_c\,\theta \qquad (48)$$

The collection efficiency, η, is $\eta \equiv (X_{1i+} - X_{1i-})/2$, where $X_{1i\pm} = L\sin\theta_{1i\pm}$. Another measure of the efficiency, which is particularly useful for nonsymmetrical trajectories, is $\eta_1 = -(\theta_{1i+} - \theta_{1i-})/2\sin^{-1}(1/L)$. Values of $\theta_{1i\pm}$ are found by solving Equation 47, after identifying $\Psi_1(\theta_{1i\pm};L,\theta_{1i\pm}) = \Psi_1(\theta_{1i\pm};R^*,\theta_{1i\pm})$ from Equation 48. Values of Ψ_1 for the limiting trajectories can be found in the same manner as values of $\hat{X}_i$ were found for infinite flows.

For case 1, the grazing limiting trajectory values of Ψ_1 correspond to a relative maximum and relative minimum in $\Psi_1(\theta_1;R^*,\theta)$. Hence

$$\Psi_1(\theta_{1i\pm};R^*,\theta_{m\pm}) = \pm(A - K_c^{\,2})^{\frac{1}{2}} + K_c\theta_{m\pm} \qquad (49)$$

with $\theta_{m\pm}$ given by Equations 19 through 22. For point particles ($\mathcal{R} = 0$), the influence of the velocity field disappears and the same results are found for all stationary cellular flows having $h(1) = 0$ and $h(L) = 1$. With $K_c = 0$, the results can be expressed in simpler form. Equations 47 and 49 give

$$[1 + p(L)\cos\alpha]\,X_{1i\pm} - [p(L)\sin\alpha]\,Z_{1i\pm} = \pm A^{\frac{1}{2}} \qquad (50)$$

Using the rotated coordinate system $\hat{Z}_1$, $\hat{X}_1$, defined by

$$X_1 = \hat{Z}_1 \sin\phi + \hat{X}_1 \cos\phi, \quad Z_1 = \hat{Z}_1 \cos\phi - \hat{X}_1 \sin\phi \tag{51}$$

$$\sin\phi = [p(L)\sin\alpha]/B, \quad \cos\phi = [1 + p(L)\cos\alpha]/B \tag{52}$$

$$B \equiv [1 + 2p(L)\cos\alpha + p(L)^2]^{\frac{1}{2}} \tag{53}$$

reduces Equation 50 to

$$\hat{X}_{1i\pm} = \pm A^{\frac{1}{2}}/B \tag{54}$$

Values of $X_{1i\pm}$ can be found using Equation 51 and $L^2 = \hat{Z}_1^2 + \hat{X}_1^2$. Taking the limit $L \to \infty$, we find that $p(L) \to K_{ex} + K_g$, $B \to G$, $\phi \to \beta$, $\hat{X}_1 \to \hat{X}_o$, and the results found earlier for an infinite flow field are recovered. This also holds true for nonzero K_c. For point particles, Equation 54 reduces to

$$\hat{\eta}_1 = \frac{(1 + Y)K_{ex} + K_g}{[1 + 2p(L)\cos\alpha + p(L)^2]^{\frac{1}{2}}} \tag{55}$$

$$p(L) = (1 + Y/L^2)K_{ex} + K_g \tag{56}$$

and it is readily apparent that the packing density has little influence on the single fiber collection efficiency for large L.

For case 2, in general Equation 47 must be solved numerically for values of $\theta_{1i\pm}$ after identifying $\Psi_1(\theta_{1i\pm};L,\theta_{1i\pm}) = \Psi_1(\theta_{1i\pm};R_n,\theta_{n\pm})$ from Equation 48, where

$\theta_{n-} = \theta_{n+} + 2\pi$. For symmetrical trajectories ($\alpha = 0$), the equations reduce to

$$L \sin\theta_{1i+} [1 + p(L)] + K_c\theta_{1i+} = 0 \qquad (57)$$

with $\theta_{1i-} = 2\pi - \theta_{1i+}$. However, in the limit $\theta_{1i+} \rightarrow \pi$, the approximation $\theta_{1i+} = \pi - \sin\theta_{1i+}$ gives

$$\eta = -\pi K_c/[1 + p(L) - K_c/L] \qquad (58)$$

a result valid for large L or small efficiencies. Equation 58 shows that as long as $-K_c << L$, packing density has little effect on the collection efficiency. For the coulombic force alone, Stenhouse (116) has calculated collection efficiencies for Kuwabara flow by numerical integration of the particle trajectories. Comparison with values obtained from Equation 57 shows his efficiencies to be low by a few percent (for $K_c = -0.1$, η is given as 0.28 instead of 0.3010 for $\pi\alpha^*/4 = 0.15$ and as 0.30 instead of 0.3081 for $\pi\alpha^*/4 = 0.03$) and hence the influence of the packing density is exaggerated.

For case 3, θ_{1i} for the nodal limiting trajectory must be found numerically as outlined for case 2; θ_{1i} for the grazing limiting trajectory is found as described for case 1. Criteria for determining the appropriate case, when not otherwise obvious, are analogous to those given for the infinite flow case.

These results indicate that for these electrical forces

the single fiber collection efficiency decreases only slightly as the packing density increases from zero. It should be noted that collection by gravitation alone is unaffected by the packing density. For point particles, the collection efficiency and effect of packing density is the same under many conditions for all stationary cellular flows having $h(1) = 0$ and $h(L) = 1$. In this analysis, it has been assumed that the electric field about a fiber is not significantly affected by neighboring fibers, which is valid when the packing density is not high.

Formation of Chains of Adhesive Particles by Interception

It has been observed experimentally (20) that finite sized particles captured by filter fibers tend to build up chain aggregates rather than distribute themselves evenly over the surface of the fibers. In order to investigate this process, mathematical experiments were performed in which equal-sized particles, dispersed randomly but uniformly on the average in the flow field, were subjected to capture on a single fiber. The particle trajectories were given by Equation 14 using a potential flow field. The starting value, $\hat{X}_o$, for each particle was generated by a random number generator using a uniform probability distribution. Particle capture was considered to occur whenever an approaching particle intercepted a previously captured

particle or the surface of the collector; strong particle-particle and particle-surface adhesion was assumed. Particles not captured are swept downstream. In this simple model, only particle capture within a single plane is considered with the flow unaffected by captured particles.

An example of particle chain formation under conditions where particle interception is the only capture mechanism (no electrical forces) is shown in Figure 53. The collection efficiency for capture by the fiber alone, given by $\hat{\eta} = 2\mathcal{R}$ for $\mathcal{R} << 1$, is very small for small particles. At first, all particles in the flow tend to be swept downstream until one particle is finally captured by the surface of the collector. The efficiency modified by the first-captured particle's presence, given by $\hat{\eta}_p = 6\mathcal{R} \sin\theta_p$, where θ_p is the angular coordinate of the captured particle, is up to three times larger than $\hat{\eta}$ for the collector surface; hence a second particle is more likely to intercept the first-captured particle than the surface of the collector. Capture of the second particle by the first further enhances collection by the captured particles and a particle chain or cluster is formed. Additional particle capture by the surface, which will result in formation of a second chain, can only occur closer to the forward stagnation zone. The presence of a second chain will prevent particle capture at the base of the first chain, so that the first chain can only grow at branches farthest from the surface that face

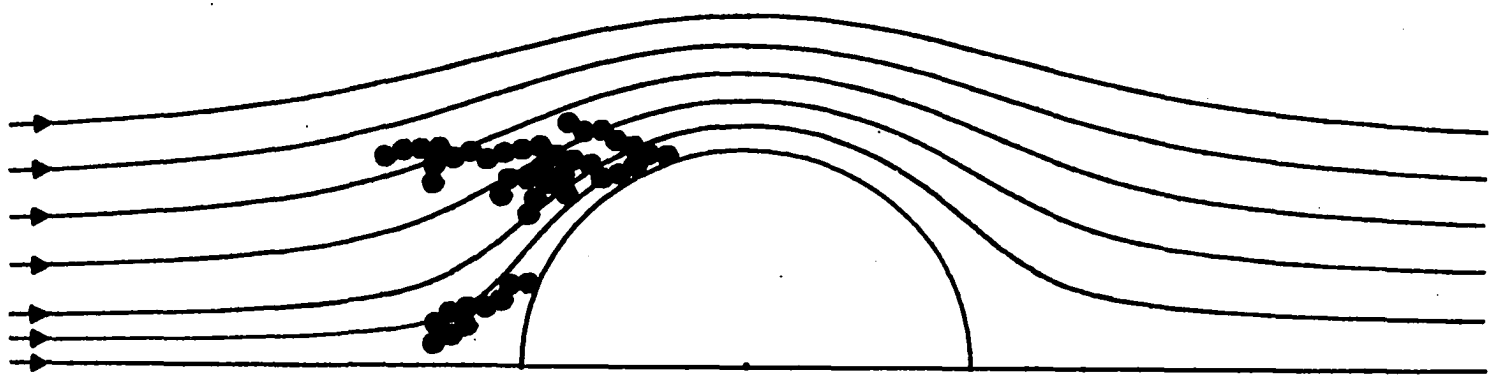

Figure 53. Particle chain formation by particle interception alone for potential flow, with $R = 0.04$. Solid lines are potential flow streamlines

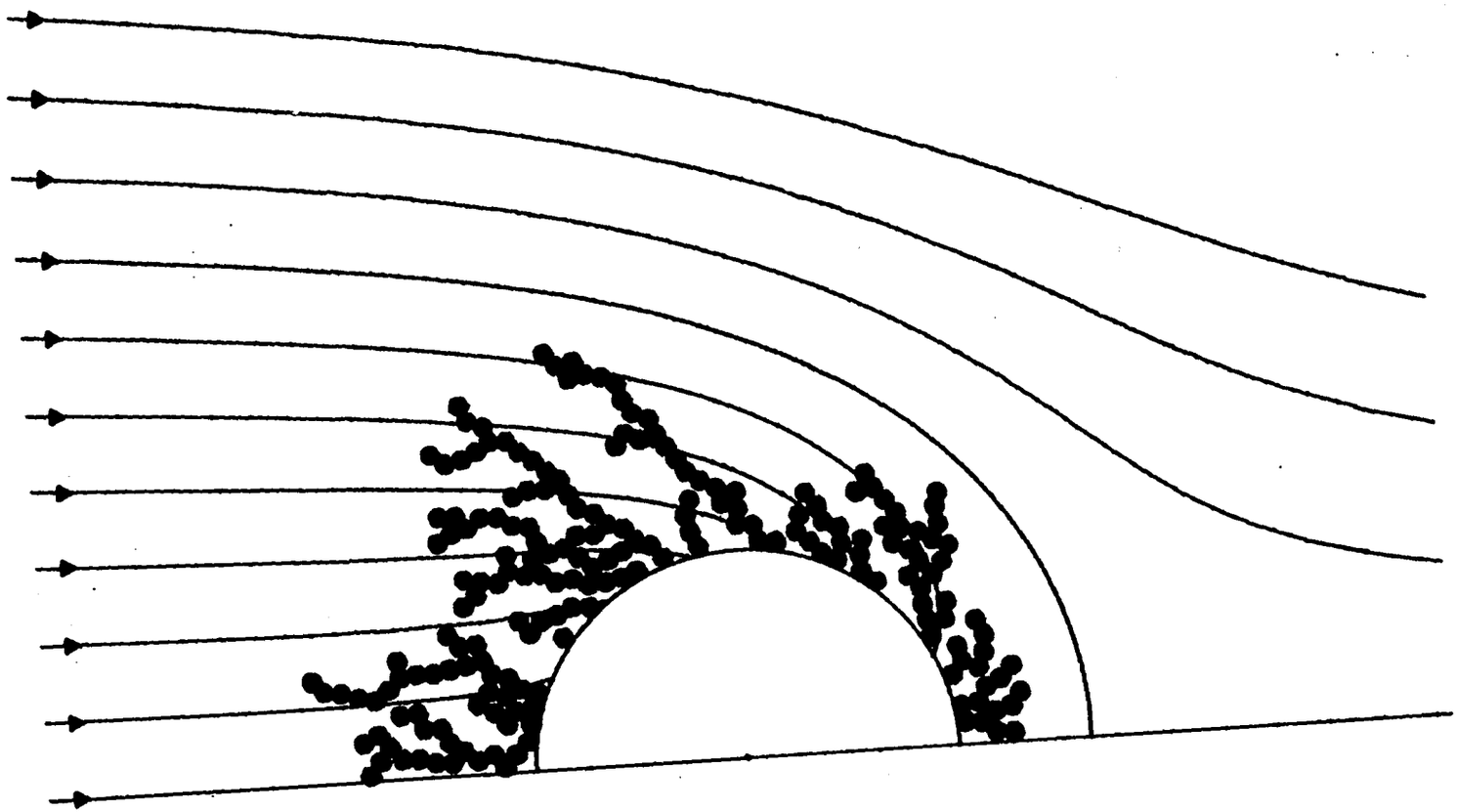

Figure 54. Particle chain formation by particle interception with a coulombic force for potential flow, with $K_c = -1.0$ and $R = 0.04$. Solid lines are particle trajectories

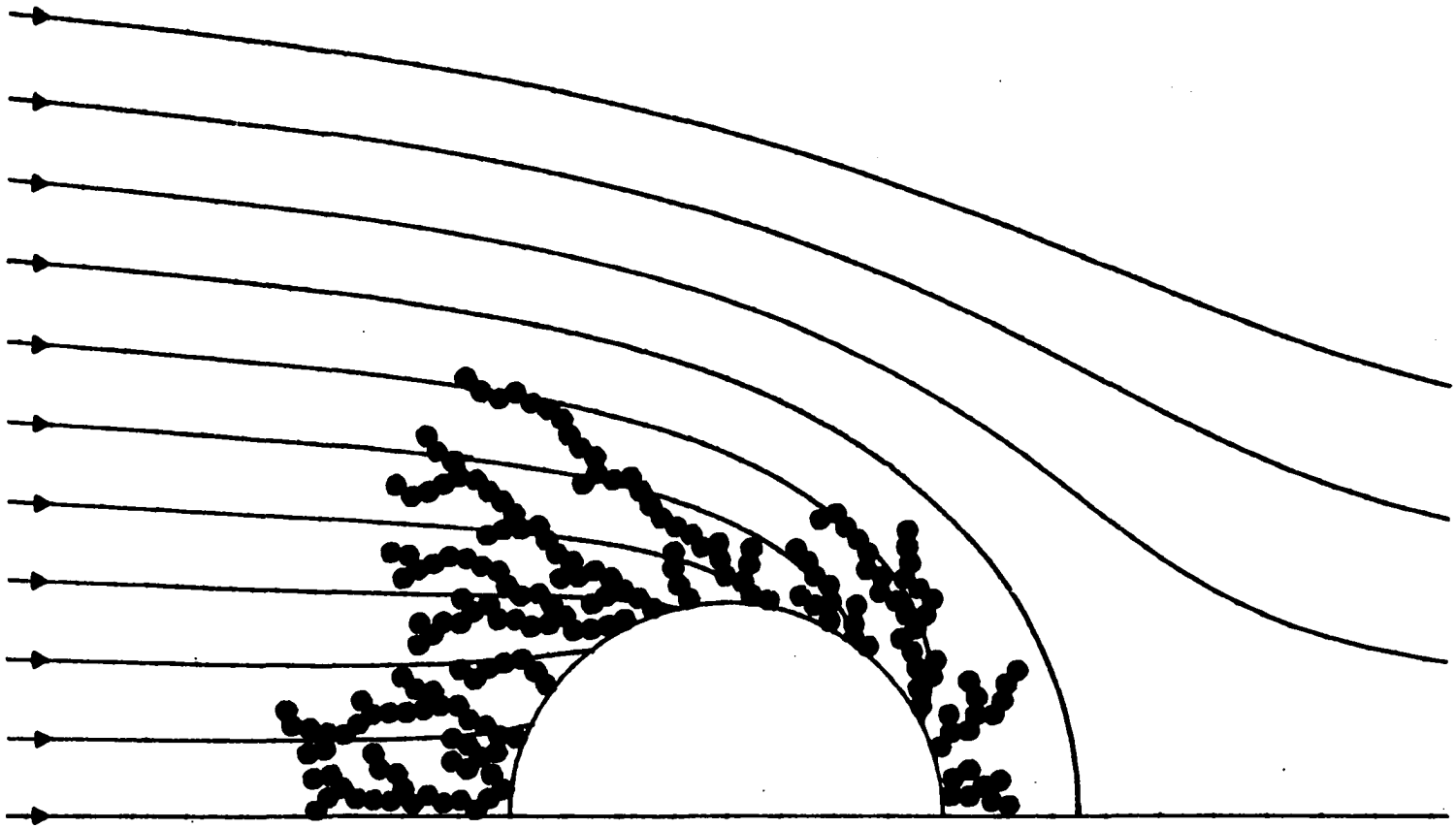

Figure 55. Particle chain formation by particle interception for the same conditions and initial particle distribution as in Figure 54, but with the addition of simulated short-range attractive forces between approaching and captured particles

into the flow.

Chain formation resulting from particle collection with a coulombic force is illustrated in Figure 54. Under the same conditions for point particles deposition would occur uniformly over the entire surface of the collector. The collection efficiency of the fiber is unaffected by particle interception. Chain initiation can occur anywhere on the surface and initially many short chains are formed. However, blocking or "shadowing" of some chains by others causes termination of some and domination of the collection by others. As chains become larger, deposition on the downstream half of the collector becomes increasingly blocked.

Also of interest in examining chain formation is the effect of short-ranged attractive (electrical image) forces between approaching and captured particles. This was simulated by expanding the effective capture surface of captured particles to one half a particle radius beyond the surface of the particles. Approaching particles were considered to be captured upon interception with the increased capture radius; the approaching particle was then "pulled" into actual contact with the capturing particle along the line between their centers at capture. The result of using this simulation of short-range forces is shown in Figure 54 for the same distribution of approaching particles and collection conditions as in Figure 55. The overall pattern of collection is basically the same but several subtle

changes have occurred. With the interparticle force the branching tendency is reduced, chains lean farther forward into the flow, are somewhat longer (and straighter) for the same number of particles, and the separation between neighboring chains is increased (interchain contact is reduced or eliminated); the average radial coordinate of the captured particles has increased from $R = 1.418$ to $R = 1.467$ and the average angular coordinate has shifted farther forward from $\theta = 109.8^{\circ}$ to $\theta = 111.6^{\circ}$.

These simple mathematical experiments have resulted in particle chain formation not unlike that observed experimentally. The major factors leading to the formation of chains as indicated by these results, are particle-particle interception and blocking or "shadowing" effects; short-range attractive forces between approaching and captured particles may modify chain formation, but they are not the primary cause of it.

Shadow Effects for a Series of Noninteracting Collectors

The particle trajectories and collection efficiencies found for a single isolated collector can be used to calculate overall efficiencies for particle collection on a series of identical noninteracting collectors. Two or more collectors are considered to be noninteracting if the flow and electrical fields within the domain of any one collector

neither influences nor is influenced by the flow and electrical fields within the domain of any other collector. The domains of neighboring collectors are connected by uniform flows and fields. This system of collectors corresponds to a filter consisting of widely-spaced parallel fibers.

Although the flow field entering the domain of a collector is recovered unaltered upon exiting (uniform flow), the same is not true for the particle field. Particles can be captured by the collector and removed from the field or their paths can be asymmetrically altered by the electrical forces. Particles entering the domains of collectors further downstream do not have the same uniform distribution assumed for the particle field approaching the first collector. Thus the efficiency of each collector must be expressed in terms of the initial particle distribution. This is facilitated by introducing the following nomenclature, which is illustrated in Figure 17:

Z^j, X^j = rectangular coordinate system centered at the jth collector

$Y^{1,k}$ = displacement coordinate of the kth collector from $X^1 = 0$; $Y^{1,1} \equiv 0$

$X_o^{j,k}$ = value of X_o for a trajectory terminating at the kth collector written in terms of the Z^j, X^j coordinate system within the domain of the jth collector

$X_i^{j,k}$ = same as $X_o^{j,k}$ but for a limiting trajectory

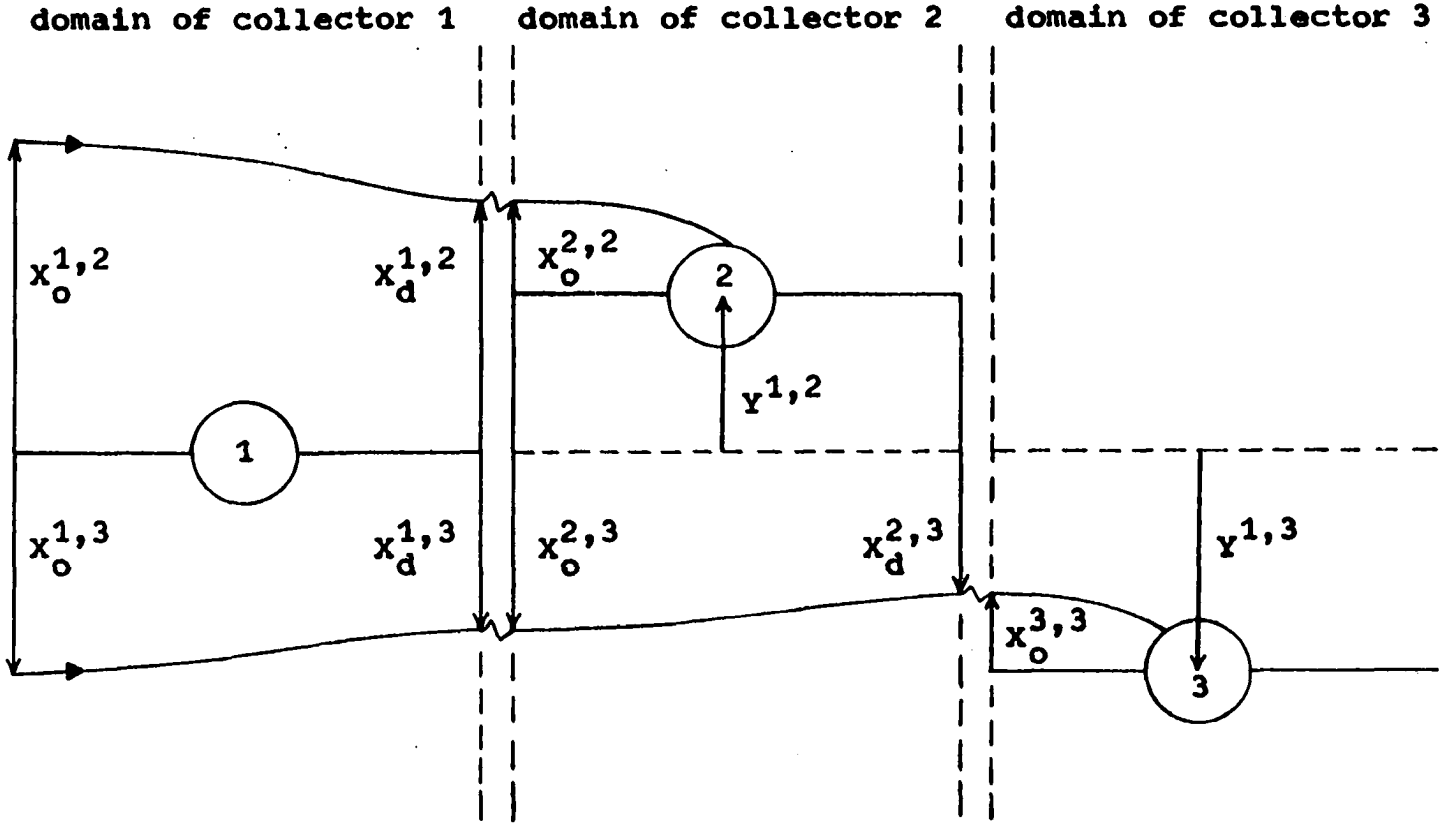

Figure 56. Coordinate systems for particle collection on a series of noninteracting cylindrical collectors

terminating at the kth collector

$X_d^{j,k}$ = displacement distance of a trajectory (terminating at the kth collector) from $X^{j'} = 0$ in the limit $Z^{j'} \to \infty$ within the domain of the jth collector

Only cases with $\alpha = \beta = 0$ will be considered.

The particle trajectories within any given domain are described by Equation 14. Taking the limit $Z^{j'} \to \infty$, Equation 14 gives the relation between $X_o^{j,k}$ and $X_d^{j,k}$ for a trajectory that merely passes through the jth domain,

$$X_o^{j,k} = X_d^{j,k} \mp \pi K_c/G \text{ for } h(Z^{j'} \to \infty) = 1 \qquad (59)$$

where the minus sign is used for $X_d^{j,k} > 0$ and the plus sign is used for $X_d^{j,k} < 0$. The matching condition between domains j and j + 1 gives

$$X_d^{j,k} = X_o^{j+1,k} + Y^{1,j+1} - Y^{1,j} \qquad (60)$$

Values of $X_{i\pm}^{k,k}$ are obtained from the solutions found for a single isolated collector. Using Equations 59 and 60, values of $X_{i\pm}^{1,k}$ can be found, from which the collection efficiency in terms of the initial particle field can be calculated, being careful to exclude portions of the particle field captured by other collectors upstream.

For particle collection under case 2 conditions, the collection efficiency is the same for each collector,

regardless of the $Y^{1,k}$ displacement values

$$\eta^{1,k} = -\pi K_c/G \text{ for all collectors } k \qquad (61)$$

This is illustrated in Figure 57 for the coulombic force, where the middle collector is displaced one collector diameter from the line-of-centers of the other two collectors. Although the efficiency of each downstream collector is the same as the first, particles captured by them may originate from unconnected portions of the initial particle field. Notice that captured portions of the particle field do not create particle-free zones downstream.

For particle collection under case 1 conditions, the collection efficiency of each downstream collector depends upon its location with respect to upstream collectors. Also, particle deposition does not occur over the entire surface of the collector, particle-free zones extend downstream, and a "shadow" effect is created which can affect deposition on other collectors downstream. This can be demonstrated as follows. Considering trajectories that are symmetrical with respect to the $Z^{k'}$-axis, a particle-free zone extends to infinity provided $X^{k'}_{d+} = X^{k'}_{i+} + \pi K_c/G > 0$. For $\alpha = \beta = 0$, Equation 22 simplifies to

$$\eta^{k'} = X^{k'}_{i+} = \{(P_0^2 - K_c^2)^{1/2} + K_c[\cos^{-1}(-K_c/P_0) - \pi]\}/G \qquad (62)$$

$$P_0 = (1 + \gamma)K_{ex} + K_g, \quad -P_0 \leq K_c \leq P_0$$

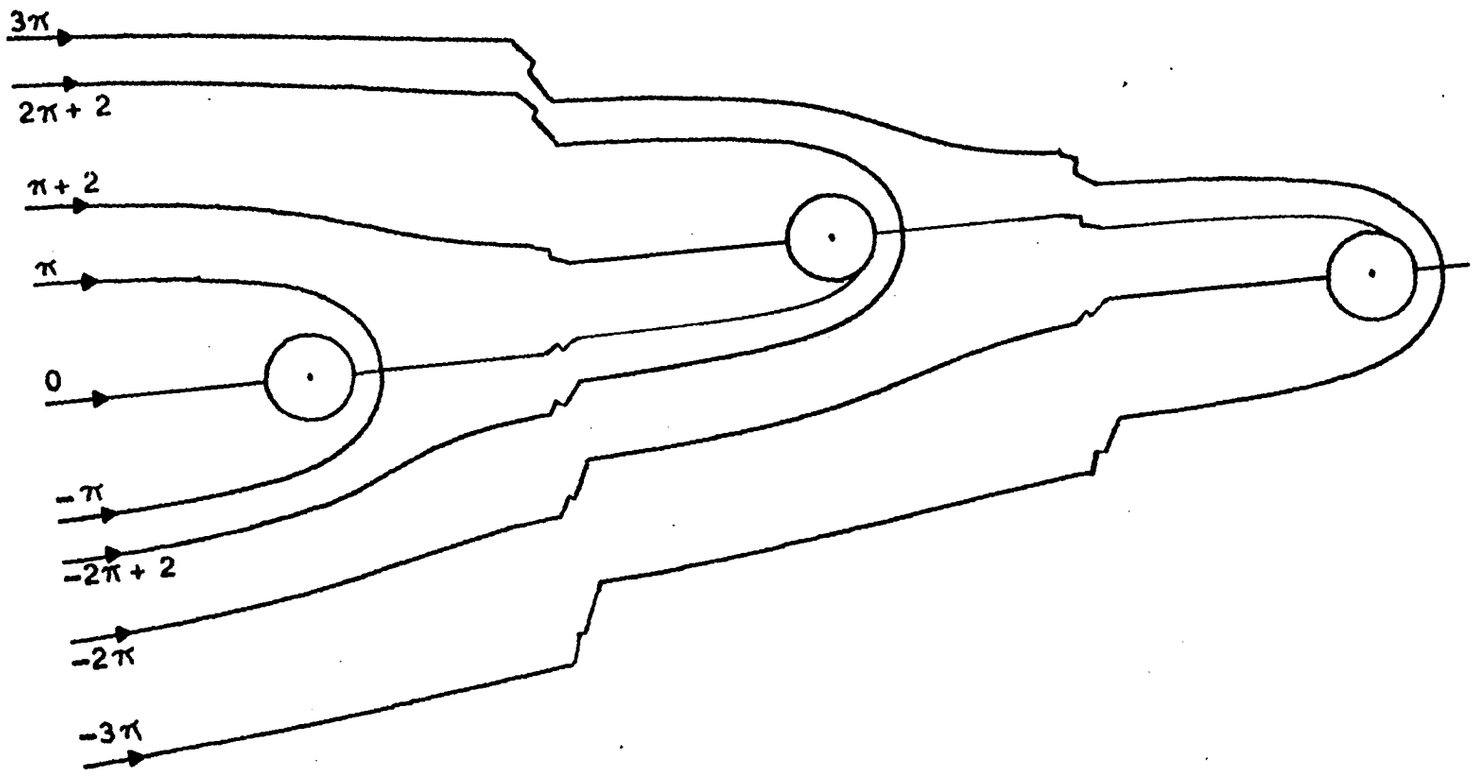

Figure 57. Particle collection on a series of noninteracting collectors for the coulombic force and potential flow, with $K_c = -1.0$

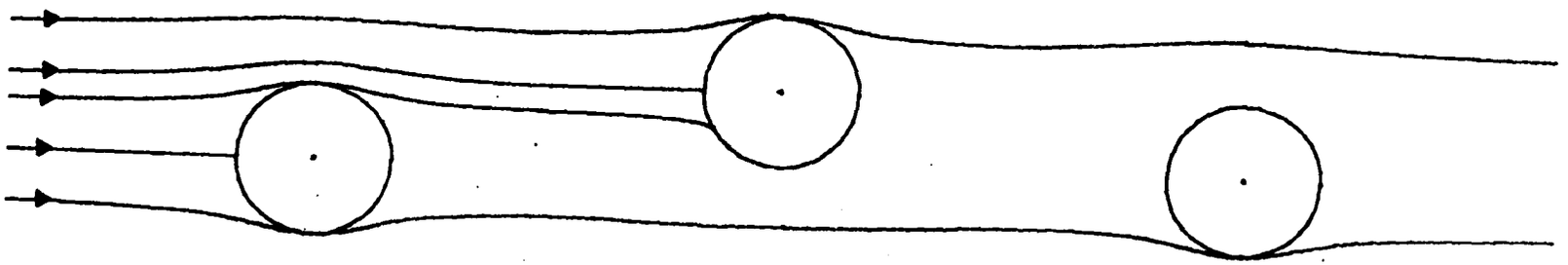

Figure 58. Particle collection on a series of noninteracting collectors for the external electric field force and potential flow, with $K_{ex} = 0.5$ and $\Upsilon = 1.0$

and hence

$$X_{d+}/P_0 = [1 - (-K_c/P_0)^2]^{\frac{1}{2}} - (-K_c/P_0)\cos^{-1}(-K_c/P_0) > 0 \quad (63)$$

$$\text{for } K_c > -P_0$$

Figure 58 illustrates collection with the external electric field force, where the middle collector is displaced one collector radius from the line-of-centers of the other two collectors. Deposition on the second collector is partially blocked by the presence of the first collector. No deposition occurs on the third collector because it lies entirely within the "shadow" of the first two. The collection efficiency of the second collector is given in general form ($K_c = 0$) by

$$\begin{aligned} \eta^{1,2} &= \tfrac{1}{2}Y^{1,2} \text{ for } 0 \leq \tfrac{1}{2}Y^{1,2} \leq X_{i+}^{1,1} \\ \eta^{1,2} &= \eta^{1,1} = P_0/G \text{ for } \tfrac{1}{2}Y^{1,2} \geq X_{i+}^{1,1} \end{aligned} \quad (64)$$

Conclusions

The results presented show that with a combination of the coulombic force, external electric field force, and gravitation, the collection efficiency and deposition density are the same under many conditions for a wide variety of flow velocity profiles, which includes potential, Oseen, and stationary-vortex flows. For the last two flows the

collection efficiency is independent of the Reynolds number. Moreover, the deposition density and radial velocity at impaction are uniform over the surface of the collector for the coulombic force case. Under some conditions interception has no effect, since the limiting trajectories end at a velocity node located away from the surface of the collector. For the external electric field and gravitational forces, the collection efficiency is a minimum when the external and flow fields are aligned, and it increases with angle of separation to a maximum when they are perpendicular. With a coulombic force and an external electric field force perpendicular to the flow direction, collection does not necessarily occur over the entire attractive force region on the collector surface. Joint use of the external electric field and coulombic forces will not necessarily lead to an increased efficiency over the single force case.

For point particles, the collection efficiency and effect of fiber packing density is the same under many conditions for stationary cellular flows having $h(1) = 0$ and $h(L) = 1$. The single fiber collection efficiency decreases only slightly as the packing density increases from zero.

PARTICLE COLLECTION ON ELLIPTICAL CYLINDERS

Introduction

The results of the previous section show that for circular cylinders, under many conditions the collection efficiency of inertialess, charged, point particles is the same for a wide variety of flow velocity profiles and independent of the Reynolds number. In light of these unusual results, it is of interest to learn how the collection efficiency is affected by fiber geometry. Actual fibers are not necessarily circular in cross-section, and nonuniform deposition of particles over time leads to distortion from circularity.

In this section, collection efficiencies are calculated for the capture of inertialess, charged, point particles on a single elliptical-cylinder collector. The forces and conditions used are the same as those used for circular cylinders with the exception that the flow field is now directed at an arbitrary angle to the major axis of the elliptical cylinder. Also considered are the limiting case of collection on a ribbon and generalizations that can be made to collection on cylinders of irregular geometry.

Equation of Motion

The equation of motion for a small, inertialess, spherical particle

$$\underset{\sim}{v} = \underset{\sim}{u} + (C/6\pi\mu R_p) \sum_e \underset{\sim}{F}_e \qquad (65)$$

is written in terms of the elliptical-cylinder coordinate system, shown in Figure 59. The surface describing the elliptical cylinder collector is denoted by $\xi = \xi_0$. Geometric quantities associated with this surface are shown in Figure 60, along with fixed and rotated rectangular coordinate systems and other quantities used in solving for the particle motion. Useful relationships between a, the length of the major semiaxis, b, the length of the minor semiaxis, c, one half the focal distance, and ξ_0 are

$$a = c\cosh\xi_0,\ a/b = \coth\xi_0,\ c^2 = a^2 - b^2$$
$$\xi_0 = \tfrac{1}{2}\ln[(a/b + 1)/(a/b - 1)] \qquad (66)$$

The fixed Z, X rectangular coordinate system is centered at the elliptical cylinder with the Z-axis parallel to the major axis. The free-stream velocity U_o is directed at an angle δ to the Z-axis; in this section its orientation is restricted to $-\pi/2 \leq \delta \leq 0$. The external electric field and gravity are both directed at an angle α to the Z-axis; their orientation is restricted to $\delta - \pi/2 \leq \alpha \leq \delta + \pi/2$. Far upstream the particles approach the collector at an angle β to the Z-axis. The particle approach angle β always lies between δ and α.

Equation 65 is made dimensionless with the use of a

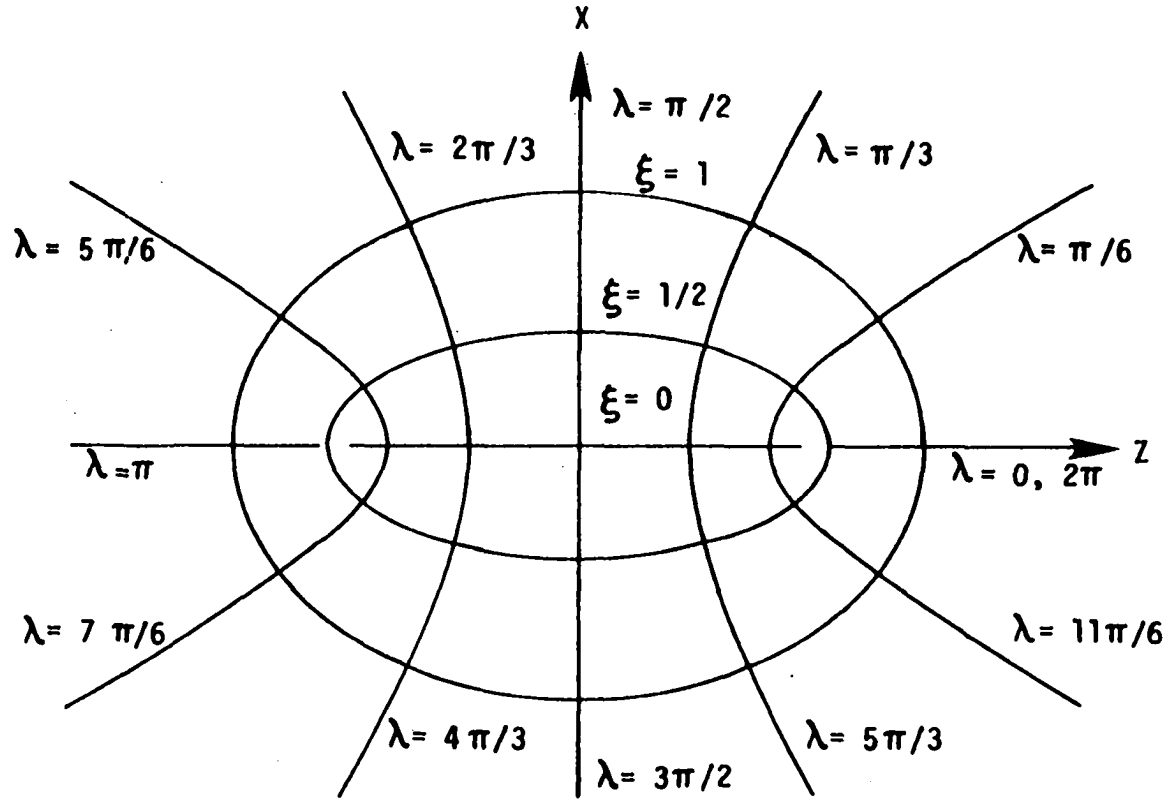

Figure 59. Elliptical cylinder coordinate system

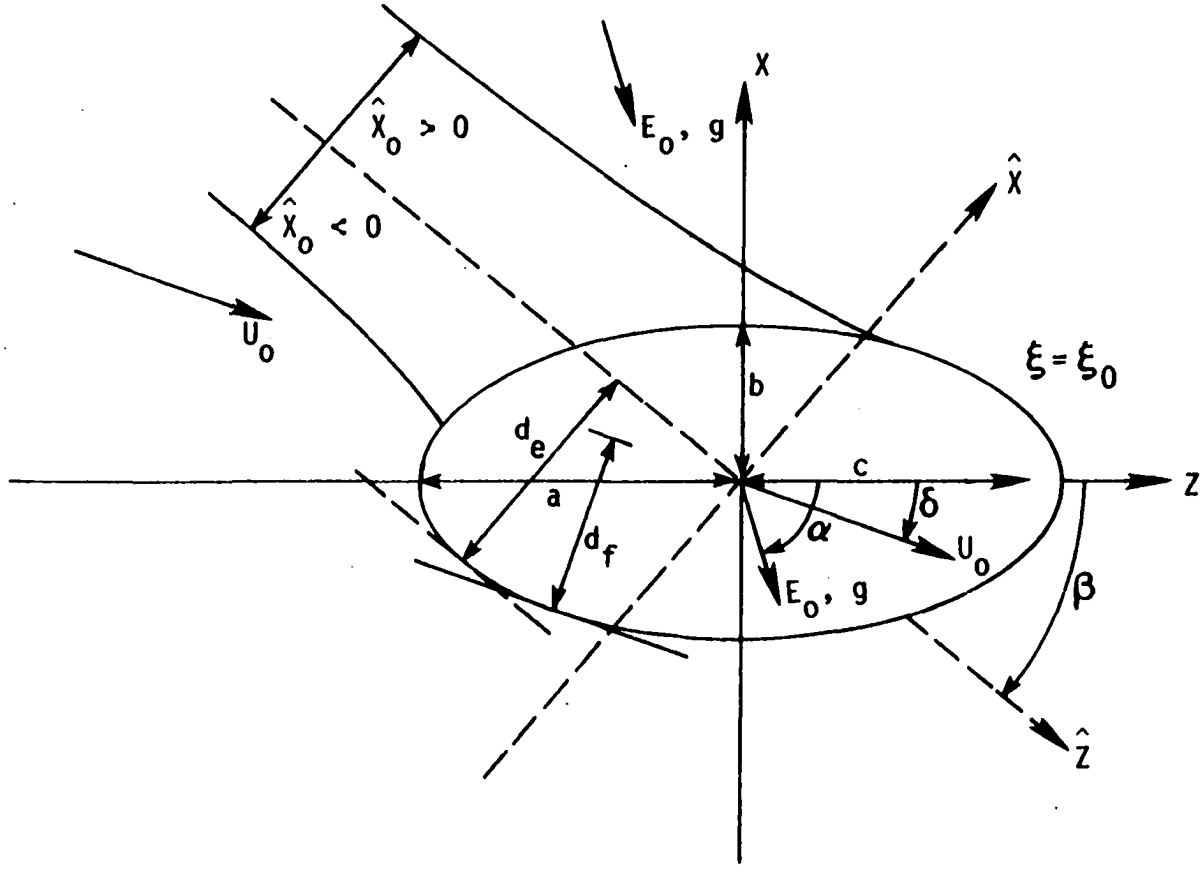

Figure 60. Geometric quantities used in the mathematical model of particle collection on an elliptical cylinder

generalized reference collector half-width d and undisturbed free-stream velocity U_o, to obtain

$$\underset{\sim}{V} = \underset{\sim}{U} + \sum_e K_e \underset{\sim}{f}_e \tag{67}$$

Two obvious choices for d are the lengths of the major and minor semiaxes, a and b. Two other choices, which are useful when the flow and external fields are not parallel to either of the semiaxes, are d_δ, defined as one half the width of the cross-sectional area of the collector projected in the direction of the flow, and d_β, defined as one half the width of the cross-sectional area of the collector projected in the direction of particle approach. The generalized dimensionless reference length parameter is $D \equiv d/c$, with $D_a \equiv a/c = \cosh\xi_0$, $D_b \equiv b/c = \sinh\xi_0$, and

$$D_\delta \equiv d_\delta/c = (\sinh^2\xi_0\cos^2\delta + \cosh^2\xi_0\sin^2\delta)^{1/2} \tag{68}$$

$$D_\beta \equiv d_\beta/c = (\sinh^2\xi_0\cos^2\beta + \cosh^2\xi_0\sin^2\beta)^{1/2} \tag{69}$$

in particular. In terms of the elliptical-cylinder coordinates ξ, λ, the dimensionless rectangular coordinates Z, X are given by

$$Z = (\cosh\xi\ \cos\lambda)/D,\quad X = (\sinh\xi\ \sin\lambda)/D \tag{70}$$

Because only point particles are considered, the method of solution is developed in terms of the potential flow field, but the solution is easily generalized to include

other stationary incompressible flows possessing a stream function. The stream function is defined by

$$U_\xi \equiv \frac{D}{\Omega}\frac{\partial \Psi_f}{\partial \lambda}, \quad U_\lambda \equiv -\frac{D}{\Omega}\frac{\partial \Psi_f}{\partial \xi} \tag{71}$$

$$\Omega \equiv (\sinh^2\xi + \sin^2\lambda)^{\frac{1}{2}} \tag{72}$$

where dimensionless variables have been used, $U_\xi = u_\xi/U_o$, $U_\lambda = u_\lambda/U_o$, $\Psi_f = \psi_f/U_o d$. The dimensionless components of the fluid velocity and the stream function for potential flow (74) are given in Table 54.

The dimensionless force expressions (77) are given in Table 54; the forces are analogous to those considered previously. However, there are now two collector polarization coefficients, Γ_0 and Γ_{90}, that are directional and a function of a/b. The coulombic force parameter K_c is inversely proportional to d but K_{ex} and K_g are independent of d.

The initial conditions for the determination of particle trajectories from Equation 67 are $V_z = \cos\delta + (K_{ex} + K_g)\cos\alpha$ and $V_x = \sin\delta + (K_{ex} + K_g)\sin\alpha$ far upstream.

Trajectory Equation

As before, the stream function Ψ for particle trajectories is given by superposition of the fluid and force stream functions, taken from Table 54

Table 54. Elliptical cylinder flow and force expressions

POTENTIAL FLOW

$$U_\xi = \sinh\xi \cos\lambda \cos\delta \,[1 - (\coth\xi - 1)/(\coth\xi_0 - 1)]/\Omega$$

$$+ \cosh\xi \sin\lambda \sin\delta \,[1 - (1 - \tanh\xi)/(1 - \tanh\xi_0)]/\Omega$$

$$U_\lambda = -\cosh\xi \sin\lambda \cos\delta \,[1 - (\tanh\xi - 1)/(\coth\xi_0 - 1)]/\Omega$$

$$+ \sinh\xi \cos\lambda \sin\delta \,[1 - (1 - \coth\xi)/(1 - \tanh\xi_0)]/\Omega$$

$$\Psi_f = \sinh\xi \sin\lambda \cos\delta \,[1 - (\coth\xi - 1)/(\coth\xi_0 - 1)]/D$$

$$- \cosh\xi \cos\lambda \sin\delta \,[1 - (1 - \tanh\xi)/(1 - \tanh\xi_0)]/D$$

CHARGED-COLLECTOR AND CHARGED-PARTICLE (COULOMBIC) FORCE

$$K_c = \rho_c Q_p C/12\pi^2 \epsilon_f dR_p \mu U_o$$

$$f_c^{\xi} = D/\Omega$$

$$f_c^{\lambda} = 0$$

$$\Psi_c = K_c \lambda$$

EXTERNAL ELECTRIC FIELD FORCE

$$K_{ex} = Q_p E_o C/6\pi\mu R_p U_o$$

$$f_{ex}^{\xi} = \sinh\xi \cos\lambda \cos\alpha \,[1 + \Gamma_0(\coth\xi - 1)/(\coth\xi_0 - 1)]/\Omega$$

$$+ \cosh\xi \sin\lambda \sin\alpha \,[1 + \Gamma_{90}(1 - \tanh\xi)/(1 - \tanh\xi_0)]/\Omega$$

Table 54. (Continued)

$$f_{ex}^{\lambda} = -\cosh\xi \sin\lambda \cos\alpha [1 - \Gamma_0(1 - \tanh\xi)/(\coth\xi_0 - 1)]/\Omega$$

$$+ \sinh\xi \cos\lambda \sin\alpha [1 - \Gamma_{90}(\coth\xi - 1)/(1 - \tanh\xi_0)]/\Omega$$

$$\Psi_{ex} = K_{ex}\sinh\xi \sin\lambda \cos\alpha [1 + \Gamma_0(\coth\xi - 1)/(\coth\xi_0 - 1)]/D$$

$$- K_{ex}\cosh\xi \cos\lambda \sin\alpha [1 + \Gamma_{90}(1 - \tanh\xi)/(1 - \tanh\xi_0)]/D$$

$$\Gamma_0 \equiv (\epsilon_c/\epsilon_f - 1)/[(b/a)\epsilon_c/\epsilon_f + 1]$$

$$\Gamma_{90} \equiv (\epsilon_c/\epsilon_f - 1)/[(a/b)\epsilon_c/\epsilon_f + 1]$$

GRAVITATIONAL FORCE

$$K_g = 2R_p^2\rho_p gC/9\mu U_o$$

$$f_g^{\xi} = (\sinh\xi \cos\lambda \cos\alpha + \cosh\xi \sin\lambda \sin\alpha)/\Omega$$

$$f_g^{\lambda} = (-\cosh\xi \sin\lambda \cos\alpha + \sinh\xi \cos\lambda \sin\alpha)/\Omega$$

$$\Psi_g = K_g(\sinh\xi \sin\lambda \cos\alpha - \cosh\xi \cos\lambda \sin\alpha)/D$$

$$\Psi = \Psi_f + \Psi_c + \Psi_{ex} + \Psi_g \tag{73}$$

The upstream or initial value Ψ_o is found by the same method used for circular cylinders, taking into consideration the arbitrary orientation of the flow field, which gives

$$\Psi_o = \hat{X}_o G + K_c(\beta + \pi) \tag{74}$$

$$G \equiv [1 + 2(K_{ex} + K_g)\cos(\alpha - \delta) + (K_{ex} + K_g)^2]^{\frac{1}{2}} \tag{75}$$

Therefore, the particle trajectory is completely defined by

$$\begin{aligned}\hat{X}_o = \{&\sinh\xi \sin\lambda \cos\delta [1 - (\coth\xi - 1)/(\coth\xi_0 - 1)] \\ &- \cosh\xi \cos\lambda \sin\delta [1 - (1 - \tanh\xi)/(1 - \tanh\xi_0)] \\ &+ \sinh\xi \sin\lambda \cos\alpha [K_{ex} + K_g + \Gamma_0 K_{ex}(\coth\xi - 1)/(\coth\xi_0 - 1)] \\ &- \cosh\xi \cos\lambda \sin\alpha [K_{ex} + K_g + \Gamma_{90} K_{ex}(1 - \tanh\xi)/(1 - \tanh\xi_0)] \\ &+ DK_c(\lambda - \beta - \pi)\}/DG\end{aligned} \tag{76}$$

where

$$\begin{aligned}\beta &= -\cos^{-1}\{[\cos\delta + (K_{ex} + K_g)\cos\alpha]/G\} \text{ for } -\pi \leq \alpha \leq 0 \\ \beta &= \sin^{-1}\{[\sin\delta + (K_{ex} + K_g)\sin\alpha]/G\} \text{ for } 0 \leq \alpha \leq \pi/2\end{aligned} \tag{77}$$

Notice that since K_{ex}, K_g, and C are independent of d, the choice of reference length does not affect the particle approach angle β.

Limiting Trajectories and Collection Efficiencies

In this section, the efficiency of particle collection is defined as the width of the cross-sectional area perpendicular to the particle paths far upstream from which all particles of a given size are collected, divided by 2d. The collection efficiency, $\hat{\eta}$, is then $\hat{\eta} \equiv (\hat{X}_{i+} - \hat{X}_{i-})/2$, where $\hat{X}_{i+}$ ($\hat{X}_{i-}$) is the dimensionless initial displacement from the $\hat{Z}$-axis of the limiting trajectory most positive (negative) in $\hat{X}_o$.

Since the boundary condition for collection by interception is not of simple form when written in elliptical-cylinder coordinates, only collection of point particles is considered. As with circular cylinders, there are two types of limiting trajectories: grazing limiting trajectories, which graze the surface of the collector; and nodal limiting trajectories, which end at a particle velocity node located away from the surface of the collector whereat the particle velocity goes to zero. This leads to three different cases of particle collection behavior.

Case 1: Two grazing limiting trajectories

Impaction of a point particle occurs when $\xi = \xi_0$, and Equation 76 reduces to

$$\hat{X}_o = [\omega_0 \sin\lambda - \omega_{90}\cos\lambda + DK_c(\lambda - \beta - \pi)]/DG \qquad (78)$$

$$\omega_0 \equiv [(1 + \Gamma_0)K_{ex} + K_g] \sinh\xi_0 \cos\alpha \tag{79}$$

$$\omega_{90} \equiv [(1 + \Gamma_{90})K_{ex} + K_g] \cosh\xi_0 \sin\alpha \tag{80}$$

Notice that terms due to the velocity field go to zero in getting Equation 78.

The grazing limiting trajectory values of $\hat{X}_o$ correspond to a relative maximum and relative minimum in $\hat{X}_o$ versus λ. The angular location of impaction of either of the limiting trajectories is denoted by λ_m; in particular, λ_{m+} corresponds to $\hat{X}_{i+}$ and λ_{m-} to $\hat{X}_{i-}$. The two values of λ_m can be found from

$$DG\ d\hat{X}_o/d\lambda = 0 = \omega_0\cos\lambda_m + \omega_{90}\sin\lambda_m + DK_c \tag{81}$$

Solving for $\cos\lambda_m$ and $\sin\lambda_m$ gives

$$\cos\lambda_{m\pm} = [-DK_c\omega_0 \mp \omega_{90}(A - D^2K_c^2)^{1/2}]/A \equiv W_{\pm} \tag{82}$$

or, equivalently,

$$\sin\lambda_{m\pm} = [-DK_c\omega_{90} \pm \omega_0(A - D^2K_c^2)^{1/2}]/A \equiv Y_{\pm} \tag{83}$$

$$A \equiv \omega_0^2 + \omega_{90}^2 \tag{84}$$

where the top signs correspond to λ_{m+} and the bottom signs correspond to λ_{m-}. Notice that λ_m is independent of the choice for d.

The values of $\hat{X}_i$ for the grazing limiting trajectories

are given by

$$\hat{X}_{i\pm} = \hat{X}_o(\lambda_{m\pm}) = [\pm(A - D^2K_c^2)^{\frac{1}{2}} + DK_c(\lambda_{m\pm} - \beta - \gamma)]/DG \quad (85)$$

subject to the condition $-A^{\frac{1}{2}} \leq DK_c \leq A^{\frac{1}{2}}$. Values of λ_m for different ranges of the parameters α and K_c are given in Table 55. From Equation 85 the collection efficiency is readily calculated as $\hat{\eta} = (\hat{X}_{i+} - \hat{X}_{i-})/2$. As was found for circular cylinders, for elliptical cylinders the grazing limiting trajectory values of $\hat{X}_i$ for point particles are the same for all stationary flows having $\Psi_f = 0$ at the surface of the collector and approaching the collector at the same orientation angle δ. The limiting trajectories intersect the collector at points where the force normal to the surface changes from attraction to repulsion.

Considering only the external electric field and gravitational forces ($K_c = 0$), the collection efficiency is given by

$$\hat{\eta} = (\omega_0^2 + \omega_{90}^2)^{\frac{1}{2}}/DG \quad (86)$$

For constant K_{ex} and K_g, the efficiency increases from a minimum when the flow and external fields are parallel to a maximum when they are perpendicular. With $\delta = \alpha = 0$ and $D = D_b$, Equation 86 reduces to

$$\hat{\eta} = [(1 + \Gamma_0)K_{ex} + K_g]/(1 + K_{ex} + K_g) \quad (87)$$

Table 55. Values of λ_m

Range of parameters α, K_c	λ_{m+} and range	λ_{m-} and range
$\delta - 90^\circ \leq \alpha \leq -90^\circ$		
$0 \leq DK_c \leq A^{\frac{1}{2}}$	$\sin^{-1}Y_+$ $(-90^\circ \rightarrow 90^\circ)$	$\cos^{-1}W_-$ $(0 \rightarrow 180^\circ)$
$-A^{\frac{1}{2}} \leq DK_c \leq 0$	$-\cos^{-1}W_+$ $(-180^\circ \rightarrow 0)$	$\pi - \sin^{-1}Y_-$ $(90^\circ \rightarrow 270^\circ)$
$-90^\circ \leq \alpha \leq 0$		
$0 \leq DK_c \leq A^{\frac{1}{2}}$	$\cos^{-1}W_+$ $(0 \rightarrow 180^\circ)$	$\pi - \sin^{-1}Y_-$ $(90^\circ \rightarrow 270^\circ)$
$-A^{\frac{1}{2}} \leq DK_c \leq 0$	$\sin^{-1}Y_+$ $(-90^\circ \rightarrow 90^\circ)$	$2\pi - \cos^{-1}W_-$ $(180^\circ \rightarrow 360^\circ)$
$0 \leq \alpha \leq \delta + 90^\circ$		
$0 \leq DK_c \leq A^{\frac{1}{2}}$	$\pi - \sin^{-1}Y_+$ $(90^\circ \rightarrow 270^\circ)$	$2\pi - \cos^{-1}W_-$ $(180^\circ \rightarrow 360^\circ)$
$-A^{\frac{1}{2}} \leq DK_c \leq 0$	$\cos^{-1}W_+$ $(0 \rightarrow 180^\circ)$	$2\pi + \sin^{-1}Y_-$ $(270^\circ \rightarrow 450^\circ)$

For constant K_{ex} and K_g, $\hat{\eta}$ increases with the length of the major axis because greater charge separation occurs in the collector. Similarly, with $\delta = \alpha = -90^\circ$ and $D = D_a$, Equation 86 reduces to

$$\hat{\eta} = [(1 + \Gamma_{90})K_{ex} + K_g]/(1 + K_{ex} + K_g) \qquad (88)$$

Equations 87 and 88 are of the same form as for circular cylinders. In general, with the external electric field force alone ($K_g = 0$), the amount of collection is greater with the field and flow both parallel to the minor axis than with both parallel to the major axis, but the collection becomes the same for all orientations when the collector is perfectly conducting. In fact in this limit ($\epsilon_c/\epsilon_f \to \infty$), Equation 86 becomes

$$\hat{\eta} = \frac{K_{ex}(a + b)/d}{[1 + K_{ex}\cos(\alpha - \delta) + K_{ex}^2]^{\frac{1}{2}}} \qquad (89)$$

and the collection is the same for all (constant) values of $\alpha - \delta$. From Equation 89, the maximum possible collection is $(a + b)/d$, which corresponds to the particles following the electric field lines.

For circular cylinders, with the external electric field in the same direction as potential flow, for K_{ex} equal to the inverse of the collector polarization coefficient the particle motion is rectilinear and the collection efficiency is not affected by particle inertia. Similar

behavior occurs with elliptical cylinders: with $\delta = \alpha = 0$ and $K_{ex} = 1/\Gamma_0$, $V_x = 0$; with $\delta = \alpha = -90^\circ$ and $K_{ex} = 1/\Gamma_{90}$, $V_z = 0$ for all Stokes numbers.

Case 1 occurs whenever $-A^{1/2} \leq DK_c \leq A^{1/2}$ and a velocity node does not exist; when a velocity node does exist, either case 2 or case 3 applies.

Case 2: Two nodal limiting trajectories

With $DK_c > A^{1/2}$, collection does not occur.

With $DK_c < -A^{1/2}$, both limiting trajectories end at the same velocity node located downstream from the collector. Therefore, using Equation 76 and $\lambda_{i-} = \lambda_{i+} + 2\pi$, $\xi = \xi_0$ (or $\lambda_{n-} = \lambda_{n+} + 2\pi$, $\xi = \xi_n$) gives the collection efficiency as

$$\hat{\eta} = -\pi K_c/G \tag{90}$$

This result, which is the same as for circular cylinders, has unusual features. Both $\hat{\eta}$ and K_c are inversely proportional to the generalized reference length d; hence d merely appears as a normalization constant and is completely arbitrary in Equation 90. The amount of collection, as given by $\hat{\eta}d$, is independent of the collector length parameters, the form of the flow field, the eccentricity and dielectric constant of the collector, and the orientation of the flow and external fields (provided the angle between them is held constant).

For the coulombic force alone, Equation 90 reduces to $\hat{\eta} = -\pi K_c$. The quantity $d\hat{X}_o/d\lambda$ at $\xi = \xi_0$ is uniform with respect to the elliptical angle λ, but the particle density on a unit area basis varies with position, as does V_ξ at impaction.

For $-A^{\frac{1}{2}} \leq DK_c \leq 0$, it is also possible to have two nodal limiting trajectories. Under this condition both attractive and repulsive forces occur at the surface of the collector, but deposition does not occur over the entire attractive force region. The collection efficiency is still given by Equation 90. Criteria for determining the appropriate case, when not otherwise obvious, follow consideration of case 3.

Case 3: One grazing and one nodal limiting trajectory

In order to calculate the collection efficiency, it is necessary to determine the values of $\hat{X}_i$ for both types of limiting trajectories. The solution for the grazing limiting trajectory is the same as in case 1. The value of $\hat{X}_i$ for the nodal limiting trajectory can be found by a procedure analogous to that outlined for circular cylinders.

An analytical solution for the nodal limiting trajectory is possible for potential flow because Equation 76 is quadratic in $\sinh\xi$. The result of solving for $\sinh\xi$ is given in Table 56, where the correct sign depends upon the location of the particle along the trajectory. The equation

Table 56. Solution of the trajectory equation for potential flow around an elliptical cylinder

$$\sinh\xi = [-B^* \pm (B^{*2} - 4A^*C^*)^{1/2}]/2A^*$$

$$A^* \equiv (J_0\sin\lambda - L_{90}\cos\lambda)^2 - (J_{90}\cos\lambda + L_0\sin\lambda)^2$$

$$B^* \equiv 2D\,[K_c(\lambda - \beta - \pi) - \hat{X}_o G]\;(J_0\sin\lambda - L_{90}\cos\lambda)$$

$$C^* \equiv D^2\,[K_c(\lambda - \beta - \pi) - \hat{X}_o G]^2 - (J_{90}\cos\lambda + L_0\sin\lambda)^2$$

$$J_0 \equiv (1 - b/a)^{-1}\cos\delta + \{[1 - \Gamma_0/(a/b - 1)]K_{ex} + K_g\}\cos\alpha$$

$$J_{90} \equiv -(a/b - 1)^{-1}\sin\delta + \{[1 + \Gamma_{90}/(1 - b/a)]K_{ex} + K_g\}\sin\alpha$$

$$L_0 \equiv (\cos\delta - \Gamma_0 K_{ex}\cos\alpha)/(a/b - 1)$$

$$L_{90} \equiv (\sin\delta - \Gamma_{90}K_{ex}\sin\alpha)/(1 - b/a)$$

$$\beta = -\cos^{-1}\{[\cos\delta + (K_{ex} + K_g)\cos\alpha]/G\} \quad \text{for } -\pi \le \alpha \le 0$$

$$\beta = \sin^{-1}\{[\sin\delta + (K_{ex} + K_g)\sin\alpha]/G\} \quad \text{for } 0 \le \alpha \le \pi/2$$

for $\sinh\zeta$ has a double root at the point along the trajectory where $V_\lambda = 0$. The value of λ at this double root location will be denoted by λ_r. The requirement that $B^{*2} - 4A^*C^* = 0$ gives the locus of values of λ_r for different trajectories as

$$\hat{X}_o(\lambda_r) = [DK_c(\lambda - \beta - \pi) \pm (-A^*)^{\frac{1}{2}}]/DG \qquad (91)$$

where the plus sign is used if $K_c < 0$, and the minus sign is used if $K_c > 0$. The limiting trajectory corresponds to the maximum (or minimum) value of $\hat{X}_o(\lambda_r)$, giving $\lambda_r = \lambda_n$ and $\hat{X}_i = \hat{X}_o(\lambda_n)$ from Equation 91. Therefore, λ_n can be found from

$$DG\, d\hat{X}_o/d\lambda_r = 0 = DK_c \pm (-dA^*/d\lambda_r)/2(-A^*)^{\frac{1}{2}} \qquad (92)$$

In general, Equation 92 must be solved numerically for λ_n.

Collection efficiency: Case criteria

Since only point particles are being considered, complications introduced by interception do not occur, and criteria in terms of K_c, A, δ, α, $\hat{X}_o(\lambda_m)$, and $\hat{X}_o(\lambda_n)$ are more straightforward.

1) For $DK_c < -A^{\frac{1}{2}}$, case 2 always applies and $\hat{\eta}$ is given by Equation 90.

2) For $-A^{\frac{1}{2}} \leq DK_c < 0$, any of the cases may apply. If there is no velocity node present, case 1 always applies, and $\hat{\eta}$ is given by Equation 85. If a velocity node is pres-

ent, either case 2 or case 3 applies: if $\delta - \pi/2 \leq \alpha \leq \delta$, then $-\pi \leq \lambda_{n+} \leq 0$, $\lambda_{n-} = \lambda_{n+} + 2\pi$, $\hat{X}_{i-}$ is the most negative of $\hat{X}_o(\lambda_{n-})$ and $\hat{X}_o(\lambda_{m-})$, and $\hat{X}_{i+} = \hat{X}_o(\lambda_{n+})$; if $\delta \leq \alpha \leq \delta + \pi/2$, then $3\pi/2 \leq \lambda_{n-} \leq 5\pi/2$, $\lambda_{n+} = \lambda_{n-} - 2\pi$, $\hat{X}_{i+}$ is the most positive of $\hat{X}_o(\lambda_{n+})$ and $\hat{X}_o(\lambda_{m+})$, and $\hat{X}_{i-} = \hat{X}_o(\lambda_{n-})$.

3) For $K_c = 0$, case 1 always applies, and $\hat{\eta}$ is given by Equation 86.

4) For $0 < DK_c \leq A^{\frac{1}{2}}$, either case 1 or case 3 applies. If a velocity node is not present, case 1 always applies, and $\hat{\eta}$ is given by Equation 85. If a velocity node is present, case 3 always applies: if $\delta - \pi/2 \leq \alpha \leq \delta$, then $0 \leq \lambda_{n-} \leq \pi$, $\hat{X}_{i-} = \hat{X}_o(\lambda_{n-})$, and $\hat{X}_{i+} = \hat{X}_o(\lambda_{m+})$; if $\delta \leq \alpha \leq \delta + \pi/2$, then $\pi/2 \leq \alpha \leq 3\pi/2$, $\hat{X}_{i+} = \hat{X}_o(\lambda_{n+})$, and $\hat{X}_{i-} = \hat{X}_o(\lambda_{m-})$.

5) For $DK_c > A^{\frac{1}{2}}$, no collection occurs.

Cases With Interception

With just the external forces ($K_c = 0$), for the special cases of the external fields and the flow parallel to either the major axis or the minor axis of the collector, the condition for collection by interception can be written in simple form. For $\alpha = \delta = 0$, the interception condition for the limiting trajectories is $X^* = \pm(1 + \mathcal{R})$ at $Z = 0$, where $\mathcal{R} \equiv R_p/b$ is the interception parameter. Use of $D_b = \sinh\xi_0$ and Equation 70 gives the interception value of ξ as $\xi^* = \sinh^{-1}[(1 + \mathcal{R})\sinh\xi_0]$ with $\lambda_i = \pi/2$ or $3\pi/2$. Substi-

tuting these values into Equation 76 gives the collection efficiency for potential flow

$$\hat{\eta} = (1 + \mathcal{R}) \left[1 + \frac{(\Gamma_0 K_{ex} - 1)}{(1 + K_{ex} + K_g)} \frac{(\coth\xi^* - 1)}{(\coth\xi_0 - 1)}\right] \qquad (93)$$

Similarly, for $\alpha = \delta = -90^\circ$, the interception condition becomes $Z^* = \pm(1 + \mathcal{R})$ at $X = 0$, $\mathcal{R} \equiv R_p/a$; using $D_a = \cosh\xi_0$ gives $\xi^* = \cosh^{-1}[(1 + \mathcal{R})\cosh\xi_0]$ with $\lambda_i = 0$ or π, and

$$\hat{\eta} = (1 + \mathcal{R}) \left[1 + \frac{(\Gamma_{90} K_{ex} - 1)}{(1 + K_{ex} + K_g)} \frac{(1 - \tanh\xi^*)}{(1 - \tanh\xi_0)}\right] \qquad (94)$$

Particle Trajectories

The particle trajectories for an elliptical cylinder are analogous to those for a circular cylinder and will not be discussed in detail. A new factor affecting the form of the trajectories is the reduced symmetry of the collector, which introduces effects arising from changing the orientation of the flow field. Figure 61 shows particle trajectories for flow at an oblique angle to the major and minor axes with both an external electric field perpendicular to the flow and an attractive coulombic force. In this particular case there are two nodal limiting trajectories. The grazing trajectory corresponding to $\hat{X}_o(\lambda_{m-})$ intersects the collector at two locations, creating a layer void of particles between them. There is a large variation in the

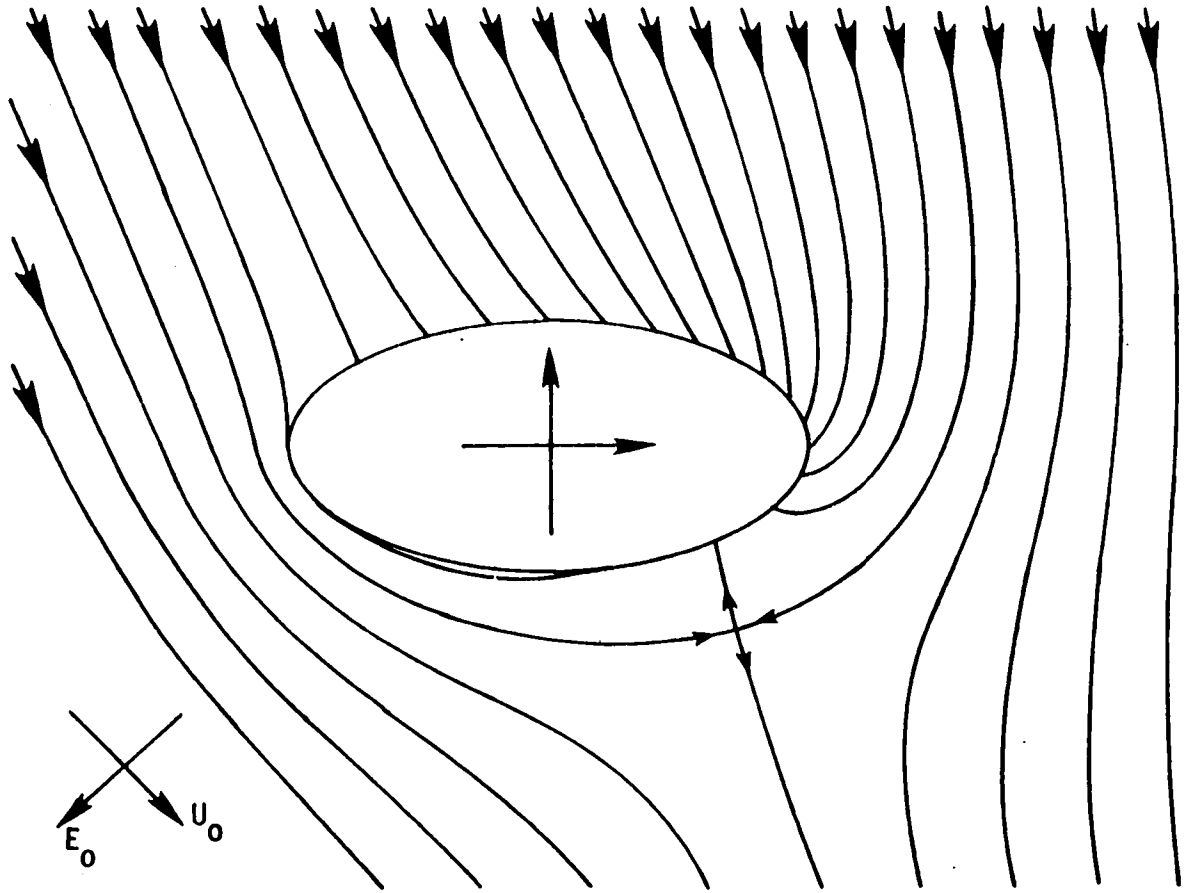

Figure 61. Particle trajectories for combined coulombic and external electric field forces in potential flow, with a/b = 2.0, $\delta = -45^{\circ}$, $\alpha = -135^{\circ}$, $\beta = -71.6^{\circ}$, $K_{ex} = 0.5$, $DK_C/A^{1/2} = -0.90$, and $\epsilon_c/\epsilon_f = \infty$

deposition density over the surface of the collector; much collection occurs at one end, but the deposition is quite sparse at the other.

Particle Collection on a Ribbon

In the limit $\xi_0 = 0$, the elliptical cylinder becomes a ribbon of width 2a lying in the X = 0 plane, and the following simplifications apply

$$b = \Gamma_{90} = \Gamma_0/(a/b - 1) = \omega_0 = \sinh\xi_0 = 0$$
$$a = c,\ \cosh\xi_0 = 1,\ d = a,\ D = 1 \tag{95}$$

The stream functions for the potential flow field and the external electric field simplify to

$$\Psi_f = \sinh\xi \sin(\lambda - \delta) \tag{96}$$

$$\Psi_{ex} = K_{ex}(X \cos\alpha - Z \sin\alpha) \tag{97}$$

Uniform flow exists parallel to the ribbon for $\delta = 0$. Since the ribbon only has an infinitesimal thickness, no polarization of the collector occurs, and the external electric field force is uniform for all orientations. The normal component of the force is uniform over the surface of the ribbon, with one side of the ribbon attractive and the other repulsive.

The coulombic force lines due to a charged ribbon are the lines of constant λ shown in Figure 59. The coulombic

force strength varies across the ribbon surface as $1/\sin\lambda$; the force is infinite at the edges of the ribbon but drops off quickly to a minimum at the center. Therefore, although the external electric field force is uniform, with both forces present both attractive and repulsive force regions can be present on a single side of the ribbon.

With the simplifications given in Equation 95, the results found for an elliptical cylinder also apply to a ribbon. Since there is only one characteristic length, collection efficiencies are normalized using a. Equation 86 for the external electric field and gravitational forces reduces to

$$\hat{\eta} = -[(K_{ex} + K_g)\sin\alpha]/G \qquad (98)$$

With the external fields parallel to the ribbon, no collection occurs regardless of the flow field orientation. The efficiency is maximum with the fields perpendicular to the ribbon. Equation 90 for collection with two nodal limiting trajectories remains unchanged.

Particle Collection on Irregular Cylinders

The approach used to solve Equation 67 depends upon the electrical forces $\underset{\sim}{f}_e$ and the fluid motion $\underset{\sim}{U}$ being solenoidal with respect to particle position coordinates. This allows the force and flow stream functions to be combined by superposition in Equation 73 to give the stream

function for particle trajectories. The unrestrictive nature of these conditions has considerable ramification: this method of solution can be applied to particle collection on any cylinder of irregular geometry having a continuous surface. By Maxwell's equations, $\underset{\sim}{f}_e$ for uniform external electric field and coulombic type forces is always solenoidal regardless of the geometry of the collector. Furthermore, some observations on the expected nature of the collection can be made without reference to a specific collector geometry. For instance, for a given collector geometry (and the same electrical force strength), the values of the grazing limiting trajectories for point particles (found from a case 1 analysis) will be the same for all stationary incompressible flows (of the same orientation) having $\Psi_f = 0$ at the surface of the collector (transpiration does not occur). Likewise, the deposition density will be independent of the flow (in case 3 situations, for portions of the surface over which deposition occurs for all flows considered).

For the external electric field force alone, Equation 86 can be written in the form

$$\hat{\eta} = K_{ex}\hat{\eta}_{max}/G \tag{99}$$

where $\hat{\eta}_{max}$ is the maximum possible efficiency for a given field orientation, which corresponds to the particles following the external field lines. $\hat{\eta}_{max}$ is a function only

of geometric constants, collector dielectric constant, and field orientation angle. The fact that the numerator dependence on K_{ex} is simply linear for all elliptical-cylinder eccentricities (the K_{ex} dependence of G is independent of the collector) and that K_{ex} is itself independent of geometric parameters or any collector reference length, leads to speculation that Equation 99 may hold for other collector geometries as well. A similar expression can be written for collection by gravitation alone.

The insensitivity of the collection in case 2 to boundary conditions at the surface of the collector allows a general result to be formulated. If it is hypothesized that two nodal limiting trajectories occur (ending at the same velocity node downstream from the collector) whenever only net attractive forces are present at the surface, then it follows that Equation 90 applies to cylindrical collectors of any cross-sectional geometry. This occurs when the attractive coulombic force is the predominant force for collection. The weaker external electric field force only affects collection through the factor G in Equation 90, which is determined by conditions at infinity and governs the approach velocity of the particle (and hence the average time of interaction with the collector).

From the insensitivity of collection with a coulombic force to the shape of the collector, it follows that the rate of particle collection should be unaffected by both

nonuniform temporal deposition of particles on a fiber and an apparent increase in size of the fiber. This, of course, assumes that deviations from a two-dimensional system do not occur, as would be the case if deposition is the same along the length of the fiber. Also, the accumulated line charge density of captured particles must be much less than the original line charge density of the fiber. It should be noted that the collection efficiency with a coulombic force is independent of particle interception, provided particle sizes are small compared to the displacement distance of the velocity node from the surface of the collector.

PARTICLE COLLECTION ON SPHEROIDS

Introduction

In this section, several analyses are presented for electrostatic particle collection on spheroids with coulombic, external electric field, and gravitational forces. In the first part of this section, results are obtained for prolate and oblate spheroids and disks for the case of two-dimensional (axisymmetric) particle trajectories. In the second part, results are obtained for spheroids, spheres, and collectors of arbitrary geometry for cases of three-dimensional (nonaxisymmetric) particle trajectories using a generalization of a method originally proposed by Dukhin and Deryagin (25). The results found for cylinders are also generalized to include three-dimensional cases. In the final part, the influence of droplet density in wet scrubbers is investigated using a cellular model of flow around a sphere.

The results found in this section are useful for predicting particle collection in electrified wet scrubbers for conditions in which particle inertia is negligible. Since spherical water droplets become prolate spheroids in a strong external electric field, the solutions for spheroids are particularly useful. Recently Knutson (45) has summarized known approximate results for collection on oblate spheroids, including electrical image forces but not exter-

nal electric field forces. Results for two-dimensional cases of collection on spheres have already been given by Nielsen (80) and Nielsen and Hill (81).

Two-Dimensional Trajectories

Equation of motion

The equation of motion for a small, inertialess, spherical particle in a gas has been given previously as

$$\underset{\sim}{v} = \underset{\sim}{u} + (C/6\pi\mu R_p) \sum_e \underset{\sim}{F}_e \qquad (100)$$

where $\underset{\sim}{v}$ is the particle velocity, $\underset{\sim}{u}$ the local mean fluid velocity, and the $\underset{\sim}{F}_e$'s the electrical and gravitational forces on the particle. For collection on spheroids, Equation 100 is solved using the prolate and oblate spheroidal coordinate systems shown in Figure 62, with the collector surface being given by $\xi = \xi_0$. Geometrical quantities associated with the collector surface are shown in Figure 63. Useful relationships between a, the length of the major semiaxis, b, the length of the minor semiaxis, c, one half the focal distance, and ξ_0 are

$$c^2 = a^2 - b^2, \; a/c = \cosh\xi_0, \; b/c = \sinh\xi_0$$
$$\xi_0 = \tfrac{1}{2} \ln[(a/b + 1)/(a/b - 1)] \qquad (101)$$

By using the reference length b (a) for prolate (oblate) spheroids and the undisturbed free-stream velocity U_o, the

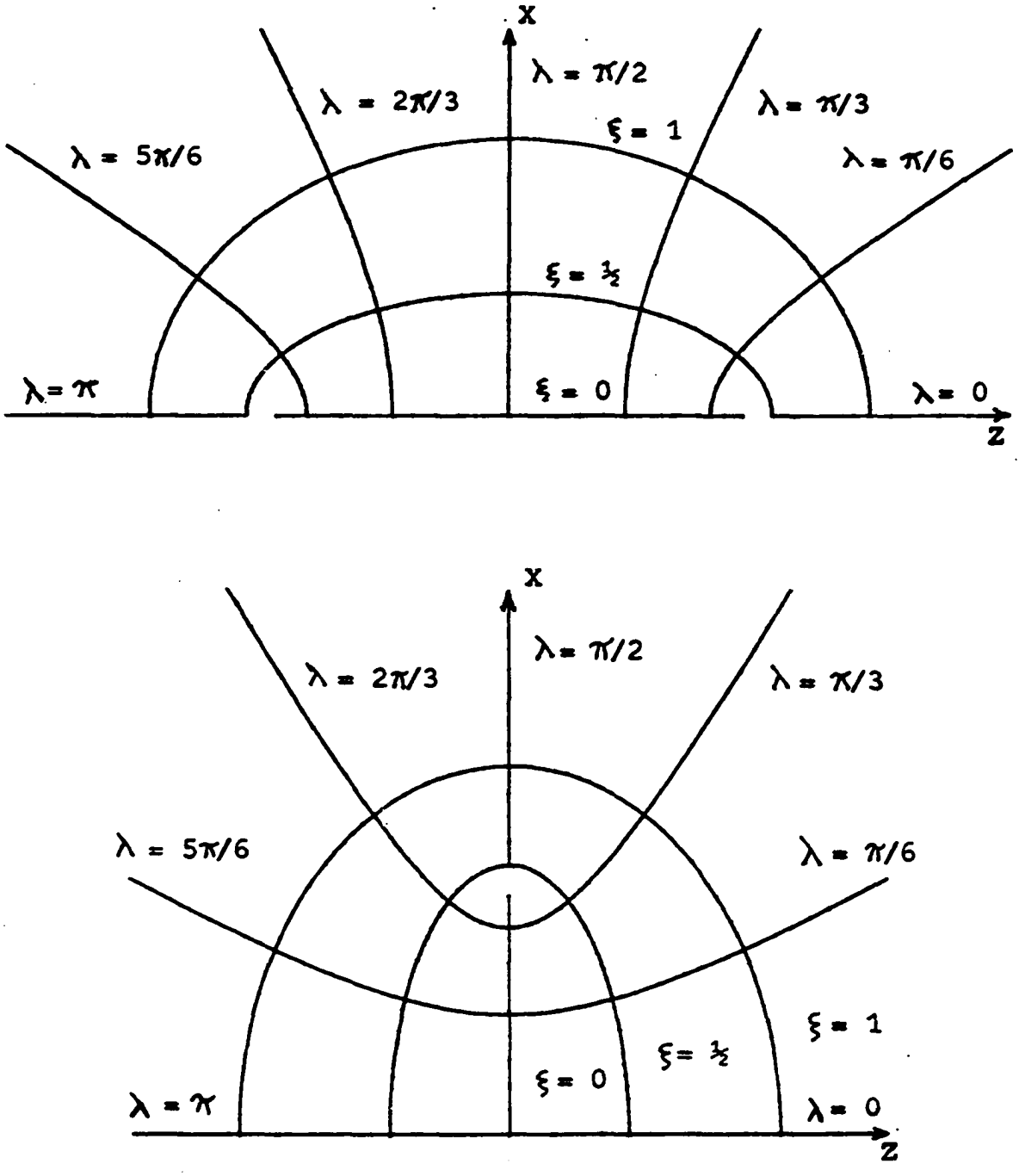

Figure 62. Prolate spheroidal (above) and oblate spheroidal (below) coordinate systems where Z-axis is axis of revolution

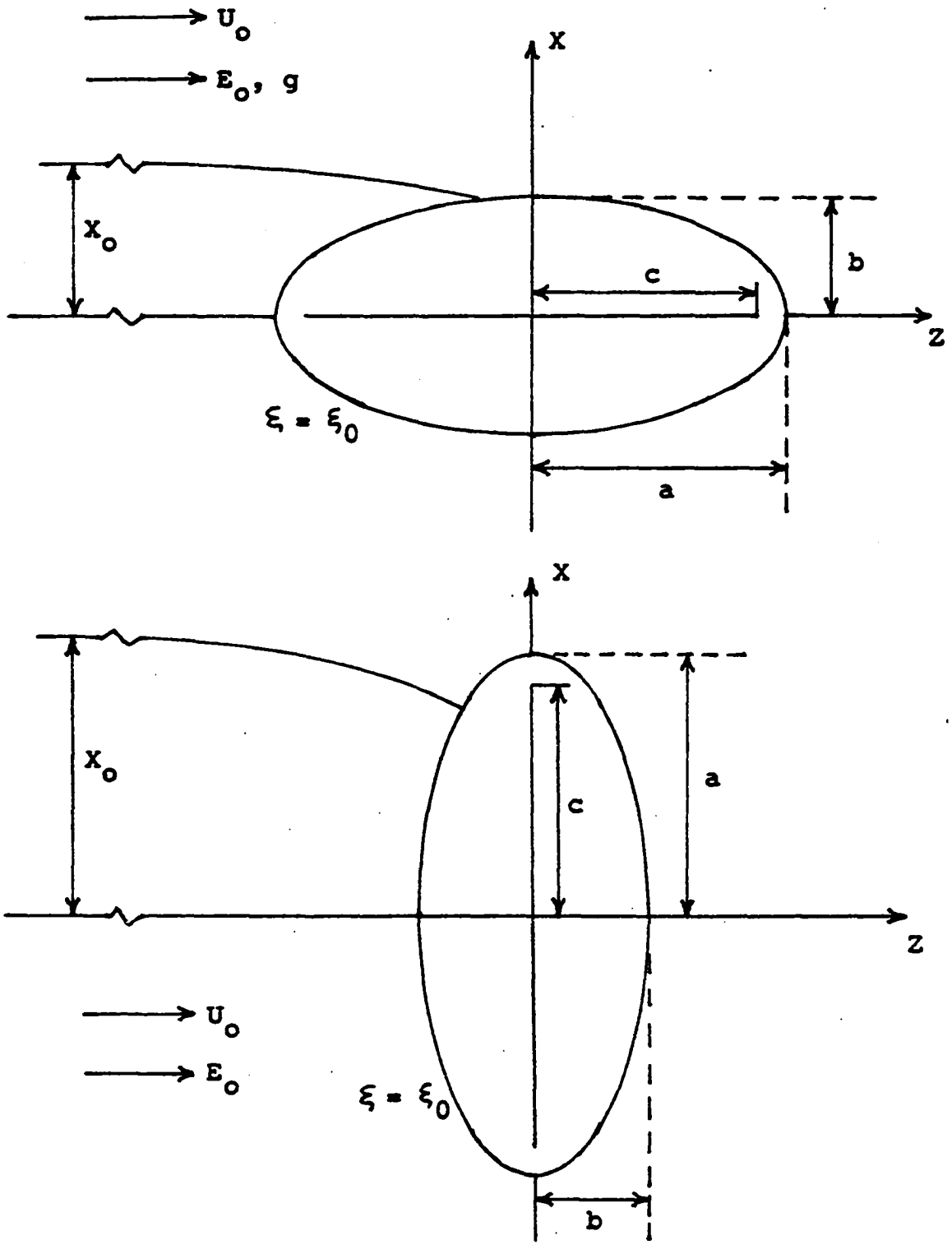

Figure 63. Geometrical quantities used in the mathematical model of particle collection on prolate spheroids (above) and oblate spheroids (below)

equation of motion can be written in the dimensionless form

$$\underset{\sim}{V} = \underset{\sim}{U} + \sum_e K_e \underset{\sim}{f}_e \tag{102}$$

where K_e is a dimensionless characteristic particle mobility corresponding to $\underset{\sim}{F}_e$, which has dimensionless spatial dependence $\underset{\sim}{f}_e$. In terms of the spheroidal coordinates ξ, λ, the dimensionless rectangular coordinates Z, X are given by

Prolate spheroid

$$Z = \cosh\xi \cos\lambda / \sinh\xi_0, \quad X = \sinh\xi \sin\lambda / \sinh\xi_0 \tag{103}$$

Oblate spheroid

$$Z = \sinh\xi \cos\lambda / \cosh\xi_0, \quad X = \cosh\xi \sin\lambda / \sinh\xi_0 \tag{104}$$

Two flow fields that can be used to describe the fluid motion in Equation 102 are Stokes flow (31) and potential flow (74) parallel to the axis of revolution. For these and any other axisymmetric, steady, incompressible flows, the fluid velocity field can be written in terms of the Stokes stream function,

Prolate spheroid

$$U_\xi = \frac{\sinh^2\xi_0}{\Omega \sinh\xi \sin\lambda} \frac{\partial\Psi_f}{\partial\lambda}, \quad U_\lambda = \frac{-\sinh^2\xi_0}{\Omega \sinh\xi \sin\lambda} \frac{\partial\Psi_f}{\partial\xi} \tag{105}$$

$$\Omega \equiv (\sinh^2\xi + \sin^2\lambda)^{1/2} \tag{106}$$

Oblate spheroid

$$U_\xi = \frac{\cosh^2\xi_0}{\Lambda \cosh\xi \sin\lambda} \frac{\partial \Psi_f}{\partial \lambda}, \quad U_\lambda = \frac{-\cosh^2\xi_0}{\Lambda \cosh\xi \sin\lambda} \frac{\partial \Psi_f}{\partial \xi} \tag{107}$$

$$\Lambda \equiv (\cosh^2\xi - \sin^2\lambda)^{1/2} \tag{108}$$

where dimensionless variables have been used, $U_\xi = u_\xi/U_o$, $U_\lambda = u_\lambda/U_o$, $\Psi_f = \psi_f/bU_o$ (prolate spheroid), $\Psi_f = \psi_f/aU_o$ (oblate spheroid). The dimensionless fluid velocities and stream functions for Stokes flow and potential flow are given in Tables 57 and 58. The stream function for an arbitrary symmetrical flow field can be written in the general form

Prolate spheroid

$$\Psi_f = \frac{\sinh^2\xi \sin^2\lambda}{2 \sinh^2\xi_0} h(\xi) \tag{109}$$

Oblate spheroid

$$\Psi_f = \frac{\cosh^2\xi \sin^2\lambda}{2 \cosh^2\xi_0} h(\xi) \tag{110}$$

where $h(\xi)$ satisfies the boundary conditions

$$h(\xi_0) = 0, \quad \lim_{Z \to -\infty} h(\xi) = 1 \tag{111}$$

for both spheroidal coordinate systems; the definition of $h(\xi)$ for Stokes flow and potential flow is given in Tables

Table 57. Prolate spheroid dimensionless fluid velocities and stream functions for flow parallel to the axis of revolution

$$U_\xi = \frac{\sinh\xi \cos\lambda}{\mathcal{Q}} h(\xi)$$

$$U_\lambda = -\frac{\cosh\xi \sin\lambda}{\mathcal{Q}} k(\xi)$$

$$\Psi_f = \frac{\sinh^2\xi \sin^2\lambda}{2\sinh^2\xi_0} h(\xi)$$

POTENTIAL FLOW

$$h(\xi) = 1 - \frac{\ln[\tanh(\xi/2)] + \cosh\xi/\sinh^2\xi}{\ln[\tanh(\xi_0/2)] + \cosh\xi_0/\sinh^2\xi_0}$$

$$k(\xi) = 1 - \frac{\ln[\tanh(\xi/2)] + 1/\cosh\xi}{\ln[\tanh(\xi_0/2)] + \cosh\xi_0/\sinh^2\xi_0}$$

STOKES FLOW

$$h(\xi) = 1 - \frac{(\cosh^2\xi_0 + 1)\ln[\tanh(\xi/2)] + \cosh\xi \sinh^2\xi_0/\sinh^2\xi}{(\cosh^2\xi_0 + 1)\ln[\tanh(\xi_0/2)] + \cosh\xi_0}$$

$$k(\xi) = 1 - \frac{(\cosh^2\xi_0 + 1)\ln[\tanh(\xi/2)] + \cosh^2\xi_0/\cosh\xi}{(\cosh^2\xi_0 + 1)\ln[\tanh(\xi_0/2)] + \cosh\xi_0}$$

Table 58. Oblate spheroid dimensionless fluid velocities and stream functions for flow parallel to the axis of revolution

$$U_\xi = \frac{\cosh\xi \cos\lambda}{\mathcal{N}} h(\xi)$$

$$U_\lambda = -\frac{\sinh\xi \sin\lambda}{\mathcal{N}} k(\xi)$$

$$\Psi_f = \frac{\cosh^2\xi \sin^2\lambda}{2\cosh^2\xi_0} h(\xi)$$

POTENTIAL FLOW

$$h(\xi) = 1 - \frac{\cot^{-1}(\sinh\xi) - \sinh\xi/\cosh^2\xi}{\cot^{-1}(\sinh\xi_0) - \sinh\xi_0/\cosh^2\xi_0}$$

$$k(\xi) = 1 - \frac{\cot^{-1}(\sinh\xi) - 1/\sinh\xi}{\cot^{-1}(\sinh\xi_0) - \sinh\xi_0/\cosh^2\xi_0}$$

STOKES FLOW

$$h(\xi) = 1 - \frac{(\sinh^2\xi_0 - 1)\cot^{-1}(\sinh\xi) - \sinh\xi \cosh^2\xi_0/\cosh^2\xi}{(\sinh^2\xi_0 - 1)\cot^{-1}(\sinh\xi_0) - \sinh\xi_0}$$

$$k(\xi) = 1 - \frac{(\sinh^2\xi_0 - 1)\cot^{-1}(\sinh\xi) - \sinh^2\xi_0/\sinh\xi}{(\sinh^2\xi_0 - 1)\cot^{-1}(\sinh\xi_0) - \sinh\xi_0}$$

Table 59. Prolate spheroid force expressions with external fields parallel to the axis of revolution

---

COULOMBIC FORCE

$$K_c = CQ_cQ_p/24\pi^2\epsilon_f R_p b^2 \mu U_o$$

$$f_c^{\xi} = \sinh^2\xi_0/\mathfrak{N} \sinh\xi$$

$$f_c^{\lambda} = 0$$

$$\Psi_c = -K_c \cos\lambda$$

EXTERNAL ELECTRIC FIELD FORCE

$$K_{ex} = CQ_pE_o/6\pi R_p \mu U_o$$

$$f_{ex}^{\xi} = \frac{\sinh\xi \cos\lambda}{\mathfrak{N}} p(\xi)$$

$$f_{ex}^{\lambda} = -\frac{\cosh\xi \sin\lambda}{\mathfrak{N}} q(\xi)$$

$$\Psi_{ex} = K_{ex} \frac{\sinh^2\xi \sin^2\lambda}{2\sinh^2\xi_0} p(\xi)$$

$$p(\xi) = 1 + 2\Gamma \frac{\ln[\tanh(\xi/2)] + \cosh\xi/\sinh^2\xi}{\ln[\tanh(\xi_0/2)] + \cosh\xi_0/\sinh^2\xi_0}$$

$$q(\xi) = 1 + 2\Gamma \frac{\ln[\tanh(\xi/2)] + 1/\cosh\xi}{\ln[\tanh(\xi_0/2)] + \cosh\xi_0/\sinh^2\xi_0}$$

$$\Gamma \equiv (\epsilon_c/\epsilon_f - 1)/[\bar{\Phi}(\xi_0)\epsilon_c/\epsilon_f + 2]$$

Table 59. (Continued)

$$\Phi(\xi_0) \equiv -2\,\frac{\ln[\tanh(\xi_0/2)] + 1/\cosh\xi_0}{\ln[\tanh(\xi_0/2)] + \cosh\xi_0/\sinh^2\xi_0}$$

GRAVITATIONAL FORCE

$$K_g = 2R_p^2\rho_p gC/9\mu U_o$$

$$f_g^{\xi} = (\sinh\xi\,\cos\lambda)/\Omega$$

$$f_g^{\lambda} = -(\cosh\xi\,\sin\lambda)/\Omega$$

$$\Psi_g = K_g\,(\sinh^2\xi\,\sin^2\lambda)/2\sinh^2\xi_0$$

Table 60. Oblate spheroid force expressions with external fields parallel to the axis of revolution

COULOMBIC FORCE

$$K_c = CQ_cQ_p/24\pi^2\epsilon_f R_p a^2\mu U_o$$

$$f_c^{\xi} = \cosh^2\xi_0/\Omega\,\cosh\xi$$

$$f_c^{\lambda} = 0$$

$$\Psi_c = -K_c\,\cos\lambda$$

EXTERNAL ELECTRIC FIELD FORCE

$$K_{ex} = CQ_pE_o/6\pi R_p\mu U_o$$

Table 60. (Continued)

$$f_{ex}^{\xi} = \frac{\cosh\xi \cos\lambda}{\Omega} p(\xi)$$

$$f_{ex}^{\lambda} = -\frac{\sinh\xi \sin\lambda}{\Omega} q(\xi)$$

$$\Psi_{ex} = K_{ex} \frac{\cosh^2\xi \sin^2\lambda}{2\cosh^2\xi_0} p(\xi)$$

$$p(\xi) = 1 + 2\Gamma \frac{\cot^{-1}(\sinh\xi) - \sinh\xi/\cosh^2\xi}{\cot^{-1}(\sinh\xi_0) - \sinh\xi_0/\cosh^2\xi_0}$$

$$q(\xi) = 1 + 2\Gamma \frac{\cot^{-1}(\sinh\xi) - 1/\sinh\xi}{\cot^{-1}(\sinh\xi_0) - \sinh\xi_0/\cosh^2\xi_0}$$

$$\Gamma \equiv (\epsilon_c/\epsilon_f - 1)/[\Xi(\xi_0)\epsilon_c/\epsilon_f + 2]$$

$$\Xi(\xi_0) \equiv -2 \frac{\cot^{-1}(\sinh\xi_0) - 1/\sinh\xi_0}{\cot^{-1}(\sinh\xi_0) - \sinh\xi_0/\cosh^2\xi_0}$$

GRAVITATIONAL FORCE

$$K_g = 2R_p^2 \rho_p g C/9\mu U_o$$

$$f_g^{\xi} = (\cosh\xi \cos\lambda)/\Omega$$

$$f_g^{\lambda} = -(\sinh\xi \sin\lambda)/\Omega$$

$$\Psi_g = K_g (\cosh^2\xi \sin^2\lambda)/2\cosh^2\xi_0$$

Table 61. Values of $\mathfrak{L}(\xi_0)$ for prolate and oblate spheroids

a/b	ξ_0	$\mathfrak{L}(\xi_0)$	
		prolate	oblate
1.000	∞	1.0000	1.0000
1.001	3.8007	0.9988	1.0012
1.010	2.6516	0.9881	1.0120
1.050	1.8568	0.9430	1.0601
1.100	1.5223	0.8914	1.1205
1.150	1.3313	0.8444	1.1810
1.200	1.1989	0.8016	1.2418
1.250	1.0986	0.7624	1.3027
1.300	1.0184	0.7264	1.3638
1.400	0.8959	0.6624	1.4864
1.500	0.8047	0.6075	1.6095
1.750	0.6496	0.4993	1.9189
2.000	0.5493	0.4200	2.2301
2.500	0.4236	0.3125	2.8562
3.000	0.3466	0.2439	3.4853
4.000	0.2554	0.1631	4.7486
5.000	0.2027	0.1182	6.0155
7.500	0.1341	0.0646	9.1898
10.000	0.1003	0.0414	12.3683
20.000	0.0500	0.0136	25.0935
∞	0	0	∞

57 and 58.

The dimensionless forces are expressed in terms of ξ and λ components as $K_e \underset{\sim}{f}_e = K_e(f_e^{\xi} \underset{\sim}{a}_{\xi} + f_e^{\lambda} \underset{\sim}{a}_{\lambda})$, with the parameters K_e and force components f_e^{ξ} and f_e^{λ} given in Tables 59 and 60 for the coulombic force, the external electric field force, and the gravitational force. Because these forces are both axisymmetric (for the external fields parallel to the axis of revolution) and solenoidal, the force components can also be written in terms of Stokes stream functions Ψ_e, which are also included in Tables 59 and 60; f_e^{ξ} and f_e^{λ} are recovered from Ψ_e by using Equations 105 and 107, with obvious changes in nomenclature. In Tables 59 and 60, the polarization coefficient of the collector in the direction of the axis of revolution, Γ, is a function of the geometrical parameter $\Phi(\xi_0)$, which changes with collector eccentricity. Values of $\Phi(\xi_0)$ are compared in Table 61 for prolate and oblate spheroids. The uniform external electric field E_o and gravity are both parallel to the free-stream velocity; E_o and g are considered positive when in the same direction as U_o, and negative when in the opposite direction.

Solution for the trajectory equation

Because the fluid motion and forces are stationary, axisymmetric, and solenoidal, a Stokes stream function, Ψ, also exists for the particle trajectories and is found by

superposition

$$\Psi = \Psi_f + \Psi_c + \Psi_{ex} + \Psi_g \tag{112}$$

Since Ψ is constant along a particle trajectory, the upstream or initial value Ψ_o is used to evaluate the left hand side of Equation 112. In the limit $Z \to -\infty$, $X \to X_o$, $\lambda \to \pi$, and $\xi \to \infty$; using Equations 103 and 104 gives

$$\Psi_o = \tfrac{1}{2}X_o^2(1 + K_{ex} + K_g) + K_c \tag{113}$$

for both prolate and oblate spheroids. Combining Equations 112 and 113 gives the particle trajectory equations

Prolate spheroid

$$X_o^2 = \frac{\sinh^2\xi \sin^2\lambda [h(\xi) + K_{ex}p(\xi) + K_g]}{\sinh^2\xi_0 (1 + K_{ex} + K_g)} - \frac{2K_c(\cos\lambda + 1)}{(1 + K_{ex} + K_g)} \tag{114}$$

Oblate spheroid

$$X_o^2 = \frac{\cosh^2\xi \sin^2\lambda [h(\xi) + K_{ex}p(\xi) + K_g]}{\cosh^2\xi_0 (1 + K_{ex} + K_g)} - \frac{2K_c(\cos\lambda + 1)}{(1 + K_{ex} + K_g)} \tag{115}$$

where the external electric field force function $p(\xi)$, defined in Tables 59 and 60, has the limits $p(\xi_0) = 1 + 2\Gamma$ and $p(\infty) = 1$.

Collection efficiencies

The efficiency of particle collection, η, is defined as the cross-sectional area perpendicular to the particle paths

far upstream from which all particles of a given size are collected, divided by the reference area πb^2 (prolate spheroid) or πa^2 (oblate spheroid). For axisymmetric particle trajectories the undisturbed cross-sectional area is circular, and the efficiency is given by $\eta = X_i^2$, where X_i is the value of X_o for the limiting trajectory for particle collection. The collection efficiency of point particles in rectilinear motion parallel to the axis of revolution is one.

For a combination of the coulombic and external forces, the boundary condition for collection by particle interception is not of simple form when written in spheroidal coordinates, and only solutions for point particles will be considered. For point particles, impaction occurs when $\xi = \xi_0$, and Equations 114 and 115 both reduce to

$$X_o^2 = \frac{[(1 + 2\Gamma)K_{ex} + K_g]}{(1 + K_{ex} + K_g)} \sin^2\lambda - \frac{2K_c\,(\cos\lambda + 1)}{(1 + K_{ex} + K_g)} \qquad (116)$$

The limiting trajectory for impaction is determined by identifying the value of $\lambda = \lambda_i$ for which X_o^2 is a maximum in Equation 116, that is

$$(1 + K_{ex} + K_g)\frac{dX_o^2}{d\lambda} = 0 = \{[(1 + 2\Gamma)K_{ex} + K_g]\cos\lambda_i + K_c\}\sin\lambda_i \qquad (117)$$

Therefore, λ_i is given either by $\sin\lambda_i = 0$ or $\cos\lambda_i = W_0$, where

$$W_0 \equiv -K_c/[(1 + 2\Gamma)K_{ex} + K_g] \qquad (118)$$

Substituting the values of λ_i into Equation 116 gives the following results.

$\underline{(1 + 2\Gamma)K_{ex} + K_g \geq 0}$

Under this condition, the force at the surface of the collector due to the external fields is attractive for the upstream half of the collector but repulsive for the downstream half. Addition of the coulombic force leads to the following force distributions and collection efficiencies.

1) For $W_0 \leq -1$, only repulsive forces are present and collection does not occur; $\lambda_i = \pi$, $\eta = 0$.

2) For $-1 < W_0 < 1$, both attractive and repulsive forces are present, with collection occurring over the entire attractive force region. The limiting trajectory grazes the collector at $\lambda_i = \cos^{-1}W_0$, where the force changes from attraction to repulsion,

$$\eta = \frac{[(1 + 2\Gamma)K_{ex} + K_g - K_c]^2}{[(1 + 2\Gamma)K_{ex} + K_g](1 + K_{ex} + K_g)} \qquad (119)$$

3) For $W_0 \geq 1$, only attractive forces are present and collection occurs over the entire collector. The limiting trajectory ends at a velocity node (where the particle velocity goes to zero due to a balance of the drag and electrical forces) located downstream from the collector along the axis of revolution; $\lambda_i = 0$,

$$\eta = -4K_c/(1 + K_{ex} + K_g) \qquad (120)$$

$$\underline{(1 + 2\Gamma)K_{ex} + K_g < 0,\ 1 + K_{ex} + K_g > 0}$$

Under these conditions, the external fields oppose the motion of the particle, and the particle velocity far upstream, given by $1 + K_{ex} + K_g$, is less than the free-stream velocity. At the surface of the collector, the forces due to the external fields are repulsive for the upstream half of the collector but attractive for the downstream half.

1) For $K_c > 0$, although portion of the downstream half of the collector is attractive (for $0 < W_0 < 1$), the repulsive forces upstream prevent collection from occurring. The collector is entirely surrounded by a space void of particles, which is delineated by the paths of particles diverted from the axis of revolution upstream and extends to infinity in the downstream direction.

2) For $K_c = 0$, for symmetrical flows a spheroidal surface surrounds the collector that has $V_\xi = 0$; hence a layer void of particles exists and no collection occurs.

3) For $K_c < 0$, although the external forces oppose the motion of the particle, the presence of an attractive coulombic force makes this action advantageous; the slower approach velocity of the particles increases the time of interaction with the coulombic force. Repulsive forces are present over portion of the upstream half of the collector (for $-1 < W_0 < 0$), but particles diverted upstream from the

axis of revolution intersect the collector at $\lambda = \lambda_0$, where, from setting $X_o^2 = 0$ in Equation 116, $\cos\lambda_0 = 1 + 2W_0$. Collection does not occur over the entire attractive force region and under some conditions occurs exclusively on the downstream half of the collector. The limiting trajectory ends at a velocity node downstream from the collector; hence $\lambda_i = 0$ and η is given by Equation 120.

Equations 119 and 120 give the collection efficiency for both prolate and oblate spheroids when the appropriate value of Γ is used; in the limit $\xi_0 \to \infty$, the collector becomes spherical, $\tilde{\Phi}(\xi_0) \to 1$, Γ reduces to the polarization coefficient of a sphere, and the results found previously for spheres are recovered. Trajectories for spheroids that illustrate the different cases above are similar in form to those given by Nielsen (80) and Nielsen and Hill (81) for spheres, with obvious differences. In deriving Equation 116 for point particles, the influence of the velocity field completely disappears, and for a given collector eccentricity, the collection efficiency and distribution of collection over the surface of the collector are the same for all stationary, axisymmetric, incompressible flows having $\Psi_f = 0$ (the stagnation streamline) at the surface of the collector. Furthermore, whenever the limiting trajectory ends at a velocity node, the collection efficiency, given by Equation 120, is independent of collector eccentricity and particle interception (provided particle sizes are small compared to

the displacement distance of the velocity node from the surface of the collector). In fact, because by Maxwell's equations the electrical forces are solenoidal for any collector shape, Equation 120 holds for any body of revolution.

With just the external forces ($K_c = 0$), the condition for collection by interception can be written in simple form because $\lambda_i = \pi/2$ always holds. The interception condition for the limiting trajectory is $X^* = 1 + \mathcal{R}$ at $Z = 0$, where $\mathcal{R} \equiv R_p/b$ (prolate spheroid) or $\mathcal{R} \equiv R_p/a$ (oblate spheroid) is the interception parameter. Using Equation 103 or 104 gives the interception value of ξ as $\xi^* = \sinh^{-1}[(1 + \mathcal{R})\sinh\xi_0]$ for prolate spheroids and $\xi^* = \cosh^{-1}[(1 + \mathcal{R})\cosh\xi_0]$ for oblate spheroids. Substituting $\xi = \xi^*$ and $\lambda = \pi/2$ into Equations 114 and 115 gives

$$\eta = \frac{(1 + \mathcal{R})^2[h(\xi^*) + K_{ex}p(\xi^*) + K_g]}{(1 + K_{ex} + K_g)} \qquad (121)$$

An interesting situation arises with potential flow, for when $K_{ex} = 1/2\Gamma$, $V_x = 0$ and $V_z = 1 + K_{ex} + K_g$; the viscous and electrical forces exactly cancel each other and particles remain in rectilinear motion. Under this condition the collection efficiency, given by $\eta = (1 + \mathcal{R})^2$, is unaffected by particle inertia. Similar behavior has been found for spheres (82), circular cylinders, and elliptical cylinders and ribbons.

Results for particle collection on disks can be obtained from the solutions found for oblate spheroids by taking the limit b = 0. In this limit considerable simplification is achieved since $\xi_0 = 0$, $\bar{\Phi}(\xi_0) \to \infty$, and $\Gamma = 0$; no polarization of the collector occurs and the external electric field lines are uniform.

Three-Dimensional Trajectories

The method of solution used in the first part of this section and in the previous analyses can only be applied to incompressible flows and solenoidal forces in cases where particle trajectories are two-dimensional, so that the stream function or Stokes stream function exists. However, for three-dimensional cases collection efficiencies can be found using a generalization of the method of solution originally proposed by Dukhin and Deryagin (25). In Dukhin and Deryagin's method, instead of finding particle trajectories and defining collection in terms of limiting trajectories, the total particle flux to the collector is found using the force distribution at the collector, and the collection efficiency is defined with respect to a reference particle flux. The method was originally proposed for point particles and used the forces at the surface of the collector, but it can also be applied to collection with interception of finite sized particles, using the force distribution at the surface surrounding the collector that

is defined by the centers of particles at capture. Although this can be an extremely useful technique, it must be applied with caution to avoid erroneous results: using just conditions at the surface of the collector, it is not possible in all cases to distinguish between the flux of particles coming from upstream and the flux of particles on closed trajectories originating elsewhere on the surface of the collector.

Method of solution

The collection efficiency, $\hat{\eta}$, is defined as the ratio of total particle flux (of particles from upstream) at the surface of interception surrounding the collector to a reference particle flux, taken to be the flux of particle centers through a reference area S_{rf}, where S_{rf} is perpendicular to the particle paths far upstream where uniform conditions exist. Dukhin and Deryagin (25) have shown that for stationary incompressible flows and solenoidal forces, the concentration of particles is constant along the particle trajectories and can be expressed as n_o, the particle concentration under uniform conditions upstream. Therefore, the reference particle flux is given by $I_{rf} = n_o v_o S_{rf}$, where v_o is the particle approach velocity far upstream. For collection on bodies of revolution, it is convenient to set $S_{rf} = \pi R_{rf}^2$, where R_{rf} is some reference length. This gives $I_{rf} = n_o v_o \pi R_{rf}^2$.

If it is assumed that collection occurs over the entire attractive force region at the surface of interception, then the total particle flux to the surface of interception is given by

$$I = -n_o \iint_s v_n ds \tag{122}$$

where v_n is the particle velocity normal to the surface and the integration area s is over the region of attractive normal force (including the drag force) at the surface. Since the external electric field force and the coulombic force are of the form $Q_p \underset{\sim}{E}$, Equation 100 can be written as

$$\underset{\sim}{v} = \underset{\sim}{u} + (C/6\pi\mu R_p)[Q_p(\underset{\sim}{E}_c + \underset{\sim}{E}_{ex}) + \underset{\sim}{F}_g] \tag{123}$$

Substituting Equation 123 into Equation 122 and dividing I by I_{rf} gives

$$\hat{\eta} = -(1/v_o \pi R_{rf}^2) \iint_s \left\{ u_n + \frac{Q_p(E_{n,c} + E_{n,ex}) + F_{n,g}}{(6\pi\mu R_p/C)} \right\} ds \tag{124}$$

At this point it is convenient to make Equation 124 dimensionless using the dimensionless variables

$$V_o \equiv v_o/U_o, \quad dS \equiv ds/R_{rf}^2, \quad E'_{n,ex} \equiv E_{n,ex}/E_o$$
$$E'_{n,c} \equiv 4\pi\epsilon_f R_{rf}^2 E_{n,c}/Q_c, \quad F'_{n,g} \equiv F_{n,g} 3/4\pi R_p^3 \rho_p g \tag{125}$$

where $E'_{n,c}$ is defined using as a reference the electrical field intensity at a distance R_{rf} away from a point charge

Q_c, where Q_c is the collector charge. This gives the general expression for calculating the collection efficiency as

$$\hat{\eta} = -(1/\pi V_o) \iint_S (U_n + K_c E'_{n,c} + K_{ex} E'_{n,ex} + K_g F'_{n,g}) dS \quad (126)$$

where

$$K_c \equiv CQ_c Q_p / 24\pi^2 \epsilon_f R_p \mu U_o R_{rf}^2 \quad (127)$$

$$K_{ex} \equiv CQ_p E_o / 6\pi R_p \mu U_o \quad (128)$$

$$K_g \equiv 2R_p^2 \rho_p g C / 9\mu U_o \quad (129)$$

are the force parameters. Notice that K_{ex} and K_g are independent of the reference length. The integration area S in Equation 126 is determined from

$$V_n = U_n + K_c E'_{n,c} + K_{ex} E'_{n,ex} + K_g F'_{n,g} = 0 \quad (130)$$

With the external electric field and gravity parallel to each other, the dimensionless particle approach velocity is given by

$$V_o = [1 + 2(K_{ex} + K_g)\cos\alpha + (K_{ex} + K_g)^2]^{\frac{1}{2}} \quad (131)$$

where α is the angle between $\underset{\sim}{U}_o$ and $\underset{\sim}{E}_o$.

Solution for point particles

For point particles, integration of Equation 126 is over the attractive force region at the surface of the collector. Since $U_n = 0$ for all flows, from Equations 123 and 126 it can be seen that for any given collector, the deposition over the surface of the collector and the collection efficiency are independent of the form of the flow (provided collection occurs over the entire attractive force region for all flows considered). Equation 126 can be used to generalize the results found in the first part of this section for collection on prolate and oblate spheroids and spheres. With the external fields remaining parallel to the axis of revolution, for the flow field at an arbitrary angle α to the axis of revolution Equation 119 becomes

$$\hat{\eta} = \frac{[(1 + 2\Gamma)K_{ex} + K_g - K_c]^2}{[(1 + 2\Gamma)K_{ex} + K_g]V_o} \qquad (132)$$

with V_o given by Equation 131. For circular and elliptical cylinders, for a combination of the coulombic force with the external field forces perpendicular or nearly perpendicular to the flow, it was found that instead of only having grazing limiting trajectories when both attractive and repulsive forces are present at the surface of the collector, it is also possible to have a combination of grazing limiting trajectories and limiting trajectories that end at a velocity node. When both types of limiting trajectories are

present, collection does not occur over the entire attractive force region; the area over which deposition occurs, and hence the collection efficiency, varies with the flow field. Furthermore, even with a region of repulsion present, it is possible to have only limiting trajectories ending at a velocity node, and grazing limiting trajectories need not occur (in this case a layer void of particles exists over part of the surface). Similar behavior can occur for spheroids and other geometries. Therefore, Equation 132 does not hold if a velocity node is present. For a given flow field, the existence of a velocity node can not be determined from the force distribution at the surface of the collector, but can be found by determining (by systematic means) if $\underset{\sim}{V}$, given by Equation 102, goes to zero at any point away from the collector.

Under the condition that an attractive force is present over the entire surface of the collector, a general result can be obtained using Gauss's law of electrostatics (34), which says that the electrical flux passing through any closed surface is equal to the total charge within the surface. This gives

$$Q_c = \epsilon_f \iint_s E_{n,c} ds, \quad 0 = \epsilon_f \iint_s E_{n,ex} ds \tag{133}$$

When made dimensionless, the coulombic force integral becomes

$$4\pi = \iint_S E'_{n,c}\,dS \tag{134}$$

Like the external electric field force, the integral of the gravitational force over the entire surface of the collector is zero. Therefore, substitution of Equation 134 into Equation 126 gives

$$\hat{\eta} = -4K_c/V_o \tag{135}$$

This result is independent of the shape of the collector, the form of the stationary and incompressible flow field, and the orientation of the flow and external fields to each other and the collector. Equation 135 also holds for finite particles if attractive forces are present over the entire interception surface. For the coulombic force alone, Equation 135 reduces to $\hat{\eta} = -4K_c$. This result was found for an arbitrary collector shape by Levin (61).

Equation 126 can also be used to obtain a general form for $\hat{\eta}$ for collection with the external electric field force alone. For a given orientation of the external electric field with respect to a collector of arbitrary shape, integration of Equation 126 over the region of attractive force gives

$$\hat{\eta} = -(K_{ex}/\pi V_o) \iint_S E'_{n,ex}\,dS \tag{136}$$

But $E'_{n,ex}$, the dimensionless spatial dependence of the electric field, is independent of the field strength.

Therefore, for an infinite field strength, the particles follow the electric field lines to the collector, and the maximum possible collection efficiency is given by

$$\hat{\eta}_{max} = -(1/\pi) \iint_S E'_{n,ex} dS \qquad (137)$$

Substituting Equations 131 and 137 into Equation 136 gives

$$\hat{\eta} = K_{ex} \hat{\eta}_{max} / (1 + 2K_{ex}\cos\alpha + K_{ex}^2)^{\frac{1}{2}} \qquad (138)$$

which is valid for all stationary incompressible flows. $\hat{\eta}_{max}$ is only a function of collector geometry, dielectric constant, and orientation with respect to E_o.

For collection with the gravitational force alone, if R_{rf} is taken to be the equivalent radius of the cross-sectional area of the collector projected in the direction of the gravitational field, then $\hat{\eta}_{max} = 1$, and the collection efficiency is given by

$$\hat{\eta} = K_g / (1 + 2K_g\cos\alpha + K_g^2)^{\frac{1}{2}} \qquad (139)$$

for all collector geometries and flows.

Solution for spheres with interception

Equation 126 can be used to obtain collection efficiencies for particle collection with interception and with the external fields at an arbitrary angle α to the flow direction. The surface of interception is a sphere of

radius $R^* = 1 + \mathcal{R}$, where $\mathcal{R} \equiv R_p/R_c$ is the interception parameter, and Equation 126 becomes

$$\hat{\eta} = -(R^{*2}/\pi V_o) \iint_S (U_r + K_c f_c{}^r + K_{ex} f_{ex}{}^r + K_g f_g{}^r) \sin\theta \, d\theta \, d\phi \tag{140}$$

The spherical coordinate system used in the mathematical model is shown in Figure 64. Dimensionless fluid velocities for potential flow and Stokes flow around a sphere and the force components used in Equation 140 are given in Table 62. It is convenient to express the radial velocity for these and other symmetrical flows in the general form $U_r = h(R) \cos\theta$, where the definition of h(R) for potential flow and Stokes flow is obvious from Table 62. Substituting the radial fluid velocity and force components into Equation 140 gives

$$\hat{\eta} = -(R^{*2}/\pi V_o) \iint_S [(H + P\cos\alpha)\cos\theta + (P\sin\alpha)\sin\theta\cos\phi + Q] \sin\theta \, d\theta \, d\phi \tag{141}$$

with $H \equiv h(R^*)$, $Q \equiv K_c/R^{*2}$, and $P \equiv K_{ex}(1 + \Upsilon/R^{*3}) + K_g$, where Υ is the polarization coefficient for a sphere. The force parameters are given by Equations 127 - 129 with the collector radius R_c as the reference length.

The boundary for integration over the area of attrac-

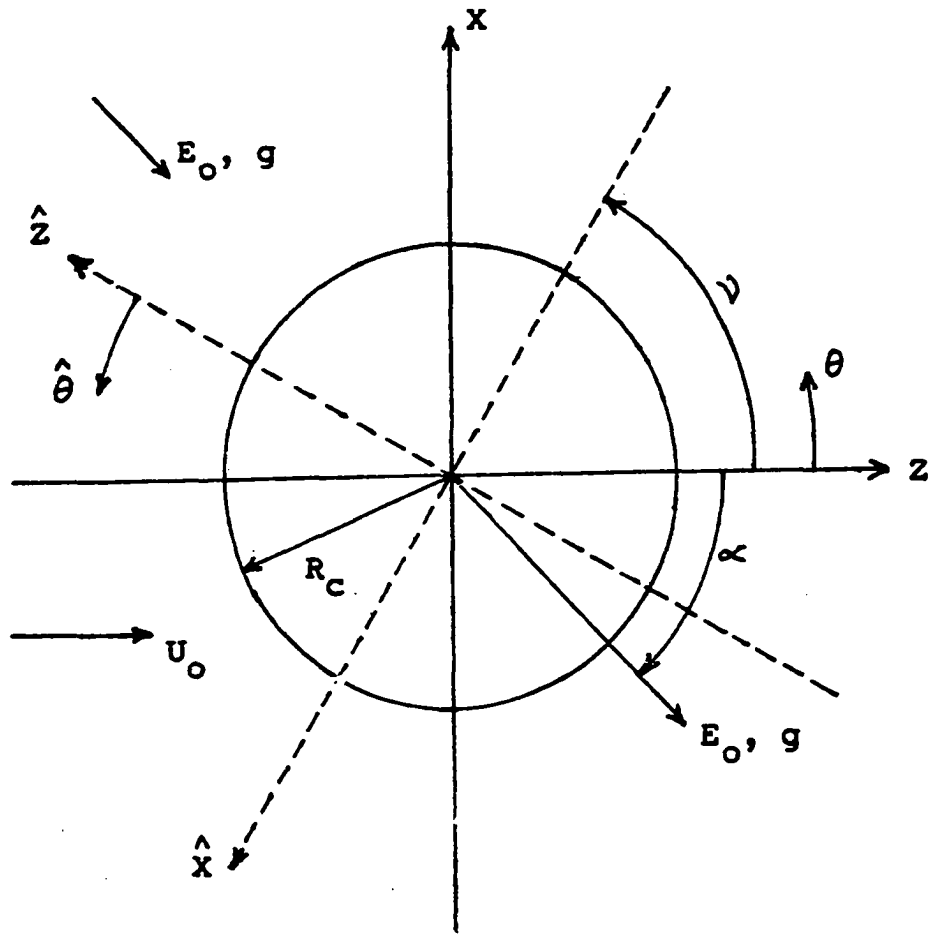

Figure 64. Fixed and rotated spherical and rectangular coordinate systems for particle collection on a sphere. The Y-axis and $\hat{Y}$-axis coincide and extend out from the figure. Surfaces of constant ϕ ($\hat{\phi}$) are half-planes bounded by the Z-axis ($\hat{Z}$-axis), with the angle ϕ ($\hat{\phi}$) measured from the positive X-axis ($\hat{X}$-axis)

Table 62. Spherical collector dimensionless fluid velocities and force components, with the external fields at an angle α to the flow

POTENTIAL FLOW

$$U_r = (1 - 1/R^3)\cos\theta$$

$$U_\theta = -(1 + 1/2R^3)\sin\theta$$

STOKES FLOW

$$U_r = (1 - 3/2R + 1/2R^3)\cos\theta$$

$$U_\theta = -(1 - 3/4R - 1/4R^3)\sin\theta$$

COULOMBIC FORCE

$$f_c^r = 1/R^2$$

$$f_c^\theta = f_c^\phi = 0$$

EXTERNAL ELECTRIC FIELD FORCE

$$f_{ex}^r = (1 + 2\Upsilon/R^3)(\sin\theta\cos\phi\sin\alpha + \cos\theta\cos\alpha)$$

$$f_{ex}^\theta = (1 - \Upsilon/R^3)(\cos\theta\cos\phi\sin\alpha - \sin\theta\cos\alpha)$$

$$f_{ex}^\phi = -(1 - \Upsilon/R^3)\sin\phi\sin\alpha$$

$$\Upsilon \equiv (\epsilon_c - \epsilon_f)/(\epsilon_c + 2\epsilon_f)$$

GRAVITATIONAL FORCE

$$f_g^r = \sin\theta\cos\phi\sin\alpha + \cos\theta\cos\alpha$$

$$f_g^\theta = \cos\theta\cos\phi\sin\alpha - \sin\theta\cos\alpha$$

$$f_g^\phi = -\sin\phi\sin\alpha$$

tive radial force is found from

$$V_r = (H + P\cos\alpha)\cos\theta + (P\sin\alpha)\sin\theta\cos\phi + Q = 0 \quad (142)$$

This boundary condition can be expressed in simpler form by using a spherical coordinate system that is rotated about the Y-axis (see Figure 64) by the angle $\nu + \pi/2$, where

$$\sin\nu = (H + P\cos\alpha)/A, \quad \cos\nu = -(P\sin\alpha)/A \quad (143)$$

$$A \equiv (H^2 + 2HP\cos\alpha + P^2)^{1/2} \quad (144)$$

The transformation between the fixed θ, ϕ coordinate system and rotated $\hat{\theta}, \hat{\phi}$ coordinate system is given by

$$\sin\theta\cos\phi = \cos\hat{\theta}\cos\nu - \sin\hat{\theta}\cos\hat{\phi}\sin\nu \quad (145)$$

$$\cos\theta = -\cos\hat{\theta}\sin\nu - \sin\hat{\theta}\cos\hat{\phi}\cos\nu \quad (146)$$

Substituting Equations 143 - 146 into Equation 142 gives

$$V_r = -A\cos\hat{\theta}_i + Q = 0 \quad (147)$$

The boundary condition is given by the intersection of the spherical surface $R = R^*$ and the cone about the rotated $\hat{Z}$-axis defined by $\hat{\theta} = \hat{\theta}_i$. This circular boundary lies on the plane $Z_i = QR^*/A$. For $Q = 0$, only the external forces are present and collection occurs over one half of the collector.

Rewriting Equation 141 in terms of the rotated $\hat{\theta}, \hat{\phi}$

coordinate system gives

$$\hat{\eta} = (R^{*2}/\pi AV_o)\int_0^{\hat{\theta}_i}\int_0^{2\pi} [A^2\cos\hat{\theta} - 2(H + P\cos\alpha)(P\sin\alpha)\sin\hat{\theta}\cos\hat{\phi} - AQ]\sin\hat{\theta}\, d\hat{\phi}\, d\hat{\theta} \tag{148}$$

Integration of Equation 148 gives the final result

$$\hat{\eta} = R^{*2}(A - Q)^2/AV_o \tag{149}$$

valid for $-1 \leq Q/A \leq 1$. In the limit $\hat{\theta}_i = \pi$ (corresponding to $Q/A = -1$), collection occurs over the entire surface of the collector and Equation 135 is recovered. With the external fields parallel to the flow ($\alpha = 0$), the particle trajectories are two dimensional and Equation 148 gives the same results found earlier by Nielsen and Hill (80, 81). Equation 149 only holds if a velocity node is not present outside the interception surface, so that it is known that collection occurs over the entire attractive force region. The presence of a velocity node can only be determined using Equation 102 and the velocity and force components in Table 62. This method of solution can also be used with nonsymmetrical flows such as Oseen flow or flows with standing vortices downstream, but the integration boundary becomes more complex.

Extension of solutions for cylinders

Applying this method of solution (for cases in which it is valid) to circular and elliptical cylinders gives the same results found using stream functions. However, for point particles it can now be shown that some of the two-dimensional results also apply to three-dimensional cases. For instance, in deriving the two-dimensional solutions, the relative orientations of the flow field and the external electric field were subject to the constraint that both be perpendicular to the axis of the collector. Because the force distribution at the surface of the collector is unaffected by the flow, however, the requirement that the flow be perpendicular to the axis can be removed, provided the external fields remain perpendicular. Gauss's law of electrostatics can be used to generalize the result, found originally for cylinders of arbitrary cross-section, that is given by Equation 90. With the coulombic force parameter defined in terms of the average line charge density along the collector, the same result applies to collectors having a cross-section that varies along the axis and to flows that are not perpendicular to the axis. Furthermore, for collection of fine particles with the coulombic type force, the average rate of particle collection is unaffected by deviations from a two-dimensional system caused by temporal particle deposition that is not uniform along the length of the collector.

Equation 126 can also be used to justify Equation 99, given for collection with just the external electric field force, and to extend its validity to include fibers that are not uniform along the axis. Notice that Equation 99 and Equation 138 are of the same form.

Particle Collection With Cellular Flows

The influence of droplet density in wet scrubbers can be investigated using a cellular flow model for flow around spheres. Kuwabara (56) has developed such a model for a system of equal sized droplets dispersed at random and homogeneously throughout the flow. Boundary conditions for the flow around a single droplet are $U_r = \cos\theta$ with zero fluid vorticity at $R = L \equiv R_{cl}/R_c$, where R_{cl} is the radius of the outer surface of the cell; $U_r = U_\theta = 0$ at the surface of the collector. The cell radius L is found from $4\pi L^3/3 = 1/N$, where N is the number of droplets per unit volume. Using the Stokes approximation of a zero collector Reynolds number, the stream function is found to be

$$\Psi_f = \tfrac{1}{2} R^2 h(R) \sin^2\theta \qquad (150)$$

$$h(R) = A/R^3 + B/R + C + DR^2 \qquad (151)$$

$$h(1) = 0, \; h(L) = 1 \qquad (152)$$

$$A \equiv (1 - 2/5L^3)/2Ku \qquad (153)$$

$$B \equiv -3/2Ku \tag{154}$$

$$C \equiv (1 + 1/2L^3)Ku \tag{155}$$

$$D \equiv -3/10L^3Ku \tag{156}$$

$$Ku \equiv 1 - 9/5L + 1/L^3 - 1/5L^6 \tag{157}$$

The stream functions for the forces are given by

$$\Psi_c = -K_c \cos\theta \tag{158}$$

$$\Psi_{ex} = \tfrac{1}{2} K_{ex}R^2(1 + 2Y/R^3)\sin^2\theta \tag{159}$$

$$\Psi_g = \tfrac{1}{2} K_gR^2\sin^2\theta \tag{160}$$

The stream function for particle trajectories is obtained by substituting the flow and force stream functions into Equation 112

$$\Psi = \tfrac{1}{2} R^2P(R)\sin^2\theta - K_c\cos\theta \tag{161}$$

$$P(R) \equiv h(R) + K_{ex}(1 + 2Y/R^3) + K_g \tag{162}$$

The constant value of Ψ for a given particle trajectory, Ψ_1, is defined using the upstream boundary conditions $R = L$, $\theta = \theta_1$,

$$\Psi_1 = \tfrac{1}{2} L^2P(L)\sin^2\theta_1 - K_c\cos\theta_1 \tag{163}$$

Defining $X_1 = L \sin\theta_1$, Equation 163 can be written as

$$\Psi_1 = \tfrac{1}{2} X_1^2 P(L) + K_c(1 - X_1^2/L^2)^{\frac{1}{2}} \tag{164}$$

Solving Equation 164 for X_1^2 gives

$$X_1^2 = 2\{[P(L)\Psi_1 - K_c^2/L^2] - K_c P(L)[1 - 2\Psi_1/L^2P(L) + K_c^2/L^4P(L)^2]^{\frac{1}{2}}\}/P(L)^2 \tag{165}$$

For $X_1 << L$, Equation 165 reduces to

$$X_1^2 = 2(\Psi_1 - K_c)/[P(L) - K_c/L^2] \tag{166}$$

The collection efficiency is defined by $\eta = X_{1i}^2$, where X_{1i} is the value of X_1 for the limiting trajectory. Impaction of particles with interception parameter R occurs for $R = R^* \equiv 1 + R$, and Equation 161 gives

$$\Psi_1 = \tfrac{1}{2} R^{*2} P(R^*)\sin^2\theta - K_c\cos\theta \tag{167}$$

The limiting trajectory value of Ψ_1, denoted by Ψ_{1i}, is determined by identifying the value of $\theta = \theta_i$ for which Ψ_1 is a maximum in Equation 167. From

$$d\Psi_1/d\theta = 0 = [R^{*2}P(R^*)\cos\theta_i + K_c]\sin\theta_i \tag{168}$$

θ_i is given by either $\sin\theta_i = 0$ or $\cos\theta_i = W \equiv -K_c/R^{*2}P(R^*)$. Therefore, considering only positive values of K_{ex} and K_g, for $W \leq -1$, $\Psi_{1i} = K_c$; for $-1 < W < 1$,

$$\Psi_{1i} = [R^{*4}P(R^*)^2 + K_c^2]/2R^{*2}P(R^*) \tag{169}$$

and for $W \geq 1$, $\Psi_{1i} = -K_c$.

The collection efficiency is found by substitution of Ψ_{1i} into either Equation 165 or 166. For $W \leq -1$, Equations 165 and 166 both give $\eta = 0$; for $-1 < W < 1$, Equation 166 gives the approximate result

$$\eta = R^{*2}[P(R^*) - K_c/R^{*2}]^2/P(R^*)[P(L) - K_c/L^2] \quad (170)$$

and for $W \geq 1$, Equation 165 gives the exact result

$$\eta = -4K_c[1 + K_c/L^2P(L)]/P(L) \quad (171)$$

The effect of droplet density can be seen more clearly from the single force results. For the external electric field force alone, Equations 165 and 169 give

$$\eta = R^{*2} \frac{[h(R^*) + K_{ex}(1 + 2\gamma/R^{*3})]}{[1 + K_{ex}(1 + 2\gamma/L^3)]} \quad (172)$$

The coulombic force result is

$$\eta = -4K_c(1 + K_c/L^2) \quad (173)$$

From these results, it is readily apparent that for large L, the droplet density in a wet scrubber has little influence on the single droplet collection efficiency. Furthermore, for point particles these results apply to all cellular flows having $h(L) = 1$ and $h(1) = 0$. In the limit of an

infinite cell radius, the results for a single isolated droplet are recovered. For collection by gravitation alone, it should by noted that the collection efficiency is unaffected by droplet density in the scrubber even for finite particle sizes; Equation 165 reduces to

$$X_{1i}^2 = \frac{R^{*2}[h(R^*) + K_g]}{(1 + K_g)} \qquad (174)$$

CONCLUSIONS

In this study particle trajectories and collection efficiencies are predicted for the collection of fine, inertialess, charged particles on a single isolated filter fiber by the combined actions of coulombic and external electric field forces, gravity, and particle interception. The results reveal how the collection efficiency is affected by such factors as the form of the flow field, the orientation of the external fields and the flow, fiber geometry, and an accumulation of previously collected particles. Using a cellular flow model, the fiber packing density in filters was shown to have little effect on single fiber collection provided the fiber separation distances are large. However, in actual filters interfiber distances are not large and fiber configuration affects both the flow and electrical forces around individual fibers. Also, as indicated by the simple analysis of shadow effects for a series of noninteracting fibers, the particle field entering a filter is soon distorted by the first-encountered fibers, so that single fiber collection efficiencies for interior fibers loose meaning unless they are connected to the particle field entering the filter. Therefore, the next problem at hand is to extend the techniques used in this study to solve for total electric field filter collection efficiencies for different configurations of fibers using

actual flows and electrical fields for interacting neighboring fibers.

For particle collection on droplets in electrified wet scrubbers, previous results for collection on spheres in which the trajectories are two-dimensional are extended to include three-dimensional trajectories (corresponding to the external electric field being at an angle to the flow) and nonspherical droplets. Using a cellular model of flow around a sphere, droplet density in scrubbers is shown to have little effect on droplet collection efficiencies, which is an assumption that is often made since droplet separation distances are often large.

LIST OF REFERENCES

1. Ajmera, P. 1970. Chemical reactions and turbulent mixing. Ph.D. Thesis. Carnegie-Mellon University, Pittsburgh, Pennsylvania. 401 pp.

2. Batchelor, G. K. 1947. Kolmogorov's theory of locally isotropic turbulence. Proceedings of the Cambridge Philosophical Society 43: 533-559.

3. Batchelor, G. K. 1949. The role of big eddies in homogeneous turbulence. Proceedings of the Royal Society (London) A195: 513-532.

4. Batchelor, G. K. 1959. Small-scale variation of convected quantities like temperature in turbulent fluid. Part 1. General discussion and the case of small conductivity. Journal of Fluid Mechanics 5: 113-133.

5. Batchelor, G. K. 1960. The theory of homogeneous turbulence. Cambridge University Press, Cambridge. 197 pp.

6. Batchelor, G. K., I. D. Howells, and A. A. Townsend. 1959. Small-scale variation of convected quantities like temperature in turbulent fluid. Part 2. The case of large conductivity. Journal of Fluid Mechanics 5: 134-139.

7. Beek, J., and R. S. Miller. 1959. Turbulent transport in chemical reactors. Chemical Engineering Progress Symposium Series Number 25, Volume 55: 23-28.

8. Brodkey, R. S. 1967. The phenomena of fluid motions. Addison-Wesley, Reading, Massachusetts. 737 pp.

9. Brodkey, R. S., ed. 1975. Turbulence in mixing operations. Academic Press, New York.

10. Corrsin, S. 1951. On the spectrum of isotropic temperature fluctuations in an isotropic turbulence. Journal of Applied Physics 22: 469-473.

11. Corrsin, S. 1951. The decay of isotropic temperature fluctuations in an isotropic turbulence. Journal of Aeronautical Science 18: 417-423.

12. Corrsin, S. 1957. Simple theory of an idealized turbulent mixer. AIChE Journal 3: 329-330.

13. Corrsin, S. 1958. Statistical behavior of a reacting mixture in isotropic turbulence. Physics of Fluids 1: 42-47.

14. Corrsin, S. 1961. The reactant concentration spectrum in turbulent mixing with a first-order reaction. Journal of Fluid Mechanics 11: 407-416.

15. Corrsin, S. 1962. Some statistical properties of the product of a turbulent, first-order reaction. Pages 105-123 in J. B. Diaz and S. I. Pai, eds. Proceedings of the 1961 Symposium on Fluid Dynamics and Applied Mathematics. Gordon and Breach, New York, New York.

16. Corrsin, S. 1964. Further generalization of Onsager's cascade model for turbulent spectra. Physics of Fluids 7: 1156-1159.

17. Corrsin, S. 1964. The isotropic turbulent mixer: Part II. Arbitrary Schmidt Number. AIChE Journal 10: 870-877.

18. Danckwerts, P. V. 1952. The definition and measurement of some characteristics of mixtures. Applied Scientific Research 3A: 279-296.

19. Dash, R. 1973. Structure of the reactant and product of a turbulent second-order reaction at large wave numbers. Journal of Applied Physics 44: 197-200.

20. Davies, C. N. 1973. Air filtration. Academic Press, New York.

21. Donaldson, C. duP., and G. R. Hilst. 1972. Chemical reactions in inhomogeneous mixtures: The effect of the scale on turbulent mixing. Pages 253-261 in R. B. Landis and G. J. Hordemann, eds. Proceedings of the 1972 Heat Transfer and Fluid Mechanics Institute. Stanford University Press, Stanford, California.

22. Donaldson, C. duP., and G. R. Hilst. 1972. Effect of inhomogeneous mixing on atmospheric photochemical reactions. Environmental Science and Technology 6: 812-816.

23. Dopazo, C. 1973. Non-isothermal turbulent reactive flows: Stochastic approaches. Ph. D. Thesis. State University of New York, Stony Brook, New York. 134 pp.

24. Dopazo, C., and E. E. O'Brien. 1973. Isochoric turbulent mixing of two rapidly reacting chemical species with chemical heat release. Physics of Fluids 16: 2075-2081.

25. Dukhin, S. S., and B. V. Deryagin. 1958. K metodike rascheta osazhdeniia dispersnykh chastits iz potoka na prepiatstviia (On the method of calculating the precipitation of disperse particles from a stream of an obstacle). Kolloidnyi Zhurnal 20: 326-328.

26. Fisher, D. A. 1974. Development and application of a model for fast reactions in turbulently mixed liquids. Ph.D. Thesis. University of Minnesota, Minneapolis, Minnesota. 198 pp.

27. Fuchs, N. A. 1964. The mechanics of aerosols. Pergamon Press, New York.

28. Gibson, C. H. 1968. Fine structure of scalar fields mixed by turbulence. I. Zero-gradient points and minimal gradient surfaces. The Physics of Fluids 11: 2305-2315.

29. Gibson, C. H. 1968. Fine structure of scalar fields mixed by turbulence. II. Spectral theory. The Physics of Fluids 11: 2316-2327.

30. Gibson, C. H., and P.A. Libby. 1972. On turbulent flows with fast chemical reactions. Part II. The distribution of reactants and products near a reacting surface. Combustion Science and Technology 6: 29-35.

31. Happel, J., and H. Brenner. 1965. Low Reynolds number hydrodynamics. Prentice-Hall, Englewood Cliffs, New Jersey.

32. Harris, I. J., and R. D. Shrivastava. 1968. The simulation of single phase tubular reactors with incomplete reactant mixing. Canadian Journal of Chemical Engineering 46: 66-69.

33. Havlicek, V. 1961. The improvement of efficiency of fibrous dielectric filter by application of an external electric field. International Journal of Air and Water Pollution 4: 225-236.

34. Hayt, W. H. 1967. Engineering electromagnetics. 2nd ed. McGraw-Hill, New York.

35. Heisenberg, W. 1948. On the theory of statistical and isotropic turbulence. Proceedings of the Royal Society (London) A195: 402-406.

36a. Hill, J. C. 1970. Zero diffusivity invariance for turbulent chemical reaction. The Physics of Fluids 13: 1394-1396.

36b. Hill, J. C. 1976. Homogeneous turbulent mixing with chemical reaction. Annual Review of Fluid Mechanics 8: 135-161.

37. Hilst, G. R., C. duP. Donaldson, M. Teske, R. Contiliano, and J. Freiberg. 1973. A coupled two-dimensional diffusion and chemistry model for turbulent and inhomogeneously mixed reaction systems. U. S. Environmental Protection Agency Report EPA-R4-73-016c. (Aeronautical Research Associates of Princeton, Princeton, New Jersey)

38. Hinze, J. O. 1959. Turbulence. McGraw-Hill, New York, New York. 586 pp.

39. Hochrainer, D., G. M. Hidy, and G. Zebel. 1969. Creeping motion of charged particles around a cylinder in an electrical field. Journal of Colloid and Interface Science 30: 553-567.

40. Iinoya, K., and K. Makino. 1974. Application of electric field effects to dust collection filters. Journal of Aerosol Science 5: 357-372.

41. von Karman, T., and C. C. Lin. 1949. On the concept of similarity in the theory of isotropic turbulence. Reviews in Modern Physics 21: 516-519.

42. Kattan, A., and R. J. Adler. 1967. A stochastic mixing model for homogeneous, turbulent, tubular reactors. AIChE Journal 13: 580-585.

43. Keeler, R. N., E. E. Petersen, and J. M. Prausnitz. 1965. Mixing and chemical reaction in turbulent flow reactors. AIChE Journal 11: 221-227.

44. Kirisch, A. A. 1972. The influence of an external electric field on the deposition of aerosols in fibrous filters. Journal of Aerosol Science 3: 25-29.

45. Knutson, E. O. 1976. Approximate formulas for electrostatic collection of aerosol particles by spheroids. Journal of Colloid and Interface Science 54: 453-455.

46. Kolmogorov, A. N. 1941. Dissipation of energy in the locally isotropic turbulence. Comptes Rendus (Doklady) de l'Academie des Sciences URSS 32: 16-18.

47. Kolmogorov, A. N. 1941. The local structure of turbulence in incompressible viscous fluid for very large Reynolds numbers. Comptes Rendus (Doklady) de l'Academie des Sciences URSS 30: 301-305.

48. Kraemer, H. G. 1954. Properties of electrically charged aerosols. Ph.D. Thesis. University of Illinois, Urbana, Illinois. 140 pp.

49. Kraichnan, R. H. 1959. The structure of isotropic turbulence at very high Reynolds numbers. Journal of Fluid Mechanics 5: 497-543.

50. Kraichnan, R. H. 1968. Small-scale structure of a scalar field convected by turbulence. The Physics of Fluids 11: 945-953.

51. Kraichnan, R. H. 1974. Convection of a passive scalar by a quasi-uniform random straining field. Journal of Fluid Mechanics 64: 737-762.

52. Kumar, P., and S. R. Patel. 1974. First-order reactant in homogeneous turbulence before the final period of decay. Physics of Fluids 17: 1362-1368.

53. Kumar, P., and S. R. Patel. 1975. On first-order reactants in homogeneous turbulence. International Journal of Engineering Science 13: 305-315.

54. Kumar, P., and Y. Paul. 1969. Structure of the reactant and product of a turbulent first-order reaction at large wave numbers. Proceedings of the National Institute of Science of India 35A: 118-125.

55. Kumar, P., and Y. Paul. 1970. Structure of a turbulent multicomponent mixture with first-order reactions at large wave numbers. Indian Journal of Pure and Applied Mathematics 1: 142-152.

56. Kuwabara, S. 1959. The forces experienced by randomly distributed parallel circular cylinders or spheres in a viscous flow at small Reynolds numbers. Journal of the Physical Society of Japan 14: 527-532.

57. Lamb, H. 1945. Hydrodynamics. 6th ed. Dover Publications, New York.

58. Lee, J. 1966. Isotropic turbulent mixing under a second-order chemical reaction. Physics of Fluids 9: 1753-1763.

59. Lee, J. 1973. Analytical structure of a generalized direct interaction approximation. Quarterly of Applied Mathematics 31: 155-176.

60. Leslie, D. C. 1973. Developments in the theory of turbulence. Oxford University Press, London. 368 pp.

61. Levin, L. M. 1959. Electrostatic precipitation of aerosol particles from a flow upon large bodies. Bulletin of the Academy of Sciences, USSR Geophysics Series 1959: 766-767.

62. Libby, P. A. 1972. On turbulent flows with fast chemical reactions. Part I. The closure problem. Combustion Science and Technology 6: 23-28.

63. Lin, C.-H. 1971. Stochastic chemical reaction with molecular diffusion. M.S. Thesis. State University of New York, Stony Brook, New York. 73 pp.

64. Lin, C.-H. 1974. Dynamically passive turbulent mixing of chemically reacting species. Ph.D. Thesis. State University of New York, Stony Brook, New York. 93 pp.

65. Lin, C.-H., and E. E. O'Brien. 1972. Two species isothermal reactions in homogeneous turbulence. Astronautica Acta 17: 771-781.

66. Lin, C.-H., and E. E. O'Brien. 1974. Turbulent shear flow mixing and rapid chemical reactions: An analogy. Journal of Fluid Mechanics 64: 195-206.

67. Loeffler, A. L., and R. G. Deissler. 1961. Decay of temperature fluctuations in homogeneous turbulence before the final period. International Journal of Heat and Mass Transfer 1: 312-324.

68. Lundgren, D. A. , and I. T. Whitby. 1965. Effect of particle electrostatic charge on filtration by fibrous filters. Industrial and Engineering Chemistry, Process Design and Development 4: 345-349.

69. Makino, K., and K. Iinoya. 1968. Experiments on collection efficiency of a dielectric fibre mat filter. Kagaku Kogaku 32: 99-104.

70. Mao, K. W., and H. L. Toor. 1970. A diffusion model for reactions with turbulent mixing. AIChE Journal 16: 49-52.

71. Mao, K. W., and H. L. Toor. 1971. Second-order chemical reactions with turbulent mixing. Industrial and Engineering Chemistry Fundamentals 10: 192-197.

72. McKelvey, K. N. 1968. Turbulent mixing with chemical reaction. Ph.D. Thesis. Ohio State University, Columbus, Ohio. 123 pp.

73. Menkes, J., and C. M. Tchen. 1968. Spectrum of turbulence and concentration fluctuations with chemical mixing and reactions. Institute for Defense Analyses Research Paper P-407. AD-67037. (Institute for Defense Analysis, Arlington, Virginia)

74. Milne-Thomson, L. M. 1969. Theoretical hydrodynamics. 4th ed. Macmillan and Company, New York.

75. Miyairi, Y., M. Kamiwano, and K. Yamamoto. 1971. Turbulent mixing in a turbulent flow reactor. International Chemical Engineering 11: 344-352.

76. Miyawaki, O., H. Tsujikawa. and Y. Uraguchi. 1974. Turbulent mixing in a multi-nozzle injection tubular mixer. Journal of Chemical Engineering of Japan 7:52-56.

77. Moon, P., and D. E. Spencer. 1961. Field theory for engineers. Van Nostrand, Princeton, New Jersey.

78. Murthy, S. N. B., ed. 1975. Turbulent mixing in nonreactive and reactive flows. Plenum Press, New York.

79. Natanson, G. L. 1957. Osazhdenie aerozolnykh chastits na obtekaemom tsilindre pod deistviem elektrostaticheskogo pritiazheniia (The condensation of aerosol particles by electrostatic attraction on a cylinder around which they are streaming). Doklady Akademii Nauk SSSR 112: 696-699; Proceedings of the Academy of Science of the USSR, Physical Chemistry Section 112: 95-98.

80. Nielsen, K. A. 1974. Effect of electrical forces on target efficiencies for spheres. Engineering Research Institute Technical Report 74127. Iowa State University, Ames, Iowa. 391 pp.

81. Nielsen, K. A., and J. C. Hill. 1976. Collection of inertialess particles on spheres with electrical forces. Industrial and Engineering Chemistry, Fundamentals 15: 149-157.

82. Nielsen, K. A., and J. C. Hill. 1976. Capture of particles on spheres by inertial and electrical forces. Industrial and Engineering Chemistry, Fundamentals 15: 157-163.

83. Nye, J O., and R. S. Brodkey. 1967. The scalar spectrum in the viscous-convective subrange. Journal of Fluid Mechanics 29: 151-163.

84. O'Brien, E. E. 1960. On the statistical behavior of a dilute reactant in isotropic turbulence. Ph.D. Thesis. Johns Hopkins University, Baltimore, Maryland. 76 pp.

85. O'Brien, E. E. 1965. The second-order isothermal reaction in isotropic turbulence. AIAA Paper 65-812 presented at the AIAA Aerothermochemistry of Turbulent Flows Conference, San Diego, California. American Institute of Aeronautics and Astronautics, New York, New York.

86. O'Brien, E. E. 1966. Closure approximations applied to stochastically distributed second-order reactants. Physics of Fluids 9: 1561-1565.

87. O'Brien, E. E. 1966. Decaying second-order isothermal reaction in final period turbulence. Physics of Fluids 9: 215-216.

88. O'Brien, E. E. 1968. Closure for stochastically distributed second-order reactants. Physics of Fluids 11: 1883-1888.

89. O'Brien, E. E. 1968. Lagrangian history direct interaction equations for isotropic turbulent mixing under a second-order chemical reaction. Physics of Fluids 11: 2328-2335, 12: 1960.

90. O'Brien, E. E. 1968. Quantitative test of the direct interaction hypothesis. Physics of Fluids 11: 2087-2088.

91. O'Brien, E. E. 1969. Postulate of statistical independence for decaying reactants in homogeneous turbulence. The Physics of Fluids 12: 1999-2005.

92. O'Brien, E. E. 1971. Turbulent mixing of two rapidly reacting chemical species. Physics of Fluids 14: 1326-1331.

93. O'Brien, E. E. 1971. Very rapid, isothermal, two-species reactions in final period turbulence. Physics of Fluids 14: 1804-1806.

94. O'Brien, E. E. 1974. Turbulent diffusion of rapidly reacting chemical species. Advances in Geophysics 18B: 341-348.

95. O'Brien, E. E., and R. M. Eng. 1970. Closure for stochastically distributed reactants. Physics of Fluids 13: 1393-1394.

96. O'Brien, E. E., and G. C. Francis. 1962. A consequence of the zero fourth cumulant approximation. Journal of Fluid Mechanics 13: 369-382.

97. O'Brien, E. E., and C.-H. Lin. 1972. Numerical examination of two species reactions in final period turbulence. Physics of Fluids 15: 931-933.

98. Obukhov, A. M. 1949. Structure of the temperature field in turbulent flow. Izvestiia Akademii Nauk SSSR, Seriia Geograficheskaia i Geofizicheskaia 13: 58.

99. Onsager, L. 1945. The distribution of energy in turbulence. Physical Review 68: 286.

100. Onsager, L. 1949. Statistical hydrodynamics. Nuovo Cimento, Supplement 6: 279.

101. Orszag, S. A. 1969. Numerical methods for the simulation of turbulence. The Physics of Fluids 12, Supplement II: 250-257.

102. Pao, Y.-H. 1962. Diffusive quantities in turbulent fluid. Ph.D. Thesis. Johns Hopkins University, Baltimore, Maryland. 118 pp.

103. Pao, Y.-H. 1964. Statistical behavior of a turbulent multicomponent mixture with first-order reactions. AIAA Journal 2: 1550-1559.

104. Pao, Y.-H. 1965. Structure of turbulent velocity and scalar fields at large wavenumbers. Physics of Fluids 8: 1063-1075.

105. Pao, Y.-H. 1968. Transfer of turbulent energy and scalar quantities at large wavenumbers. Physics of Fluids 11: 1371-1372.

106. Patel, S. R. 1974. Multi-point, multi-time concentration correlations and decay of homogeneous turbulence. International Journal of Engineering Science 12: 159-178.

107. Patel, S. R. 1976. On first-order reactants in homogeneous turbulence - numerical results. International Journal of Engineering Science 14: To appear.

108. Paul, Y. 1966. Reactant and product concentration spectrum functions in turbulent mixing with a first-order reaction. Tensor 17: 308-312.

109. Pavlica, R. T. 1968. The effect of viscoelasticity upon reaction rates in turbulent systems. M.S. Thesis. University of Delaware, Newark, Delaware. 91 pp.

110. Proudman, I., and J. R. A. Pearson. 1957. Expansions at small Reynolds numbers for the flow past a sphere and a circular cylinder. Journal of Fluid Mechanics 2: 237-262.

111. Rao, D. P., and I. J. Dunn. 1970. A Monte Carlo coalescence model for reaction with dispersion in a tubular reactor. Chemical Engineering Science 25: 1275-1282.

112. Rao, D. P., and L. L. Edwards. 1971. Conversion in turbulent tubular reactors with unmixed feed. Industrial and Engineering Chemistry Fundamentals 10: 398-400.

113. Rao, D. P., and L. L. Edwards. 1971. On the diffusion model of Mao and Toor. AIChE Journal 17: 1264-1265.

114. Rosenhead, L., ed. 1963. Laminar boundary layers. Oxford University Press, London.

115. Singh, M. 1973. Chemical reactions in one and two dimensional turbulent flow systems. Ph.D. Thesis. Carnegie-Mellon University, Pittsburgh, Pennsylvania. 314 pp.

116. Stenhouse, J. I. T. 1974. The influence of electrostatic forces in fibrous filtration. Filtration and Separation 11: 25-26.

117. Tchen, C. M. 1953. On the spectrum of energy in turbulent shear flow. Journal of Research of the National Bureau of Standards 57: 51-62.

118. Tchen, C. M. 1965. Spectral theory of turbulent mixing processes with applications to reactions. Space Sciences Laboratory Report R65SD66. General Electric Company, King of Prussia, Pennsylvania.

119. Thomas, J. W., and E. J. Woodfin. 1959. Electrified fibrous air filters. Transactions of the American Institute of Electrical Engineers II, 78: 276-278.

120. Tomotika, S., and T. Aoi. 1950. The steady flow of viscous fluid past a sphere and circular cylinder at small Reynolds numbers. Quarterly Journal of Mechanics and Applied Mathematics 3: 140-161.

121. Toor, H. L. 1962. Mass Transfer in dilute turbulent and nonturbulent systems with rapid irreversible reactions and equal diffusivities. AIChE Journal 8: 70-78.

122. Toor, H. L. 1967. The invariance of the scalar decay law. AIChE Journal 13:616.

123. Toor, H. L. 1969. Turbulent mixing of two species with and without chemical reactions. Industrial and Engineering Chemistry Fundamentals 8: 655-659.

124. Toor, H. L., and S. H. Chiang. 1959. Diffusion-controlled chemical reactions. AIChE Journal 5: 339-344.

125. Toor, H. L., and M. Singh. 1973. The effect of scale on turbulent mixing and on chemical reaction rates during turbulent mixing in a tubular reactor. Industrial and Engineering Chemistry Fundamentals 12: 448-451.

126. Torrest, R. S., and W. E. Ranz. 1970. Concentration fluctuations and chemical conversion associated with mixing in some turbulent flows. AIChE Journal 16: 930-942.

127. Vassilatos, G., and H. L. Toor. 1965. Second-order chemical reactions in a nonhomogeneous turbulent fluid. AIChE Journal 11: 666-673.

128. Walkenhorst, W. 1970. Reflections and research on the filtration of dust from gases with special consideration of electrical forces. Journal of Aerosol Science 1: 225-242.

129. Walkenhorst, W., and G. Zebel. 1964. Über ein neues Schwebstoffilter hoher Abscheideleistung und Geringen Strömungswiderstandes (A new aerosol filter that has both high collection efficiency and low flow resistance). Staub Reinhaltung der Luft 24: 444-448.

130. Whipple, F. J. W., and J. A. Chalmers. 1944. On Wilson's theory of the collection of charge by falling drops. Quarterly Journal of the Royal Meteorological Society 70: 103-119.

131. Yieh, H. 1970. Turbulent mixing with chemical reaction. Ph.D. Thesis. Ohio State University, Columbus, Ohio. 135 pp.

132. Yoshioka, N., H. Emi, M. Hattori, and I. Tamori. 1968. Effect of electrostatic force on the filtration efficiency of an aerosol. Kagaku Kogaku 32: 815-820.

133. Zebel, G. 1965. Deposition of an aerosol flowing past a cylindrical fiber in a uniform electric field. Journal of Colloid Science 20: 522-543.

ACKNOWLEDGMENTS

The author wishes to express his deep appreciation to Dr. James C. Hill for his continuing encouragement, advise, and interest in this work.

Thanks to Dr. William H. Abraham, Dr. Richard C. Seagrave, Dr. Robert J. Angelici, and Dr. Lennox N. Wilson for serving on the doctoral committee.

Special appreciation is expressed to the author's wife, Linda M. Nielsen, for her patience, encouragement, perseverance, and understanding throughout the course of this investigation; to the author's daughter, Annette Marie, who throughout this work had to miss being with her daddy more than should have been; to the author's parents, LaVerne and Howard A. Nielsen, for their constant encouragement; and to the author's inlaws, Mary and D. Hugh Miller, whose Iowa farm provided a pleasant retreat from this work. This dissertation is dedicated to the memory of the author's paternal grandparents, Agnes and Andreas Nielsen-Muurmand, and maternal grandparents, Marie and Hans Wentzer Møller-Nielsen, who sought freedom of opportunity in a new land and thereby set the stage for this work.

Computer funds provided by the Engineering Research Institute of Iowa State University and by an Exxon Grant in Aid to the Chemical Engineering Department at Iowa State University are gratefully acknowledged.

The author was supported during this work by a National Defense Education Act Title IV Fellowship, Procter and Gamble Company Fellowship, and American Oil Company Fellowship.

November 18, 1976

„Glücklich ist,
Wer vergisst,
Das was nicht zu ändern ist."